

UNIVERSITY OF PADOVA
Department of Civil, Environmental and
Architectural Engineering



**SIMPLIFIED DISPLACEMENT-BASED APPROACHES
FOR SEISMIC DESIGN AND VULNERABILITY
ASSESSMENT OF MULTI-SPAN RC BRIDGES**

A dissertation submitted in partial fulfillment
of the requirements for the degree of
DOCTOR OF PHILOSOPHY
in Civil and Environmental Engineering

By
Giovanni Tecchio

Padova, January 2013



UNIVERSITÀ
DEGLI STUDI
DI PADOVA

Sede Amministrativa: Università degli Studi di Padova

Dipartimento di
INGEGNERIA CIVILE, EDILE ED AMBIENTALE (DICEA)

DOTTORATO DI RICERCA IN : SCIENZE DELL'INGEGNERIA CIVILE ED AMBIENTALE
CICLO XXV

TITOLO TESI: **SIMPLIFIED DISPLACEMENT-BASED APPROACHES FOR SEISMIC
DESIGN AND VULNERABILITY ASSESSMENT OF MULTI-SPAN RC BRIDGES**

Coordinatore : Ch.mo Prof. Stefano Lanzoni

Supervisore : Ch.mo Prof. Claudio Modena

Dottorando : Giovanni Tecchio

© Giovanni Tecchio, 2012

All rights reserved

SUMMARY

Simplified methods of seismic verification, using equivalent single degree of freedom systems for the response prediction, have been the subject of great emphasis on research in the field of earthquake engineering particularly since the mid-1990s. This interest is justified still today by the great uncertainty characterizing the prediction of the seismic response: the variability of the parameters influencing the structural capacity and the seismic input definition, makes the use of sophisticated models not always effective and warranted. Furthermore, the extensive use of Non Linear Time-History (NLTH) analyses requires a calibration of the hysteretic model parameters and ground motions that seems still to date hardly applicable to day to day engineering practice.

At the same time in last decade the design for earthquake resistance has undergone a critical review, triggered by the concept of Performance-Based Design. Performance objectives represent the attainment of certain damage levels for a given seismic intensity, and it has been widely recognized that the damage measure for a structure is directly related to deformations: displacements are the fundamental index of structural damage in seismic events and the achievement of the target displacement in relation to the different limit states should be the main objective of the verification procedure.

Displacement-Based methods for seismic verification of structures hold together the two aspects evidenced so far, being simplified procedures which rely on a substitute SDOF structure and use as reference control parameter the target limit displacement for the system under exam.

At present Displacement-Based Design (DBD) methods for new structures have reached a degree of formalization almost complete, with the recent publication of a Model Code for their adoption into seismic codes (Calvi and Sullivan, 2009). However, several aspects related to the method calibration are still matter of research, being the representativeness of the substitute linear structure a critical issue, in particular the formulation of equivalent viscous damping and the definition of the target displacement profile for a given structural system.

With regard to the appraisal of existing structures, the development of Displacement-Based Assessment (DBA) approach represents the state of the art of research in this field, since so far the calibration of the methods dealt essentially with new structures only. The specific problems of the development of DBA methodologies include the prediction of the possible collapse mechanisms due to brittle rupture of members (which may be substantially different from those of the new ductile structures, designed following capacity design criteria), and the inclusion of local damage effects caused by nodes not adequately confined.

In this context the research activity focuses on the evaluation, calibration and development of simplified Displacement-Based approaches for seismic verification of bridge structures, with particular reference to their use in a probabilistic framework, represented by vulnerability analyses and risk calculation on a large scale.

In the first part the thesis addresses the methodological aspects of the DBD procedures focusing on the error sources of the simplified methods. In particular the current design methods for new structures with flexural ductile behaviour are evaluated, with reference to the formulations of the equivalent viscous damping and target displacement profile to be adopted in the analysis.

A first study investigates the accuracy of the current Direct Displacement-Based Design (DDBD) procedure applied to simple SDOF systems (with specific reference to multi-span simply supported rc bridge piers), the main error sources being the approximation of the substitute linear structure characterized by the equivalent viscous damping, and the scaling of the displacement elastic spectrum through the modification damping factor. Using different formulations proposed in literature for equivalent viscous damping and spectrum reduction factor, a parametric study is carried out on an ample set of SDOF systems (previously designed with the DDBD method and subsequently verified with NLTH analyses), and an average error chart is obtained, allowing the prediction of the expected error for the design cases of multi-span simply supported bridge piers.

A second work investigates the representativeness of the equivalent SDOF structure related to the estimation of the design displacement profile within a displacement-based framework. In the case of transverse response prediction for continuous rc girder bridges, the accuracy of the current iterative Direct Displacement-Based method (called DBD-IT in this work) is evaluated, and compared to an alternative direct design method (named DBD-DEM) herein proposed. The alternative methods combine in a non-iterative procedure the DBD framework with a Response Spectrum Analysis carried out with effective stiffness.

In the second part the methodological aspects are addressed with regard to the specific issues of the existing bridge structures, not seismically designed (and not satisfying capacity design principles), and thus characterized by failure modes, limit states, hysteretic behaviour, and local ductility of the nodes that are different from those characterizing new seismically designed structures. In particular the calibration effort regards the assessment of pier capacity, piers generally representing the most vulnerable elements in existing bridges. A simplified numerical model is defined for the aggregation of phenomenological non linear shear behaviour and fiber representation of flexural behaviour for piers, calibrated by using experimental results on rc columns with flexure and shear failure extracted from on line databases (PEER database). A parametrical study is then developed for single bent and multiple bent piers (cantilever, walls frame), considering all main geometrical and material properties that can influence the pier capacity, aiming at the determination of the effective properties for existing rc bridge piers, to be used in a Displacement-Based framework. The effective ranges of the selected parameters were determined by a preliminary statistical analysis on the bridges of the reference database (the Veneto Region road network bridge stock, named VR stock).

With regard to the appraisal of existing structures, the specific advantage in the use of simplified analytical procedures becomes apparent when a probabilistic seismic risk estimation is carried out on a large-scale. In this study, in the final part, the DBA method previously calibrated, is applied to assess the seismic vulnerability of the bridge stock under exam on a regional scale. A limited number of bridges are

chosen as reference examples for each homogeneous subclass of multi-span bridges, comparing simplified DBA procedures with NLTH analyses for the development of analytical fragility curves, and an extensive vulnerability analysis for the class of multi-span rc bridges of the VR stock is then developed, using the previously calibrated DB fragility curves.

Finally regional seismic risk maps are drafted including all the multi-span rc bridges of the VR stock, for three different scenarios of damage: the seismic risk is obtained by the convolution of hazard functions, defined on the base of the PGA exceedance probabilities provided by the current Italian seismic code, and the analytical fragility curves calculated with the Displacement-Based approaches.

An immediate extension of the research on existing rc bridges, may be represented by the development of fragility curves for the whole classes of multi-span structures: these fragility functions could be obtained considering the variability in the range of geometrical and mechanical characteristics obtained from the statistical analysis of the VR database for that specific classes, and the envelope curves obtained could than be applied for the vulnerability evaluation of typical bridges of the Italian or European stocks.

A long-term development of the work may regard the extension of the simplified Displacement-Based procedures to the evaluation of different classes of structures, particularly of single span rc bridges and masonry arch bridges, which represent the other major category of existing bridges, to complete as much as possible the scenario of seismic risk for the infrastructure network under examination. In this context it will be possible to calibrate the seismic input for risk analysis through the use of hazard curves, obtained from micro-zonation studies in the areas of interest.

Keywords: *simplified methods, Displacement-Based approaches, seismic design of bridges, vulnerability assessment, large-scale risk analysis.*

SOMMARIO

I metodi semplificati di verifica sismica, che utilizzano sistemi equivalenti ad un grado di libertà per la predizione della risposta, hanno avuto larga diffusione nello scorso decennio, non solo per il progetto di nuove opere ma soprattutto in relazione alla valutazione del comportamento strutturale dell'esistente. Parallelamente, con l'affermazione di approcci alla progettazione basati su criteri di performance, si è consolidato il concetto che il parametro più adeguato di misura della risposta sismica è rappresentato dallo spostamento, e il raggiungimento dello spostamento target in relazione ai diversi stati limite rappresenta il vero obiettivo della procedura di verifica.

Le metodologie semplificate di progetto e valutazione basate sugli spostamenti (Displacement-Based), tengono insieme questi due aspetti, basandosi nella formulazione corrente su un sistema equivalente lineare ad un grado di libertà rappresentativo del sistema non lineare reale, e utilizzando come parametro di controllo della procedura lo spostamento limite accettabile per quel dato sistema strutturale.

Per quanto riguarda gli aspetti del progetto di nuove strutture, tali metodologie hanno ormai raggiunto un grado di formalizzazione pressoché completo, con la pubblicazione in tempi molto recenti della proposta finale di un Model Code (Settembre 2012) per il loro recepimento nei codici normativi. Restano tuttavia oggetto di ricerca e sperimentazione gli aspetti legati alla calibrazione del metodo, in relazione alla rappresentatività del sistema equivalente lineare ad un grado di libertà, legata alle caratteristiche di smorzamento viscoso equivalente e al profilo di spostamento target da assumere per le diverse tipologie di strutture. Per quanto riguarda il tema della valutazione delle strutture esistenti, lo sviluppo di approcci agli spostamenti rappresenta lo stato dell'arte della ricerca in quest'ambito, avendo la taratura del metodo riguardato sinora sostanzialmente le sole nuove strutture. Le problematiche specifiche dei metodi di valutazione riguardano la necessità di estendere la previsione dei possibili meccanismi globali di rottura per crisi di tipo fragile degli elementi, che possono essere del tutto dissimili da quelli delle nuove strutture duttili progettate secondo i criteri del capacity design, e l'inclusione degli effetti locali dovuti a fenomeni di danneggiamento per crisi dei nodi non adeguatamente confinati. E' di attualità inoltre l'applicazione dei metodi di valutazione basati sugli spostamenti nelle analisi di rischio sismico a larga scala, in molti studi sinora basate sulle metodologie di analisi statica non lineare, che presentano molti aspetti comuni ai metodi displacement-based.

In questo contesto si inserisce il lavoro di ricerca sulle strutture da ponte, che si focalizza nella prima parte sull'aspetto dell'affidabilità dei metodi di progetto per le nuove opere (Displacement-Based Design) e nella seconda sulle procedure di valutazione dell'esistente (Displacement-Based Assessment) con metodi deterministici e stime in ambito probabilistico della vulnerabilità sismica.

Per quanto riguarda il tema del design, un primo studio affronta la valutazione dell'errore del metodo semplificato DDBD per strutture ad un grado di

libertà, individuando come principale fonti di approssimazione del metodo la formulazione dello smorzamento viscoso per il sistema 1gdl lineare equivalente, e la taratura del fattore di riduzione dello spettro elastico in spostamento. Sulla base di un'estesa analisi parametrica su un campione di sistemi SDOF, progettati con il metodo DDBD e verificati con analisi dinamiche non lineari in time history, si è pervenuti alla determinazione di un abaco semplificato e alla stima dell'errore per sistemi reali, rappresentati da pile da ponte in c.a. per impalcati in semplice appoggio.

Un secondo lavoro sulle procedure di progetto riguarda la risposta sismica in direzione trasversale dei ponti continui a travata, e la valutazione dell'attuale procedura iterativa, in relazione alla regolarità strutturale. La predizione della risposta trasversale con un approccio Displacement-Based presenta alcuni aspetti critici legati alla rappresentatività del sistema equivalente 1gdl rispetto al sistema mgdl di partenza, e in particolare alla difficoltà di una corretta stima del profilo di spostamento di progetto per ponti irregolari. La procedura corrente viene comparata con una procedura proposta (non iterativa) che utilizza in modo diretto l'output del metodo DBD in termini di stima delle rigidezze della struttura per effettuare un'analisi spettrale con rigidezze effettive, e che consente di combinare l'effetto dei modi superiori nella risposta.

Per quanto attiene al metodo di valutazione dell'esistente, l'interesse specifico dell'utilizzo di procedure semplificate affidabili ed efficienti dal punto di vista computazionale rispetto a metodi più complessi quali analisi dinamiche non lineari nel dominio del tempo, risulta del tutto evidente con analisi probabilistiche per stime di rischio a larga scala. In quest'ambito il lavoro si è incentrato sulla valutazione di vulnerabilità sismica di opere da ponte con i metodi agli spostamenti, utilizzando come caso studio di riferimento il sistema della rete stradale della regione Veneto, che consta di circa 2700km di strade provinciali e regionali in cui si inseriscono 495 opere da ponte considerate strategiche, collocate prevalentemente in zona sismica 2 e 3.

Un'approfondita analisi statistica preliminare è stata svolta nell'ambito del lavoro di tesi per la determinazione delle caratteristiche dello stock di ponti oggetto dell'indagine: il database disponibile raccoglie i dati dei ponti oggetto di verifiche sismiche svolte nel periodo 2007-2010 dall'Università di Padova per gli enti gestori della rete, e della campagna di indagini strutturali svolta a supporto. A partire da alcuni dati di anagrafica generale e utilizzando le informazioni disponibili su ciascun manufatto, è stato possibile individuare con specifico riferimento ai ponti a travata in c.a., che rappresentano il 70% circa dei manufatti dello stock, le caratteristiche geometriche, meccaniche e di armatura per classi omogenee di strutture, ottenendo un inventario di dati con un livello di dettaglio molto più approfondito dei comuni database utilizzati per le analisi di rischio a larga scala. Questo lavoro preparatorio ha rappresentato la base di dati necessari per svolgere una serie di analisi parametriche per la caratterizzazione delle curve di capacità dei ponti esistenti in c.a., che rappresentano il primo step di calcolo per la valutazione sismica con procedure semplificate agli spostamenti. Dallo studio parametrico è stato inoltre possibile calibrare con maggior precisione gli stati limite da assumere con riferimento a predefiniti livelli di danno, e ottenere una miglior taratura delle formulazioni dello smorzamento equivalente per le pile in c.a. esistenti.

La seconda parte del lavoro sulle strutture esistenti riguarda lo studio di vulnerabilità per i ponti a travata in c.a. costituenti lo stock e la successiva analisi di rischio: i metodi semplificati DBA sono stati utilizzati per la creazione di curve di fragilità per i ponti a travata in c.a. per 3 prefissati livelli di danno, e l'analisi di rischio è stata ottenuta come convoluzione con le curve di pericolosità sismica fornite dalla normativa italiana vigente, ottenendo delle mappe di scenario di danno atteso a larga scala. Tali mappe costituiscono il primo esempio della mappatura estesa del rischio sismico applicata alla rete infrastrutturale della Regione Veneto, con la particolarità di essere state ottenute sulla base di curve di fragilità analitiche con metodi semplificati di valutazione agli spostamenti, calibrate sulle caratteristiche specifiche di queste tipologie di ponti esistenti, che sono del tutto rappresentative dei ponti stradali realizzati in Italia dal secondo dopoguerra ad oggi. Altri studi analoghi svolti negli ultimi anni per la valutazione del rischio infrastrutturale a larga scala si sono basati su procedure consolidate quali il metodo HAZUS (RISK-UE), che non sono tarati sulle caratteristiche specifiche dei ponti italiani non essendo generalmente disponibili database per studi a larga scala con informazioni di dettaglio tali da consentire una calibrazione delle curve di fragilità come in questo studio.

Un'estensione dello studio sull'esistente è rappresentato dalla costruzione di curve di fragilità per intere classi omogenee di strutture per ponti esistenti in c.a.: tali curve sono state ottenute a partire dalle curve di fragilità analitiche calcolate per una serie di opere master scelte come rappresentative delle classi omogenee di ponti del database, utilizzando la variabilità sui range delle caratteristiche geometriche e meccaniche ottenute dall'analisi statistica del database di riferimento precedentemente descritta.

Sviluppi futuri del lavoro riguardano infine l'estensione delle procedure proposte di valutazione a classi diverse di strutture rispetto ai ponti in c.a., in particolare ai ponti ad arco in muratura che rappresentano l'altra categoria rilevante di opere dello stock, per arrivare ad una definizione il più possibile completa del rischio sismico sulle opere della rete in esame e ad una taratura di curve di fragilità specifiche per queste classi di opere. Sarà inoltre possibile calibrare in modo più puntuale la definizione dell'input sismico attraverso l'utilizzo di curve di hazard ottenute da mappe di pericolosità sismica locale mediante studi di micro zonazione per le aree di interesse.

*Ad Elisabetta:
se non fosse per lei, non sarei giunto sin qui*

ACKNOWLEDGEMENTS

My first and utmost gratitude is to my tutor, Prof. Claudio Modena for his supervision and suggestions during my PhD study. His generous encouragements and great enthusiasm have always stimulated me to face challenges with confidence.

My thanks also go to Dr. Eng. Francesca Da Porto, and Dr. Eng. Carlo Pellegrino. The extensive discussions and close cooperation with them resulted in many of the ideas presented in this work.

I also wish to express my special thanks to all the friends and colleagues I met during the doctoral program, who have given with their efforts and enthusiasm a great contribution to the realization of this thesis, in particular Marco Donà, who deserves my special gratitude, Daniele Ali Santoro, Paolo Zampieri.

I am also indebted to all friends at SM Ingegneria for the constant support and understanding they all have provided.

The final acknowledgement is for my English teacher; her professional proofreading and kind assistance was of great help during all the work.

*Giovanni Tecchio
January 2013, Padova, Italy*

TABLE OF CONTENTS

SUMMARY	iii
SOMMARIO	vii
ACKNOWLEDGEMENTS	xii
LIST OF FIGURES	xix
LIST OF TABLES	xxiii
LIST OF SYMBOLS	xxix
CHAPTER 1	
INTRODUCTION	1
1.1 BACKGROUND OF DISPLACEMENT-BASED SEISMIC VERIFICATION PROCEDURES	
1.1.1 Criticisms of Force-Based seismic design approaches	4
1.2 RESEARCH MOTIVATION	8
1.3 RESEARCH OBJECTIVES	9
1.4 RESEARCH CONTENTS	9
1.4.1 Methods of investigation	11
1.4.2 Restrictions	11
1.5 OUTLINE OF THE THESIS	12
CHAPTER 2	
REVIEW OF CURRENT DISPLACEMENT-BASED METHODS FOR SEISMIC DESIGN AND ASSESSMENT OF BRIDGES	15
2.1 FUNDAMENTALS OF THE DIRECT DISPLACEMENT-BASED DESIGN METHOD	15
2.1.1 Performance levels: section and structure limit states	17
2.1.2 Displacement response spectra	21
2.1.3 Equivalent Damping models	24
2.1.4 Elastic Spectrum Reduction Factor	30
2.1.5 Stiffness and material and properties of rc sections	32
2.2 DISPLACEMENT-BASED DESIGN OF GIRDER BRIDGES	34
2.2.1 SDOF bridge structures	36
2.2.2 MDOF bridge structures: continuous bridges	37
2.3 DISPLACEMENT-BASED APPROACHES FOR SEISMIC ASSESSMENT OF EXISTING STRUCTURES	45
2.3.1 Specific issues for DBA	45

2.3.2 Displacement Based Assessment procedures	46
2.4 CLOSING REMARKS	48
CHAPTER 3	
DIRECT DISPLACEMENT-BASED DESIGN METHOD: ERROR PREDICTION FOR MULTI-SPAN SIMPLY SUPPORTED BRIDGES	51
3.1 INTRODUCTION	51
3.2 ERROR SOURCES OF THE DDBD METHOD FOR SDOF SYSTEMS	52
3.3 PARAMETRICAL ANALYSIS FOR IDEAL SDOF SYSTEMS	53
3.3.1 Elastic Displacement Response spectrum	53
3.3.2 Equivalent viscous damping models	54
3.3.3 Response spectrum reduction factors	57
3.3.4 Evaluation algorithm	58
3.3.5 DDBD verification.....	60
3.4 PREDICTION ERROR FOR DIRECT DISPLACEMENT-BASED DESIGN OF CANTILEVER BRIDGE RC BRIDGE PIERS	67
3.4.1 Input data and design limitations.....	67
3.4.2 Design process of cantilever rc piers and limits check.....	68
3.4.3 Relationship between drift and ductility.....	72
3.5 CONCLUSIONS	73
CHAPTER 4	
DISPLACEMENT-BASED DESIGN FOR TRANSVERSE RESPONSE OF CONTINUOUS RC GIRDER BRIDGES: ITERATIVE VS DIRECT PROCEDURES	75
4.1 INTRODUCTION	75
4.2 ISSUES RELATED TO THE PROPOSAL OF THE DBD-DEM PROCEDURE	77
4.3 DBD-IT AND DBD-DEM PROCEDURE.....	79
4.4 CASE-STUDIES AND REGULARITY OF BRIDGES.....	82
4.5 GROUND MOTION AND PERFORMANCE CRITERIA	85
4.6 VERIFICATION STUDY	86
4.7 SUMMARY OF DBD-IT VS DBD-DEM RESULTS.....	91
4.8 CONCLUSIONS	95
CHAPTER 5	
DISPLACEMENT-BASED ASSESSMENT OF EXISTING BRIDGES: PARAMETRICAL ANALYSIS FOR CAPACITY OF RC PIERS	97
5.1 INTRODUCTION	97
5.2 SIMPLIFIED PHENOMENOLOGICAL MODEL FOR AGGREGATION OF FLEXURE BEHAVIOUR AND NON-LINEAR SHEAR EFFECTS	99
5.2.1 Aggregation of non-linear shear effects	100
5.2.2 Shear-Cracking equations.....	103
5.2.3 Shear capacity envelope	105
5.2.4 Implementation in the F.E. model	106

5.2.5	Experimental database	108
5.2.6	Calibration of Equivalent Viscous Damping expression for shear- failure mechanisms	115
5.3	PARAMETRICAL ANALYSIS	119
5.3.1	Single bent (cantilever) piers with circular section	119
5.3.2	Multiple bent (frame) piers with circular section	134
5.4	CONCLUSIONS	148

CHAPTER 6

DISPLACEMENT-BASED APPROACHES FOR THE VULNERABILITY ASSESSMENT OF RC BRIDGES: APPLICATION ON A REGIONAL-SCALE CASE STUDY		151
6.1	INTRODUCTION	151
6.2	THE VENETO REGION ROAD NETWORK BRIDGE STOCK	154
6.2.1	General characteristic of the stock –SET1-	156
6.2.2	Rc bridge stock –SET2-	160
6.2.3	Material properties of the existing rc bridges (SET4)	173
6.2.4	Extent of the database	180
6.2.5	Reference Bridge structures	183
6.3	DISPLACEMENT-BASED ASSESSMENT OF REFERENCE BRIDGE STRUCTURES: DETERMINISTIC APPROACH	187
6.3.1	F.E. model	187
6.3.2	Seismic action	188
6.3.3	Performance levels and damage indexes	191
6.3.4	Comparison of results between DBA approach and TH verification	192
6.4	METHODS FOR FRAGILITY CURVE DEVELOPMENT	203
6.4.1	Fragility curves obtained with NLTH analysis (THFr)	205
6.4.2	Displacement-Based fragility curves (DBFr)	206
6.4.3	System fragility curves for bridges	209
6.5	EVALUATION OF SEISMIC RISK	211
6.5.1	Seismic hazard	211
6.5.2	Seismic risk	212
6.6	DISPLACEMENT-BASED FRAGILITY CURVES FOR REFERENCE BRIDGES	214
6.6.1	Seismic input	214
6.6.2	Bridge model simulation	216
6.6	Fragility curves and risk assessment for RBs: DBA and TH approach	218
6.6.1	Fragility curves for RBs: comparison with RISK-UE curves	228
6.7	EXPECTED SEISMIC DAMAGE	232
6.7.1	Maps of the expected damage for the Veneto Region stock	232
6.8	CONCLUSIONS	238

CHAPTER 7

CONCLUSIONS 241

 7.1 GENERAL OBSERVATIONS 241

 7.2 INNOVATIVE ASPECTS OF THE RESEARCH..... 242

 7.3 FUTURE DEVELOPMENTS AND RECCOMENDATIONS FOR
 FURTHER RESEARCH 243

REFERENCES 245

APPENDIX A

DBD PROCEDURES FOR TRANSVERSE RESPONSE OF CONTINUOUS
BRIDGES (DBD-IT) AND (DBD-DEM) RESULTS AND NLTH VERIFICATIONS.
..... 253

APPENDIX B

PARAMETRIC STUDY FOR CAPACITY AND PIER EFECTIVE PROPERTIES:
SINGLE AND MULTIPLE BENT RECTANGULAR PIERS AND WALL PIERS 275

APPENDIX C

VENETO REGION (VR) BRIDGE STOCK..... 280

LIST OF FIGURES

Fig. 1.1 – Performance objectives defined by the Vision 2000 report ^[O1]	2
Fig. 1.2 – Limit states related to lateral deformations for a ductile structure (Fib Report 7-2).....	3
Fig. 1.3 – Typical moment-curvature relationship for a bridge pier with moderate axial load and bi-linear approximation.....	5
Fig. 1.4 – Interdependency of strength and stiffness ^[P3]	5
Fig. 1.5 – Displacement ductility capacity approximation based on the equal-displacement rule.....	6
Fig. 1.6 – Influence of height on displacement ductility capacity.....	7
Fig. 2.1 – Fundamentals of DDBD procedure.....	16
Fig. 2.2 – Direct Displacement-Based Design flowchart for a SDOF structure.....	17
Fig. 2.3 – Elastic ($\xi=5\%$) acceleration response spectra a) and Displacement Response Spectra for different ground types (A,B,C,D,E). Spectrum type 1, ($M_w > 5,5$), $a_g = 0.35$ [g], according to EC8 ^[X2]	22
Fig. 2.4 – Influence of M_w and r on 5% damped displacement spectra for firm ground (type B), according to Faccioli et al ^[F1]	24
Fig. 2.5 – Equivalent damping for bilinear (BI) and RPP hysteretic models.	25
Fig. 2.6 – Hysteresis rules considered for calibration of Eq.2.35 ^[P11]	27
Fig. 2.7 – Comparison of the hysteretic component ξ_{hyst} formulations as function of displacement ductility μ for the JDSS, D.K. and G.B.P. models.....	28
Fig. 2.8 – Damping modifiers to elastic spectral displacements:.....	31
Fig. 2.9 – a) Dimensionless Nominal Moment and b) Yield Curvature for circular piers.....	32
Fig. 2.10 – Dimensionless Nominal Moment and Yield Curvature for: c) and d) rectangular columns, e) walls with distributed reinforcement.....	33
Fig. 2.11 – Possible transverse displacement profile for girder bridges ^[P1]	40
Fig. 2.12 – Flowchart of the current DDBD procedure for transverse design of continuous bridges ^[P1]	44
Fig. 2.13 – Overview of the DBA/C procedure: a) Estimate of inelastic displacement shape, b) Equivalent SDOF representation, c) Identification of seismic intensity that would cause limit state to develop, d) Risk estimate.....	48
Fig. 3.1 – Substitute structure for a cantilever bridge pier (SDOF system).....	52
Fig. 3.2 – a) Acceleration response spectra from time histories set compared with code acceleration spectrum (EC8-type 1, $a_g = 0.35$, ground type C), b) code displacement elastic response spectrum (5% damping).....	54
Fig. 3.3 – Takeda Thin (TT) hysteretic model parameters.....	54
Fig. 3.4 – a) Period dependency of hysteretic component for equivalent damping models (D.K.) and (G.B.P.), plotted for different ductility levels (TT hysteretic model). b) Equivalent viscous damping ratio provided by the four models based on the TT hysteretic rule: (JDSS), (D.K.), (G.B.P.) for $T_{eff}=4s$ and (D.K.G.) for $T_{eff}>1s$	56
Fig. 3.5 – Flowchart of the evaluation algorithm used in the parametrical analysis.	59
Fig. 3.6 – Relative error obtained (Eq.3.16), using different EVD models for the pre-fixed spectrum reduction factor $R_\xi = EC8-2003$. Case studies presented: a) $\mu=1.25$, b) $\mu=1.5$, c) $\mu=2.0$, d) $\mu=3.0$	62

Fig. 3.7 – Relative error obtained (Eq.3.16) between the DDBD design displacement Δ_u^d and the maximum displacement demand Δ_u^{TH} , using different EVD models for the pre-fixed spectrum reduction factor $R_\xi=EC8-2003$. Case studies presented: e) $\mu=4.0$, f) $\mu=5.0$	62
Fig. 3.8 – Relative error obtained (Eq.3.16) using different expression for the spectrum reduction factor R_ξ , for a pre-fixed EVD model, $\xi_{eq}=(D.K.G.)$. Case studies presented: a) $\mu=1.25$, b) $\mu=1.5$, c) $\mu=2.0$, d) $\mu=3.0$,	63
Fig. 3.9 – Relative error obtained (Eq.3.16) between the DDBD target displacement Δ_u^d and the required maximum displacement Δ_u^{TH} , by using different expression for the spectrum reduction factor R_ξ , for a pre-fixed EVD model, $\xi_{eq}=(D.K.G.)$. Examples presented: e) $\mu=4.0$, f) $\mu=5.0$	64
Fig. 3.10 – Design displacements μ_Δ^d of the DDBD method compared with the average inelastic displacement spectra obtained by TH analyses, following the procedure of Fig. 3.2, for all ductility levels ($\mu=1.25-5.0$). Case study: $\xi_{eq}=(D.K.G.)$, $R_\xi=EC8-2003$	65
Fig. 3.11 – Relative error obtained for design displacements Δ_u^d of Fig. 3.8 with the average inelastic displacement spectra obtained by TH analyses. Case study: $\xi_{eq}=(D.K.G.)$, $R_\xi=EC8-2003$	65
Fig. 3.12 – Relative error obtained for design displacements Δ_u^d of Fig. 3.8 with the average inelastic displacement spectra obtained by TH analyses. Case study: $\xi_{eq}=(D.K.G.)$, $R_\xi=EC8-2003$	66
Fig. 3.13 – Realistic SDOF designs obtained for cantilever rc piers with tributary mass $M_{eff}=250t$	70
Fig. 3.14 – Realistic SDOF designs obtained for cantilever rc piers with tributary mass $M_{eff}=500t$	70
Fig. 3.15 – Relative error prediction (%) for the DDBD method applied to the design of cantilever rc bridge piers (SDOF systems). The medium error diagram in the background refers to Fig.3.12, while the design points for realistic cases are extracted from Figs.3.13, 3.14.	71
Fig. 3.16 – Intervals for ductility demand, μ_D , versus drift θ , obtained for the realistic design cases analyzed, and interpolating line approximating values corresponding to medium T_{eff} values of the design intervals.	72
Fig. 3.17 – Approximate relation μ_D , versus drift θ , and curves obtained for some pre-defined values of L/D (Eq. 3.30).....	73
Fig. 4.1 –Flowchart of the proposed DBD-DEM procedure for transverse design of continuous bridges	81
Fig. 4.2 –Acceleration and displacement smoothed design response spectrum superimposed with spectra generated by synthetic compatible ground motions.....	85
Fig. 4.3 –Conceptual model considered for the TH analyses.	87
Fig. 4.4 –Conceptual model considered for the TH analyses.	88
Fig. 4.5 – Series 1-2 bridges with SC deck ($\theta_L=1\%$). DBD-IT and DBD-DEM deformed shaped comparison in respect to THA medium displacement results.	92
Fig. 4.6 – Series 5-6 bridges with PRC deck ($\theta_L=4\%$). DBD-IT and DBD-DEM deformed shaped comparison in respect to THA medium displacement results	93
Fig. 4.7 – DDBD-IT and DDBD-DEM methods: relative errors respect to THA medium displacement results.	94
Fig. 5.1 – Shear failure in reinforced concrete piers: a) Hanshin expressway, Kobe earthquake, Japan, 1995, b) Northridge earthquake, California, 1994.....	98
Fig. 5.2 – Classification of rc column failure modes according to the ATC-6 ^[A6]	100
Fig. 5.3 – Flexure-shear aggregation with the simplified phenomenological approach proposed by Miranda et al. ^[M8] , 2005.	101
Fig. 5.4 – Fiber cross section; typical arrangement of fibers for a solid circular section	106
Fig. 5.5 – Constitutive laws adopted in the F.E. model: a) concrete, Kent and Park ^[K8] model, b) reinforcement steel, Menegotto and Pinto model, 1973.	108
Fig. 5.6 – Typical test setup for the selected specimen	109

Fig. 5.7 – Specimen C01F: a) experimental and numerical Force-Displacement curves of the column subjected to quasi-static cycles with displacement control, superimposed with Pushover curve; b) numerical pushover and shear envelope; c) comparison of Moment-curvature plots obtained with Opensees and Cumbia	111
Fig. 5.8 – Specimen R04S: a) experimental and numerical Force-Displacement curves of the column subjected to quasi-static cycles with displacement control, superimposed with Pushover curve; b) numerical pushover and shear envelope; c) comparison of Moment-curvature plots obtained with Opensees and Cumbia	112
Fig. 5.9 – Experimental and numerical Force-Displacement cycles for specimens C02, R01F, R02S, R03S, R05S	114
Fig. 5.10 – Definition of equivalent damping ratio according to the area-based approach by Jacobsen[J1,J2]	115
Fig. 5.11 – Pre-peak and post-peak stabilized hysteresis loops considered for the specimens R03S and R04S, corresponding to cycles 2 and 5.....	117
Fig. 5.12 – Evaluation of Equivalent Viscous Damping as a function of lateral drift θ : pre-peak, post-peak experimental results and proposed interpolating law	117
Fig. 5.13 – Superposition with Logarithmic interpolating laws obtained for evaluation of EVD for flexural columns	118
Fig. 5.14 – Logarithmic interpolating laws obtained for evaluation of EVD for flexural and shear critical columns	118
Fig. 5.15 – Adimensional capacity curves (resistant acceleration vs displacement ductility): a) shear flexure (FS) piers, b),c),d) flexure (F) piers	120
Fig. 5.16 – Adimensional capacity curves (resistant acceleration vs drift): a) shear (S) piers, b), c) shear flexure (FS) piers, d),e),f) flexure (F) piers.....	121
Fig. 5.17 – Failure mechanisms chart. λ_c represents the value of the limit confinement parameter	122
Fig. 5.18 – Steel and concrete deformation: a) PL1, b) PL3.....	123
Fig. 5.19 – Drift at failure (θ_u) for flexural(F), shear-flexural (FS), and shear (S) piers.	124
Fig. 5.20 – Interpolating laws for ultimate drift, θ_u : a) flexural(F) piers, b) shear-flexural (FS), and shear (S) piers.	124
Fig. 5.21 – Nominal drift for flexure-shear (FS) and flexure (F) cantilever piers	125
Fig. 5.22 – Drift at shear cracking for shear critical piers (S, FS).....	125
Fig. 5.23 – Single bent circular pier: dimensionless nominal moment and yield curvature (FeB44k steel type): a) $f_c=30\text{MPa}$, b) $f_c=40\text{MPa}$, c) $f_c=55\text{MPa}$	127
Fig. 5.24 – Single bent circular pier: dimensionless nominal moment and yield curvature (AQ50-60 steel type): a) $f_c=30\text{MPa}$, b) $f_c=40\text{MPa}$, c) $f_c=55\text{MPa}$	128
Fig. 5.25 – Single bent circular pier: effective stiffness ratio (FeB44k steel type).....	129
Fig. 5.26 – Single bent circular pier: effective stiffness ratio (AQ50-60 steel type)	129
Fig. 5.27 – Single bent circular pier: post yielding slope for (F) and (SF) piers. a) FeB44k steel type, b) AQ50-60 steel type.....	130
Fig. 5.27 – Single bent circular pier: slope after shear cracking for (S) piers. a) FeB44k steel type, b) AQ50-60 steel type.....	131
Fig. 5.29 – Effective stiffness at ultimate displacement for (F), (FS), (S).	132
Fig. 5.30 – Effective stiffness as function of ductility for (F), (FS) piers.	133
Fig. 5.31 – Adimensional capacity curves (resistant acceleration vs displacement ductility): a), b) shear flexure (FS) piers, c),d),e) flexure (F) piers.....	135
Fig. 5.32 – Adimensional capacity curves (resistant acceleration vs drift): a), b) shear (S) piers, c),d) shear flexure (FS) piers, e), f), g) flexure (F) piers.....	136
Fig. 5.33 – Failure mechanisms chart. λ_c represents the confinement parameter	137
Fig. 5.34 – Steel and concrete deformation: a) PL1, b) PL3.....	138
Fig. 5.35 – Drift at failure (θ_u) for flexural(F), shear-flexural (FS), and shear (S) piers.	139
Fig. 5.36 – Interpolating laws for ultimate drift, θ_u : a) flexural(F) piers, b) shear-flexural (FS), and shear (S) piers.	140
Fig. 5.37 – Nominal drift for flexure-shear (FS) and flexure (F) cantilever piers	140

Fig. 5.38 – Drift at shear cracking for shear critical piers (S, FS).....	141
Fig. 5.33 – Multiple bent circular pier: M_n and nominal yield curvature, χ_n (FeB44k steel type) : a) $f_c=30\text{MPa}$, b) $f_c=40\text{MPa}$, c) $f_c=55\text{MPa}$	142
Fig. 5.34 – Multiple bent circular pier: dimensionless nominal moment and yield curvature (AQ50-60 steel type)	143
Fig. 5.35 – Multiple bent circular pier: effective stiffness ratio (FeB44k steel type)	144
Fig. 5.42 – Multiple bent circular pier: effective stiffness ratio (AQ50-60 steel type)	144
Fig. 5.43 – Multiple bent circular pier: post yielding slope for (F) and (SF) piers. a) FeB44k steel type, b) AQ50-60 steel type.....	145
Fig. 5.44 – Single bent circular pier: slope after shear cracking for (S) piers. a) FeB44k steel type, b) AQ50-60 steel type.....	146
Fig. 5.45 – Effective stiffness at ultimate displacement for (F), (FS), (S)	147
Fig. 5.46 – Effective stiffness as function of ductility for (F), (FS) piers.	148
Fig. 6.1 – Localization of the bridges and classification on the base of deck/pier material: DC- reinforced concrete, DPC- prestressed reinforced concrete, DM-masonry (or unreinforced concrete, deck or piers), DCS-composite/steel, ND-not classified.	155
Fig. 6.2 – On site tests on rc bridges: a) pachometer test, b) sclerometric test.....	156
Fig. 6.3 – Laboratory tests: a) core borings and compressive strength tests on concrete samples. b) extraction of reinforcements bars and traction test.....	156
Fig. 6.4 – Normal pdf of yield strength f_y , for prior distribution, distribution obtained by test values on specimen, and updated pdf with Bayesian approach: a) smooth bars (Aq50- 60), b) deformed bars (FeB44K).....	179
Fig. 6.5 – Reference Bridge structures: a) 2.1.1a-RBs1, b)2.1.1b-RBs2, c)2.1.2a-RBs3, d) 2.1.3a-RBs4, e)2.1.3b-RBs5, f) 2.1.3b-RBs6, g)2.1.4a-RBs7, h)2.1.4b-RBs8	184
Fig. 6.6 – Reference Bridges structures for class 2.2 (gerber structures): a) 2.2.1-RBs9, b)2.2.2 –RBs10	185
Fig. 6.7 –Reference Bridges: a) 2.3.1b3-RBs11, b) 2.3.1.a3 –RBs12, c) 2.3.1a4 -RBs13, d) 2.3.2b1-RBs14, e) 2.3.2a2-RBs15, f)2.3.3a1-RBs16, g)2.4.1-RBs17	186
Fig. 6.8 –Analytical model of a typical continuous bridge structure: a) column model geometry, b) 3D spine model.....	188
Fig. 6.9 – Smooth elastic acceleration and displacement response spectra for PL1, PL2, PL3 according to Eq. 6.5 for Campelli Bridge construction site (Longarone-BL-, Zone 2, ground type B).....	189
Fig. 6.10 – Ground motions compatible with the elastic smooth spectra PL3 ($P_{vr}=1\%$ in 50years) for the Campelli bridge (Fig. 6.8).....	191
Fig. 6.11 – Smooth elastic acceleration and displacement response spectra for PL1, PL2, PL3 according to Eq. 6.5 for Campelli Bridge construction site (Longarone-BL-, Zone 2, ground type B).....	191
Fig. 6.12 – Medium error trend for C/D ratio calculated according to Eq. 6.7, for PL1, PL2, PL3 limit states for RBs of classes 2.1,2.2.	203
Fig. 6.13 – Linear Regression in the bi-logarithmic plane for the probabilistic model of Damage Measure (Intensity Measure is given in this case by PGA, with maximum value $PGA=1g$).....	205
Fig. 6.14 – Mean displacement response spectrum and mean ± 1 standard deviation	207
Fig. 6.15 – Pdf of damage functions for different value of IM (PGA) and lognormal CDF curve obtained, associated to a pre-defined PL	208
Fig. 6.16 – Hazard map of the Veneto region supplied by INGV (PGA, 10% probability of exceeding in 50 years on a soil type A) and exposure of the analyzed bridge stock.....	212
Fig. 6.17 – Hazard curve supplied by INGV: Campelli Bridge (Longarone-BL-, seismic zone 2), Botteon Bridge (Fadalto-TV- seismic zone 2), Ivach Bridge (San Tommaso Agordino-BL- seismic zone 3), Fener Bridge (Alano di Piave-BL-, seismic zone 2).	212
Fig. 6.18 – Generation of seismic input suites according to Multi Straip Analysis technique	215

Fig. 6.19 – <i>a) f_c normal distribution ($\mu=32.2$ MPa, $\sigma=9.0$ MPa), and corresponding 5 realizations used in bridge samples, b) f_y normal distribution for Aq50-60 steel ($\mu=330$ MPa, $\sigma=17$ MPa) and 3 realizations adopted for fragility analysis.</i>	216
Fig. 6.20 – <i>Error obtained by comparing the medium value $c[g]$ of DBFr and THFr curves for the Reference Bridge structures analyzed.....</i>	227
Fig. 6.21 – <i>Seismic Risk for multi-span rc bridges (classes 2.1, 2.1) in the VR stock. Damage state corresponding to PL1</i>	234
Fig. 6.22 – <i>Seismic Risk for multi-span rc bridges (classes 2.1, 2.1) in the VR stock. Damage states corresponding to PL2 and PL3.</i>	235

LIST OF TABLES

Tab. 1.1 – Drift limits suggested by the Vision 2000 report ^[O1]	3
Tab. 2.1 – Structural Drift limits (after DBD09 Model Code ^[C2])	19
Tab. 2.2 – Permanent Drift limits (after DBD09 Model Code ^[C2]).....	19
Tab. 2.3 – Material strain limits for rc structures (after DBD09 Model Code ^[C2])	19
Tab. 2.4 – Assessment limit states.....	20
Tab. 2.5 – Values of the parameters describing the recommended Type 1 elastic response spectra according to EC8 ^[X2]	22
Tab. 2.6 – Values of the parameters describing the recommended Type 1 elastic response spectra.....	23
Tab. 2.7 – Values of EVD coefficients used by D.K. formulation.....	26
Tab. 2.8 – Values of EVD coefficients for hysteretic component using Eq. 2.25, proposed by Grant et al ^[P11]	27
Tab. 2.9 – Secant stiffness correction factors $\lambda^{[G1]}$ for elastic damping.....	29
Tab. 2.10 – Equivalent viscous damping coefficients Cs for tangent-stiffness damping[P1].	30
Tab. 2.11 – Displacement shape for regular continuous deck bridges ^[C2]	40
Tab. 4.1 – Properties of the PRC deck and the equivalent steel box, substitutive of the composite SC deck.....	83
Tab. 4.2 – Relative Stiffness index RS calculated for 4-spans and 6-spans bridges configurations with PRC and SC deck.....	83
Tab. 4.3 – Bridge configurations.....	84
Tab. 4.4 – Concrete02 model. Stress-strain relations with loading and unloading paths for confined and unconfined concrete.....	87
Tab. 4.5 – Menegotto-Pinto model for steel reinforcement.....	87
Tab. 4.6 – Typical output obtained for one bridge for different Drift Levels θ_L	89
Tab. 5.1 – Classification of rc pier type, according to failure model.....	100
Tab. 5.2 – Summary of stiffness components (Simplified Approach ^[M8]).....	103
Tab. 5.3 – Steel02 material model parameters.....	108
Tab. 5.4 – Concrete02 material model parameters.....	108
Tab. 5.5 – Experimental database.....	109
Tab. 5.6 – Geometric and reinforcement characteristic of the specimens.....	110
Tab. 5.7 – Properties of the specimens in the experimental database.....	110
Tab. 5.8 – Flexural columns: characteristics of the analyzed hysteretic cycles.....	116
Tab. 5.9 – Shear critical columns: characteristics of the analyzed hysteretic cycles	116
Tab. 5.10 – Single bent circular piers: 1440 pier samples studied in total.....	119
Tab. 5.11 – Dimensionless yield curvature for circular bridge columns.....	129
Tab. 5.12 – Multiple bent circular piers: 2376 pier samples studied in total.....	134
Tab. 5.13 – Dimensionless yield curvature for circular bridge columns.....	144
Tab. 6.1 – SET 1 statistics: general properties of the whole bridge stock.....	157
Tab. 6.2 – Parameters used for the classification of rc girder bridges.....	162
Tab. 6.3 – Identification of homogeneous classes for rc and prc bridges’ stock.....	163
Tab. 6.4 – SET 2 statistics: rc and prc bridges general properties.....	164
Tab. 6.5 – SET 3a statistics: multi-span rc girder bridges properties.....	166
Tab. 6.6 – SET 3b statistics: pier geometric properties of multi-span rc girder bridges.....	168
Tab. 6.7 – SET 3c statistics: pier reinforcement ratio and confinement parameter.....	172

Tab. 6.8 – <i>SET 4 statistics: R_{cm} values obtained from laboratory tests on concrete specimens</i>	174
Tab. 6.9 – <i>SET 4 statistics: R_{cm} values obtained for different pier types</i>	175
Tab. 6.10 – <i>SET 4 statistics: R_{cm} values obtained for different pier types</i>	175
Tab. 6.11 – <i>SET 4b statistics: F_{ym}, F_{tm}, Elongation 5ϕ values obtained from laboratory test on reinforcement bar specimens</i>	176
Tab. 6.12 – <i>SET 4 statistics: F_{ym}, F_{tm}, Elongation 5ϕ values obtained from laboratory test on reinforcement bar specimens separately specimen individuated as FeB44k bars and Aq50-60 bars</i>	176
Tab. 6.13 – <i>Requirements for reinforcement bars according to different Italian Codes of past decades.</i>	178
Tab. 6.14 – <i>Updating of Normal pdf distribution parameters for smooth bars (type Aq50-60) and deformed bars (type FeB44k)</i>	179
Tab. 6.15 – <i>Significant parameters of the VR stock – single bent circular piers-: a) effective ranges, b) representative values individuated for parametrical analysis</i>	181
Tab. 6.16 – <i>Significant parameters of the VR stock – single bent square piers-: a) effective ranges, b) representative values individuated for parametrical analysis</i>	181
Tab. 6.17 – <i>Significant parameters of the VR stock –wall piers: a) effective ranges, b) representative values individuated for parametrical analysis</i>	181
Tab. 6.18 – <i>Significant parameters of the VR stock – multiple bent circular piers-: a) effective ranges, b) representative values individuated for parametrical analysis</i>	182
Tab. 6.19 – <i>Significant parameters of the VR stock – multiple bent square piers-: a) effective ranges, b) representative values individuated for parametrical analysis</i>	182
Tab. 6.20 – <i>Characteristics of reinforcement steel</i>	182
Tab. 6.21 – <i>Reference Bridge structures: Macro-class 2. Classes 2.1, 2.2, 2.3, 2.4</i>	183
Tab. 6.22 – <i>Design intensity (Probability of Exceedance P_{vr}) for Structural Category and Performance Level according to Calvi et al.^[C1], 2009 for Importance Class III</i>	188
Tab. 6.23 – <i>Definition of limit states for the assessment of rc bridge piers</i>	192
Tab. 6.24 – <i>RBs1: Capacity curves of a single column of the pier bent: a) longitudinal b) transverse direction</i>	194
Tab. 6.25 – <i>RBs1: long. direction (L), comparison between DBA and TH results</i>	194
Tab. 6.26 – <i>RBs7: transverse. direction (T), comparison between DBA and TH results</i>	194
Tab. 6.27 – <i>RBs2: Capacity curve of the pier: a) longitudinal and transverse direction</i>	195
Tab. 6.28 – <i>RBs 2: long. and transverse direction, comparison between DBA and TH results</i>	195
Tab. 6.29 – <i>RBs 3: Capacity curves of the pier: a) longitudinal direction</i>	196
Tab. 6.30 – <i>RBs 3: long. direction (L), comparison between DBA and TH results</i>	196
Tab. 6.31 – <i>RBs7: Capacity curves of a single column of the pier bent: a) longitudinal b) transverse direction</i>	197
Tab. 6.32 – <i>RBs7: long. direction (L), comparison between DBA and TH results</i>	197
Tab. 6.33 – <i>RBs7: transverse. direction (T), comparison between DBA and TH results</i>	197
Tab. 6.34 – <i>RBs7: Capacity curves of a single column of the pier bent: a) longitudinal b) transverse direction</i>	198
Tab. 6.35 – <i>RBs5: long. direction (L), comparison between DBA and TH results</i>	198
Tab. 6.36 – <i>RBs5: transverse direction (T), comparison between DBA and TH results</i>	198
Tab. 6.37 – <i>RBs7: Capacity curves of a single column of the pier bent: a) longitudinal b) transverse direction</i>	199
Tab. 6.38 – <i>RBs6: long. direction (L), comparison between DBA and TH results</i>	199
Tab. 6.39 – <i>RBs6: transverse direction (T), comparison between DBA and TH results</i>	199
Tab. 6.40 – <i>RBs7: Capacity curves of a single column of the pier bent: a) longitudinal b) transverse direction</i>	200
Tab. 6.41 – <i>RBs7: long. direction (L), comparison between DBA and TH results</i>	200
Tab. 6.42 – <i>RBs7: transverse direction (T), comparison between DBA and TH results</i>	200

Tab. 6.43 – RBs7: Capacity curves of a single column of the pier bent: a) longitudinal b) transverse direction.....	201
Tab. 6.44 – RBs7: long. direction (L), comparison between DBA and TH results.....	201
Tab. 6.45 – RBs7: transverse direction (T), comparison between DBA and TH results.....	201
Tab. 6.46 – RBs7: Capacity curve of the pier: a) longitudinal direction.....	202
Tab. 6.47 – RBs7: long. direction, comparison between DBA and TH results.....	202
Tab. 6.48 –RBs1, Botteon Bridge. DBFr and THFr fragility curves and medium error: a) Long. Direction-single pier-, b) Transv. Direction-single pier-, c) System fragility curves for the bridge.....	218
Tab. 6.49 –RBs1, Botteon Bridge: a) hazard curve b) Seismic Risk.....	218
Tab. 6.50 –RBs 2, Rio Ghisel Bridge. DBFr and THFr fragility curves and medium error: a), b) Long. and Transverse Direction-single pier-, b) c) System fragility curves for the bridge.....	219
Tab. 6.51 –RBs 2, Rio Ghisel Bridge: a) hazard curve b) Seismic Risk.....	219
Tab. 6.52 –RBs 3, Torrente Frison Bridge. DBFr and THFr fragility curves and medium error: a), b) Long. and Transverse Direction-single pier-, c) System fragility curves for the bridge.....	220
Tab. 6.53 –RBs 3, Torrente Frison Bridge: a) hazard curve b) Seismic Risk.....	220
Tab. 6.54 –Rbs 4, A27 Bridge. DBFr and THFr fragility curves and medium error: a) Long. Direction-single pier-, b) Transv. Direction-single pier-, c) System fragility curves for the bridge.....	221
Tab. 6.55 –Rbs3, A27 Bridge: a) hazard curve b) Seismic Risk.....	222
Tab. 6.56 –RBs5, Campelli Bridge. DBFr and THFr fragility curves and medium error: a) Long. Direction-single pier-, b) Transv. Direction-single pier-, c) System fragility curves for the bridge.....	222
Tab. 6.57 –RBs 5, Campelli Bridge: a) hazard curve b) Seismic Risk.....	223
Tab. 6.58 –RBs6, Vittorio Veneto (Fener) Bridge. DBFr and THFr fragility curves and medium error: a) Long. Direction-single pier-, b) Transv. Direction-single pier-, c) System fragility curves for the bridge.....	223
Tab. 6.59 –RBs 6, FenerBridge: a) hazard curve b) seismic risk.....	224
Tab. 6.60 –RBs7, Schiavonesca Bridge. DBFr and THFr fragility curves and medium error: a) Long. Direction-single pier-, b) Transv. Direction-single pier-, c) System fragility curves for the bridge.....	224
Tab. 6.61 –RBs7, Schiavonesca Bridge: a) hazard curve b) Seismic Risk.....	225
Tab. 6.62 –RBs 8, Reghena Bridge. DBFr and THFr fragility curves and medium error: a) Long. Direction-single pier-, b) Transv. Direction-single pier-, c) System fragility curves for the bridge.....	225
Tab. 6.63 –RBs 8, Reghena Bridge: a) hazard curve b) Seismic Risk.....	226
Tab. 6.64 –RBs10, Canal Bianco Bridge. DBFr and THFr fragility curves and medium error: a), b) Long. and Transverse Direction-single pier-, b) c) System fragility curves for the bridge.....	226
Tab. 6.65 –RBs 10, Canal Bianco Bridge: a) hazard curve b) Seismic Risk.....	226
Tab. 6.66 – RISK-UE method: bridge classes individuated on the base of material, column bent type, deck static scheme, structural code adopted for design.....	228
Tab. 6.67 – Parameters for fragility curves development according to RISK-UE method ...	228
Tab. 6.68 –Seismic risk associated to PL1, PL2, PL3 for multi-span rc continuous bridges (Classes 2.1).....	237
Tab. 6.69 –Seismic risk associated to PL1, PL2, PL3 for multi-span rc continuous bridges (Classes 2.2).....	238

LIST OF SYMBOLS

- A_g gross section area
- A_c area of the concrete section
- A_s area of tension reinforcement in concrete section
- A_{sh} area of transverse reinforcement in section perpendicular to the direction considered
- A_s effective shear area of uncracked section
- $a_{(T,5)}$ absolute acceleration (expressed in units of g) of a 5% damping DRS
- A_1 Area of a complete stabilized hysteretic loop
- a_g peak ground acceleration for a rock soil (type A)
- a_u^d ultimate design acceleration
- a_y yield acceleration
- b_c width of rectangular column section
- c viscous damping coefficient
- C generic constant
- C_M center of mass of the superstructure
- C_S coefficient applied to peak response displacement for different soils
- D diameter of circular section
- d effective depth of section
- d_{bl} longitudinal reinforcement diameter
- $E_{I_{cr,i}}$ stiffness of the member i , obtained considering the cracked section
- $E_{I_{gross,i}}$ stiffness of the member i , obtained considering the gross section
- E_s steel modulus of elasticity
- e generic eccentricity
- f'_c compressive strength of unconfined concrete
- f'_{cc} compressive strength of confined concrete
- f_t tension strength
- f_y characteristic yield strength of steel
- f'_{ye} expected yield strength of steel for DDBD
- f_u steel ultimate stress
- F_D force produced by a damper device
- F_i generic force acting on member “ i ”
- F_u generic ultimate force
- F_u^d ultimate force/strength relative to the design displacement Δ_u^d .
- F_y yield force
- G shear modulus
- g acceleration due to gravity
- H_{eff} effective height of the equivalent SDOF system
- $H_{P,i}$ pier height
- h_b beam section depth
- h_c column section depth

- I_P pier moment of inertia
- I_S moment of inertia of the bridge superstructure
- I_{cr} moment of inertia of cracked concrete section
- I_g moment of inertia of un-cracked concrete section
- j (subscript) structural element contributing to seismic resistance
- K structure stiffness
- K_A abutment stiffness for transverse displacement
- K_S superstructure stiffness for transverse displacement
- $K_{f,i}$ flexural pier stiffness during phase “i”
- $K_{s,i}$ shear pier stiffness during phase “i”
- K_{eff} structure effective stiffness for DDBD
- K_{el} initial elastic stiffness
- k correction factor for elastic damping
- L_b beam length
- L_P plastic hinge length
- L_S deck (superstructure) span length
- L_{SP} strain penetration length
- M moment
- M_{base} sum of moments at the base level
- M_D design bending moment
- M_{DN} adimensional design bending moment
- M_e effective mass participating in the fundamental mode
- M_N nominal moment capacity
- M_u ultimate moment capacity
- M_w earthquake moment magnitude
- M_Y first-yield flexural strength
- m mass
- N_{ED} design axial load
- n number of dof for a MDOF structure
- n_p number of piers
- P axial force on section (also N)
- r distance of the site from the nearest “fault plan”
- R force reduction factor
- r_Δ post-yielding displacement bilinear factor
- r_ϕ post-yielding curvature bilinear factor
- r_ψ post-yielding rotational bilinear factor
- R_ξ reduction factor applied to displacement spectrum for damping ξ
- $S_{De}(T)$ relative spectral displacement
- $S_e(T)$ absolute spectral acceleration
- T period
- T_B period at the beginning of the maximum spectral response acceleration plateau
- T_C period at the end of the maximum spectral response acceleration plateau
- T_c corner period of a DRS
- T_{eff} effective period of the SDOF system at its design displacement
- T_{el} elastic period of the SDOF substitute system
- t time
- V_c shear strength from concrete shear-resisting mechanisms
- V_y yield shear force

- \mathbf{V}_{base} base shear force
- \mathbf{V}_{srss} SRSS of the modal base shears
- \mathbf{x} fraction of the transverse inertial forces carried by the abutments
- \mathbf{x}_{NEW} estimate of the fraction of the transverse inertial forces carried by the abutments (current iteration)
- \mathbf{x}_{OLD} estimate of the fraction of the transverse inertial forces carried by the abutments (previous iteration)
- $\mathbf{x}(\mathbf{t})$ relative displacement of a SDOF system
- $\ddot{\mathbf{x}}_g(\boldsymbol{\tau})$ ground acceleration time history
- $\{\mathbf{u}_m\}$ structure displacement associated to mode m

Greeks

- $\{\Phi_m\}$ mode shape relative to eigenvalue m
- α unloading stiffness factor in the modified Takeda model
- β reloading stiffness factor in the modified Takeda model
- β_m global equivalent modal damping (in the S.S. substitute structure method)
- $\beta_{s,i}$ local equivalent damping (in the S.S. substitute structure method)
- Γ_m modal mass participation factor
- $\Delta_{(T,5)}$ relative displacement of a 5% damping DRS
- Δ_a transverse displacement of the abutments
- Δ_c design displacement at the critical mass
- $\Delta_{c \text{ CALC}}$ ultimate displacement of the critical mass
- Δ_{eff}^d effective design displacement of the SDOF substitute structure
- Δ_f displacement resulting from foundation flexibility
- Δ_{high} displacement at the critical pier due to higher modes
- Δ_i displacement at mass i
- $\Delta_{i \text{ NEW}}$ target displacement shape of the current iteration
- $\Delta_{i \text{ OLD}}$ target displacement shape of the previous iteration
- δ_c dimensionless inelastic mode shape at the critical mass c
- δ_i dimensionless inelastic mode shape at mass i
- Δ_p plastic displacement
- Δ_u ultimate displacement
- Δ_u^{DDBD} target displacement of the of the DDBD method obtained for the equivalent SDOF system
- $\Delta_u^{\text{T-H}}$ ultimate displacement obtained by using NLTH analysis.
- Δ_u^d, ϕ target displacement obtained using curvature limit ϕ_m .
- Δ_u^d, ν target displacement obtained using drift limit ν_p o ν_d .
- Δ_u^d ultimate target displacement
- Δ_y yield displacement
- $\Delta_{y, \text{eff}}$ effective yield displacement of the SDOF substitute structure.

- ε_{cm} maximum concrete compression strain for a specific damage level
- ε_{cu} ultimate compression strain in concrete
- ε_m maximum reinforcement strain for a specific damage level
- ε_{sm} maximum reinforcement strain for a specific damage level
- ε_{su} ultimate reinforcement strain
- ε_y yield reinforcement stress
- η ARS and DRS damping reduction coefficient
- ϑ rotation; drift angle (displacement/height); angle
- ϑ_d design drift
- ϑ_Δ stability index in P- Δ design
- ϑ_P plastic rotation of the structural element
- ϑ_r permanent or residual drift
- ϑ_u section ultimate rotation
- ϑ_Y yield drift
- ϑ_y section yield rotation
- λ_{lim} limit value of slenderness coefficient
- λ coefficient of slenderness
- μ_Δ displacement ductility factor
- $\mu_{\Delta,eff}$ displacement ductility factor of the equivalent SDOF system
- μ_Δ^d design displacement ductility factor
- μ_Δ^u ultimate displacement ductility factor
- μ_ϕ curvature ductility factor
- μ_ϑ rotation ductility factor
- ν normalized axial load
- ξ fraction of critical damping
- ξ_a coefficient of equivalent viscous damping related to bridge abutments
- ξ_{eff} equivalent viscous damping coefficient of the substitute SDOF structure.
- ξ_{el} elastic viscous damping
- ξ_{eq} equivalent viscous damping
- ξ_{hyst} hysteretic component of equivalent viscous damping ratio
- ξ_s elastic damping of the superstructure (assumed equal to 5%)
- ρ_l [%] area ratio of longitudinal reinforcement
- ρ_v [%] volumetric ratio of transverse reinforcement
- Φ_{Dy} Dimensionless yield curvature
- Φ_m Maximum admissible curvature $\Phi_m = \min(\Phi_{mc}; \Phi_{ms})$.
- Φ_P Plastic curvature capacity
- Φ_u Ultimate curvature
- Φ_y Nominal yield curvature
- Φ_y' First yield curvature.
- ψ phase angle or phase at the initial time (of a sinusoidal response).
- ω angular frequency
- ω_D damped natural frequency
- ω_m undamped natural frequency of the system (for mode m)

- ω_{ν} higher-mode drift reduction factor

CHAPTER 1

INTRODUCTION

1.1 BACKGROUND OF DISPLACEMENT-BASED SEISMIC VERIFICATION PROCEDURES

In past decades design for seismic resistance has been undergoing a critical review during triggered by an increasing emphasis on the concept of *performance level* for a given structure; a new seismic design approach has been developing, called Performance-Based-Design, PBD (or Performance-Based-Earthquake Engineering, PBEE), aiming at realizing structural systems able to sustain a pre-defined damage level under a pre-fixed earthquake intensity.

The development of the PBD approach was in the 1990's the natural outgrowth of the assessment and retrofit procedures for existing buildings. Initially, the practice of meeting performance-based objectives was rather informal, nonstandard, and somewhat qualitative. In 1992 the Federal Emergency Management Agency (FEMA) sponsored the development of national consensus guidelines for the seismic retrofit of buildings, the ATC-40 project^[A1]. That project standardized the qualitative descriptions of performance previously used into a series of quantifiable performance levels that could be predicted through the use of specific design parameters (in terms of element forces and displacement demands). The same attempt to standardize the performance-based approach was addressed by SEAOC's (Structural Engineers Association of California) Vision 2000 project^[O1], including the design of new buildings. The seismic performance objectives were defined as the coupling of expected performance levels with expected levels of seismic ground motion in the Vision 2000 document^[O1]. A predefined performance level describes the damage condition considered acceptable for a certain structure in relation to its importance and the desired post-earthquake serviceability, depending on both the non-structural and structural damage levels, which are treated independently and then combined in order to give a comprehensive performance target.

In the Vision 2000 document four performance levels and four levels of seismic excitation were considered. Performance levels are defined as:

- *Level I: Operational* (Fully operational). The building retains its original stiffness and strength. Non-structural components operate, and the building is available for normal use.

- *Level II: Immediate occupancy* (Operational). Only minor structural and non structural damage has occurred. Facility continues in operation with minor disruption in non essential services. The structure retains nearly all its original stiffness and strength.

-Level III: *Life safety*. Significant structural and non-structural damage has occurred. The building retains some lateral strength against collapse. The risk of life threatening injury during the earthquake is low.

-Level IV: *Structural Stability (Near Collapse)*. Damage is severe for structural and non structural components. Structural collapse is prevented.

The relation between these performance levels and earthquake design levels is summarized in Fig. 1.1, where the line *Basic Objective* identifies a series of performance targets for normal structures, the other two lines (*Essential* and *Safety Critical Objective*) relate performance levels to seismic intensity for two structural classes of increasing importance^[P1].

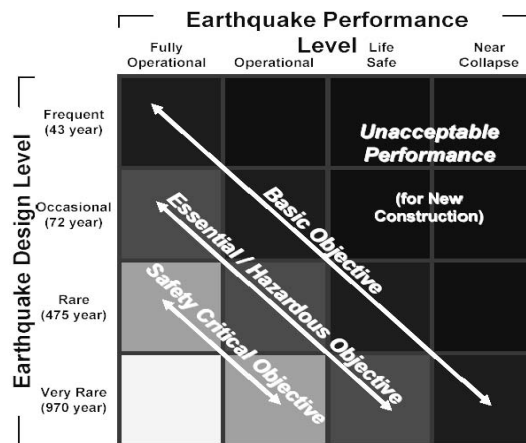


Fig. 1.1 – Performance objectives defined by the Vision 2000 report^[O1]

Together, the FEMA-273 NEHRP (National Earthquake Hazard Reduction Program) Guidelines for Seismic Rehabilitation of Buildings^[F3], resulting from the ATC-40 project, and the Vision 2000 report defined the current state of practice in performance-based engineering. Although using a slightly different terminology, the ATC-40 and the Vision 2000 report suggested the same building performance levels, the latter introducing a direct relation between required performance and maximum tolerable drift limits: the interdependency between a predetermined damage level and the maximum displacement profile attained by the structure was recognized, and the design criteria defined on the base of different attainable displacements at different limit states.

The relation introduced by the Vision 2000 document between predetermined damage levels and permissible drift limits, was the first translation of this fundamental concept into design requirements and represented a turning point for the seismic design philosophy, establishing the base for a complete application into engineering practice of the Displacement-Based seismic Design approach that was pioneered in those years by Priestley and his co-workers [P2, P3, P5, P9, K1].

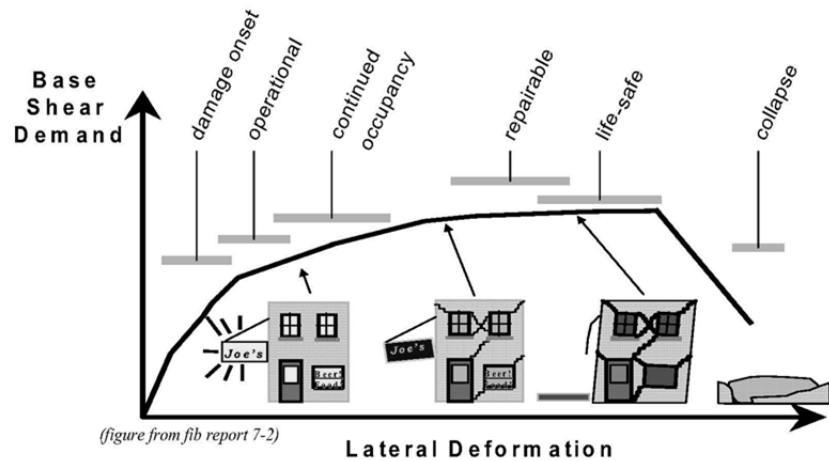


Fig. 1.2 – Limit states related to lateral deformations for a ductile structure (Fib Report 7-2)

Tab. 1.1 – Drift limits suggested by the Vision 2000 report^[O1]

Building Limit States	Maximum	Permanent
Operational	0.2	negligible
Immediate Occupancy	0.5	negligible
Life Safety	1.5	0.5
Structural Stability	2.5	2.5

At the end of the 1990's, the growing emphasis on the Performance-Based approach, tied to the application of capacity design principles, led to the development of a new design process [among others P3, P5, C3, K1, K3], assuming as starting point the limit design displacement and obtaining as result the base shear force, and the distribution of strength in the structure (see §2.1).

This approach (displacements lead to strength), was proposed as the opposite of the traditional (Force-Based, FB) design approach, where strength leads to an estimate of displacement^[P1], and which was based upon a pure linear elastic analysis and a rough reduction of the initial design forces by a predetermined force-reduction factor (assumed to be related with the desired level of displacement ductility capacity).

The theorists of the new Displacement-Based-Design (DBD) method raised a series of criticisms to traditional FB design methods, which can be summarized as follows [P3]:

- interdependency of strength and stiffness, and as a consequence iterative design required (stiffness cannot be adequately determined until the structure is fully designed);
- inappropriate definition of behaviour factors for whole categories of structures;
- invalid assumptions for the relationship between elastic and inelastic displacements;
- inadequate representation of structural performance of systems where inelastic action develops in different members at different level of structural response (e.g. bridges with piers of different heights), or system with dual

load path (e.g. transverse response of continuous girder bridges with fixed abutments).

- inadequate representation of variations of hysteretic characteristics of different structural systems.

A quick overview of the most important problems concerning Force-Based design philosophy, is herein reported. The reader is referred to other textbooks [P1, P3] for an exhaustive discussion of the topic.

1.1.1 Criticisms of Force-Based seismic design approaches

1.1.1.1 Interdependency of strength and stiffness of concrete members

In force-based design, the stiffness of the structural members is required at the beginning of the entire process in order to define the natural elastic periods of the structure, and subsequently to distribute the global inertia force. It is common practice to perform this first step using the gross-section properties of the members, but current codes also allow the use of reduced values [e.g. D2, E1, N1], resulting from concrete cracking: typically reduction factor values around 0.3÷0.5 is suggested.

Regardless of what assumption is made, a constant relation between the gross moment of inertia of section I_g and the corresponding cracked value I_{cr} is assumed: this approach states that the structural stiffness is independent of both flexural strength (mainly given by the amount of flexural reinforcement) and axial load. To examine this assumption, the flexural rigidity estimated from the moment-curvature relationship can be considered:

$$EI = \frac{M_N}{\phi_Y} \quad (1.1)$$

where M_N is the nominal moment capacity of the section ($\varepsilon_c=0.004$, $\varepsilon_s=0.015$) and ϕ_Y is the associated yield curvature of the equivalent bilinear representation, as shown in Fig. 1.4 for a typical bridge pier.

Eq. 1.1 therefore reveals that the common assumption in force-based design, considering the member stiffness independent of strength, implies a direct proportional relationship between M_N and ϕ_Y . Experimental evidence indicates that this assumption is not valid: yield curvature is effectively independent of strength, and hence the stiffness EJ is directly proportional to flexural strength M_N , with ϕ_Y a constant in Eq. 1.1. The correct relationship is then represented in Fig.2.4d^[P3]. As a consequence of these simple considerations, it clearly results impossible to perform an accurate analysis of the structure until the final element reinforcement, and hence the final member strength, is determined. In other words, the traditional force-based design results in the end to be an iterative process in which the members stiffness must be upgraded at each iteration.

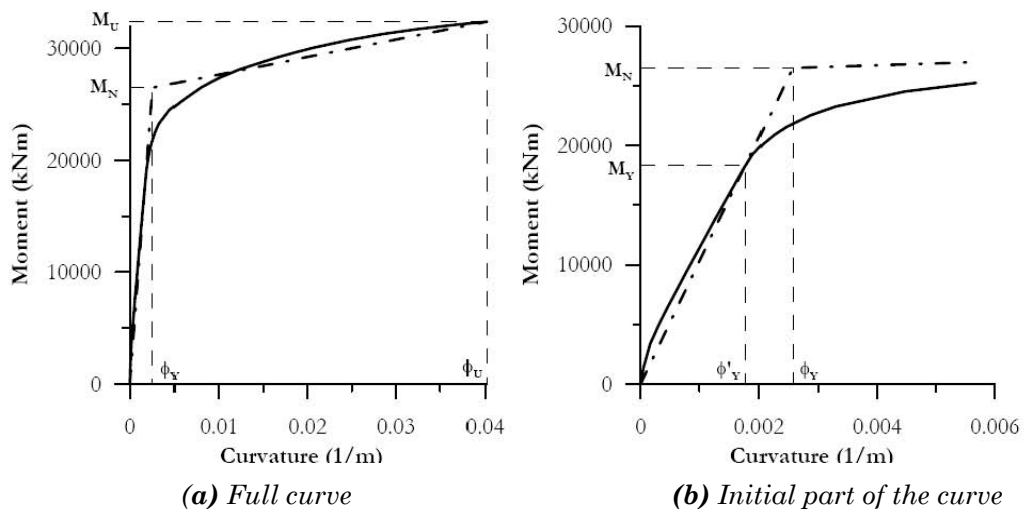


Fig. 1.3 – Typical moment-curvature relationship for a bridge pier with moderate axial load and bi-linear approximation

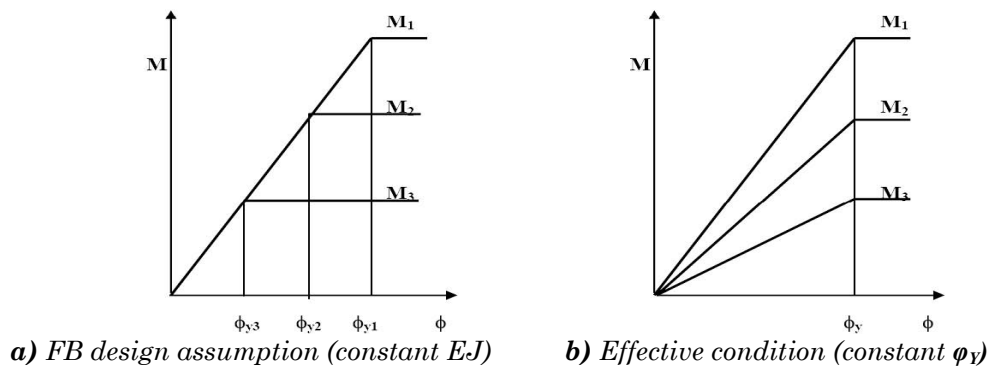


Fig. 1.4 – Interdependency of strength and stiffness^[P3]

1.1.1.2 Force-Reduction Factors and ductility capacity

In the traditional force-based design approach, after having performed the modal analysis of the structure and computed the total elastic inertia force, the design of the members is achieved by introducing a force-reduction factor formally linked with the desired ductility capacity level. This is a very simple procedure that leads correctly to design a structure behaving inelastically at the ultimate limit state under a certain (severe) seismic event, but at the same time reveals conceptual fallacies and inappropriate definitions of behaviour factors for whole categories of structures. The subsequent observations need to be taken into account:

- Relationships between ductility and force reduction factor are not well established, leading to inaccurate calculations of the inelastic displacement as a function of the elastic ones.

The force-reduction factor (R) is often related to the displacement ductility capacity μ_A :

$$\mu_{\Delta} = \frac{\Delta_u}{\Delta_y} \quad (1.2)$$

following the “equal displacement” rule, which states that the displacement of the inelastic system Δ_u is equal to that of the respective elastic system Δ_0 characterized by the same initial stiffness and unlimited strength. This approximation is graphically shown in Fig.1.4a, and it implies the formal equivalence between the force-reduction factor R , and the displacement ductility capacity μ , as reported in Eq. 1.3.

$$\mu_{\Delta} = \frac{\Delta_u}{\Delta_y} = \frac{F_0}{F_y} = R \quad (1.3)$$

Introducing the approximate relationship between peak acceleration and displacement response (based on a steady-state sinusoidal response), it is possible to estimate the design displacement as a function of the peak acceleration:

$$\Delta_u = \Delta_0 = \frac{T^2}{4\pi^2} a_0 \quad (1.4)$$

It has been recognized that equal displacement approximation is non-conservative for short-period structures (the increase in displacement response from period elongation is less than the decrease resulting from augmented damping); as a consequence, some design codes, apply the equal energy approximation when determining peak displacement [P1]. According to this second approach, the area under the line which represents the perfect linear elastic behavior must be the same as that defined by the elastic perfectly-plastic approximation.

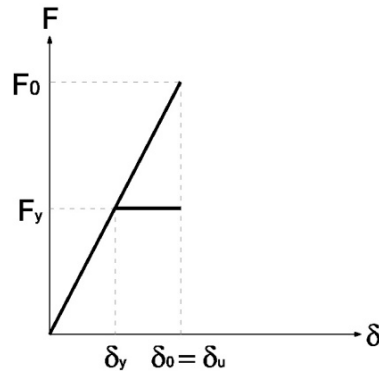


Fig. 1.5 – Displacement ductility capacity approximation based on the equal-displacement rule

$$\Delta_u = \Delta_0 \frac{R^2 + 1}{2R} = \frac{T^2}{4\pi^2} a_0 \frac{R^2 + 1}{2R} \quad (1.5)$$

However, if the real structure has a behavior considerably different from the ideal elastic perfectly plastic one, also the aforementioned procedure is no longer

valid.

-The behaviour factors for whole categories of structures are defined in a simplistic manner, without recognizing that ductility capacity varies widely within a structural class. This can be simply demonstrated with reference to an example [P1], that compares the ductility capacity of two bridge piers of identical cross section, axial load and longitudinal reinforcement, but with different heights, 3 and 8m respectively (see Fig.1.6).

The two piers have the same yield and ultimate curvatures ϕ_y and ϕ_u , and hence, the same curvature ductility factor $\mu_\phi = \phi_u / \phi_y$. The lateral displacement of the deck (at height H), and the displacement ductility can be quickly derived from the following well-known relations:

$$\Delta_y = \phi_y \frac{H^2}{3} \quad (1.6)$$

$$\Delta_p = \phi_p \cdot L_p \cdot H \quad (1.7)$$

$$\mu_\Delta = \frac{\Delta_u}{\Delta_y} = \frac{\Delta_y + \Delta_p}{\Delta_y} = 1 + 3 \cdot \frac{\phi_p \cdot L_p}{\phi_y \cdot H} \quad (1.8)$$

L_p being the plastic hinge length that will form at the pier base.

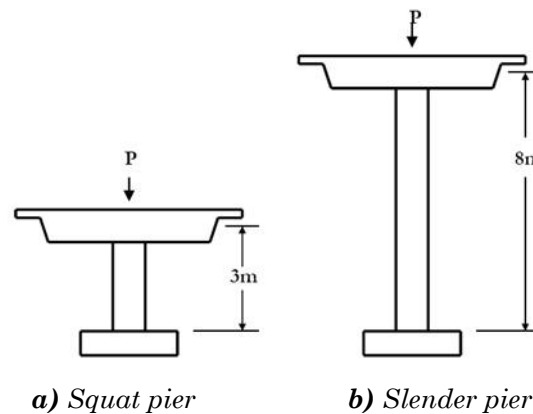


Fig. 1.6 – Influence of height on displacement ductility capacity

Using this approach, and an appropriate computation of the yield curvature, it can be found that the displacement ductility capacities of the two columns approximately differ by a factor of 2. The use of a unique force reduction factor, irrespectively to the different ductility demands, results in this case in a different safety value obtained for the two structures (non-uniform risk design).

Despite the criticisms leveled at the FB design process, it should be recognized that it generally leads to safe and satisfactory designs when combined with capacity-design rules; however the degree of protection obtained is different from structure to structure. Direct Displacement-Based Design approach was meant to overcome the deficiencies previously emphasized. As an alternative, more rational, seismic design approach, DBD aims at designing uniform-risk structures,

which would achieve, rather than be bound by, a given performance limit state under a pre-defined seismic action ^[P1].

The state of the art of the current Displacement-Based procedures is reported hereafter in Chapter 2, with specific reference to the application to bridge design and assessment.

1.2 RESEARCH MOTIVATION

It has been previously outlined that in the past decades design for earthquake resistance has undergone a critical review, shifting towards the perspective of a Performance-Based approach. Parallely simplified methods of seismic verification, using equivalent single degree of freedom systems for response prediction, have been the object of a great effort of research in the field of earthquake engineering particularly since the mid-1990s (Fajfar and Krawinkler^[F5], 1997).

This specific interest in simplified procedures can be justified still today, as a citation by P. Fajfar (2002) well explains: *“Structural response to strong earthquake ground motion cannot be accurately predicted due to large uncertainties and the randomness of structural properties and ground motion parameters. Consequently, excessive sophistication in structural analysis is not warranted.”* Furthermore, from a professional point of view, the extensive use of more complex approaches for seismic analysis such as Non Linear Time-History (NLTH) analyses, requires calibration of the hysteretic model parameters and an accurate selection of ground motions, that seems to date hardly applicable to everyday engineering practice. From a research perspective, the specific advantage in the use of simplified analytical procedures is still evident when seismic verification is carried out in a probabilistic framework (i.e. fragility analysis), explicitly accounting for uncertainties in mechanical model and input parameters (and leading to a multiplication of the analyses to be performed in respect to a deterministic approach). When a probabilistic risk estimation based on analytical approaches has to be developed on a large-scale model (e.g. on a regional infrastructure system as in this study), the use of simplified and reliable procedures for the development of fragility curves is strongly suggested, NLTH analyses being very time-consuming, despite the continuous enhancement of computational capacities.

In the last decade displacement-based (DB) methods have become increasingly established assessment procedures that use strain and displacement measures as structural damage indexes and seismic performance control parameters. Displacement-Based together the two aspects evidenced so far: they are simplified procedures which rely on a substitute SDOF structure for the prediction of seismic response, and are fully developed in a Performance-Based framework, the target limit displacement being used as reference control parameter (damage index) for a pre-defined performance level.

At present Displacement-Based Design (DBD) methods for new structures have reached a degree of formalization almost complete (Priestley, Calvi and Kowalsky^[P1], 2007) and have been proposed for code-implementation (Calvi and Sullivan^[C2], 2009). However, several aspects related to the method calibration are still matter of research, the representativeness of the substitute linear structure being

a critical issue, in particular the formulation of equivalent viscous damping and the definition of the target displacement profile for a given structural system.

With regard to the appraisal of existing structures, the development of the Displacement-Based Assessment (DBA) approach represents the state of the art of research in this field, since so far the calibration of the methods dealt essentially only with new structures. The specific problems of the development of DBA methodologies include the prediction of the possible collapse mechanisms due to brittle rupture of members (which may be substantially different from those of the new ductile structures, designed according to capacity design criteria), and the inclusion of local damage effects caused by nodes not adequately confined.

1.3 RESEARCH OBJECTIVES

In this context the research activity focuses on the evaluation, calibration and development of simplified Displacement-Based (DB) approaches for seismic verification of bridge structures, with particular reference to their use in a probabilistic framework, such as vulnerability analyses and risk calculation on a large scale.

In the first part, the thesis addresses the methodological aspects of the DB procedures focusing on the error sources of the simplified methods, with reference to their application on bridge structures represented by simple SDOF systems or MDOF systems. In particular the accuracy of current methods for the design of new structures with flexural ductile behaviour is evaluated, with special reference to the formulation of the equivalent viscous damping and the target displacement profile to be adopted in the analysis.

In the second part the methodological aspects are considered with regard to the specific issues of existing bridge structures, not seismically designed (and not satisfying capacity design principles), and thus characterized by failure modes, limit states, hysteretic behaviour, and local ductility of nodes different from those of new seismically designed structures. In particular the calibration effort focuses on the assessment of pier capacity, piers generally representing the most vulnerable elements in existing bridges. The aim is to provide proper indications about the effective properties of existing piers to be adopted in a Displacement-Based assessment framework.

Finally, the DBA method previously calibrated, is applied for the seismic vulnerability assessment on large scale of a reference bridge stock, the stock of rc multi-span bridges belonging to the Veneto regional road network (VR stock). Seismic risk maps are plotted in order to supply different scenarios of the expected damage for the class of bridges under exam in a low-medium seismicity area, like the Veneto Region (N-E of Italy), and can be used for prioritization of seismic retrofit interventions.

1.4 RESEARCH CONTENTS

As regards the first part of the research, more closely related to the design of new structures, at the beginning the accuracy of the current Direct Displacement-Based Design (DDBD) procedure applied to simple SDOF systems (with specific

reference to multi-span simply supported rc bridge piers) is investigated, the main error sources being the approximation of the substitute linear structure characterized by the equivalent viscous damping, and the scaling of the displacement elastic spectrum through the modification damping factor. Using different formulations proposed in literature for equivalent viscous damping and spectrum reduction factor, a parametric study is carried out on an ample set of SDOF systems (previously designed with the DDBD method and subsequently verified with NLTH analyses), and an average error chart is obtained, predicting the expected error for the design cases of multi-span simply supported bridge piers.

Next the representativeness of the equivalent SDOF structure related to the estimation of the design displacement profile within a displacement-based framework is examined. In the case of transverse response prediction for continuous rc girder bridges, the accuracy of the current iterative Direct Displacement-Based method (called DBD-IT in this work) is evaluated, and compared to an alternative direct design method (named DBD-DEM) herein proposed. The alternative method combines in a non-iterative procedure the DBD framework with a Response Spectrum Analysis carried out with effective stiffness.

In the second part of the thesis the focus is on the calibration of the Displacement-Based method for the assessment of rc existing bridges. Using a shear-flexure non linear model calibrated on experimental data derived by the PEER database, an extensive study is carried out, aiming to identify the possible collapse mechanisms due to brittle rupture of members, specify the corresponding limit states in terms of material strain and global drift and define the effective stiffness and equivalent viscous damping for the corresponding limit states. A series of plots are derived, that can be used directly for the capacity evaluation of existing piers and the definition of the main structural parameters used in the DBA procedure.

The parametrical study is developed for single bent and multiple bent piers (represented by cantilever, walls and frame piers), considering all the main properties that can influence the pier capacity. The effective ranges of these parameters were identified by a preliminary statistical analysis on the bridges of the reference bridge inventory (the VR stock), which includes about 500 bridges structures belonging to the Veneto regional road network. The bridge inventory data, and in particular the class of multi-span rc bridges, were the object of a detailed statistical survey within the thesis work, which allowed to get information about members' structural characteristics (e.g. static schemes, piers dimensions, effective reinforcement content, material properties), aiming at setting the actual ranges of the main pier parameters.

Finally an extensive vulnerability analysis for the class of multi-span rc bridges of the VR stock is subsequently developed, using the previously calibrated DBA procedures for the calculation of analytical fragility curves. A limited number of bridges are chosen as reference examples for each homogeneous subclass of multi-span bridges, and a direct comparisons of simplified DBA procedures with NLTH analyses is made on this restricted set of structures in connection to the development of fragility curves.

Regional seismic risk maps are drafted including all the multi-span rc bridges of the VR stock, for three different scenarios of damage (slight damage,

severe damage and collapse): the seismic risk is obtained by the convolution of hazard functions, defined on the base of the PGA exceedance probabilities provided by the current Italian seismic code, and the analytical fragility curves calculated with the Displacement-Based approach.

1.4.1 Methods of investigation

The numerical analyses were carried out using finite element models created with the software Opensees, exploiting the potentiality of the program for the fiber modeling of flexural behaviour and the aggregation of the non-linear shear effects. Through the development of specific scripts and the use of parametric datasheet for input and output, a considerable number of parametric analyses both in the linear and non linear field (simplified Displacement-Based approaches and NLTH analyses respectively) were easily managed. Other models made with commercial software were developed for the purpose of comparing results.

Regarding the calibration of the numerical models, in particular for the analyses on the existing structures, experimental results for rc columns which had experienced flexure and shear failure were used. The experimental hysteretic cycles were extracted from databases available on line (Structural Performance Database, of the Pacific Earthquake Engineering Research Center, PEER), which included specimens with both circular and rectangular solid sections.

Finally, as regards the statistical survey on the VR bridge inventory, the work involved the arrangement and statistical analysis of a large amount of data, extrapolated from the original projects, or obtained from the results of laboratory or on-site tests and geometrical surveys.

1.4.2 Restrictions

In this work some restrictions have been necessarily introduced to limit the field of investigation:

- in the parametric study on the error prediction of Direct-Displacement-Based and subsequent analyses, only the current widespread approach, in which the hysteretic energy absorption is represented by equivalent viscous damping, is considered. Other formulations using inelastic displacement spectra are not investigated;
- in the vulnerability study of multi-span rc bridges, piers are individuated as the only vulnerable components of the bridge lateral resisting system. Soil-structure interaction is considered only as linear effect to include the increment in pier lateral drift.
- in the risk analysis hazard curves are derived directly from Italian seismic hazard maps obtained by INGV (Meletti and Montaldo^[M7], 2007) using log-normal interpolation. No specific micro-zonation studies were used for the assessment of the local (regional) seismic hazard.

1.5 OUTLINE OF THE THESIS

The thesis is organized into the following chapters:

- Chapter 1: “Introduction”.
- Chapter 2: “Review of current Displacement-Based methods for seismic design and assessment of bridges” .
- Chapter 3: “Direct Displacement-Based Design method: error prediction for multi-span simply supported bridges”.
- Chapter 4: “Displacement-Based Design for transverse response of continuous rc bridges: iterative vs direct procedure”
- Chapter 5: “Displacement-Based Assessment of existing bridges: parametrical analysis for capacity of rc piers”.
- Chapter 6: “Displacement-Based approaches for vulnerability assessment of rc bridges: application on a regional-scale case study.
- Chapter 7: “Conclusions”

Chapter 1 describes the framework of the work, and identifies the main research objectives.

Chapter 2 contains a state-of-the-art literature review of Displacement-Based methods for seismic design and assessment, with specific reference to bridge structures.

Chapter 3 investigates the accuracy of the current Direct Displacement-Based Design (DDBD) procedure applied to simple structures that can be represented by Single Degree Of Freedom systems. In the first part of the study a parametrical analysis is developed on a large sample of ideal SDOF oscillators, considering the influence of different equivalent damping models for the linearization of non linear system. As a final result a mean error chart is presented, characterizing the scatter in the results as a function of design ductility $\mu_{\Delta d}$ and effective period T_{eff} . In the second part a displacement-based design process for an ample set of realistic cantilever rc piers with flexural ductile behaviour is developed. Using the mean error diagram previously obtained, the error range for reinforced concrete bridge piers is derived with reference to the realistic design cases analyzed. Finally an approximate relationship between ductility and drift is derived, and parametric curves are plotted for pre-fixed values of pier height/diameter ratio.

Chapter 4 investigates the representativeness of the equivalent SDOF structure in respect to the original MDOF system, in the case of transverse response prediction for continuous rc girder bridges within a displacement-based framework, with particular reference to the estimation of the design displacement profile. The accuracy of the current iterative Direct Displacement-Based method (called DBD-IT in this work) applied to the prediction of the transverse response of multi-span continuous girder bridges is evaluated, and compared to a non-iterative (direct) design method, named DBD-DEM, herein proposed with the aim of simplifying the current procedure for everyday design use. In the DBD-DEM method the effective stiffness of the linearized system at the target displacement is predicted by using

the DBD framework, and subsequently a Spectrum Response Analysis (RSA) with the effective stiffnesses of members previously derived is used for the estimation of the target displacement shape and the final design of piers.

Chapter 5 addresses some critical issues for the calibration of displacement-based assessment procedure (Displacement-Based Assessment, DBA) applied to existing rc bridges. A simplified numerical model is used for the aggregation of phenomenological non linear shear behaviour and fiber representation of flexural behaviour for piers, and an equivalent damping formulation (EVD) for shear critical column is proposed, expressing the hysteretic component of EVD as a function of the pier lateral drift. A parametrical study is then developed for bridge piers with different static scheme (cantilever, frame, walls), considering the effective ranges of main parameters influencing the bridge capacity, determined from the statistical analysis on the VR stock carried out in Chapter 6. A series of charts are obtained for flexural and shear pier capacity, collapse mechanisms, ultimate deformations, drift, secant-to-yielding stiffness, effective stiffness, that can be directly used for the capacity evaluation of existing piers and the definition of the main structural parameters used in the DBA procedure.

Chapter 6 presents the application of Displacement-based methods for the vulnerability assessment and calculation of seismic risk for multi-span rc bridges. A large-scale case study is addressed, with reference to the stock of bridges belonging to the Veneto Region road network (VR stock). A preliminary extensive statistical survey is carried out, to characterize the bridge properties in terms of static scheme, material properties, geometrical parameters and aiming at providing the effective ranges of the main pier parameters, essential for the calculation of rc pier capacity for multi-span bridges (longitudinal and transverse reinforcement ratio, confinement parameters, normalized axial load, etc.).

An extensive vulnerability analysis of the entire multi-span rc bridge stock is subsequently developed, using the previously calibrated DBA procedures for the calculation of analytical fragility curves. A comparison with analytical curves obtained with TH analysis is presented for a restricted number of structures (selected as reference structures for the corresponding homogeneous classes of bridges), discussing the reliability of the method for the development of fragility curves. A direct comparison with fragility functions obtained with tabular methods (RISK-UE) is also presented, showing how these methods, usually adopted in the absence of detailed information on large-scale stocks, are decidedly inaccurate for the vulnerability prediction of Italian (or European) typical bridge structures. Finally seismic risk maps are plotted for all the multi-span rc bridges of the VR stock, for three different scenarios corresponding to light damage, severe damage and collapse of bridges.

In Chapter 7 the outcomes of the thesis are summarized and future work is considered.

CHAPTER 2

REVIEW OF CURRENT DISPLACEMENT-BASED METHODS FOR SEISMIC DESIGN AND ASSESSMENT OF BRIDGES

2.1 FUNDAMENTALS OF THE DIRECT DISPLACEMENT-BASED DESIGN METHOD

Different displacement-based design approaches have been developed in recent years^[F4,C1], all aiming at designing structures capable of reaching a pre-fixed lateral deflection under a given seismic excitation. In the Direct Displacement-Based Design method (called “direct” because no iteration is required in its basic formulation^[P1]), the achievement of a given performance (expressed in terms of target displacement) is obtained by analyzing an equivalent elastic single-degree-of-freedom (SDOF) model. The equivalent elastic SDOF model, is directly derived from the real inelastic system through some basic working equivalences, and characterized by an effective mass m_e , equivalent secant stiffness K_{eff} (with respect to the maximum allowable displacement), and an equivalent viscous damping ξ_{eq} , representative of the combined elastic damping and hysteretic energy dissipated during the seismic response. This concept is based on the considerations developed in the Substitute Structure approach initially proposed by Shibata and Sozen^[S1].

The design process can be seen as a “reverse” procedure with respect to the Force-Based approach: at the beginning it requires the selection of a performance level by the choice of a target displacement, and ends with the calculation of the stiffness characteristics and required design lateral force. The seismic input is given by an elastic Displacement Response Spectrum (DRS) rather than an Acceleration Response Spectrum (ARS). For multi-degree of freedom (MDOF) systems, the estimate of a consistent deflected shape considering the inelastic contribution given by the formation of plastic hinges is also required.

The whole analysis is carried out focusing on the substitute equivalent linear SDOF system (see Fig. 2.1): first, its *equivalent mass* m_e , design and yield displacements are determined (Δ_d and Δ_y respectively); then, the *displacement ductility capacity* μ_Δ and the corresponding *equivalent viscous damping* ξ_{eq} are easily derived. Finally, using the damped Displacement Response Spectrum (DRS), with the design displacement at maximum response determined, the *effective period* T_e is directly calculated, and the *effective stiffness* K_e of the equivalent SDOF system is easily obtained by the classical relations for the period of a SDOF oscillator:

$$K_e = 4\pi^2 \frac{m_e}{T_e^2} \quad (2.1)$$

while the design lateral force is given by:

$$F = V_{base} = K_e \Delta_d \quad (2.2)$$

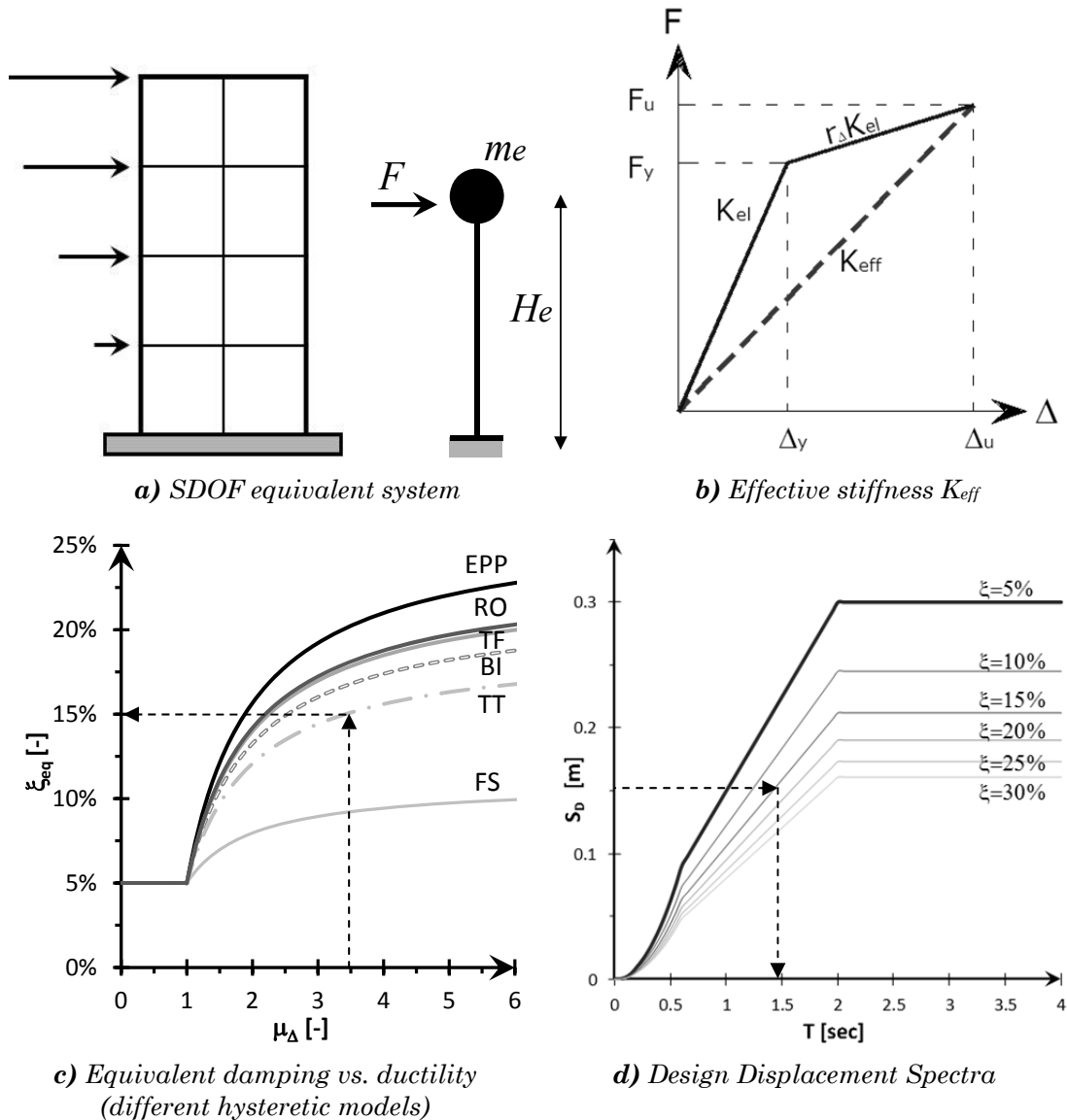


Fig. 2.1 – Fundamentals of DDBD procedure

The formulation presented above has the advantage of characterizing the effects of ductility on seismic demand independently from hysteretic characteristics: different damping equations are generated separately for different hysteretic models (e.g. the Takeda Thin, TT model, is used for rc columns with high axial load, while the Flanged-Shaped, FS model, is appropriate for pre-stressed structures, see Fig. 2.6c). It is possible, anyhow, to combine the damping/ductility

relationship in a single inelastic displacement response spectra set^[P1]: this simplifies one step of the procedure, but requires the ductility modifiers to be determined for each hysteretic rule considered.

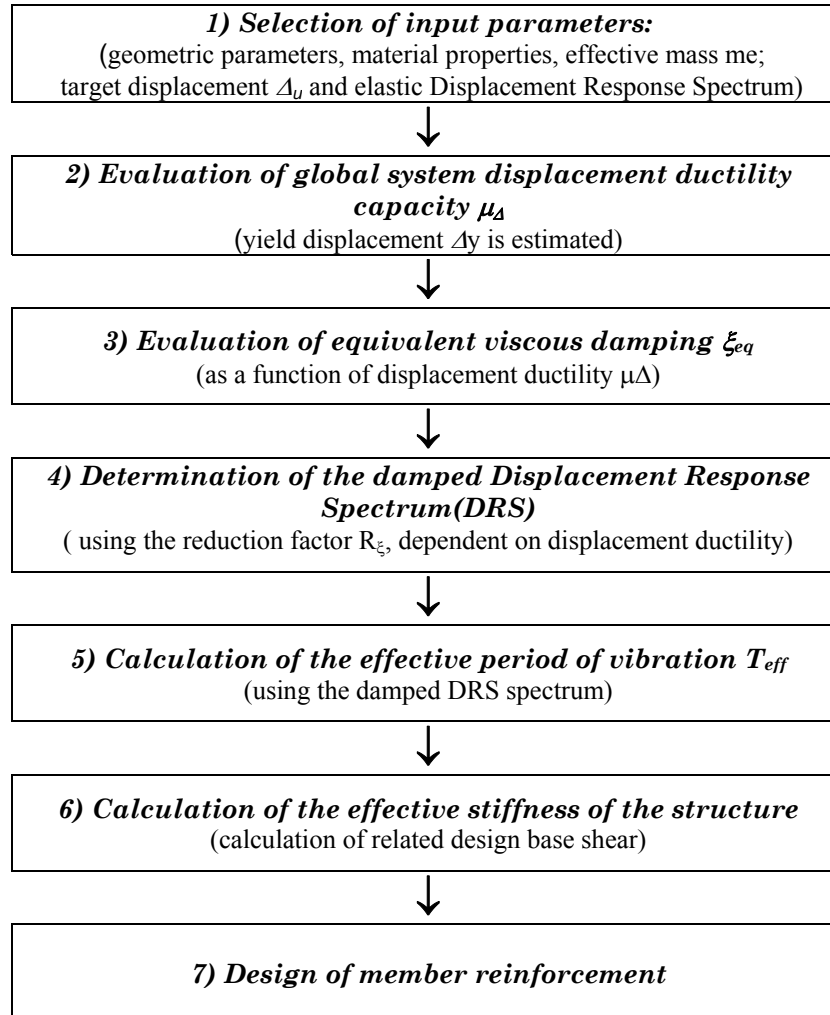


Fig. 2.2 – Direct Displacement-Based Design flowchart for a SDOF structure

2.1.1 Performance levels: section and structure limit states

The definition of physical damage is one of the key aspects of Performance-Based Earthquake Engineering, whether it is applied to the design of new structures or to the assessment of existing constructions. As stated earlier, the most significant damage index for a structure is represented by a displacement measure: the damage estimation based on the maximum displacement attained by the system during a pre-defined event is a challenging topic, and is still a subject of research work (see among others Priestley^[P7], 1997, Priestley et al.^[P4], 1996, Priestley et al.^[P1], 2007, Crowley et al.^[C4], 2006).

The focus of the present paragraph is the definition of appropriate limit states for ductile rc structures, and more in specifically for rc bridges. Additional considerations should be addressed for assessment purposes, being existing structures often characterized by inadequately confined members and different failure mechanisms in respect to newly designed structures.

1.1.1.1 Performance objectives

A *performance objective* has been defined in the Vision 2000^[O1] document as the “coupling of expected performance with expected level of seismic ground motion”, and represents the performance level of the structure to be addressed in the design, related to a predefined seismic hazard.

The Vision 2000 guidelines are useful for general reference, having introduced the concept that performance objective have to be more demanding (i.e. there should be less damage) for a high probability earthquake (one that may occur several times during the life of the structure) or for an important structure or dangerous occupancy. However, to better relate the structural response to the performance level, it is necessary to define sectional (member) and global (structure) limit states, the former to be used in displacement-based capacity equations.

Design limit states

A comprehensive summary of material strain limits, maximum drift limits and residual drifts criteria for different structures is presented in the DBD09 Model Code^[C2], by Calvi and Sullivan, 2009, drawing on earlier studies, and extending the information provided. Three limit states are set for design reference:

- **LS1, Serviceability:** only insignificant damage can be expected and any necessary repair can be carried out without affecting normal operations;
- **LS2, Damage Control:** damage should be economically repairable;
- **LS3, Collapse prevention(near collapse):** no collapse is required.

The drift ratio θ , used for maximum and permanent drifts, is defined as:

$$\theta_i = \frac{\Delta_{i+1} - \Delta_i}{x_{i+1} - x_i} \quad (2.3)$$

where Δ_i and Δ_{i+1} are the maximum displacements of levels i and $i+1$ respectively and $(x_{i+1} - x_i)$ represents the distance between levels.

The target displacement for a bridge pier can be characterized by either *serviceability* or *ultimate* criteria, which are likely to be based on the local drift limits for the piers, derived from accepted ductility limits or, more correctly, from accepted strain limits.

Serviceability limit state might be taken to be the onset of concrete cover crushing (related to extreme compression fibre concrete strain), or the development of crack widths of a size that might require injection grouting (related to limit strain in reinforcing bars).

Ultimate conditions may be taken as corresponding to a damage control limit state beyond which structural repair is not economically feasible, or

alternatively to a true “collapse” limit state^[K1]; a maximum fibre compression strain can be set based on the volumetric ratio of the transverse reinforcement (e.g. according to Mander^[M3] model), while reinforcement strain limits will be provided for adequate protection against bar buckling or extreme deformations.

Tab. 2.1 – Structural Drift limits (after DBD09 Model Code^[C2])

Drift Limit	LS1	LS2	LS3
<i>Buildings with brittle non structural elements</i>	0.004	0.025	No limit
<i>Buildings with ductile non structural elements</i>	0.007	0.025	No limit
<i>Building with non-structural elements detailed to sustain building displacements</i>	0.010	0.025	No limit
<i>Framed Timber walls</i>	0.010	0.020	0.030
<i>RC Bridge Piers</i>	θ_Y	0.030	0.040
<i>Isolated bridges</i>	$2/3*\vartheta_Y$	$2/3*\vartheta_Y$	ϑ_Y

Tab. 2.2 – Permanent Drift limits (after DBD09 Model Code^[C2])

Drift Limit	LS1	LS2	LS3
<i>Building Structures</i>	0.002	0.004	No limit
<i>Bridge Structures</i>	0.002	0.004	No limit
<i>Retaining walls</i>	0.005	0.010	No limit

The “first yield” is defined as the point when the section first attains the longitudinal reinforcement yield strain of $\varepsilon_y = f_y/E_s$, or a concrete compression of the extreme fiber of 0.002. Even if it was common in the past to require for LS1 near elastic response, implying a reinforcement strain equal to the yield strain, this is currently felt to be excessive conservative, as a strain of several times the yield value can be sustained without creating damage involving repair. The nominal yield point (M_N, ϕ_y) is thus defined by an extreme fibre compression strain of 0.004 or an extreme reinforcing bar strain of 0.015, whichever occurs first [P3].

For confined concrete members the damage control limit states, can be characterized as follows:

$$\varepsilon_{c,dc} = 0.004 + \frac{1.4\rho_v f_{yh} \varepsilon_{su}}{f'_{cc}} \quad (2.4)$$

$$\varepsilon_{sm} = 0.6 \varepsilon_{su} \quad (2.5)$$

Tab. 2.3 – Material strain limits for rc structures (after DBD09 Model Code^[C2])

Material	LS1	LS2	LS3
Concrete comp. strain	0.004	$\varepsilon_{c,dc} < 0.02$	$1.5*\varepsilon_{c,dc}$
Rebar tension strain	0.015	$0.6\varepsilon_{su} < 0.05$	$0.9\varepsilon_{su} < 0.08$

The limits are proposed for bridge piers with fixed-pinned end conditions.

The target performance consists in obtaining a displacement shape, where at least one column or abutment reaches its desired damage level^[K3]. The

displacements at the other columns or abutments are obtained with reference to the effective modal shape.

Tab. 2.4 – Assessment limit states

	LS1	LS2	LS3
	(Serviceability/Slight Damage)	(Damage Control/Severe Damage)	(Survival/Collapse)
Description	Spalling of concrete, residual crack widths = 1.0mm	Certain amount of repairable damage may be permissible: formation of wide flexural cracks requiring injection grouting	Collapse does not take place; extensive damage, repair may not be economically or technically feasible
Strain Limit	$\varepsilon_c = 0.004$ $\varepsilon_s = 0.015$		
Displ.Ductility	$\mu_N = 1-2$		
Description	Limited ductility developed, cracks widths reach 1.0mm	$\mu_N = 3-6$ (4 for European bridges) Significant repair required (still feasible), wide flexural or shear cracks, buckling of longitudinal reinforcement may occur	Repair of building not feasible either physically or economically due to shear failure of vertical elements or excess flexural displacement
Strain Limit	$\varepsilon_c(\text{LS1}) = 0.002$ $\varepsilon_s(\text{LS1}) = \varepsilon_y$	$\varepsilon_c(\text{LS2}) = 0.004-0.005^\dagger$ $\varepsilon_s(\text{LS2}) = 0.010-0.015^\dagger$ Member flexural strength achieved, limited ductility developed	$\varepsilon_c(\text{LS3}) = 0.005-0.01^{**}$ $\varepsilon_s(\text{LS3}) = 0.015-0.03^{**}$ Wide flexural and/or shear cracks occur, buckling of longitudinal reinforcement may happen
Description	Serviceability: loss of linear elastic response, flexural or shear type hairline cracks (<1.0mm)		
Strain Limit	$\varepsilon_c(\text{LS1}) = 0.002$ $\varepsilon_s(\text{LS1}) = \varepsilon_y$	$\varepsilon_c(\text{LS2}) = 0.004-0.005$ $\varepsilon_s(\text{LS2}) = 0.010-0.015$	$\varepsilon_c(\text{LS3}) = 0.005-0.010$ $\varepsilon_s(\text{LS3}) = 0.015-0.030$
Description	Loss of linear elastic response, yielding in section	$\varepsilon_{c,dk} = 0.004 + \frac{1.4 \rho_v f_{yh} \varepsilon_{su}}{f'_{cc}}$	$\varepsilon_s = 0.6 \varepsilon_{su}$
Strain Limit	$\varepsilon_c = 0.004^\dagger$ $\varepsilon_s = 0.015^\dagger$		
Description		Member flexural strength achieved, limited ductility developed	Wide flexural and/or shear cracks occur, buckling of longitudinal reinforcement may happen
Strain Limit	$\varepsilon_c(\text{LS1}) = 0.002$ $\varepsilon_s(\text{LS1}) = \varepsilon_y$	$\varepsilon_c(\text{LS2}) = 0.0035$ $\varepsilon_s(\text{LS2}) = 0.015$	$\varepsilon_c(\text{LS3}) = 0.075$ $\varepsilon_s(\text{LS3}) = 0.035$
Strain Limit		$\varepsilon_{c,dk} = 0.004 + \frac{1.4 \rho_v f_{yh} \varepsilon_{su}}{f'_{cc}}$	es = 0.6es_u
Strain Limit	$\varepsilon_c = 0.0035$ $\varepsilon_s = 0.01$	$\varepsilon_c = 0.0035$ $\varepsilon_s = 0.04$	$\varepsilon_c = 0.004$ $\varepsilon_s = 0.06$
Drift/Rotation limits	θ_y		Survival: 3/4 θ_u Collapse: θ_u

[†] Limits valid for inadequately confined members, checked at the outer fibers of core concrete

** Limits valid for inadequately confined members, checked at the most outer fibers

Assessment limit states

For existing structures, the definition of physical damage is one of the key aspects of loss estimation appraisal. In this work, dealing with bridge rc structures with inadequately confined members in a displacement-based framework, references for sectional damage limit states were derived from the works by Priestley et al. ^[P4], 1996, Priestley ^[P9], 1997, Calvi ^[C1,C7], 1997 and Crowley ^[C8], 2006. References to current seismic codes in force (Italian and Turkish codes) were also considered. Structure limit states are individuated in terms of strain limits on materials, displacement ductility values or limit drift/rotations for single members.

2.1.2 Displacement response spectra

As briefly outlined before, DDBD methods use elastic Displacement Response Spectra for different levels of equivalent viscous damping, rather than the classical elastic Acceleration Response Spectrum. Design spectra were typically defined as a spectral shape related to soil condition, modified by the *PGA* value reflecting the seismicity of the region. To date, only some seismic codes ^[X1,X4] give more detailed information, providing spectral acceleration ordinates at two or three key periods for different probabilities of occurrence, and thus enabling design data based on site longitude and latitude to be extracted. In any case in most codes, following the definition of the standard 5% damping ARS as a function of the probability of occurrence of a certain event and the soil characteristics, the related 5% damping DRS is directly generated using the following approximate relationships:

$$S_{De}(T) \cong \frac{1}{\omega^2} S_e(T) \quad (2.6)$$

$$\Delta_{(T,5)} \cong \frac{1}{\omega^2} a_{(T,5)} g = \frac{T^2}{4\pi^2} a_{(T,5)} g \quad (2.7)$$

where S_{De} is the *spectral relative displacement*, S_e the *spectral absolute acceleration* and $a_{(T,5)}$ represents the *spectral design acceleration* (expressed in units of g) with reference to a SDOF system with an elastic period T and a viscous damping of 5%. Ideally the elastic displacement spectra should be developed separately, by using a set of time history records, and deriving the exact DRS directly through Duhamel's integral, in which $\omega_D = \omega\sqrt{1-\xi^2}$ represents the damped frequency of the system.

$$S_{De} = |x(t)|_{max} = \left| -\frac{1}{\omega_d} \int_0^t \ddot{x}_g(\tau) e^{-\xi\omega(t-\tau)} \sin\omega_d(t-\tau) d\tau \right|_{max} \quad (2.8)$$

Fig. 2.3 shows the ARS and the respective DRS, derived with regard to the EC8 ^[X2] formulation in the case of a peak ground acceleration $a_g=0.35g$, and soil type from A to E.

The equations used to derive the ARS spectra are the following:

$$0 \leq T \leq T_B: S_e(T) = a_g \cdot S \cdot \left[1 + \frac{T}{T_B} \cdot (\eta \cdot 2,5 - 1) \right] \quad (2.9)$$

$$T_B \leq T \leq T_C: S_e(T) = a_g \cdot S \cdot \eta \cdot 2,5 \quad (2.10)$$

$$T_C \leq T \leq T_D: S_e(T) = a_g \cdot S \cdot \eta \cdot 2,5 \cdot \left[\frac{T_C}{T} \right] \quad (2.11)$$

$$T_D \leq T \leq 4s: S_e(T) = a_g \cdot S \cdot \eta \cdot 2,5 \cdot \left[\frac{T_C \cdot T_D}{T^2} \right] \quad (2.12)$$

where:

$S_e(T)$ is the acceleration elastic response spectrum;

a_g is the design ground acceleration on type A ground;

T_B is the lower limit of the period of the constant spectral acceleration branch;

T_C is the upper limit of the period of the constant spectral acceleration branch;

T_D is the value defining the beginning of the constant displacement range;

S is the soil factor;

η is the damping correction factor $\eta = \sqrt{10/(5 + \xi)} \geq 0,55$;

The corresponding DRS spectra are obtained using Eq. (2.6).

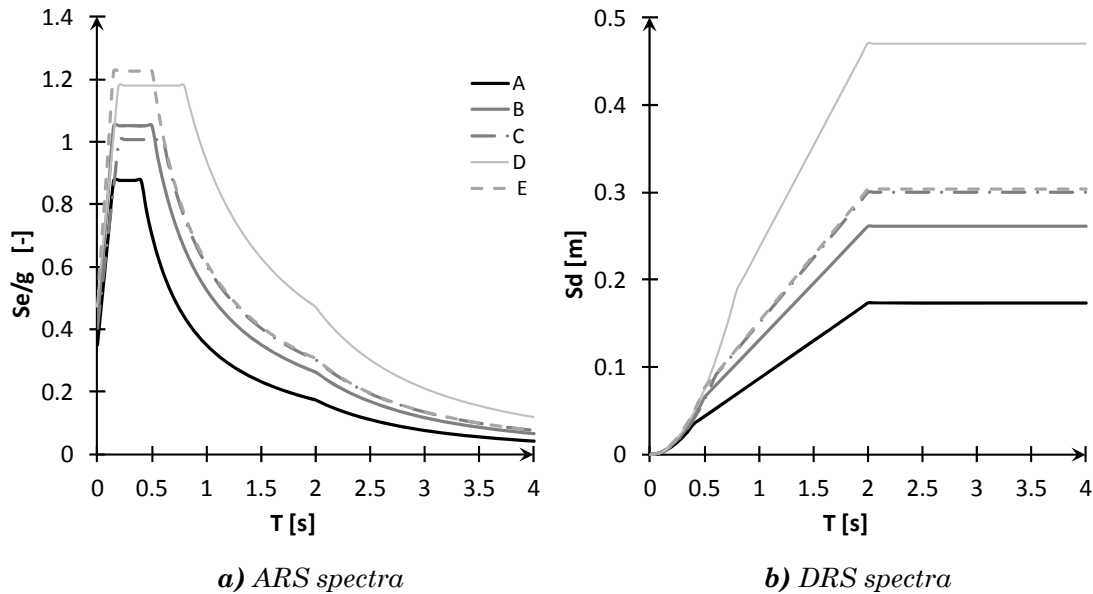


Fig. 2.3 – Elastic ($\xi=5\%$) acceleration response spectra **a)** and Displacement Response Spectra for different ground types (A,B,C,D,E). Spectrum type 1, ($M_w > 5,5$), $a_g = 0.35$ [g], according to EC8^[X2].

Tab. 2.5 – Values of the parameters describing the recommended Type 1 elastic response spectra according to EC8^[X2].

Ground type	S [-]	T_B [s]	T_C [s]	T_D [s]
A	1.00	0.15	0.4	2.0
B	1.20	0.15	0.5	2.0
C	1,15	0.20	0.6	2.0
D	1.35	0.20	0.8	2.0
E	1.40	0.15	0.5	2.0

The current EC8^[X2] regulations specify that the corner period T_D is taken as 1.2s for causative earthquakes with magnitude $M_w < 5.5$ (Type 2 spectra), and as 2.0 for $M_w \geq 5.5$ (Type 1 spectra). Recent studies by Boore and Bommer^[B2] have suggested that this low corner period is the result of data from analogue records which were processed with low-order filters set at periods making interpretations unreliable at periods above 2 seconds^[P1].

Recent work by Faccioli et al. ^[F1,F2], analyzing high-quality digital records, has shown the possibility of generating DRS directly from the moment magnitude M_w of the seismic event and the distance r of the site under consideration, from the nearest “fault plan”.

The corner period appears to increase almost linearly with magnitude, and the following conservative relationship is proposed:

$$T_c = 1,0 + 2,5(M_w - 5,7), \quad M_w \geq 5.7 \quad (2.13)$$

For the peak response displacement, $\Delta_{c,max}$, the following relationship is derived for firm ground conditions:

$$\log_{10} \Delta_{c,max} = -4,46 + 0,33 \log_{10} \Delta\sigma + M_w - \log_{10} r \quad (cm) \quad (2.14)$$

where $\Delta\sigma$ is the stress drop, expressed in MPa, and r is the epicentral distance, expressed in km. Using an average value of $\Delta\sigma = 6$ MPa, the following expression is obtained:

$$\Delta_{c,max} = C_s \cdot \frac{10^{(M_w - 3,2)}}{r} \quad (mm) \quad (2.15)$$

The authors^[F1,F2] proposed some tentative coefficient C_s for different ground condition, as reported in Tab.2.3.

Tab. 2.6 – Values of the parameters describing the recommended Type 1 elastic response spectra.

Ground	Type	C_s
Rock	(A)	0.7
Firm Ground	(B)	1.0
Intermediate Soil	(C)	1.4
Very soft Soil	(D)	1.8

Other findings of the above mentioned study are the following:

- the 5% damped spectra tends to increase almost linearly with T up to the corner period value; beyond this is conservative to assume a constant spectral displacement;
- the measure of the peak ground displacement can be considered the value corresponding to $T=10$ s in the 5% damped displacement spectrum;
- soft soil amplification is more pronounced at longer distances (30-50km).

The DRS formulation proposed by Faccioli (Eqs. 2.21 and 2.23) is plotted below for M_w values from 7.5 to 6.0 and for values of epicentral distance r equal to 10 and 20km.

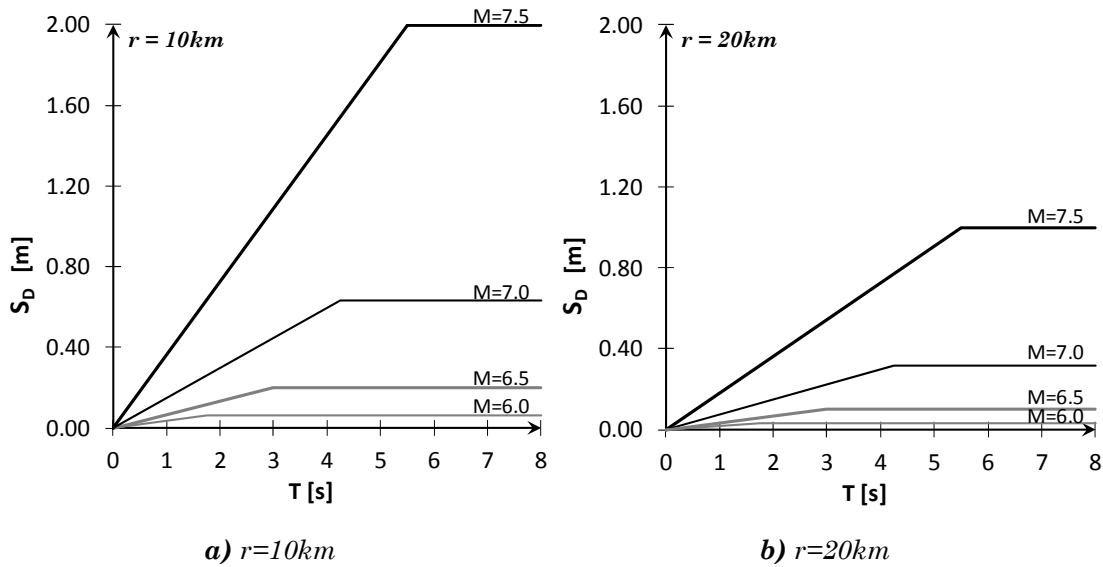


Fig. 2.4 – Influence of M_w and r on 5% damped displacement spectra for firm ground (type B), according to Faccioli et al.^[F1].

2.1.3 Equivalent Damping models

DDBD approach involves replacing the non linear structure with an equivalent linear structure whose maximum displacement response is approximately equal to the non linear structure response (equivalent secant stiffness K_{eff}), and whose Equivalent Viscous Damping (EVD) is given as a combination of elastic and hysteretic components:

$$\xi_{eq} = \xi_{el} + \xi_{hyst} \quad (2.16)$$

where the hysteretic damping ξ_{hyst} depends on the hysteresis rule appropriate for the structure to be designed and is generally related to the displacement ductility capacity μ_{Δ} , while the viscous-elastic ratio ξ_{el} is generally, for concrete structures, taken as 5%, related to critical damping. Many significant studies have been conducted on equivalent damping over the past decades (Jennings^[J3], 1968, Gulkan and Sozen^[G2], 1974, Ivan and Gates^[I1], 1979, Kowaksy et al.^[K1], 1995, Miranda and Garcia^[M2], 2002); recently much effort has been addressed to find EVD expressions coherent with DDBD assumptions [G1,P11,D1]. A brief discussion on this topic and a summary of the main findings is reported in the following paragraphs.

2.1.3.1 Hysteretic damping

The equivalent structure approach was first suggested by Jacobsen^[J1,J2], equating the energy absorbed by hysteretic steady-state cyclic response of a non linear oscillator to the EVD of the equivalent linear oscillator. This concept leads to the well-known relationship:

$$\xi_{hyst} = \frac{A_h}{2\pi F_m \Delta_m} = \frac{2}{\pi} \frac{A_h}{2F_m 2\Delta_m} = \frac{2}{\pi} R_{ia} \quad (2.17)$$

where A_h is the area of one complete stabilized hysteretic cycle (also defined as energy dissipated per cycle) and R_{la} is the so-called loop area ratio.

The whole discussion, here presented, refers to a $F-\Delta$ diagram, but it can be demonstrated that the same considerations can be made by looking at the classic moment-curvature hysteretic loop.

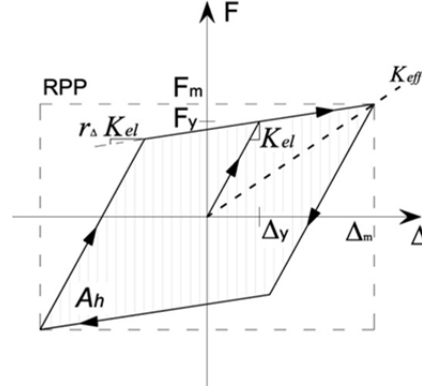


Fig. 2.5 – Equivalent damping for bilinear (BI) and RPP hysteretic models.

While Jacobsen's original approach was tied to the initial stiffness of the system, the DDBD application of his approach has been tied to secant stiffness at peak response, resulting in an equal period shift (T_{eff}/T_i) for each hysteretic model considered:

$$\frac{T_{eff}}{T_i} = \sqrt{\frac{\mu_{\Delta}^d}{1 + r_{\Delta}\mu_{\Delta}^d - r_{\Delta}}} \quad (2.18)$$

with reference to a bilinear hysteretic model (as shown in Fig. 2.13), with initial stiffness K_{el} , secondary stiffness $r_{\Delta}K_{el}$, and displacement ductility $\mu_{\Delta}^d = \Delta_m / \Delta_y$.

Applying the Jacobsen's approach in conjunction with the secant stiffness at peak response (JDSS approach) for the theoretical case of a Rigid-Perfectly-Plastic (RPP) loop (see Fig. 2.13), leads to the maximum value of the equivalent damping, $\xi_{hyst}=2/\pi$ (Jennings^[13], 1968); Eqs. 2.19-2.23 are therefore obtained for the hysteretic damping as a function of displacement ductility, with reference to hysteretic models presented in Figs. 2.5 and 2.6a,b,d.

- *Elasto-Plastic Bi-linear Hysteretic Model (BI):*

$$\xi_{hyst} = \frac{2 (\mu_{\Delta} - 1)(1 - r_{\Delta})}{\pi \mu_{\Delta}(1 + r_{\Delta}\mu_{\Delta} - r_{\Delta})} \times 100\% \quad (2.19)$$

- *Flag Shaped Hysteretic Model (FS) ($r_{\Delta}=0.1$; $r_l=0.04$; $r_s=1.0$):*

$$\xi_{hyst} = \frac{217}{\pi} \left[\frac{5\mu_{\Delta}^2 + 95\mu_{\Delta} - 100}{\mu_{\Delta}(10\mu_{\Delta} + 90)} \right] \times 100\% \quad (2.20)$$

- *Takeda's Hysteretic Model:*

$$\xi_{hyst} = \left(\frac{2}{\pi}\right) \left\{ 1 - \frac{3}{4} \mu_{\Delta}^{\alpha-1} \gamma - \frac{1}{4} \left[\frac{r_{\Delta} \beta \mu_{\Delta}}{\mu_{\Delta}} \left(1 - \frac{1}{\mu_{\Delta}}\right) + 1 \right] \left[2 - \beta \left(1 - \frac{1}{\mu_{\Delta}}\right) - \mu_{\Delta}^{\alpha-1} \gamma \right] - \frac{1}{4} \left[\frac{r_{\Delta} \beta^2 \mu_{\Delta}}{\gamma} \left(1 - \frac{1}{\mu_{\Delta}}\right)^2 \right] \right\} \times 100\% \quad (2.21)$$

where $\gamma = r_{\Delta} \mu_{\Delta} - r_{\Delta} + 1$.

With $\alpha=0.5$, $\beta=0$ and $r_{\Delta}=0$, the *Takeda Thin (TT)* model is expressed as:

$$\xi_{hyst} = \frac{1}{\pi} \left(1 - \frac{1}{\sqrt{\mu_{\Delta}}}\right) \times 100\% \quad (2.22)$$

and with $\alpha=0$, $\beta=0.6$ e $r_{\Delta}=0$, *Takeda Fat (TF)* model can be simplified as follows:

$$\xi_{hyst} = \left(\frac{2}{\pi}\right) \left\{ 1 - \frac{3}{4} \mu_{\Delta}^{-1} - \frac{1}{4} \left[2 - 0.6 \left(1 - \frac{1}{\mu_{\Delta}}\right) - \mu_{\Delta}^{-1} \right] \right\} \times 100\% \quad (2.23)$$

Later works ^[P11,D1], in order to evaluate the displacement-prediction capability of equivalent linear structures (ELS), used specific accelerograms, rather than equating steady-state response to sinusoidal excitation. Dwairi et al. (2007), made an extensive evaluation of the JDSS approach, indicating an overestimation of the EVD for intermediate to long periods, in particular for systems with high energy absorption, confirming the results of previous studies (Chopra ^[C1], 2001).

Tab. 2.7 – Values of EVD coefficients used by D.K. formulation.

Hysteretic model	C($T_{eff} < 1s$)	C($T_{eff} \geq 1s$)
<i>Elasto-Plastic (EPP)</i>	$85 + 60(1 - T_{eff})$	85
<i>Takeda Fat (TF)</i>	$65 + 50(1 - T_{eff})$	65
<i>Takeda Thin (TT)</i>	$50 + 40(1 - T_{eff})$	50
<i>Flag Shaped, $\beta=0.35$ (FS)</i>	$30 + 35(1 - T_{eff})$	30

In addition new equivalent viscous damping formulations for different hysteresis rules were calibrated, presenting the hysteretic component in the following general form (herein called Dwairi and Kowalsky, *D.K.*, formulation):

$$\zeta_{hyst} = C \left(\frac{\mu - 1}{\mu \pi} \right) \% \quad (2.24)$$

where the coefficient C depended on the hysteresis rule, and a period-dependency was found for $T_{eff} < 1.0s$ (see Tab. 2.8).

Another refined formulation for hysteretic damping has been recently proposed by Grant et al. ^[P11], with a period dependency related to variable coefficients in accordance with the various hysteresis rules investigated (see Fig.2.14):

$$\xi_{hyst} = a \left(1 - \frac{1}{\mu_{\Delta}^b} \right) \left[1 + \frac{1}{(T_{eff} + c)^d} \right] \times 100\% \quad (2.25)$$

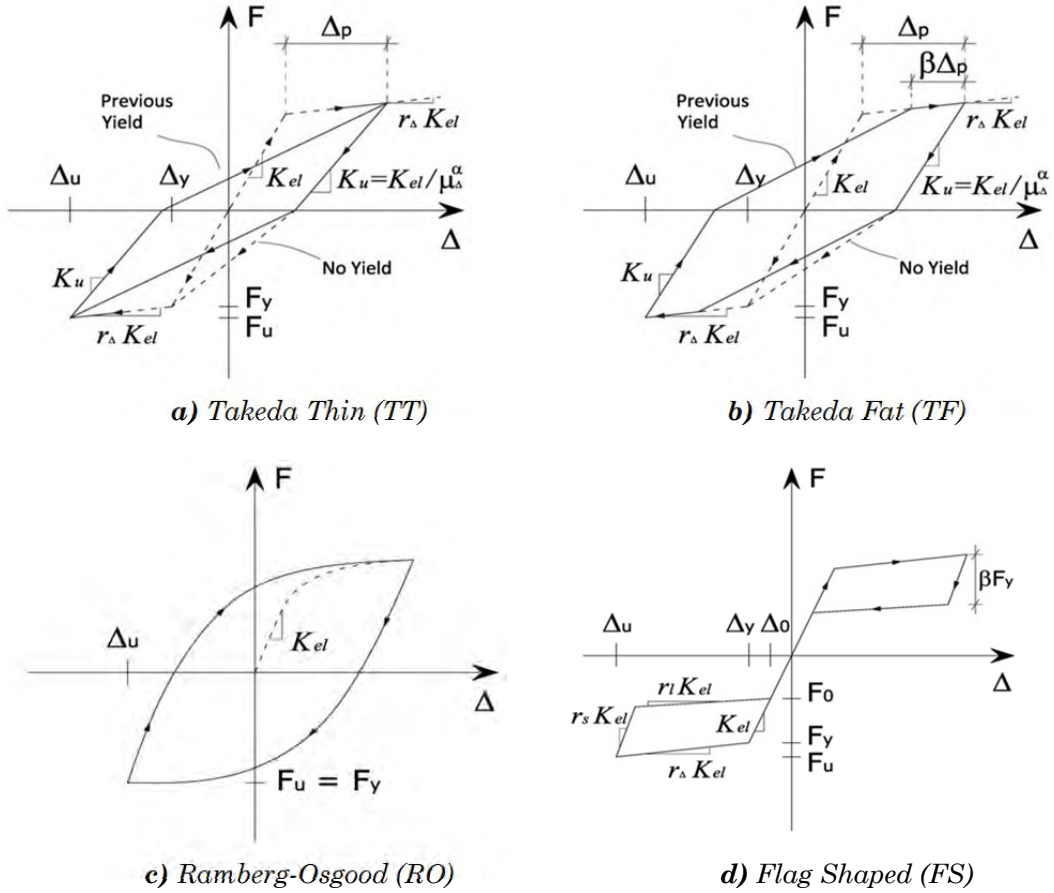


Fig. 2.6 – Hysteresis rules considered for calibration of Eq.2.35^[P11].

The values of the coefficients a, b, c, d used in Eq. 2.35 are listed in Table 2.9 (herein called Grant-Blandon-Priestley, *G.B.P.*, formulation).

A final comparison of the different formulations proposed is presented in Fig. 2.7: the hysteretic component ξ_{hyst} is plotted as function of displacement ductility μ ; D.K. and G.B.P models are plotted eliminating the period-dependency (a value of $T_{eff}=4s$ is assumed for both models).

Tab. 2.8 – Values of EVD coefficients for hysteretic component using Eq. 2.25, proposed by Grant et al^[P11].

Hysteretic model	a	b	c	d
Elasto-Plastic (EPP)	0.224	0.336	-0.002	0,250
Bilinear, $r_{\Delta}=0.2$ (BI)	0.262	0.655	0.813	4.890
Takeda Thin (TT)	0.215	0.642	0,824	6.444
Takeda Fat (TF)	0.305	0.492	0.790	4.463
Flag Shaped, $\beta=0.35$ (FS)	0.251	0.148	3.015	0.511
Ramberg-Osgood (RO)	0.289	0.622	0.856	6.460

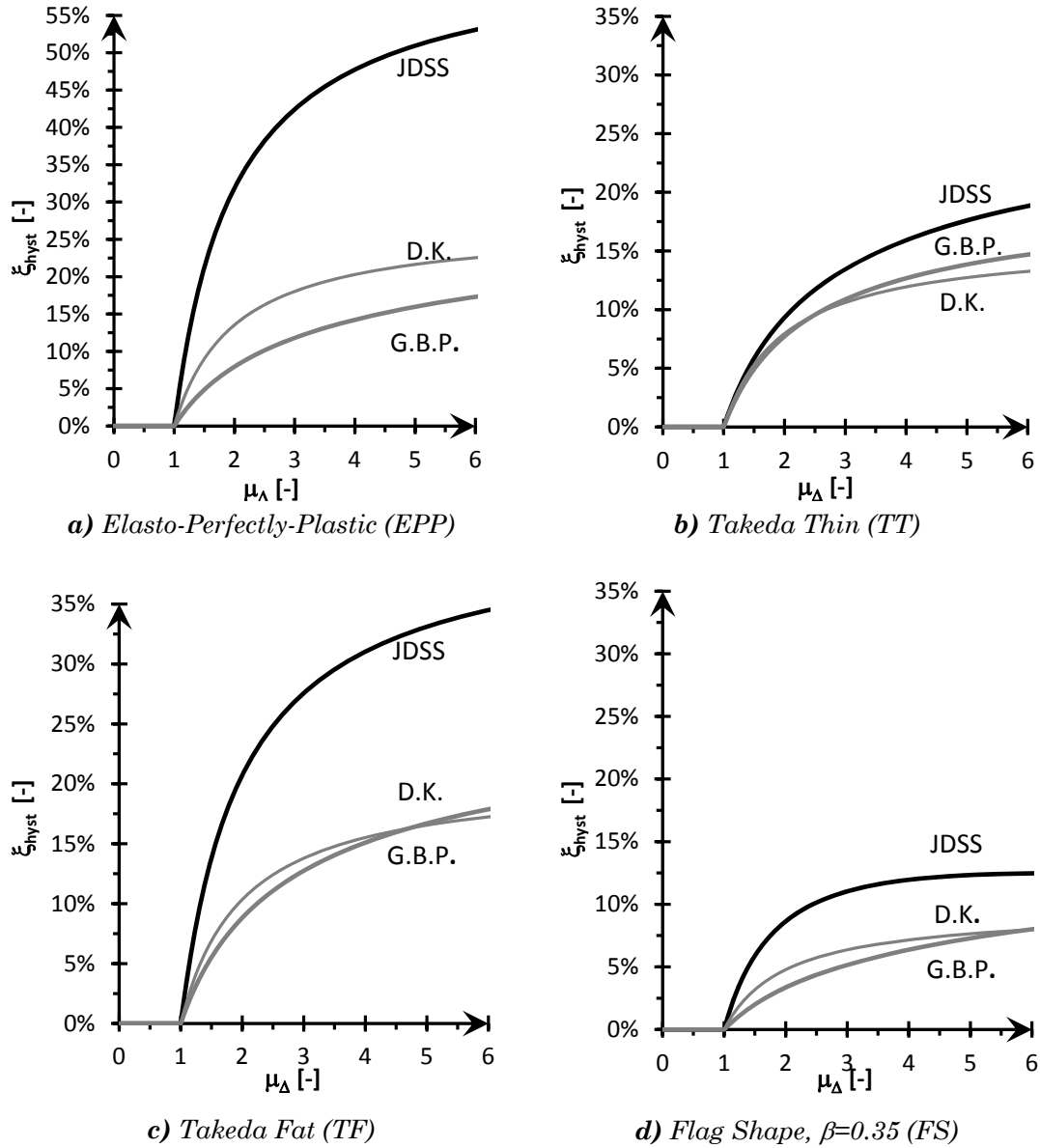


Fig. 2.7 – Comparison of the hysteretic component ξ_{hyst} formulations as function of displacement ductility μ for the JDSS, D.K. and G.B.P. models

2.1.3.2 Elastic damping

In Eq.2.16, the fraction of critical damping referred to the elastic component ξ_{el} is generally assumed to be 5% for rc structures, as noted above. In SDOF systems dynamic analysis, the elastic damping coefficient c , is derived by the well known equations:

$$m \ddot{x} + c \dot{x} + kx = -m \ddot{x}_g \quad (2.26)$$

$$c = 2 m \omega_d \xi = 2 \xi \sqrt{m k} \quad (2.27)$$

where m , k , are mass and stiffness, ξ the fraction of critical damping and ω_i the circular frequency; hence the value of the damping coefficient is assumed constant, related to the initial-elastic stiffness K_i , or less commonly, as a variable associated to a tangent-stiffness, and updated at each step when the stiffness degrades.

However, it is apparent that there is a possible inconsistency, the damping coefficient of the substitute structure being in the DDBD method related to secant stiffness to maximum displacement K_{eff} ($K_{eff}=K_i/\mu$ for low post-yield stiffness).

Grant et al.^[G1,P11] determined a correction factor k to be multiplied by the elastic damping ξ_{el} to ensure compatible assumptions when elastic damping is used in the DDBD framework to characterize the equivalent substitute structure.

The form of Eq. 2.16 is slightly changed:

$$\xi_{eq} = \kappa \xi_{el} + \xi_{hyst} \quad (2.28)$$

$$k = \mu^\lambda \quad (2.29)$$

Tab. 2.9 – Secant stiffness correction factors λ ^[G1] for elastic damping.

Hysteretic model	Initial stiffness	Tangent stiffness
<i>Elasto-Plastic</i> (EPP)	0.127	-0.341
<i>Bilinear</i> , $r_\Delta=0.2$ (BI)	0.193	-0.808
<i>Takeda Thin</i> (TT)	0.340	-0.378
<i>Takeda Fat</i> (TF)	0.312	-0.313
<i>Flag Shaped</i> , $\beta=0.35$ (FS)	0.387	-0.430
<i>Ramberg-Osgood</i> (RO)	-0.060	-0.617

The coefficient λ depends on the hysteresis rule, and the elastic damping assumption, while μ is the displacement ductility factor. Values for λ are listed in Tab. 2.9^[G1]; the modification factor for secant stiffness EVD model is generally $k > 1$ (for $\mu > 1$) when referred to initial stiffness damping (except for the RO hysteretic model), while it's always $k < 1$ for tangent stiffness damping.

2.1.3.1 Design recommendations

In the final table herein presented, the ductility dependency of the elastic damping of Eq. 2.27 is included inside the basic form of the equivalent viscous damping equations. It can be observed that the period-dependency of Eq. 2.23 can be ignored for most of the structures, since it will be unusual for regular structures such as frame, wall buildings and bridges to have $T_{eff} < 1.0s$ ^[P1]. With this simplification, Eq. 2.22 provides almost identical results to the more complete expressions of Eq. 2.23, and the coefficient C are adjusted, so the final value taken for ξ_{el} is 0.05:

$$\xi_{eq} = 0.05 + C_s \left(\frac{\mu - 1}{\mu \pi} \right) \quad (2.30)$$

where the coefficient C_s depended on the hysteresis rule.

Tab. 2.10 – *Equivalent viscous damping coefficients C_s for tangent-stiffness damping[P1].*

Structural member	Hysteretic model	C_s (tangent-stiffness)
<i>Friction slider</i>	<i>Elasto-Plastic (EPP)</i>	0.670
<i>Bilinear isolation system</i>	<i>Bilinear, $r_\Delta=0.2$ (BI)</i>	0.519
<i>Rc wall, bridge pier</i>	<i>Takeda Thin (TT)</i>	0.444
<i>Rc frame</i>	<i>Takeda Fat (TF)</i>	0.565
<i>Prc frame</i>	<i>Flag Shaped, $\beta=0.35$ (FS)</i>	0.186
<i>Steel frame</i>	<i>Ramberg-Osgood (RO)</i>	0.577

2.1.4 Elastic Spectrum Reduction Factor

The DDBD method uses a secant stiffness representation of structural response, and requires a modification to the elastic DRS spectrum to account for the ductile behaviour of the system under design; the influence of ductility can be represented either by equivalent viscous damping or directly by inelastic displacement spectra for different ductility levels. Some authors have proposed for DDBD the use of inelastic spectra instead of elastic design spectra^[C1], but it is current practice to use the equivalent viscous damping approach^[P1], considering that inelastic spectra based on displacement ductility must be calibrated for each different hysteretic rule.

However some uncertainty remains in the calibration of the EVD model (as discussed in the previous section), and in the definition of the spectrum reduction factor R_ξ to be applied to the DRS spectrum for different levels of damping ξ_{eq} . In this work three different forms (among the most widely used) for the R_ξ expression are presented:

1. Newmark e Hall^[N1], 1982:

$$R_\xi = [1.31 - 0.19 \ln(100\xi)] \quad (2.31)$$

2. EC8^[X3], 1998:

$$R_\xi = [0.07 / (0.02 + \xi)]^{0.5} \quad (2.32)$$

3. EC8^[X2], 2003:

$$R_\xi = [0.10 / (0.05 + \xi)]^{0.5}$$

(2.33)

The three expressions are compared in Fig. 2.10 for different values of damping ratio ξ_{eq} ; the Newmark-Hall form implies higher values of the damping factor R_ξ , so less reduction to elastic displacement are required, while the other two expressions are comparable, having the same tendency.

It has been recently demonstrated by Faccioli and Villani^[F2], 2009, that the modification factor R_ξ shall be obtained considering the local seismicity and earthquake characteristics; on the basis of a study on spectral displacement

variations in Italy the following expressions are proposed for sites where near-field effects are not expected:

$$R_{\xi} = \left(\frac{0.10}{0.05 + \xi} \right)^{0.5} \quad \text{for } T \leq 7\text{s} \quad (2.34)$$

$$R_{\xi L} = \frac{1}{18} \left[(1 - R_{\xi 0})T + 25R_{\xi 0} - 7 \right] \quad \text{for } 7 < T < 25\text{s} \quad (2.35)$$

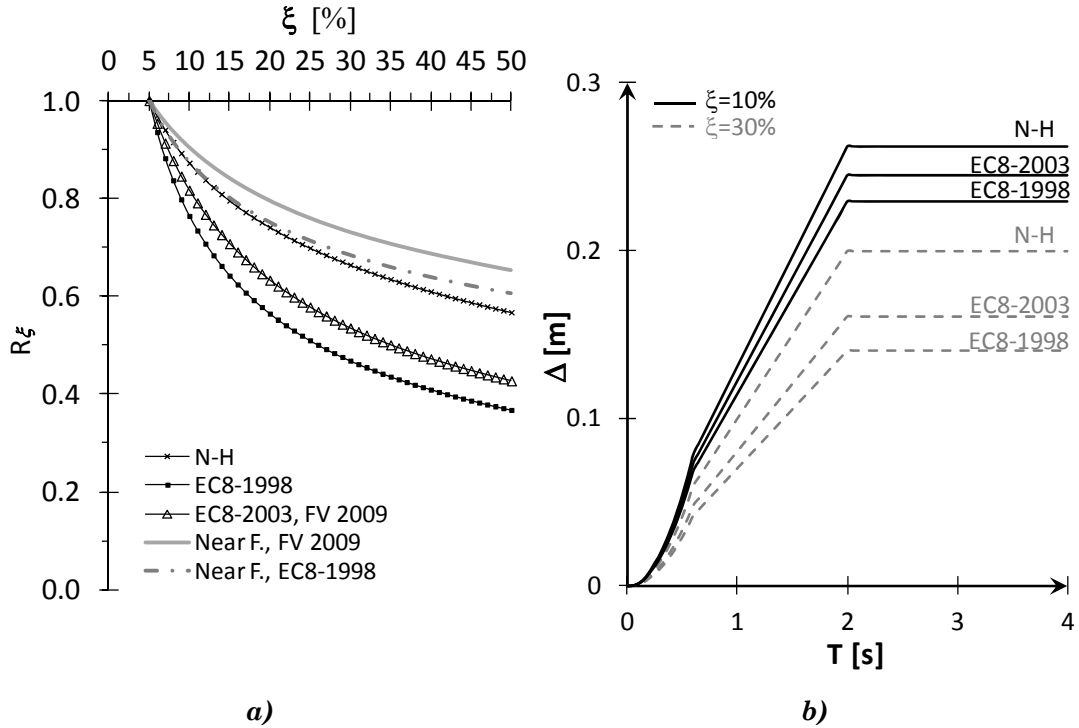


Fig. 2.8 – Damping modifiers to elastic spectral displacements:
a) comparison of different expressions for R_{ξ} . **b)** EC8 type 1 Displacement Spectra ($a_g/g=0.35$, type C ground), reduced by R_{ξ} factors for damping values $\xi=10, 30\%$

For near-field sites where forward directivity is possible, being energy dissipation not so effective in reducing seismic response, a lower reduction factor is suggested:

$$R_{\xi 0} = \left(\frac{0.10}{0.05 + \xi} \right)^{0.25} \quad (2.36)$$

Previously, an equivalent expression for site where forward directivity pulse characteristics might be expected Priestley^[P3] had been suggested by Priestley^[P3], 2003, modifying the EC8-1998 expression:

$$R_{\xi} = \left(\frac{0.07}{0.02 + \xi} \right)^{0.25} \quad (2.37)$$

2.1.5 Stiffness and material and properties of rc sections

It was stated in Chapter 1, that the elastic stiffness of cracked sections is essentially proportional to strength (see Eq. 1.3). The concept of a constant yield curvature ϕ_y independent of strength is fundamental for the direct-displacement based approach. In the following figures, a summary of the research^[P3] results obtained from Moment-Curvature analysis, is reported.

The following yield curvature are applicable for the “corner” of the equivalent bilinear approximation of force-deformation response:

$$\phi_y = 2.25 \varepsilon_y / D \quad \text{for circular rc column} \quad (2.38)$$

$$\phi_y = 2.10 \varepsilon_y / h_c \quad \text{for rectangular rc column} \quad (2.39)$$

$$\phi_y = 2.00 \varepsilon_y / l_w \quad \text{rectangular concrete walls} \quad (2.40)$$

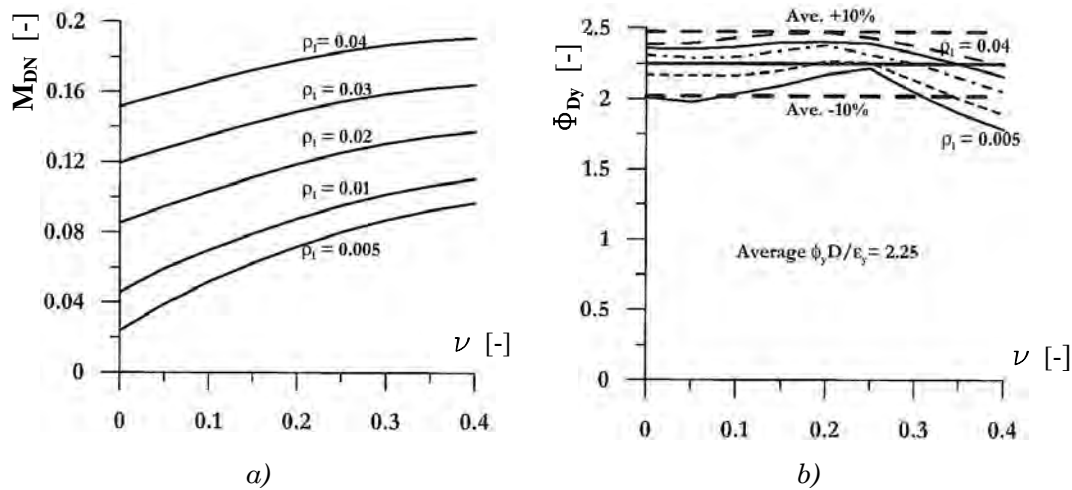


Fig. 2.9 – a) Dimensionless Nominal Moment and b) Yield Curvature for circular piers

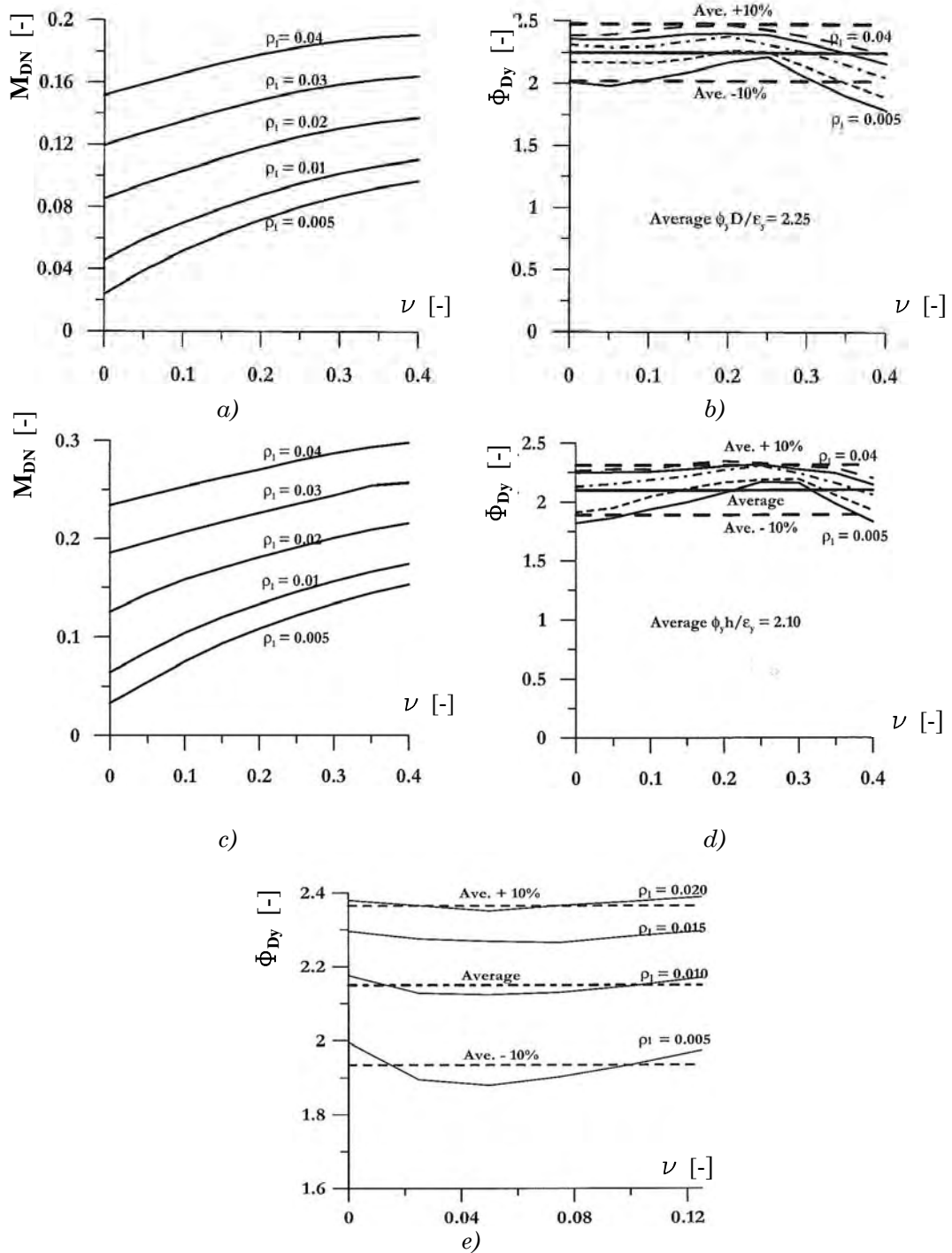


Fig. 2.10 – Dimensionless Nominal Moment and Yield Curvature for: c) and d) rectangular columns, e) walls with distributed reinforcement

2.1.5.1 Material Design Strengths

For gravity load design of structures, a lower bound value for material strength is generally used when determining the nominal strength of sections. This

is combined with partial material factors to ensure a conservative estimate of the section strength.

$$\phi_f M_N \geq M_R \quad (2.41)$$

where ϕ_f is the flexural strength reduction factor and M_N , M_R are the designed and required moment capacities. However in seismic design it is expected that the moment capacity will be considerably less than the demand resulting from an elastic response, when designing locations of intended plastic hinging. Consequently it is recommended that flexural strength reduction factors not be used when designing locations of intended plastic hinging. The following design material strengths can be adopted^[P1, C2]:

$$f'_{ce} = 1.3f'_c \quad \text{for concrete} \quad (2.42)$$

$$f_{ye} = 1.1f_y \quad \text{for steel} \quad (2.43)$$

2.2 DISPLACEMENT-BASED DESIGN OF GIRDER BRIDGES

Girder bridges are structures composed of few structural elements to be designed for seismic response, in specific foundations, piers, abutments, bearings and joints, while in general the superstructure is dimensioned by vertical dead and traffic loads, and is supposed to remain elastic under seismic inertial forces. Nevertheless, bridges can exhibit a highly irregular behaviour, comparatively more complex than that of wall-frame buildings, due to variable column heights, non-uniform span lengths, transverse flexibility of the superstructure, and sometimes to the horizontal or vertical curvature of the deck.

Furthermore, in bridge seismic design, specific aspects have to be considered, that can significantly influence the longitudinal and transverse response of the structure and which can be effectively included in the DDBD approach:

- *P-Delta effects*: these effects are particularly important for bridges, as piers can be very high. Thus, although it is uncommon for buildings to be designed for drifts exceeding 0.025, bridges may be designed for a response drift of 0.04 or even higher^[P1, C2], generally governed by material strain limit. In the DDBD the design displacement is known at the beginning of the design process and hence the $P-\Delta_d$ moment is known before the required strength is determined; a *stability index* θ_Δ can be introduced:

$$g_\Delta = P \Delta_d / M_D \quad (2.44)$$

where M_D is the base moment capacity. When θ_Δ exceeds a pre-fixed value (e.g. 0.085 for rc frame structures), the design base moment capacity should be amplified:

$$V_b = K_e \Delta_d + C \frac{P \Delta_d}{H} \quad (2.45)$$

$$M_b = K_e \Delta_d H + C P \Delta_d \quad (2.46)$$

where C is a constant to account for the hysteresis loop ($C=1$ is suggested for steel structures, while $C=0.5$ seems suitable for rc members^[P1]).

- *Soil-structure interaction* and foundation flexibility affect the damping, elastic period and ductility demand on the structure, in relation to the different support conditions (Spread footing, Column/Pile Shaft, Pile-supported Footing). Foundation effects can be more easily integrated in Displacement-Based design, including the additional displacement resulting from rotation at the pier base.

- *Dual load paths*: for bridges with lateral restraints at the abutments, some of the transverse inertia forces will be carried back by the superstructure bending to the abutments, proportionally to the intensity increase, the superstructure responding elastically and the pier response being ductile.

- *Seismic isolation and added damping*: adapting the procedure to include additional damping sources it is quite straightforward in the DDBD framework. First the design displacement has to be decided: normally it can be based on the isolator displacement capacity, which may be equated to the plateau displacement of the displacement response spectrum, for the system damping level. This results in a minimum-strength design. In this case the system design displacement will be equal to the superstructure displacement, and can be considered the same in both the longitudinal and the transverse direction; capacity design procedures will be used to ensure that the piers remain elastic under the design level of excitation. The effective damping of each pier/isolator combination can be expressed as:

$$\zeta = \frac{\zeta_{pier} \Delta_{pier} + \zeta_{iso} \Delta_{iso}}{\Delta_{pier} + \Delta_{iso}} \quad (2.47)$$

where the displacement of the pier, Δ_{pier} is reduced from the pier yield displacement by about 20% to allow for possible overstrength in the isolator devices. Investigation of the DDBD approach to incorporate seismic isolation or added damping in bridge design is beyond the scope of this work.

A discussion on this topic and related design details can be found in Priestley et al^[P1], 2007.

- *Influence of abutment design*: often a monolithic connection between the superstructure and the abutment is provided, especially for shorter bridges of few spans. In this case the inertial response will be often related to a short effective period, and the design will be dictated by strength characteristics more than ductility properties. Damping, however, can be higher than the 5% generally adopted by force-based elastic design.

- *Degree of fixity at column top*: the pier-top degree of fixity can influence the expected moment pattern for transverse response, and affect the yield displacement and the plastic hinge length. If the pier consists of two or more columns, it can be considered fully fixed at the top, with equal moments at top and bottom of the columns. For a single-column bent, both in the case of monolithic connection with the superstructure or multiple support on two or more bearings, though it would appear that behaviour will always be that of a simple cantilever, if the superstructure is torsionally stiff and restrained against uplift at the abutment, then a reversal moment may develop over the height of the pier.

2.2.1 SDOF bridge structures

In the case of multi-span girder bridges, if the superstructure consists of simple-supported spans with rotational flexibility at the movement joints about the vertical axis, it is reasonable to consider the design of each pier individually, based on the tributary superstructure mass and the pier displacement capacity. Essentially the seismic design of a regular bridge under transverse excitation becomes a series of independent systems, and the assumption of a SDOF approximation is generally accepted^[P1]: the deformation of the pier with a concentrated mass on the top, is assumed to be controlled by a first-mode response.

2.2.1.1 Design displacement

Generally for a bridge structure, for any given limit state, structural performance will be governed by limiting material strain (see Sec. 2.1.1). For serviceability limit state, LS1, the nominal moment capacity is required, defined by an extreme fibre compression strain of 0.004 or an extreme tension strain of 0.015 of the reinforcing bars. The two limit strain do not generally occur simultaneously, consequently there are two possible limit state curvatures:

$$\phi_{mc} = \varepsilon_{cm}/c ; \quad \phi_{ms} = \varepsilon_{sm}/(d - c) \quad (2.48)$$

and the lesser governs the structural design $\phi_U = \min(\phi_{mc}, \phi_{ms})$. Once the limit curvature ϕ_m is known, the design displacement $\Delta_{u,\phi}^d$ can be estimated as a function of the yield curvature ϕ_y , and the *plastic hinge length* L_p . For a cantilever the following relation is valid:

$$\Delta_{u,\phi}^d = \Delta_y + \Delta_p = \frac{\phi_y(H + L_{SP})^2}{3} + (\phi_u - \phi_y)L_p H \quad (2.49)$$

where the plastic hinge length is:

$$L_p = \max[(k H + L_{SP}); (2L_{SP})] \quad (2.50)$$

with:

$$k = 0,2 \left(\frac{f_u}{f_y} - 1 \right) \leq 0,08 \quad (2.51)$$

and L_{sp} representing the strain penetration length:

It should be noted that Eq. 2.46 requires the knowledge of the neutral axis depth, which is a function of axial load ratio and longitudinal reinforcement, typically not known at the first stage of design; dimensionless expressions based only on material properties and geometric dimensions^[P3] are reported in Sec. 2.1.5.

An alternative design approach would assume a pre-fixed tolerable value for plastic rotation ϑ_p , according to element detailing, or for global design drift, and then design the detail to ensure that the strain limits will be achieved. This simplifies the design process.

$$\vartheta_p = (\phi_u - \phi_y)L_p \quad (2.52)$$

$$\vartheta_d = \vartheta_Y + \vartheta_p \quad (2.53)$$

$$\Delta_{u,\vartheta}^d = \Delta_y + \Delta_p = \frac{\varphi_y(H+L_{sp})^2}{3} + \vartheta_p H = (\vartheta_y + \vartheta_p) H = \vartheta_d H \quad (2.54)$$

2.2.1.2 SDOF design process

The general DDB framework (see Fig. 2.8) can be applied straightforwardly directly for a SDOF system represented by a reinforced concrete pier cantilever. The procedure can be summarized as follows:

- step 1: select a level of performance and obtain the target-displacement Δ_u^d based on strain or drift criteria (see Sec. 2.1.1);
- step 2: estimate the yield displacement Δ_y , and evaluate the displacement ductility capacity μ_{Δ}^d :

$$\Delta_y = \varphi_y (H + L_{sp})^2 / 3 \quad (2.55)$$

$$\mu_{\Delta}^d = \Delta_u^d / \Delta_y \quad (2.56)$$

- step 3: evaluate the equivalent viscous damping values ξ_{eq} as a function of displacement ductility (e.g. using Eq. 2.28 with Cs defined for the TT hysteretic model)

$$\xi_{eq} = 0.05 + 0.444 \left(\frac{\mu - 1}{\mu \pi} \right) \quad (2.57)$$

- step 4: determine the damped displacement elastic spectrum, using the reduction factor R_{ξ} , dependent on the value ξ_{eq} calculated in the previous step. The EC8-2003 form is suggested:

$$R_{\xi} = \left(\frac{0.10}{0.05 + \xi} \right)^{0.5} \quad (2.58)$$

- step 5: enter the damped displacement elastic spectrum with Δ_u^d and calculate the effective period T_{eff} ;
- step 6: compute effective stiffness K_{eff} using Eq. 2.1, and calculate design base shear, accounting for P- Δ effects if required:

$$V_{eff} = K_{eff} \Delta_u^d + 0.5 \frac{P \Delta_u^d}{H} \quad (2.59)$$

- step 7: design the structure for the base shear demand obtained at the previous step.

2.2.2 MDOF bridge structures: continuous bridges

For MDOF structures the initial part of the design process requires the determination of the substitute SDOF system characteristics: equivalent mass m_e , design displacement Δ_d and effective damping ξ_e .

Once the *substitute structure* has been determined, the global design base shear is calculated following the same procedure as for SDOF systems (reported in

Fig.2.8); subsequently the base shear is distributed among the masses of the original structure as inertia forces, and the structure is analyzed under these forces calculating design moments at locations of potential plastic hinges.

2.2.2.1 Design Displacement

The design displacement of the equivalent SDOF structure (the generalized displacement coordinate) is based on the inelastic mode shape of the bridge considered, and is calculated as:

$$\Delta_d = \frac{\sum_{i=1}^n (m_i \Delta_i^2)}{\sum_{i=1}^n (m_i \Delta_i)} \quad (2.60)$$

where m_i and Δ_i are the masses and displacements of the n significant mass locations respectively. The equation is based on the requirement that the work done by the equivalent SDOF system be equivalent to the work done by the MDOF force system, (Calvi, et al.^[C3], 1995).

The design displacement depends on the limit state displacement of the critical pier, and on the assumed displacement shape for the structure.

With a knowledge of the displacement of the critical element and the design displacement shape, the displacement of individual masses is given by^[P1]:

$$\Delta_i = \delta_i \left(\frac{\Delta_c}{\delta_c} \right) \quad (2.61)$$

where δ_i is the inelastic first mode shape, Δ_c is the design displacement at the critical mass c , and δ_c is the value of the mode shape. Generally a discretization of deck with masses lumped at the top of piers and at abutments is considered; a portion of column masses and the cap beam masses can also be lumped at the top^[P4].

If higher modes are expected to determine a significant overall increase in displacement and superstructure transverse moments (and consequently in abutment reactions), as in the case of irregular bridge structures, simplified methods should be used to account for their effects, in two possible forms: use of simple conservative design rules or use of modified methods for modal superposition (see the related *Capacity Design Requirements* section). In this case it is suggested^[C2] to reduce the design drift limit:

$$\Delta_i = \omega_\theta \delta_i \left(\frac{\Delta_c}{\delta_c} \right) \quad (2.62)$$

where $\omega_\theta = (1 - \Delta_{high}/\Delta_c) < 1$ with Δ_{high} is the displacement at the critical pier caused by higher mode response (modal response spectrum analysis can be used to estimate displacement contributions due to higher modes at potentially critical pier locations), or alternatively $\omega_\theta = 0.7$ if non linear time history analysis is performed to verify the bridge behaviour.

2.2.2.2 Displacement Shape

The determination of the displacement shape is one of the most critical points of the design process: in the case of a straight continuous bridge

superstructure, integrally connected with the piers, the displacements of all superstructure masses will generally be identical for the longitudinal response, while for the transverse response the displacement of each bent will vary in accordance with the modal response of the system^[K3]. The mode shape will depend on the relative transverse stiffness of the piers, the presence or absence of internal movement joints, the degree of lateral restraint provided at abutment supports and the superstructure lateral stiffness.

Some indexes can be utilized to characterize the relative stiffness of the superstructure in respect to pier stiffness; according to the index proposed by Calvi and Sullivan^[C2], the deck can be considered “stiff” if the ratio of its lateral stiffness to the pier sectional stiffness EI_s/EI_p satisfies the following relationship:

$$48 \frac{EI_s}{C_p n_p EI_p} \left(\frac{H_p}{L_s} \right)^3 \geq 0,02 \quad (2.63)$$

where n_p is the number of piers, H_p can be taken as the average pier height, L_s is the distance between the abutments, C_p is a factor accounting for pier fixity (3 for pinned-fixed, 12 for fixed-fixed piers).

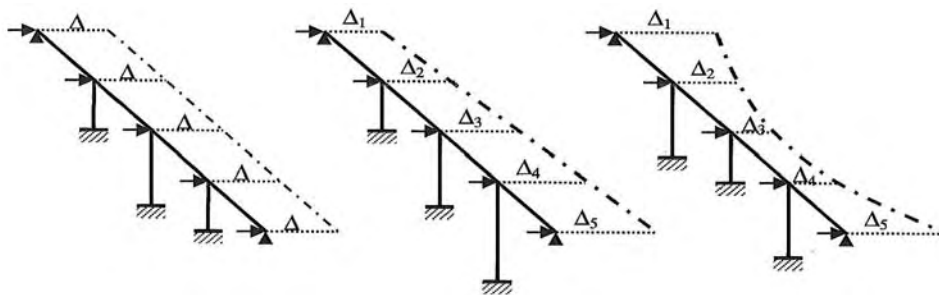
For bridges without restraint at the abutments and with fixed pier tops, the superstructure can be considered effectively rigid according to Dwairi et Kowalsky^[D2], 2006, evaluating the relative stiffness index RS :

$$RS = \frac{K_s}{\sum_{j=1}^m K_{Pj}} = \frac{384I_s}{5L_s^3} \cdot \sum_{j=1}^m \frac{H_{Pj}^3}{C_{Pj}I_{Pj}} \geq 0,6 \quad (2.64)$$

where I_s and l_s are the superstructure transverse moment of inertia and length respectively, while H_{Pj} and I_{Pj} are pier effective height and moment of inertia respectively. The superstructure is assumed to be uncracked (elastic response), while pier stiffness is based on cracked-section stiffness (ductile response).

In general there are three kinds of possible transverse displacement, corresponding to a fully restrained abutment, a completely unrestrained abutment, and the case where the abutment is restrained, but has significant transverse flexibility.

In the first instance, if the superstructure is rigid in the transverse direction, there is a simplification of the displacement pattern for symmetric structures, all columns translating by the same displacement (Fig. 2.11a), and the target system displacement is limited to the lateral single pier capacity; in the case of irregular systems, this translation may be accompanied by a rotational component (Fig. 2.11b).



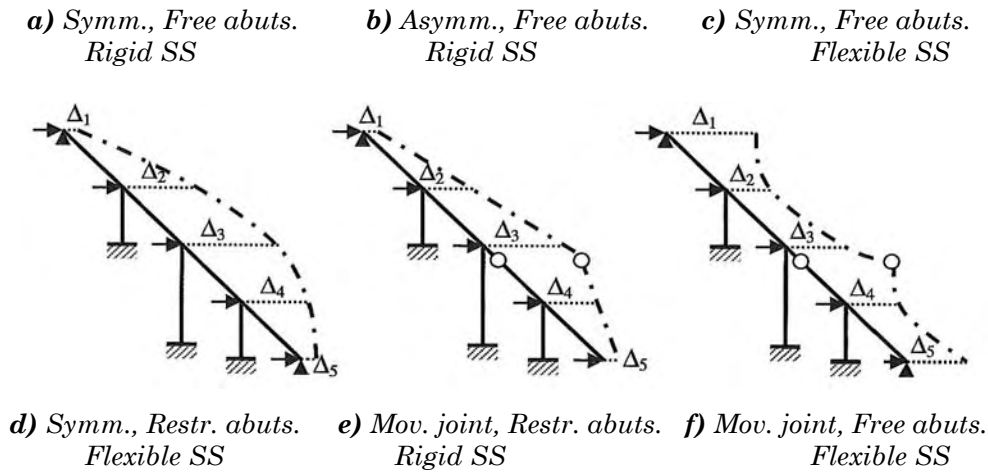


Fig. 2.11 – Possible transverse displacement profile for girder bridges^[P1]

For a fully or partial restraint at the abutments, in the case of a symmetric structure (Fig. 2.11d) with flexible superstructure, the displacement shape can be approximated by a sine function (Alfawakhiri et al^[A4], 2000):

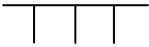
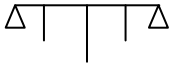
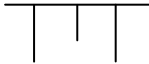
$$\varphi_1 = \frac{\sin(\pi x / L_s) + \pi^3 B}{1 + \pi^3 B}, \quad B = \frac{E I_s}{K_a L_s^3} \quad (2.65)$$

where x is the longitudinal coordinate, L_s is the bridge length, B a coefficient calculated on the base of the elastic abutment stiffness. Also a parabolic function can be utilized, as reported in Tab. 2.12^[C2].

For irregular bridges that do not match the simple configuration of pier distribution and support restraint reported in Tab 2.12, the displaced shape at peak response (i.e. the inelastic first mode shape^[P1]) should be calculated. The displacement pattern, as discussed above, depends on the elastic properties of the superstructure (elastic lateral stiffness), known at the start of the seismic design, and on the effective piers' properties, (effective stiffnesses related to strengths and ductilities), which are not initially known, hence an iterative design approach is usually required. A good estimation of the overall displaced shape has been proved^[K3] to be obtainable considering an *Effective Mode Shape (EMS)* modal analysis: elastic properties are used for the superstructure to solve the eigenvalue problem, while secant stiffness at maximum response is used for columns and abutment. If an iterative procedure is applied, an initial assumption of 10% of the uncracked section stiffness can be applied to columns expected to exceed their yield displacement, a value of 50% can be used for the other columns, while 30% of the initial elastic stiffness is suggested for the abutments^[K3].

Tab. 2.11 – Displacement shape for regular continuous deck bridges^[C2]

Pier configuration	Abutment	Displacement shape
Uniform $\Delta \left \begin{array}{ c c c } \hline & & \\ \hline \end{array} \right. \Delta$	Pinned	$\delta_i = \frac{16}{5L_a^4} (x^4 - 2L_a x^3 + L_a^3 x)$

Uniform		Free	$\delta_i / \delta_c = 1$
Valley		Pinned	$\delta_i = \frac{16}{5L_d^4}(x^4 - 2L_d x^3 + L_d^3 x)$
Valley Ridge		Free	$\delta_i = 1,5 - \frac{8}{5L_d^4}(x^4 - 2L_d x^3 + L_d^3 x)$

2.2.2.3 Design process for longitudinal response

The design process is in this case straightforward: the deck is typically assumed to be axially rigid, imposing the same displacement demand along the length of the bridge in the longitudinal direction. The design displacement shall then be limited by the critical pier or abutment member deformation.

The total base shear force is found from Eq.2.2, and distributed to the piers. The way in which this distribution is effected is a designer's choice, but will normally be based on the assumption of equal moment capacity (and hence identical reinforcement details) at the base of all piers (note that this is markedly different from force-based design, where the design moments would be inversely proportional to the squared pier heights). The system damping is then found as the average of damping ratios of the individual elements, weighted by shear force and displacement. For longitudinal response the design displacements will be equal, and hence: if the decision to assume equal moment capacity at the base of all piers is made at the start of the design process, then the relative fractions of shear force carried by the piers is known, and Eq.(6) can be solved even though the absolute magnitudes of piers' shears are still unknown.

2.2.2.4 Design process for transverse response

As discussed earlier, the transverse response of multi-span bridges is inherently more complex than longitudinal response, and the following issues must be considered:

- transverse design displacements profiles;
- dual seismic load paths;
- effective system damping;

An iterative procedure is currently proposed to overcome this intrinsic complexity, and two initial assumptions are required: the fraction x of the load carried by the superstructure bending back to abutments, and the displacement profile. The procedure is articulated in the following steps^[P1]:

a) *Estimate the initial displacement profile*, which should reproduce the inelastic displaced shape. Choose the limit-state target displacement for the critical pier (strain-based or drift-based). A parabolic or sine-based displacement shape (see Tab.2.12) may be assumed for the initial iteration. The initial displacement profile is thus obtained by Eq.2.61, and the displacement of each pier or abutment Δ_i is estimated.

b) Estimate the fraction of lateral force x carried by the superstructure bending (based on experience: possible choice could be $x=0.5$ for restraint at the abutments, $x=0$ for unrestrained abutments).

c) Determine the SDOF equivalent system properties.

c.1) Determine the equivalent system displacement Δ_d , given by Eq.2.60.

c.2) Determine the effective mass m_e , including the appropriate contribution from pier mass (typically $1/3^{\text{rd}}$):

$$m_e = \sum_{i=1}^n m_i \Delta_i / \Delta_d \quad (2.66)$$

c.3) Determine the effective height H_e :

$$H_e = \sum_{i=1}^n (m_i \Delta_i H_i) / \sum_{i=1}^n m_i \Delta_i \quad (2.67)$$

c.4) Compute the yield displacement of all piers, using Eq.2.55, and then their displacement ductility demand with Eq.1.4.

c.5) Determine the system damping ξ_e :

when different structural elements with different strengths and damping factors contribute to seismic resistance, the global damping may be found by weighting the individual components by the work done:

$$\xi_e = \sum_{i=1}^n (V_i \Delta_i \xi_i) / \sum_{i=1}^n (V_i \Delta_i) \quad (2.68)$$

where V_j , Δ_j are the shear force and the design displacement of the j^{th} element, while ξ_j can be evaluated from Eq.2.54. Since shear force distribution is unknown at this stage of design procedure, some realistic assumption should be made. In general, as a matter of convenience, the designer may choose the same section and reinforcement ratio of the pier diameter, even if sometimes it might not be possible or convenient (design may be governed by different load combination, not by seismic action). However, Eq. 2.68 can be simplified by assuming for DDBD design a shear force distribution in inverse proportion to height. This relation can be easily derived when the same flexural strength (with zero post-yield stiffness) to all pier bases is provided^[K3], but it can also be used if a different flexural strength is adopted, introducing the factor α_j , ratio of flexural strength of a pier to the flexural strength of the critical pier^[A5]:

$$V_j \propto \frac{\alpha_j}{H_j} \text{ (ductile piers), } V_j \propto \frac{\alpha_j \mu_j}{H_j} \text{ (elastic piers)}$$

(2.69)

Combining all the contributions from superstructure damping ξ_{ss} , abutment damping ξ_{ss} and pier damping ξ_i , the equivalent system damping is derived as:

$$\xi_e = \frac{x(\Delta^d - \Delta_a^d)\xi_{ss} + x\Delta_A^d\xi_A + (1-x)\left(\sum_{j=1}^{n^{\circ} \text{ piers}} \frac{C}{H_j} \cdot \Delta_j \xi_j\right) / \sum_{j=1}^{n^{\circ} \text{ piers}} \frac{C}{H_j}}{x(\Delta^d - \Delta_a^d) + x\Delta_A^d(1-x)\left(\sum_{j=1}^{n^{\circ} \text{ piers}} \frac{C}{H_j} \cdot \Delta_j\right) / \sum_{j=1}^{n^{\circ} \text{ piers}} \frac{C}{H_j}} \quad (2.70)$$

the coefficient $C = \alpha_j \mu_j$ being used for elastic piers, $C = \alpha_j$ for yielded piers.

d) Calculate the effective period, effective stiffness and total base shear V_{base} for the ESDOF system, entering the design spectrum, damped with ξ_e , and using Eq.2.1, 2.2.

e1) Distribute the base shear as inertia forces to the masses in accordance with the assumed target displacement profile:

$$F_i = V_{base} (m_i \Delta_i) / \sum_{i=1}^n m_i \Delta_i \quad (2.71)$$

e2) Estimate the effective stiffness of pier and abutments by distributing shear forces from Eq.2.67 and calculating

$$K_{eff,i} = V_i / \Delta_i \quad (2.72)$$

f) Execute a linear static analysis using the load vector computed at step e1) and the member stiffness at step e2) to estimate the displacement of critical pier $\Delta_{c,CALC}$, and the new displacement profile $\Delta_{i,NEW}$.

g) Revise the critical pier displacement Δ_c , $\Delta_c = \Delta_{c,CALC}$

h) Revise the design displacement profile $\Delta_{i,OLD} = \Delta_{i,NEW}$, and iterate to convergence.

i) Use $\Delta_{i,NEW}$ and $K_{eff,i}$ to calculate design strength required to each pier.

l) Design reinforcement for critical section and apply capacity design principle for other sections.

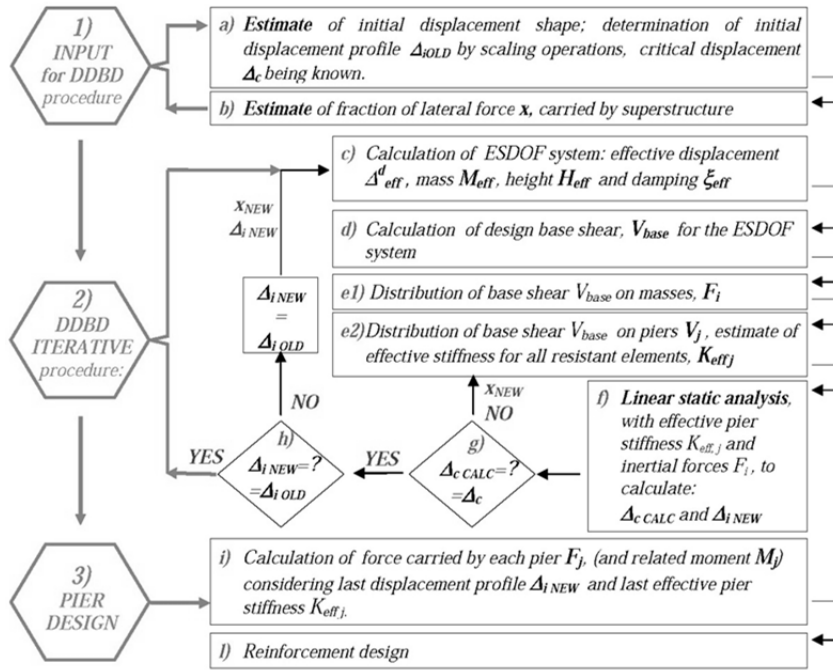


Fig. 2.12 – Flowchart of the current DDBD procedure for transverse design of continuous bridges^[P1]

2.2.2.5 Capacity design issues

The purpose of capacity design is to ensure that undesirable modes of inelastic deformation and brittle collapses may occur. To this aim, overstrength factors are used, and the general requirement for capacity protection is defined by the following relation:

$$\phi_S S_D \geq S_R = \phi^0 \omega S_E \quad (2.73)$$

where S_E is the design action, ϕ^0 is the ratio of overstrength moment capacity to required capacity, S_D is the design strength, ϕ_S is a strength reduction factor (related to partial material factors..). Furthermore, the influence of higher mode effects can be included in Eq. 2.35, using a dynamic amplification factor $\omega \geq 1$. This is a simplified approach, also applied by some current seismic codes^[X4], to take into account possible amplification of moments and shears due to secondary modes. Alternatively a more consistent estimation of the higher mode effects can be obtained with the ModifiedModalSuperposition (MMS) method, using an appropriate combination rule (CQC or SRSS), combining the inelastic first-mode design forces, $S_{1D,i}$ with the elastic forces $S_{i,e}$ related to higher mode periods (calculated with the elastic stiffness of the members), applying the basic equation:

$$S_{CD,i} = \sqrt{S_{1D,i}^2 + S_{2,e}^2 + S_{3,e}^2 + \dots S_{n,e}^2} \quad (2.74)$$

A simple modification of the previous approach is introduced by the EffectiveModalSuperposition method^[O2,P1,A5]: a Response Spectrum Analysis is carried out after the completion of the DDBD procedure, whereby stiffness of members with plastic hinges (e.g. piers) is represented by secant stiffness to the

peak displacement response, while elastic members (e.g. the superstructure) are modelled by initial stiffness value, and seismic hazard is defined by a 5% damped elastic design spectrum (Adhikari et al. ^[A5], 2010). Final results are obtained by combining the higher mode-elastic forces from SRA with the DDBD inelastic first mode design forces:

$$S_{CD,i} = \sqrt{(\phi^0 S_{1D,i})^2 + S_{2,i}^2 + S_{3,i}^2 + \dots S_{n,i}^2} \quad (2.75)$$

Both overstrength at plastic hinges and higher mode effects may have a significant influence on the maximum transverse moment developed in the superstructure and on the maximum abutment reaction.

2.3 DISPLACEMENT-BASED APPROACHES FOR SEISMIC ASSESSMENT OF EXISTING STRUCTURES

As outlined in Chapter 1, the development of an assessment procedure in a displacement-oriented framework is the natural development of a performance-based approach for the evaluation of existing structures. The major difficulty in such a methodology is based on the initial definition of displacement values (drifts/rotations) as damage indexes, is the determination of the structure displaced shape at collapse. For new structures, typical displacement profiles can be generally used, but they can be inappropriate for older substandard structures^[P1], where different inelastic mechanisms may develop, due to inappropriate location of plastic hinges and premature failure of non-ductile members.

2.3.1 Specific issues for DBA

A series of issues has to be addressed for the development of an appropriate DBA approach, because additional problems arise interpreting the structural behaviour compared to newly design structures, related to the appropriate identification of the collapse mechanism and the displacement shape. The main specific aspects related to the assessment procedure can be summarized as follows:

- *Definition of performance limit state*: less conservative expressions could be applied in respect to design estimates, but different (generally poorer) material properties are expected, and low confinement levels are usually provided for existing rc members.
- *Identification of the collapse mechanism*: different behaviour can be expected compared to new structures, which are designed accordingly to capacity designed principles. In terms of local collapse of members, hierarchy of strength for ductile and brittle mechanisms could not be respected. In terms of global capacity of the structure the inelastic mechanism can be beam-sway type, column-sway, or mixed. In this context the effects related to higher modes and torsional behaviour can be of considerable importance. They can be evaluated in the characteristic displacement formulation Δ_D with simplified conservative expression, or

computed with a more consistent analysis in the determination of the inelastic mode shape.

- *Identification of the likely hysteretic model:* appropriate cyclic models should be calibrated for structures with different level of dissipation capacity. Structures affected by shear failure, are not characterized by fat hysteretic cycles, anyhow a residual energy dissipation is still present, and the equivalent viscous damping expression has to be calibrated accordingly.
- *Local collapse of nodes:* in existing structures premature local collapse and increment of stiffness degradation can be due to unconfined joints, lap-splices in hinge zones, bond slip effects between reinforcement bars and concrete, buckling of vertical bars (which are non effectively tied by stirrups), or foundation failure (vertical, overturning or sliding).

For a detailed coverage on this topic, reference can be made to Priestley et al. ^[P4], 1996, Priestley ^[P9], 1997.

2.3.2 Displacement Based Assessment procedures

Two methods are proposed by Priestley et al. ^[P1] as displacement-based seismic assessment procedures, both complying with the principles of DDBD. In this text they will be recalled as *DBA/D*, *DBA/C* procedures, the first varying iteratively the displacement demand Δ_{Dem} , and comparing its final estimate with the capacity Δ_{cap} , the latter calculating the elastic capacity $\Delta_{cap,el}$ and comparing it with the elastic demand $\Delta_{Dem,el}$.

The methods have many similarities to non linear static methods proposed in the last decade by Fajfar and others ^[F4], requiring at the initial stage of the procedure the development of the force-displacement response being, based on available structural details. In the DBA procedures the use of the equivalent substitute structure characterized by an equivalent damping allows a better inclusion of the hysteretic properties of the system; in addition, a direct estimation of the risk for the assessed structure can be carried out.

The *DBA/D* procedure is recognized by the author valid only for a pass/fail assessment, but not adequate to determine risk for structures that do not pass the criterion $\Delta_{cap} \geq \Delta_{cap}$: in fact the damping values corresponding to capacity and demand differ (ductilities for the two displacements are different), and hence the two damped spectra are not directly comparable. The method *DBA/C* seems more consistent: it determines the equivalent elastic spectral displacement corresponding to the assessed displacement capacity and associated damping; the step by step procedure ^[P1] is described in the next paragraph.

2.3.2.1 *DBA/C procedure*

1. Estimate the inelastic mechanism and the related displacement capacity, e.g. through the assessment of the global Force-Displacement (pushover) curve.
2. Calculate the equivalent SDOF displacement Δ_{cap}^d and Δ_y , the effective height h_e , the effective mass m_e .

$$\Delta_{cap}^d = \frac{\sum_{i=1}^n (m_i \Delta_i)^2}{\sum_{i=1}^n m_i \Delta_i}, \quad m_e = \frac{\sum_{i=1}^n m_i \Delta_i}{\Delta_d},$$

$$H_e = \frac{\sum_{i=1}^n m_i \Delta_i H_i}{\sum_{i=1}^n m_i \Delta_i} \quad (2.76)$$

where m_i e Δ_i are the masses and displacements of the significant mass locations.

3. Determine the displacement ductility capacity:

$$\mu = \Delta_{cap}^d / \Delta_y \quad (2.77)$$

4. Determine the effective damping ξ_A corresponding to μ from Eq. 2.30.

5. Calculate the spectral reduction factor R_ξ corresponding to ξ_A , e.g. from Eq. 2.32, (repeated here for simplicity):

$$R_\xi = \left(\frac{0.07}{0.02 + \xi_A} \right)^{0.5} \quad (2.78)$$

6. Calculate the equivalent elastic spectral displacement capacity:

$$\Delta_{Cap,el} = \frac{\Delta_{Cap}^d}{R_\xi} \quad (2.79)$$

7. Determine the effective assessment stiffness $K_A = F / \Delta_{cap}$, including P- Δ effects, corresponding to the displacement capacity (the displacement capacity depends on what performance level is chosen).

8. Calculate the effective stiffness by the SDOF equation:

$$K_e = \frac{V_b}{\Delta_{cap}^d} \quad (2.80)$$

8. Calculate the effective period from the SDOF equation:

$$T_e = 2\pi \sqrt{\frac{m_e}{K_e}} \quad (2.81)$$

9. If a suite of elastic displacement spectra for different annual probabilities of exceedance is available, the appropriate spectrum can be matched to $\Delta_{cap,e}$; if not, the equivalent elastic “code” displacement demand $\Delta_{dem,el}$ can be read off the code elastic spectrum at the period T_e .

10. The capacity/demand displacement ratio C/D can be estimated:

$$C/D = \Delta_{Cap,el} / \Delta_{Dem,el} \quad (2.82)$$

11. The C/D ratio can be used to determine the risk from a plot giving the annual probability of exceedance as a function of displacement.

At present hazard curves are generally available as measure of the seismic intensity PGA related to annual probability of exceedance p ; however if the spectral shape is considered independent of intensity (but there are many restrictions to this assumption), the C/D ratio represents also the ratio corresponding to

$$PGA_{Cap,el} / PGA_{Dem,el} \quad (2.83)$$

and the hazard curve can be directly used.

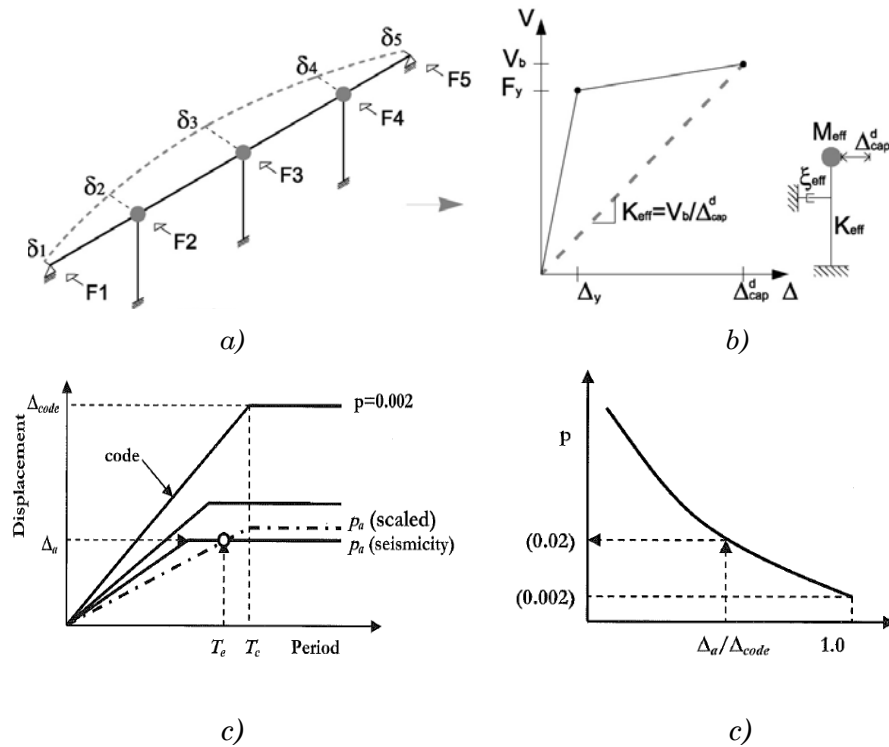


Fig. 2.13 – Overview of the DBA/C procedure: a) Estimate of inelastic displacement shape, b) Equivalent SDOF representation, c) Identification of seismic intensity that would cause limit state to develop, d) Risk estimate

2.4 CLOSING REMARKS

The basic Direct Displacement-Based design and assessment procedures are simple and straightforward for the user, but complexity is implicit in many of the assumptions required by the procedure.

In the specific case of the assessment method, the direct approach of the DB method is further made complex by the uncertainties in material strength, the absence of pre-defined hierarchies between flexural and shear strength of members, and the limited capacity of the structure, related to possible no-ductile global mechanisms.

There are still several aspects, common to the design and assessment methods, that need a detailed evaluation and possibly further development. The following aspects have to be highlighted:

1a. *Selection of target displacement*: the selection of appropriate performance levels in terms of sectional limit states and global structural limit states, is still an open field of research for many structural typologies^[C2]. Estimation of damage can be related to maximum attained strain, drift/chord rotation limit, global behaviour (e.g. displacement related to a certain percentage decrease of the total strength). For assessment purposes, specific limits have to be individuated considering material properties and reinforcement detailing of sections.

1b. *Selection of seismic input*, in the form of an elastic Displacement Response Spectrum: the DRS spectra provided by many current seismic codes are inadequate for DDBD design.

2. *Estimate of the collapse mechanism and design displacement shape*: the method requires the estimate of the design displacement shape for MDOF systems, which is not easy to be assessed for irregular structures (e.g. bridges with piers of variable heights). In the evaluation of existing structures further uncertainties are related to development of non-ductile local and global mechanisms.

3.,4. *Evaluation of equivalent viscous damping (EVD) and the related spectrum reduction factor R_{ξ}* : different formulations for ξ_{eq} exist, relating the hysteretic energy component to ductility values, and there is still emphasis in research activity about its appropriate form^[D1,P11]. A related aspect is the *identification of the likely hysteretic mode* for existing structures, which may be characterized by a reduced hysteretic dissipation, thus appropriate cyclic models should be calibrated for existing rc members with different level of dissipation capacity.

Furthermore, there is continuing debate over the correct formulation of the spectral displacement reduction factor R_{ξ} ^[C2] to be taken into account, especially for near field-site design cases.

CHAPTER 3

DIRECT DISPLACEMENT-BASED DESIGN METHOD: ERROR PREDICTION FOR MULTI-SPAN SIMPLY SUPPORTED BRIDGES

3.1 INTRODUCTION

In this chapter a research work investigating the accuracy of the current Direct Displacement-Based Design (DDBD) procedure applied to simple Single Degree Of Freedom (SDOF) systems is presented, with specific reference to multi-span simply supported rc bridge piers. The seismic design of a regular girder bridge under transverse excitation is usually considered as a series of independent systems, and the assumption of a SDOF approximation is generally accepted.

In the first part of the work a parametrical analysis is carried out, aimed at the design with the current DDBD procedure, of a considerable amount of simple ideal oscillators, and at the verification by dynamic inelastic time history analysis of the previously designed systems. A range of effective periods T_{eff} between 0.2 and 4.0 seconds are considered for the SDOF ideal systems, and values of displacement ductility μ_{Δ}^d between 1.25 and 5.0 are assumed to include possible low, medium and high ductile behaviours. Four different Equivalent Viscous Damping models ξ_{eq} are evaluated, associated to three forms of the R_{ξ} scaling factor for the elastic Displacement Response Spectrum (DRS). In total 4212 SDOF ideal systems were designed, and subsequently compared with the results obtained from Non Linear Time History (NLTH) analyses, performed for the same set of non linear simple oscillators based on the Takeda Thin hysteretic model. On the basis of these results, the more appropriate forms of EVD models and the R_{ξ} factor to be adopted in the current DDBD procedure are discussed. The relative error of the DDBD method is thus obtained, and by interpolating the medium error curves, a simplified abacus of the expected approximation error of the simplified design method is derived.

In the second part of the work a sensitivity study is performed, to obtain realistic design values in terms of T_{eff} and μ_d for cantilever rc piers with flexural behaviour, all having different values of slenderness and reinforcement amount; such columns are designed for drift values θ between 1.5% and 4.0%. Using the medium error diagram previously obtained, it is shown that in the realistic design cases of rc bridge piers, the DDBD method has good accuracy for low and medium ductility design levels ($\mu_{\Delta}^d < 1.5$), while for high displacement ductility values

($1.5 \leq \mu_{\Delta}^d \leq 3.5$) the relative error results higher, though always acceptable considering that DDBD method generally overestimates.

3.2 ERROR SOURCES OF THE DDBD METHOD FOR SDOF SYSTEMS

Approximate solutions for non linear structures have gained a good reputation for performance-based design procedures in the last two decades^[F4]; one of these techniques is the concept of equivalent linearization, initially developed by Shibata e Sozen^[S1], 1976, and later implemented in the current form of the DDBD method by Priestley et al.^[P3, P1, C2], 2007. It requires the use of an equivalent elastic structure (Equivalent Single Degree of Freedom, ESDOF) substitutive of the real inelastic systems (SDOF or MDOF). The Substitute structure is characterized by the effective stiffness K_{eff} , which is the secant stiffness at maximum displacement Δ_u , the effective damping ξ_{eq} , related to the hysteretic energy absorbed, and the effective mass m_e , which is the effective mass of the structure participating in the fundamental mode of vibration.

It is of interest to identify the error range prediction for the simplified DDBD procedure, so that its attractiveness may be evaluated as much for its conceptual coherency as for the balancing of accuracy against reduced computational effort.

One of the most realistic structures conforming to the assumptions of a SDOF approximation is a cantilever pier of a regular isostatic bridge under transverse excitation^[P1] (when the soil-structure interaction can be neglected): its structural behaviour under cyclic loads can be characterized by a simple oscillators, represented by a cantilever with a concentrated mass on the top.

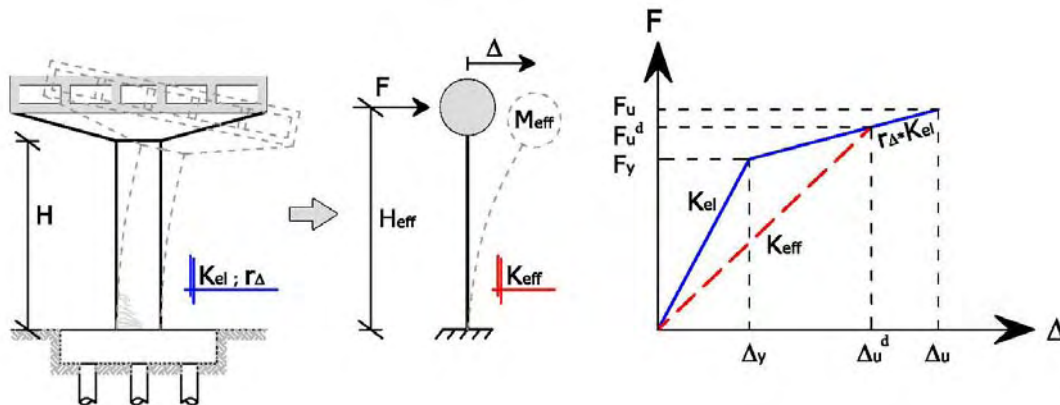


Fig. 3.1 – Substitute structure for a cantilever bridge pier (SDOF system)

In order to assess the accuracy of DDBD method when applied to simple SDOF inelastic systems, it is necessary to focus on the critical assumptions introduced by the method, namely:

1. the equivalent linearization process, with the estimation of an equivalent viscous damping ξ_{eq} ;
2. the use of overdamped displacement elastic spectra.

The equivalence of a simple non linear oscillator with an elastic system, is based on the response of a system whose period T_{eff} is related to the secant stiffness

at maximum displacement Δ_u . The energy absorbed by the hysteretic steady-state cyclic response of the non linear oscillator is equated to ξ_{eq} of the linear oscillator, and the maximum displacement response of the two systems is considered approximately to be equal. The appropriate calibration of the EVD model depends on the hysteresis cycles of the real system during seismic excitation, and represents the first source of approximation of the simplified design method.

Another source of uncertainty in the design process is represented by the use of overdamped displacement elastic spectra to represent the peak response of ductile inelastic systems; since the effective properties of the ESDOF systems are elastic, the current DDBD method uses damped elastic response spectra for the design, but debate is going on over the correct formulation of the reduction factor R_ξ . Alternative methods, such as the use of inelastic design spectra proposed by some authors (Chopra^[C1], 2001) are not examined in this study.

This work aims to quantify the scatter in the results of the approximate solutions obtained through equivalent linearization of non linear systems as applied to the DDBD method, if compared to non linear time-history analysis (NLTH) for the prediction of SDOF structures response. The approximations highlighted above are intrinsic in the simplified method also when it is applied to MDOF systems, in which case further assumptions, in particular the target-displacement shape adopted, introduce additional uncertainties.

Other limitations of the current DDBD design procedure discussed in Chapter 2, related to the initial choice of the target displacement and to the appropriate definition of 5% damping elastic displacement spectrum (associated with the magnitude and fault plan distance, Facciole & Villani^[F2], 2009) are not considered herein.

3.3 PARAMETRICAL ANALYSIS FOR IDEAL SDOF SYSTEMS

3.3.1 Elastic Displacement Response spectrum

The seismic action for the design of SDOF systems is obtained from the elastic response spectrum proposed by EC8(2003): the horizontal component of "type 1" spectrum (5% damping) is selected as reference acceleration response spectrum for a ground of medium stiffness (type C, $S=1.15$, $T_B=0.20s$, $T_C=0.6s$, $T_D=2.0s$), with a $PGA=0.35g$.

The corresponding horizontal displacement response spectrum is derived with the following relation:

$$S_D(T) = S_a(T) \left[\frac{T}{2\pi} \right]^2 \quad (3.1)$$

where $S_D(T)$ is the spectral elastic displacement response.

A set of 7 synthetic accelerograms compatible with the EC8 spectrum were generated with the SIMQKE program (Gasparini and Vanmarcke, 1976). In Fig. 3.2 the acceleration response spectra for the 7 generated accelerograms compared with the code horizontal acceleration response spectrum and the code elastic displacement spectrum, are plotted.

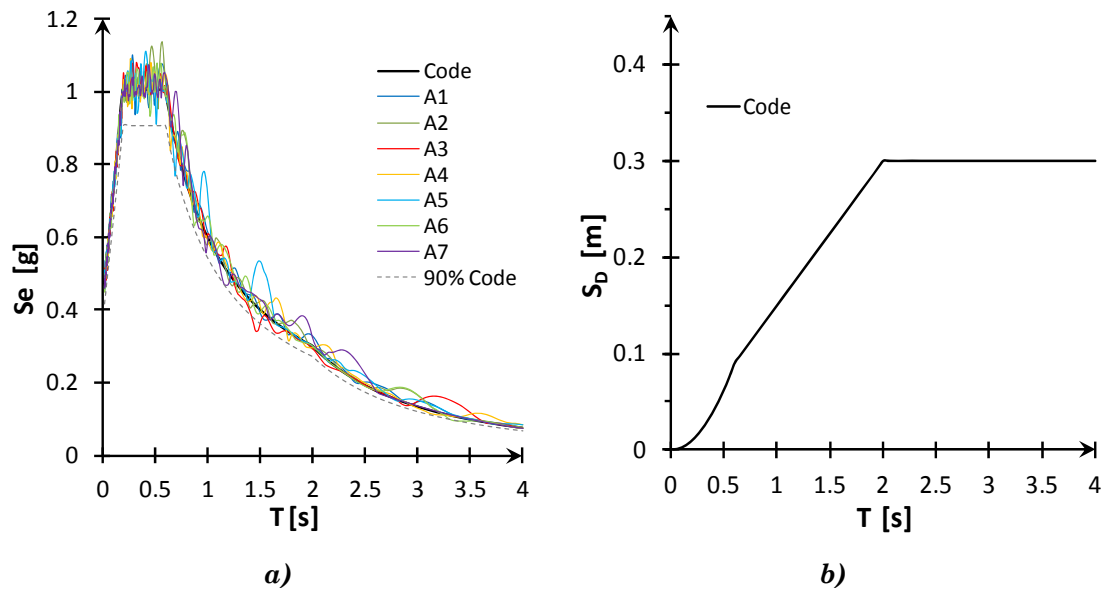


Fig. 3.2 – a) Acceleration response spectra from time histories set compared with code acceleration spectrum (EC8-type 1, $a_g=0.35$, ground type C), **b)** code displacement elastic response spectrum (5% damping)

3.3.2 Equivalent viscous damping models

The DDBD design procedure requires the estimation of an equivalent viscous damping for the substitute linear structure; the damping relationships used in the parametric analysis consider the effect of ductility on damping, and are obtained as a combination of elastic and hysteretic components (see Eq. 2.16, here reported for simplicity):

$$\xi_{eq} = \xi_{el} + \xi_{hyst} \quad (3.2)$$

a value $\xi_{el}=0.05$ is generally adopted for concrete structures, and ξ_{hyst} is calibrated taking into account the appropriate hysteresis rule for the structure to be designed.

<i>Takeda Thin (TT)</i>			
r_Δ	α	β	
0.0	0.5	0.0	

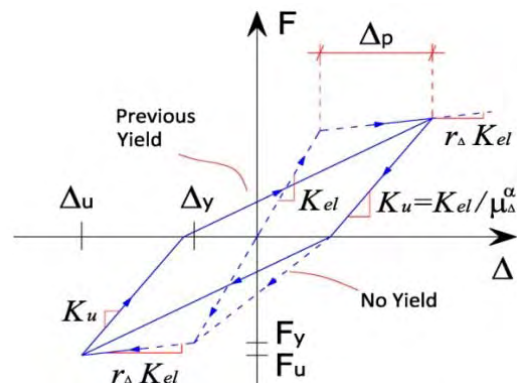


Fig. 3.3 – Takeda Thin (TT) hysteretic model parameters

In this case the Takeda Thin (TT) hysteretic model was used as a good representation of structural elements with significant axial load, such as bridge piers. An unloading stiffness factor $\alpha=0.5$ and a bilinear stiffness ratio $r_{\Delta}=0.0$ were adopted (see Fig.3.3).

Four different EVD models are compared in the numerical analyses, all calibrated for the TT hysteretic model, with the parameters r_{Δ} , α , β taken as specified above. The first one, the JDSS model, is the original Jacobsen's model^[J1,J2], tied to the initial stiffness of the non linear system, while the other expressions (D.K., G.B.P., D.K.G.) have been developed in the past years^[G1,P11,D1] more coherently with DDBD assumptions, by relating the model to secant stiffness at peak response (this results in an equal period shift T_{eff}/T_i for any of the hysteretic models considered). For further details see considerations in §2.1.3.

The EVD expressions adopted in this study are reported in Eqs. 3.3-3.8:

1. Jacobsen's Model^[J1,J2] (JDSS):

$$\xi_{eq} = \xi_{el} + \xi_{hyst} = \xi_{el} + \frac{2}{\pi} \left(1 - \frac{3}{4} \mu_{\Delta}^{\alpha-1} \gamma - \frac{1}{4} \right) \quad (3.3)$$

The expression can be simplified as follows with the values reported in Fig. 3.3:

$$\xi_{eq} = \xi_{el} + \xi_{hyst} = \xi_{el} + \frac{1}{\pi} \left(1 - \frac{1}{\sqrt{\mu_{\Delta}}} \right) \% \quad (3.4)$$

2. Model by Dwairi^[P1] et al. (D.K):

$$\xi_{eq} = \xi_{el} + \xi_{hyst} = \xi_{el} + C_{TT} \left(\frac{\mu_{\Delta} - 1}{\pi \mu_{\Delta}} \right) \% \quad (3.5)$$

where:

$$C_{TT} = 50 + 40(1 - T_{eff}) \text{ for } T_{eff} \leq 1 \text{ s} \quad (3.6)$$

$$C_{TT} = 50, \quad T_{eff} > 1 \text{ s} \quad (3.7)$$

3. Model by Grant^[G1,J2] et al. (G.B.P) :

$$\begin{aligned} \xi_{eq} &= k \xi_{el} + \xi_{hyst} = \\ &= k \xi_{el} + 0,215 \left(1 - \frac{1}{\mu_{\Delta}^{0,642}} \right) \left[1 + \frac{1}{(T_{eff} + 0,824)^{6,444}} \right] \% \end{aligned} \quad (3.8)$$

where:

$$\begin{aligned} k &= 1 & \mu_{\Delta} < 1 \\ k &= \mu_{\Delta}^{\lambda} & \mu_{\Delta} \geq 1, \end{aligned}$$

$\lambda=0.340$ for the initial stiffness damping model (TT hysteresis rule, Tab. 2.10)

The factor λ is the secant stiffness correction factor proposed by Grant et al.^[G1,P11], and is related to the hysteresis rule selected (in this case the TT hysteretic model): it introduces an adjustment that was proved to be necessary because in DDBD, the initial elastic damping is related to the secant stiffness to maximum displacement, whereas in inelastic time-history analysis, it is conventional practice to relate the elastic damping to the initial stiffness. Without such an adjustment the verification of DDBD by NLTH analysis would be based on an incompatible assumption (§2.1.3).

4. Model by Dwairi et al. with the correction factor for elastic damping^[P1] (D.K.G.):

$$\xi_{eq} = k \xi_{el} + \xi_{hyst} = \mu_{\Delta}^{\lambda} \xi_{el} + C_{TT} \left(\frac{\mu_{\Delta} - 1}{\pi \mu_{\Delta}} \right) \% \quad (3.9)$$

where: $C_{TT} = 50$, $\kappa = \mu_{\Delta}^{\lambda}$ has the same value as in Eq.(8).

The Eq.3.9 modifies Eq.3.5 introducing the correction factor for elastic damping suggested by Grant et al.^[G1,P11], with the same value of term λ used in Eq.3.8.

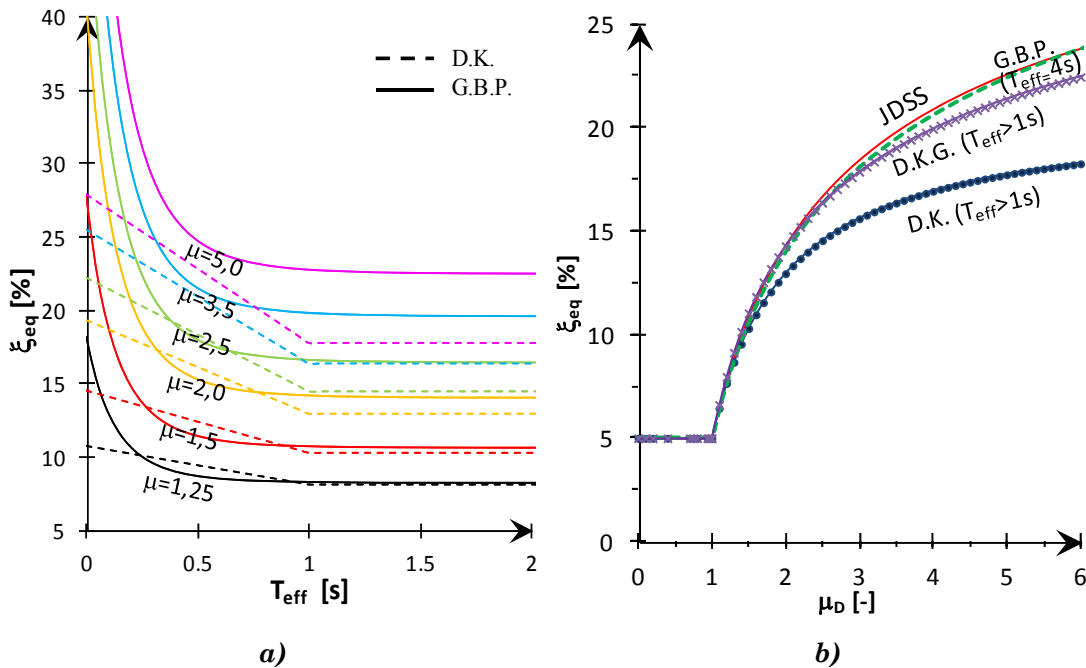


Fig. 3.4 – a) Period dependency of hysteretic component for equivalent damping models (D.K.) and (G.B.P.), plotted for different ductility levels (TT hysteretic model). **b)** Equivalent viscous damping ratio provided by the four models based on the TT hysteretic rule: (JDSS), (D.K.), (G.B.P.) for $T_{eff}=4s$ and (D.K.G.) for $T_{eff}>1s$.

The (D.K.) and (G.B.P.) equivalent viscous damping models have a period dependency, which leads to an evident increase of damping for $T_{\text{eff}} < 1\text{s}$, but which is not significant for periods greater than 1.0 seconds in both cases; this dependency can be seen in Fig.3.4a for various ductility levels. To compare the different damping formulas only as functions of the displacement ductility, the expressions for D.K. and (G.B.P.) models have been plotted for $T_{\text{eff}} \geq 1\text{s}$ and $T_{\text{eff}} = 4\text{s}$ respectively in Fig. 3.2b. First it can be observed that a significant difference is represented by the (D.K.) model, due to the absence of the correction factor $\kappa = \mu_{\Delta}^{\lambda}$ for the elastic damping, which leads to a damping ratio underestimation, increasing for high ductility values. Moreover the highest damping values are given by the JDSS model, which represents a sort of upper envelope, even if does not present a correction factor for elastic damping. The JDSS model high overestimation has been proved by different authors^[C1,D1]; in this specific case, being the TT hysteresis rule associated with the (JDSS) model, its trend seems to be very close to more “advanced” models like (G.B.P) and (D.K.G.). Thus the scatter in the results is expected to be lower than in other cases, in which “fatter” hysteretic models are adopted (for example the Takeda-Fat or the Elasto-Plastic model, see also Fig. 2.6).

3.3.3 Response spectrum reduction factors

The basic elastic displacement response spectrum (corresponding to an elastic damping ratio of $\xi_{eq} = 0.05$) shall be damped with regard to the calculated structural equivalent viscous damping ξ_{eq} , by multiplying spectral ordinates with the reduction factor R_{ξ} .

$$S_{\Delta\xi}(T) = R_{\xi} S_{\Delta 0.05}(T) \quad (3.10)$$

To date seismologists are still debating about the appropriate form of the damping modifier R_{ξ} to elastic spectral displacement, as previously discussed in §2.1.4. In this study three commonly used expressions presented in §2.1.4 are compared: the first was proposed by Newmark and Hall^[N1] in 1987, while the second was presented in the 1998 edition of Eurocode 8^[X3], and was subsequently replaced by the third in the 2003 revision of EC8^[X4]. Eqs 2.31, 2.32 and 2.33 are reproduced for convenience here below:

1. Newmark e Hall (NH):

$$R_{\xi} = [1,31 - 0,19 \ln(100\xi)] \quad (3.11)$$

2. EC8-1998:

$$R_{\xi} = [0,07 / (0,02 + \xi)]^{0,5} \quad (3.12)$$

3. EC8-2003:

$$R_{\xi} = [0,10 / (0,05 + \xi)]^{0,5} \quad (3.13)$$

Other expressions for the R_{ξ} coefficient have been recently proposed by some authors^[F2] for near-field sites (see §2.1.4); such effects on spectral displacements are not addressed in this study.

3.3.4 Evaluation algorithm

The parametric analysis was performed with the aim of comparing the DDBD target displacements with T-H response for a wide range of SDOF systems. The analysis is based primarily on the definition of a series of simple nonlinear oscillators, obtained by “inverting” the current DDBD procedure: by choosing a set of initial input parameters to address the design and the EVD models previously presented (Eqs. 3.3-3.8), the overdamped displacement spectra can be determined by scaling the elastic spectrum with the reduction factor R_ξ . The capacity curve for each ideal oscillator is derived on the basis of the pre-fixed design ductility μ_Δ^d and the design displacement Δ_u^d , calculated by entering the damped spectra with the input effective period T_{eff} . At this point the design of the ideal SDOF system can be considered complete; once the key features of each non linear SDOF system have been defined by means of the capacity curve, and the hysteresis rule is associated (Takeda Thin model, Fig.3.3), the inelastic response in terms of ultimate displacements can be evaluated using non linear analysis in the time domain, and the relative error compared to the design displacement.

The evaluation procedure is articulated in the following steps:

(i) DEFINE INITIAL INPUT PARAMETERS

- a) Select the basic response spectrum $S_{\Delta 0.05}(T)$.
- b) Select a value for design displacement ductility μ_Δ^d and effective period T_{eff} of the SDOF ideal oscillator.

(ii) DETERMINE THE DAMPED RESPONSE SPECTRUM

- c) Calculate the equivalent viscous damping ξ_{eq} as a function of ductility, choosing one of the models given by Eqs.3.3, 3.5, 3.8, 3.9;
- d) Obtain the response spectrum reduction factor R_ξ using one of the formulas 3.11, 3.12, 3.13.
- e) Multiply the basic response spectral ordinates with the reduction factor R_ξ and obtain the design displacement response spectrum $S_{\Delta \xi}(T)$ in accordance with the Eq.3.9.

(iii) CALCULATE THE TARGET RESPONSE

- f) Enter the damped displacement spectrum $S_{\Delta \xi}(T)$ with T_{eff} , and calculate the target displacement Δ_u^d .
- g) Calculate the design acceleration a_u^d entering the acceleration response spectrum $S_{a \xi}(T)$ with T_{eff} .

(iv) OBTAIN THE CAPACITY CURVE FOR SDOF OSCILLATOR

- h) Calculate the yield displacement Δ_y for the SDOF system as $\mu_\Delta^d = \Delta_u^d / \Delta_y$
- i) Calculate the elastic period with the following equation:

$$T_{el} = T_{eff} \sqrt{(1 + r_\Delta \mu_\Delta^d - r_\Delta) / \mu_\Delta^d} \quad (3.14)$$

where r_Δ is the bilinear stiffness ratio of Fig.3.1

- l) Calculate the yield acceleration as

$$a_y = \frac{4\pi^2}{T_d^2} \Delta_y \quad (3.15)$$

The capacity curve has thus been obtained and can be plotted in the acceleration-displacement (A-D) plane.

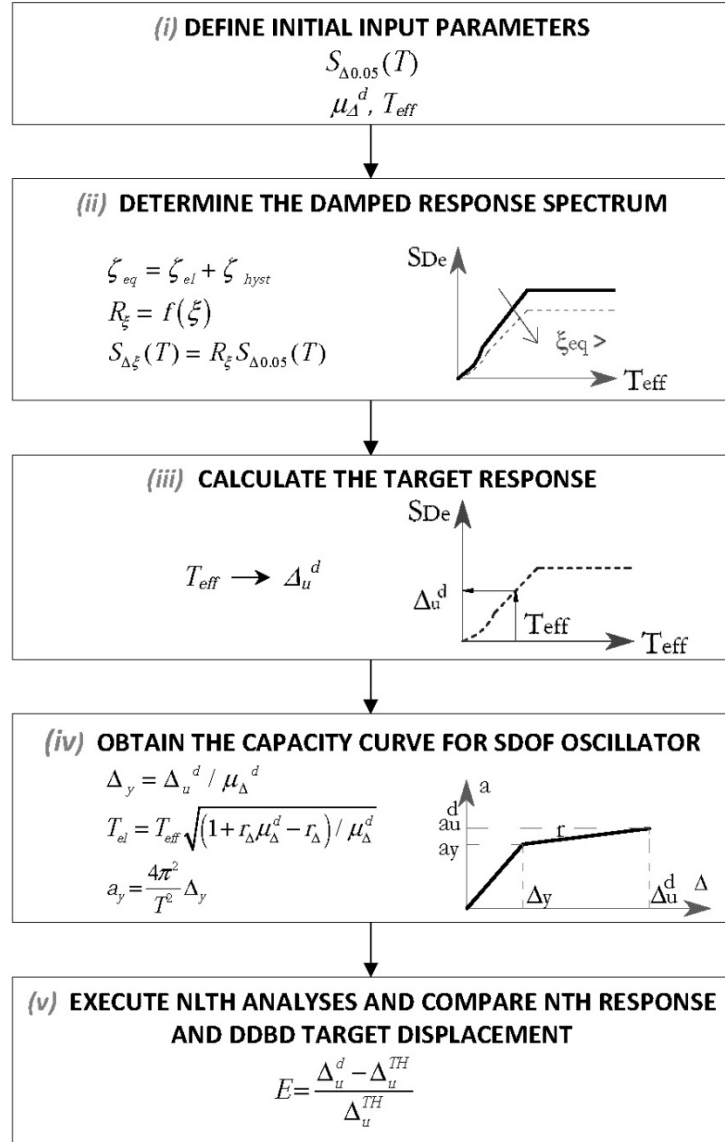


Fig. 3.5 – Flowchart of the evaluation algorithm used in the parametrical analysis.

(v) EXECUTE NLTH ANALYSES

m) Run the TH analyses using the SDOF non linear system defined by the capacity curve and adopting the Takeda Thin hysteretic model (with the parameters specified in Fig.3.3; the value $\xi_{el}=5\%$ is to be assumed for the elastic viscous damping.

(vi) COMPARE NLTH RESPONSE AND DDBD TARGET DISPLACEMENT

n) Plot the displacement Δ_u^{TH} obtained as the average of maximum displacement demands calculated for the 7 spectrum compatible time histories represented in Fig.3.2, and compute the relative error:

$$E [\%] = \frac{\Delta_u^d - \Delta_u^{TH}}{\Delta_u^{TH}} \quad (3.16)$$

Following the procedure described from point (i) to (vi) a parametric study was carried out by considering as input parameters 39 different values of effective period T_{eff} , defined between 0.2 and 4 seconds, by stepping 0.1s, and 9 different ductility levels μ_{Δ}^d in the range [1.25, 5]; consequently for a single design spectrum 351 analyses were performed. Each spectrum was obtained scaling the basic response spectrum after choosing among 4 types of equivalent damping models ξ_{eq} (§3.3.2), associated to three different scaling factors R_{ξ} (§3.3.3). In total 4212 SDOF non linear systems were designed, and subsequently verified in terms of displacement demands through dynamic non linear analyses in the time domain.

3.3.5 DDBD verification

In this section a synthesis of the results obtained from the parametrical analyses on ideal SDOF systems is reported. Figs. 3.6, 3.7 show the comparison of results for different EVD models, for a pre-fixed form of the damping modification factor R_{ξ} . Here the single case of $R_{\xi} = EC8-2003$ is reproduced, but the following considerations are based also on similar results obtained for the other R_{ξ} formulas, (NH) and (EC8-1998). The relative errors between the design displacement of the DDBD method and the mean value of the TH peak displacements value are represented for constant displacement ductility values μ_{Δ}^d .

It is apparent that for all EVD models errors increase with high ductility values, in particular overestimation errors: this seems reasonable, being the prediction of a “near” elastic response more easily reproduced by a linearized system, than an inelastic behaviour requiring a deep excursion into the plastic field.

Problems related to the overestimation errors of the JDSS model are not so evident as in other studies, and this is due to the shape of the hysteretic model adopted (Takeda Thin model) for the non-linear cyclic behaviour of bridge piers, as already anticipated before.

The graphs show that three of the different EVD models evaluated, give very similar results for $T_{eff} > 0.75s$, and consequently the same trend of the relative error plot is obtained for all ductility levels. The exception is represented by the (D.K.) model, to which is tied the greatest inaccuracy in this range, due to the absence of the elastic damping correction.

For $T_{eff} < 0.75s$ the (JDSS) and (D.K.G.) models sensibly underestimate the EVD required to the linear SDOF system to equate the non linear peak displacements obtained with TH analyses. This is due to the absence of a dependence on the effective period T_{eff} , that on the contrary is accounted for by (D.K.) and (G.B.P) model. In particular best results are obtained for all ductility levels by the (G.B.P.) model, even if it is not accurate in the low-period range.

Finally it can be observed that it will be unusual for normal structures (wall and frame buildings or bridges) to have effective period values less than 0.75-1s, and this is confirmed also by the results of the sensitivity analysis on realistic piers design developed in the second part of the work.

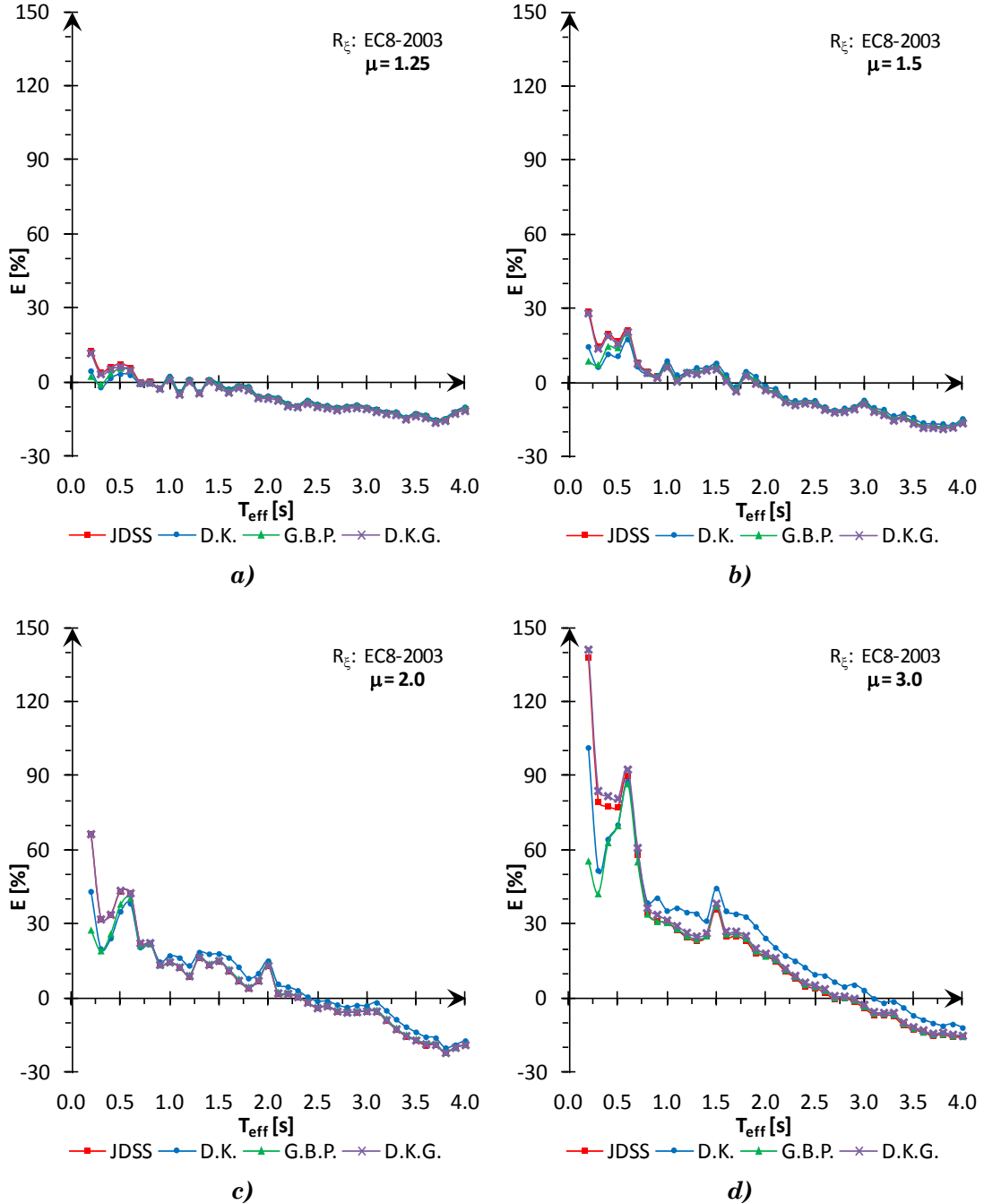


Fig. 3.6 – Relative error obtained (Eq.3.16), using different EVD models for the prefixed spectrum reduction factor R_{ξ} =EC8-2003. Case studies presented: **a)** $\mu=1.25$, **b)** $\mu=1.5$, **c)** $\mu=2.0$, **d)** $\mu=3.0$

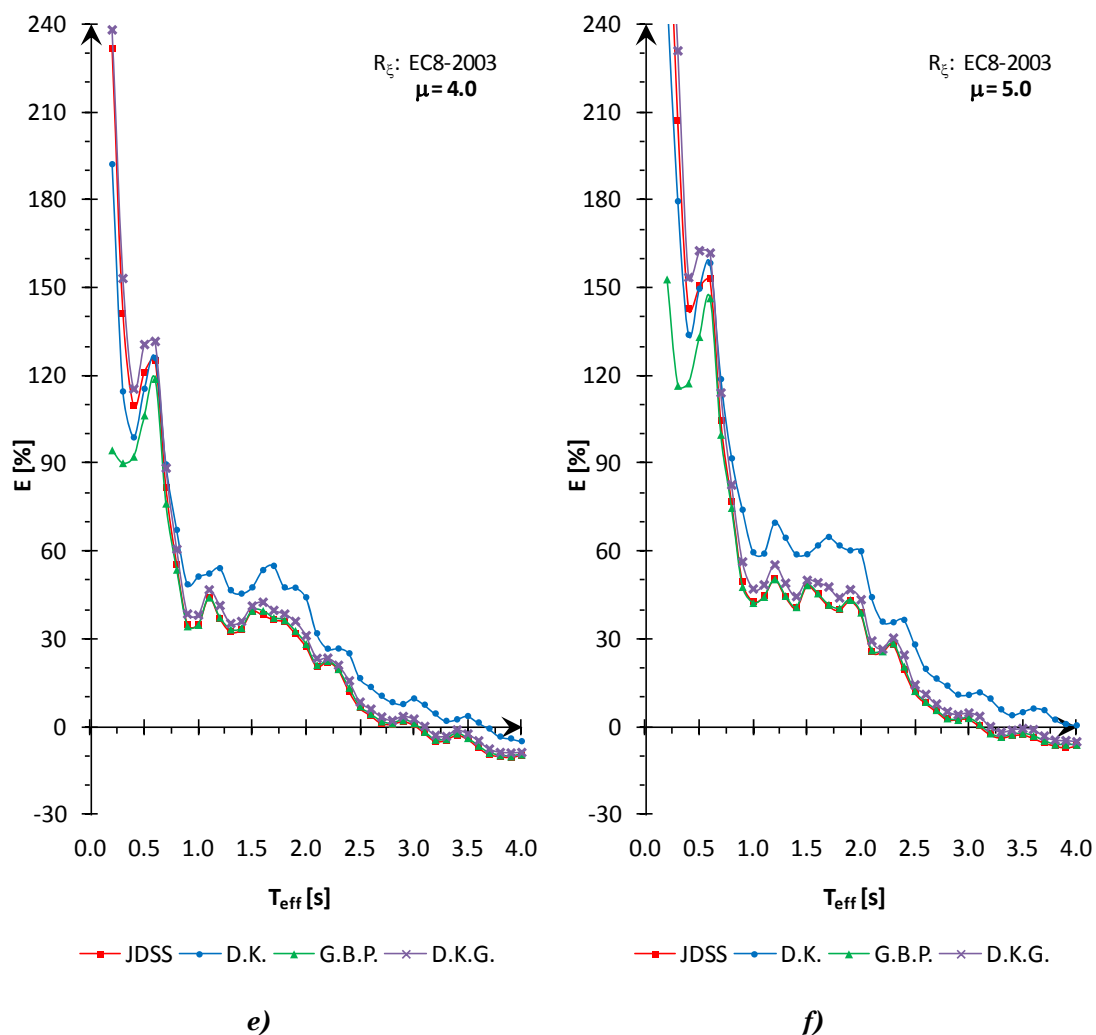


Fig. 3.7 – Relative error obtained (Eq.3.16) between the DDBD design displacement Δ_u^d and the maximum displacement demand Δ_u^{TH} , using different EVD models for the pre-fixed spectrum reduction factor $R_\xi = EC8-2003$. Case studies presented: **e)** $\mu=4.0$, **f)** $\mu=5.0$.

Since T_{eff} is greater than 1 in most of real design cases, and since the (DKG) model requires as input data only the ductility value μ_Δ^d (unlike the GBP model, that needs also T_{eff} , an output of the DDBD method, leading to an iterative procedure), it can be concluded that the (DKG) model is effectively the most convenient.

In Figs. 3.8, 3.9 the comparison of relative errors obtained on the design displacement prediction using different forms for the spectral reduction factor R_ξ is presented. The same equivalent damping model (D.K.G.) is used in these cases, with reference to some pre-fixed ductility levels, $\mu = 1.25, 1.5, 2.0, 3.0, 4.0, 5.0$. It can be observed that accuracy diminishes with the increase of the ductility demand for all the R_ξ forms considered.

The formula that leads to more conservative results (greatest overestimation errors) is by Newmark-Hall, which results to be too cautious; as for the other two,

EC8-2003 and EC8-1998, can be observed an overall reduction of the relative error as the period increases, with a quite comparable trend for $T_{eff} > 1s$.

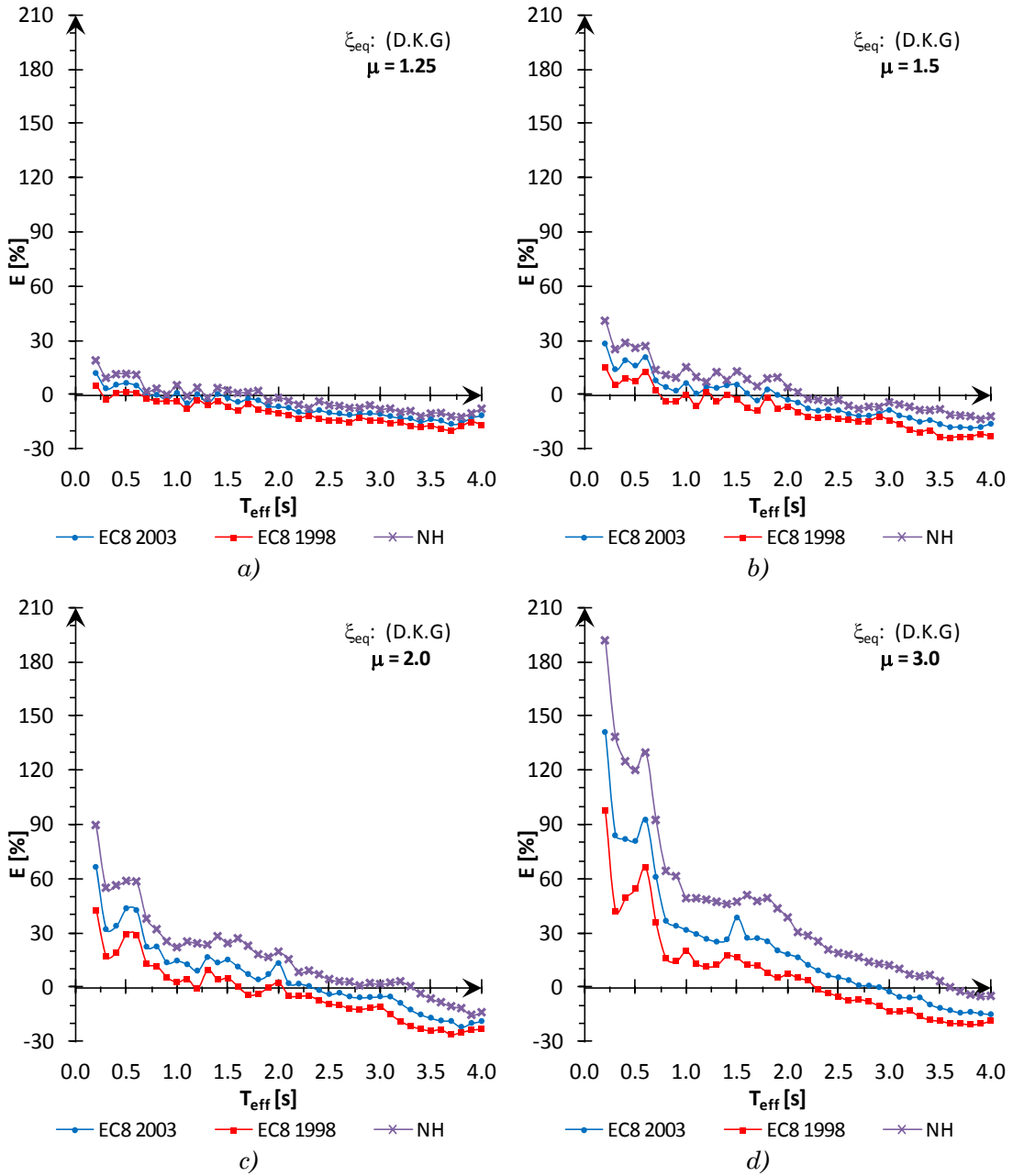


Fig. 3.8 – Relative error obtained (Eq.3.16) using different expression for the spectrum reduction factor R_{ξ} , for a pre-fixed EVD model, $\xi_{eq}=(D.K.G)$. Case studies presented: **a)** $\mu=1.25$, **b)** $\mu=1.5$, **c)** $\mu=2.0$, **d)** $\mu=3.0$,

The most precise equivalent spectral elastic displacement, seems to be obtained using the $R_{\xi} = EC8-1998$ factor but the EC8-2003 curve remains always above the corresponding EC8-1998 curve, consequently the underestimation error is smaller for $T_{eff} > 2s$; this consideration can justify the preference for the EC8-2003 formula, currently adopted by Calvi et al.^[C2], 2009.

The results obtained for the other damping models and ductility levels are not reported here for brevity's sake, but same conclusions can be drawn.

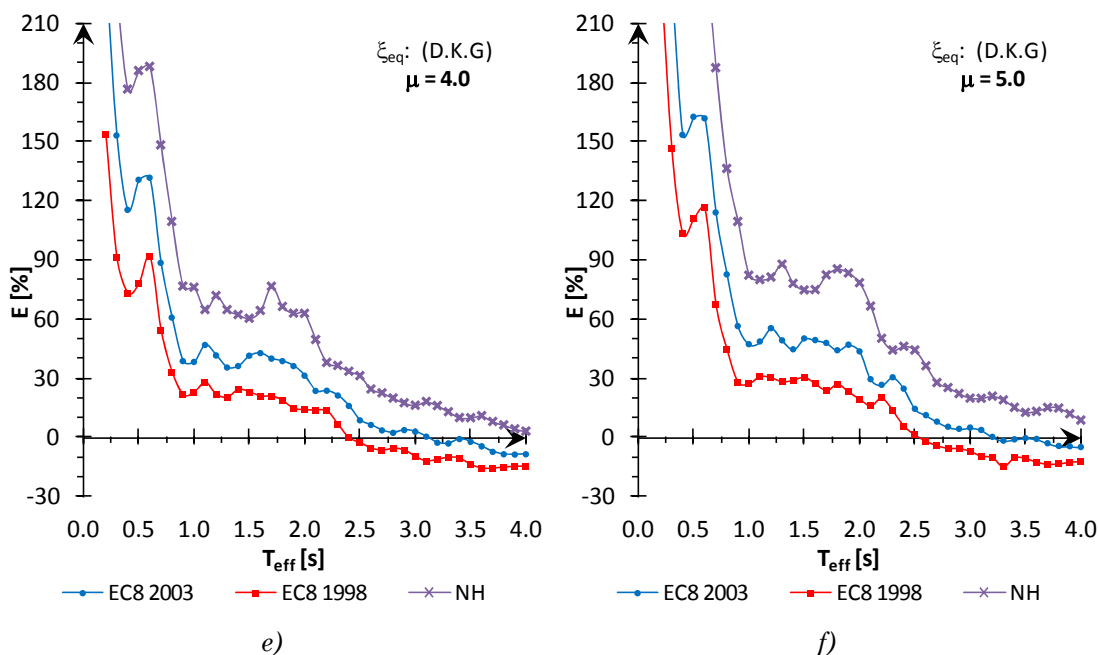


Fig. 3.9 – Relative error obtained (Eq.3.16) between the DDBD target displacement Δ_u^d and the required maximum displacement Δ_u^{TH} , by using different expression for the spectrum reduction factor R_ξ , for a pre-fixed EVD model, $\xi_{eq}=(D.K.G.)$. Examples presented: **e)** $\mu=4.0$, **f)** $\mu=5.0$.

Following the verification process described by the flowchart in Fig. 3.5 it is possible to plot the iso-ductility displacement design spectra, and compare them with the inelastic displacement spectra obtained by NLTH analysis. An example of this comparison is given in Fig.3.10 for the choice of EVD model $\xi_{eq}=(D.K.G.)$, and $R_\xi=EC8-2003$. In Fig.3.11 the relative error according to Eq.3.16 is plotted with the same assumptions for the entire periods range, considering all the different ductility levels.

In Fig. 3.10 it can be observed that the DDBD target displacements, corresponding to the inelastic displacement response spectra, are generally higher than the TH average peak displacement demands, at least up to the corner point of the spectra: being the displacement that results from the non linear analysis of bridges smaller, it can be deduced that the method tends to overestimate the response.

The point of intersection between the DDBD design displacement spectrum and the curve of the effective peak displacement demand (obtained with TH analysis for the non linear SDOF system) shifts towards higher values of T_{eff} for increasing ductility levels. This means that the overestimation error of the DDBD method increases for higher μ_d^A values, consequently the method is proved to be more conservative for high-ductility design cases.

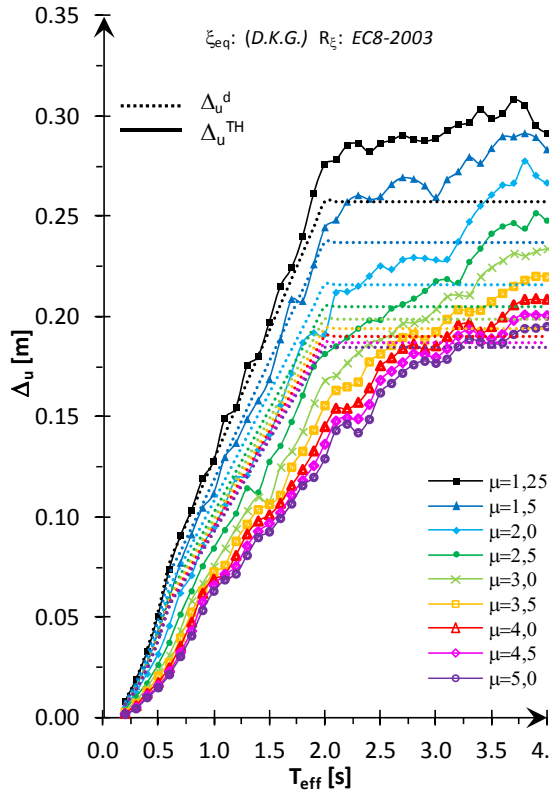


Fig. 3.10 – Design displacements μ_{Δ}^d of the DDBD method compared with the average inelastic displacement spectra obtained by TH analyses, following the procedure of Fig. 3.2, for all ductility levels ($\mu=1.25-5.0$). Case study: $\xi_{eq}=(D.K.G.)$, $R_{\xi}=EC8-2003$.

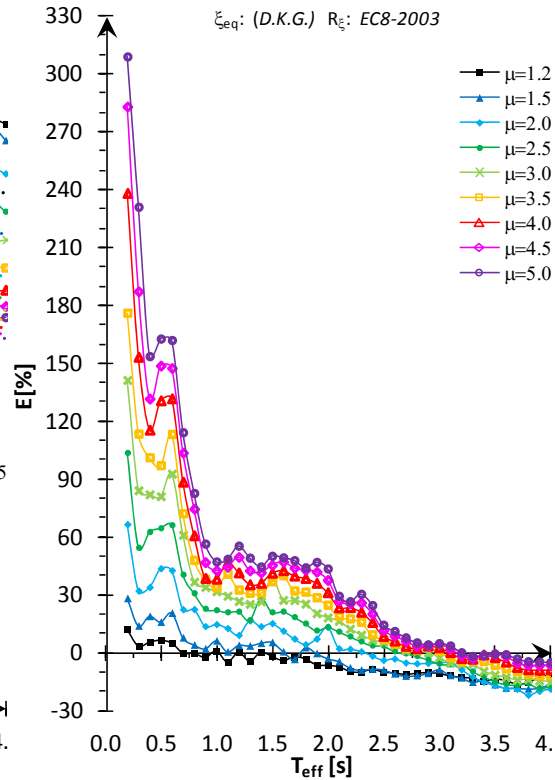


Fig. 3.11 – Relative error obtained for design displacements Δ_u^d of Fig. 3.8 with the average inelastic displacement spectra obtained by TH analyses. Case study: $\xi_{eq}=(D.K.G.)$, $R_{\xi}=EC8-2003$.

The method is generally conservative, at least for structures with $T_{eff} < 2.5-3.0s$, with overestimation errors for ideal SDOF oscillators significantly dependent on the design ductility level, while underestimation errors are of small relevance.

As previously noted, it should be evidenced that the effective periods T_{eff} below 0.7s do not correspond to real pier designs with flexural behaviour (see also subsequent Figs. 3.13-3.14), thus the high errors committed by the simplified DDBD method in this range are of small significance and no practical interest.

It could be useful to know “prior” the accuracy of the DDBD method when applied to SDOF systems, namely the error that the simplified procedure introduces using the approximations of a substitute linear structure characterized by the equivalent viscous damping ξ_{eq} and the scaling of the displacement elastic spectrum through the modification damping factor R_{ξ} . With this aim, a diagram of the mean relative error is plotted in Fig.3.12. A polynomial interpolation of the relative error curves plotted in Fig.3.11 for constant ductility levels is obtained, and the average prediction error is expressed as a function of design displacement ductility μ_{Δ}^d (which is an input of the DDBD method), and T_{eff} .

The error ranges identified in Fig. 3.12 define the design areas in which all the possible SDOF systems designed with the simplified DDBD method are affected by medium errors included between the extreme values of the range.

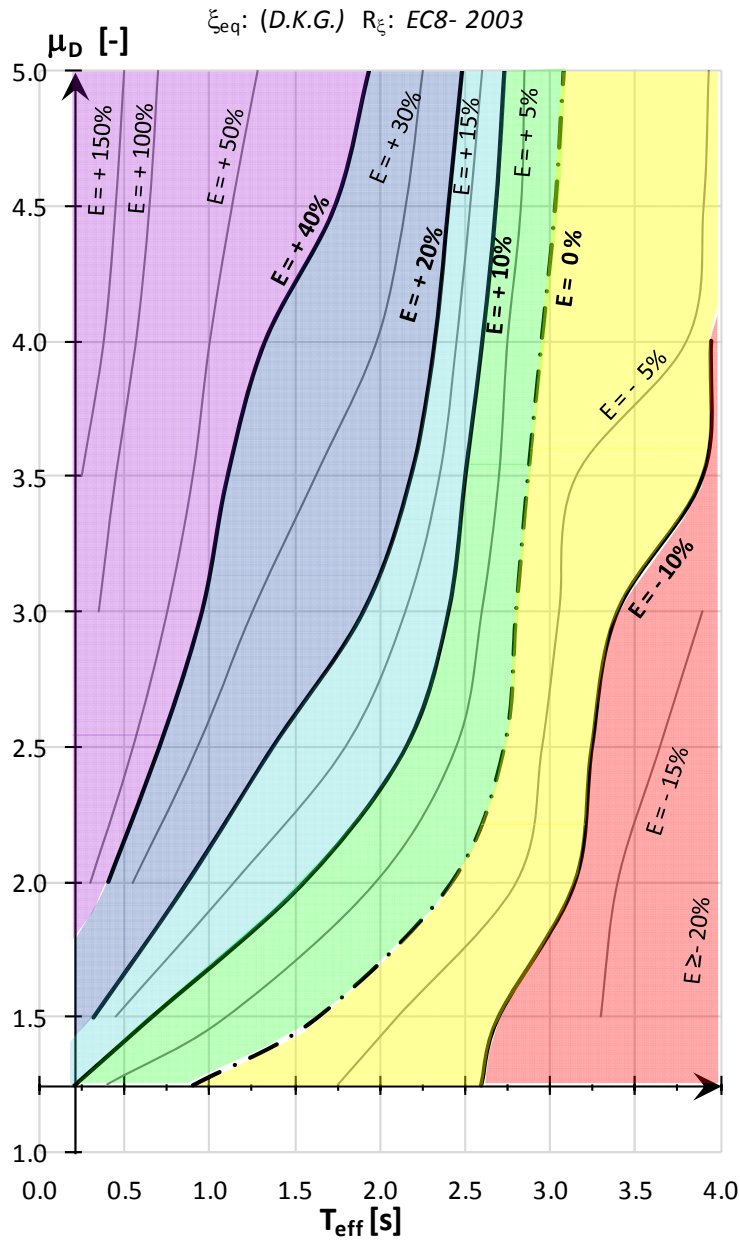


Fig. 3.12 – Relative error obtained for design displacements Δ_u^d of Fig. 3.8 with the average inelastic displacement spectra obtained by TH analyses. Case study:
 $\xi_{eq}=(D.K.G.)$, $R_{\xi}=EC8-2003$

3.4 PREDICTION ERROR FOR DIRECT DISPLACEMENT-BASED DESIGN OF CANTILEVER BRIDGE RC BRIDGE PIERS

This chapter deals with a sensitivity analysis on realistic SDOF structures, namely cantilever rc piers of simply-supported bridges. The study was carried out with the aim of identifying the ranges of all possible combinations of displacement ductility μ_{Δ}^d and effective periods T_{eff} for such structures.

3.4.1 Input data and design limitations

The input data for the sensitivity analysis are listed below:

- *Seismic action*: the reference elastic spectrum is the same used for the parametrical analysis in the first part of the work, i.e. EC8-2003 spectrum “type 1”, Ground type C ($S=1.15$, $T_B=0.20s$, $T_C=0.6s$, $T_D=2.0s$), $a_g=0.35g$, 5% damping.

- *Effective mass* of the SDOF system: 2 values of tributary mass are considered, $m_{1eff}=250$ t; $m_{2eff}=500$ t;

- *Materials*: effective properties are used for concrete and reinforcement. Concrete C32/40: $f_{ce}=1,3$ $f'_c=43,2$ MPa. Reinforcement steel B450C: $f_{ye}=1,1f_y=495$ MPa.

- *Pier geometry, bar diameter*: circular section, concrete cover: 3.5 cm, bar diameter $d_{bf}=30$ mm;

The following limits relating to geometry (D,L), reinforcement ratio ρ_l , slenderness λ , and normalized axial load are introduced to address the design of circular cantilever piers for typical multi-span simply supported girder bridges:

1. Longitudinal reinforcement ratio: $0,5\% < \rho_l < 4\%$ (3.17)

2. Maximum value of the dimensionless axial load:

$$\nu = N_{Ed} / f'_c A_c < 0.6 \quad (3.18)$$

3. Pier slenderness (limit suggested by NTC'08, for linear analysis)

$$\lambda < \lambda_{lim} = 15.4 \frac{C}{\sqrt{\nu}} \quad (3.19)$$

where the coefficient C is expressed by $C = 1,7 - r_m$, with the limits $0,7 \leq C \leq 2,7$, depending on the first order distribution of flexural moments at the pier top and bottom $r_m = M_{01}/M_{02}$ (set equal to 0 for a cantilever pier).

4. Geometric parameters (to individuate an appropriate geometric range for bridge piers and guarantee a flexural behaviour):

Minimum diameter : $D \geq 1$ m (3.20)

Height/ Diameter ratio: $H/D \geq 3.5$ (3.21)

Adequate confinement and sufficient transverse reinforcement are supposed to be used, ensuring a ductile flexural response of the piers.

3.4.2 Design process of cantilever rc piers and limits check

A series of circular cantilever columns are designed with the DDBD method, considering as target design drift limits $\theta_d = 0.015-0.04$, and stepping 0.005 (6 values); 9 levels of design displacement ductility are addressed: $\mu_{\Delta}^d = 1.25, 1.5, 2.0, 2.5, 3.0, 3.5, 4.0, 4.5, 5.0$,

The realistic design limits fixed above in terms of slenderness, amount of reinforcement, and height-diameter ratio are implemented: design cases not satisfying the previous limits are considered “unrealistic”, and excluded from the number of possible solutions.

Numerical analyses are carried out by considering as equivalent viscous damping the (D.K.G.) model (Eq. 3.9), and as spectrum reduction factor the *EC8-2003* formula (Eq. 3.13).

The design procedure is articulated in the following steps:

- a) Initial input: choice of the effective mass value m_e , selection of the target drift level $\theta_d = 0.015-0.04$ among the 6 pre-fixed values, choice of the displacement ductility level μ_{Δ}^d .
- b) Construction of the damped displacement response spectrum using Eqs.3.10,3.13..
- c) Choice of the T_{eff} for the selected μ_{Δ}^d and θ_d values (the same period range of 0.2-4.0s used in the parametrical analysis of ideal SDOF systems was considered).
- d) The damped displacement spectrum $S_{\Delta\xi}(T)$ is entered with T_{eff} , and the target displacement Δ_d is calculated.
- e) The yield displacement is obtained as:

$$\Delta_y = \Delta_d / \mu_{\Delta}^d \quad (3.22)$$

- f) The pier height is estimated with the relation:

$$H = \Delta_u^d / \theta_d \quad (3.23)$$

- g) The yield curvature ϕ_y is calculated, the strain penetration length L_{sp} being known:

$$L_{sp} = 0.022 f_{ye} d_{bl} \quad (3.24)$$

$$\phi_y = 3\Delta_y / (H + L_{sp})^2 \quad (3.25)$$

- g) Calculation of pier design diameter, using a simplified relation for dimensionless yield curvature ϕ_y , (Priestley^[P3], 1993):

$$\phi_y = 2,25 \varepsilon_y / D \rightarrow D = 2,25 \varepsilon_y / \phi_y \quad (3.26)$$

- h) First design check for minimum diameter requirement and expected flexural behavior, according to Eqs.3.18, 3.20; if the limits are not satisfied the design case is excluded as possible realistic solution, and the process is interrupted.

- i)** Second design check for pier slenderness λ according to Eq.3.18; if the limit is not respected the procedure is stopped.
- j)** If h) and i) requirements are satisfied, the effective stiffness K_{eff} is calculated:

$$K_{eff} = 4\pi^2 M_{eff} / T_{eff}^2 \quad (3.27)$$

- k)** Determination of the design shear (including P- Δ effects), and bending moment at the pier base:

e:

$$F_u^d = K_{eff} \Delta_d + 0,5 P \Delta_d / H \quad (3.28)$$

$$M_{base} = F_u^d H \quad (3.29)$$

- l)** Determination of the minimum longitudinal reinforcement; for the calculated M_{base} , (and acting axial load ν), the minimum reinforcement ratio is computed for symmetric reinforcement, imposing as strain limits $\varepsilon_c=0.004$, $\varepsilon_s=0.015$. Only reinforcement ratio percentage according to Eq.3.17 are accepted.

The research of the realistic design cases was carried out by determining the extreme values of the effective period admissible range, $T_{eff, min}$ and $T_{eff, max}$, for a pre-fixed drift θ_d and an established ductility level μ_{Δ}^d .

In Figs.3.13-3.14 the realistic designs obtained are plotted for the case of tributary mass M_e : for a better graphic result the occurrences corresponding to single designs are represented with a step of T_{eff} 0.1- 0.15s. The design ductility μ_{Δ}^d values are plotted versus effective period T_{eff} , and the obtained ranges for pier slenderness λ are superimposed.

It can be observed that typical design values for rc cantilevers piers are obtained for a range of $\mu_{\Delta}^d=1.25-5.0$, and effective periods vary from a minimum of 0.75s to almost 3.0s.

The range of slenderness considered varies from $\lambda=28$ to $\lambda=69$.

In order to better compare the final results obtained with target ductility values commonly accepted in Europe for bridge design, it seems appropriate to consider the range of the parameter μ_{Δ}^d according to the maximum values of behaviour factors q currently proposed by seismic codes [X1],[X2] for reinforced concrete piers design (implicitly assuming the validity of the “equal displacement” rule, $q = \mu_{\Delta}^d$, for the typical range of periods considered). Two classes have been defined: low-medium (DCM) design ductility, $1.5 \leq \mu_{\Delta}^d < 2.0$, and high design ductility (DCH), $2.0 \leq \mu_{\Delta}^d \leq 3.5$.

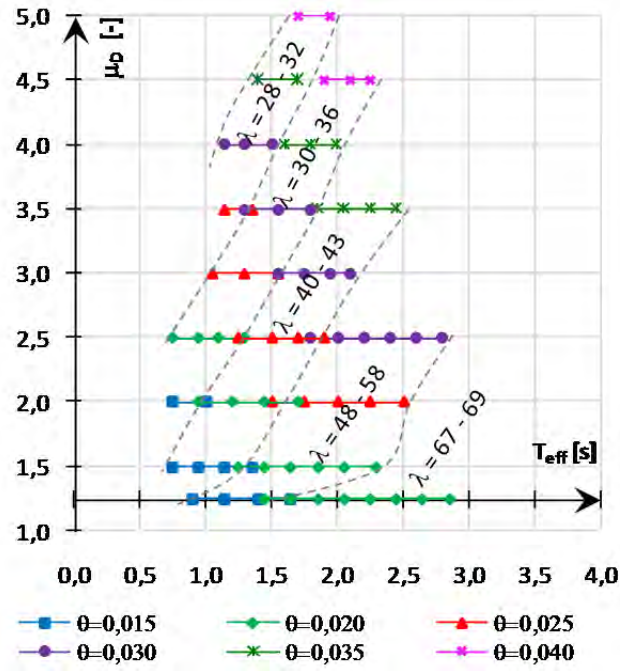


Fig. 3.13 – Realistic SDOF designs obtained for cantilever rc piers with tributary mass $M_{eff}=250t$.

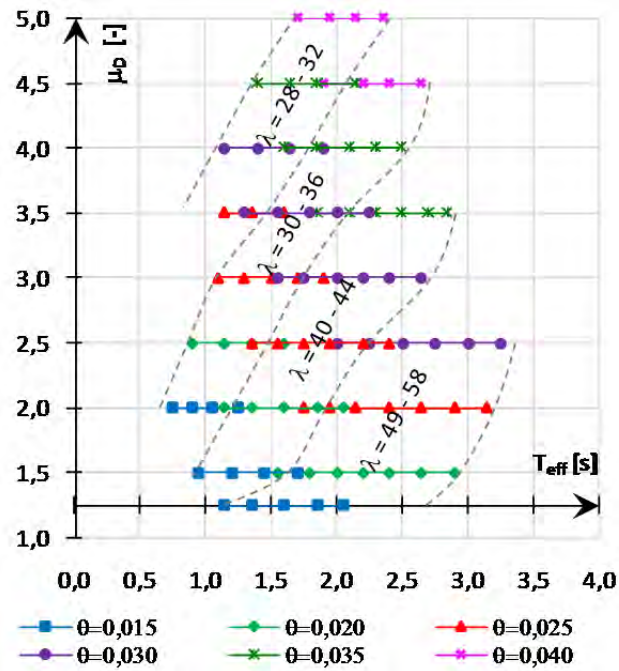


Fig. 3.14 – Realistic SDOF designs obtained for cantilever rc piers with tributary mass $M_{eff}=500t$.

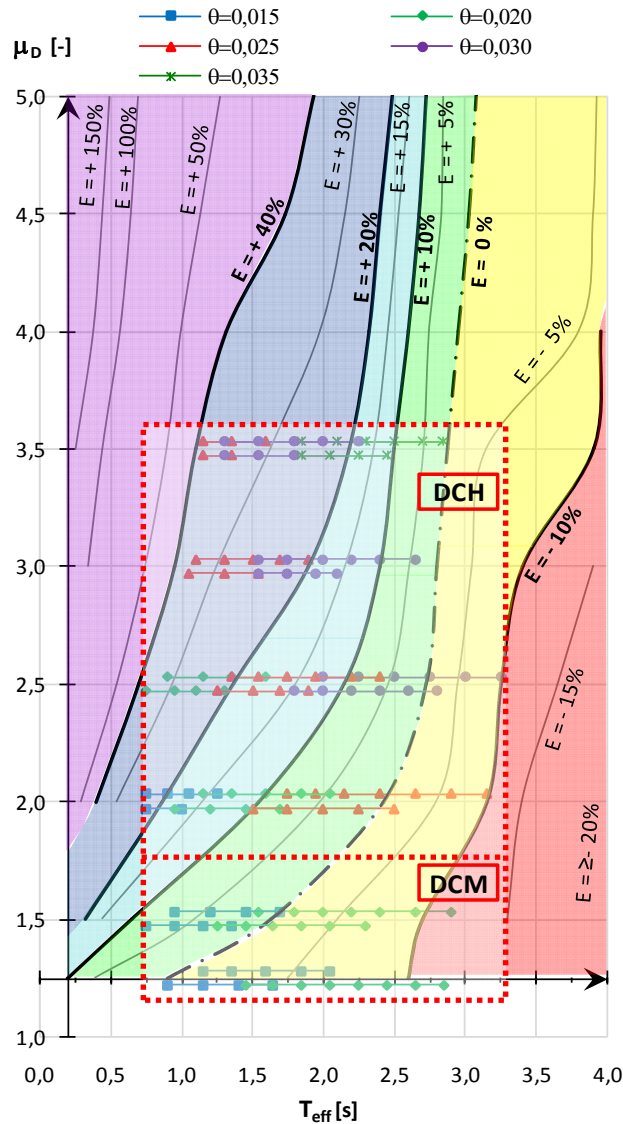


Fig. 3.15 – Relative error prediction (%) for the DDBD method applied to the design of cantilever rc bridge piers (SDOF systems). The medium error diagram in the background refers to Fig.3.12, while the design points for realistic cases are extracted from Figs.3.13, 3.14.

A final plot is proposed superimposing the “realistic “ design points to the medium error diagram previously obtained in the $(T_{eff}, \mu_{\Delta}^d)$ plane (see Fig.3.13): it is possible to derive the error prediction of the DDBD method when applied to the design of cantilever piers of simply supported rc bridges (SDOF systems).

It can be observed that the DDBD method is generally conservative: underestimation errors are limited for any realistic design, almost always less than 10% , with few cases (6%) with relative error just slightly higher ($E_m < 12\%$).

As regards the overestimation error range, as already observed for ideal SDOF systems, the accuracy is dependent on design ductility:

- for low-medium ductility design cases ($\mu_d \leq 1.5$), the DDBD method is again very accurate, with a low error range calculated for the single pier design, $E_m < +10\%$;

- for high ductility values, ($1.5 < \mu_d \leq 3.5$), the relative error results higher, even if most of the samples attain errors levels that can be considered still acceptable ($E_m < 20\%$ in 63% and $E_m < +30\%$ in 90% of design cases), considering that is an overestimation inaccuracy, and that the design process is a simplified direct method. Anyhow there is a not negligible percentage of structures (10%) with higher errors, with a maximum lower than 40%.

3.4.3 Relationship between drift and ductility

A key point of the displacement-based procedure is the definition of the accepted drift, which implies an evaluation of the relationship between drift and ductility, the latter being often adopted as a damage measure.

With reference to the realistic design cases analyzed, it was possible to plot the interval of ductilities corresponding to prefixed drift values (see Fig. 3.16).

It can be observed that higher drifts θ are tied to high displacement ductility μ_d values, and drifts $\theta \geq 2.5-3\%$, corresponds to $\mu > 3.5$, that is the upper limit currently adopted by seismic codes for bridge piers, so higher drift design requirements imply a strong inelastic behaviour of the rc members.

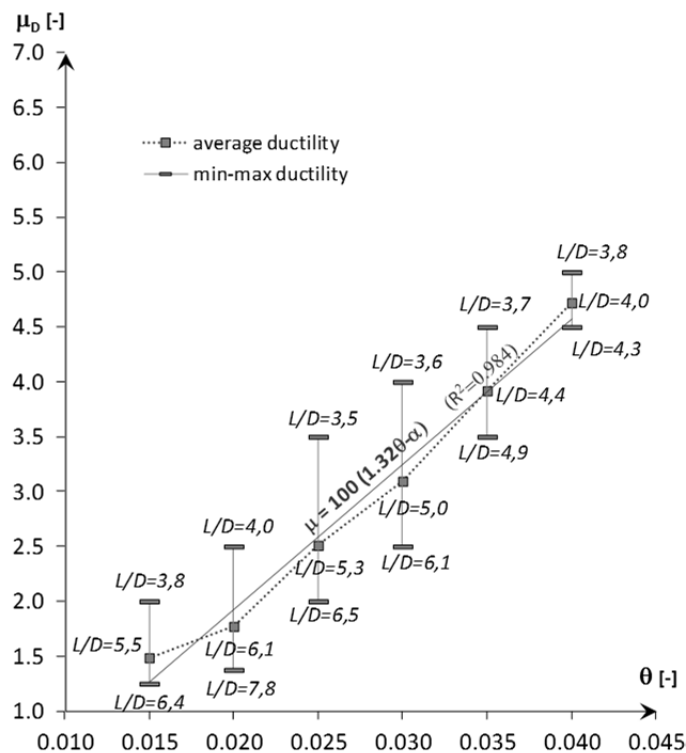


Fig. 3.16 – Intervals for ductility demand, μ_d , versus drift θ , obtained for the realistic design cases analyzed, and interpolating line approximating values corresponding to medium T_{eff} values of the design intervals.

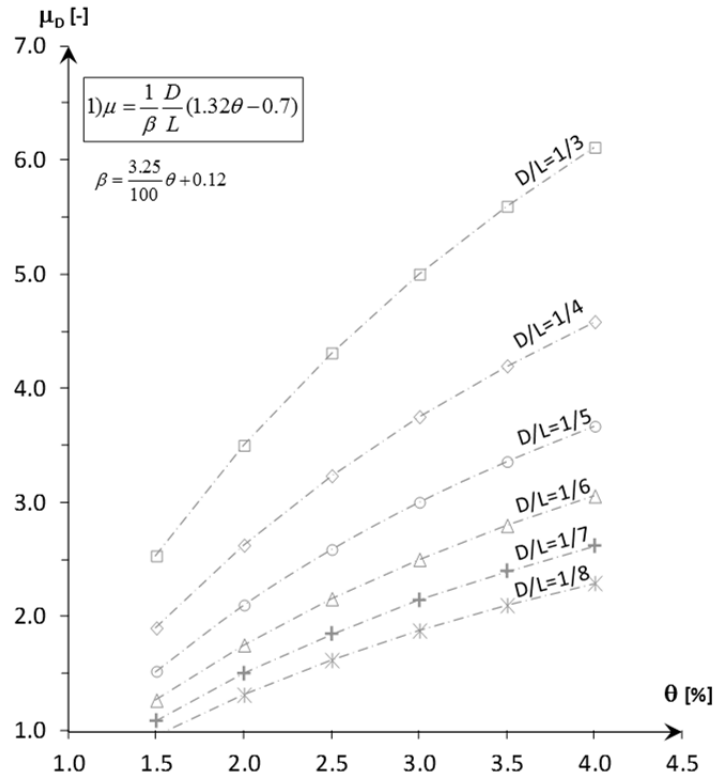


Fig. 3.17 – Approximate relation μ_D , versus drift θ , and curves obtained for some pre-defined values of L/D (Eq. 3.30)

Observing that the ductility ratio between the medium value, represented by the interpolating line, and the an extreme value of the interval, corresponds approximately to the (D/L) ratio of the corresponding columns, it was possible to derive the more general relation, given by (Eq. 3.30), and plot a series of curves for prefixed (D/L) values, extending the ranges previously obtained (see Fig. 3.14).

$$\mu = \frac{1}{\beta} \frac{D}{L} (1.32\theta - 0.7) \quad (3.30)$$

where $\beta = \frac{3.25}{100} \theta + 0.12$, and θ expressed as (%).

3.5 CONCLUSIONS

This work provides an estimate of the medium error committed by the current DDBD method for the design of SDOF structures, with specific reference to isostatic bridge piers (cantilever piers conform to the assumption of SDOF systems). It could be useful to know “prior” the accuracy of the method, namely the error that the simplified procedure introduces, the main error sources being the approximation of a substitute linear structure characterized by the equivalent viscous damping ξ_{eq} , and the scaling of the displacement elastic spectrum through the modification damping factor R_ξ .

In the first part of the study a parametrical analysis has been developed on a large sample of ideal SDOF oscillators (4212), discussing the influence of different equivalent damping models ξ_{eq} [D1], [G1], [J1] for the linearization of non linear system.

The SDOF ideal systems were designed according to the DDBD procedure, and subsequently verified with Non Linear Time History (NLTH) analyses, performed for the same set of non linear simple oscillators (based on Takeda Thin hysteretic model). The effect on the scaling of elastic spectra with different reduction factors R_ξ is also discussed, with reference to current formulations [N1],[X1],[X2].

The method is shown to be generally conservative, at least for structures with $T_{eff} < 2.5-3.0s$, with overestimation errors for ideal SDOF oscillators significantly dependent on design ductility level, while underestimation errors are almost never relevant. As final result a medium error diagram [T1] is presented, which summarizes the scatter in the results as a function of design ductility μ_Δ^d and effective period T_{eff} .

In the second part a realistic displacement-based design process for cantilever rc piers with flexural behaviour is carried out, to investigate the range of the variables μ_Δ^d and T_{eff} within the possible design solutions. An ample set of circular columns were designed for drift values between 1.5 and 4.0%, and “realistic” design limits have been fixed in terms of slenderness, amount of reinforcement, normalized axial load and height-diameter ratio. Using the medium error diagram previously obtained, the error range for reinforced concrete bridge piers is derived for the realistic design cases analyzed.

It can be observed that underestimation errors are modest for any realistic design, almost always less than 10%, with few cases (6%) with relative error just slightly higher ($E_m < 12\%$); as regards the overestimation error range, as already evidenced for ideal SDOF systems, the accuracy is strongly dependent on design ductility. For low-medium ductility design cases ($\mu_d \leq 1.5$), the DDBD method is again very accurate, $E_m < +10\%$, while for high ductility values, ($1.5 < \mu_d \leq 3.5$), the relative error is higher, even if most still acceptable in most of the design cases ($E_m < +30\%$ in 90% of design cases).

Finally an approximate relationship between ductility and drift is derived, and parametric curves are plotted for pre-fixed values of D/L ratio.

CHAPTER 4

DISPLACEMENT-BASED DESIGN FOR TRANSVERSE RESPONSE OF CONTINUOUS RC GIRDER BRIDGES: ITERATIVE VS DIRECT PROCEDURES

4.1 INTRODUCTION

Transverse response prediction for continuous rc girder bridges in a displacement-based framework presents some critical issues related to representativeness of the equivalent SDOF structure in respect to the original MDOF system, particularly in the estimation of the design displacement profile in the case of irregular bridges (see also § 2.2).

Transverse seismic response of multi-span continuous bridges is more complex to evaluate than that of multi-span simply-supported bridges. The presence of a continuous deck precludes the possibility of separating the responses of single piers, which cannot be studied independently as SDOF systems.

In its current formulation (Priestley et al.^[P1], 2007) the Direct Displacement-Based Design method uses a substitute linear equivalent structure (ESDOF), characterized by a secant stiffness K_{eff} , and an appropriate level of equivalent viscous damping ζ_{eq} , in order to represent the seismic behavior of a MDOF system. The equivalent damping value ζ_{eq} , is used to scale the elastic displacement-spectrum through the correction factor R_{ξ} , and consequently to calculate the effective period T_{sys} and the effective stiffness K_{sys} of the ESDOF system. The calibration of the equivalent damping value ζ_{eq} and related factor R_{ξ} , which has to be tied to the hysteretic energy dissipated by the structure in the non linear field, introduces a first approximation^[T1]. Another error component is introduced into the method related to the representation of the real system (MDOF) with an equivalent SDOF, through the definition of the target displacement profile.

In the transverse response of a continuous bridge the relative stiffness between deck and piers affects the ultimate displacement profile, depending on the deck transverse stiffness and the type of bearings at the abutments^[T3]. If the superstructure is effectively rigid and the bearings are very deformable transversally

to the bridge axis, the deck reacts like a rigid body, and the design displacement profile is simplified, being a combination of rigid translation and rotation (Dwairi and Kowalsky, 2006). Conversely, when the abutment bearings are fixed transversally, the superstructure is subjected to a transverse global deformation for the entire length of the bridge (with fixed points at the abutments), restraining the pier top displacements proportionally to its transversal stiffness. Deck flexural stiffness under lateral force is generally higher than that of piers. The superstructure is assumed to be elastic, and the only elements undergoing plasticity are the piers.

The inelastic displacement profile is also conditioned by the pier transverse stiffness relative ratios, depending on the pier strengths and ductilities, that are not initially known (Priestley et al., 2007). For this reason, in the case of continuous bridges the current suggested procedure is iterative, being the ultimate displacement shape an input value of the DDBD method.

It seems evident that the system regularity can significantly affect the reliability of the DDBD simplified method, based on the assumption that the structural response is represented by a simple ESDOF system, and controlled by the fundamental mode (inelastic first mode). For highly irregular structures several modes should be considered to determine the kinematic mechanism of the structure, and this could be certainly the case of girder bridges with non-symmetric distribution of piers, especially with long spans, thus higher mode effects are of necessity to be incorporated in the DDBD procedure to estimate flexural strengths^[A5]. Moreover, if concentrations of nonlinearity are very high, the system deformed shape forecast by modal analysis (i.e. based on the superposition of the deformed shapes associated with the modes of the elastic structure) may be very different from the actual deformation sustained by the bridge during a seismic event and this nullifies the prediction of deformation and force distribution^[G3].

This chapter investigates the accuracy of the current iterative Direct Displacement-Based method (called DBD-IT in this work) when applied to the prediction of the transverse response of multi-span continuous girder bridges, and compares it to a non-iterative (direct) design method, named DBD-DEM, herein proposed with the aim of simplifying the current procedure for everyday design use.

The numerical analyses are carried out considering multiple configurations of regular and irregular continuous bridges with 4 to 6 spans, designed with target drift limits of 1% to 4%, and subsequently checked with non linear time history analysis. The parametric study is performed on the transverse response of multi-span continuous bridges with the abutment bearings transversally fixed; the aim is to quantify the errors for a wide range of bridge configurations in respect to non-linear Time-History analysis, and try to evidence the error components related to equivalent viscous damping calibration (ESDOF system) and the inelastic displacement shape estimation.

At the same time, the DBD-DEM procedure, implemented in a non-iterative fashion, is evaluated. The DDBD process based on a substitute equivalent SDOF structure is applied in one direct step, by assuming an initial estimate of the displacement profile Δ_{1i} and obtaining the effective pier stiffnesses $K_{eff,j}$ and the system damping ξ_{eq} . Subsequently the values $K_{eff,j}$ are assigned to calibrate the piers' stiffnesses in a spectral response analysis, where the design spectrum is damped according to the ξ_{eq} value. In this way a better estimation Δ_{2i} of the inelastic displacement profile is obtained by normalizing the displacement shape δ_{2i} calculated by SRA, to the critical displacement Δ_c , while shear forces and moments are calculated consequently. Using SRSS superposition, the effects of higher modes can be included when they are significant; it is assumed that ductility substantially influences only the first-mode response (Priestley et al., 2007), and the higher mode effects are the same in the inelastic range as in the elastic range.

It has to be noted that the proposed DDBD-DEM method has the relevant advantage of being a direct procedure, maintaining and also enhancing the accuracy of the DBD-IT approach when compared on the same case-studies set.

4.2 ISSUES RELATED TO THE PROPOSAL OF THE DBD-DEM PROCEDURE

The displacement-based method herein presented, called DirectEffectiveMethod (DBD-DEM), descends from the Effective Modal Superposition (EMS) initially proposed by Alvarez^[A3], 2004, Ortiz^[O2], 2006, subsequently supported by Priestley et. al^[P1], 2007, and recently adopted also by Adhikari et al.^[A5], 2010.

The EMS method uses a ResponseSpectrumAnalysis (RSA) after completion of the DDBD (iterative) procedure, whereby stiffness of members with plastic hinges (e.g. piers) is represented by secant stiffness to the peak displacement response, while elastic members (e.g. superstructure) are modeled by initial stiffness value, and seismic hazard is defined by a 5% damped elastic design spectrum (see also §2.2). In the EMS procedure the final results are obtained combining the higher mode-elastic forces from SRA with the DDBD inelastic first mode design forces, using SRSS or CQC combination rule. In previous approaches^[A3,O2,P1] higher mode effects were considered only for determining the design elastic responses (e.g. transverse moment at deck, abutment shear force, etc.), and flexural strength at plastic hinges was taken from the inelastic first mode, while recently^[A5] higher mode effects have been incorporated in the DDBD procedure for estimating flexural strengths too.

The above mentioned procedures were anticipated by another work^[K3], by Kowalsky M.J., 2002, where the concept of an *effective mode shape* was already introduced: the displacements of columns and abutments were obtained by an

appropriate combination of modes, such as SRSS, and the effective shape was used iteratively in the DDBD framework to calculate the ESDOF properties at the target displacement. Once the base shear global force was calculated, the force distribution was assigned according to Eq. 2.67 (with $\alpha=1$), under the hypothesis of all columns having the same longitudinal steel ratio and column diameter. In the work by Kowalsky, there wasn't yet the idea of subdividing explicitly the lateral force x carried by the superstructure bending load path, which was introduced later (see the procedure in §2.2.2.4); moreover high errors were evidenced at abutment locations.

The modifications introduced by the DBD-DEM procedure described below address the following issues:

- Simplification of the design process, the proposed method relying on a non-iterative procedure. In its original aim DDBD was to be a direct and simplified design method (hence the name "Direct" DB procedure), while the current form (but also the previous versions mentioned above) requires iterations for transverse bridge design, otherwise than the simplified approach used for all other kinds of structures. Even if the specific reasons that led to the current definition were well grounded, of an iterative design process, it seems to the author the attractiveness of a direct method should be maintained also for the design of continuous girder bridges..

- Use of a general ResponseSpectrumAnalysis to account for higher mode effects in the prediction of the inelastic displacement pattern. Recently several authors have demonstrated that simplified methods based on the ESDOF representation of MDOF systems, relying on the assumption that inelastic behaviour can be controlled only by a single mode, suffer shortcomings when applied to highly irregular structures^[K5, A5]. The RSA represents the most general approach for the linear analyses of irregular structures and can conveniently be adopted also in Displacement-Based Design. In DBD-DEM method the effective stiffness of the linearized system at the target displacement is predicted by using the DBD framework, and subsequently the contribution of higher mode effects is added with an appropriate combination of modes, such as SRSS (assuming that higher mode effects in the inelastic range are the same as in the elastic range).

- Possibility of assigning different flexural strengths to piers: the current DBD-IT procedure allows the irregular distribution of flexural strength among piers with the modification proposed by Adhikari et al.^[A5], 2010, introduced in Eq.2.67 with factor α_j .

In the end the DEM procedure uses the DDBD framework to calibrate the estimate of effective pier stiffness $K_{eff,j}$ and global damping ξ_e , which are subsequently used to execute a ResponseSpectrumAnalysis, where the usual approximations related to the choice of element stiffness and spectrum reduction factor are eliminated or at least reduced on the base of DDBD results.

4.3 DBD-IT AND DBD-DEM PROCEDURE

The current iterative DDBD procedure^[P1] for transverse design of continuous bridges has been described in detail in §2.2.2.4, and the flowchart of the process represented in Fig. 2.11. The reader is addressed to Chapter 2 for a detailed coverage of this topic.

In the DirectEffectiveMethod (DEM) herein proposed, the DDBD procedure based on a substitute equivalent SDOF structure is applied only in one direct step. The procedure needs the support of an elastic F.E. model, because linear static analyses (LSA) and a spectral response analysis have to be carried out.

The design process can be summarized as follows:

a) Initial displacement shape estimate. The initial displacement vector δ_{1i} is assumed as an initial estimate of the first modal shape. The objective is to obtain a displaced shape, wherein the performance target is reached by the pier (or abutment), identified as the critical member.

It is suggested to perform a modal analysis with a cracked stiffness for piers (elastic properties should be used for the superstructure), reducing it uniformly for all piers, or better (as in the examples presented in this paper) taking as yield secant stiffness the initial value reduced to 60%, and then scaling it for each pier through the displacement ductility factor μ_{Δ}^j (that can be obtained directly from the design drift). Abutment stiffness can be assumed as 30% of the initial elastic stiffness.

This displacement shape is then normalized to the critical displacement Δ_c , to obtain the initial displacement profile:

$$\Delta_{1i} = \delta_{1i} \left(\frac{\Delta_c}{\delta_c} \right) \quad (4.1)$$

b) Estimate of the lateral force fraction carried by superstructure. The value of the lateral force fraction x , carried by the superstructure, can be calculated through a static analysis (LSA) of the system with imposed transverse displacements Δ_{1i} and pier stiffness calculated before.

$$V_{a1} + V_{a2} = x V_{base} \quad (4.2)$$

c) Determination the ESDOF system properties and displacement. In order to characterize the multi-span continuous bridge as a corresponding SDOF structure, various equivalent system properties have to be identified: effective displacement Δ_{eff}^d , mass M_{eff} , height H_{eff} and damping ξ_{eff} of ESDOF system have to be evaluated as in the typical DDBD design process, by using the following expressions:

$$\Delta_{eff}^d = \frac{\sum_{i=1}^{n^o} mass(m_i \Delta_i^2)}{\sum_{i=1}^{n^o} mass(m_i \Delta_i)} \quad (4.3)$$

$$M_{eff} = \frac{\sum_{i=1}^{n^o} mass(m_i \Delta_i)}{\Delta_{eff}^d} \quad M_{eff} = \frac{\sum_{i=1}^{n^o} mass(m_i \Delta_i)}{\Delta_{eff}^d} \quad (4.4)$$

$$H_{eff} = \sum_{i=1}^n (m_i \Delta_i h_i) / \sum_{i=1}^n (m_i \Delta_i) \quad (4.5)$$

where m_i , Δ_i , h_i are respectively the i -th mass, its displacement and height (the offset due to the deck height is accounted for in the calculation of h_i in respect to H_j of the pier).

$$\xi_{eff} = \frac{x \Delta_{eff}^d \cdot 0,05 + (1 - x) \left(\sum_{j=1}^{n^{\circ} piers} \frac{C}{H_j} \cdot \Delta_j \xi_j \right) / \sum_{j=1}^{n^{\circ} piers} \frac{C}{H_j}}{x \Delta_{eff}^d + (1 - x) \left(\sum_{j=1}^{n^{\circ} piers} \frac{C}{H_j} \cdot \Delta_j \right) / \sum_{j=1}^{n^{\circ} piers} \frac{C}{H_j}} \quad (4.6)$$

where H_j , Δ_j , ξ_j , are the height, top displacement and damping, calculated with Eq.(2.2), of the j -th pier . Elastic damping (5%) is adopted for the superstructure, and its displacement is assumed to be equal to the system displacement Δ_d^{eff} .

The coefficient $C = \alpha_j$ is taken for yielded piers, while the modifying factor $C = \alpha_j \mu_j$ has to be assumed for piers remaining elastic under seismic excitation, with α_j representing the assumed ratio of the flexural strength of a pier to the strength of the critical pier (often $\alpha_j = 1$ for all pier for convenience).

d) Determination of the design base shear of the ESDOF system. To determine the effective period T_{eff} , entering the displacement spectra (damped trough the R_ξ factor) are entered with Δ_{eff}^d . The effective stiffness K_{eff} and the total base shear V_{base} (considering the P- Δ effects) are calculated as follows:

$$K_{eff} \cong 4\pi^2 \frac{M_{eff}}{T_{eff}^2} \quad (4.7)$$

$$V_{base} = K_{eff} \Delta_{eff}^d + 0,5 P \Delta_{eff}^d / H_{eff} \quad (4.8)$$

e) Estimate of the effective stiffness of piers. Distributing total base shear V_{base} for each pier in a simplified way (proportional to “ $1/H_j$ ” for yielded piers, and to “ μ_Δ/H_j ” for elastic piers), the i -th pier effective stiffness estimate $K_{eff,j}$, is obtained as follows:

$$V_j = (1 - x) V_{base} \left(\frac{C}{H_j} / \sum_{j=1}^{n^{\circ} piers} \frac{C}{H_j} \right) \quad (4.9)$$

$$K_{eff,j} = V_j / \Delta_{1j} \quad (4.10)$$

f) Estimate of the modal effective shape. A spectral response analysis (SRA) is performed to obtain a better estimate of the inelastic effective shape δ_{2i} . $K_{eff,j}$ values for piers and a displacement spectrum damped by the factor $R_\xi(\xi_{eff})$ are used.

g) Estimate of the inelastic design profile and related effective stiffnesses of piers. The modal effective shape δ_{2i} determined at the previous step, is normalized with Eq. 4.1 to the critical displacement Δ_c , in order to obtain the inelastic design profile estimate Δ_{2i} while the related final estimate of pier effective stiffness is obtained as:

$$K'_{eff,j} = K_{eff,j} \left(\frac{\delta_c}{\Delta_c} \right) \quad (4.11)$$

in the simplified hypothesis that the post-yield stiffness of global Force-displacement curve is zero (extensions can be easily derived for a residual constant post-yield stiffness).

h) Estimate of the design strength required. Shear force F_j carried by each pier is calculated considering the obtained displacement profile Δ_{2i} , and the final estimate of pier effective stiffness $K'_{eff,j}$ (Eq. 4.10). The design moment M_j is finally calculated.

$$F_i = K'_{eff,i} \Delta_{2i} \quad (4.12)$$

$$M_{base,i} = F_i H_i \quad (4.13)$$

i) Reinforcement design. Reinforcement in critical sections is designed for forces estimated in the previous step and capacity design principles are applied for the design of other sections.

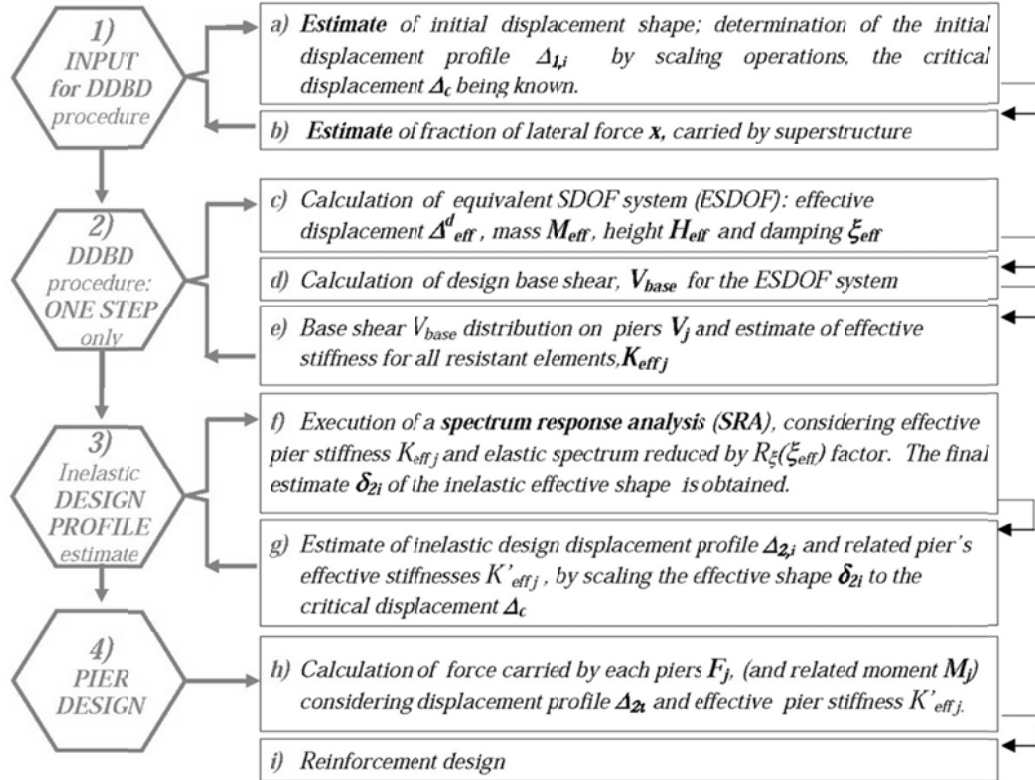


Fig. 4.1 –Flowchart of the proposed DBD-DEM procedure for transverse design of continuous bridges

4.4 CASE-STUDIES AND REGULARITY OF BRIDGES

In the parametric study, a set composed by 36 different bridge configurations was analyzed; 8 different four-spans bridge geometries and other 10 six-spans were considered, with terminal span of 40m and central ones 50m long. Two different deck types were adopted^[T1], a PrestressReinforcedConcrete (PRC) box girder deck, and a composite SteelConcrete (SC) deck. The PRC deck is characterized by a transverse bending stiffness $E_C J_{22}$ about three times higher than the SC deck (for simplicity the SC deck was replaced in the F.E. model with an equivalent steel box section, $J_{22,PRC} \approx 15J_{22,SC}$). Concrete C40/45 and reinforcement steel B450C were used for piers, while concrete C75/85 for PRC deck and structural steel S355 were used for deck materials.

Deck properties are reported in Table 4.1, and all bridge geometrical configurations are presented in Table 4.2. Each bridge is identified by the deck code and the specific sequence of piers height values (e.g. PRC132), where $H=1$ is the reference height equal to 4.0m. All piers are single cantilevers, with circular sections of variable diameter D (specified in Table 4.2); in the transverse direction the superstructure is assumed to be connected to the piers with fixed bearings, and lateral restraints are provided at the abutments.

The case study set was chosen considering regular and irregular configurations: the structural regularity of a continuous bridge is difficult to be evaluated before the analysis with reference to the transverse response, since the elastic behaviour of the deck interact with the non linear response of piers during the seismic excitation. Some authors evaluated structural regularity through various approaches that resulted in different regularity indexes: some studies refers to the participating modal mass as a parameter of regularity (Calvi et al.^[C5], 1989), whereas other use parameters comparing the modal behaviour of the single deck and of the whole bridge in linear phase (Calvi and Pinto^[C6], 1996).

In this study a relative stiffness index, RS , is introduced to relate superstructure and piers' transversal stiffness (Priestley et al.^[P1], 2007):

$$RS = K_s / \sum_{i=1}^n K_{pi} \quad (4.14)$$

where K_s is the transversal stiffness of the deck, derived from the static scheme of a simply-supported beam spanning between the abutments and undergoing a uniform load:

$$K_s = 384/5 \cdot (EI)_s / L_s^3 \quad (4.15)$$

and K_{pi} is the transverse pier stiffness

$$K_{pi} = 1 / (1 / K_f + 1 / K_v) \quad (4.16)$$

$$K_{fi} = 3(EI)_{pi} / H_{pi}^3 \text{ and } K_{vi} = GA_{pi} / H_{pi} \text{ (negligible for slender piers).}$$

In this paper the RS index is calculated considering the effective pier stiffness $K_{pi,e}$, taking as yield secant stiffness the initial value reduced to 60% and then scaling it by the ductility factor μ_{Δ}^j for a drift level $\theta=3\%$. The ductility is calculated considering Δ_u^j as obtained directly from the design drift for a sine-based displacement shape, and estimating the yield displacement Δ_y^j .

Tab. 4.1 – Properties of the PRC deck and the equivalent steel box, substitutive of the composite SC deck.

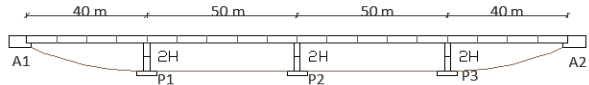
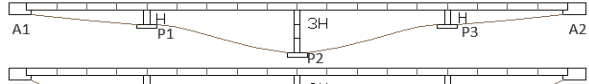
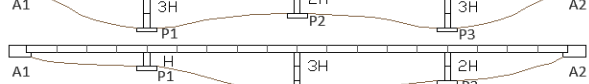
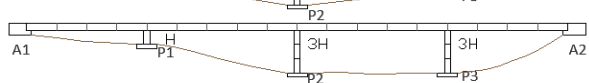
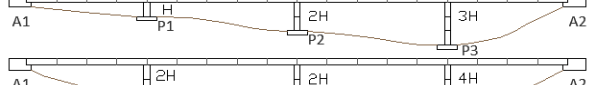
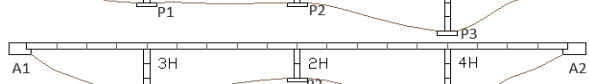
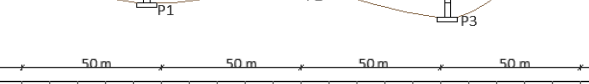
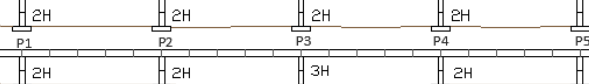
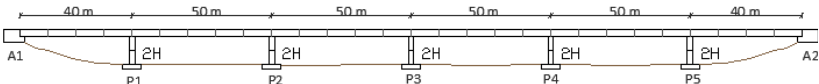
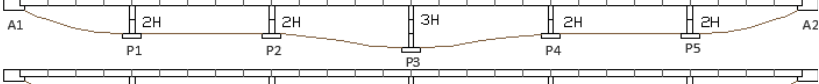
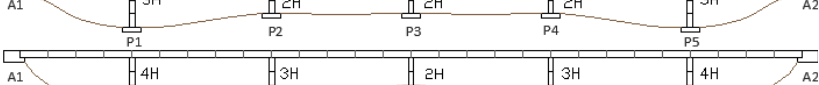
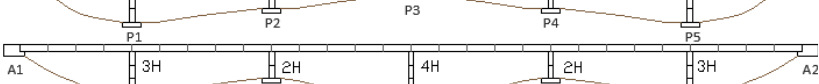
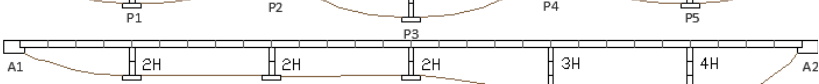
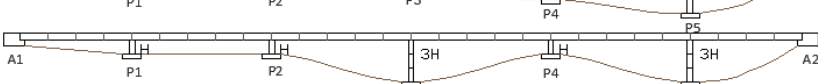
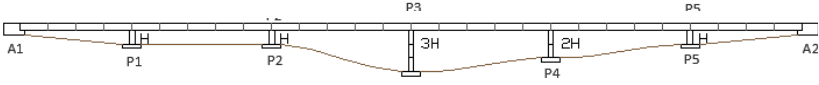
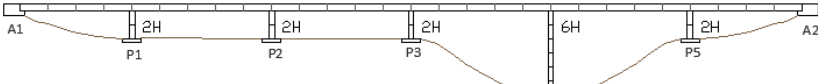
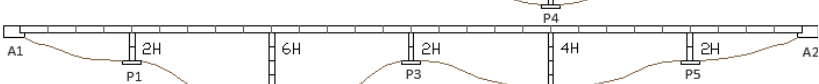

<p>PRC deck- $A=7.3m^2$ $J_{22}=81m^4$, $J_{11}=8.0m^4$, $J_t=15.53m^4$, $E_c=40.82GPa$ $W=220$ kN/m</p>	<p>SC deck- $A=0.75m^2$ $J_{22}=5.4m^4$, $J_{22}=0.61m^4$, $J_t=1.8m^4$, $E_s=206GPa$ $W=150$ kN/m</p>

In Tab. 4.2 the values of the coefficient RS for the different bridge configuration is reported.

Tab. 4.2– Relative Stiffness index RS calculated for 4-spans and 6-spans bridges configurations with PRC and SC deck.

	RS_{PRC}	RS_{SC}
222	4.2	1.6
131	5.0	2.2
323	5.0	1.8
132	3.5	1.5
133	3.9	1.7
123	3.2	1.3
224	3.8	1.5
324	4.1	1.6
22222	1.7	0.8
22322	2.2	0.9
32223	2.1	1.0
43234	2.2	1.0
32423	2.2	1.0
22234	1.3	0.6
11313	1.1	0.4
11321	1.6	0.6
22262	1.7	0.7
26242	1.1	0.4

Tab. 4.3 – Bridge configurations.

Geometric configuration	Bridge	D_{pier} [m]
	PRC/SC 222	1.95/1.85
	PRC/SC 131	1.65/1.50
	PRC/SC 323	2.00/1.95
	PRC/SC 132	1.95/1.80
	PRC/SC 133	2.00/1.85
	PRC/SC 123	2.00/1.90
	PRC/SC 224	2.30/2.20
	PRC/SC 324	2.30/2.20
	PRC/SC 22222	2.00/1.80
	PRC/SC 22322	2.05/1.85
	PRC/SC 32223	2.00/1.80
	PRC/SC 43234	2.30/2.10
	PRC/SC 32423	2.20/1.95
	PRC/SC 22234	2.50/2.30
	PRC/SC 11313	2.00/2.00
	PRC/SC 11321	1.90/1.80
	PRC/SC 22262	2.65/2.55
	PRC/SC 26242	2.70/2.55

4.5 GROUND MOTION AND PERFORMANCE CRITERIA

The reference design spectrum used for the parametrical analysis was derived from the smoothed elastic spectrum “Type 1” presented in EN 1998-1:2004, with the following assumptions: type C soil ($S=1.15$, $T_B=0.20s$, $T_C=0.6s$, $T_D=2.0s$), peak ground acceleration $PGA=0.35g$, return period $T_R=475$ years (reference occurrence probability $P_{LR}=10\%$ in a reference period $T_L=50$ years).

According to the modifications proposed by Faccioli et al.(2004) and supported by Calvi et al. (2009), the corner period value T_c was modified in order to correlate it to the effective magnitude value acting in situ (a magnitude $M_w = 6,9$ was assumed), using Eq.2.13.

The reference spectrum was subsequently scaled in order to fit the seismic design intensity levels required for a Class of Importance III, that has to be adopted for bridge structures (Calvi et al. [C2], 2009):

Level 1 (L_1): $p=20\%$ in 50years

Level 2 (L_2): $p=4\%$ in 50years

Level 3 (L_3): $p=1\%$ in 50years

The coefficient of importance given in EN 1998-1:2004^[X2] was used to scale the reference PGA, obtaining:

$PGA_1=0,28g$ for L_1

$PGA_2=0,49g$ for L_2

$PGA_3=0,77g$ for L_3

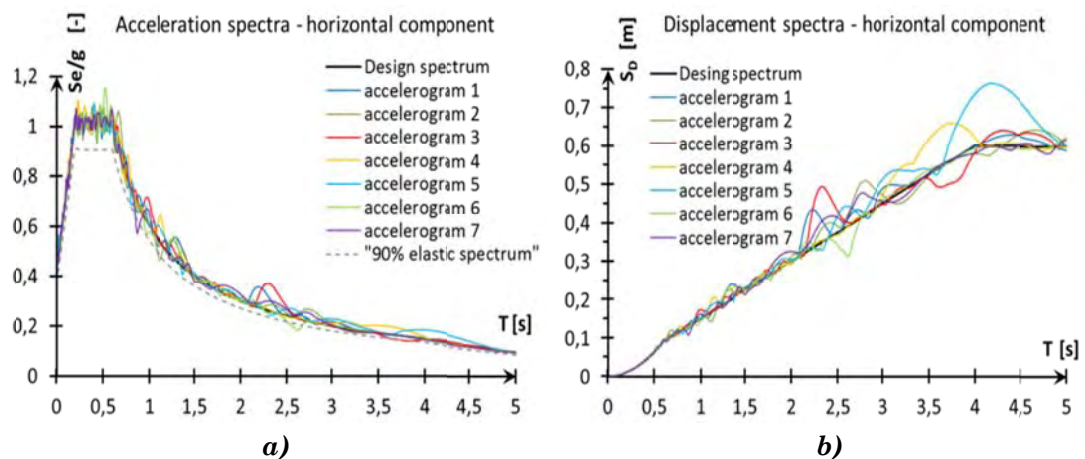


Fig. 4.2 –Acceleration and displacement smoothed design response spectrum sumperimposed with spectra generated by synthetic compatible ground motions

In the present study the displacement elastic response spectra, are reduced by a scaling factor R_{ξ} , according to an equivalent viscous damping model ξ_{eq} calibrated with reference to the Takeda Thin hysteretic law (well-representative of structural elements with significant axial loads, such as bridge piers).

Eqs. 2.55, 2.56 are used for the formulation of ξ_{eq} and R_{ξ} respectively.

Seven synthetic acceleration records, compatible with the proposed design spectra were generated with SIMQKE program (Gasparini and Vanmarke^[G4], 1976), and used as input ground motions in non-linear Time History analyses for the verification study. The seismic input to all piers was assumed coherent and in phase: possible effects due to spatial variability of ground motion were not considered.

Two limit drift values θ were considered for of each sample in the case-study set as performance criteria for high-ductility design, according to the reference values proposed by Calvi and Sullivan^[C2], 2009: drift limit $\theta_L=3\%$ was defined for Level 2 (damage-control) of earthquake design intensity, while value $\theta_L=4\%$ was chosen for Level 3 (collapse prevention), though probably representing an upper limit for usual design. In addition a very low drift $\theta_L=1\%$ was considered for serviceability limit state (Level1) in order to obtain low ductility design cases, with pier mean ductility value close to 1.

In the end the series of models investigated in the parametrical analyses are the following:

Series 1: $\theta_L=1\%$, symmetric bridge configuration with PRC and SC deck, 4-spans (PRC/SC 222, 131, 323) and 6-spans (PRC/SC 22222, 22322, 32223, 43234, 32423).

Series 2: $\theta_L=1\%$, asymmetric bridges with PRC and SC deck, 4-spans (PRC/SC 132, 133, 123, 224, 324) and 6 spans (PRC/SC 22234, 11313, 11321, 22262, 26242).

Series 3: $\theta_L=3\%$, same bridge configurations as Series 1.

Series 4: $\theta_L=3\%$, same bridge configurations as Series 2.

Series 5: $\theta_L=4\%$, same bridge configurations as Series 1.

Series 6: $\theta_L=4\%$, same bridge configurations as Series 2.

4.6 VERIFICATION STUDY

In order to verify the procedures in terms of meeting the design displacement and hence damage levels, the bridges were subjected to NonLinearTimeHistoryAnalyses (NLTHA). The accuracy of the DBD-IT and DBD-DEM procedures were evaluated through NLTHA using the free available software Opensees (2006); numerical models reproduce the 3D real bridges' geometries, incorporating the realistic distribution of mass and stiffness, and using elastic elements for the superstructure and fiber discretization for piers with the implicit Force-Based element representation. (see Fig.4.3).

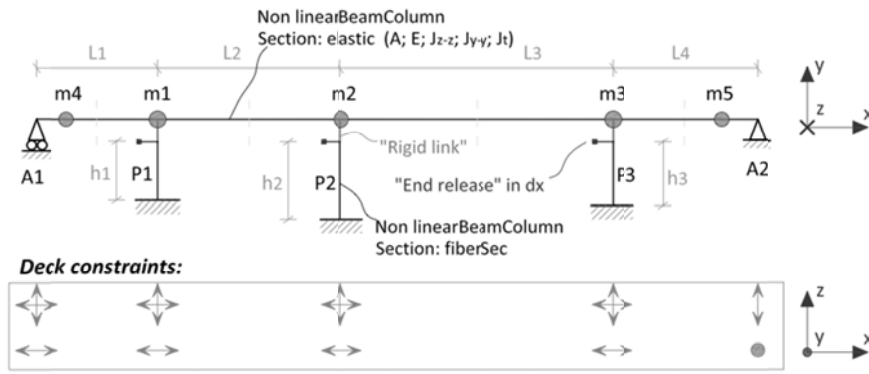
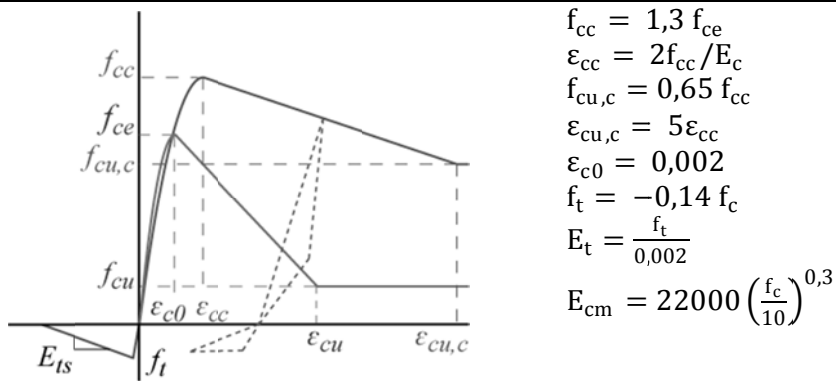


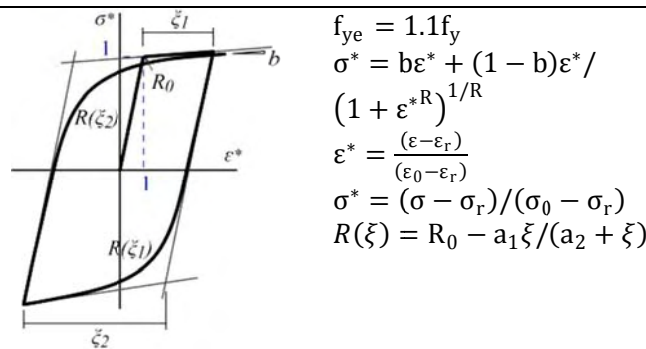
Fig. 4.3 – Conceptual model considered for the TH analyses.

The material models adopted are reported in Tables 4.3, 4.4; for confined and unconfined concrete the model *Concrete 02* was used (implemented in Opensees), calibrated on the Mander model, with the parameters set as reported in Table 4.3. The Menegotto-Pinto model was used for cyclic behaviour of steel reinforcement (see also §5.2.4 for more detail on constitutive laws for materials).

Tab. 4.4 – *Concrete02* model. Stress-strain relations with loading and unloading paths for confined and unconfined concrete.



Tab. 4.5 – Menegotto-Pinto model for steel reinforcement



In the verification process, each of the 36 bridge samples (18 geometrical configurations for pier sections and heights and 2 deck types being used, as described before) was previously designed according to the DDBD-IT and DDBD-DEM procedure, for the 3 different performance levels adopted ($\theta=1,3,4\%$), 216 structural designs being executed on the whole. Subsequently each bridge, detailed with longitudinal reinforcement in accordance with the previous step, was subjected to a suite of 7 ground motions (3 accelerograms series for the 3 different design spectra adopted), for a total of 1512 non-linear Time-History analyses.

The average error, indicating whether the displacement design shape is on the whole a reliable representation of the real inelastic displacement profile, is calculated as follows:

$$E_m = \text{mean}_{i=1..N_p} \frac{|\Delta_i^D - \Delta_i^{TH}|}{\text{mean}_{i=1..N_p} \Delta_i^{TH}} \quad (4.17)$$

where N_p is piers' number, Δ_i^D is the i -th pier design displacement of the DBD procedure, Δ_i^{TH} is the i -th pier top displacement obtained by THA (mean value of the 7 accelerograms).

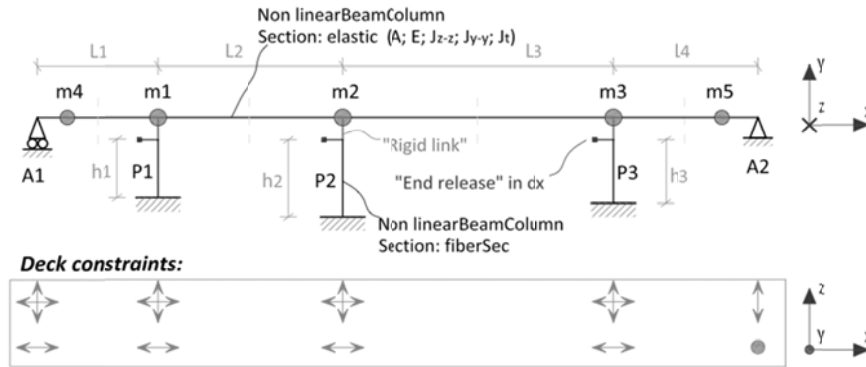


Fig. 4.4 –Conceptual model considered for the TH analyses.

The minimum and maximum error for each pier was also calculated, as:

$$E_{\max, \min} = \max, \min_{i=1..N_p} \frac{\Delta_i^D - \Delta_i^{TH}}{\Delta_i^{TH}} \quad (4.18)$$

In particular the minimum error could be significant to prove whether the simplified method is conservative for the design of each member.

The E_{esdor} error is related to the equivalent viscous damping calibration, and it was introduced with the aim of evidencing the component of the global approximation related to the linearized single degree of freedom system behaviour, by analogy with the study developed in Chapter 3.

The error is evaluated by comparing the ultimate design displacement of the equivalent SDOF system with THA displacement:

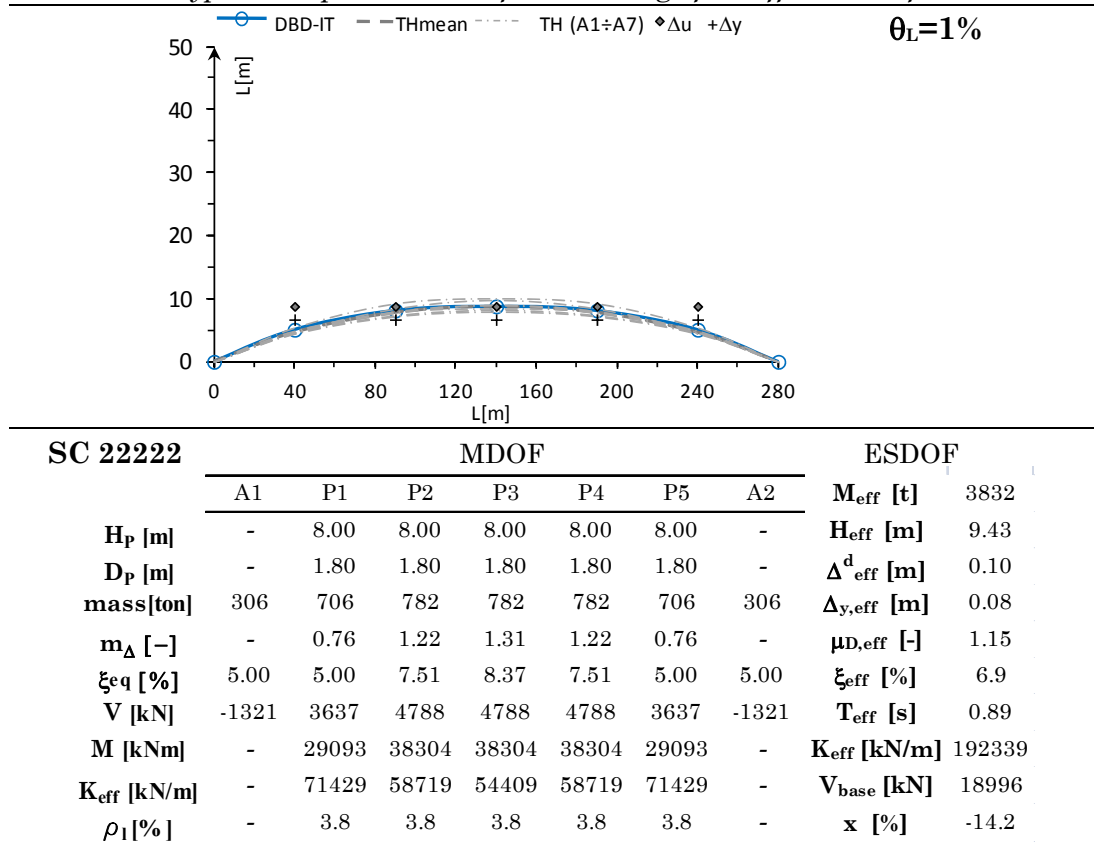
$$E_{esdof} = (\Delta_{esdof}^D - \Delta_{esdof}^{TH}) / (\Delta_{esdof}^{TH}) \quad (4.19)$$

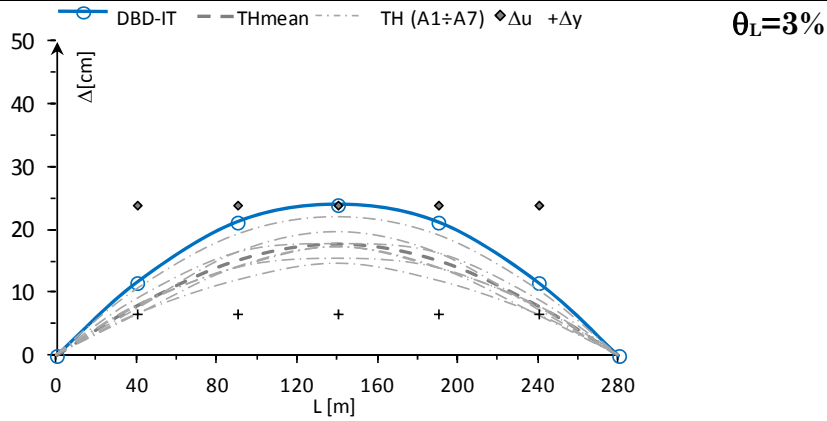
where Δ_{esdof}^D is the design displacement of DDBD procedure, while Δ_{esdof}^{TH} is the ultimate displacement obtained by the ESDOF with non-linear THA (an elastic-perfectly plastic Takeda Thin model is assumed for the ESDOF hysteretic law-see Fig. 3.3).

A typical example of the complete output obtained for the DDBD-IT and DDBD-DEM verification study is reported in Tab.4.6, for the case of a symmetric bridge (PRC22222). The main properties of the ESDOF system are reported (K_{eff} , ξ_{eq}), as well as the piers' required ductility and the piers' design shear and moment for the different Performance Levels adopted ($\theta=1\%,3\%,4\%$).

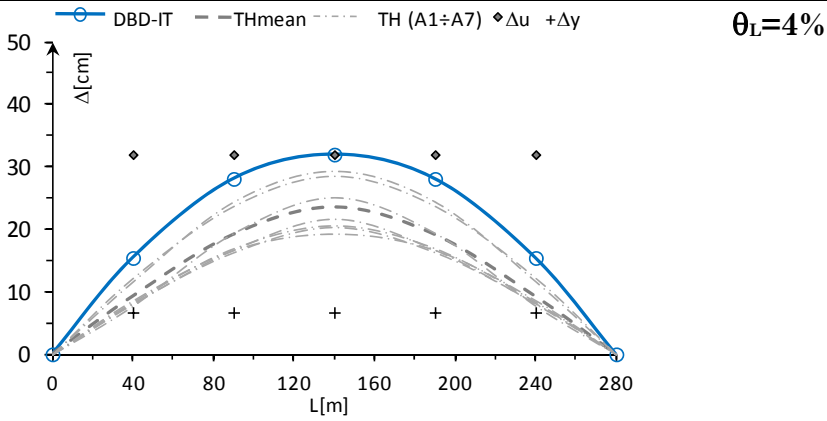
For easiness of reading other detailed results are inserted in Appendix A, with reference to the design procedures DBD-IT and DBD-DEM and NLTH verification for the bridges of Series 3 and 4 ($\theta=3\%$).

Tab. 4.6 – Typical output obtained for one bridge for different Drift Levels θ_L





SC 22222	MDOF							ESDOF	
	A1	P1	P2	P3	P4	P5	A2	M_{eff} [t]	3735
H_P [m]	-	8.00	8.00	8.00	8.00	8.00	-	H_{eff} [m]	9.46
D_P [m]	-	1.80	1.80	1.80	1.80	1.80	-	Δ_{eff}^d [m]	0.25
mass [t]	306	706	782	782	782	706	306	$\Delta_{y,eff}$ [m]	0.10
μ_D [-]	-	1.73	3.17	3.58	3.17	1.73	-	$\mu_{D,eff}$ [-]	2.44
ξ_{eq} [%]	5.00	10.97	14.67	15.19	14.67	10.97	5.00	ξ_{eff} [%]	13.3
V [kN]	-93	2958	2958	2958	2958	2958	-93	T_{eff} [s]	1.62
M [kNm]	-	23667	23667	23667	23667	23667	-	K_{eff} [kN/m]	56241
K_{eff} [kN/m]	-	25506	13943	12327	13943	25506	-	V_{base} [kN]	14606
ρ_1 [%]	-	2.0	2.0	2.0	2.0	2.0	-	x [%]	-1.2



SC 22222	MDOF							ESDOF	
	A1	P1	P2	P3	P4	P5	A2	M_{eff} [t]	3662
H_P [m]	-	8.00	8.00	8.00	8.00	8.00	-	H_{eff} [m]	10.60
D_P [m]	-	1.80	1.80	1.80	1.80	1.80	-	Δ_{eff}^d [m]	0.38
mass [ton]	306	706	782	782	782	706	306	$\Delta_{y,eff}$ [m]	0.14
m_Δ [-]	-	2.30	4.19	4.77	4.19	2.30	-	$\mu_{D,eff}$ [-]	2.68
ξ_{eq} [%]	5.00	13.00	15.76	16.17	15.76	13.00	5.00	ξ_{eff} [%]	13.9
V [kN]	-715	5432	5432	5432	5432	5432	-715	T_{eff} [s]	1.58
M [kNm]	-	43456	43456	43456	43456	43456	-	K_{eff} [kN/m]	57929
K_{eff} [kN/m]	-	35186	19329	16975	19329	35186	-	V_{base} [kN]	22637
ρ_1 [%]	-	4.0	4.0	4.0	4.0	4.0	-	x [%]	-9.2

4.7 SUMMARY OF DBD-IT VS DBD-DEM RESULTS

The verification study results for the two compared methods DDBD-IT and DDBD-DEM are presented in Fig.4.6 in terms of relative errors in respect to TH verification.

It can be observed that the DDBD-IT method is almost always conservative, being $E_{min}(DDBD-IT) > 0$ except in single cases, and the overestimation error tending to increase in the inelastic range for high ductility design cases (i.e. for high drift limit design cases).

The accuracy of the DDBD-IT method appears to be closely related to structural regularity: when applied to very regular bridges, corresponding to uniform or “v-shaped” symmetric configurations with high values of RS index (approximately $RS > 2$), the method is reliable, with a low error range with respect to TH analyses. For low-ductility design cases ($\theta = 1\%$), the mean error range is $E_M(DDBD-IT) < 20\%$, and remains less than 35% for high ductility design cases corresponding to $\theta = 3\%$, ($E_M < 45\%$ for drift $\theta = 4\%$, but this represents a drift upper limit for common design).

Considering all symmetric bridges (on the left of the graphs in Fig.6) the mean error range is $E_M < 25\%$ for $\theta = 1\%$ and $E_M < 50\%$ for high ductility design cases; this overestimation could be considered still acceptable on the basis of the significant approximations introduced by the simplified method. The same error range is valid also for non symmetric bridges with $RS > 2$; this means that the ESDOF system is quite representative also for non-symmetric bridges with a very rigid superstructure dominating the response. For other cases a verification with non linear THA is required; in particular for non-symmetric bridges with $RS < 1$ the error range is unacceptable, being more than 80%. Results show also that E_{esdof} is a small component of the total error, rarely exceeding the value of 10%.

As regards the DDBD-DEM method herein proposed, the results show that, though it's a direct method, it enhances the accuracy of the current procedure, especially for high-ductility design cases. As can be seen from the general error trend, DDBD-DEM generally leads to better results, not only for symmetric bridges (with a decrease of 20-25% of the mean error E_M), for which the iterative current method is already accurate enough, but in particular for irregular cases, being the medium error $E_M(DDBD-DEM)$ always within the range of 55% in respect to THA results. However, the direct estimate obtained with the DDBD-DEM method could not be still satisfactory for irregular cases. A further enhancement can be obtained by modifying the DDBD-DEM method proposed into a two-step procedure: the final displacement shape calculated at the first step, can be used to redistribute more precisely the total effective stiffness K_{eff} of the entire system among piers, obtained with DBD framework (step e). In this way a second, partial step can be

implemented, in which the RSA is carried out again with the new values of stiffnesses for piers.

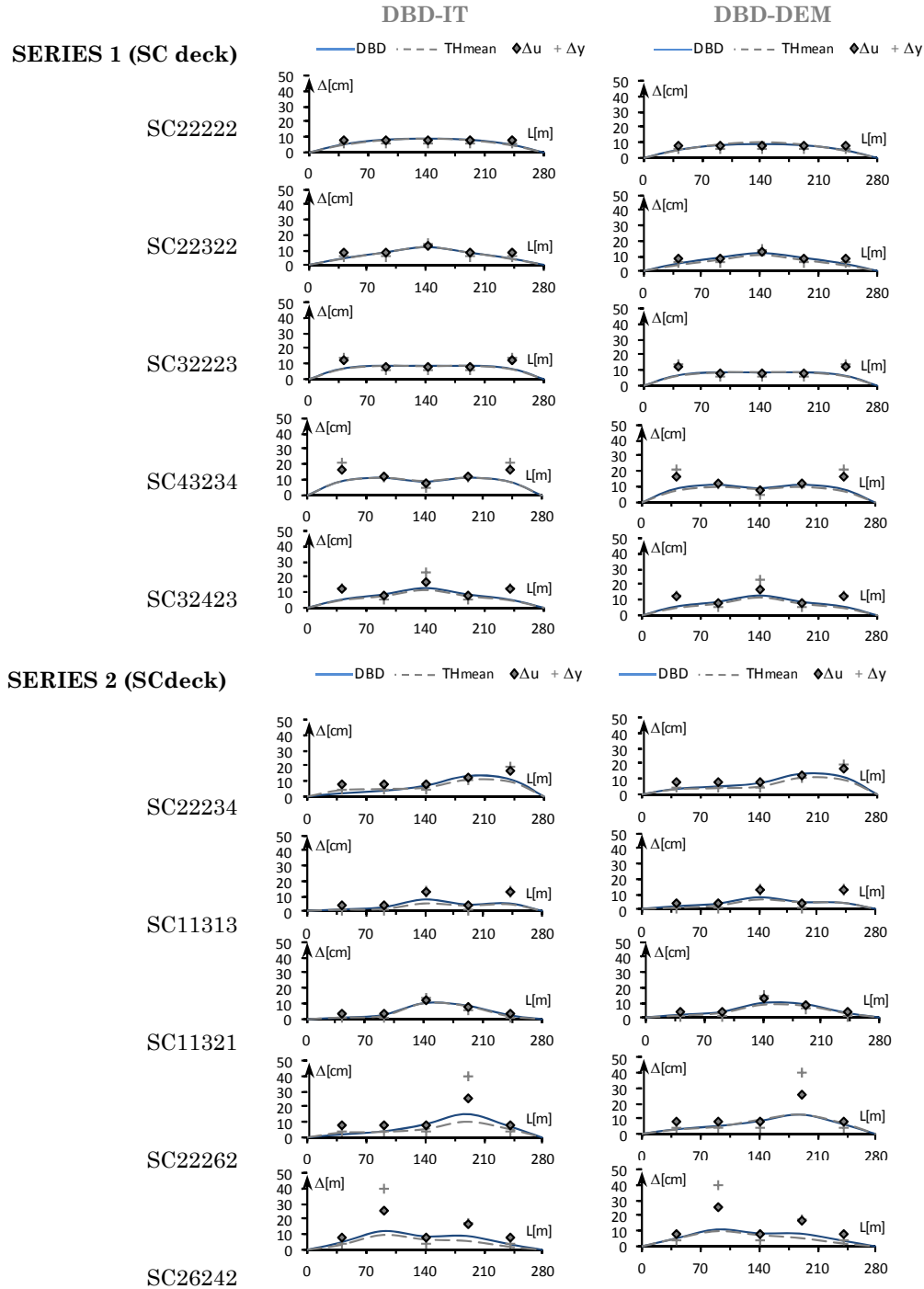


Fig. 4.5 – Series 1-2 bridges with SC deck ($\theta_L=1\%$). DBD-IT and DBD-DEM deformed shaped comparison in respect to THA medium displacement results.

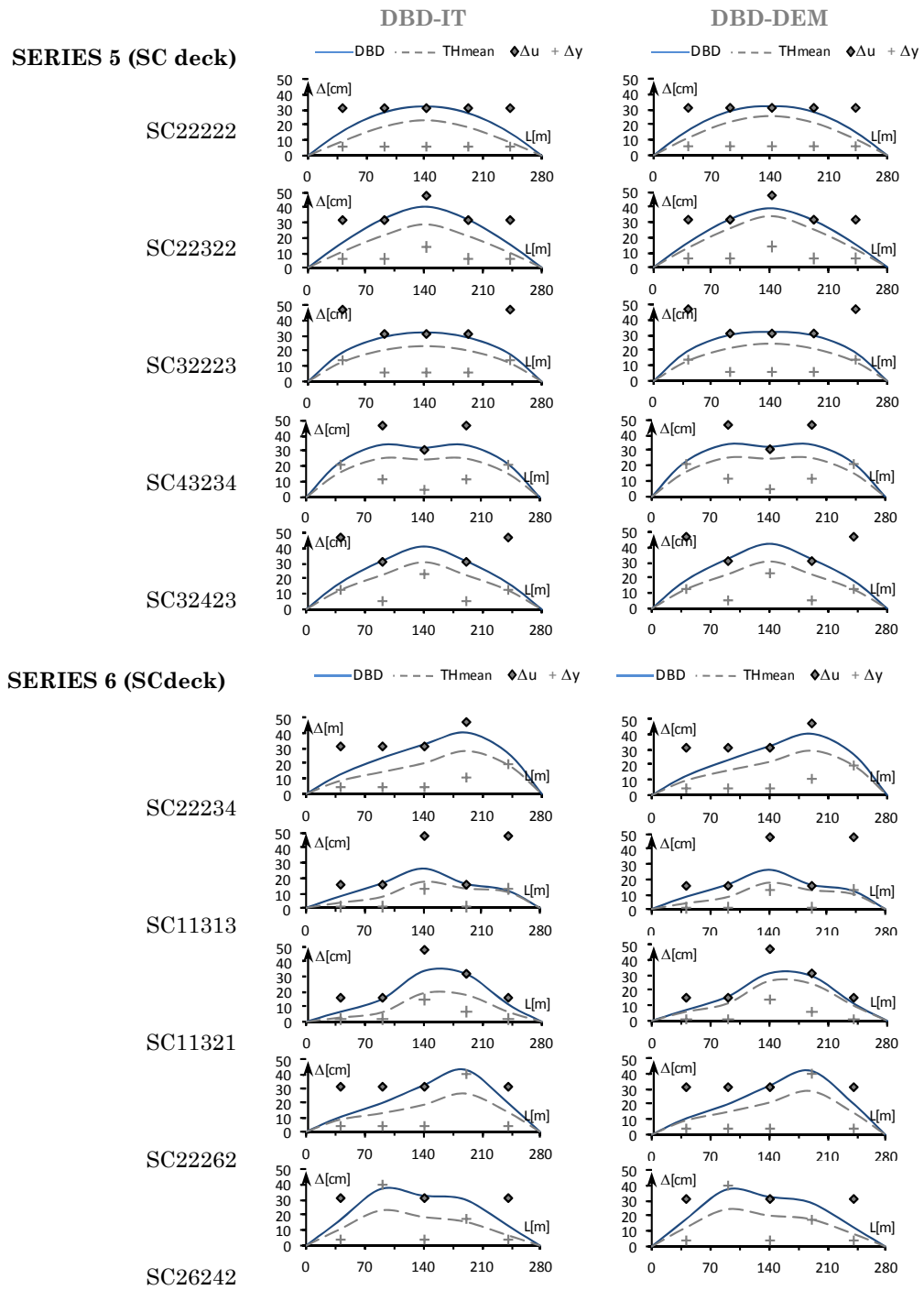


Fig. 4.6 – Series 5-6 bridges with PRC deck ($\theta_L=4\%$). DBD-IT and DBD-DEM deformed shaped comparison in respect to THA medium displacement results

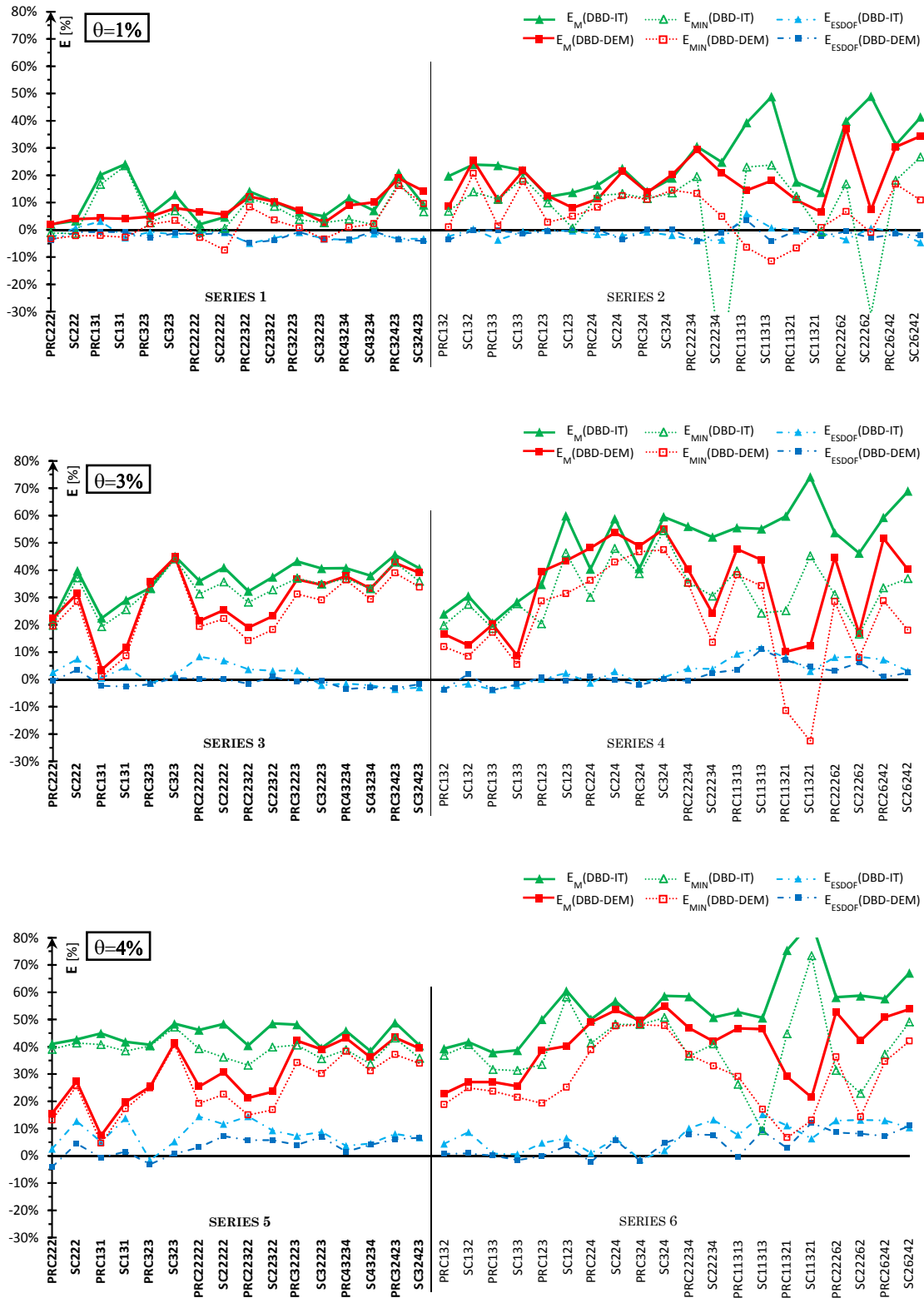


Fig. 4.7 – DDBD-IT and DDBD-DEM methods: relative errors respect to THA medium displacement results.

4.8 CONCLUSIONS

The research study presented in this chapter investigates the accuracy of the current iterative Direct Displacement-Based method (called DBD-IT in this work) when applied to the prediction of the transverse response of multi-span continuous girder bridges, comparing it with a non-iterative (direct) design method, named DBD-DEM, herein proposed with the aim of simplifying the current procedure for everyday design use.

Parametric analyses were carried out by considering multiple configurations of regular and irregular continuous girder bridges, with 4 to 6 spans. Each of the 36 bridge samples was previously designed according to the DDBD-IT and DDBD-DEM procedure, for the 3 adopted different performance levels ($\theta=1,3,4\%$), and subsequently each bridge, detailed with longitudinal reinforcement accordingly with the previous step, was subjected to a suite of 7 ground motions (3 accelerograms series for the 3 different design spectra adopted), for a total of 1512 non-linear Time-History analyses carried out.

The results indicate that the bridges designed with direct displacement-based design globally follow their target displacement pattern when subjected to TH analyses, and it should be noted that even if there are excess displacements, they are almost always less than design limits.

It can be observed that the DDBD-IT leads to design overestimations for the transverse response of RC continuous bridges, with a variable error trend: the mean error $E_M(\text{DDBD-IT})$, with respect to TH, increases significantly with the ductility demand, and although it is relevant, in most cases it can be considered acceptable on the basis of the significant approximations introduced by the simplified design method. The best results were obtained for very regular bridges (uniform or “v-shaped” symmetric pier configurations with high values of RS index (approximately $RS>2$). In these cases the substitute ESDOF system is still representative of the MDOF original structure, and the mean error value E_M is lower than 25% for low-ductility design cases ($\theta=1\%$), and remains less than 35% for high ductility design cases corresponding to $\theta=3\%$ (that is the reference value when damage-control considerations govern the design for ultimate limit states). Higher errors can be obtained for higher drift values, $\theta=4\%$ ($E_M <45\%$) but this represents a drift upper limit for common design also for the collapse limit state.

For irregular structures there is a problem of representativeness of the global displacement shape: it seems apparent that the system regularity affect significantly the reliability of the DDBD simplified method, based on the assumption that structural response is represented by a simple ESDOF system, and controlled by the fundamental mode (inelastic first mode). In particular for non-symmetric bridges with $RS<1$ the error range is unacceptable, reaching more than 80%. Results show also that E_{esdof} (the error related to the SDOF system, tied to the choice of

equivalent damping ξ_{eq} and spectrum reduction factor R_{ξ}) is a small component of the total error, rarely exceeding the value of 10%. This is consistent with the results of investigations carried out in chapter 3, because medium ductility values μ_{eff}^A obtained for ESDOF system (see Tab 4.6) rarely exceed the value 2.5.

As regards the non-iterative procedure (DDBD-DEM) proposed, it offers the advantages of a direct design, generally leading also to better estimates too. The results show that the suggested method enhances the accuracy of the current DDBD-IT procedure not only for symmetric bridges, with a decrease of the 20-25% of the mean error in respect to $E_M(\text{DDBD-IT})$, but also for irregular cases, where the iterative procedure DDBD-IT leads to very high overestimates, and a verification with non linear THA is consequently required. This can be related to the use of a general ResponseSpectrumAnalysis in the DDBD-DEM method, accounting for higher mode effects in the forecast of the inelastic displacement pattern. If the estimate obtained is still not satisfactory, in particular for irregular structures, a further enhancement can be obtained by modifying the proposed DDBD-DEM method into a two-step procedure. The final displacement shape calculated at the first step can be used to redistribute more precisely the total effective stiffness K_{eff} among piers (step e), by implementing a second, partial step, in which the RSA is carried out again with the new values of pier stiffness derived by the design process in the first step.

CHAPTER 5

DISPLACEMENT-BASED ASSESSMENT OF EXISTING BRIDGES: PARAMETRICAL ANALYSIS FOR CAPACITY OF RC PIERS

5.1 INTRODUCTION

Appropriate seismic assessment of reinforced concrete bridges is an important challenge in economically advanced countries where the majority of road bridges have been constructed between the 50s and the 70s, when many areas had not yet been recognised to be earthquake prone and seismic provisions were not enforced.

In past earthquakes, many older reinforced concrete bridges failed catastrophically due to design deficiencies of piers, related to the reduced confinement, inadequate shear reinforcement especially in plastic hinge regions, insufficient length of lap splices. Most failures observed in concrete structures were related to shear (see some examples in Figs. 5.1 a, b). The deficiencies in amount, distribution and anchorage of transverse reinforcement led to brittle and unsafe modes of failure, that are precluded in new seismically designed structures, in which the application of capacity design principles protect columns from inelastic action by implementing an adequate member strength hierarchy. The characteristics of a large class of existing bridge piers make them vulnerable to shear failure, and they are referred to as “shear-critical” columns.

A rational assessment of existing bridges may require a revision of limit states and methods to calculate strength and deformation capacity of members^[C9]. The on-going interest towards a displacement-based approach to seismic assessment of reinforced concrete structures has shifted the focus on the study of the deformation characteristics of members. In terms of displacements, the total member response is not only influenced by the sectional behaviour, but also by other sources of flexibility like rotation at foundation level, bond-slip in the member boundary, and for shear-critical columns also the formation of a stable diagonal shear cracks has been suggested as the source of flexibility that triggers the additional member displacement^[M8]. For this type of columns, generally a linear-elastic force-deformation response is assumed up to flexural yield, and generally the assessment implies failure at very low displacements, with a too conservative approach respect to the evidences of experimental tests (see among others Sezen and Mohele^[S5], 2004, Calvi et al.^[C9], 2005). The use of a more accurate model

could have a significant influence on the assessed level of seismic action that a structure can sustain. When the induced shear force reaches the shear strength at a value lower than the nominal yield strength, experimental results show that rarely does shear failure occur at lateral drifts below 1%, and force-deformation response exhibits a considerable loss of stiffness before the actual failure occurs^[M8].



Fig. 5.1 – Shear failure in reinforced concrete piers: a) Hanshin expressway, Kobe earthquake, Japan, 1995, b) Northridge earthquake, California, 1994

From a Displacement-Based approach perspective, the evaluation of displacement capacity of reinforced concrete piers with limited shear resistance represent a fundamental topic, since so far the calibration of the methods dealt essentially with new ductile structures only. The specific problems of the development of DBA methodologies include the prediction of the possible collapse mechanisms due to brittle rupture of members, the evaluation of the influence of shear deformability and the inclusion of local damage effects caused by nodes not adequately confined. Also the estimate of energy dissipation in shear-dominated columns represents in this context an important goal: the majority of equivalent damping ratios have been proposed to date on the basis of experimental or numerical investigations on ductile structural members, while an equivalent damping model for columns with limited shear resistance is still undefined.

In this chapter these specific issues of the Displacement-Based methodology applied to existing bridge structures are addressed. In particular the calibration effort regards the assessment of pier capacity.

A simplified numerical model^[M8] is adopted for the aggregation of phenomenological non linear shear behaviour and fiber representation of flexural behaviour for piers, and validated using experimental results on rc columns with flexure and shear failure extracted from on line databases. An equivalent damping formulation for shear critical column is then proposed on the base of the results directly obtained from the reference experimental database, expressing the hysteretic component of EVD as a function of the pier lateral drift, and not as function of the displacement ductility as generally proposed^[D1,P1] for flexural columns.

A parametrical study is subsequently developed for single bent and multiple bent piers (cantilever, walls frame), and represents the core part of the Chapter 5. All main geometrical and material properties that can influence the pier capacity, including the aspect ratio of the section, the normalized axial load, the percentage of longitudinal reinforcement, the level of confinement, the strength of concrete and

steel are considered. The effective ranges of the selected parameters are determined by the preliminary statistical analysis conducted on the bridges of the reference database adopted in this study (the Veneto Region road network bridge stock), presented in Chapter 6. The parametric study aims at the determination of the effective properties for existing rc bridge piers, to be used in a Displacement-Based framework: pier flexural and shear capacity, collapse mechanisms, ultimate deformations, drift, secant-to-yielding stiffness, effective stiffness are defined and calibrated with the help of non linear static and dynamic analyses. Parametrical analysis are performed for a large number of pier configurations, and the results are summarized in a series of charts and proposed expressions that can be directly used within the DBA framework, giving the equivalent properties of piers.

These extensive numerical analyses supply a sound mechanical background to the Displacement-Based assessment methodology implemented in Chapter 6 for the vulnerability analysis and seismic risk evaluation of the Veneto Region bridge stock.

5.2 SIMPLIFIED PHENOMENOLOGICAL MODEL FOR AGGREGATION OF FLEXURE BEHAVIOUR AND NON-LINEAR SHEAR EFFECTS

In the 1981 Seismic Design Guidelines for Highway Bridges^[A6], named (ATC-6), the Applied Technology Council proposed a conceptual model that describes the relationship between shear strength and displacement ductility, recognizing that the strength is reduced with increasing ductility as lateral drift increases, the flexure-shear cracks widen and the concrete mechanism of shear transfer degrades due to loss of aggregate interlock. Three possible failure modes of columns subjected to lateral displacement were individuated, described in Tab. 5.1 and represented in Fig.5.2.

The conceptual model proposed in ATC-6 gave rise to several ductility dependent shear capacity models. Among others, the more recent and extensively used are the *Modified UCSD model*, proposed by Kowalsky and Priestley^[K7], 2000, and the Sezen and Mohele model^[SS], 2004.

Since ductility can be related to lateral drift, the ductility dependent shear models can be used to determine the “drift at shear failure”^[M8]. Priestley et al.^[P4] (1996), stated that the drift at shear failure can be taken as that corresponding to the ductility level at which the flexural strength response curve intersects the shear strength envelope.

In this study, following the work of Calvi et al.^[C9], 2005, the level of drift at failure is carried out using the shear capacity model approach. The Sezen model is adopted for calculation of the shear strength envelope, described in §5.2.2.

Experimental observations also indicate that the force level at which the flexural force-deformation response curve starts to deviate from the measured hysteretic response usually coincides with the formation of diagonal shear cracks in the column^[M8]. Calvi et al.^[C9], 2005, based on test results of shear columns, evidenced that there is a considerable loss of stiffness after shear cracking, and constructed a semi-empirical force-deformation by independently calculating the flexural and shear stiffness of the column and then properly combining the two

components. In this study an updated, simplified approach of the conceptual framework proposed in [C9] is adopted, as suggested by Miranda et al.^[M8], 2005. The formalization of the conceptual framework is described in §5.2.1; however, the implementation of the model (see §5.2.4), was done differently from [M8], because a fiber-discretization was used for the modeling of the flexural behaviour and shear effects were subsequently aggregated using the non linear Force-Displacement curve proposed in [M8]. For the shear cracking expression the experimental formula obtained by Calvi et al.^[C9], 2005, is adopted, which is derived from ACI 318-02^[A7], and applicable for assessment purposes, requiring the transverse reinforcement spacing ratio s/d (see Eq. 5.14).

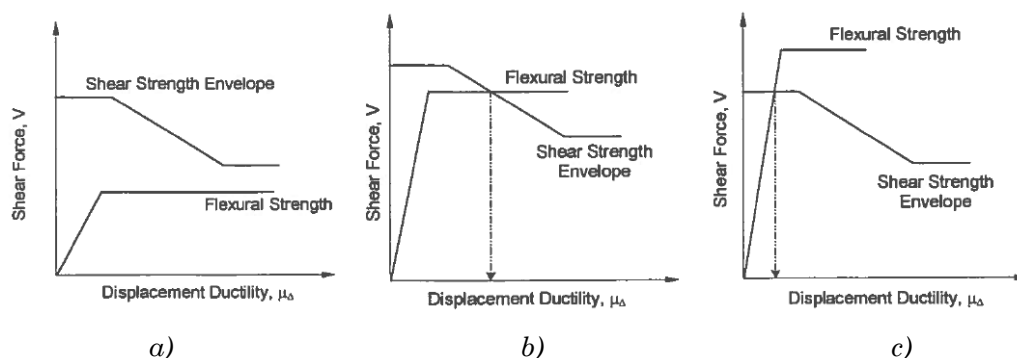


Fig. 5.2 – Classification of rc column failure modes according to the ATC-6^[A6]

Tab. 5.1 – Classification of rc pier type, according to failure model

Code	Failure	Description
(F)	<i>Flexure</i>	Take place if the shear force corresponding to the nominal flexural strength is less than the shear capacity for any value of ductility
(FS)	<i>Flexure-Shear</i>	Occurs when the column reaches its nominal flexural capacity first, but as ductility increases the corresponding shear force exceeds the shear strength envelope
(S)	<i>Brittle Shear</i>	The shear capacity of column is reached prior to the development of the nominal flexural strength

5.2.1 Aggregation of non-linear shear effects

In the model proposed by Miranda, Calvi, Pinho, Priestely^[M8] (named herein M.C.P.P, 2005) adopted in this study, the total stiffness that characterizes each phase of response is derived from the sum of the flexural stiffness and shear stiffness that correspond to each particular phase. In each loading phase the global stiffness can be calculated assuming the flexure and shear components as two springs working in series, thus the following relation can be adopted:

$$K_{Ti} = \frac{1}{\frac{1}{K_{fi}} + \frac{1}{K_{si}}} \quad (5.1)$$

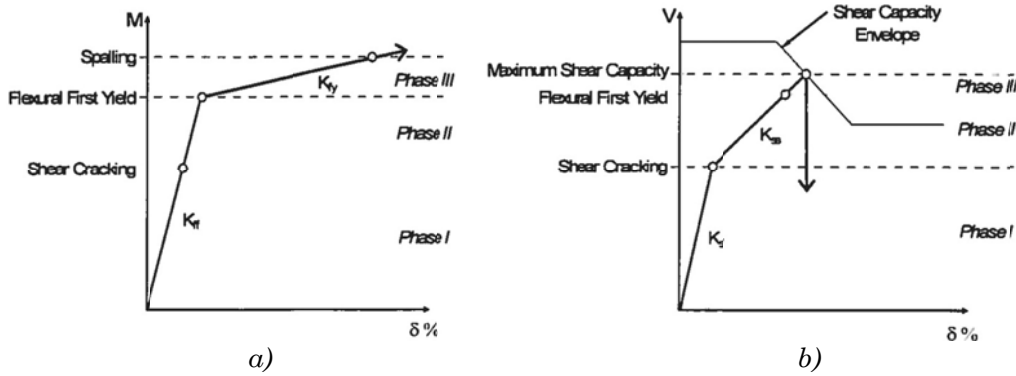


Fig. 5.3 – Flexure-shear aggregation with the simplified phenomenological approach proposed by Miranda et al.^[M8], 2005.

Phase 0: elastic response

In the elastic range, flexural stiffness is proportional to the product $E_c I_g$. The sectional moment of inertia I_g is based on gross section properties, and the elastic modulus of concrete is usually estimated as $E_{cm} = 22000(f_{cm}/10)^{0.3}$

$$K_{fe} = \frac{3E_c I_g}{H^3}, \quad K_{se} = \frac{12E_c I_g}{H^3} \quad (5.2)$$

The member shear stiffness and the elastic shear modulus are given by:

$$K_{se} = \frac{G A_v}{H}, \quad G = \frac{E_c}{2(1+\nu)} \quad (5.3)$$

the shear area A_v , depends on the shape of the cross section under consideration.

Phase I: flexurally cracked response (prior to shear cracking)

In general it is assumed that the flexural stiffness after flexural cracking is also proportional to the product $E_c I_e$. In this case the sectional moment of inertia I_e , is based on effective section properties rather gross section properties. The member flexural stiffness again depends on the boundary condition, namely:

$$K_{ff} = \frac{3E_c I_e}{H^3}, \quad K_{fs} = \frac{12E_c I_e}{H^3} \quad (5.4)$$

Charts giving the cracked stiffness in the form $I_e = \lambda I_g$ have been proposed by Priestley^[P3]. With a more consistent methodology, the effective stiffness product, $E_c I_e$, can be determined from a moment curvature analysis, assuming that the elastic phase is represented by constant flexural section stiffness of:

$$EI_{eff} = M_N / \phi_N \quad (5.5)$$

The evaluation of shear stiffness after flexural cracking is carried out according to recommendation by Priestley et al.^[P4], 1996, whereby the shear stiffness is proportional to the product GA_{ve} , and the reduction in shear stiffness is proportional to the reduction of flexural stiffness (after flexural cracking). The member shear stiffness in phase II is given by:

$$K_{sf} = \frac{GA_{ve}}{H}, \quad A_{ve} = A_v \frac{I_e}{I_g} = A_v \frac{E_c I_e}{E_c I_g} \quad (5.6)$$

the additional displacement component related to the shear, at onset of diagonal cracking is thus:

$$\Delta_{sl} = V_{cr} / k_{sf} \quad (5.7)$$

Phase II: stiffness cracked in shear

In the proposed simplified approach the flexural stiffness remains unchanged after shear cracking occurs. In order to seek agreement with Park and Pauly^[P10] model, the stiffness K_{ff} governs flexural response both in Phase I and II (see Fig.5.1).

The shear stiffness in phase II is evaluated according to the work by Park and Pauly^[P10], 1975. In their analysis the diagonally cracked member was idealized as an elastic truss, following the same principles of the Ritter-Morsch truss mechanism for reinforced concrete. The expression given by Park and Pauly for the unitary shear stiffness makes allowance for different compressions strut inclinations and stirrup orientations.

$$k_v = \frac{\rho_x \sin^4 \alpha_s \sin^4 \beta_h (\cot \alpha_s + \cot \beta_h)^2}{\sin^4 \alpha_s + n \rho_x \sin^4 \beta_h} E_s b_w d \quad (5.8)$$

where ρ_x is the volumetric transversal reinforcement ratio, α_s is the inclination of compression struts, from member axis, β_h the inclination of stirrups from member axis, n the steel to concrete module ratio.

$$\rho_x = \frac{A_{st}}{s b_w \sin \beta_h} \quad n = \frac{E_s}{E_c} \quad (5.9)$$

When the stirrups are placed perpendicular to the axis of the column ($\beta_h=90^\circ$), as in practically all seismic applications, Eq. 5.7 simplifies as follows:

$$k_v = \frac{\rho_x \sin^2 \alpha_s \cos^2 \alpha_s}{\sin^4 \alpha_s + n \rho_x} E_s b_w d \quad (5.10)$$

The member shear stiffness after the opening of diagonal cracks is finally given as:

$$K_{ss} = \frac{k_v}{H} \quad (5.11)$$

The diagonal compression struts usually forms at 45° angles, and then tend to flatten towards 30° as yielding of the member progresses. In this study a 45° compression strut inclination was used in the calculation of stiffness after shear cracking. It can be observed that the proposed approach does not take into

consideration the effects that flexure-shear interaction has on the shear deformations; however a brittle shear failure can be assumed to preclude flexural effects from taking over the member response.

At nominal flexural strength the shear deformation is thus:

$$\Delta_{sN} = \Delta_{sI} + (V_N - V_{cr}) / K_{ss} \quad (5.12)$$

V_N is the shear corresponding to nominal moment, $V_N = M_N/H$ for a cantilever.

Phase III: after nominal yield

The next event for a Shear-Flexure pier may be the nominal yielding of bars, before the attainment of shear ultimate force. There could be also the case in which the flexural collapse is reached after the shear cracking, in both cases the yield point produces an abrupt change in the flexural stiffness. The result is a simplified bilinear Force-displacement curve for simple flexural piers and tri-linear global capacity curve in the case of Shear-Flexure (SF) piers.

In this work, the flexural behaviour is obtained directly by fiber schematization, so the change in stiffness after yielding is directly obtained by uniaxial stress-strain laws of materials. Anyhow in the original (M.C.P.P) formulation this point is defined on the base of the idealized moment –curvature diagram: after the yielding, the post yielding slope is given by:

$$k_{fy} = \frac{M_U - M_N}{\phi_U - \phi_N} \quad (5.13)$$

and consequently the flexural displacement component is obtained by a simple modification of Eq. 2.49 (introducing $\Delta_y (M_U/M_y)$ instead of Δ_y and $\phi_U - \phi_y (M_U/M_y)$ instead of $\phi_U - \phi_y$).

Evaluation of the shear stiffness after flexural yield was performed under the assumption the flexural yield does not affect the shear stiffness^[M8]. Under this assumption, the shear stiffness after shear cracking K_{ss} governs the response in both Phase II and Phase III, and shear deformation, as a fraction of total reformation remains essentially constant.

Other authors^[P1] suggest to increment shear deformation in proportion to flexural deformation after yield, however the significance to total deformation in this phase is typically small.

Tab. 5.2 –*Summary of stiffness components (Simplified Approach [M8])*

Phase	Flexure	Shear	Total Stiffness
Phase I	K_{ff}	K_{sf}	$1/(1/K_{ff} + 1/K_{sf})$
Phase II	K_{ff}	K_{ss}	$1/(1/K_{ff} + 1/K_{ss})$
Phase III	K_{fy}	K_{ss}	$1/(1/K_{fy} + 1/K_{ss})$

5.2.2 Shear-Cracking equations

The phenomenological model introduced for the description of shear additional deformations, require the definition of both the cracking conditions and the post-cracking stiffness reduction.

The aspect of diagonal shear–flexure cracking has been explored since the early 60s (Park and Paulay^[P10], 1975). Experimental tests on 194 solid section beams with little or no shear reinforcement had been used for the definition of the concrete contribution to the shear strength used in the ACI 318-02^[A7] formulation:

$$V_{cw} = v_{cw}(b_w d) \quad (5.14)$$

$$V_{cw} = \begin{cases} (0.29\sqrt{f'_c} + 0.3f_{pc})b_w d \\ \leq 0.41\sqrt{f'_c} b_w d \end{cases} \quad (5.15)$$

where

$$f_t = 0.33\sqrt{f'_c} \text{ concrete tension strength} \quad (5.16)$$

$$f_{pc} = P / A_g \text{ average axial stress} \quad (5.17)$$

v_{wc} is the cracking shear stress corresponding to the opening of the web shear cracks, which initiates when the principal tension stress induced by the applied loading or deformation increases to a value that is equal to the tension strength of the concrete.

Different formulations have been successively adopted by other codes, maintaining the general expression and meaning of Eq. 5.12, with similar formulation of the cracking shear stress, here reported only for comparison:

Eurocode 2:

$$v_{cr} = \beta_p \tau_{rd} k_s (1.2 + 40\rho_l) + 0.15P / A_g \quad (5.18)$$

where $\beta_p=1$ (for member without concentrated loads near support), $\tau_{rd}=0.25f_{ck0.05}$, $k_s=(1.6-d/1000)\geq 1.0$

Australian Concrete Design Standard AS-3600:

$$v_{cr} = \beta_1 \beta_2 \beta_3 \left(\frac{A_{st} f'_c}{b_w d} \right)^{1/3} \quad (5.19)$$

where $\beta_1=1.1(1.6-d/1000)\geq 1.1$, $\beta_2=1+P/(14A_g)$ for members with axial compression, $\beta_3=1$ (for member without concentrated loads near support).

5.2.2.1 Miranda, Calvi, Pinho, Priestley formulation (M.C.P.P.)

Miranda et al.^[M8] observed that there is a sensible variation in the accuracy of shear cracking force prediction using the previous expression (Eqs. 5.12-5.17), and all of the equations appear to generate a considerable variability when applied to a shear critical column experimental database, constituted by solid and hollow sections. They proposed a modified formulation to obtained results that better matched with experimental values:

$$V_{cr} = 0.215 \left(\frac{s}{d} \right)^{-0.57} v_{cr} A_w \quad (5.20)$$

$$A_w = b_w d \quad v_{cr} = 0.5\sqrt{f'_c} \sqrt{1 + \frac{P}{0.5\sqrt{f'_c} A_g}}$$

(5.21)

Differently from the other formulations this expression reflects an influence of the transverse reinforcement, thus its application is straightforward for assessment purposes (not for design), transverse reinforcement details being already known.

In this study the (M.C.P.P) formulation is adopted to characterize the shear force level corresponding to the beginning of Phase II (stiffness cracked in shear) described in §5.2.1.

5.2.3 Shear capacity envelope

The shear strength capacity is calculated in this study using the predictive model by Sezen. Ideally the shear strength envelope should coincide with the cyclic lateral force deformation curve at the lateral drift corresponding to maximum capacity, and should represent a higher bound to the strength developed by the column at higher ductility levels. In general terms it can be observed that the modified UCSD model^[K7], resulted in higher estimations of the shear strength^[M8]. For the reference column database used in this research it was observed that the Sezen model provided a better correlation with experimental results, generally being more conservative than UCSDS model.

5.2.3.1 The Sezen shear model (2004)

In this predictive model, the shear capacity is given as the sum of two components: the concrete mechanism and the steel truss mechanism. The effect of the axial load is included in the concrete component. The shear strength provided by steel truss is also assumed to be ductility-dependent, and degrade with increasing ductility due to transverse reinforcement misalignment and anchorage degradation (which occurs especially in older columns with non seismic detailing). Shear strength is given by:

$$V_n = k_{\Delta}(V_c + V_s) \quad (5.22)$$

$$V_s = \frac{A_{sh}f_yh d}{s} \quad (5.23)$$

$$V_c = \frac{0.5\sqrt{f_{c0}}}{a/d} \sqrt{1 + \frac{P}{0.5\sqrt{f_{c0}}A_g}} (A_e) \quad 2 \leq a/d \leq 4 \quad (5.24)$$

where

$$k_{\Delta} = \begin{cases} 1,0 & \mu_{\Delta} \leq 2 \\ 1 - 0,3 \cdot \frac{\mu_{\Delta} - 2}{4} & 2 < \mu_{\Delta} < 6 \\ 0,7 & \mu_{\Delta} > 6 \end{cases} \quad (5.25)$$

The non-dimensional parameters k_{Δ} relates the shear strength with the ductility level. The effective shear area is taken as $A_e=0.8A_g$. The term a/d appears because it was recognize that the column aspect ratio has an influence in the shear strength associated to the concrete mechanism; Sezen proposed a linear reduction for increasing aspect ratios in the range between 2.0 and 4.0. Outside this range the

author suggests the relation could be non linear and cautions has to be used in applying the formula.

5.2.4 Implementation in the F.E. model

In the parametrical study presented in this Chapter for the analysis of capacity of existing rc piers, rc members are modeled by using the finite element code Opensees (McKenna et al.^[Y1], 2007) developed for seismic non linear structural analysis able to take into account all nonlinearity sources in a reinforced concrete structure.

The section of each element is subdivided in fibers such that it is possible to assign the constitutive model for each of the three modeled material (unconfined concrete for section cover, confined concrete for the core of the section, and steel for reinforcement bars) and the exact position and dimension of the bars.

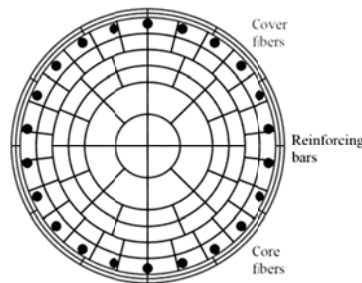


Fig. 5.4 – *Fiber cross section; typical arrangement of fibers for a solid circular section*

The use of fibers with uniaxial material behaviour to model sectional response emerged in last two decades as a viable alternative to the classical plastic hinge hysteretic models. Fiber models have the advantage that inelastic deformations can be distributed along the element length rather than taking place at predefined locations of the members, and calibration of hysteretic parameters of plastic hinges (accounting for moment-axial load interaction) is not required, being sufficient the definition of materials' non linear constitutive relations. Moreover, the direct access to sectional strain values could be very useful for mechanics-based loss assessment studies if the damage definitions are based on strain exceeding certain levels of pre-defined limit-states. On the other hand, in fiber models the coupling between the effects of normal and shear forces is not straightforward. The complexity of the problem is related to the different involved phenomena leading to shear failure, such as crack propagation, transfer of the compressive stresses from the point of load application to the supports, aggregate interlock, dowel action of the longitudinal steel, and slip between concrete and steel.

The shear mechanism has been modeled using the simplified phenomenological relation^[M8] (M.C.C.P), 2005, described in §5.2.1. In particular, the shear relation is implemented by using the option Section Aggregator which groups different materials behaviour into a single section force-deformation model. Thus only the shear component was aggregated using a V- γ (shear-strain) hysteretic relation, the flexural behaviour being directly obtained with fiber-section discretization. The shear-strain relation consists of bilinear envelope curve with

stiffness degrading, defined accordingly with (M.C.C.P) model^[M8], with the V_{cr} point corresponding to cracking level defined by Eqs. 5.18-5.19.

Another aspect taken into account in the model is the bond-slip effect in proximity of the section of plastic hinges. This phenomenon is due to the difference between the deformation of the bars and concrete which yields a typical crack. It is worth to point out that this effect may be pronounced for plain bars due to the low adhesion between concrete and steel. Following the approach proposed by Zhao and Sritharan^[Z1] (2007), a way to account for the bond-slip effect consists of concentrating the rotation due to the slip in a section. This is done in Opensees by using a *zeroLengthSection* element which has a length equal to 1 with a single integration point, thus element deformations correspond to section deformations and then the moment-curvature is equivalent to moment-rotation relation. In this way, the rotation due to bond slip effect may be evaluated by defining a properly stress-slip relation for the steel, describing the interaction between concrete and bar.

5.2.4.1 Material constitutive laws

The reinforcing steel bars are modeled according to Menegotto-Pinto constitutive law (Menegotto and Pinto^[M9], 1973), implemented in Opensees with the *Steel02* model. A modulus of elasticity equal to 205000 MPa is assumed, along with a yield stress and a hardening parameter b defined in Tab. 6.18 for Aq50-60 and FeB44k steel types. The transition parameters from elastic to plastic behavior are set according to Menegotto and Pinto, 1973.

A Kent-Scott-Park model is chosen for the concrete behavior (Kent and Park^[K8], 1971), implemented in Opensees with the *Concrete02* model. This constitutive law for uniaxial material response has a first parabolic trend up to compression peak stress equal to f_c with a corresponding strain equal to ε_0 and a decreasing linear trend up to f_{cu} , with corresponding strain ε_{cu} . The concrete contribution for tension stresses is neglected and then its constitutive law has zero strength when the strain assumes positive values, even if the model allows to implement it with linear trend till f_t , maximum tensile stress). The ratio between reloading stiffness and initial stiffness is given by the parameter λ .

To define the confined concrete, the maximum compressive strength (f'_{cc}) and concrete crushing strength (f_{cu}) are calculated according to Mander et al.^[M3], 1988, related to the unconfined compression strength f'_c and lateral confining pressure f'_i :

$$f_c = \frac{f'_{cc} x r}{r-1+x} \quad (5.26)$$

$$x = \frac{\varepsilon_c}{\varepsilon_{cc}} \quad (5.27)$$

$$r = \frac{E_c}{E_c - E_{sec}} \quad (5.28)$$

$$E_c = 5000 \sqrt{f'_c}, \quad E_{sec} = \frac{f'_{cc}}{\varepsilon_{cc}} \quad (5.29)$$

$f_{cc} = \lambda_c f_c$, where the confinement parameter λ_c is expressed as:

$$\lambda_c = 2.254 \sqrt{1 + 7.94 \frac{f_l}{f_c} - 2 \frac{f_l}{f_c} - 1.254} \quad (5.30)$$

$$f_l = \frac{1}{2} \rho_s f_{yh} \quad (\text{for circular sections with hoops or spirals}) \quad (5.31)$$

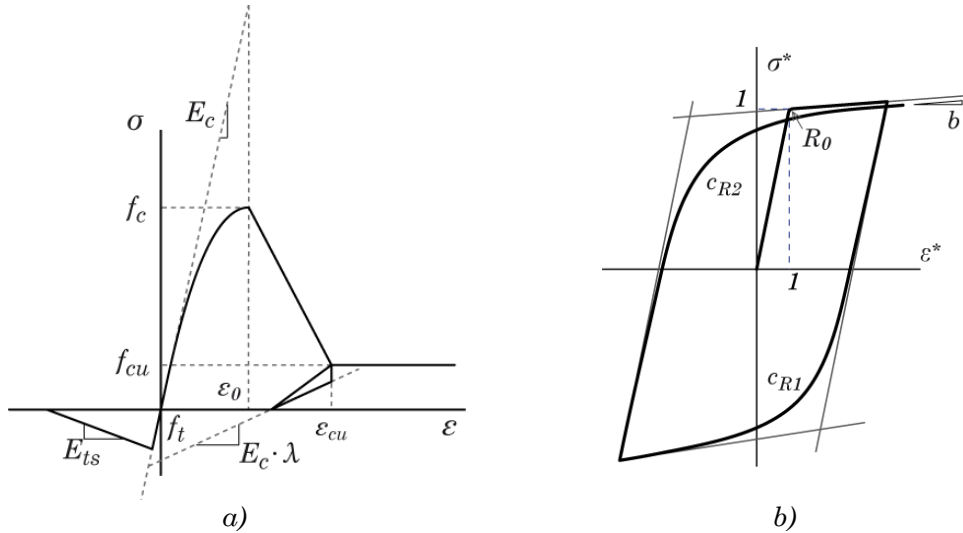


Fig. 5.5 – Constitutive laws adopted in the F.E. model: a) concrete, Kent and Park^[K8] model, b) reinforcement steel, Menegotto and Pinto model, 1973.

Tab. 5.3 – Steel02 material model parameters

Material	f_y	E_s (MPa)	b	R_0	c_{R1}	c_{R2}
Reinforcement steel	f_y^*	205000	b^*	20	0.925	0.15

f_y^* , b^* yield stress and hardening parameter defined for Aq50-6and FeB44k steel types accordingly to Tab 6.18

Tab. 5.4 – Concrete02 material model parameters

Material	f_c	ε_0	f_{cu}	ε_{cu}	λ	f_t	E_{ts}
Concrete cover	f_{c+}	$2f_c/E_c^{++}$	0	0.004	0.10	0	f_t/ε_0
Concrete core	$f_{cc^{**}}$	$2f_{cc}/E_c^{++}$	$f_{cu^{**}}$	ε_{cu}^{***}	0.10	0	f_t/ε_0

+ from test results and material characterization (see §6.2.3)

++ $E_c = 5000\sqrt{f_c}$

** Equation from Mander et al.^[M3]

*** Equation 2.4

5.2.5 Experimental database

The phenomenological model adopted in this study for interaction of flexure-shear behaviour in the piers is deduced from previous studies (Calvi et al.^[C9], 2005, Miranda et al.^[M8], 2005). However, as clarified before, its implementation differs because the flexural stiffness component is directly obtained by a fiber-discretization modeling and the shear stiffness of the (M.C.P.P.) model is

aggregated. Thus it was considered necessary to validate the modelization with experimental tests, that were also considered in the perspective of the calibration of a new equivalent viscous damping expression for shear-critical columns.

No actual experimental work was carried out during the course of the research; the validation of the model was obtained using experimental results on rc columns with flexure and shear failure extracted from on line databases.

In specific the source used for the selection of the experimental test was the *Structural Performance Database*, arranged by the Pacific Earthquake Engineering Research Center, available on line (<http://nisee.berkeley.edu/spd/>).

The scaled columns of the reference experimental database have circular and rectangular solid section, were tested with quasi-static cycles with displacement control in double bending, and had shear or flexural failure. Only column tests that explicitly reported the hysteretic response curve in terms of applied force and lateral deformation and type of failure were considered.

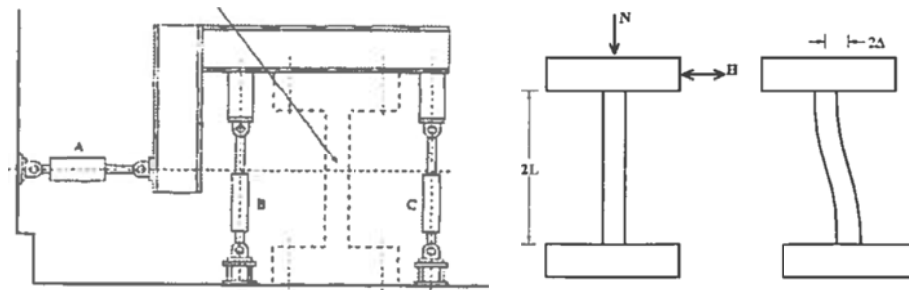


Fig. 5.6 – Typical test setup for the selected specimen

The main properties of the reference experimental database and specimens characteristics are reported in Tabs.5.3-5.5. Other details on the test setup and on the properties of the experimental database can be found in [M8].

Tab. 5.5 – Experimental database

Database ID	Source	Authors	Specimen ID	Section Type	Failure type
C01F	SPD-PEER	Lehman et al. (1998)	415	Circ.	Flex.
C02F	SPD-PEER	NIST	Full Flexure	Circ.	Flex.
R01F	SPD-PEER	Park and Paulay	Specimen No.9	Rect.	Flex.
R02S	SPD-PEER	Imai and Yamamoto (1986)	No. 1309	Rect.	Shear
R03S	SPD-PEER	Lynn et al. (1998)	3CLH18	Rect.	Shear
R04S	SPD-PEER	Lynn et al. (1998)	3CMH18	Rect.	Shear
R05S	SPD-PEER	Lynn et al. (1998)	3CMD12	Rect.	Shear

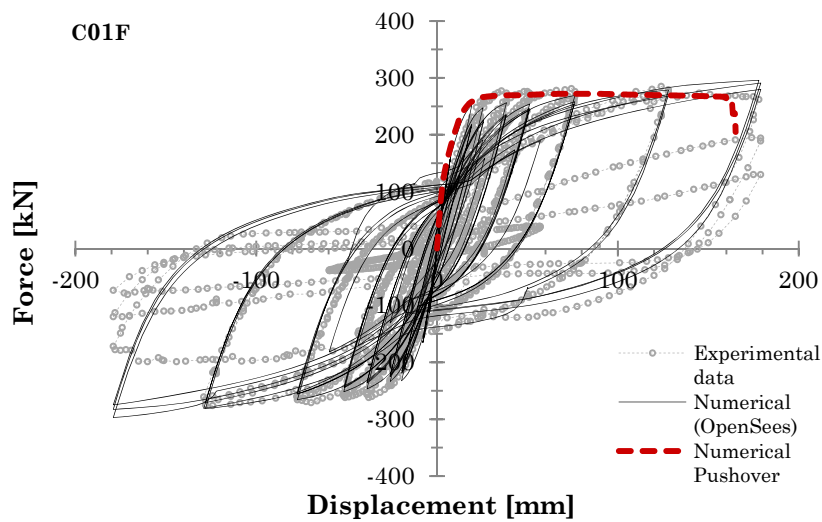
Tab. 5.6 – *Geometric and reinforcement characteristic of the specimens*

<i>ID</i>	Geometric properties				Reinforcement ratio		
	<i>d</i> (mm)	<i>s</i> (mm)	<i>a/d</i>	ρ_l (%)	ρ_s (%)		
C01F	609,6	31.75	4,00	1.49	0.698		
C02F	1520	88.9	6.01	1.99	0.630		
	<i>b</i> (mm)	<i>h</i> (mm)	<i>s</i> (mm)	<i>a/b</i>	ρ_l (%)	ρ_x (%)	ρ_y (%)
R01F	400	600	80/160	1.65	1.88	1.25	1.05
R02S	400	500	100	3.22	2.66	0.40	0.31
R03S	457	457	457	3.22	3.03	0.08	0.08
R04S	457	457	457	3.22	3.03	0.08	0.08
R05S	457	457	305	3.22	3.03	0.21	0.21

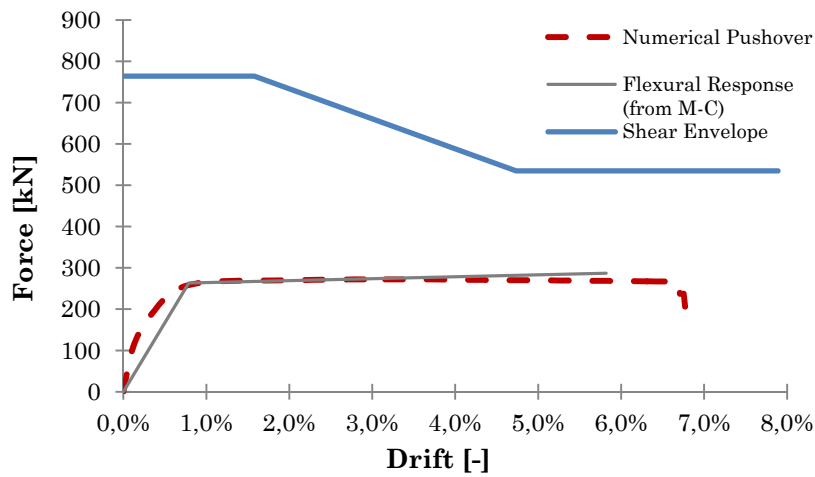
Tab. 5.7 – *Properties of the specimens in the experimental database.*

<i>Database ID</i>	Material properties			Axial load
	f'_c (MPa)	f_y (MPa)	f_{yh} (MPa)	$P/A_g f'_c$
C01F	30.3	483	607	0.072
C02F	35.8	475	493	0.069
R01F	26.9	432	305	0.100
R02S	27.1	318	336	0.072
R03S	26.9	331	400	0.089
R04S	27.6	331	400	0.262
R05S	27.6	331	400	0.262

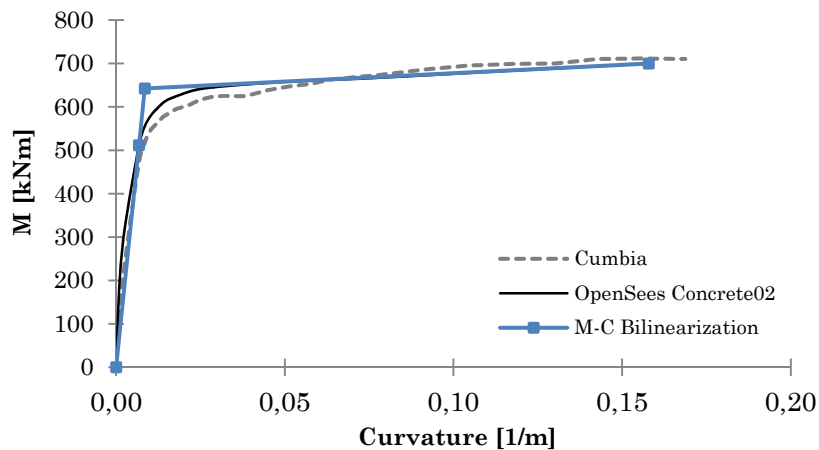
The numerical model of the specimen was implemented as described in §5.2.4, and subjected to quasi-static loads in displacement control accordingly to the loading history of the experimental tests.



a)



b)



c)

Fig. 5.7 – Specimen C01F: a) experimental and numerical Force-Displacement curves of the column subjected to quasi-static cycles with displacement control, superimposed with Pushover curve; b) numerical pushover and shear envelope; c) comparison of Moment-curvature plots obtained with Opensees and Cumbia

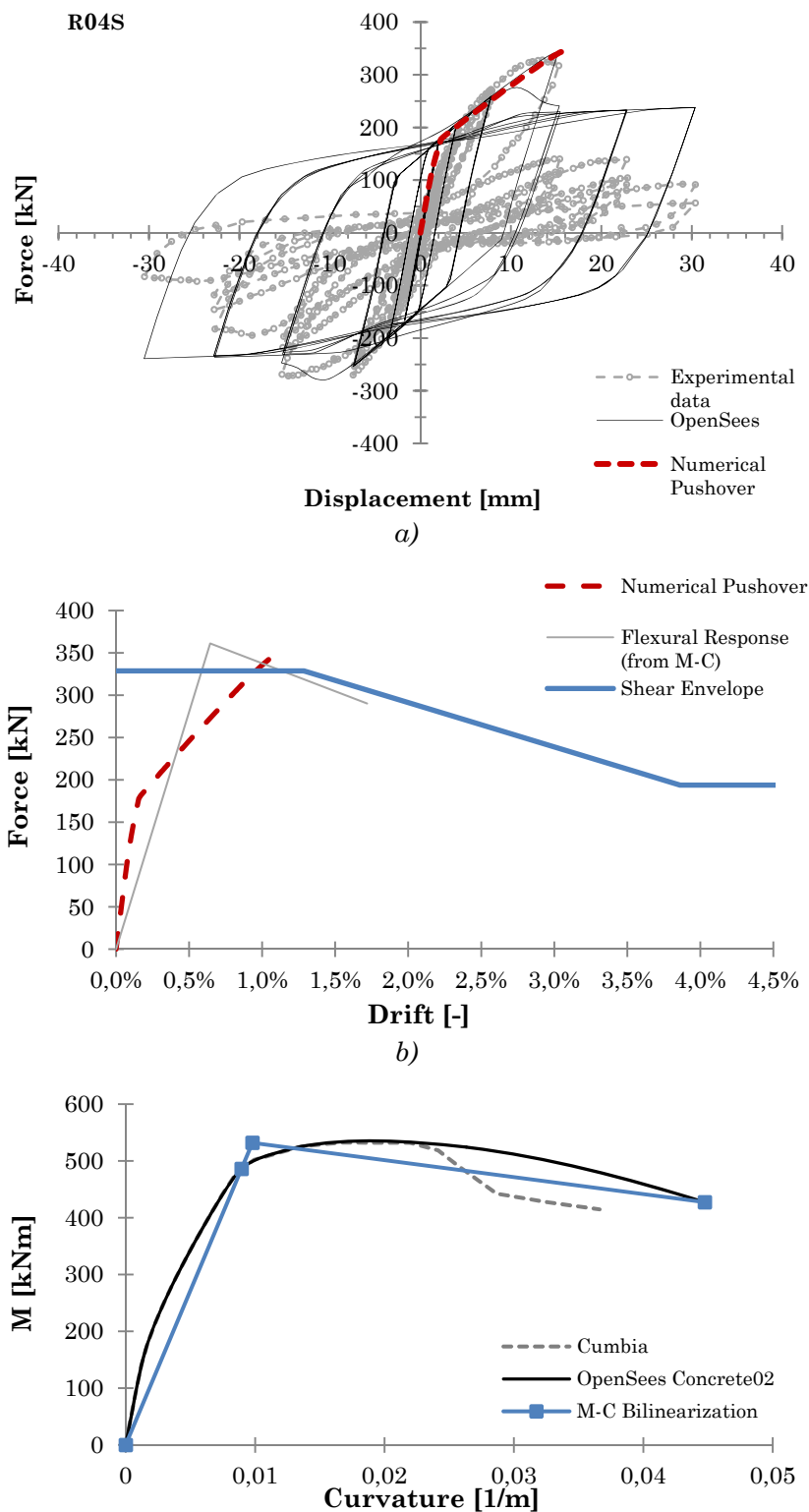
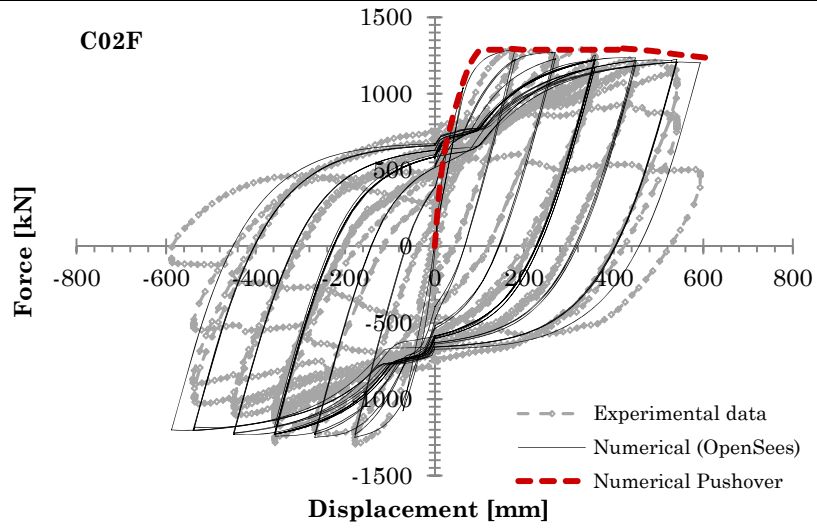
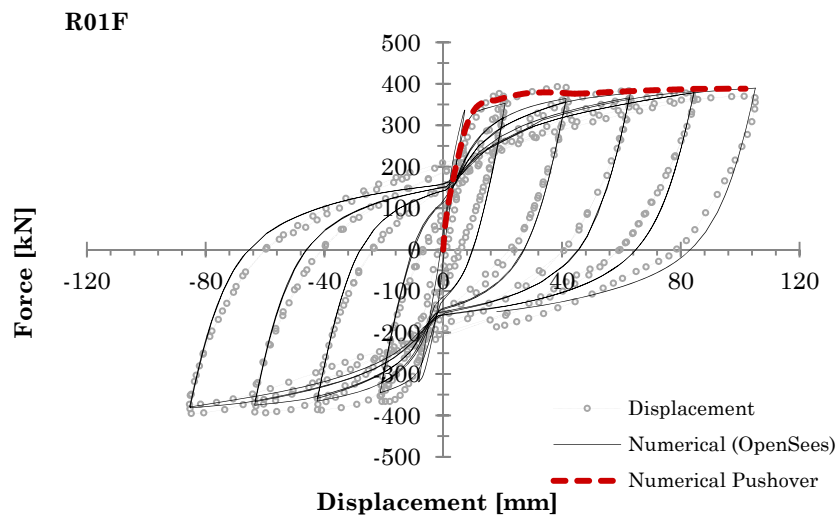


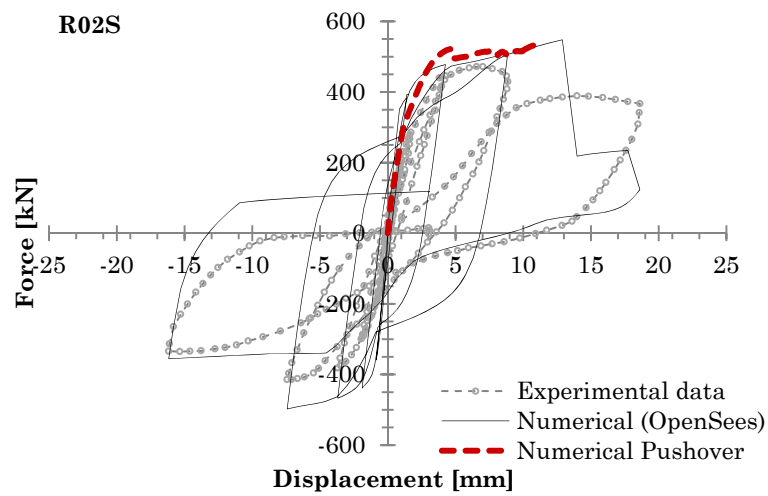
Fig. 5.8 – Specimen R04S: a) experimental and numerical Force-Displacement curves of the column subjected to quasi-static cycles with displacement control, superimposed with Pushover curve; b) numerical pushover and shear envelope; c) comparison of Moment-curvature plots obtained with Opensees and Cumbia



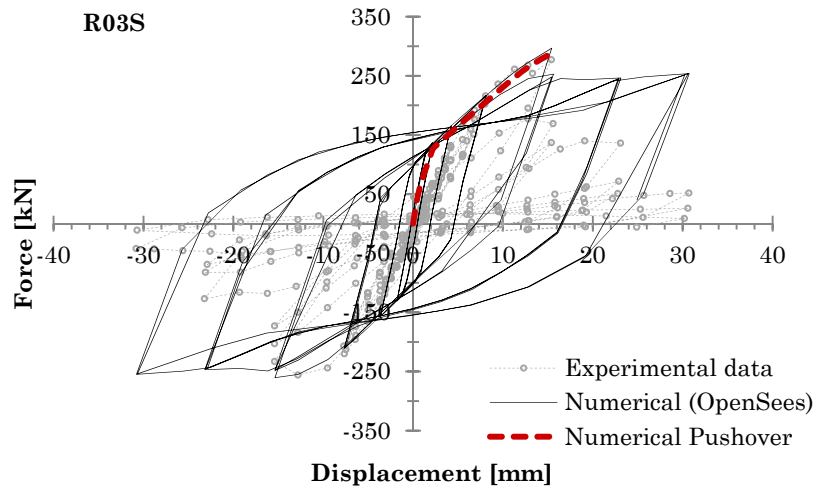
a)



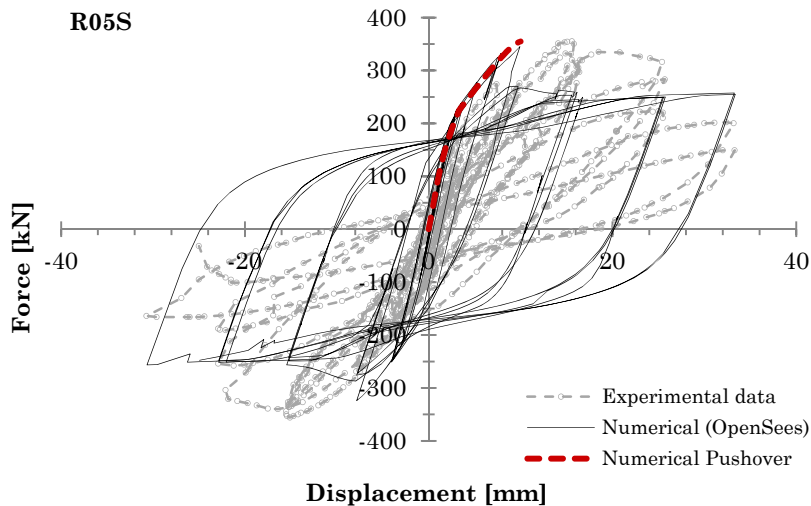
b)



c)



d)



e)

Fig. 5.9 –Experimental and numerical Force-Displacement cycles for specimens C02, R01F, R02S, R03S, R05S

5.2.5.1 Summary of results on tested columns

In the following Figs. 5.7-5.9 the experimental cycles superimposed with the numerical hysteretic loops obtained are reported for all the specimens.

The response of the models to cyclically imposed displacements is quite satisfactory: it matches well the experimental response of the physical model till the attainment of the maximum displacement at failure, and also the stiffness in the reloading phase is accurately reproduced till the drift at failure. In the cases where a flexure (F) or flexure-shear (FS) behaviour is obtained for the specimen, the numerical model reproduces the experimental cycles quite well also after the drop of resistance corresponding to failure, in the post-peak response. However, when a

brittle shear failure (S) is reproduced after the reaching of shear strength, the post peak numerical cycles show an overestimation of the residual strength.

The definition of the drift at shear failure and corresponding effective properties (stiffness) being the aim of the experimental calibration, the numerical model is judged adequate, even the post-shear failure behaviour is not always accurately reproduced.

5.2.6 Calibration of Equivalent Viscous Damping expression for shear-failure mechanisms

It has already been discussed in §2.1.3 that the Substitute Structure approach implemented in the Displacement-Based framework requires the definition of an equivalent viscous damping ratio, reflecting the energy dissipation characteristics of the real structure at maximum response, and various expression proposed by different authors were presented [D1,P1,D11]. Subsequently in Chapter 3 it was demonstrated how the choice of different EVD expressions and related spectrum reduction factor affects the accuracy of DDBD procedure.

It has to be observed that most of the equivalent damping models proposed to date [D1,P1], were developed on the basis of theoretical, experimental or numerical investigations on ductile members, and the displacement ductility μ was used as the reference parameter to express the hysteretic energy dissipation, depending the dissipated energy in one hysteretic cycle on the amplitude of the displacement. However, for shear-critical columns, shear precludes the development of a stable ductile hysteretic response, and existing bridge piers are often affected by a limited shear resistance. Moreover, the yield strength is often not attained by columns failing in shear.

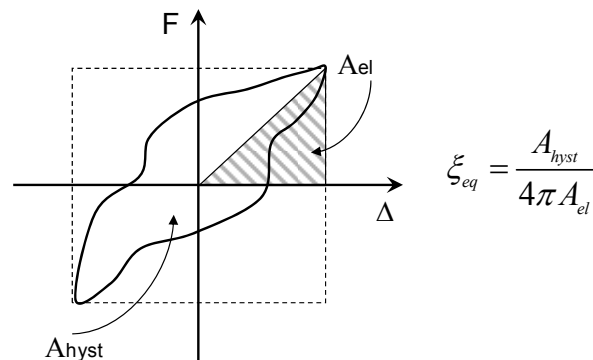


Fig. 5.10 – Definition of equivalent damping ratio according to the area-based approach by Jacobsen[J1,J2]

In the work by Miranda et al.^[M8], to which this study refers for the EVD evaluation approach based on experimental results, a preliminary hypothesis for columns failing in shear is done, relating the EVD to the expression of the lateral drift, θ . It was observed that in general there appears to be less scatter when the experimental damping estimation are reported in terms of lateral drift rather than μ , and that the relationship between EVD and a measure of the lateral deformation amplitude is better expressed as a function of drift, since it has a unique definition, while ductility is capable of many interpretation^[M8]. However a formalization of

these consideration is not presented in [M8], and to the extent of the author's knowledge, currently there is no EVD expression validated specifically for shear-critical columns to be adopted in the DBA approach.

In this paragraph a new formulation of EVD is proposed on the base of the evaluation of the experimental results extracted from the reference database described in the previous paragraph. The interpolating law is based on a restricted number of experimental tests analyzed, the expression representing a first proposal that may be tested and calibrated on a more ample set of specimens.

5.2.6.1 Evaluation of EVD component from experimental force-deformation cycles

A study on the damping characteristics of reinforced concrete columns with limited shear resistance was performed using the experimental force-deformation curves from the specimens of the reference database reported in Tab. 5.3.

Following the area-based approach introduced by Jacobsen^[J1,J2], the equivalent viscous damping ratio ξ_{eq} can be defined in terms of the proportion between the area enclosed by one complete hysteretic cycle and the area under a linear elastic response curve evaluated to the same displacement amplitude (see Fig. 5.7).

The equivalent viscous damping ratio was evaluated using a number of cycles (4 or 5), belonging to the experimental force-deformation response curve for the all the specimens in the reference database (7 specimens, 3 with flexural failure, individuated with the final "F" letter in the database ID, and 4 failing in shear). The equivalent viscous damping ratio ξ_{eq} was calculated using standard area comparison through the Eq. 2.17.

Tab. 5.8 – Flexural columns: characteristics of the analyzed hysteretic cycles

ID - F	Cycle 1		Cycle 2		Cycle 3		Cycle 4	
	θ	ξ_{eq}	θ	ξ_{eq}	θ	ξ_{eq}	θ	ξ_{eq}
C01F	0.79%	2.39%	1.58%	12.13%	3.15%	20.66%	5.27%	25.96%
C02F	0.74%	6.80%	1.96%	8.46%	2.94%	19.20%	3.92%	24.78%
R01F	1.18%	16.95%	2.35%	21.67%	3.55%	28.04%	4.76%	28.90%

Tab. 5.9 – Shear critical columns: characteristics of the analyzed hysteretic cycles

ID - S	PRE-Peak cycles				POST-Peak cycles - Not stabilized		POST-Peak cycles - Stabilized			
	Cycle 1		Cycle 2		Cycle 3		Cycle 4		Cycle 5	
	θ	ξ_{eq}	θ	ξ_{eq}	θ	ξ_{eq}	θ	ξ_{eq}	θ	ξ_{eq}
R02S	0.22%	6.74%	0.48%	8.19%	0.99%	17.51%	0.99%	17.51%	2.11%	21.28%
R03S	0.14%	5.50%	0.53%	5.17%	1.05%	12.69%	1.56%	13.39%	1.82%	15.58%
R04S	0.13%	5.95%	0.52%	5.31%	1.04%	13.86%	1.55%	14.01%	1.81%	16.17%
R05S	0.14%	5.62%	0.25%	5.54%	1.07%	10.48%	1.64%	16.53%	2.17%	18.18%

In the shear-critical columns, the hysteresis loops evidenced the presence of two or three cycles to the same displacement amplitude prior to the peak response (see Tab. 5.8, cycles 1 and 2), corresponding to the attainment of the maximum shear capacity.

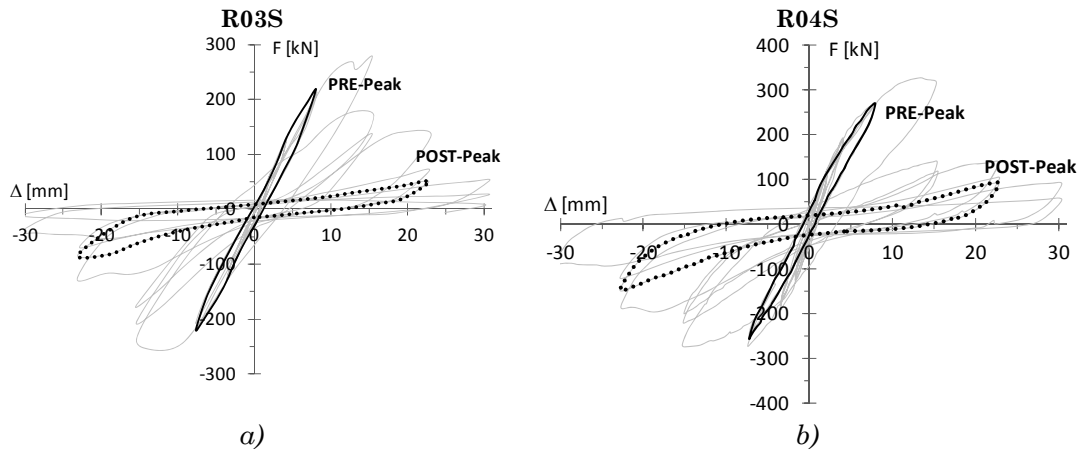


Fig. 5.11 – Pre-peak and post-peak stabilized hysteresis loops considered for the specimens R03S and R04S, corresponding to cycles 2 and 5

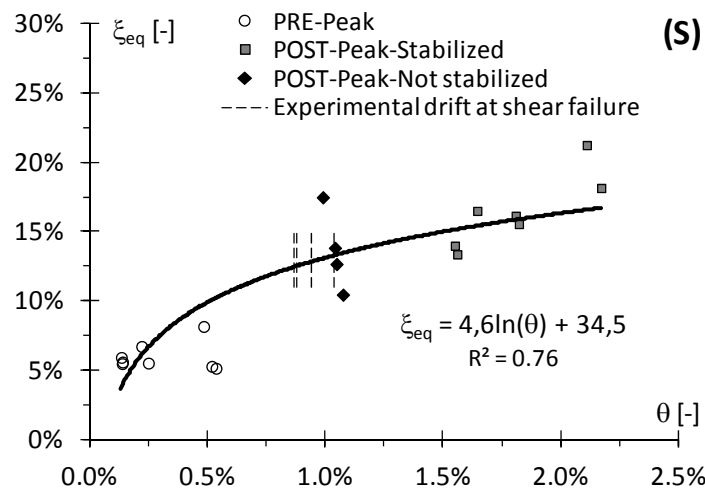


Fig. 5.12 – Evaluation of Equivalent Viscous Damping as a function of lateral drift θ : pre-peak, post-peak experimental results and proposed interpolating law

In the DBA approach the effective stiffness is calculated to maximum displacement, evaluated for shear critical columns as the drift corresponding to the maximum shear capacity (peak response). Equivalent damping for the substitute linear structure has to be evaluated using hysteretic cycles whose displacement amplitude is lower than the drift at peak response (represented in Tab. 5.8 and Fig. 5.7 by pre-peak cycles) or almost equal (represented by post-peak cycles, not stabilized). To better represent the progression of hysteretic dissipation, also additional post-peak cycles were considered in the evaluation, corresponding to target displacement that are beyond that corresponding to the peak force response.

A logarithmic law interpolates quite accurately the experimental results, and the following expression is proposed for the EVD for shear-critical columns:

$$\xi_{eq} [\%] = 4.6 \ln \theta + 34.5 \quad \theta \leq 1.5\% \quad (5.32)$$

Experimental results showing that failure occurs around the 1% drift level (see Fig. 5.7), the experimentally evaluated damping ratio ξ_{eq} lies between 12-15%, and the ultimate drift value limited under 1.5% for Shear (S) columns or Flexure-Shear (FS). This values will be confirmed also by the parametric analysis developed for cantilever and frame bridge piers in next paragraphs.

It seems apparent that the hysteretic dissipation and related EVD value has to be higher at the target drift for flexural piers than for shear-critical piers. Only with the aim of comparing the absolute values of EVD obtained, a law expressing $\xi_{eq}=f(\theta)$ for flexural piers is introduced and plotted in Fig.5.7. Interpolation obtained with typical ξ_{eq} expression as function of displacement ductility (see also Eq. 2.30 and Tab. 2.10) is reported in Fig. 5.10 for flexural columns.

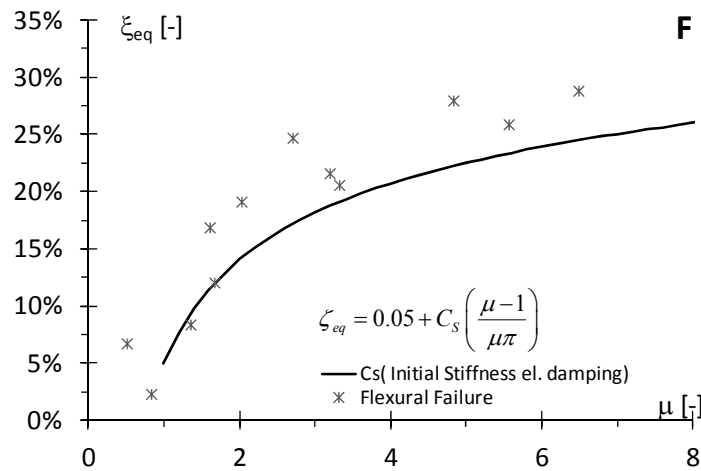


Fig. 5.13 – Superposition with Logarithmic interpolating laws obtained for evaluation of EVD for flexural columns

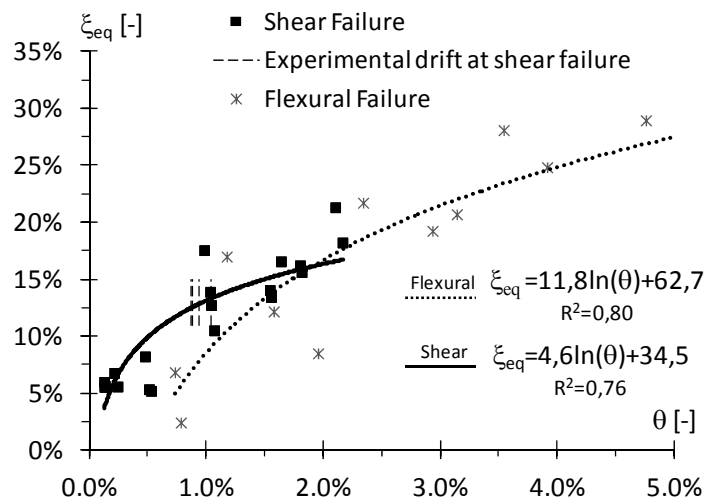


Fig. 5.14 – Logarithmic interpolating laws obtained for evaluation of EVD for flexural and shear critical columns

It can be observed that for flexural piers, with ultimate drifts of about 3- 4% corresponding ξ_{eq} values of about 20-25% are obtained.

5.3 PARAMETRICAL ANALYSIS

An extensive parametrical analysis is carried out to assess the force displacement characteristics of existing piers, accounting to shear deformation accordingly to the shear-flexural model described in previous paragraphs.

The main properties that can influence the pier capacity are considered, including the aspect ratio of the section, the normalized axial load, the percentage of longitudinal reinforcement and volumetric transverse reinforcement (tied to the level of confinement of the concrete core), the strength of concrete and steel. The values adopted for the selected parameters are determined by the statistical survey conducted on the structures of the reference VR bridge stock, presented in Chapter 6, and fall within the database extent described in Tabs. 6.15-6.20.

Single bent and multiple bent piers are analyzed represented by cantilever, walls and frame piers. In the parametrical analysis the rc member are supposed to be fully restrained at the foundations.

The parametric study aims at the determination of the effective properties for existing rc bridge piers, to be used in a Displacement-Based framework. Three different collapse mechanisms are individuated (brittle shear-S-, flexure-shear-FS- and flexure mechanism), and pier flexural and shear capacity in terms of force-displacement curves are individuated. Synthetic charts are supplied, giving adimensional yielding moment, secant-to-yielding stiffness, ultimate deformations and drifts, and ultimate effective stiffness for different pier configurations. The charts summarize the information obtained from all the capacity curves obtained in the parametric study, which were developed for each pier sample by non linear static analysis.

In the DBA framework these charts can be subsequently used, for a certain rc pier under exam, to reconstruct in a simplified manner the member capacity curve (Force-Displacement curve), that has to be known at the beginning of the procedure.

5.3.1 Single bent (cantilever) piers with circular section

In the following table the values of the parameters adopted for circular piers are reported.

Tab. 5.10 –Single bent circular piers: 1440 pier samples studied in total.

Single Bent - Circular Piers					
D	[m]	2.0	2.6	3.2	3.5
H *	[m]	4.0	6.0	8.0	12.0
ρ_l	[%]	0.20	0.35	0.50	
ρ_{st}	[%]	0.05	0.20		
ν_k	[-]	0.05	0.10	0.20	0.25
f_c	[MPa]	30	40	55	
Steel	[-]	Aq50-60	FeB44K		

* effective H/D ratios:

1.9, 2.0, 2.3, 2.5, 3.1, 3.4, 3.8, 4.0, 4.6, 6.0

The parameters (longitudinal and transverse reinforcement ρ_l , ρ_{st} respectively, and normalized axial load, v_k) are defined accordingly to the expressions reported in §6.2.4, while the steel properties are individuated in Tab.6.20 for FeB44k and AQ50-60 steel types.

The circular cantilever piers analyzed have diameters variable between 2.0 and 3.5m, with height over diameter ratios, H/D ranging between 2.0 and 6.0. This kind of existing piers have a very low reinforcement content, with a longitudinal reinforcement ratio ρ_l equal at maximum to 0.5 and volumetric transverse reinforcement content between 0.05 and 0.20. The axial load at the pier base is generally quite low, under 25% of the section concrete strength. The ranges analyzed for material characteristics are quite ample, to reflect the substantial variability of the concrete and steel properties in the reference database.

The number of pier samples obtained from the combinations of the analyzed parameters are 1440.

5.3.1.1 Capacity curves

The capacity curves obtained are reported in an adimensional fashion for (S), (SF) and (F) piers. The lateral resisting acceleration (expressed in terms of g) is expressed as a function of the total drift θ , and also as a function of the displacement ductility, μ , in the case of (SF) and (F) piers.

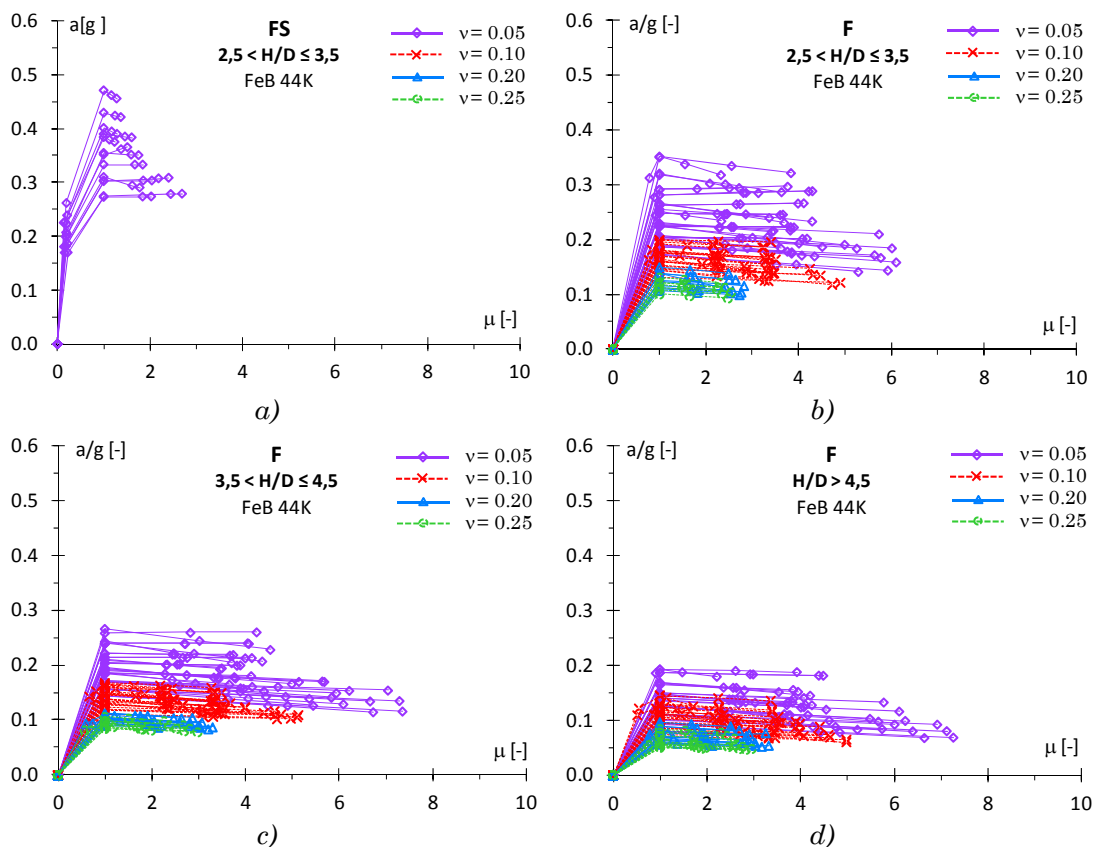


Fig. 5.15 – Adimensional capacity curves (resistant acceleration vs displacement ductility): a) shear flexure (FS) piers, b),c),d) flexure (F) piers

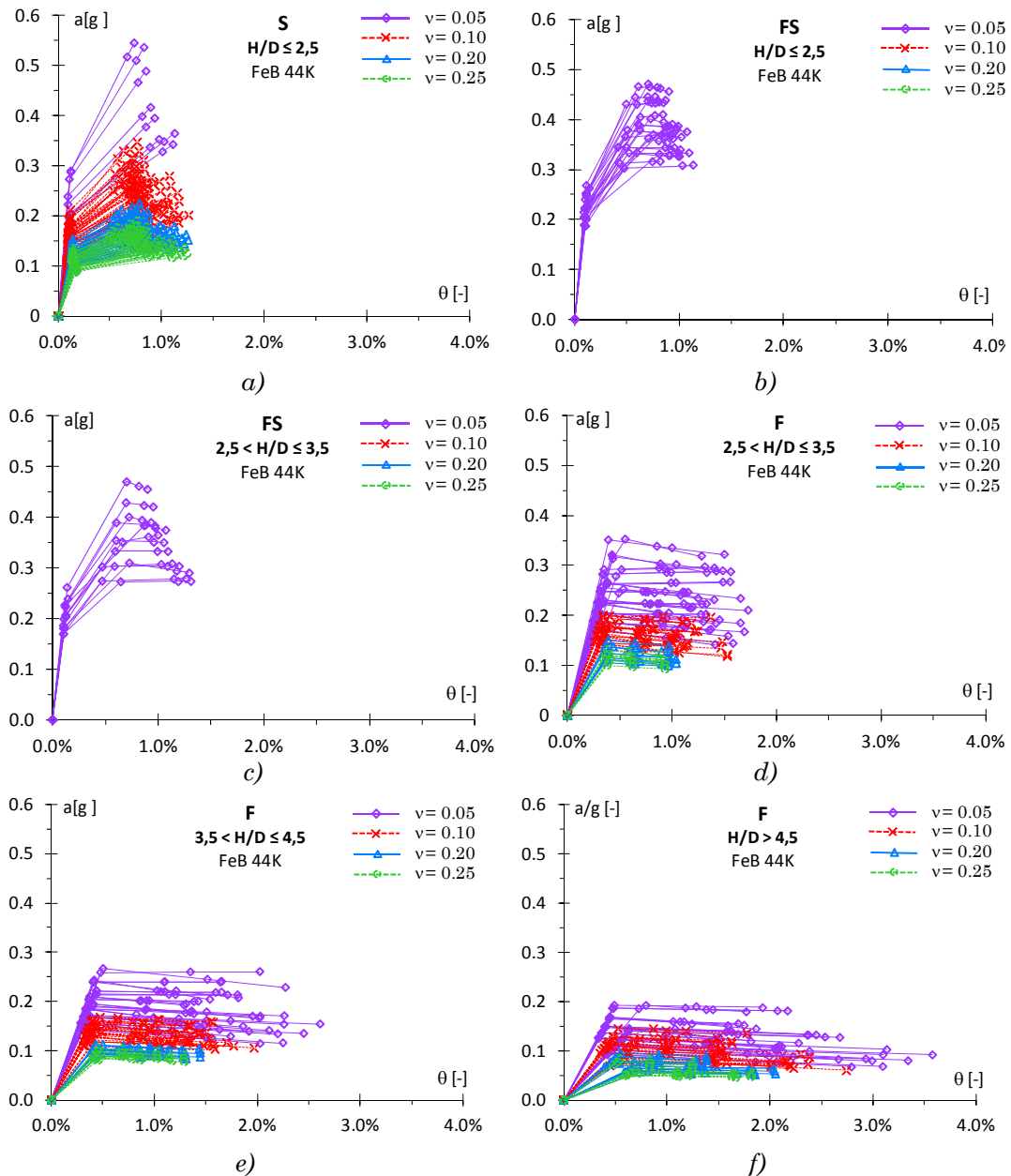


Fig. 5.16 – Adimensional capacity curves (resistant acceleration vs drift): a) shear (S) piers, b), c) shear flexure (FS) piers, d),e),f) flexure (F) piers

In the previous figures the capacity curves obtained for S,SF, F piers reinforced with FEB44k steel type are reported as general reference. The corresponding curves obtained for columns reinforced with steel AQ50-60 have a similar trend, and are omitted for brevity. However, all the significant results that can be extracted from the capacity curves, are included in the charts in the subsequent paragraphs.

The pier samples being a large number, capacity curves were divided into sub-groups in relation to failure mechanisms, and for flexural piers also in different subclasses separating medium-short piers from slender piers with higher ductility capacity.

5.3.1.1 Failure mechanism

As expected, it can be observed for the failure mechanism a strict dependence on the H/D aspect ratio. Approximate ranges individuating different collapse mechanisms for cantilever circular piers in relation to the H/D ratio are found to be the following:

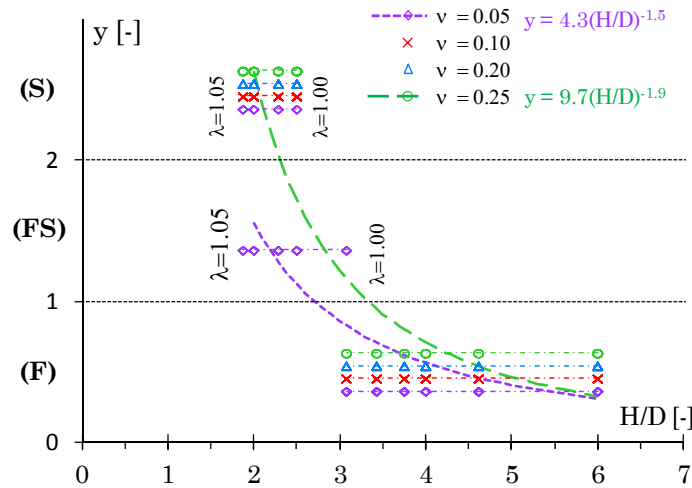


Fig. 5.17 – Failure mechanisms chart. λ_c represents the value of the limit confinement parameter

- $H/D < 2.5$ shear, shear-flexure;
- $2.5 < H/D < 3.5$ shear-flexure, flexure;
- $H/D > 3.5$ flexure

More precisely, the plot on Fig. 5.17 can be used to find the pier type collapse mechanisms, on the base of geometric aspect ratio (with low values corresponding to shear critical columns) and normalized axial load. The series of points correspond to effective H/D ratios individuated in Tab 5.10; interpolating laws are proposed for $\nu=0.05$ and $\nu=0.25$. The range 0-1 in y axis represents the range of (F) piers, 1-2 the range (FS) piers, while $y > 2$ correspond to (S) piers.

5.3.1.2 Strain limits

In Tab.2.4 a summary of the current limit states proposals for the assessment of existing rc structures is reported. The limits chosen in this work for material strain and sectional limit states are reported in Tab. 6.23.

A sensitivity analysis was carried out in order to individuate the correspondence between the selected limit states (PL1 and PL3) and the effective material strain obtained for the circular pier sections under exam.

For PL1 it can be observed that for higher normalized axial load ($\nu=0.20, 0.25$) steel strain limits are less likely to occur when the concrete strain limit has already been reached.

For PL3 it can be noted that the section failure is always related to the attainment of maximum concrete strain when steel bars are already yielded. The maximum strain at the concrete core outer fibers is always under 1%, that is typical of a poorly confined section (for seismically design rc members higher values can

be attained, see Tab.2.3). The upper limits for steel strain ($0.6\varepsilon_{su}$) is never reached.

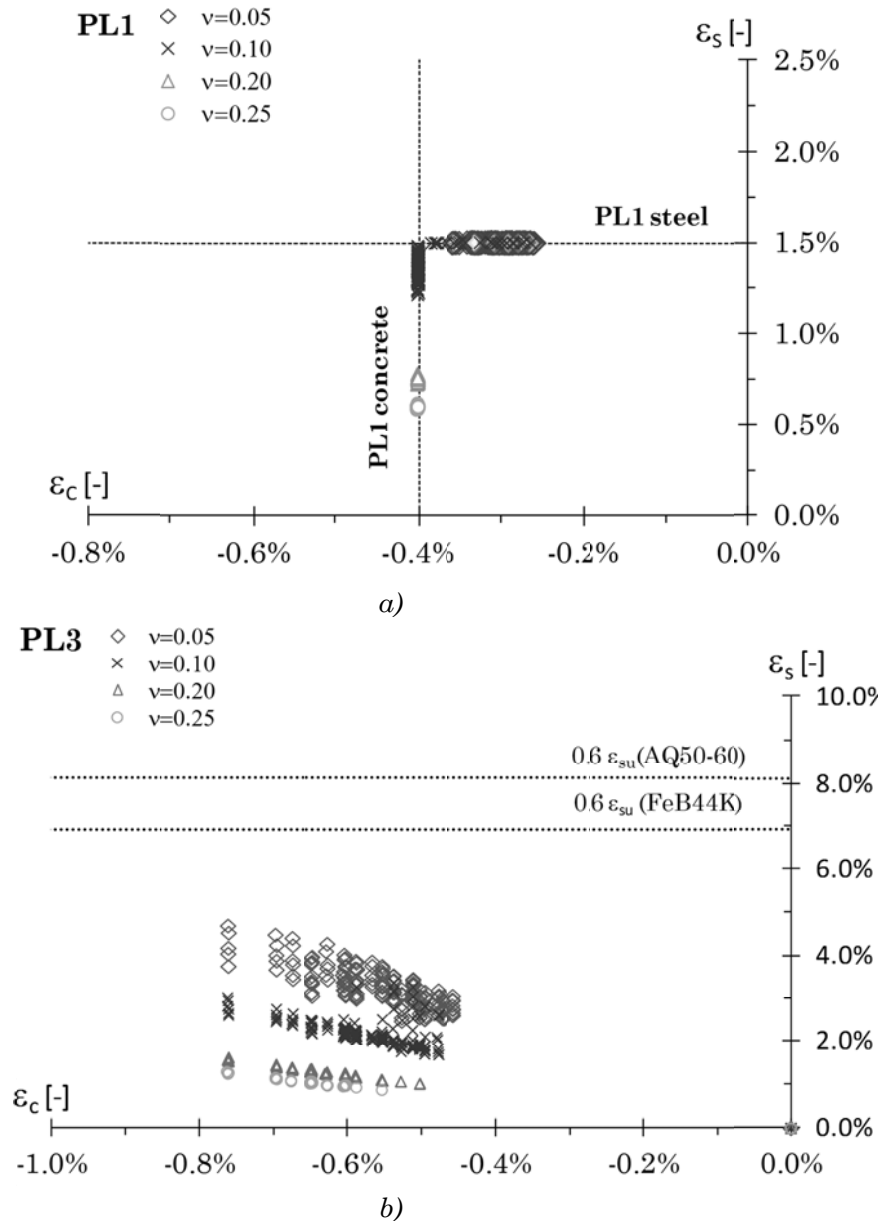


Fig. 5.18 – Steel and concrete deformation: a) PL1, b) PL3

5.3.1.3 Drift limits

In the present section the global drift limits extracted from the capacity curves reported in the paragraph §5.3.1.1 are plotted.

Drift at failure is firstly individuated. The drift values correspond to strain limits defined for PL3 (see Tab. 6.23)

- $0.5\% < \theta_u < 1.5\%$ for (S), (SF) piers. The mean value $\theta_u = 1\%$ is quite representative and confirms the experimental values reported in §5.2.4.

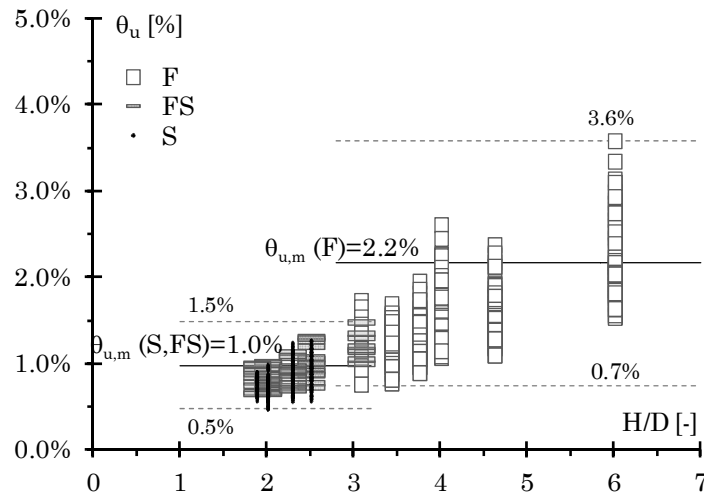


Fig. 5.19 – Drift at failure (θ_u) for flexural(F), shear-flexural (FS), and shear (S) piers.

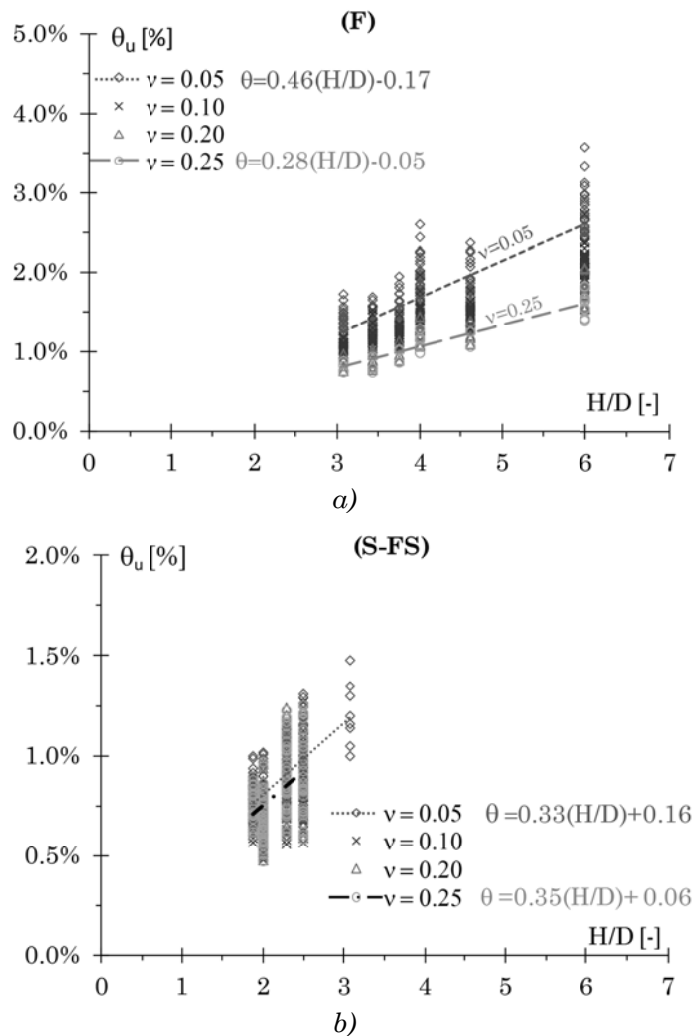


Fig. 5.20 – Interpolating laws for ultimate drift, θ_u : a) flexural(F) piers, b) shear-flexural (FS), and shear (S) piers.

- $0.7\% < \theta_u < 3.6\%$ for (F) piers, with a greater variability, and a medium value of $\theta_m = 2.2\%$.

In Fig. 5.20 interpolating curves are proposed as functions of the aspect ratio H/D and normalized axial load, and can be used to derive the ultimate drift, θ_u (and thus the ultimate displacement, D_u) for the pier under exam, whose characteristics fall within the ranges defined in Tab.5.10.

It has to be found (as for other charts reported hereafter), that other parameters like the reinforcement ratio ρ_l , have not much influence, because the actual ranges are not so variable (all piers samples have low longitudinal reinforcement content and are poorly confined by transverse hoops, with small variability).

5.3.1.4 Nominal drift and drift at shear cracking

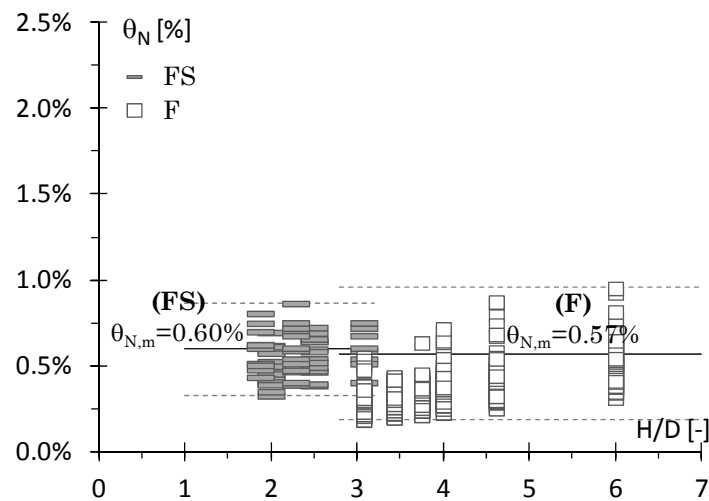


Fig. 5.21 – Nominal drift for flexure-shear (FS) and flexure (F) cantilever piers

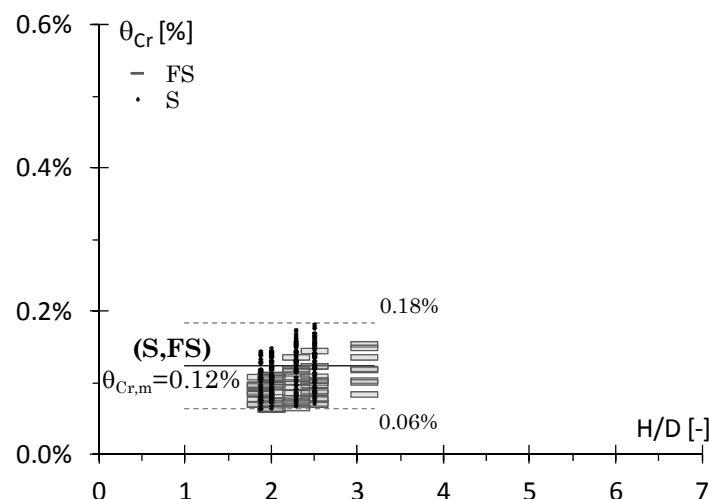


Fig. 5.22 – Drift at shear cracking for shear critical piers (S, FS).

Nominal drifts for (F) and (FS) piers are reported in Fig. 5.21, and can be used to determine the displacement associated to nominal capacity.

In particular for (F) piers the variability is significant, and the indication of the mean nominal drift $\theta_{N,m}=0.57$ obtained, is not applicable to reconstruct directly the capacity curve for a certain pier under exam. In this case the same information can be obtained from the adimensional curvature plots reported in §5.3.1 (this is possible when the (F) curves are not affected by the attainment of the Shear Cracking, thus the shear deformation is not significant and the capacity curve can be simply represented as bilinear, as can be seen in Fig.5.17).

5.3.1.5 Nominal moment and curvature

As it was mentioned in Chapter 1, a fundamental assumption in DB procedure is that the elastic stiffness of cracked concrete sections is essentially proportional to strength, on the contrary the yield curvature can be assumed independent from strength (reinforcement content). The following charts, are obtained from a moment curvature analysis with bilinear representation (see §1.1.1). The charts follows the layout of similar charts proposed by other authors^[P1, P3] for section of new seismically designed members. Here the concrete sections analyzed are typical of existing bridges piers, with material and reinforcement characteristics corresponding to the ranges individuated in Tabs. 5.10.

The results obtained, that can be used also to plot directly the capacity curve for flexural piers, are aligned but partially different from those obtained in literature for newly designed sections (reported in Fig. 2.10): e.g. the average values of yield curvature are generally lower in respect to those proposed by [P1, P3] for the section under exams, and also the stiffness ratio for cracked section at yielding is lower.

The values of adimensional nominal moment, M_n , and nominal curvature, χ_n are derived for different values of concrete strength, steel properties of longitudinal bars, and different reinforcement content ρ_l (confinement effects related to the different transverse reinforcement content ratio are evaluated, but not much significant in relation to the percentages considered).

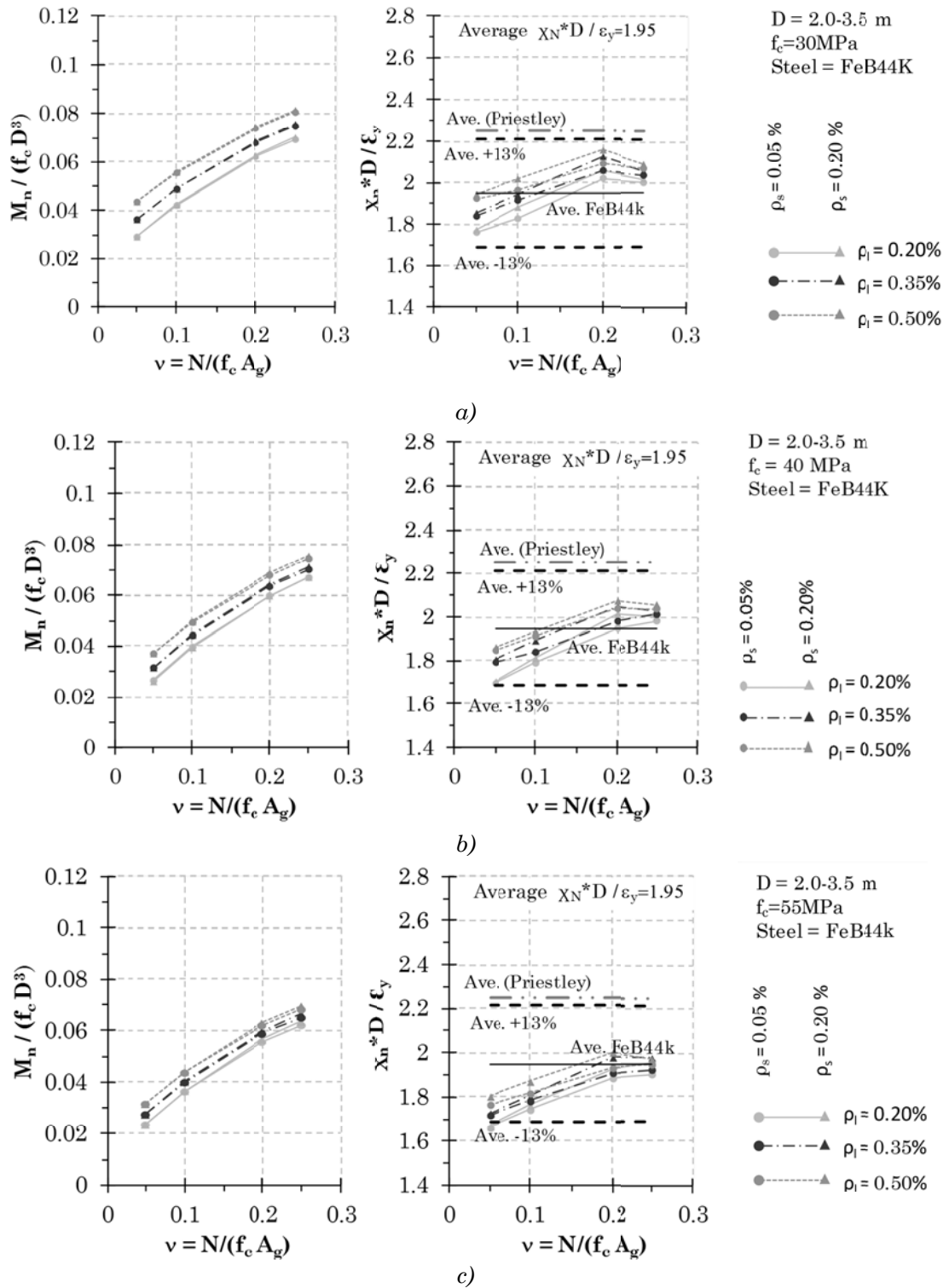


Fig. 5.23 – Single bent circular pier: dimensionless nominal moment and yield curvature (FeB44k steel type): a) $f_c=30\text{MPa}$, b) $f_c=40\text{MPa}$, c) $f_c=55\text{MPa}$

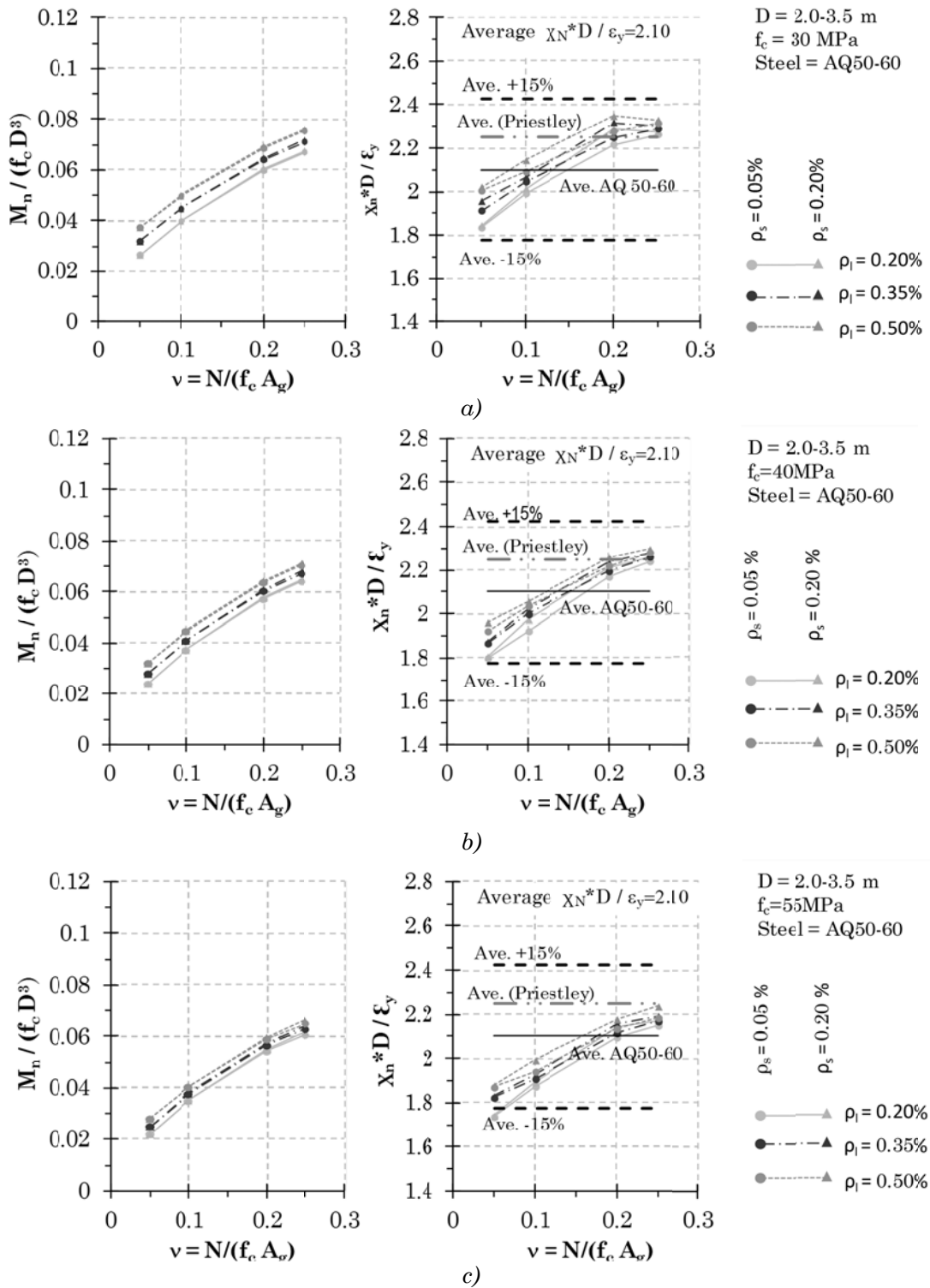


Fig. 5.24 – Single bent circular pier: dimensionless nominal moment and yield curvature (AQ50-60 steel type): a) $f_c=30\text{MPa}$, b) $f_c=40\text{MPa}$, c) $f_c=55\text{MPa}$

Tab. 5.11 – Dimensionless yield curvature for circular bridge columns

Single bent (D=2.0-3.5m)			
		FeB44k	Aq50-60
χ_{ND}/ε_y	mean	1.95	2.10
	error	0.13	0.15

5.3.1.6 Elastic stiffness (prior to shear cracking)

It has already been described in §5.2.1, that the phenomenological model adopted for pier capacity, requires in phase I an initial stiffness defined as $K_y=1/(1/K_{gf}+1/K_{sf})$ (see Tab. 5.2).

The cracked flexural stiffness given by Eq. 5.5 can be obtained directly from the charts reported in Fig. 5.26. The global initial stiffness prior to shear cracking can be thus directly obtained, using Eq.5.6., and the expression reported in Tab. 5.2.

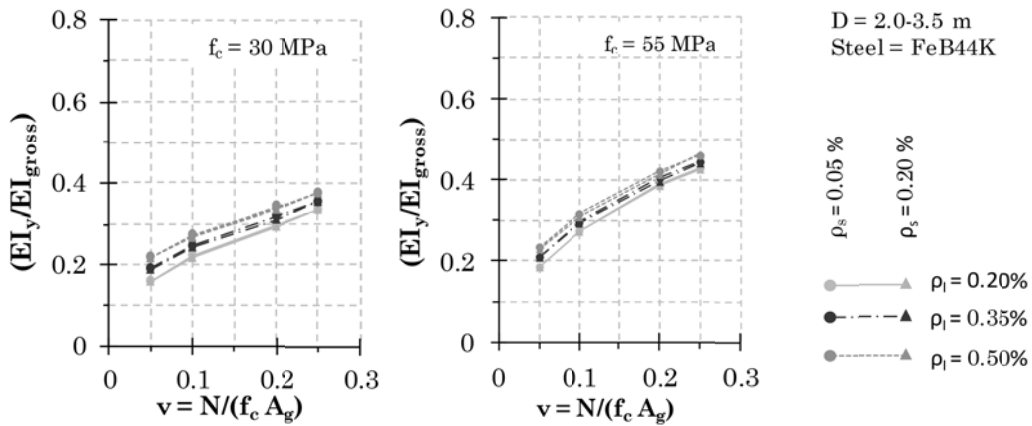


Fig. 5.25 – Single bent circular pier: effective stiffness ratio (FeB44k steel type)

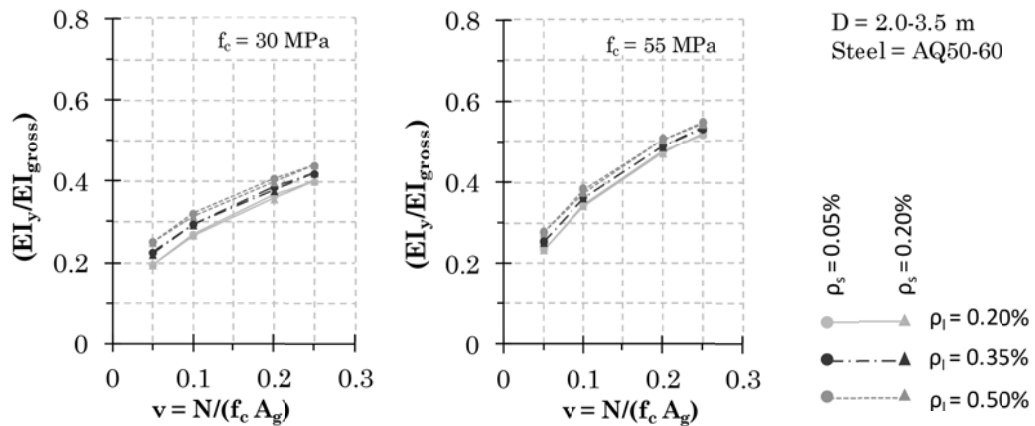


Fig. 5.26 – Single bent circular pier: effective stiffness ratio (AQ50-60 steel type)

5.3.1.7 Post-yielding and post-cracking slope

As it can be seen from Fig. 5.16, 5.17, the typical capacity curve for (F) and (FS) piers has a very low residual stiffness after yielding.

The post-yielding slope of the adimensional capacity curve ($a[g], \theta$) is around zero, sometime positive, sometime negative, as can be seen in Fig.5.16. The values obtained are reported as function of the H/D ratios in Fig. 5.27, and an interpolating law is proposed.

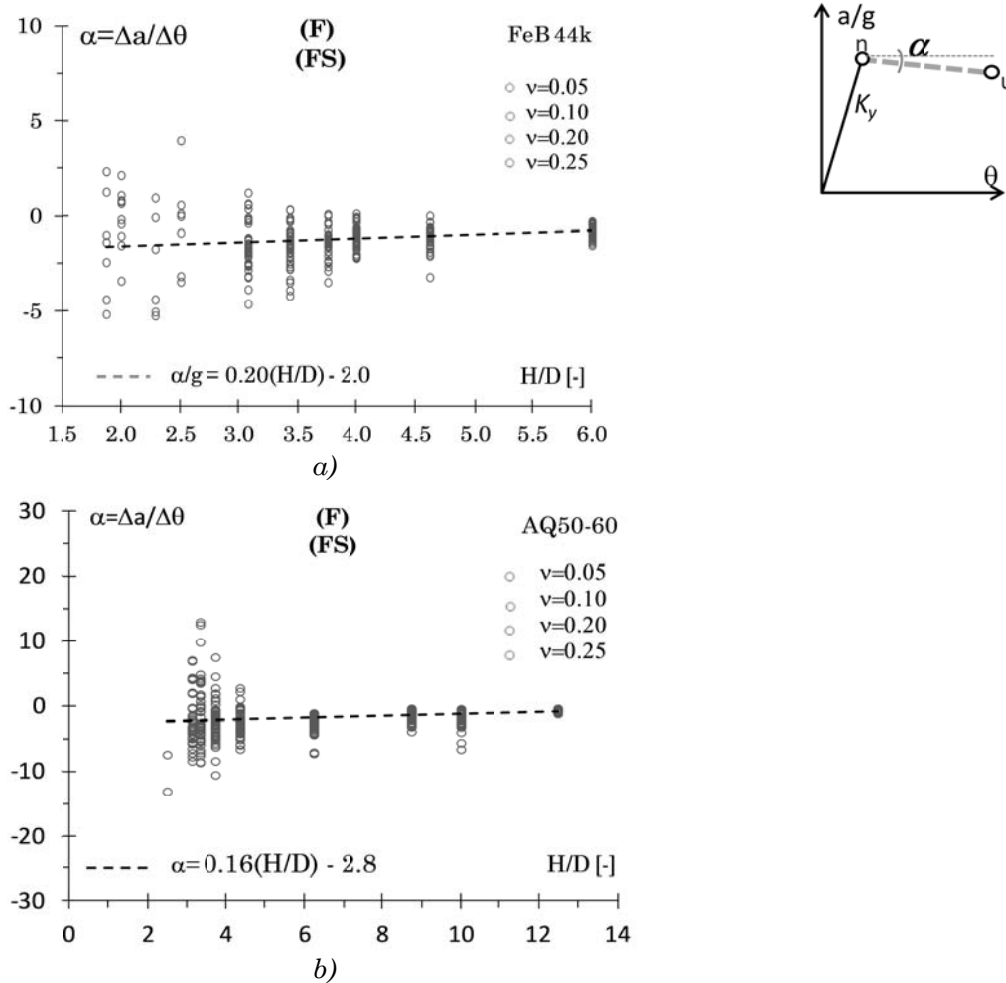


Fig. 5.27 – Single bent circular pier: post yielding slope for (F) and (SF) piers. a) FeB44k steel type, b) AQ50-60 steel type.

Similarly the capacity curve slope values are obtained for piers with brittle shear failure, (S) type. In this case there is an abrupt stiffness reduction after the shear cracking, but a significant residual stiffness is maintained till the attainment of maximum shear strength.

In this case the values that can be derived directly from the charts of Fig. 5.28 represent the slope of the adimensional capacity curves (which are plotted in Fig.5.16) between the Shear Cracking Point and the point corresponding to ultimate displacement.

These values can be directly used to get the final point of a Force-Displacement curve for a shear-critical pier, together with information relative to ultimate drift (Fig. 5.20) and ultimate stiffness (Fig. 5.28)

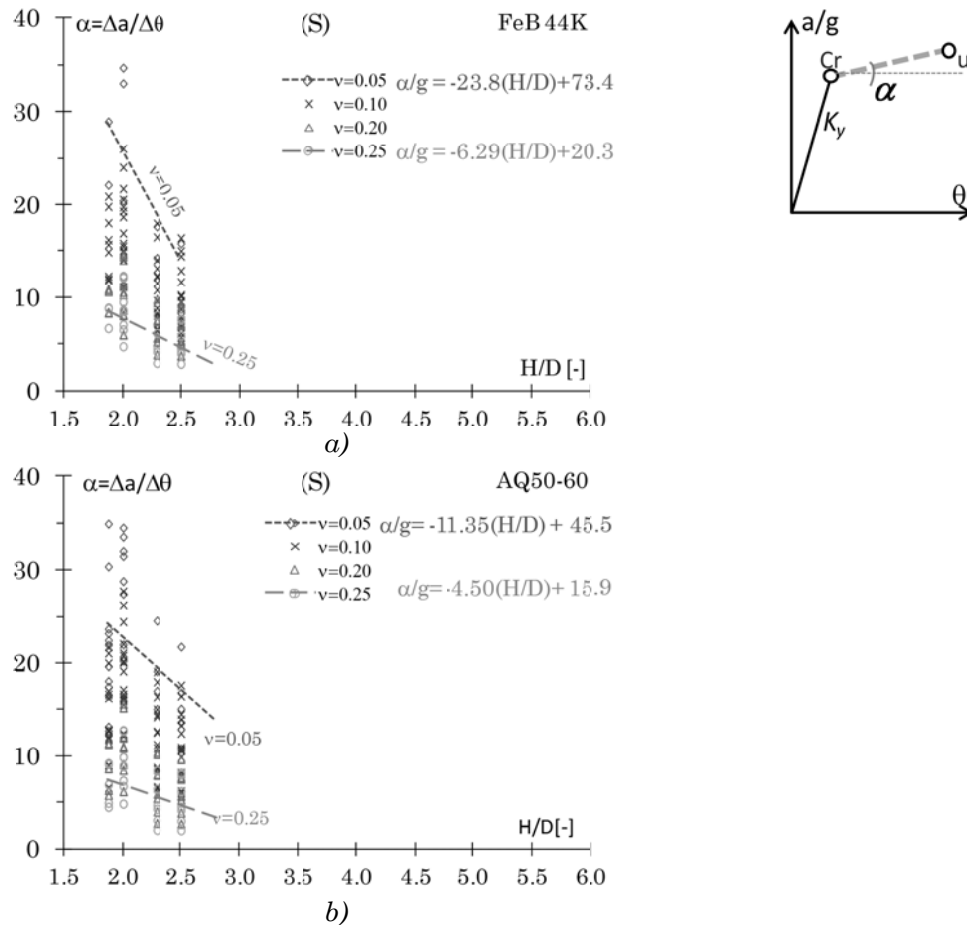


Fig. 5.28 – Single bent circular pier: slope after shear cracking for (S) piers. a) FeB44k steel type, b) AQ50-60 steel type.

5.3.1.8 Effective stiffness

The effective stiffness at ultimate (target) displacement is one of the fundamental parameters that have to be known for the applicability of the DB assessment procedure.

In the following charts the effective stiffness, K_{eff} , is expressed as a fraction of the initial stiffness K_y (prior to shear cracking). K_{eff} can be estimated as a function of the geometric aspect ratio H/D and the normalized axial load v .

It can be noted that the average value K_{eff}/K_y is not so different for (F) piers and (S) piers, at least for low value of v , but the initial stiffness K_y is generally higher for S piers (see Fig 5.16) thus also the final K_{eff} will result higher.

Effective stiffness is also expressed as a function of displacement ductility μ in Fig. 5.29. This graph can be useful, if different limit states are adopted for assessment, corresponding to lower ductility values in respect to the ultimate value.

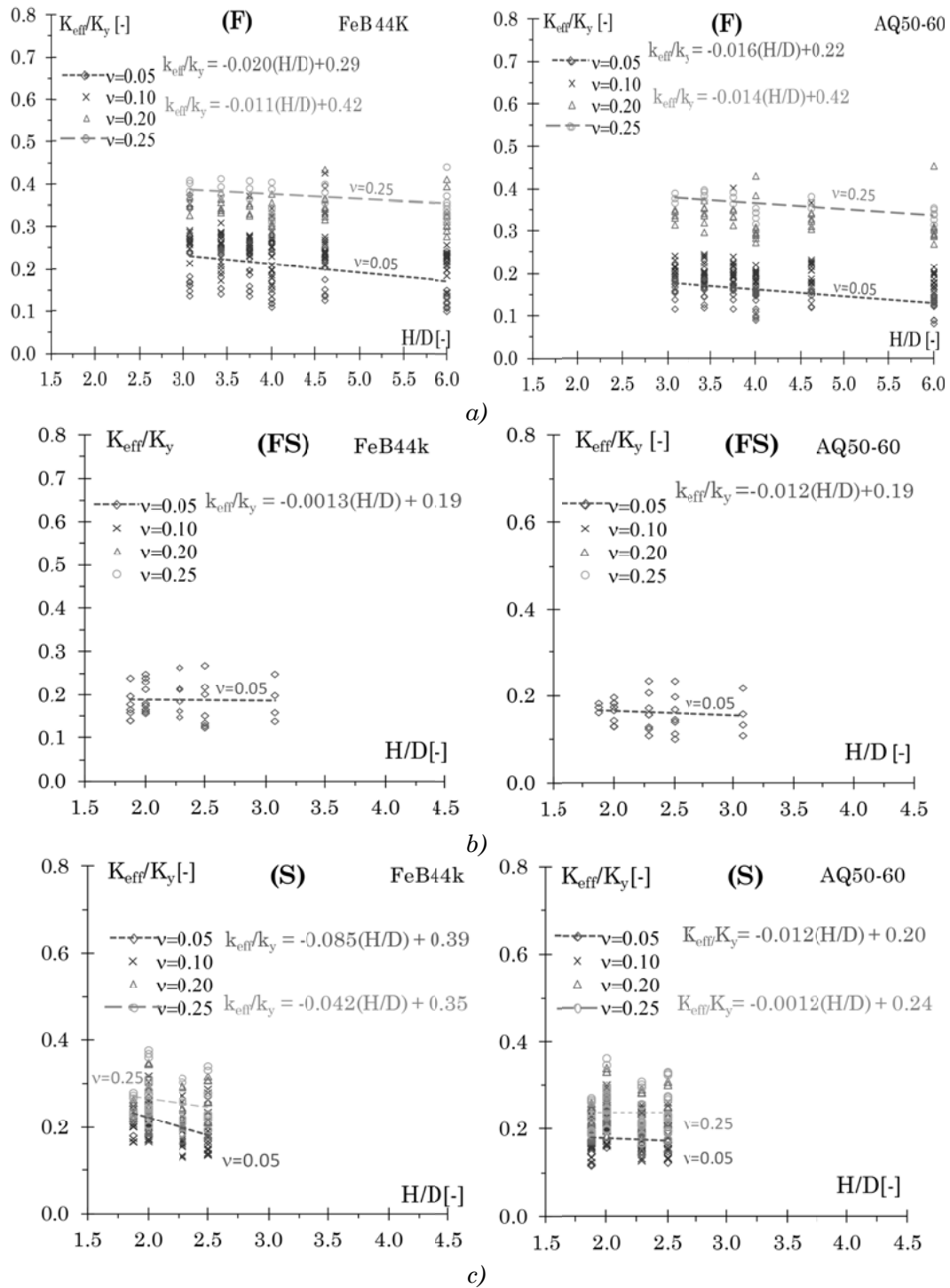


Fig. 5.29 – Effective stiffness at ultimate displacement for (F), (FS), (S).

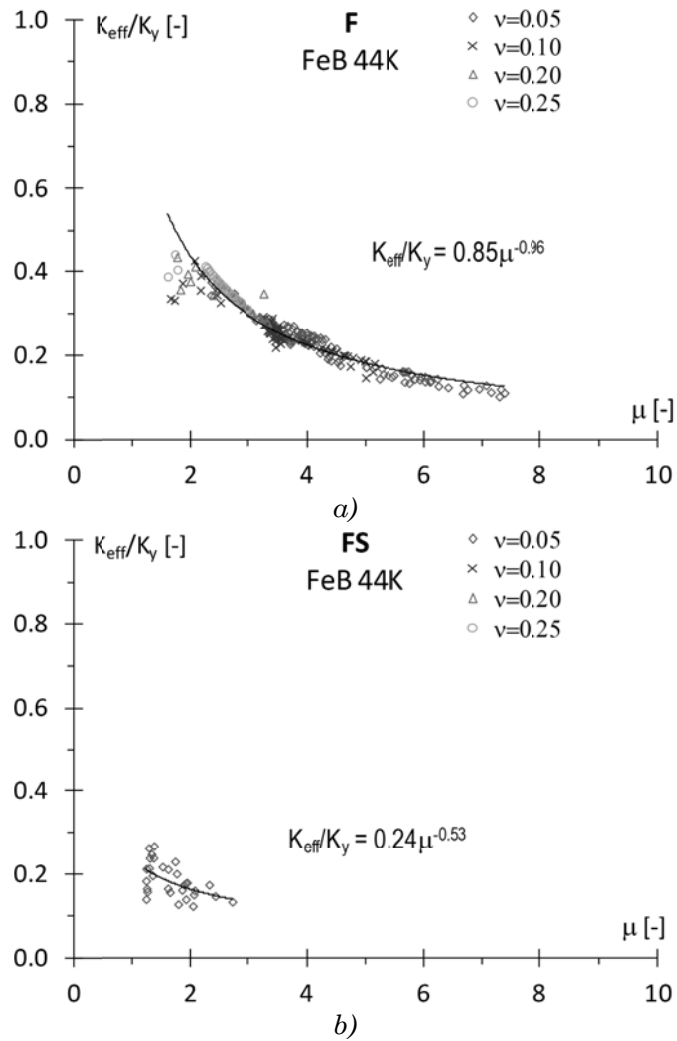


Fig. 5.30 – Effective stiffness as function of ductility for (F), (FS) piers.

5.3.2 Multiple bent (frame) piers with circular section

Multiple bent piers with circular section are also analyzed in the parametric study, with the characteristics reported in Tab.5.12, covering the ranges individuated in Tabs. 6.15-6.20.

The circular frame piers have small diameters, variable between 0.4 and 1.6m, with height over diameter ratios, H/D , ranging between about 2.0 and 12.0. Longitudinal reinforcement ratios ρ_l reaches higher values in respect to cantilever piers, within the range [0.5-1.5], the concrete section being smaller. Also the volumetric transverse reinforcement content is higher, between 0.10 and 0.30%. The axial load at the pier base is generally quite low, under 25% of the section concrete strength. The ranges analyzed for concrete strength is $30 < f_c < 55$, and two steel types are considered, FeB44k and AQ50-60.

The number of pier samples obtained from the combinations of the analyzed parameters are 2376.

Tab. 5.12 – *Multiple bent circular piers: 2376 pier samples studied in total.*

		Multiple Bent - Circular Piers					
D	[m]	0.4	0.8	1.2	1.6		
H *	[m]	2.5	3.0	4.0	5.0	7.0	12.0
ρ_l	[%]	0.50	1.00	1.50			
ρ_{st}	[%]	0.10	0.20	0.30			
ν_k	[-]	0.05	0.10	0.20	0.25		
f_c	[MPa]	30	40	55			
Steel	[-]	Aq50-60	FeB44K				

* effective H/D ratios: 1.9, 2.1, 2.5, 3.1, 3.3, 3.8, 4.4, 6.3, 8.8, 10.0, 12.5

5.3.2.1 Capacity curves

The capacity curves obtained are reported in an adimensional fashion for (S), (SF) and (F) piers. The lateral resisting acceleration (expressed in terms of g) is expressed as a function of the total drift θ , and also as a function of the displacement ductility, μ , in the case of (SF) and (F) piers.

In the previous figures the capacity curves obtained for S,SF, F piers reinforced with AQ50-60 steel type are reported as general reference. The corresponding curves obtained for columns reinforced with steel FeB44k have a similar trend, and are omitted for brevity.

As already done for cantilever piers, the samples being a large number, capacity curves were divided into sub-groups in relation to the failure mechanism, and for flexural piers also in different subclasses separating medium-short piers from slender piers with higher ductility capacity.

The adimensional capacity curves are representative in terms of resistant acceleration of a single column for a multiple pier bent. This value has to be

multiplied for the number of columns (supposed all equal) to obtain the total resistant shear of the pier bent.

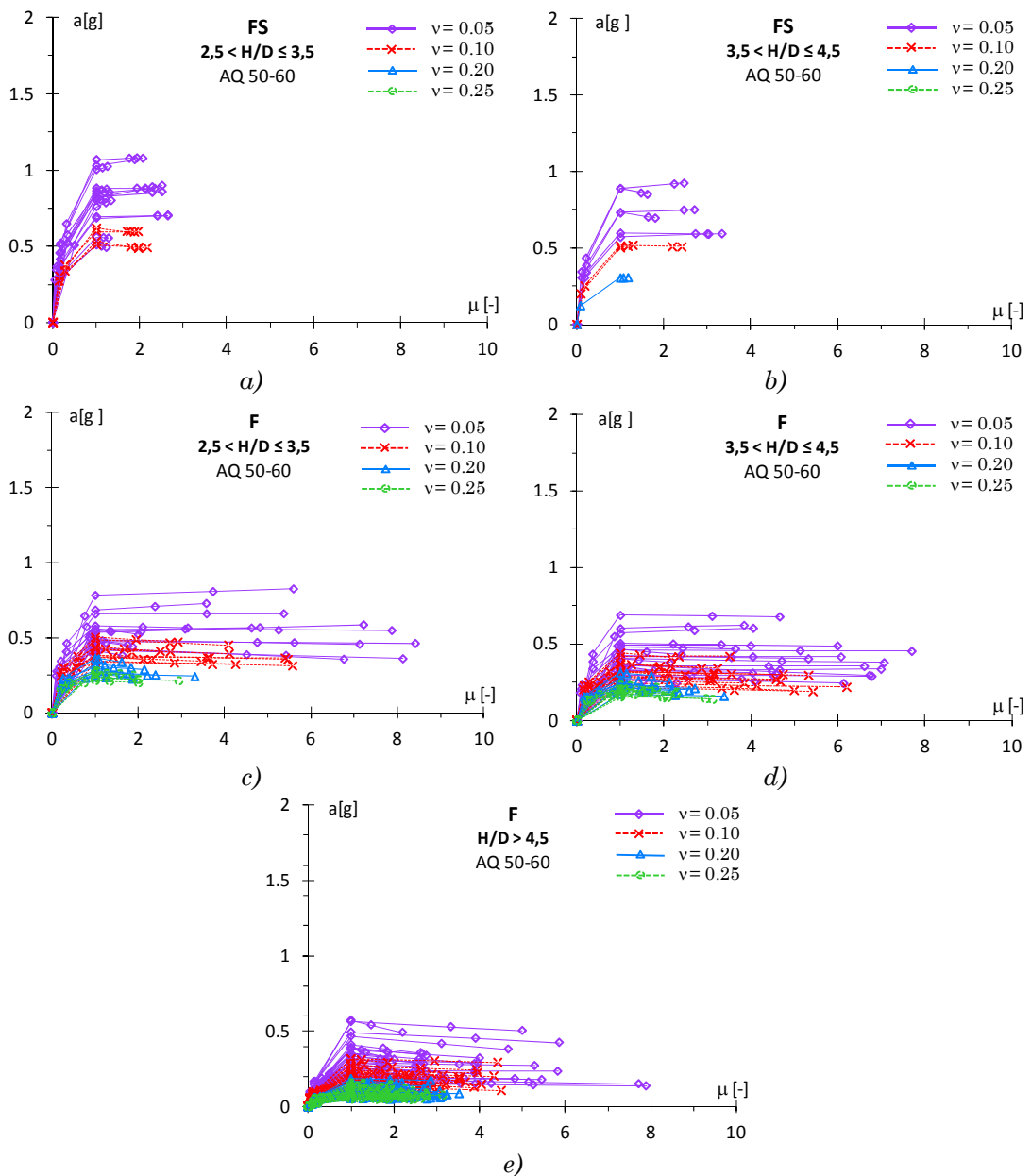


Fig. 5.31 – Adimensional capacity curves (resistant acceleration vs displacement ductility): a), b) shear flexure (FS) piers, c),d),e) flexure (F) piers

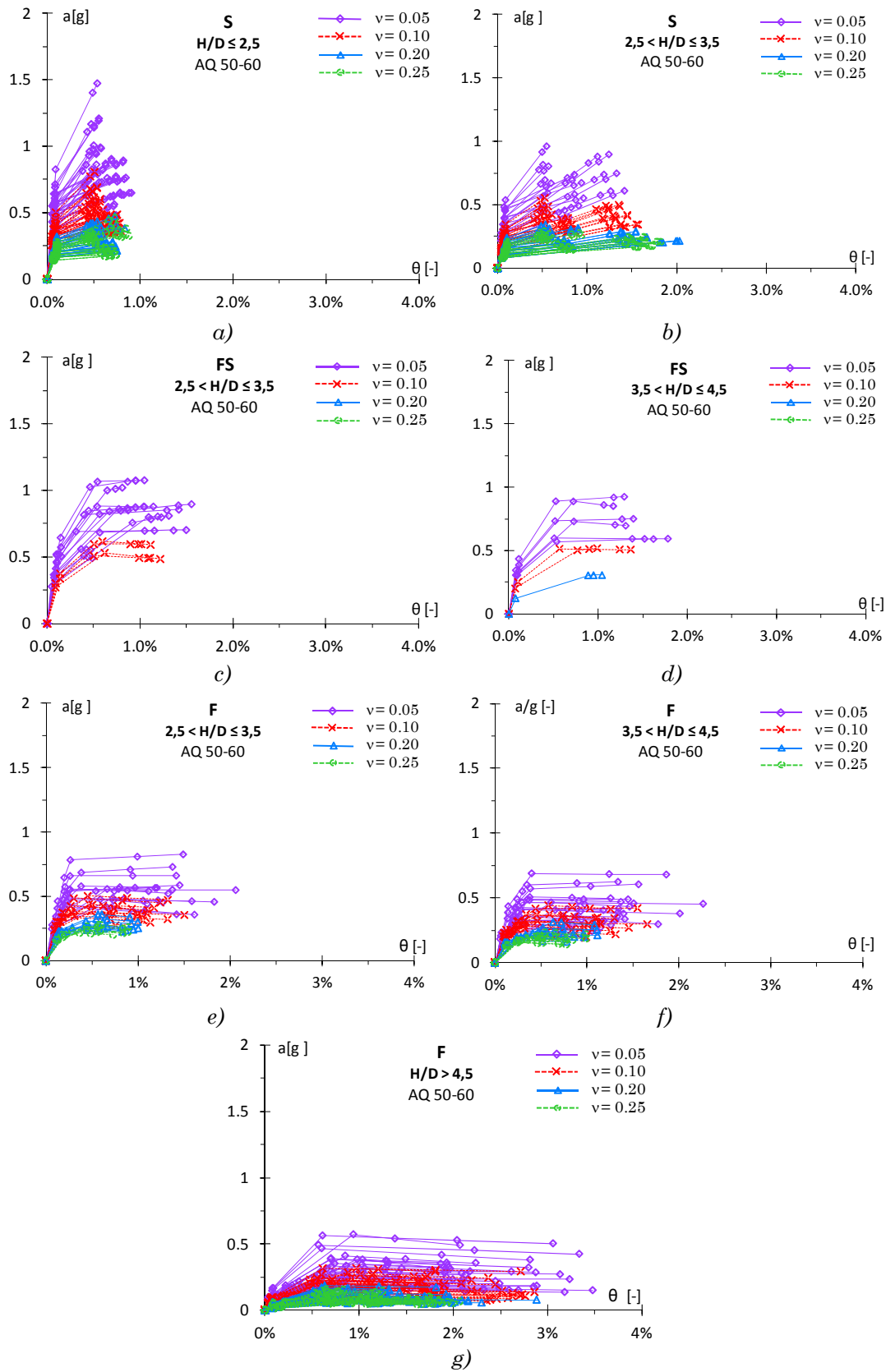


Fig. 5.32 – Adimensional capacity curves (resistant acceleration vs drift): a), b) shear (S) piers, c), d) shear flexure (FS) piers, e), f), g) flexure (F) piers

5.3.2.1 Failure mechanism

The chart represents a tool for the individuation of the failure mechanism expected for the pier under exam. Approximate ranges individuating different collapse mechanisms for cantilever circular piers in relation to the H/D ratio are found to be the following:

- $H/D < 2.5$ shear;
- $2.5 < H/D < 3.5$ shear, shear-flexure, flexure;
- $3.5 < H/D < 4.5$ shear flexure, flexure;
- $H/D > 4.5$ shear flexure, flexure

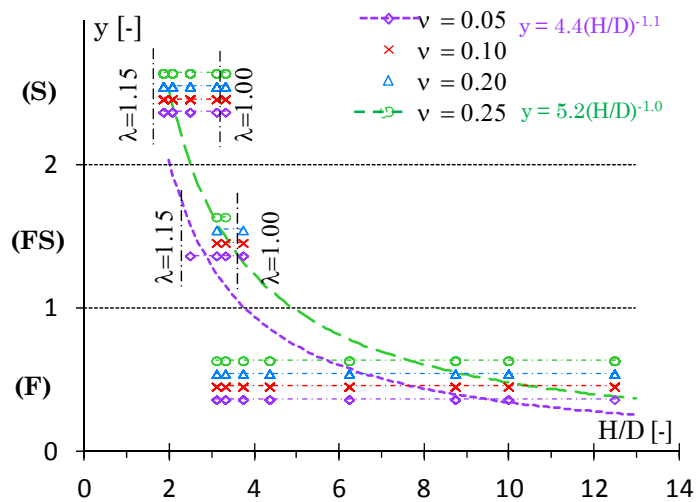


Fig. 5.33 – Failure mechanisms chart. λ_c represents the confinement parameter

The series of points correspond to effective H/D ratios individuated in Tab 5.10; interpolating laws are proposed for $\nu=0.05$ and $\nu=0.25$. The range 0-1 in y axis represents the range of (F) piers, 1-2 the range (FS) piers, while $y > 2$ correspond to (S) piers.

5.3.2.1 Strain limits

The sensitivity analysis developed in §5.3.1.2, is repeated herein for frame pier sections, to individuate the correspondence between the selected limit states (PL1 and PL3) and the effective material strains obtained.

For PL1 it can be observed that for higher normalized axial load ($v=0.20, 0.25$) steel strain limits are less likely to occur when the concrete strain limit has already been reached.

For PL3 it can be noted that the section failure is always related to the attainment of maximum concrete strain when steel bars are already yielded. The maximum strain at the concrete core outer fibers reaches higher values, but at maximum about 1.0-1.1%. The upper limits for steel strain ($0.6\varepsilon_{su}$) is never reached.

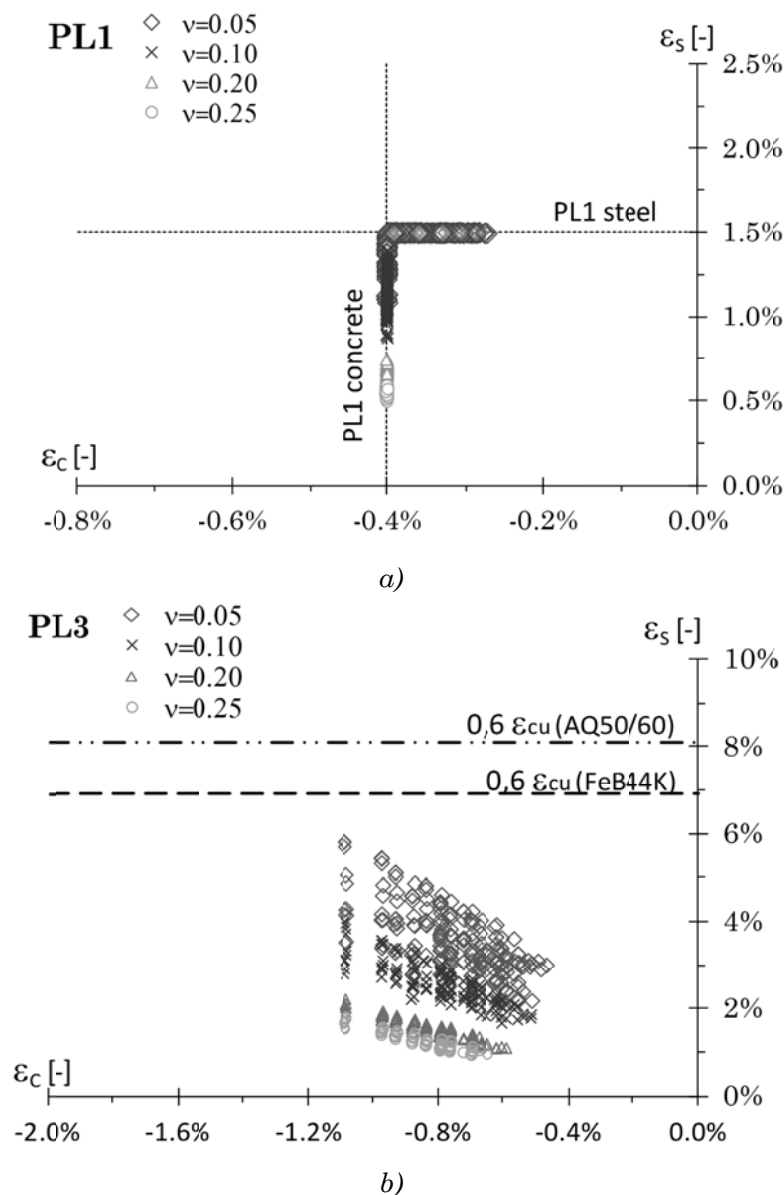


Fig. 5.34 – Steel and concrete deformation: a) PL1, b) PL3

5.3.2.2 Drift limits

In this paragraph the global drift limits extracted from the capacity curves reported in §5.3.2.1. are plotted.

Drift at failure is firstly individuated. The drift values correspond to strain limits defined for PL3 (see Tab. 6.23)

- $0.4\% < \theta_u < 2.1\%$ for (S), (SF) piers, with a mean value 1.3%.

- $0.7\% < \theta_u < 4.1\%$ for (F) piers, with a greater variability, and a medium value of $\theta_m = 2.4\%$.

In Fig. 5.25 interpolating curves are proposed as functions of the aspect ratio H/D and normalized axial load, and can be used to derive the ultimate drift, θ_u (and thus the ultimate displacement, D_u) for the pier under exam, whose characteristics fall within the ranges defined in Tab.5.10.

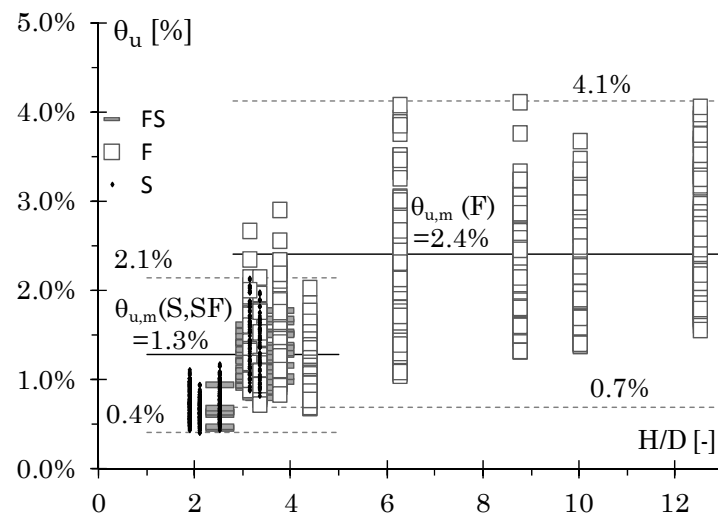


Fig. 5.35 – Drift at failure (θ_u) for flexural (F), shear-flexural (FS), and shear (S) piers.

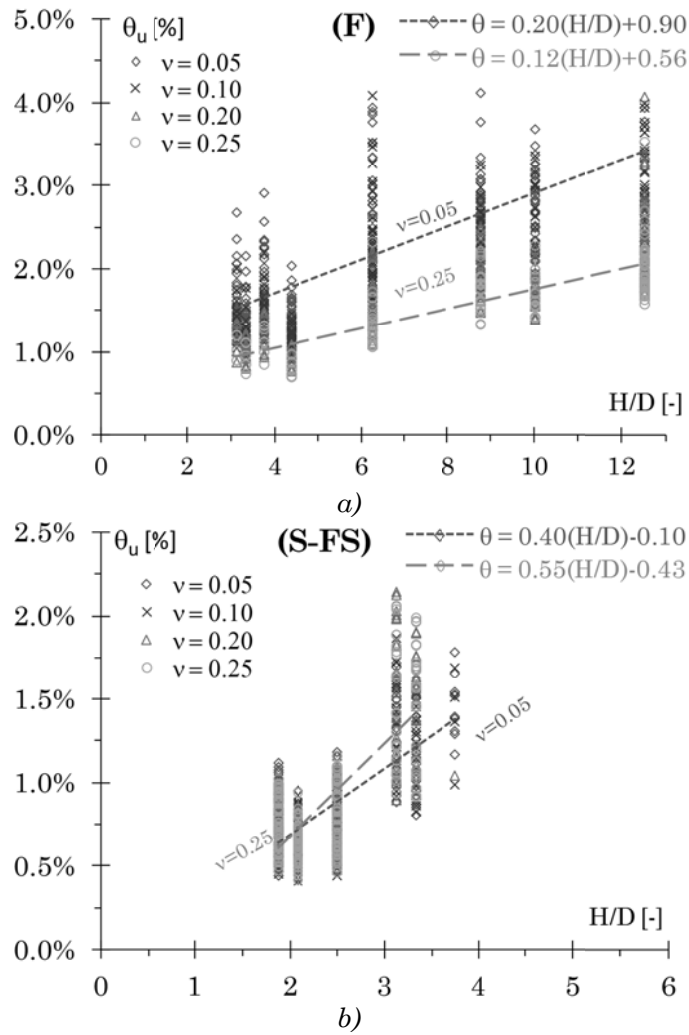


Fig. 5.36 – Interpolating laws for ultimate drift, θ_u : a) flexural (F) piers, b) shear-flexural (FS), and shear (S) piers.

5.3.2.3 Nominal drift and drift at shear cracking

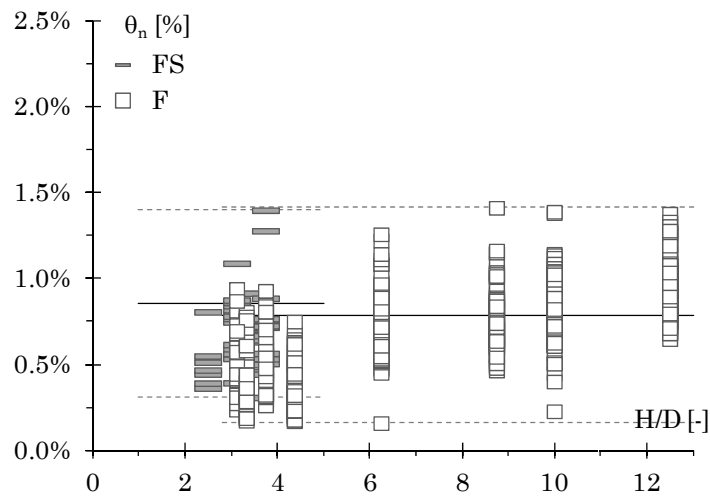


Fig. 5.37 – Nominal drift for flexure-shear (FS) and flexure (F) cantilever piers

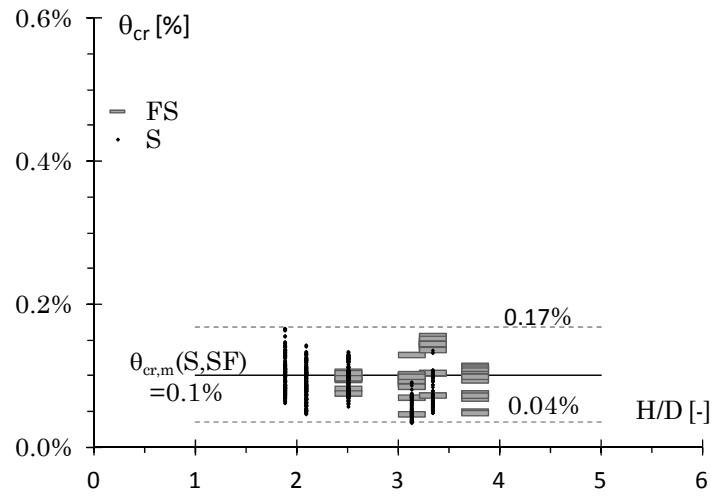


Fig. 5.38 – Drift at shear cracking for shear critical piers (S, FS).

Nominal drifts for (F) and (FS) piers are reported in Fig. 5.37. For nominal drift, same comments reported in §5.3.1.4 are valid.

Drift at shear cracking is reported in Fig. 5.38, and the medium value of 0.1% can be considered representative.

5.3.2.4 Moment-Curvature analysis

The values of adimensional nominal moment, M_n , and nominal curvature, χ_n are plot for different values of concrete strength, steel properties of longitudinal bars, and different reinforcement content ρ_l . The results obtained can be used to find directly the Nominal Yield Point in the capacity curve of flexural piers.

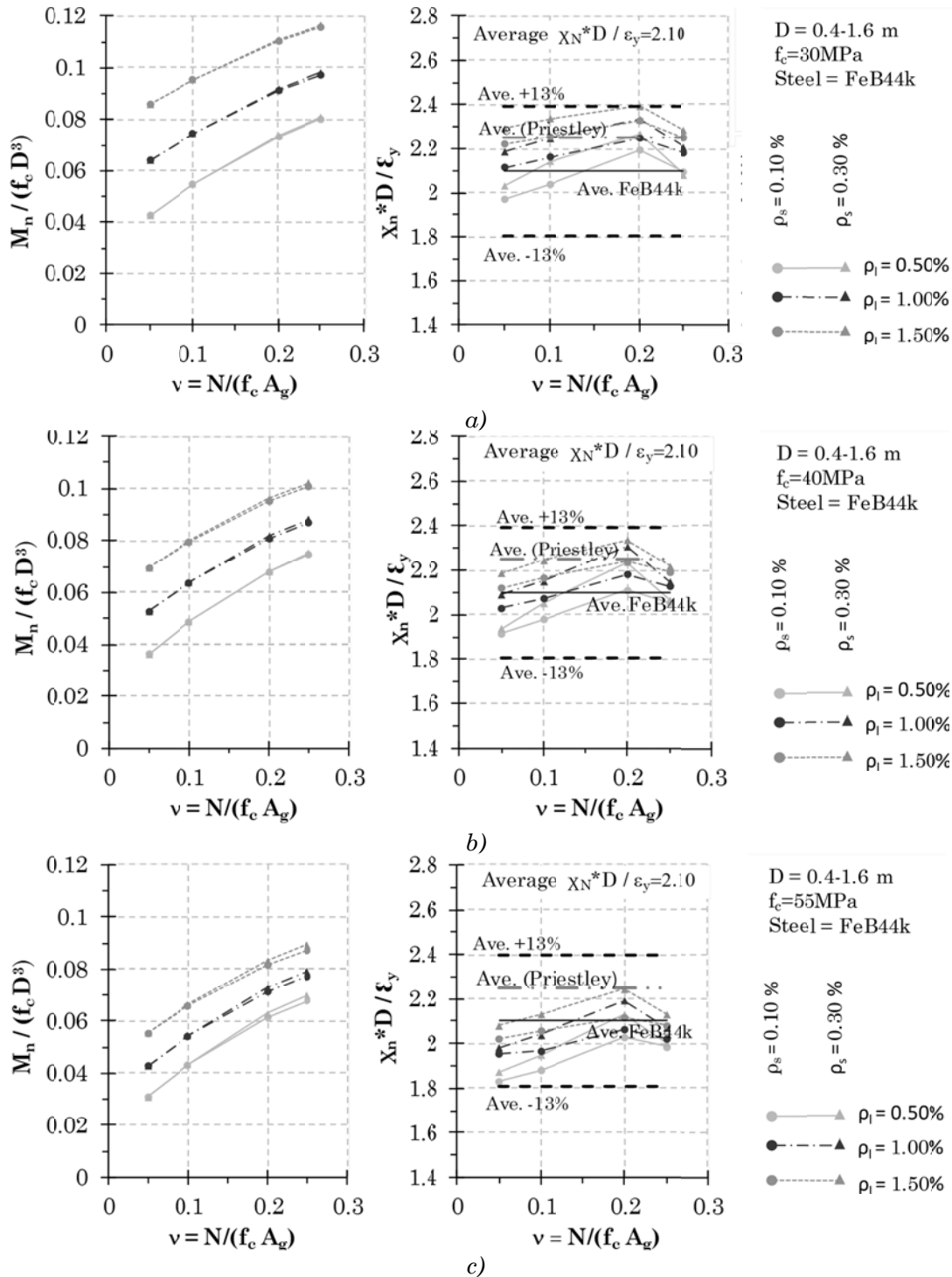


Fig. 5.39 – Multiple bent circular pier: M_n and nominal yield curvature, χ_n (FeB44k steel type): a) $f_c=30\text{MPa}$, b) $f_c=40\text{MPa}$, c) $f_c=55\text{MPa}$

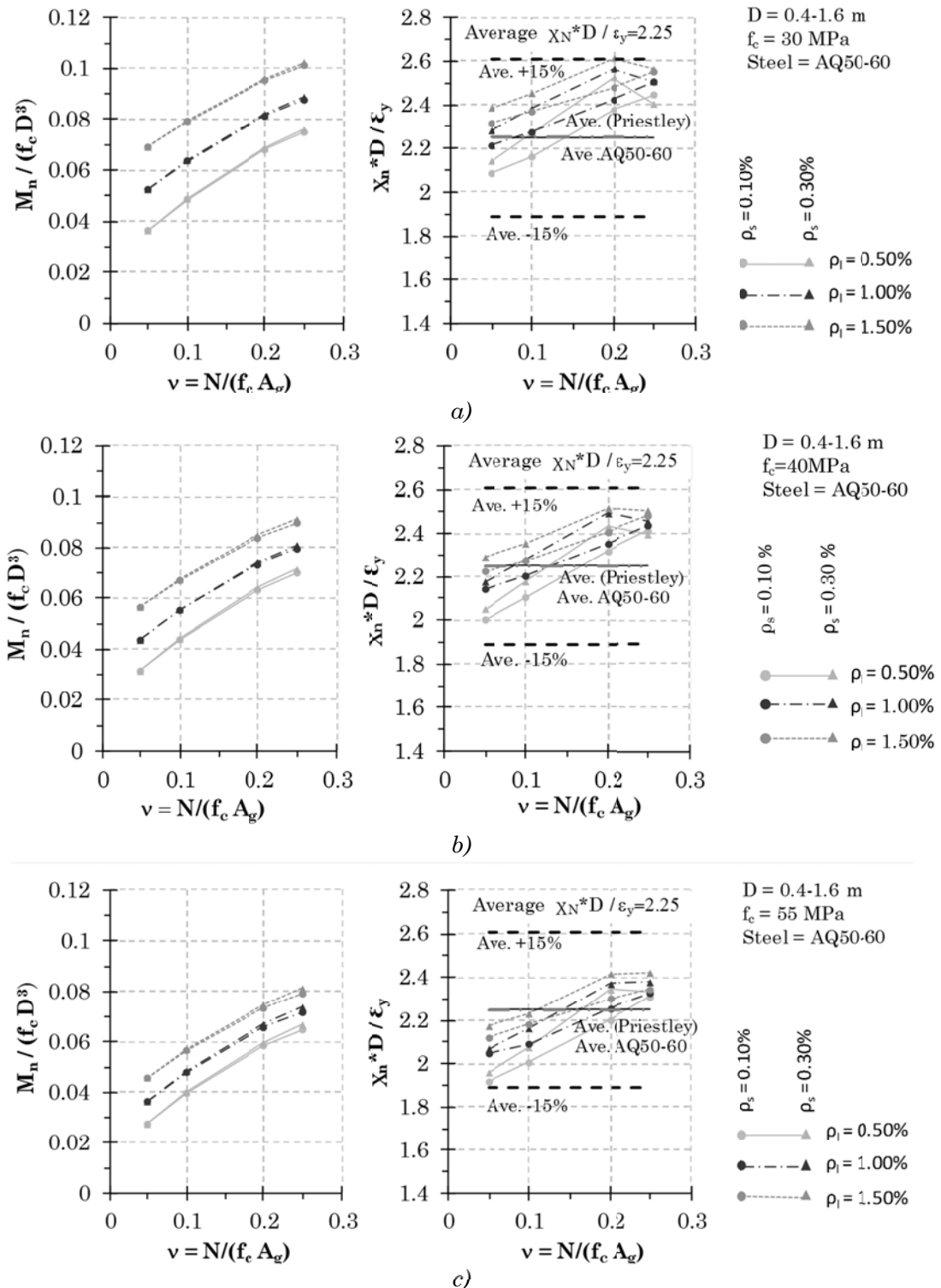


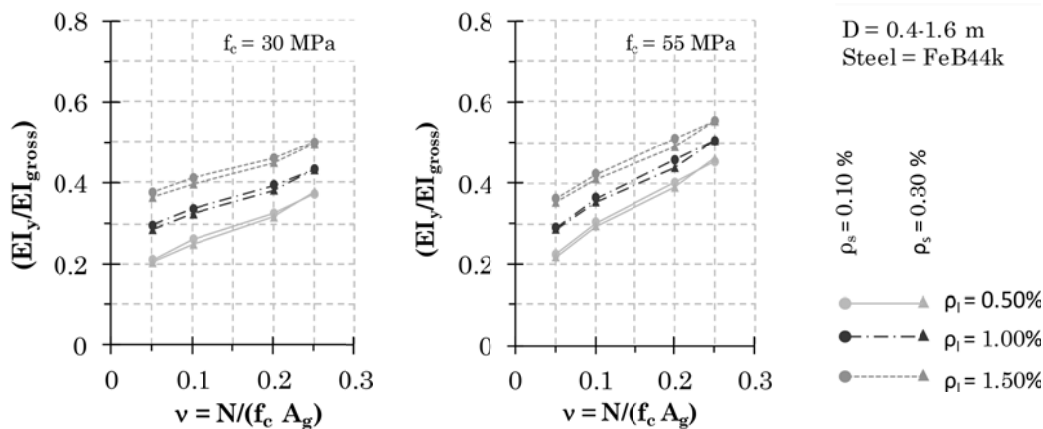
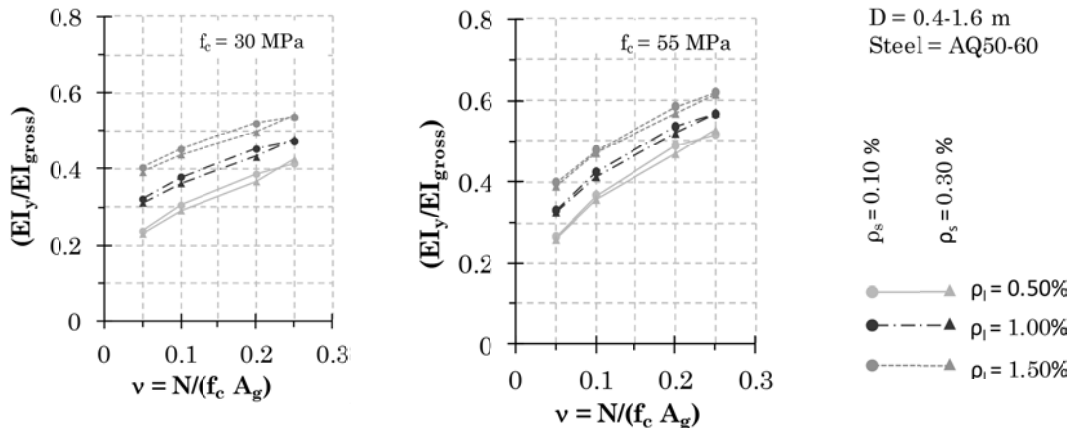
Fig. 5.40 – Multiple bent circular pier: dimensionless nominal moment and yield curvature (AQ50-60 steel type)

Tab. 5.13 – Dimensionless yield curvature for circular bridge columns

Multiple Bent (D=0.4-1.6m)			
		FeB44k	Aq50-60
$\chi_N D / \varepsilon_y$	mean	2.10	2.25
	error	0.13	0.15

5.3.2.5 Elastic stiffness (prior to shear cracking)

The cracked flexural stiffness given by Eq. 5.5 can be obtained for multiple bent circular piers directly from the charts reported in Fig. 5.42. The global initial stiffness prior to shear cracking can be thus directly obtained, using Eq.5.6., and the expression reported in Tab. 5.2.


Fig. 5.41 – Multiple bent circular pier: effective stiffness ratio (FeB44k steel type)

Fig. 5.42 – Multiple bent circular pier: effective stiffness ratio (AQ50-60 steel type)

5.3.2.1 Post-yielding and post-cracking slope

The typical capacity curve for (F) and (FS) piers has a very low residual stiffness after yielding. The values obtained are reported as function of the H/D ratios in Fig. 5.243, and an interpolating law is proposed.

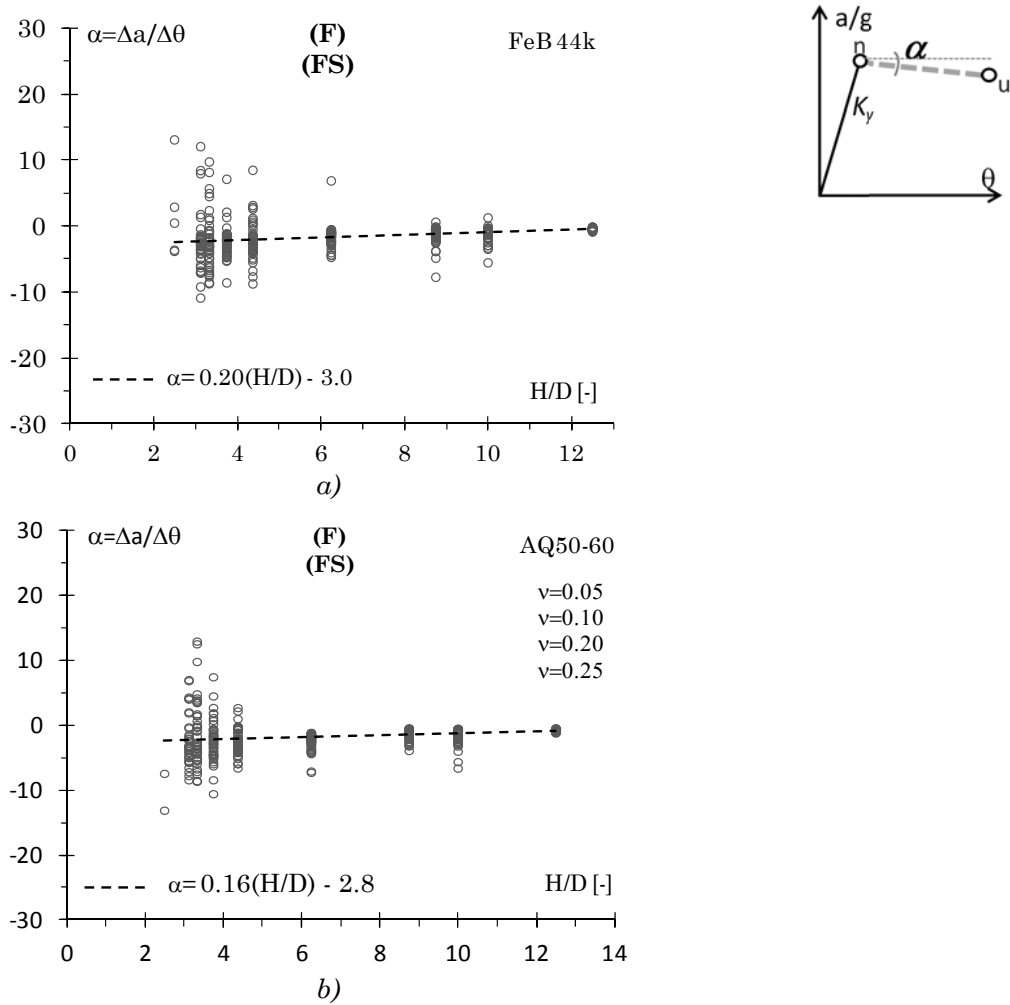


Fig. 5.43 – Multiple bent circular pier: post yielding slope for (F) and (SF) piers. a) FeB44k steel type, b) AQ50-60 steel type.

Similarly the capacity curve slope values are obtained for piers with brittle shear failure, (S) type.

In this case the values that can be derived directly from the charts of Fig. 5.44 represent the slope of the adimensional capacity curves (which are plotted in Fig.5.16) between the Shear Cracking Point and the point corresponding to ultimate displacement.

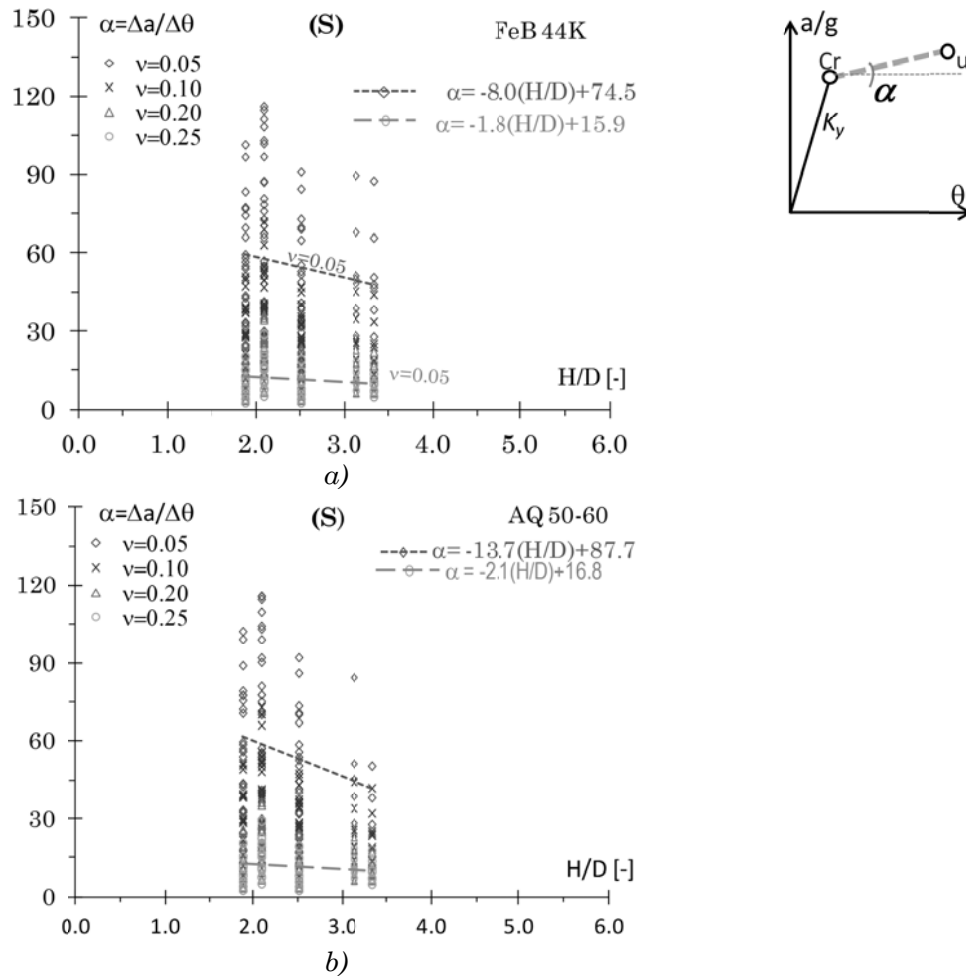
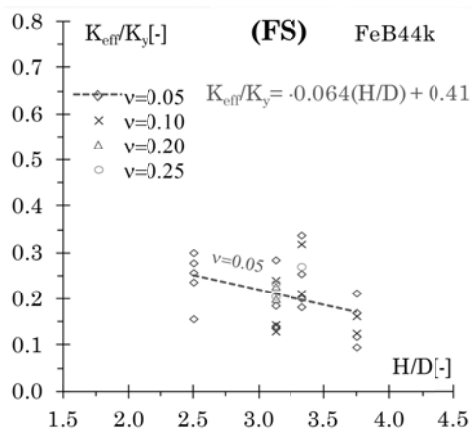
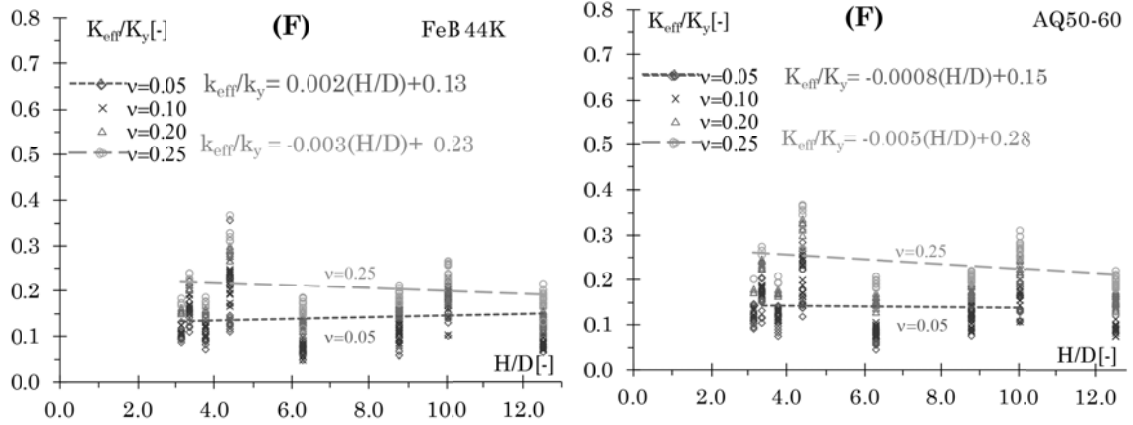


Fig. 5.44 – Single bent circular pier: slope after shear cracking for (S) piers. a) FeB44k steel type, b) AQ50-60 steel type.

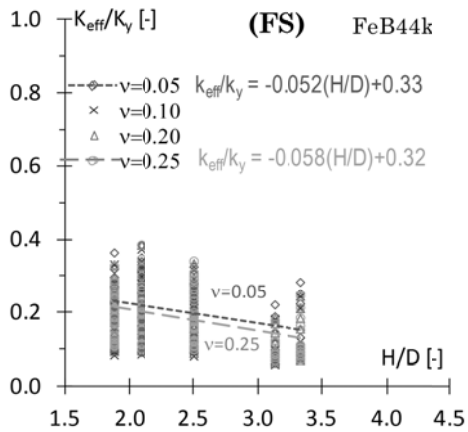
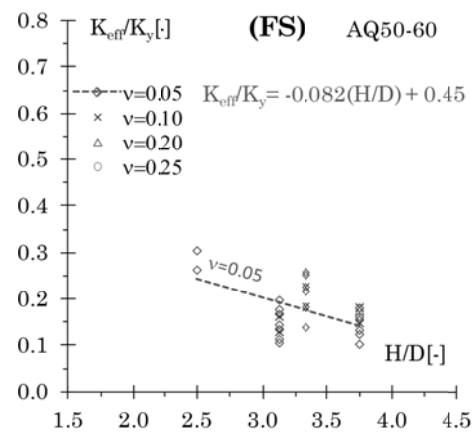
5.3.2.1 Effective stiffness

In the following charts the effective stiffness at ultimate (target) displacement, K_{eff} , is expressed as a fraction of the initial stiffness K_y (prior to shear cracking). K_{eff} can be estimated as a function of the geometric aspect ratio H/D and the normalized axial load v .

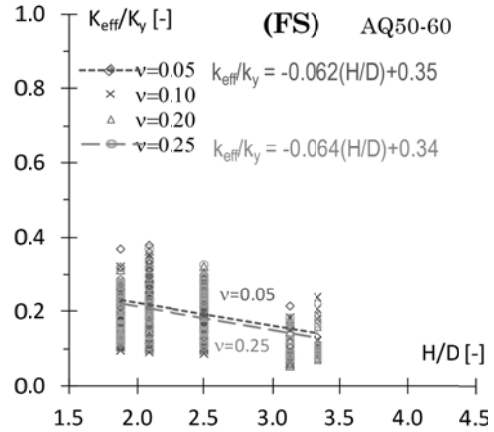
Effective stiffness is also expressed as a function of displacement ductility μ in Fig. 5.46.



a)



b)



c)

Fig. 5.45 – Effective stiffness at ultimate displacement for (F), (FS), (S).

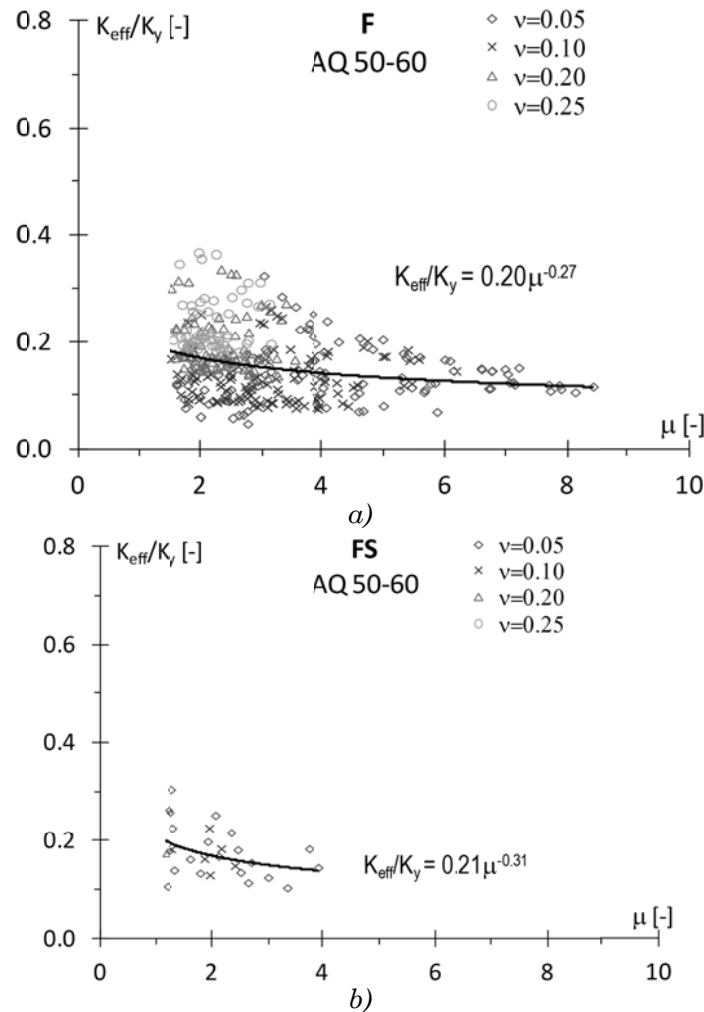


Fig. 5.46 – Effective stiffness as function of ductility for (F), (FS) piers.

For the easiness of reading, other results obtained for different kind of sections, in specific rectangular sections (cantilever and frame piers) and wall piers are reported in Appendix B.

5.4 CONCLUSIONS

Existing reinforce concrete piers exhibit generally an unsatisfactory seismic performance due to related to the reduced confinement, inadequate shear reinforcement especially in plastic hinge regions, insufficient length of lap splices. Thus a large class of existing bridge piers, especially with members with low aspect ratio, are vulnerable to shear failure.

The development of a Displacement-Based approach to seismic assessment require the study of the deformation and energy dissipation characteristics of existing members. In this context it is necessary to individuate the proper failure mechanisms, and calculate the effective displacements capacity of piers, both for flexural columns with limited ductility than for shear-critical column.

In this study the simplified phenomenological model developed by Miranda et al.^[M8], 2005, and adopted by Priestley et al.^[P1], 2007, is used to include the effects of non linear shear deformations for existing piers, by aggregating non linear shear effects to fiber modeling of flexural effects. The model is validated using experimental results of cyclic tests on scaled columns available from the .

Experimental hysteretic cycles are also used to derive a new equivalent damping expressions for shear critical column, which provides the equivalent viscous damping at failure as a function of the total drift instead of the displacement ductility as usually proposed^[D1, P1] for new ductile members.

An extensive parametric analysis is subsequently carried out to obtain the deformation characteristics and effective properties of piers. The analyses are performed for a large number of pier configurations (cantilever, frame piers, wall piers), whose effective ranges of main parameters influencing the seismic capacity were obtained from the preliminary statistical survey on the VR bridge stock described in Chapter 6.

The results are summarized in a series of charts that can be used to develop the capacity curves of piers under exam, and to obtain the pier equivalent properties that can be directly used within the DBA framework.

CHAPTER 6

DISPLACEMENT-BASED APPROACHES FOR THE VULNERABILITY ASSESSMENT OF RC BRIDGES: APPLICATION ON A REGIONAL-SCALE CASE STUDY

6.1 INTRODUCTION

In Italy, in consequence of Ordinance n.3274/2003 of the Prime Minister and its implementing provisions, Decree of the Department of Civil Protection n.21/2003, the managing authorities of road and railway networks are charged not only with the routine maintenance of all structures, but also with the seismic appraisal of the critical elements in the infrastructure systems. Retrofit interventions are required to enhance the seismic reliability of strategic structures, since they are to operational for the post-event emergency activities of the Civil Protection. Bridges play a crucial role, representing the key nodes of several road routes. Motivated by the potential vulnerability of the transportation infrastructure, many public and private managing authorities are going to incorporate seismic risk assessment in their Bridge Management Systems, as already done abroad by local Departments of Transportation (FEMA^[F4], 2003, Shinozuka et al, 2000).

In this context BMS, previously used only in relation to day-to-day upkeep of bridges, have been developing over the past years, into efficient instruments for determining the best allocation of resources to maximize the safety and functionality of the road network (Thompson et al. 1998^[T3], Bazos and Kiremidjian^[B4], 1995, Frangopol and Neves^[F5], 2004, Frangopol and Liu^[F6], 2007).

At present there is a growing demand for including in BMS tools for the appraisal of seismic bridge vulnerability, as it is of critical importance to predict the operational state of the roads in a post-earthquake scenario. This implies the formulation, for the infrastructure under examination, of an earthquake loss model, that can serve different purposes: help an efficient planning of rescue operations in an emergency situation, minimize the impact of a possible system downtime in terms of economical loss, and mitigate the risk, through a prioritization of urgent retrofit interventions for the most vulnerable structures.

The main aim of a loss model is to calculate the seismic hazard at all the sites of interest and convolute this hazard with the vulnerability of the exposed structure stock, to predict the damage distribution (Crowley et al.^[C4], 2004). The damage

ratio can be used to calculate the loss relating the cost of repair to the cost of demolition and replacement of the structure under exam.

It is current practice to assess seismic vulnerability with fragility curves, describing the conditional probability for a structure of exceeding a defined level of damage at the different levels of the seismic action intensity.

With regard to the assessment methods for existing constructions, the interest in using simplified procedures is apparent when probabilistic risk analysis is carried out on a large-scale (e.g. on a regional infrastructure system).

As estimation of vulnerability involves a large number of structures, the fragility curves have to be obtained by means of quick and reliable numerical calculations. The so-called Capacity Spectrum Method (ATC-40, 1996 and HAZUS, 1999) developed for the analytical assessment of the structural vulnerabilities has emerged as a standard tool for loss evaluation and has been implemented in several related softwares (Stafford et.al, 2007). More recently a Displacement-Based loss assessment methodology was formulated (see among others, Crowley et al.^[C4], 2006): the procedure uses mechanics-derived formulae to describe the displacement capacity of classes of buildings at three different limit states. Recent applications were proposed for the Turkish building stock (see Bal et al.^[C3], 2010).

The most extensively used tool currently available to derive vulnerability curves of large-scale systems is the Hazus methodology (FEMA, 1999^[F8], 2003^[F9]), which provides fragility curves for whole classes of structures, calibrated on databases developed in the US. The HAZUS model is sufficiently accurate when applied to a class of buildings or bridges very similar to those in the default system, but it shows deficiencies when applied to a community-specific database, where different typologies are represented. Fragility functions are not calibrated to the Italian (and more in general European) bridge typologies and construction characteristics: for example masonry arch bridges, in the Hazus database, fall within the category “other” system, not clearly defined in relation to their specific vulnerable elements, while they represent, in Italy, more than 20% of the existing road bridge database (see §6.2), and at least the 50% of all railway bridges. Other shortcomings are related to different construction methodologies also for the same structural types supplied in the original database.

Despite these considerations, the Hazus framework is reliable and has been extensively used in recent years as a tool for Earthquake Risk estimation on a large scale, as generally the possibility of modifying its parameters does not exist, for lack of a detailed comprehensive data inventory regarding European (and Italian) structure types. A step forward in this sense was made with the RISK-UE project^[M5], with definition of earthquake risk scenarios for different European towns, with supplied more specific data for the European building and bridges stock. Related to this project, a comparison study of five European earthquake loss

assessment methodologies as opposed to the unified U.S. HAZUS model, was presented by Strasser et al., 2008^[S3]. As regards fragility curves for bridges, the RISK-UE method is built using the Hazus approach, parameters and ranges, and the only difference is related to the initial classification of the structure with reference to homogeneous classes more adequate for the European bridge typologies.

Bridge inventories are generally poor, because the availability of detailed data in a Bridge Management System entails a specific campaign of inspection, a structural survey, on-site and laboratory tests, archive research for original project information, requiring an extraordinary effort for the managing authority, and costs as wells. In this work, the bridge inventory refers to the Veneto Region road network bridge stock (named VR stock), which was the object, in the years 2007-2010, of a seismic verification study, carried out by the University of Padova, according to the requirements of Decree n.21/2003, mentioned above. This activity represented a long preliminary work, and allowed to obtain detailed information of members' structural characteristics (e.g. piers dimensions, effective reinforcement content, material properties) for a significant number of structures in the inventory (with some inevitable operational restrictions, related to the possibility of execution of extensive laboratory tests).

All these data were collected within this thesis in an extensive statistical survey, described in next paragraphs. Focusing on the rc bridges' macro-class, after a preliminary subdivision of the stock into homogeneous sub-classes, it was possible to characterize the effective range of bridge properties in terms of static scheme, material characteristics, geometrical parameters and reinforcement content.

This information represented a sound base for the development of a parametrical analysis on the capacity of members (e.g. bridge piers), as previously described in Chapter 5. Owing this parametric study it was possible to calculate more precisely the limit states to be taken for shear and flexural behavior (with reference to pre-defined levels of damage), and get a better calibration of the values of equivalent damping for the existing rc piers, to be later adopted in the simplified DBA analyses.

A limited number of rc multi-span bridges were then chosen as reference samples (named Reference Bridge structures, *RBs*) for each homogeneous class, and a direct comparisons of simplified DBA procedures with NLTH analyses were carried out on this restricted set of structures. First the deterministic safety factors, represented by Capacity/Demand ratios obtained for different earthquake intensity levels were compared, and subsequently the fragility curves obtained for the bridges under exam.

An extensive vulnerability analysis of the entire stock was subsequently developed, using the previously calibrated DBA procedures: analytical fragility curves were derived with the simplified displacement-based method (DBFr curves) for all the multispan rc bridges of the VR stock (101).

Seismic risk maps were drafted in the end: the calculation of seismic risk as convolution integral of the hazard curve was explicitly derived for the *RB* structures, and tabulated for all the multi-span rc bridges. The spatial distribution of damage was represented for all the Veneto region stock superimposed on Google Earth maps.

6.2 THE VENETO REGION ROAD NETWORK BRIDGE STOCK

The first component of a reliable risk assessment model for an infrastructure system is the detailed definition of the bridge inventory, that is fundamental for the evaluation of the vulnerability characteristics of the exposed structures. The reference database of this work is represented by the stock of bridges of the Veneto Region (N-E of Italy) road network, consisting in 496 bridges belonging to the provincial and regional infrastructure systems, mostly located in medium-high seismicity areas (Zone 2 and 3 according to the Italian seismic zonation map valid for the administrative classification of the country).

A large number of these structures have been already classified in the Italian bridge Interactive Database (I.br.I.D.), arranged by the University of Padova-Department of Civil, Environmental and Architectural Engineering- (<http://ibrid.dic.unipd.it/>), which gathers information of about 500 bridges.. The database is open-source, and synthetic data for the reference structure such as, localization, geometrical and material features, photos, year of construction, are made available.

In this work, a detailed statistical analysis was carried out on the whole bridge stock, on the basis of the results of the structural survey campaign and the archival research conducted in years 2007-2010 first on the road network managed by Veneto Strade s.p.a. (km 1476,8 of regional and provincial roads in the province of Venezia, Treviso, Belluno, Padova, Verona, Rovigo, with 347 bridges located in seismic zones 2, 3 and 4) and subsequently extended to the network of Viabilità (km 1250 of provincial roads located in the province of Vicenza, with 149 bridges). The raw data were elaborated and re-organized in this thesis with the aim of defining a detailed picture of the properties of existing rc bridges, with specific reference to girder bridges, which represent about 70% of the total number of constructions in the database. The final objective of the statistical survey, was the definition of the effective ranges of properties influencing the seismic structural capacity of the different rc bridge typologies.

The statistical survey is organized on different levels: a first set (SET 1) of statistics considers the general features of the stock. At the beginning of the work only these general data were partially available. Localization, deck material, number of spans, span length, year of construction are reported in this set and described in paragraph §6.2.1.

The second set of statistics relates only the category of rc girder bridges, focusing on the geometrical and mechanical parameters that may influence the capacity of a structure. With reference to the different typological classes of bridges (which can differ for static scheme, deck properties, pier, abutment or support characteristics, etc.), described in the SET 2a, appropriate ranges for all the geometrical and mechanical parameters having an influence on the seismic response were individuated. Number of spans, deck type and geometry, span length, pier and abutment type, pier cross section type, pier aspect ratio (h/d), pier cross section geometries, foundation type etc. were recorded in SET 3a, while longitudinal reinforcement ratio, transverse reinforcement ratio, confinement parameters, normalized axial loads, foundation type etc. were catalogued in SET 3b.

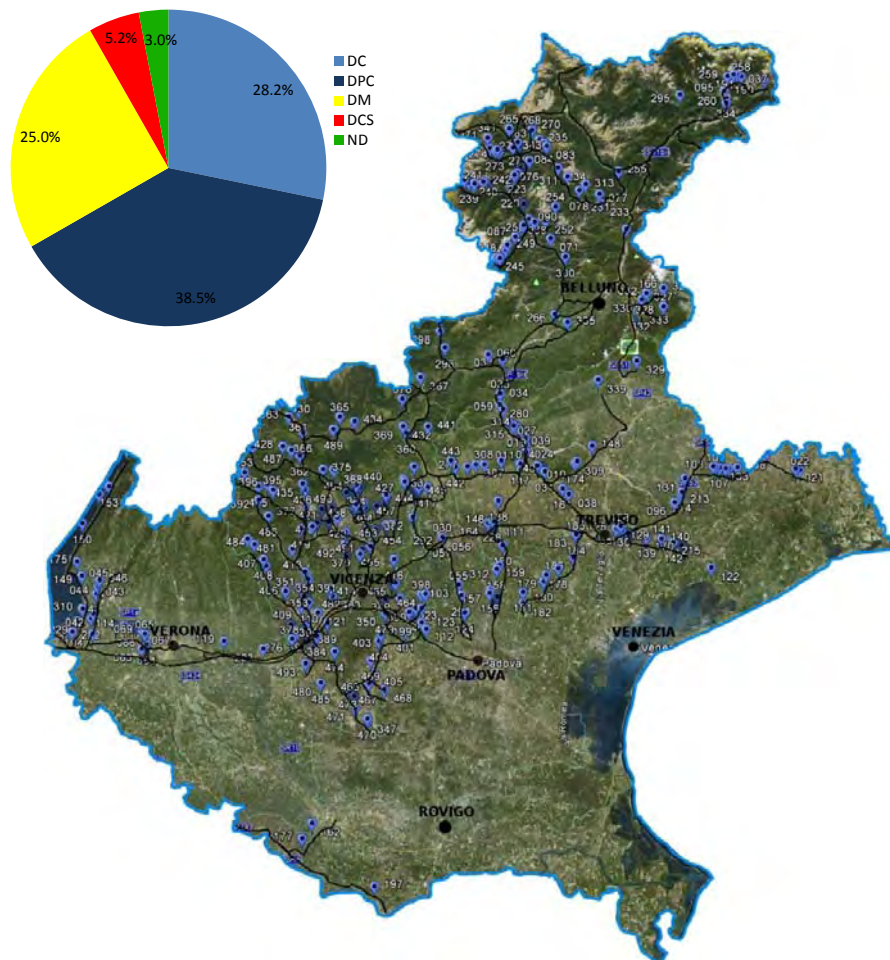


Fig. 6.1 – Localization of the bridges and classification on the base of deck/pier material: DC- reinforced concrete, DPC- prestressed reinforced concrete, DM-masonry (or unreinforced concrete, deck or piers), DCS-composite/steel, ND-not classified.

A final set of statistics (SET 4) regards material properties, for concrete and reinforcement steel. On the base of laboratory and in-situ tests, it appeared that a wide range of concrete strength were adopted for piers and substantially two types

of steel reinforcement were used, grade Aq50 used for smooth bars, representative of structures built till the middle 1970's, and grade Feb44k representative of typical deformed bars used in structures built in the last 35 years. On site tests and laboratory tests were executed on piers and abutments to determine material strengths, and reinforcement distributions. SonReb and Sclerometric Tests, Pachometric Tests were conducted on site on a limited but representative number of structures (74), to obtain an estimate of compressive concrete strength, and the reinforcement distribution and diameter of bars. Laboratory tests were carried out on a restricted number of structures to determine the compressive strength of concrete (f_{cm}), by testing rc core specimens. Tensile strength of the reinforcement bars (f_{ym} , f_{tm}), as well as maximum elongation, were derived by uniaxial traction tests. Other Non Destructive Tests or Medium Destructive Tests were carried out on masonry bridges (e.g. single and double flat jack tests, core boring...).

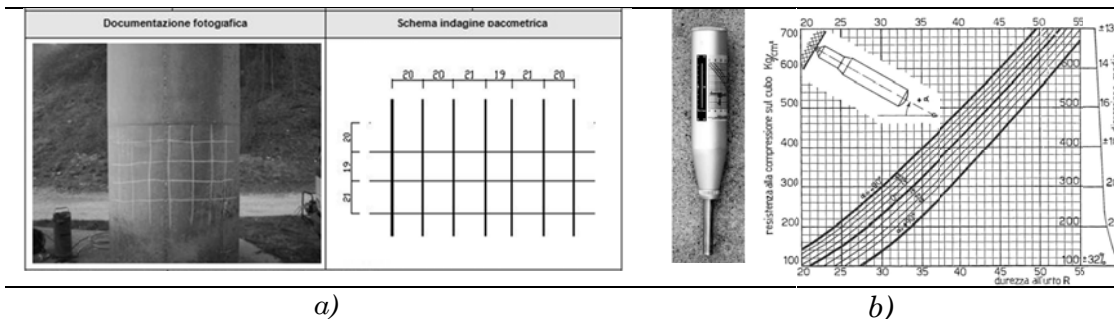


Fig. 6.2 – On site tests on rc bridges: a) pachometer test, b) sclerometric test

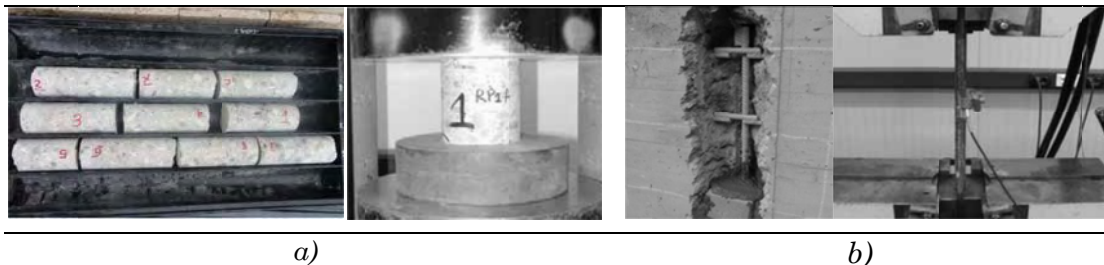


Fig. 6.3 – Laboratory tests: a) core borings and compressive strength tests on concrete samples. b) extraction of reinforcement bars and traction test

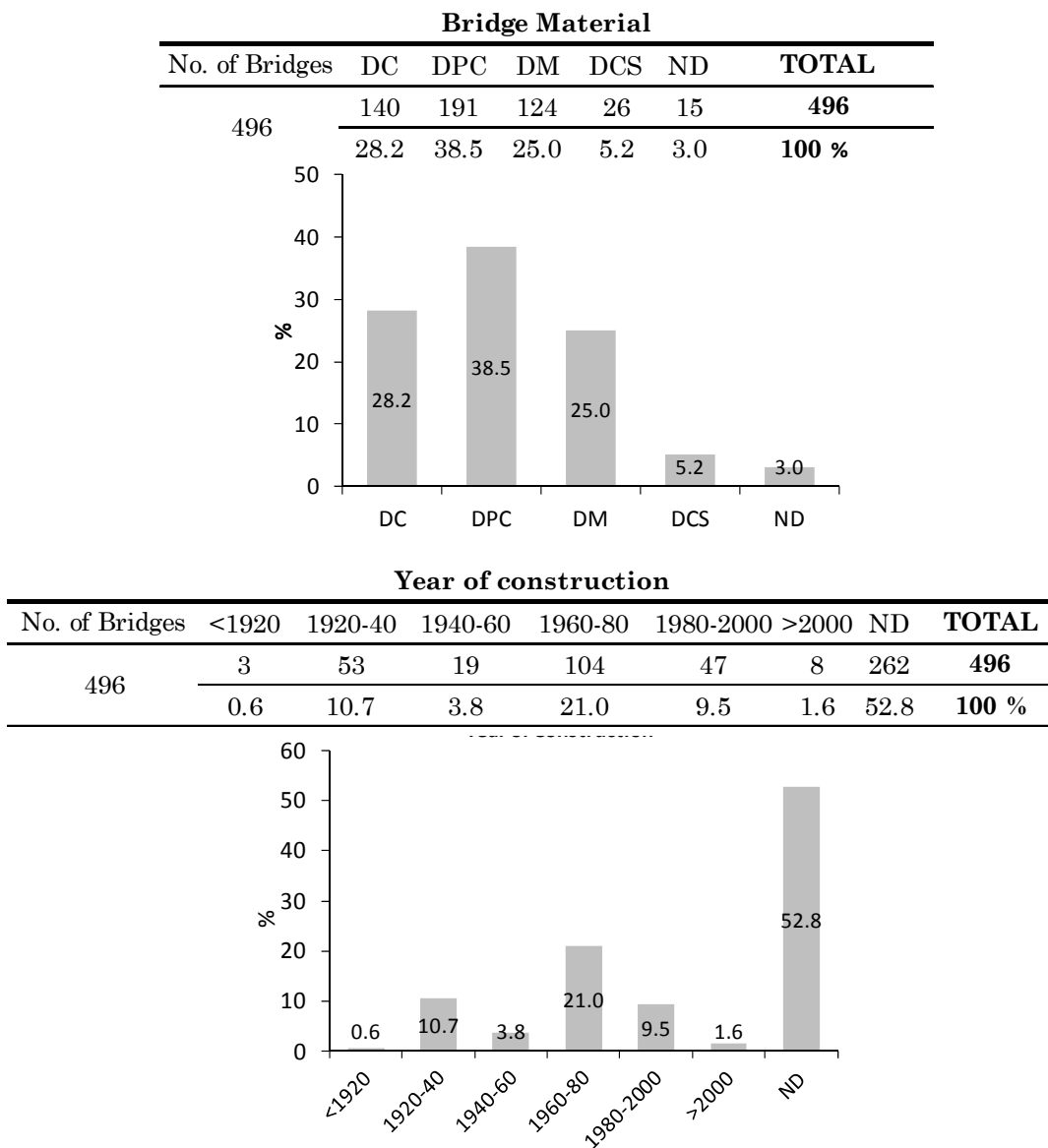
6.2.1 General characteristic of the stock –SET1-

The total number of structures contained in the bridge inventory is 496. If we consider the construction material, rc and prc bridges represent the greatest percentage of the stock, 66.7%; girder bridges, arch bridges, frame structures are included. The second greatest portion is represented by masonry structures, 25.0% (mostly arch structures, 21.8%, and a residual percentage 3.2% with deck of different material and masonry piers). Steel decks are a small percentage of the stock, and often steel girders are combined with a rc slab in composite structures, in relatively recent bridges, built since the mid-1980s.

Most of the structures are single-span (65.1%), with short-medium span lengths. Including also multi-span bridges, only 10.7% have spans longer than 30.0m, and very long structures, with total length greater than 250m are only exceptions (2%).

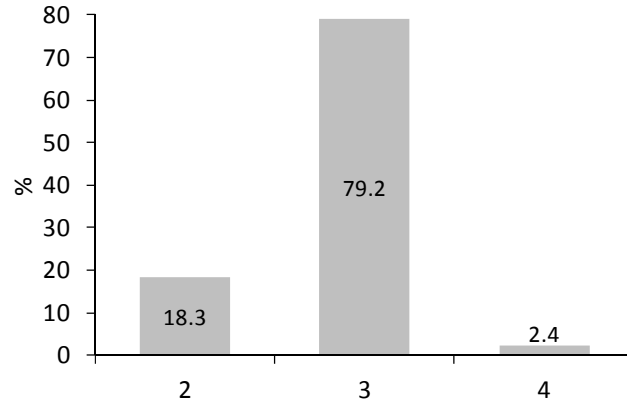
The information available for the stock is very detailed compared to usual bridge databases: the geometrical survey, regarded almost all the structures (97.6%), while on site tests were executed on a selected subset of structures (14.9%), representative of the different bridge classes. Lab tests were conducted on a limited number of bridges (35, 7.1% of the whole) to characterize material properties. In addition, an archive research allowed to recover the original projects of 87 bridges (mostly rc bridges), which represent 17.5% of the total.

Tab. 6.1 –*SET 1 statistics: general properties of the whole bridge stock.*



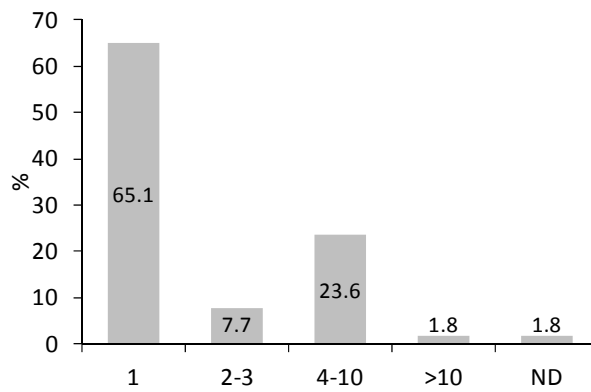
Zonation

No. of Bridges	2	3	4	TOTAL
496	91	393	12	496
	18.3	79.2	2.4	100 %



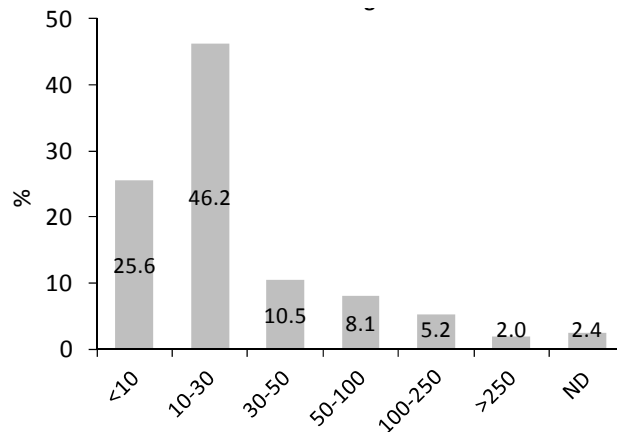
N of Spans

No. of Bridges	1	2-3	4-10	>10	ND	TOTAL
496	323	38	117	9	9	496
	65.1	7.7	23.6	1.8	1.8	100 %

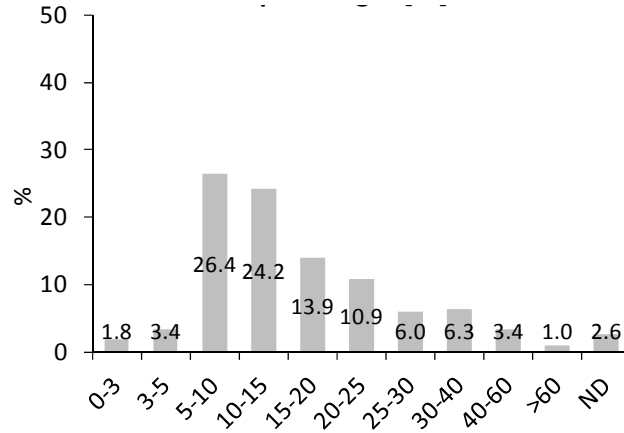


Total Length [m]

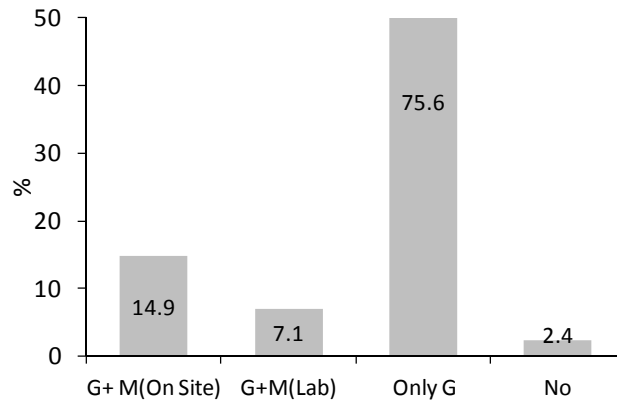
No. of Bridges	<10	10-30	30-50	50-100	100-250	>250	ND	TOTAL
496	127	229	52	40	26	10	12	496
	25.6	46.2	10.5	8.1	5.2	2.0	2.4	100 %



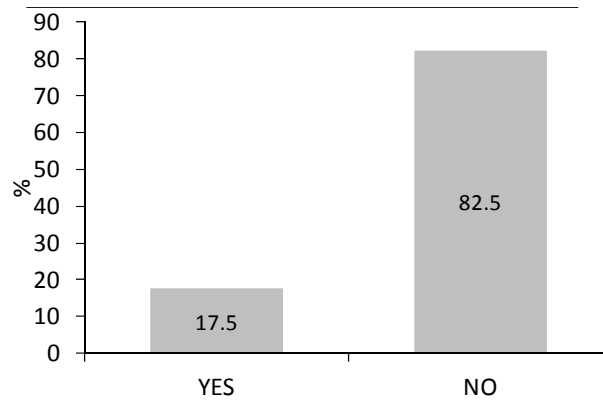
		Span Length [m]										ND	TOTAL
No. of Bridges	0-3	3-5	5-10	10-15	15-20	20-25	25-30	30-40	40-60	>60			
496	10	17	131	120	69	54	30	31	17	5	12	496	
	1.8	3.4	26.4	24.2	13.9	10.9	6.0	6.3	3.4	1.0	2.6	100 %	



Survey (Geometry+ Material)					
No. of Bridges	G+ M(On Site)	G+M(Lab)	Only G	No	TOTAL
496	74	35	375	12	496
	14.9	7.1	75.6	2.4	100 %

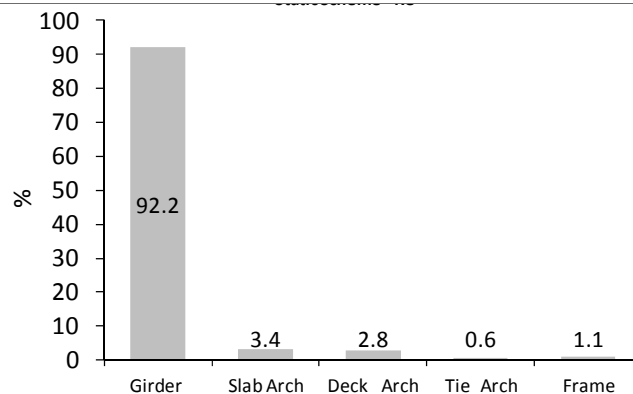


Original Project			
No. of Bridges	YES	NO	TOTAL
496	87	409	496
	17.5	82.5	100 %



Static Scheme - RC

No. of Bridges	Girder	Slab Arch	Deck_Arch	Tie_Arch	Frame	TOTAL
	329	12	10	2	4	357
357	92.2	3.4	2.8	0.6	1.1	100 %



6.2.2 Rc bridge stock –SET2-

The present study focuses mainly on the girder bridges category. The classification aiming to the seismic evaluation, composite structures are grouped with rc and prc bridges, in an overall girder bridge set, which represents the 66.3% of the whole stock (No. 329).

The data gathering is based on a preliminary subdivision of the whole population of rc bridges into different sets and subsets. This classification is useful for establishing of a number of homogeneous classes of rc girder structures, characterized by similar properties in terms of structural typology, geometric characteristics, static behaviour and finally seismic capacity.

Three different orders of classification are listed in Tab. 6.3, and indentified as follows.

-MACRO-CLASSES, with reference to deck type:

- 1) girder bridges, single span;
- 2) girder bridges, multi-span;
- 3.) arch bridges;
- 4.) frame bridges;

-CLASSES, with reference to the static scheme adopted:

Macro-class1 (single span girder bridges)

- 1.1) simply-supported bridges (S_SIMPLE);
- 1.2) integral bridges (S_INTEG);

Macro-class2 (multispan girder bridges):

- 2.1) simply supported (M_SIMPLE);
- 2.2) gerber bridges (M_GERBER);
- 2.3) continuous bridges (M_CONT);
- 2.4) simply supported with kinematic chain (M_KINEM).

Macro-class3 (arch bridges):

- 3.1) slab arches (rc bridges with barrel-vaults) (SLAB-ARCH),
- 3.2) tied arches -with horizontal tie-beams- (TIED ARCH),
- 3.3) deck arches -arch connected with pillars to the upper deck- (DECK ARCH).

Macro-class4 (frame bridges):

4.1) frames

- SUB-CLASSES, are defined with reference to the main parameters affecting the static and seismic response. The subclasses are individuated only for girder bridges, in relation to type of bearings (for Classes 1.1), pier static scheme (for Classes 2.1-2.2), number of spans and pier arrangement (Class 2.3). Parameters related to pier sections, deck material and properties, abutment and foundation characteristics, are considered for the classification, but only as internal variables for each subclass. Some classes are unique and do not have subclasses (e.g. Classes 1.2- simple span integral bridges, and 2.4 multi-span bridges with kinematic chain). The following subclasses are identified for

Class 1.1 (single span simply-supported girder bridges):

- 1.1.Iα fixed long. restraint (steel hinges, shear keys)
- 1.1.IIαa partial long. restraint-neoprene pads
- 1.1.IIαb partial long. restraint-friction support
- 1.1.IIαc partial long. restraint-seismic devices

Class 1.2: no subclasses

Class 2.1 (multi-span simply-supported girder bridges):

- 2.1.1 single bent piers
- 2.1.2 wall piers
- 2.1.3 multiple bent piers (single frame)
- 2.1.4 multiple bent piers (multiple frame)

Class 2.2 (multi-span gerber girder bridges): no subclasses

Class 2.3 (multi-span continuous girder bridges):

- 2.3.1 multi-span bridges with 2-3 spans
- 2.3.2 multi-span symmetric bridges (n>3 spans)
- 2.3.3 multi-span non symmetric bridges (n>3 spans)

Each class contains a set of structures with similar properties, and the statistics are principally aimed at determining the effective ranges of the significant parameters for each class.

The SET2 of statistics regards the general properties of girder bridges (No.329), while SET3 covers more specifically the multi-span classes (No.101 bridges), with regard to geometric properties of piers (SET3a) and reinforcement content (SET3b). In the end a final group of statistics regards material properties (SET4), referred to the limited number of structures, specified above, for which it was possible to execute on-site and lab tests.

The main parameters investigated in the statistics are listed in Tab. 6.2.

Tab. 6.2 – *Parameters used for the classification of rc girder bridges*

PARAMETER	RANGE	CODE
Static Scheme	Single Span simply supported	S_SIMPLE
	Single Span Integral	S_INTEG
	Multi-Span Simply supported	M_SIMPLE
	Multi-Span Gerber Scheme	GERBER
	Multi-Span Continuos	CONT
	Multi-Span Kinematic Chain	KINEM
	Arch	ARCH
	Frame	FRAME
N of spans	Single Span	1
	2-3 Spans	2-3
	Multi-spans	M
Span Leight		
Deck Material	Rc Deck	DC
	Prc Deck	DPC
	Composite Deck	DCS
Deck Properties	Slab	SLAB
	Concrete Double Girder	C_DOUBLE
	Concrete Multiple Girder	C_M_G
	Concrete Box	C_BOX
	Steel Double Girder	S_DOUBLE
	Steel Multiple Girder	S_M_G
	Steel Box	S_BOX
Deck geometry	Straight Deck	G-ST
	Skew Deck	G-SK
	Curved Deck	G-CV
Deck skweness	Low skweness	l-SK
	Medium skweness	m-SK
	High skweness	h-SK
Pier Type	Cantilever -Single Column-	PSC
	Cantilever -Wall-	PW
	Frame -Double Pier-	PF2
	Frame -Multiple Pier-	PFM
Pier Section	Solid Rectangular (or Poligonal)	SR
	Solid Circular	SC
	Hollow Simply-Connected	HS
	Hollow Multiply-Connected	HM
Axial Normalized Load		ν_k
Piers/Abutment height		H
Cross section long. Aspect Ratio		H/BL
Cross section transv. Aspect Ratio		H/Bt
Long. Reinforcement Ratio		ρ_l
Transverse Volumetric Reinforcement Ratio		ρ_{st}
Confinement Parameter (by Mander)		λ_c
Bearings	Neoprene pads	NEO
	Friction	FRI
	Steel-rubber devices	DEV
Foundation Type	Spread footings	S_FOOT
	Pile footings	P_FOOT
	Pile shafts	P_SHAFTS
	Caissons	CAISSONS

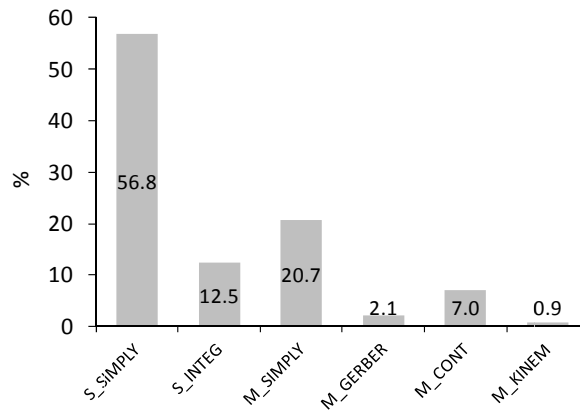
Tab. 6.3 – Identification of homogeneous classes for rc and pre bridges' stock.

MACRO CLASS (DeckType)	CLASS (Static Scheme)	SUBCLASS (PIER-ABUTMENT-SUPPORT-DECK PARAMETERS)																								
		Bearings				Pier type			Pier section			Pier Arrangement			Deck properties											
		Long. (α)/ Fixed (1) Steel hinges/ Short	Transverse (β) Partial Restraint (2)	NEO	FRI	DEV	PSC	PW	PF2	PFM	Multiple bent	Solid	Hollow	2-3 spans	Multi-span	DC	DPC	Slab	Double Girder	Multi- Box Girder	S_F	P_F	P_Shl	Cais	Foundation	
(1.) GIRDER BRIDGE	S- SIMPLY	(1.1.a1)	(1.1.a2a)	(1.1.a2b)	(1.1.a2c)																					
(1.2) SINGLE SPAN -	S-INTEG																									
(2.1)	M-SIMPLY	x	x	x	x	x	(2.1.1)	(2.1.2)	(2.1.3)	(2.1.4)	2.1.1.a	2.1.1.b	2.1.1.c	2.1.1.d	x	x	x	x	x	x	x	x	x	x	x	
(2.2)	M- GERBER	x	x	x	x	x	(2.2.1)	(2.2.2)			x	x	x	x	x	x	x	x	x	x	x	x	x	x	x	
(2.3) - SINGLE BRIDGE - MULTI SPAN -	M-CONT	2.3.1-β1	2.3.1-β2				2.3.1-β1/2_a	2.3.1-β1/2_b	2.3.1-β1/2_c	2.3.1-β1/2_d	x	x	x	x	(2.3.1)	x	x	x	x	x	x	x	x	x	x	x
(3.1)	M-KINEM	x	x	x	x	x	x	x	x	x	x	x	x	x	(2.3.2)	x	x	x	x	x	x	x	x	x	x	x
(3.2)	SLAB-ARCH	x	x	x	x	x	x	x	x	x	x	x	x	x	(2.3.3)	x	x	x	x	x	x	x	x	x	x	x
(3.3)	TIED-ARCH	x	x	x	x	x	x	x	x	x	x	x	x	x	(2.4.1)	x	x	x	x	x	x	x	x	x	x	x
(4.) FRAME*	DECK-ARCH	x	x	x	x	x	x	x	x	x	x	x	x	x	x	x	x	x	x	x	x	x	x	x	x	x
	FRAME	x	x	x	x	x	x	x	x	x	x	x	x	x	x	x	x	x	x	x	x	x	x	x	x	x

Tab. 6.4 –SET 2 statistics: rc and prc bridges general properties

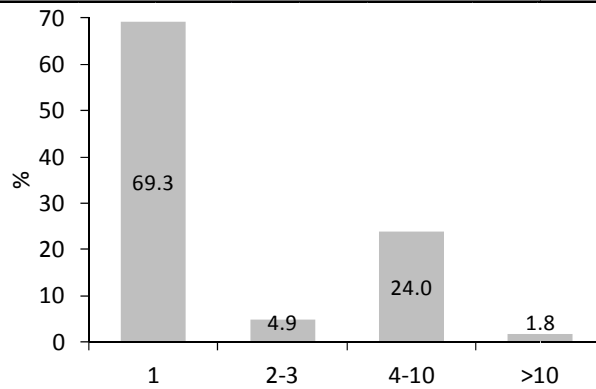
Static Scheme - RC

No. of Bridges	S_SIMPLE	S_INTEG	M_SIMPLE	M_GERBER	M_CONT	M_KINEM	TOTAL
329	187	41	68	7	23	3	329
	56.8	12.5	20.7	2.1	7.0	0.9	100 %



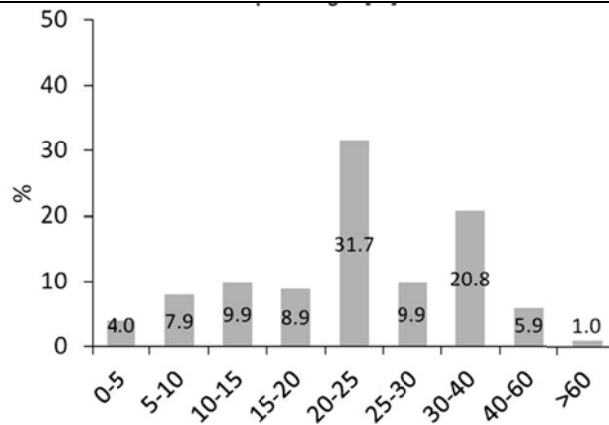
N of Spans

No. of Bridges	1	2-3	4-10	>10	TOTAL
329	228	16	79	6	329
	69.3	4.9	24.0	1.8	100 %



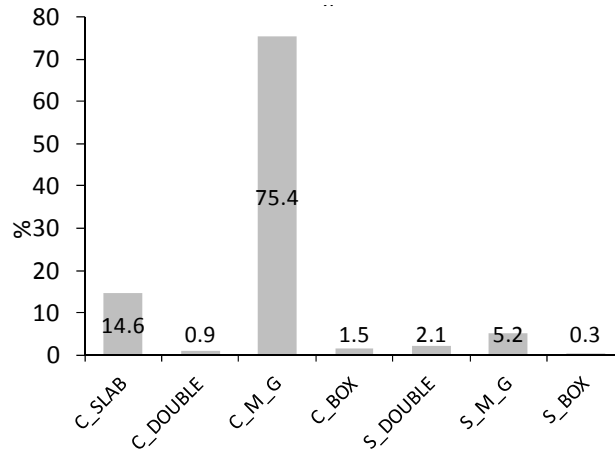
Span Length [m]

No. of Bridges	0-3	3-5	5-10	10-15	15-20	20-25	25-30	30-40	40-60	>60	TOTAL
329	1	7	76	79	51	48	25	28	12	2	329
	0.3	2.1	23.1	24.0	15.5	14.6	7.6	8.5	3.6	0.6	100 %



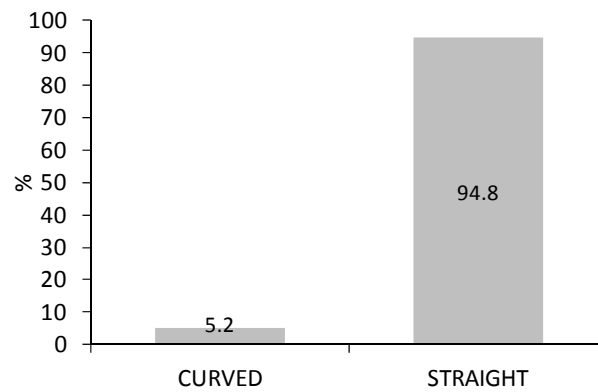
Deck Properties

No. of Bridges	C_SLAB	C_DOUBLE	C_M_G	C_BOX	S_DOUBLE	S_M_G	S_BOX	TOTAL
329	48	3	248	5	7	17	1	329
	14.6	0.9	75.4	1.5	2.1	5.2	0.3	100 %



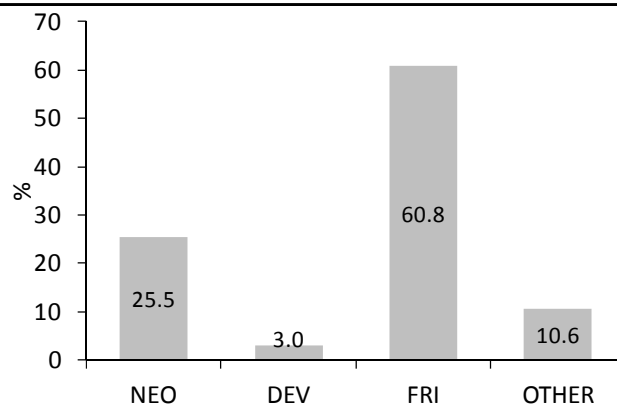
Deck geometry

No. of Bridges	CURVED	STRAIGHT	TOTAL
329	17	312	329
	5.2	94.8	100 %

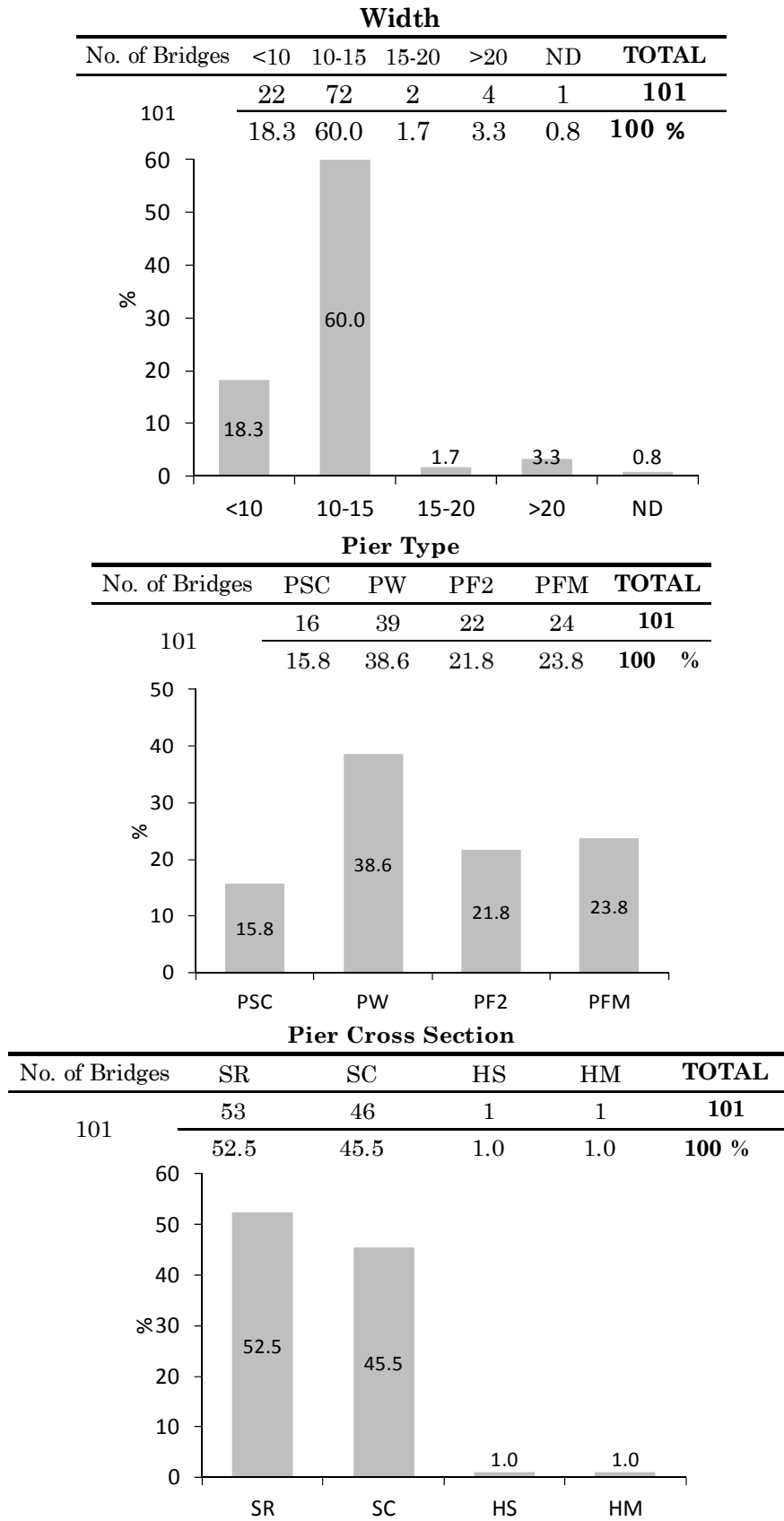


Bearings

No. of Bridges	NEO	DEV	FRI	OTHER	TOTAL
329	84	10	200	35	329
	25.5	3.0	60.8	10.6	100 %

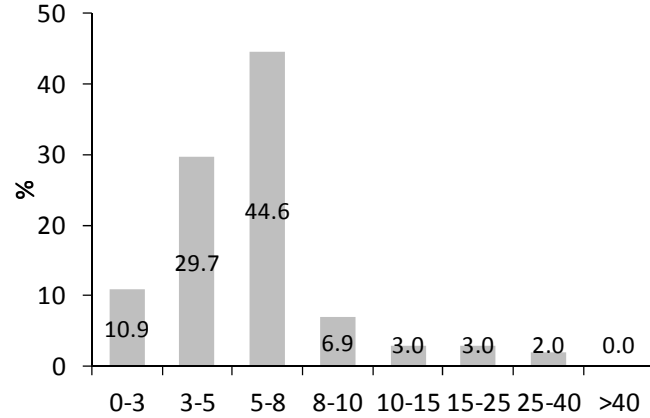


Tab. 6.5 –SET 3a statistics: multi-span rc girder bridges properties



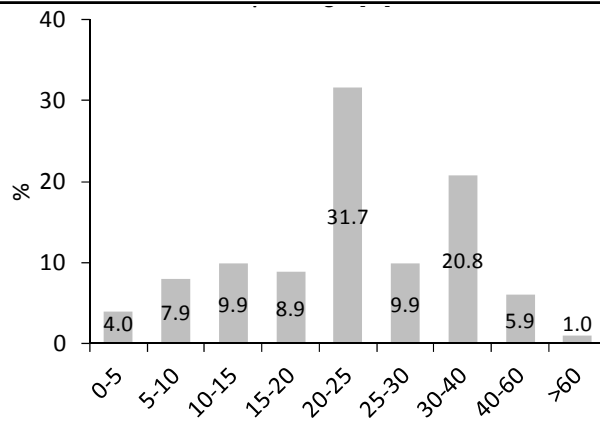
Pier Height [m]

No. of Bridges	0-3	3-5	5-8	8-10	10-15	15-25	25-40	>40	TOTAL
101	11	30	45	7	3	3	2	0	101
	10.9	29.7	44.6	6.9	3.0	3.0	2.0	0.0	100 %



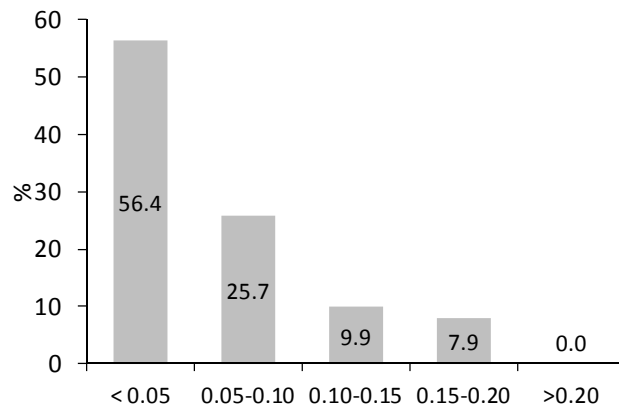
Span Length [m]

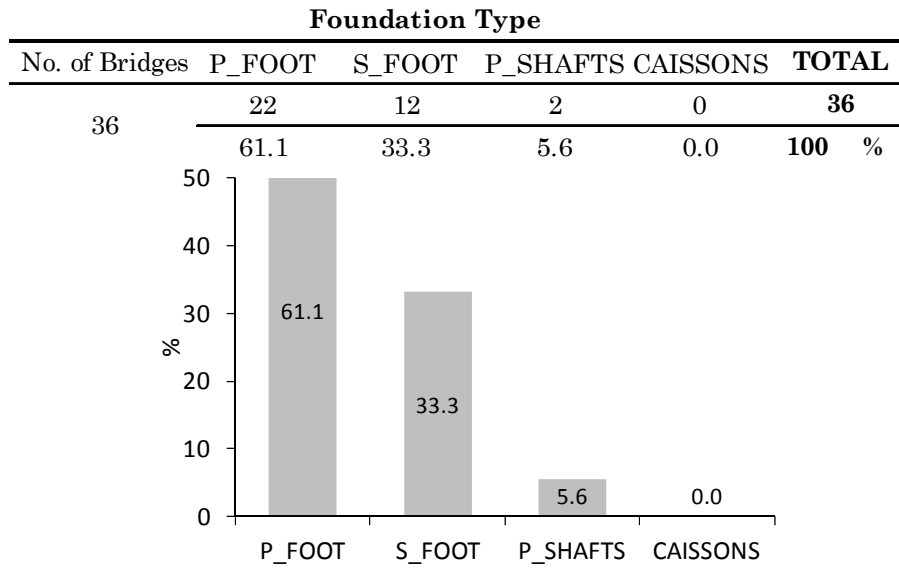
No. of Bridges	0-5	5-10	10-15	15-20	20-25	25-30	30-40	40-60	>60	TOTAL
101	4	8	10	9	32	10	21	6	1	101
	4.0	7.9	9.9	8.9	31.7	9.9	20.8	5.9	1.0	100 %



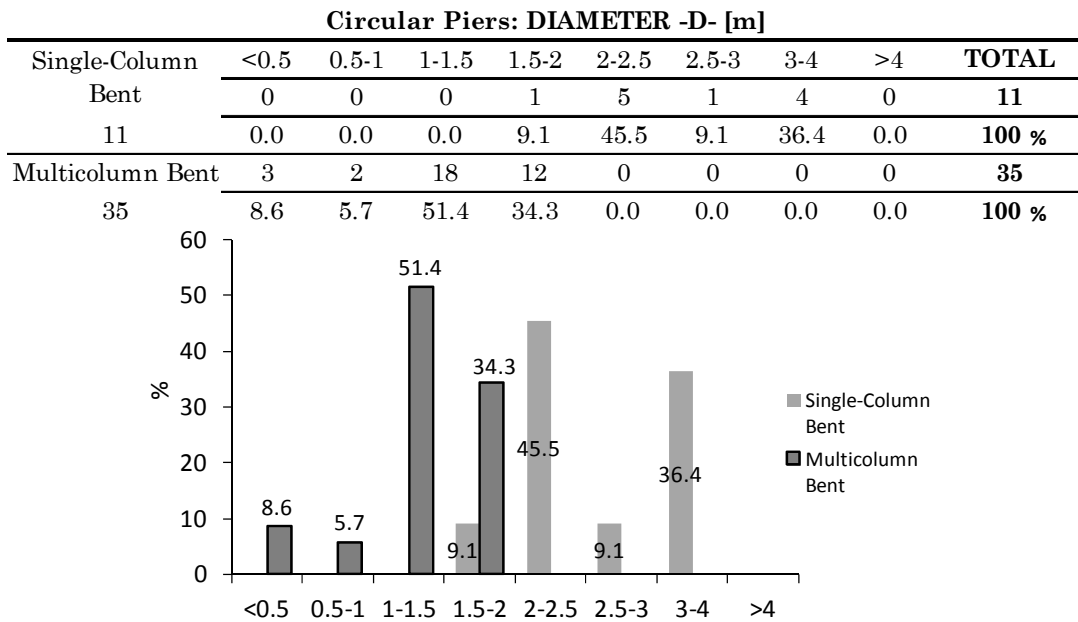
Normalized Axial Load

No. of Bridges	< 0.05	0.05-0.10	0.10-0.15	0.15-0.20	>0.20	TOTAL
101	57	26	10	8	0	101
	56.4	25.7	9.9	7.9	0.0	100 %



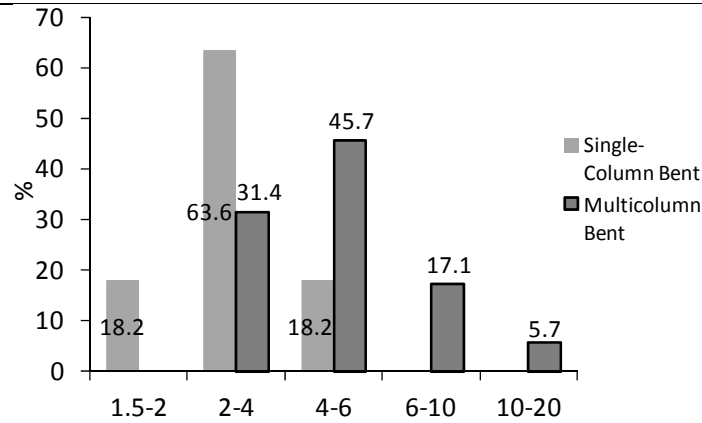


Tab. 6.6 –*SET 3b statistics: pier geometric properties of multi-span rc girder bridges*



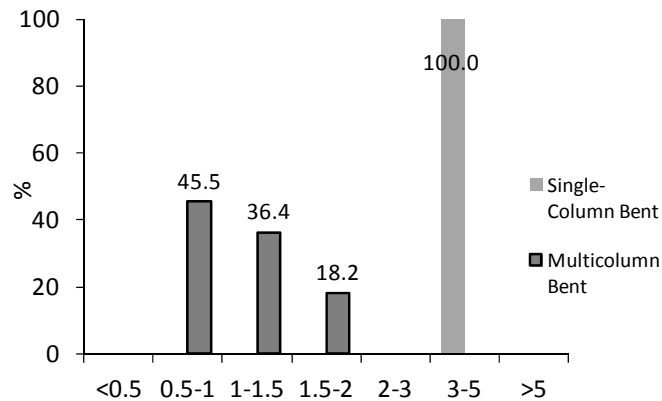
Circular piers: H/D

	1.5-2	2-4	4-6	6-10	10-20	TOTAL
Single-Column Bent	2	7	2	0	0	11
11	18.2	63.6	18.2	0.0	0.0	100 %
Multicolumn Bent	0	11	16	6	2	35
35	0.0	31.4	45.7	17.1	5.7	100 %



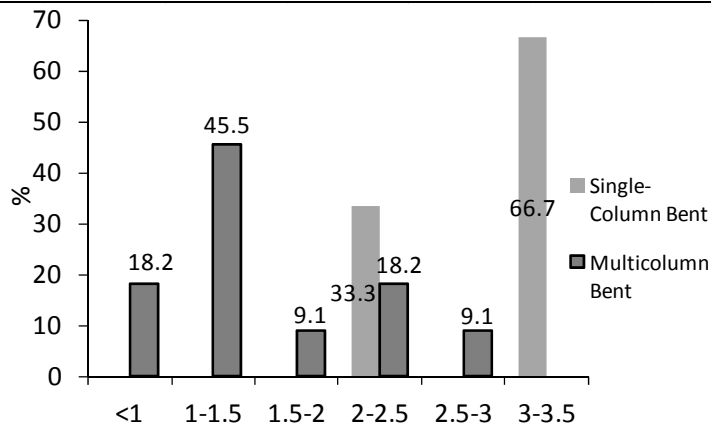
PIER DEPTH -BT- (Solid Rectangular Section) [m]

	<0.5	0.5-1	1-1.5	1.5-2	2-3	3-5	>5	TOTAL
Single-Column Bent	0	0	0	0	0	3	0	3
3	0.0	0.0	0.0	0.0	0.0	100.0	0.0	100 %
Multicolumn Bent	0	5	4	2	0	0	0	11
11	0.0	45.5	36.4	18.2	0.0	0.0	0.0	100 %



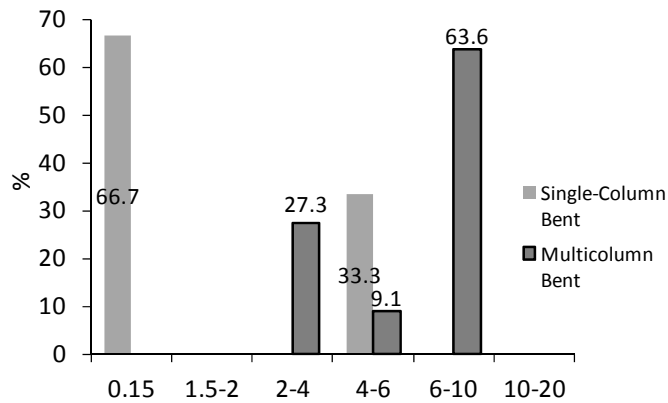
BT/BL (Solid Rect. Section)

	<1	1-1.5	1.5-2	2-2.5	2.5-3	3-3.5	TOTAL
Single-Column Bent	0	0	0	1	0	2	3
3	0.0	0.0	0.0	33.3	0.0	66.7	100 %
Multicolumn Bent	2	5	1	2	1	0	11
11	18.2	45.5	9.1	18.2	9.1	0.0	100 %



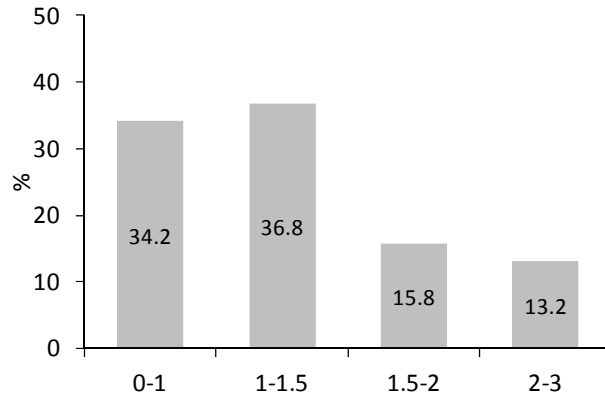
H/BT

	0-1.5	1.5-2	2-4	4-6	6-10	10-20	TOTAL
Single-Column Bent	2	0	0	1	0	0	3
3	66.7	0.0	0.0	33.3	0.0	0.0	100 %
Multicolumn Bent	0	0	3	1	7	0	11
11	0.0	0.0	27.3	9.1	63.6	0.0	100 %



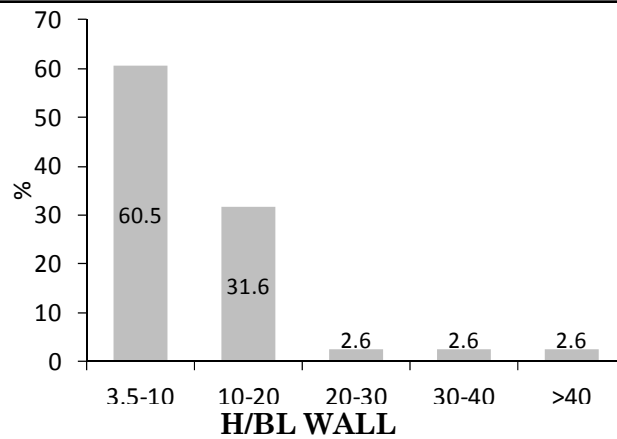
PIER THICKNESS (Wall) -BL- [m]

No. of Bridges	0-1	1-1.5	1.5-2	2-3	TOTAL
38	13	14	6	5	38
	34.2	36.8	15.8	13.2	100 %



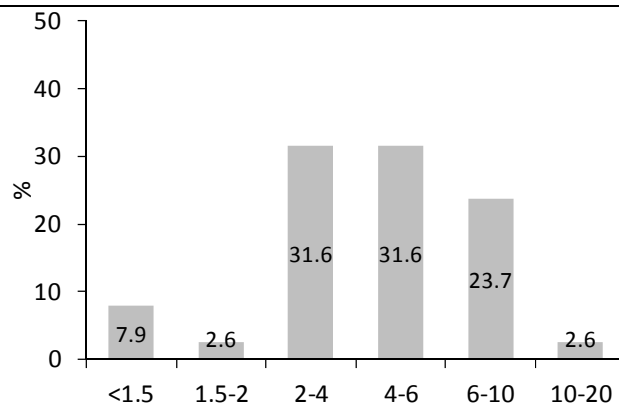
BT/BL [m] - WALL

No. of Bridges	3.5-10	10-20	20-30	30-40	>40	TOTAL
38	23	12	1	1	1	38
	60.5	31.6	2.6	2.6	2.6	100 %



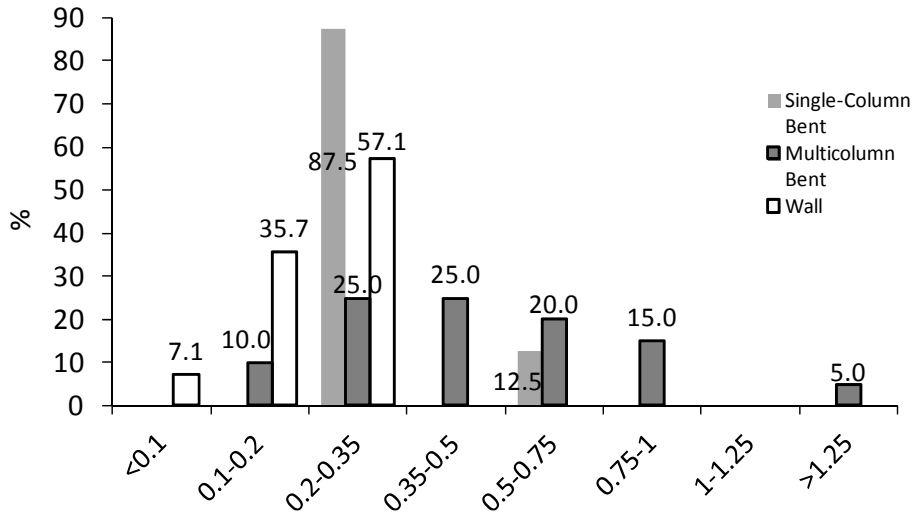
H/BL WALL

No. of Bridges	<1.5	1.5-2	2-4	4-6	6-10	10-20	TOTAL
38	3	1	12	12	9	1	38
	7.9	2.6	31.6	31.6	23.7	2.6	100 %

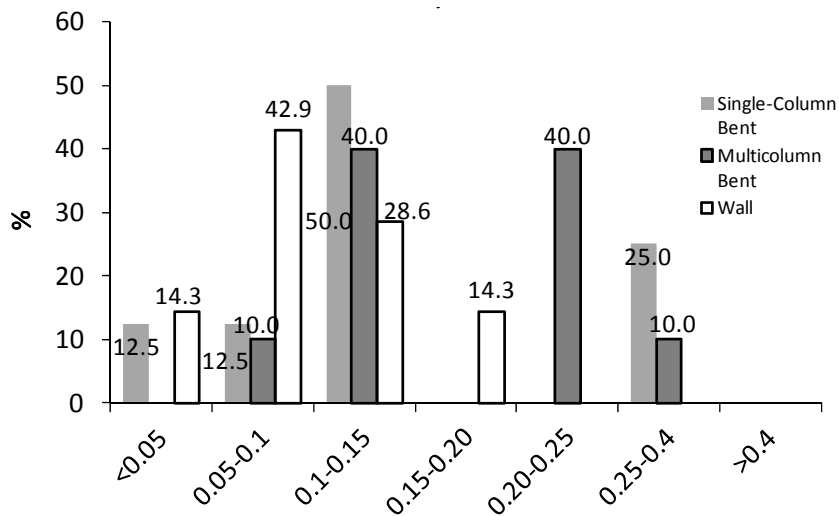


Tab. 6.7 –SET 3c statistics: pier reinforcement ratio and confinement parameter

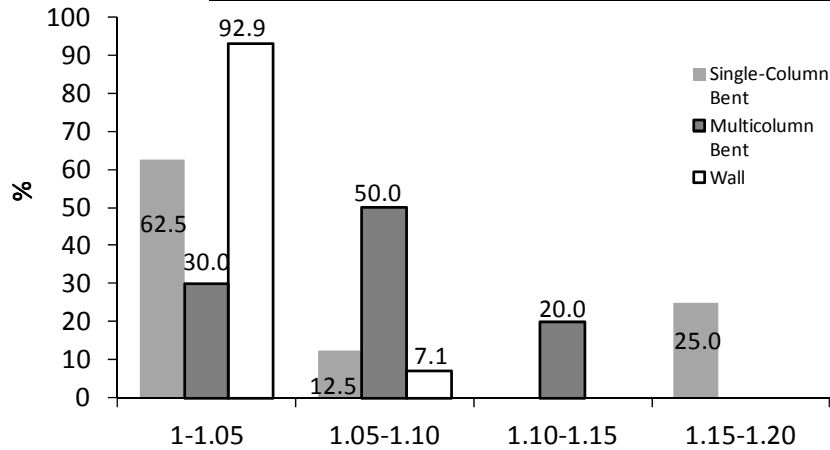
		ρ_l [%]								
Single-Column Bent		<0.1	0.1-0.2	0.2-0.35	0.35-0.5	0.5-0.75	0.75-1	1-1.25	>1.25	TOTAL
8		0	0	7	0	1	0	0	0	8
		0.0	0.0	87.5	0.0	12.5	0.0	0.0	0.0	100 %
Multicolumn Bent		0	2	5	5	4	3	0	1	20
20		0.0	10.0	25.0	25.0	20.0	15.0	0.0	5.0	100 %
Wall		1	5	8	0	0	0	0	0	14
14		7.1	35.7	57.1	0.0	0.0	0.0	0.0	0.0	100 %



		ρ_{st} [%]							
Single-Column Bent		<0.05	0.05-0.1	0.1-0.15	0.15-0.20	0.20-0.25	0.25-0.4	>0.4	TOTAL
8		1	1	4	0	0	2	0	8
		12.5	12.5	50.0	0.0	0.0	25.0	0.0	100 %
Multicolumn Bent		0	2	8	0	8	2	0	20
20		0.0	10.0	40.0	0.0	40.0	10.0	0.0	100 %
Wall		2	6	4	2	0	0	0	14
14		14.3	42.9	28.6	14.3	0.0	0.0	0.0	100 %

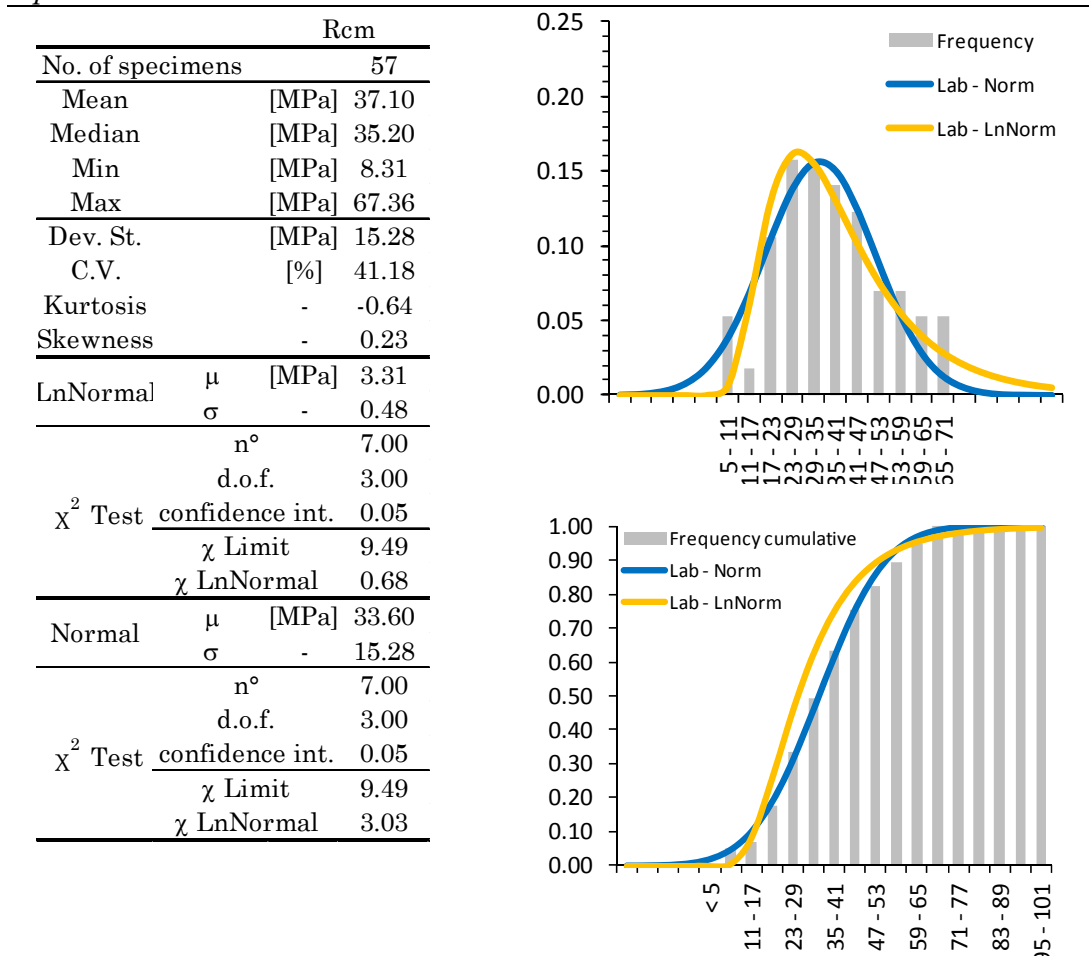


	λ_c				TOTAL
	1-1.05	1.05-1.10	1.10-1.15	1.15-1.20	
Single-Column Bent	5	1	0	2	8
8	62.5	12.5	0.0	25.0	100 %
Multicolumn Bent	6	10	4	0	20
20	30.0	50.0	20.0	0.0	100 %
Wall	13	1	0	0	14



6.2.3 Material properties of the existing rc bridges (SET4)

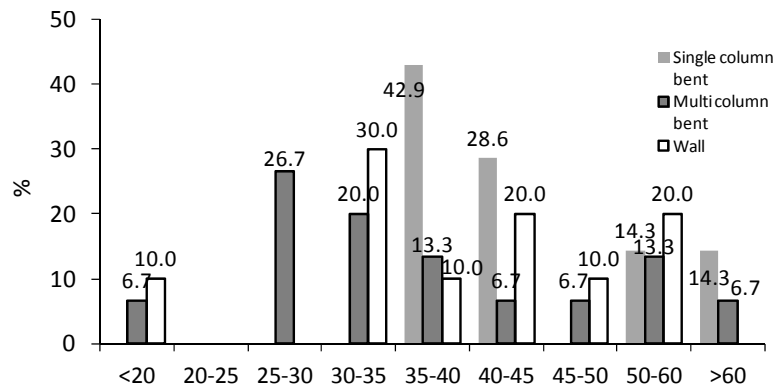
A final set of statistics regards material properties: strength properties for concrete (f_{cm} on cylindrical specimen with h/d ratio equal to 1), yield strength f_{ym} , ultimate strength f_{tm} , and elongation for steel bars were derived from the results of laboratory tests. In the following tables frequency histograms and relative probability density functions and cumulative probability curves are presented for normal and log normal distributions. A wide dispersion of values was obtained for concrete strength (from $R_{cm} < 15$ MPa to $R_{cm} > 70$ MPa), considering all the specimens together in a single set (no. 57, concrete cores extracted were generally more than one for each bridge). A mean value of 37.1 MPa and standard deviation of 15.28 MPa were obtained for normal distribution fitting the frequency histograms. Also the non symmetric lognormal distribution was found to satisfy the χ^2 test used for fitting the distribution curve, with a mean value $R_{cm} = 27.93$ MPa.

Tab. 6.8 –*SET 4 statistics: R_{cm} values obtained from laboratory tests on concrete specimens*


Dividing tests results on concrete with regard to pier types, it can be noted that there is still a wide range of strength, but some differences can be evidenced. Single column bent (cantilever) piers are generally made of good concrete ($R_{cm} \geq 30$ MPa), while wall piers exhibit the highest percentage of unsatisfactory resistance (10% of samples have $R_{cm} < 20$ MPa), and concrete strength never reach high values ($R_{cm} < 60$ MPa). Multicolumn bent show a wider dispersion, with the same percentage (6.7%) of low and high strength values ($R_{cm} < 20$ MPa and $R_{cm} > 60$ MPa respectively), while most of the samples are in a medium range, with $25 < R_{cm} < 60$.

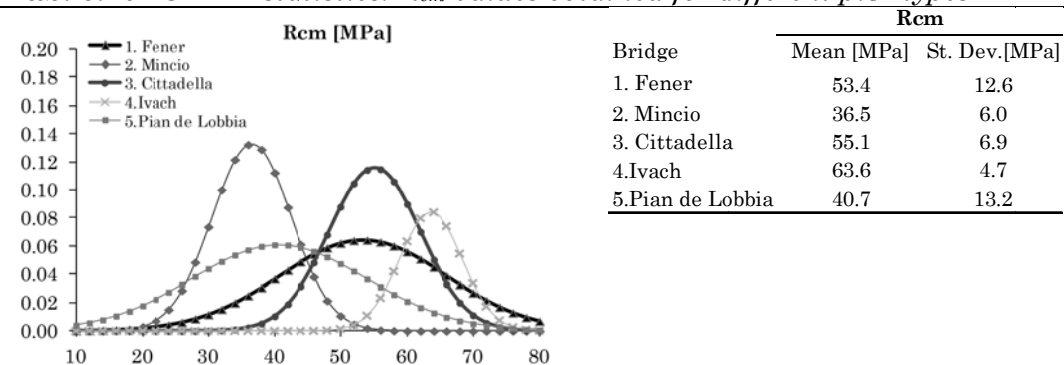
Tab. 6.9 –SET 4 statistics: R_{cm} values obtained for different pier types

		Rcm [MPa] - ALL MULTISPAN (Lab Tests)									
		<20	20-25	25-30	30-35	35-40	40-45	45-50	50-60	>60	TOTAL
Single column bent		0	0	0	0	3	2	0	1	1.0	7
	7	0.0	0.0	0.0	0.0	42.9	28.6	0.0	14.3	14.3	100 %
Multi column bent		1	0	4	3	2	1	1	2	1.0	15
	15	6.7	0.0	26.7	20.0	13.3	6.7	6.7	13.3	6.7	100 %
Wall		1	0	0	3	1	2	1	2	0.0	10
	10	10.0	0.0	0.0	30.0	10.0	20.0	10.0	20.0	0.0	100 %



Fragility analyses being the final object of the research, it is necessary to individuate an average standard deviation for concrete properties for a single construction, even for structures in which no sufficient information are present for a statistical interpretation. A value of $\sigma=9\text{MPa}$ can be assumed, on the base of comparison that can be made for structures with sufficient number of lab tests (see Tab. 6.8, the mean standard deviation obtained is 8.7MPa).

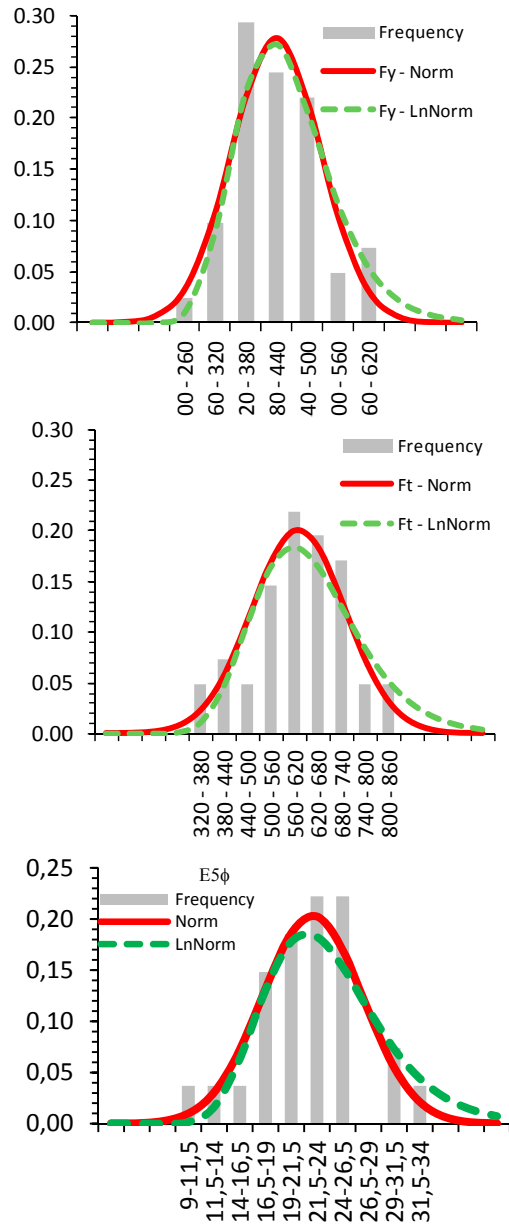
Tab. 6.10 –SET 4 statistics: R_{cm} values obtained for different pier types



Also considering available tests on steel bars all together, a wide dispersion of results is obtained (a medium value of yield strength $f_{y,M}=408.5\text{MPa}$ and $\sigma=86.1\text{MPa}$ for the normal distribution). Best results were obtained by subdividing steel

bars in two category, type Aq 50-60 and FeB44k, and subsequently updating material properties with bayesian approach.

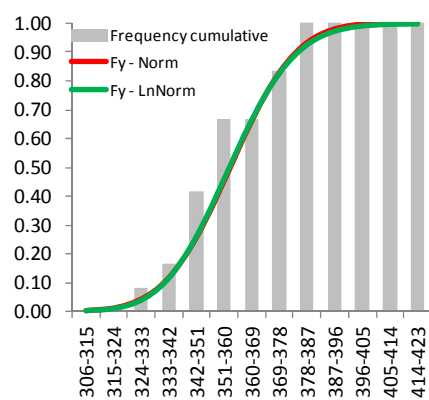
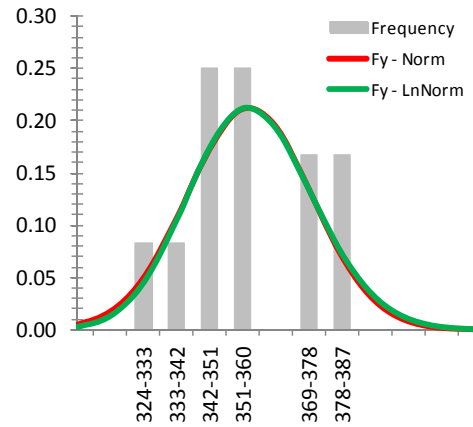
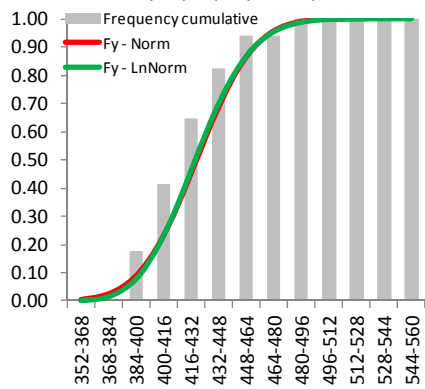
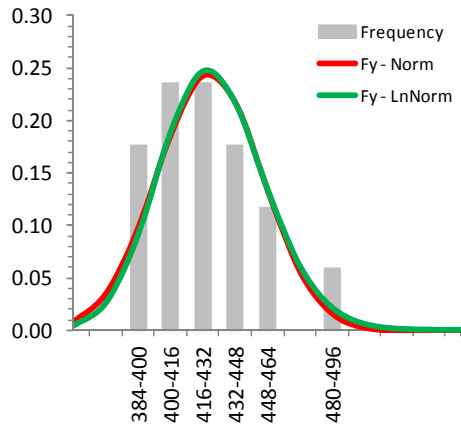
Tab. 6.11 –SET 4b statistics: F_{ym} , F_{tm} , Elongation 5ϕ values obtained from laboratory test on reinforcement bar specimens



		Fy	Ft	El. 5ϕ
No. of specimens		41	41	27
Mean	[MPa]	408.5	600.6	22.3
Median	[MPa]	407.0	603.0	23.0
Min	[MPa]	244.0	340.0	10.5
Max	[MPa]	595.0	835.0	32.0
Dev. St.	[MPa]	86.1	119.5	4.9
C.V.	[%]	21.1	19.9	22.0
Kurtosis	-	-0.2	-0.1	0.6
Skewness	-	0.3	-0.4	-0.2
LnNormal	μ [MPa]	6.0	6.4	3.1
	σ	0.2	0.2	0.2
χ^2 Test	n°	4.0	6.0	4.0
	d.o.f.	3.0	3.0	3.0
	conf.	0.1	0.1	0.1
	χ Limit	3.8	7.8	3.8
χ LnNormal	2.4	0.4	0.4	
Normal	μ [MPa]	408.5	600.6	22.3
	σ	86.1	119.5	4.9
χ^2 Test	n°	5.0	5.0	4.0
	d.o.f.	3.0	3.0	3.0
	conf.	0.1	0.1	0.1
	χ Limit	6.0	6.0	3.8
χ LnNormal	1.4	0.4	0.1	

Tab. 6.12 –SET 4 statistics: F_{ym} , F_{tm} , Elongation 5ϕ values obtained from laboratory test on reinforcement bar specimens separately specimen individuated as FeB44k bars and Aq50-60 bars

FeB44k					Aq50-60						
		Fy	Ft	El. $\delta\phi$			Fy	Ft	All. 5ϕ		
No. of specimens		24	24	16	No. of specimens		17	17	11		
Mean	[MPa]	449.00	672.94	22.56	Mean	[MPa]	357.54	551.00	27.67		
Median	[MPa]	449.00	675.00	23.00	Median	[MPa]	355.00	545.00	30.50		
Min	[MPa]	402.00	593.00	18.50	Min	[MPa]	328.91	509.00	21.50		
Max	[MPa]	533.00	761.00	32.00	Max	[MPa]	381.00	588.00	31.00		
St. Dev.	[MPa]	32.76	51.02	3.56	St. Dev.	[MPa]	16.86	28.85	5.35		
C.V.	[%]	7.30	7.58	15.77	C.V.	[%]	4.72	5.24	19.32		
Kurtosi	-	1.40	-0.79	1.65	Kurtosi	-	-1.01	-1.46	-1.10		
Skewness	-	0.82	-0.05	0.95	Skewness	-	0.06	-0.09	-1.72		
LnNormal	μ	[MPa]	6.10	6.51	3.11	LnNormal	μ	[MPa]	5.88	6.31	3.31
	σ	-	0.07	0.08	0.15		σ	-	0.05	0.05	0.21
		n°	4.00	4.00	4.00			n°	4.00	4.00	4.00
		d.o.f.	3.00	3.00	3.00			d.o.f.	3.00	3.00	3.00
X ² Test	Conf.	0.05	0.05	0.05	X ² Test	Conf.	0.05	0.05	0.05		
	χ Limit	3.84	3.84	3.84		χ Limit	3.84	3.84	3.84		
	χ LnNormal	0.88	3.78	1.48		χ LnNormal	0.82	1.46	3.34		
Normal	μ	[MPa]	449.00	672.94	22.56	Normal	μ	[MPa]	357.54	551.00	27.67
	σ	-	32.76	51.02	3.56		σ	-	16.86	28.85	5.35
		n°	4.00	4.00	4.00			n°	4.00	4.00	4.00
		d.o.f.	3.00	3.00	3.00			d.o.f.	3.00	3.00	3.00
X ² Test	Fiducia	0.05	0.05	0.05	X ² Test	Conf.	0.05	0.05	0.05		
	χ Limit	3.84	3.84	3.84		χ Limit	3.84	3.84	3.84		
	χ Normal	0.56	0.58	5.52		χ Normal	1.59	1.41	3.42		



6.2.3.1 Bayesian updating of reinforcement bars properties

Bayesian statistics provide a powerful tool to update prior information (e.g. based on code requirements) with additional information on material properties derived by in situ tests or lab tests. As material properties are often considered as normal or lognormal variables in fragility analysis, normal gamma or lognormal gamma distribution form a class of natural conjugate priors, that enable to easily update prior hyperparameters for these properties.

In this case a normal distribution was assumed as prior information:

$$f_R(R) = N(R_{m0}, \sigma_{R0}) = \frac{1}{\sigma_{R0} \cdot \sqrt{2 \cdot \pi}} \exp\left(-\frac{1}{2} \cdot \left(\frac{x - R_{m0}}{R\sigma_0}\right)^2\right) \quad (6.1)$$

where N is the probability normal function, R_{m0} is the prior mean value of the variable R (f_y, f_t), and σ_{R0} its standard deviation.

The following relationship can be assumed between characteristic and mean value:

$$R_{k0} = R_{m0} - 1.64 \cdot \sigma_{R0} \quad (6.2)$$

Characteristic values can be statistically updated on the basis of the results x_1, x_2, \dots, x_n tests, using the following equations:

$$R_m = \frac{(x_m \cdot \sigma_{R0}^2 + R_{m0} \cdot \sigma_x^2)}{(\sigma_x^2 + \sigma_{R0}^2)}, \sigma_R = \sqrt{\frac{\sigma_x^2 \cdot \sigma_{R0}^2}{\sigma_x^2 + \sigma_{R0}^2}} \quad (6.3)$$

where x_m, σ_x are the mean value and standard deviation of the specimen sample tested and R_m, σ_R , are the variable updated values.

This procedure was used for the strength parameters of reinforcement bars, smooth bars and deformed bars. On the base of prior code information, smooth bars were supposed to be applied extensively in the constructions of the VR stock realized till the beginning of the 1970s (type Aq50 was selected as reference type), and deformed bars afterwards (FeB44k type was chosen for deformed bars).

Tab. 6.13 –Requirements for reinforcement bars according to different Italian Codes of past decades.

Code	R.D.L. n° 2229/1939			LL.PP. N° 1472/1957				D.M. 30/05/1972				
	S			Aq42	S	Aq50	D	S		D		
Bar type	Dolce	Semiduro	Duro	Aq42	Aq50	Aq60	-	FeB22	FeB32	A38	A41	FeB44
F_y	≥ 225	≥ 260	≥ 300	≥ 225	≥ 260	≥ 300	-	≥ 215*	≥ 315*	≥ 375*	≥ 400*	≥ 430*
F_t	420 - 490	490 - 585	585 - 685	410 - 490	490 - 585	585 - 685	-	≥ 335*	≥ 490*	≥ 450*	≥ 490*	≥ 540*
Elongation												
A₅	-	-	-	-	-	-	-	≥ 24*	≥ 23*	≥ 14*	≥ 14*	≥ 12*
Elongation												
A₁₀	≥ 20	≥ 16	≥ 14	≥ 20	≥ 16	≥ 14	≥ 12	-	-	-	-	-
Elongation												
A_{gt}	-	-	-	-	-	-	-	-	-	-	-	-

Code	D.M. 30/05/1974				D.M. 09/01/1996				D.M. 14/01/2008	
	S		D		S	D	D	D	D	
Bar type	FeB22	FeB32	FeB38	FeB44	FeB22	FeB32	FeB38	FeB44	B450A	B450C
Fy	≥ 215*	≥ 315*	≥ 375*	≥ 430*	≥ 215*	≥ 315*	≥ 375*	≥ 430*	≥ 450*	≥ 450*
Ft	≥ 335*	≥ 490*	≥ 450*	≥ 540*	≥ 335*	≥ 490*	≥ 450*	≥ 540*	≥ 540*	≥ 540*
Elongation A ₅	≥ 24*	≥ 23*	≥ 14*	≥ 12*	≥ 24*	≥ 23*	≥ 14*	≥ 12*	-	-
Elongation A ₁₀	-	-	-	-	-	-	-	-	-	-
Elongation A _{gt}	-	-	-	-	-	-	-	-	≥ 2,5*	≥ 7,5*

S= smooth bars, D= Deformed bars

* Characteristic values referred to a 5% fractile for strength and 10% fractile for elongation

In the following tables the prior information and the updated values R_m , σ_m for Normal distribution are reported. The updated values of mean strength and standard deviation, reported in Tab. 6.13, were used in fragility analyses for the normal distribution of steel bars, type Aq 50-60 and FeB44k (for smooth bars and deformed bars respectively).

Tab. 6.14 – Updating of Normal pdf distribution parameters for smooth bars (type Aq50-60) and deformed bars (type FeB44k)

		Specimens		Prior values		Updated values		x_m/R_m [%]
		x_m	σ_{mx}	R_{m0}	σ_{m0}	R_m	σ_m	
Aq50-60	fy [MPa]	357.54	16.86	260.00	30.00	330.00	14.70	108.34
	ft [MPa]	551.00	28.85	535.00	25.00	550.00	18.89	100.18
	Elongation A ₅ [%]	27.67	5.35	16.00	1.00	16.39	0.98	168.76
FeB44k	fy [MPa]	449.00	32.76	466.93	35.00	460.00	23.92	97.61
	ft [MPa]	672.94	51.02	610.72	30.00	620.00	25.86	108.54
	Elongation A ₅ [%]	22.56	3.56	13.64	1.00	14.29	0.96	157.83

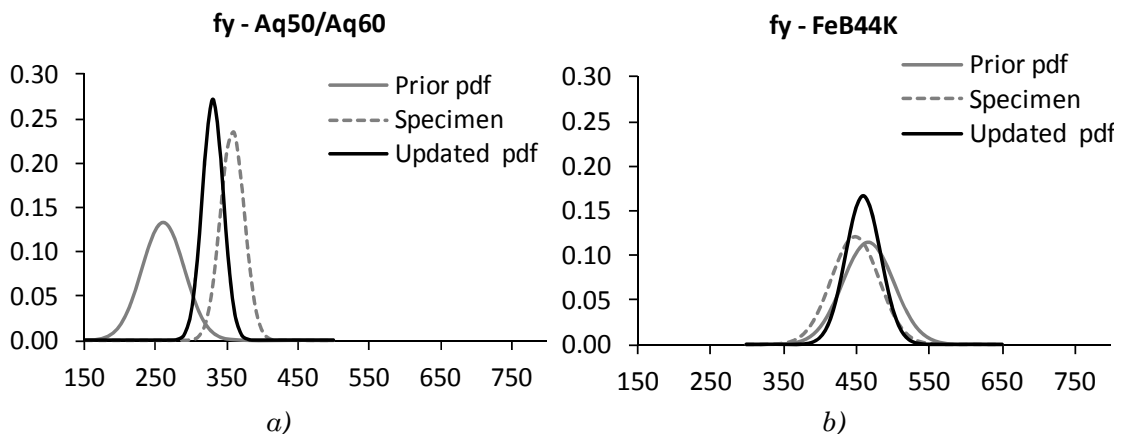


Fig. 6.4 – Normal pdf of yield strength f_y , for prior distribution, distribution obtained by test values on specimen, and updated pdf with Bayesian approach: a) smooth bars (Aq50-60), b) deformed bars (FeB44K)

6.2.4 Extent of the database

The statistical survey described in the previous paragraphs allowed to highlight the effective ranges of the main pier parameters for multi-span bridges, in terms of geometry, reinforcement content, confinement parameters, normalized axial load that are necessary for the calculation of pier capacity.

The significant values obtained directly from the VR stock are reported in the following tables. In the tables the ranges used as reference values for the parametrical analysis developed in Chapter 5 are also presented. It has to be noted that some values are extrapolated to fill some gaps of the bridge inventory, due to the small number of samples present in the database for some sub-category.

It can be noted that reinforcement content is generally very low: longitudinal reinforcement ratio ρ_l (Eq.6.1) piers has as upper bound value of 1% for single cantilever piers, that is the minimum amount generally required for columns by current seismic codes, and percentages less than 0.5% are very frequent. Transverse reinforcement volumetric ratio ρ_{st} has extremely low values (0.05-0.3%), being the standard transversal reinforcement arrangement of piers represented by perimetral hoops D10-12@25-30cm, without any internal tie legs. This leads to very low value of confinement parameter λ_c , 1.05-1.15, while generally varying for newly designed structures between 1 and 2.

Normalized axial load acting, ν_k , is always less than 0.25, so columns have limited compressive stress due to vertical loads (0.6 is the upper limit provided by most codes for ductile behaviour of columns in seismic zones).

Symbols used are reported in the following equations:

$$\rho_l = \frac{A_s}{A_c} \quad \text{longitudinal reinforcement ratio} \quad (6.4)$$

$$\rho_{st} = \frac{A_{sw}}{b_w s_L} \quad \text{transverse reinforcement volumetric ratio} \quad (6.5)$$

$$\nu_k = \frac{N_{Ed}}{A_c f_{ck}} \quad \text{normalized axial load} \quad (6.6)$$

$$\lambda_c \quad \text{confinement parameter (see Eq. 5.28)}$$

where:

A_s = total area of longitudinal reinforcement

A_c = area of concrete cross-section

A_{sw} = total area of transverse steel within a distance s_L (mm^2)

In the following tables the ranges directly obtained from the VR database for significant pier parameters are reported for cantilever and frame piers (single and multiple bent). Rounded values to be considered as representative of the effective ranges are also reported, representing the basis for the combinations adopted in the parametric analysis of Chapter 5. Values with bold characters are extrapolated and not directly found in the VR bridge inventory.

Tab. 6.15 – Significant parameters of the VR stock – single bent circular piers-: a) effective ranges, b) representative values individuated for parametrical analysis

Single Bent					Representative values for parametrical analysis					
Circular Piers	Min	Max	Mean	σ						
D [m]	1.9	3.5	2.62	0.691	2	2.3	2.6	2.9	3.2	3.5
H [m]	3.60	10.90	7.23	2.21	4	6	8	10	12	16
H/D	1.71	4.95	2.88	1.04	1.75	2	2.5	3	4	8
ρ_l [%]	0.22	0.31	0.24	0.11	0.2	0.35	0.5	0.7	1	
ρ_{st} [%]	0.04	0.27	0.18	0.12		0.05	0.1	0.2	0.3	0.4
λ_c	1.03	1.17	1.10	0.50		1	1.1	1.2		
ν_k	0.02	0.16	0.06	0.06	0.05	0.1	0.15	0.2		
Concrete	35.60	63.58	44.34	22.91	30	35	40	45	55	65
Reinf. steel	Aq50-60 FeB44K				Aq50-60		FeB44K			
	a)					b)				

Tab. 6.16 – Significant parameters of the VR stock – single bent square piers-: a) effective ranges, b) representative values individuated for parametrical analysis

Single Bent					Representative values for parametrical analysis					
Square Piers	Min	Max	Mean	σ						
BT [m]	3.30	3.50	3.40	0.14		3	3.5	5		
BT/BL	2.00	3.50	2.75	1.06		2	2.5	3	3.5	
H [m]	2.00	16.00	10.40	7.92	4	6	8	10	14	18
H/BT	1.37	4.57	2.97	2.26	2	2.5	3	4	6	
ρ_l [%]	0.26	0.71	0.48	0.31	0.2	0.35	0.5	0.7	1	
ρ_{st} [%]	0.10	0.15	0.13	0.03		0.05	0.1	0.2	0.3	0.4
λ_c	1.03	1.09	1.06	0.04		1	1.1	1.2		
ν_k	0.02	0.03	0.03	0.01		0.05	0.1	0.15		
Concrete	35.68	50.60	42.32	7.59	30	35	40	45	55	65
Reinf. steel	Aq50-60 FeB44K				Aq50-60		FeB44K			
	a)					b)				

Tab. 6.17 – Significant parameters of the VR stock – wall piers: a) effective ranges, b) representative values individuated for parametrical analysis

Wall Piers					Representative values for parametrical analysis						
Wall thick. BL[m]	Min	Max	Mean	σ							
BT/BL	3.56	43.70	10.65	8.07	3.75	4	5	10	20	40	45
H [m]	0.80	18.00	4.82	2.92	2	4	6	8	12	18	
H/BL	0.75	12.00	4.70	2.49	0.75	2	4	6	8	12	
ρ_l [%]	0.03	0.34	0.22	0.09		0.05	0.2	0.35	0.5		
ρ_{st} [%]	0.03	0.19	0.10	0.05		0.025	0.05	0.1	0.2		
λ_c	1.01	1.07	1.02	0.02		1	1.05	1.1			
ν_k	0.00	0.06	0.02	0.01			0.05	0.1			
Concrete	16.23	55.17	38.89	15.58	15	25	30	35	40	45	55
Reinf. steel	Aq50-60 FeB44K				Aq50-60		FeB44K				
	a)					b)					

Tab. 6.18 – Significant parameters of the VR stock – multiple bent circular piers: a) effective ranges, b) representative values individuated for parametrical analysis

Multiple Bent					Representative values for parametrical analysis												
Circular Piers	Min	Max	Mean	σ													
D [m]	0.30	1.60	1.22	0.36	0.3	0.6	0.9	1.2	1.5	1.8							
H [m]	2.50	18.87	5.57	2.88	2	4	6	8	10	14	18						
H/D	2.04	11.79	4.87	2.17	2	4	6	10	12								
ρ_l [%]	0.16	0.90	0.39	0.20	0.3	0.5	0.75	1	1.5	1.8							
ρ_{st} [%]	0.09	0.27	0.15	0.05	0.05	0.1	0.2	0.25	0.4								
λ_c	1.05	1.15	1.09	0.04	1	1.1	1.2	1.3									
ν_k	0.03	0.24	0.07	0.04	0.05	0.1	0.15	0.2	0.25								
Concrete	26.75	77.24	39.35	15.56	20	25	35	40	45	50	60	70					
Reinf. steel	Aq50-60 FeB44K				Aq50-60				FeB44K								

a) b)

Tab. 6.19 – Significant parameters of the VR stock – multiple bent square piers: a) effective ranges, b) representative values individuated for parametrical analysis

Multiple Bent					Representative values for parametrical analysis											
Square Piers	Min	Max	Mean	σ												
BT [m]	0.60	1.50	0.99	0.35	0.5	1	1.5	2								
BT/BL	0.60	2.50	1.38	0.63	0.75	1	1.5	2	2.5							
H [m]	3.75	10.00	5.66	1.95	2	4	6	10	14	18						
H/BT	3.20	9.50	6.25	2.36	2	4	6	10	12							
ρ_l [%]	0.36	1.82	0.81	0.55	0.3	0.5	0.75	1	1.5	1.8						
ρ_{st} [%]	0.13	0.30	0.20	0.06	0.05	0.1	0.2	0.3	0.4							
λ_c	1.02	1.06	1.04	0.01	1	1.1	1.2	1.3								
ν_k	0.01	0.17	0.09	0.05	0.05	0.1	0.15	0.2	0.25							
Concrete	17.51	50.66	35.58	13.13	20	25	35	40	45	50	60	70				
Reinf. steel	Aq50-60 FeB44K				Aq50-60				FeB44K							

a) b)

Tab. 6.20 – Characteristics of reinforcement steel

	Aq50-60	FeB44K
Fy [MPa]	330	460
Ft [MPa]	550	620
Agt [%]	13.5	11.5

6.2.5 Reference Bridge structures

A limited number of Reference Bridge structures (*RBs*) was chosen in the inventory as representative elements for each homogeneous bridge class and subclass. The listing of these structures, with reference to the corresponding class, is reported in Tab. 6.11. Brief summaries with the main characteristics of the bridges are reported in Appendix C.

In the following paragraphs, the *RBs* belonging to multi-span bridge classes 2.1-2.4, are used as bridge samples in DBA analysis and TH verification, firstly with a direct deterministic approach (see §6.3), and subsequently in a probabilistic framework for the construction of fragility curves.

Tab. 6.21 – Reference Bridge structures: Macro-class 2. Classes 2.1, 2.2, 2.3, 2.4.

CLASS	No. RBs	N°	Zone	Name	Road (S.P.- S.R.)	Km	Year	Span	L span [m]	
2.1 M_SIMPLEY	2.1.1a	RBs1	496	2	Botteon	S.S. 51	X	1978	7	24.00
	2.1.1.b	RBs2	304	3	Rio Ghisel	S.R. 203	39+056	1972	5	16.40
	2.1.2a	RBs3	334	3	Torrente Frison	S.R. 465	4+200	1967	3	48.8
	2.1.3a	RBs4	196	3	Cavalcavia A27	S.R. 89	2+778	1988	3	37.50
	2.1.3b	RBs5	59	2	Cav. Vittorio Veneto -	S.P. 32	0+429	1970	21	23.73
	2.1.3b	RBs6	5	2	Campelli	S.P. 251	103+750	1964	8	30.33
	2.1.4a	RBs7	8	2	S.P.248 "Schiavonesca"	S.R. 348	17+710	1967	3	16.14
	2.1.4b	RBs8	21	3	Fiume Reghena	S.R. 53	113+712	1970	4	24.00
2.2 GERBER	2.2.1	RBs9	35	2	Fante d'Italia	S.P. 1 bis	16+078	1969	13	34.50
	2.2.2.	RBs10	162	3	Canal Bianco	S.R. 482	59+831	1971	3	31.35
2.3 CONT	2.3.1.IIβ.c	RBs11	400	3	Autostrada A4	S.P. 21	4+846	ND	3	36.40
	2.3.1.Iβ.c	RBs12	197	3	Cavalcavia A13	S.R. 06	4+400	1967	3	26.1
	2.3.1.IIβ.d	RBs13	116	3	Cavalcavia zona città	S.R. 11	292+800	1974	2	5.00
	2.3.2.IIβ.a	RBs14	70	3	Cavalcaferrovia FF.SS	S.R. 245	2+486	2000	12	33.00
	2.3.2.IIβ.b	RBs15	292	3	Cavalcavia Borgo Vicenza	S.R. 47	29+990	1994	6	26.30
	2.3.3.Iβ.a	RBs16	299	3	Pontet l	S.R. 50	60+608	1994	6	58.00
2.4 KINEM	2.4.1	RBs17	495	3	Cavalcavia Silea	S.R. 53	X	2004	4	40

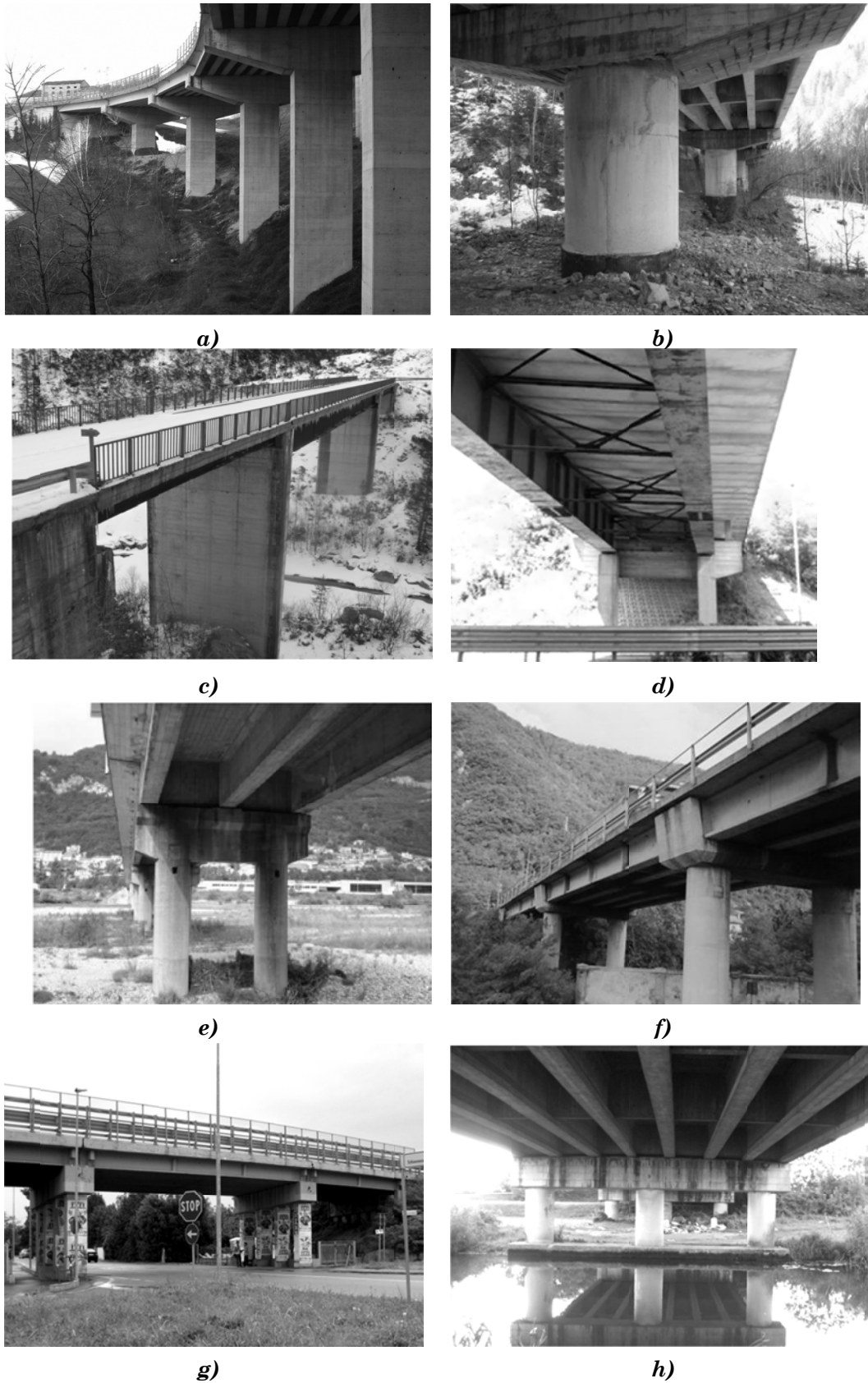


Fig. 6.5 – Reference Bridge structures: a) 2.1.1a-RBs1, b)2.1.1b-RBs2, c)2.1.2a-RBs3, d) 2.1.3a-RBs4, e)2.1.3b-RBs5, f) 2.1.3b-RBs6, g)2.1.4a-RBs7, h)2.1.4b-RBs8



Fig. 6.6 – *Reference Bridges structures for class 2.2 (gerber structures): a) 2.2.1-RBs9, b)2.2.2 –RBs10*

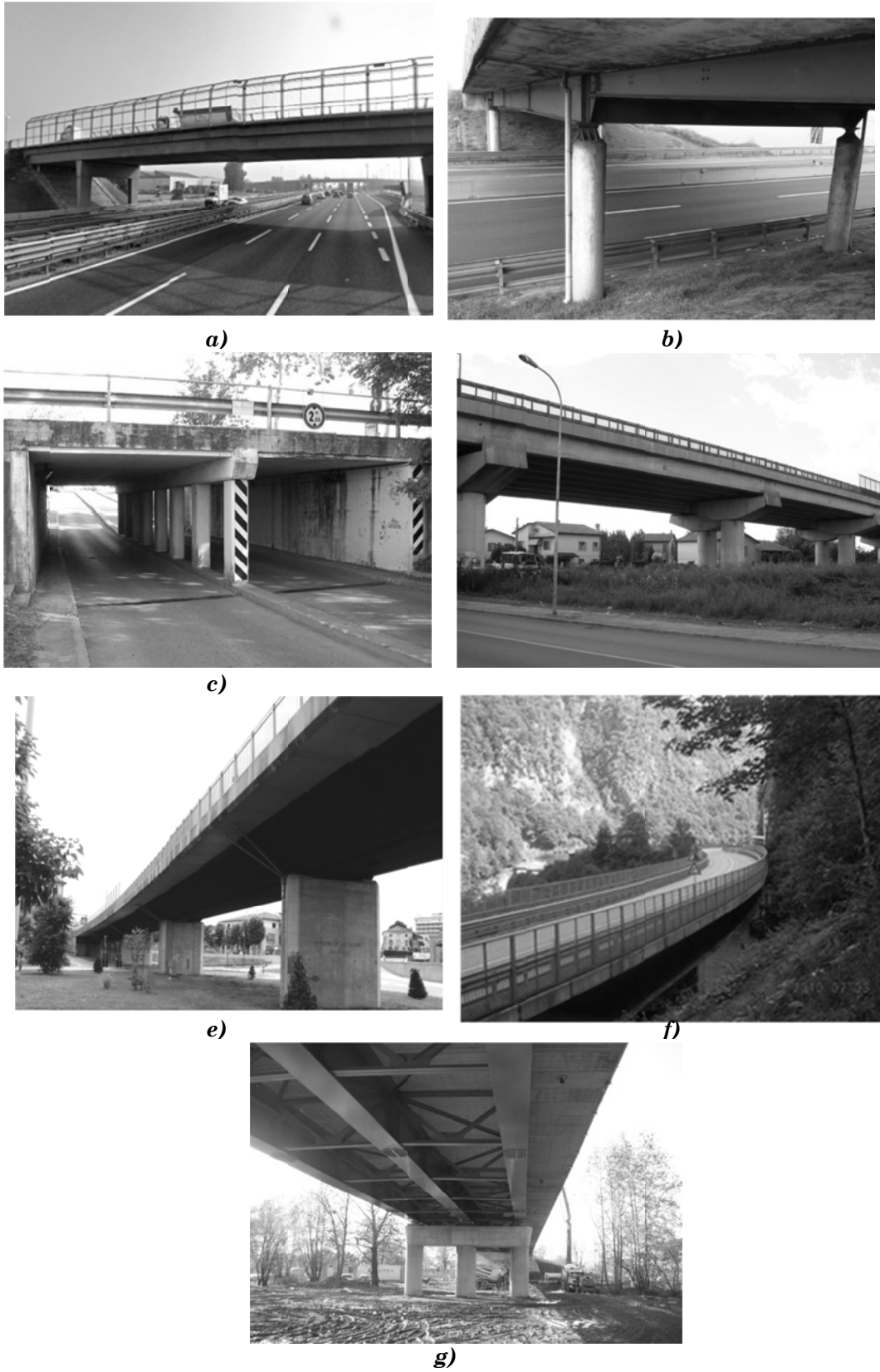


Fig. 6.7 –Reference Bridges: a) 2.3.1b3-RBs11, b) 2.3.1.a3 –RBs12, c) 2.3.1a4 -RBs13, d) 2.3.2b1-RBs14, e) 2.3.2a2-RBs15, f)2.3.3a1-RBs16, g)2.4.1-RBs17

6.3 DISPLACEMENT-BASED ASSESSMENT OF REFERENCE BRIDGE STRUCTURES: DETERMINISTIC APPROACH

In this section deterministic verifications with the DBA approach (described in §2.3.2.1) are carried out on a selected number of structures, represented by the the Reference Bridge structures(RBs) for multi-span girder bridges specified in the previous paragraph, assumed as representative samples of the respective homogeneous classes and subclasses (see Tab.6.19).

Direct applications of the *DBA/C* procedure (see §2.3.2) are carried for the three performance levels established in §6.3.6. Displacement-based approach results are subsequently compared with NLTH verifications: for each PL, Incremental Dynamic Analyses (Vamvatsikos & Cornell^[V1], 2002) were performed by scaling incrementally the set of spectrum-compatible accelerograms till the ultimate pier displacement capacity was reached for PL3, or other displacement level individuated by the corresponding PL1 or PL2.

The mean value $\bar{\alpha}_j(PL_{1,2,3})$ of the recorded seismic action scaling factors α_j is accepted as the Capacity/Demand ratio for the structure being assessed (Paskoy and Petrini^[P15], 2012). The damage index is represented by the inverse value $1/\alpha=D/C$ (see Eq. 6.6).

6.3.1 F.E. model

Incremental Dynamic Analyses and comparisons with the simplified *DBA/C* approach are implemented in the finite element code Opensees (McKenna et al.^[Y1], 2007).

Three dimensional nonlinear F.E. models were developed for the analysis. They are spine model of the bridge structure with line elements located at the centroid of the cross section following the alignment of the bridge. The frame elements representing only the single pier for multi-span simple supported bridges (Classes 2.1, 2.2), and the entire 3D structure for continuous bridges (Classes 2.3, 2.4). Pier members are modeled with non linear elements, while superstructure (deck) is modeled with linear elements.

The pier schematization is a direct applications of the flexural-shear model validated in Chapter 5 (the reader is referred to §5.2.4 for more details). The flexural behaviour is obtained with a fiber-modeling schematization: each element is subdivided in fibers, such that it is possible to assign for each material the constitutive model and exact position of reinforcing bars. A different number of element in used in dependence of the type of static scheme for pier bent (cantilever or frame) and its height. The Concrete02 model (available in the Opensees library), calibrated on Mander model, is chosen for the concrete (cover and core of the section) behavior, while the reinforcing steel bars are modeled according to Menegotto-Pinto constitutive law (see §5.2.4). In order to represent the shear

behavior the phenomenological shear-strain hysteretic model (see §5.2.2) is introduced, with the Section Aggregator function described before.

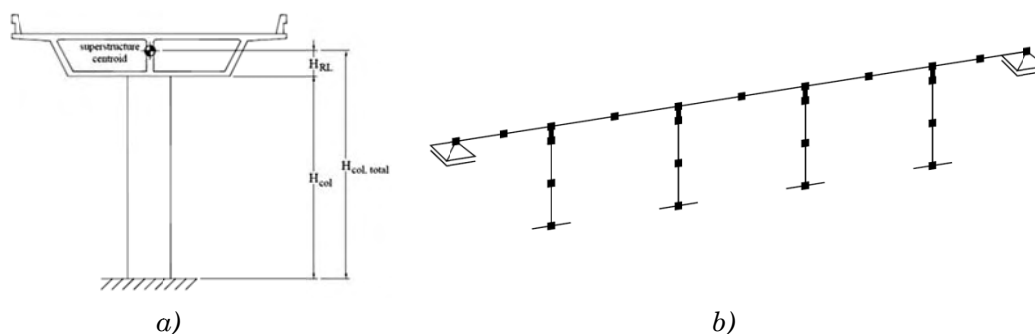


Fig. 6.8 –Analytical model of a typical continuous bridge structure: a) column model geometry, b) 3D spine model

Newmark's time-stepping integration method was used to solve numerically the system of differential equations governing the response of the bridge. The parameters of integration β and γ that define the variation of acceleration over a time step and determine the stability and the accuracy characteristics of the method are chosen to be $\beta = 0.5$ and $\gamma = 0.25$ (average acceleration method).

6.3.2 Seismic action

According to a performance-based-approach structures shall be verified so that performance criteria are met for the seismic intensity expected with a specified probability of exceedance P_{vr} in a given reference period for the structure (V_r , e.g 50 years), also taking into account the class of importance of the structure itself (which depends on structure occupancy usage and damage consequences, in a scale from I to IV, bridge structures being generally considered of importance class III).

The seismic action intensities used for the verification procedures were derived accordingly to the values reported in Tab. 6.20. This values are individuated for design purposes in a Displacement-Based framework for serviceability limit state, PL1, damage control limit state, PL2, and collapse prevention, PL3 (Calvi et al.^[C1], 2009).

Tab. 6.22 –Design intensity (Probability of Exceedance P_{vr}) for Structural Category and Performance Level according to Calvi et al.^[C1], 2009 for Importance Class III

Performance Level	V_r [years]	P_{vr} [%]
PL1	50	20
PL2	50	4
PL3	50	1

The correspondance between P_{vr} and return period T_r is defined by the well-known relationship:

$$T_R = -\frac{V_R}{\ln(1 - P_{Vr}(SL))} \quad (6.7)$$

thus the return periods associated to PL1, PL2, PL3 are $T_r=225, 1225, 4975$ years.

The seismic input used herein for the DBA method is represented by smooth response spectra defined by the Italian Seismic Code ^[X1]. The horizontal acceleration spectra are characterized by following equations:

$$\begin{aligned} 0 \leq T \leq T_B \quad S_e(T) &= a_g \cdot S \cdot \eta \cdot F_0 \cdot \left[\frac{T}{T_B} + \frac{1}{\eta \cdot F_0} \cdot \left(1 - \frac{T}{T_B} \right) \right] \\ T_B \leq T \leq T_C \quad S_e(T) &= a_g \cdot S \cdot \eta \cdot F_0 \\ T_C \leq T \leq T_D \quad S_e(T) &= a_g \cdot S \cdot \eta \cdot F_0 \cdot \left(\frac{T_C}{T} \right) \\ T_D \leq T \quad S_e(T) &= a_g \cdot S \cdot \eta \cdot F_0 \cdot \left(\frac{T_C \cdot T_D}{T^2} \right) \end{aligned} \quad (6.8)$$

where:

$$T_C = C_C \cdot T_C^*, \quad T_B = T_C/3, \quad \eta = \sqrt{\frac{10}{5+\xi}} \geq 0.55,$$

$$T_D = 4,0 \cdot \frac{a_g}{g} + 1.6 \text{ represents the corner period}$$

The corresponding displacement response spectra $S_{de}(T)$ are obtained by Eq. 2.7.

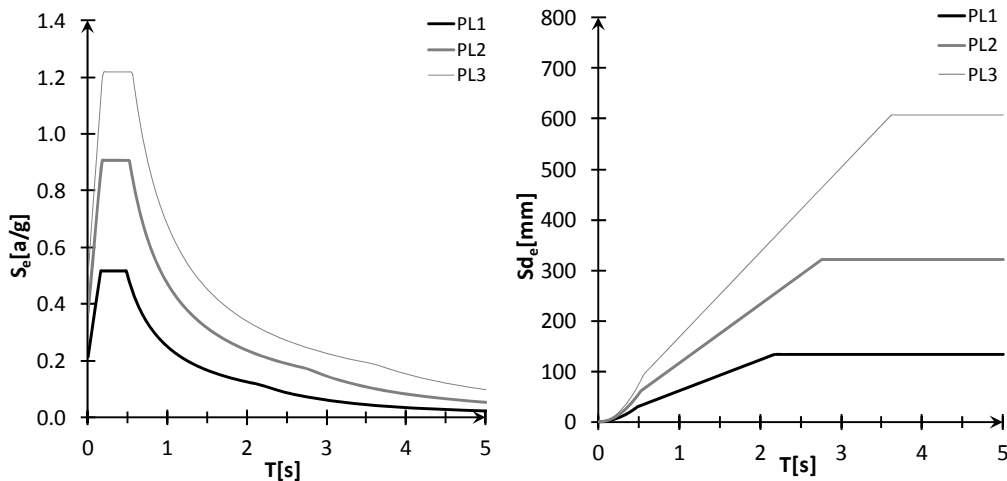
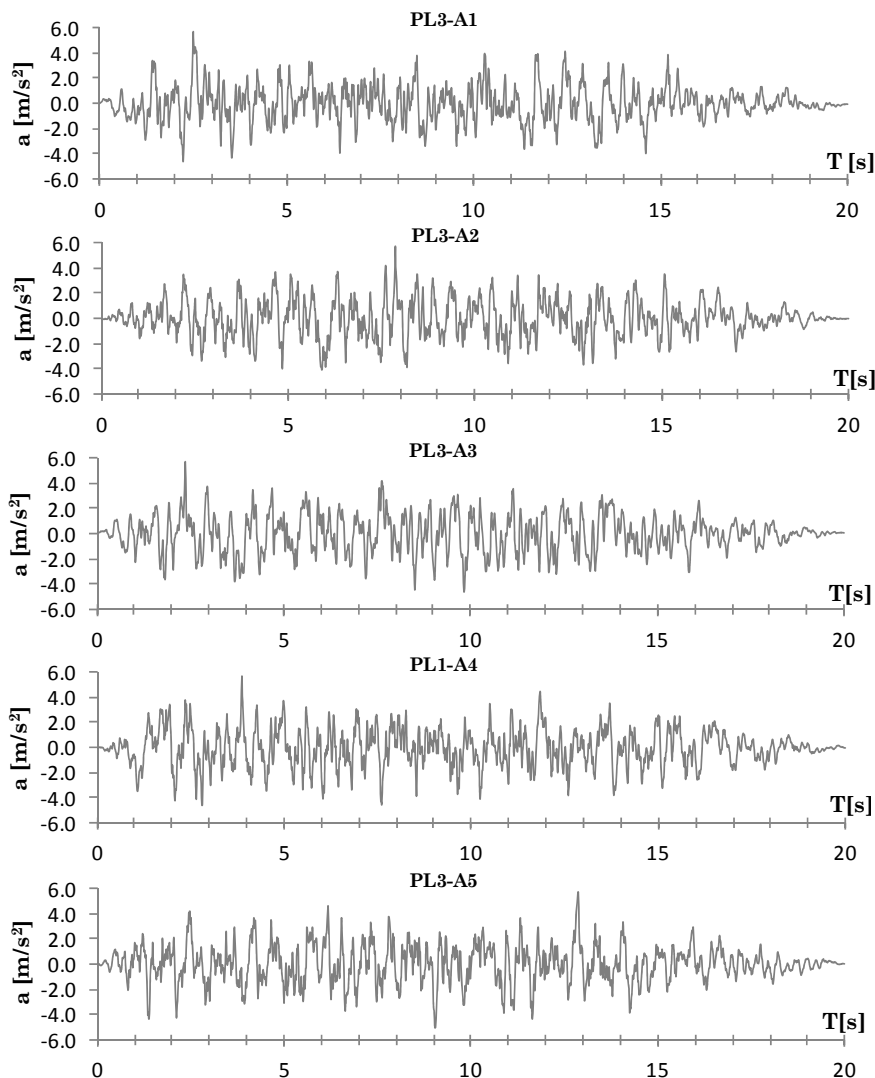


Fig. 6.9 – Smooth elastic acceleration and displacement response spectra for PL1, PL2, PL3 according to Eq. 6.5 for Campelli Bridge construction site (Longarone-BL-, Zone 2, ground type B)

The input parameters a_g , F_o , T_c are defined for the specific construction site of each bridge, by interpolating on the reference grid values supplied by the code, while the S factor varies to the ground type of ground and topographic condition of the site.

As said above, the DBA results were compared against those obtained with non linear time histories analyses for the selected RBs. Seismic input for analyses in time domain was represented by a set of 7 synthetic accelerograms compatible with the code spectrum for each PL, generated with the SIMQKE program (Gasparini and Vanmarcke[G4], 1976). In Fig. 6.10 a typical set of generated ground motions, compatible with the PL3 spectrum of Fig. 6.8 is presented. The corresponding acceleration response spectra for the 7 generated accelerograms, compared with the relative code acceleration response spectra, are plotted in Figs. 6.9 a,b



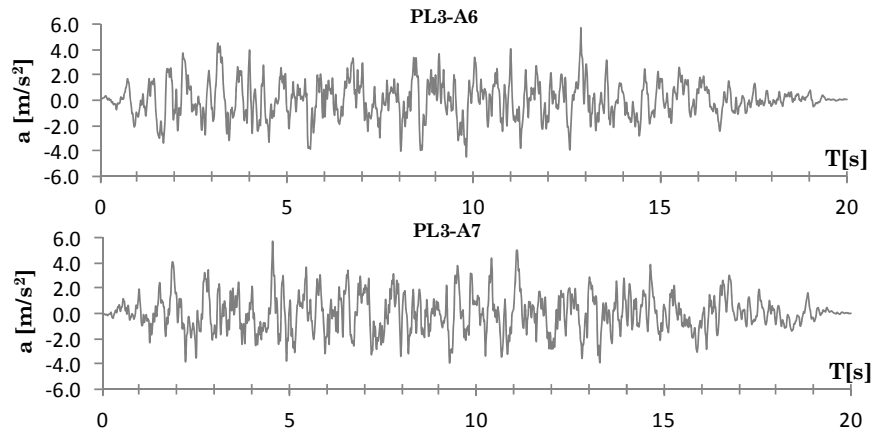


Fig. 6.10 – Ground motions compatible with the elastic smooth spectra PL3 ($P_{vr}=1\%$ in 50years) for the Campelli bridge (Fig. 6.8)

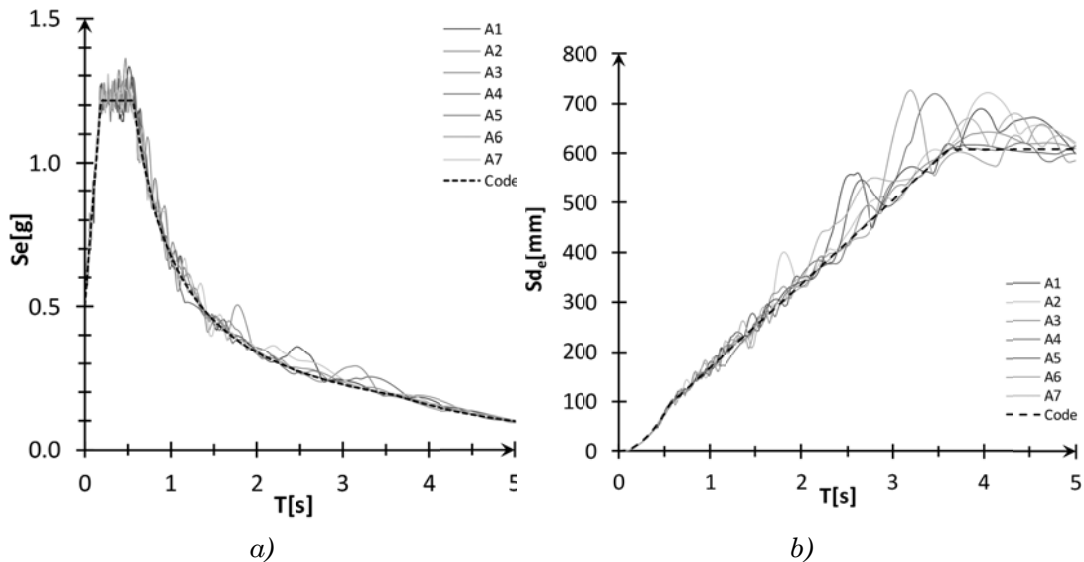


Fig. 6.11 – Smooth elastic acceleration and displacement response spectra for PL1, PL2, PL3 according to Eq. 6.5 for Campelli Bridge construction site (Longarone-BL-, Zone 2, ground type B)

6.3.3 Performance levels and damage indexes

Three performance levels are chosen in this study for the seismic assessment, following the approach of previous studies reported in §1.1.1.1. Reference values were partially adapted to the characteristics of the analyzed bridge structures population (i.e. poorly confined rc members, with piers frequently characterized by shear behaviour).

As regards sectional limits states for piers, strain and drift values are reported in Tab. 6.21.

For piers with flexural behaviour LS₁, Slight Damage, is represented by the attainment of the nominal capacity (θ_{yn}), defined by strain limits on pier base section equal to $\varepsilon_c=0.004$, $\varepsilon_s=0.015$. Extensive damage/collapse limit state, LS₃,

corresponds to the displacement (or drift) tied to strain on materials equal to $\varepsilon_c=1.5\varepsilon_{c,dc}$ and $\varepsilon_s=0.9\varepsilon_{su}$. For the intermediate severe damage limit state, a drift limit corresponding to $2/3\theta_u$, was chosen; alternatively it could be represented by the attainment of the ultimate deformation on the most outer fibers of the concrete core, $\varepsilon_c=\varepsilon_{c,dc}$ (see Eq.2.4), or a limited steel deformation $\varepsilon_s=0.6\varepsilon_{su}$.

Corresponding limit states are defined also for piers with shear behaviour; LS1 is individuated as drift (θ_{cr}) corresponding to the attainment of the shear value corresponding to shear cracking, V_{cr} , while LS2 is represented by the drift corresponding to shear ultimate resistance θ_s , and LS3 is set to $1.1\theta_s$, considering that a residual displacement capacity is still present after shear ultimate force has been reached.

Tab. 6.23 –Definition of limit states for the assessment of rc bridge piers

PIERS		LS1 (Sligth Damage)	LS2 (Severe Damage)	LS3 (Extensive/Complete)
Description		Spalling of concrete, residual crack widths max 1.0mm	Significative repair required, wide flexural or shear crack	Collapse does not take place; extensive damage, not repairable, due to shear failure of vertical elements or excess flexural
<i>Ductile flexural behaviour</i>	Strain	$\varepsilon_c=0.004$ $\varepsilon_s=0.015$		$\varepsilon_c=\varepsilon_{cdc}<0.01$ $\varepsilon_s=0.6\varepsilon_{su}<0.06$
	Drift	θ_{yn}	$2/3\theta_u$	θ_u
<i>Brittle shear behaviour</i>	Drift	θ_{cr}	θ_s	$1.1\theta_s$

Damage measures (DM) are directly defined in relation to the attainment of the limit displacement for each performance level, in terms of ratio between displacement demand and capacity

$$DM_{PLj}=(D/C)_{PLj} \quad (6.9)$$

Taking LS1 as example, for a cantilever pier of height h , the displacement capacity is expressed by $\Delta_{C,LS1}=\theta_{yn}h$, which value is directly compared with the displacement demand Δ_D in terms of elastic spectral displacement according to the procedure described in §2.3.2.1.

6.3.4 Comparison of results between DBA approach and TH verification

The result of the comparison between DBA analysis and TH verification are reported in this paragraph for each one of the Reference Bridge structures selected, as representative of multi-span rc girder bridges of classes 2.1, 2.2 (see Tab. 6.19).

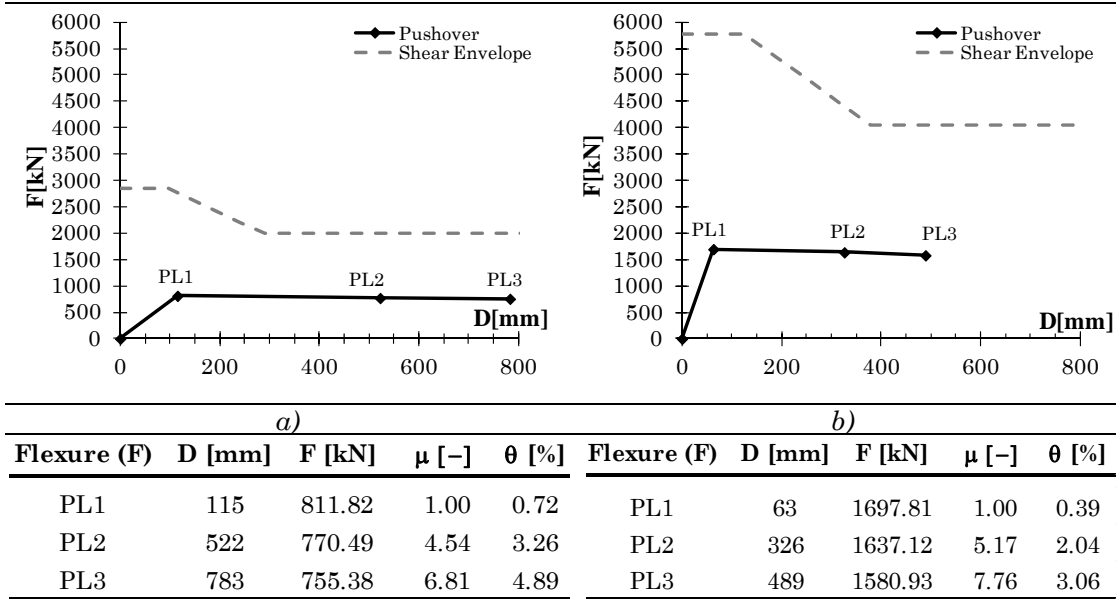
The behaviour is separately investigated in the longitudinal and transverse direction for multiple bent bridge piers, which act under horizontal inertial forces as cantilever structures along the bridge axis, and as frames (simple or multiple) in the

orthogonal direction. For wall piers the longitudinal direction is the most vulnerable, so only longitudinal behaviour is investigated.

Capacity curves are also reported, with the definition of the shear envelope and the performance levels attained. Capacity curves are plotted with reference to a single column also for multiple bents, to characterize the pier behaviour (Shear-S-, Flexure-Shear, FS, or flexure, F), and corresponding ductility values and drift values.

The mean error with reference to the C/D ratio is calculated as follows:

$$E_{mean} = \frac{(C/D)_{TH,mean} - (C/D)_{DBA}}{(C/D)_{TH,mean}} \quad (6.10)$$

RBs 1-Botteon Bridge
Tab. 6.24 – *RBs1: Capacity curves of a single column of the pier bent: a) longitudinal b) transverse direction*

Tab. 6.25 – *RBs1: long. direction (L), comparison between DBA and TH results*

<i>DBA analysis-L</i>						
Botteon-L-	Δ_c [mm]	V_b [kN]	ξ_c [-]	T_c [s]	C/D	$DM_{PL}=D/C$
PL1	115	811.82	0.050	2.264	0.558	1.793
PL2	522	770.49	0.168	3.603	2.458	0.407
PL3	783	755.38	0.177	4.217	1.740	0.575

<i>TH verification-L</i>						
Botteon-L-	TH			DBA		Error %
	C/D	σ	C.o.V[%]	$C/D \pm \sigma$	C/D	
PL1	0.539	0.049	9.093	0.490	0.588	-3.550
PL2	2.323	0.035	1.507	2.288	2.358	-5.82
PL3	1.580	0.091	5.760	1.489	1.671	-10.13

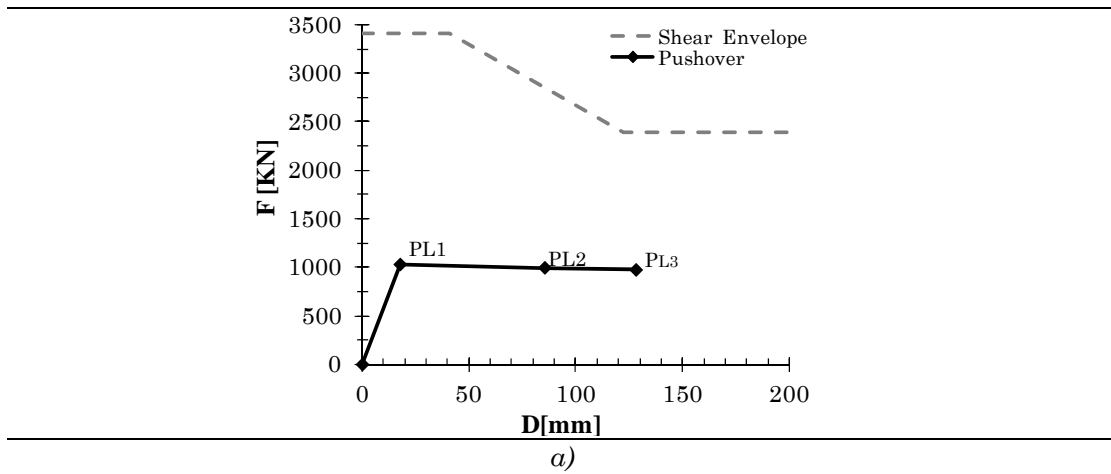
Tab. 6.26 – *RBs7: transverse. direction (T), comparison between DBA and TH results*

<i>DBA analysis-T</i>						
BOTTEON-T-	Δ_c [mm]	V_b [kN]	ξ_c [-]	T_c [s]	C/D	$DM_{PL}=D/C$
PL1	63	1697.81	0.050	1.097	0.621	1.609
PL2	326	1637.12	0.170	2.907	1.284	0.779
PL3	489	1580.93	0.186	3.726	0.954	1.048

<i>THA verification-T</i>						
Botteon-T-	TH			DBA		Error %
	C/D	σ	C.o.V[%]	$C/D \pm \sigma$	C/D	
PL1	1.740	0.069	3.965	1.671	1.809	7.53
PL2	0.891	0.117	13.127	0.774	1.008	12.60
PL3	1.261	0.126	9.996	1.135	1.387	16.86

RBs 2-Rio Ghisel Bridge

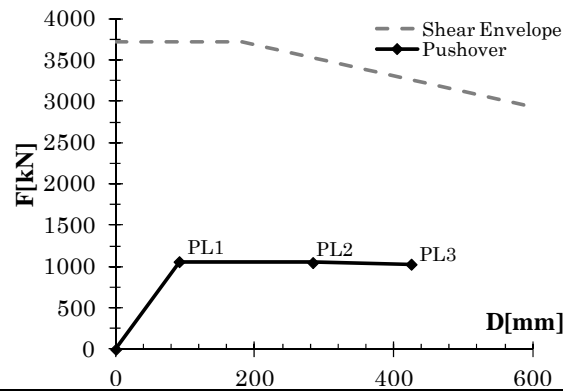
Tab. 6.27 – RBs2: Capacity curve of the pier: a) longitudinal and transverse direction



Flexure (F)	D [mm]	F [kN]	μ [-]	θ [%]
PL1	18	1030.5	1.00	0.3
PL2	85	996.2	4.83	1.3
PL3	128	974.6	7.24	2.0

Tab. 6.28 – RBs 2: long. and transverse direction, comparison between DBA and TH results

<i>DBA analysis</i>						
Rio Ghisel	Δcap	Vbase	ξ_c	T_c	C/D	DM _{PL} =D/C
	[mm]	[kN]	-	[s]	-	-
PL1	18	1030.5	0.050	0.513	1.373	0.728
PL2	85	996.2	0.162	1.146	2.197	0.455
PL3	128	974.6	0.172	1.419	1.624	0.616
<i>THA verification</i>						
Rio Ghisel	TH				DBA	Error
	C/D	σ	C.o.V	C/D $\pm \sigma$	C/D	%
	-	-	[%]	-	-	
PL1	1.383	0.125	9.004	1.259 - 1.508	1.373	0.754
PL2	2.373	0.220	9.272	2.153 - 2.592	2.197	7.412
PL3	1.828	0.133	7.259	1.695 - 1.960	1.624	11.113

RBs 3- Frison Bridge
Tab. 6.29 – *RBs 3: Capacity curves of the pier: a) longitudinal direction*


a)

Flexure (F)	D [mm]	F [kN]	μ [-]	θ [%]
PL1	91	1059.99	1.00	0.62
PL2	283	1049.28	3.11	1.91
PL3	425	1028.89	4.66	2.87

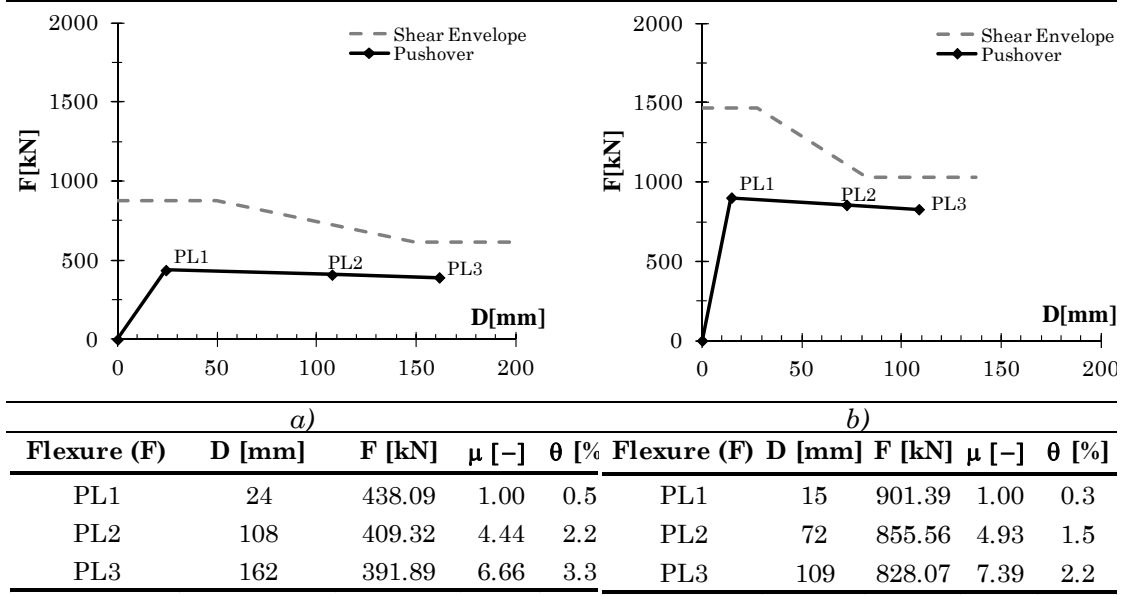
Tab. 6.30 – *RBs 3: long. direction (L), comparison between DBA and TH results*

<i>DBA analysis-L</i>						
Frison-L-	Δ_c [mm]	V_b [kN]	ξ_c [-]	T_c [s]	C/D	$DM_{PL}=D/C$
PL1	91	1060.0	0.050	1.113	1.039	0.962
PL2	283	1049.3	0.135	2.983	2.274	0.440
PL3	425	1028.9	0.154	3.699	2.034	0.492

<i>TH verification-L</i>						
Frison-L-	TH				DBA	Error
	C/D	σ	C.o.V[%]	$C/D \pm \sigma$	C/D	%
PL1	0.984	0.091	9.249	0.893 1.075	1.039	-5.60
PL2	2.480	0.083	3.346	2.397 2.563	2.274	8.32
PL3	2.229	0.138	6.192	2.091 2.367	2.034	8.74

RBs 4- A27 Bridge

Tab. 6.31 – *RBs7: Capacity curves of a single column of the pier bent: a) longitudinal b) transverse direction*



Tab. 6.32 – *RBs7: long. direction (L), comparison between DBA and TH results*

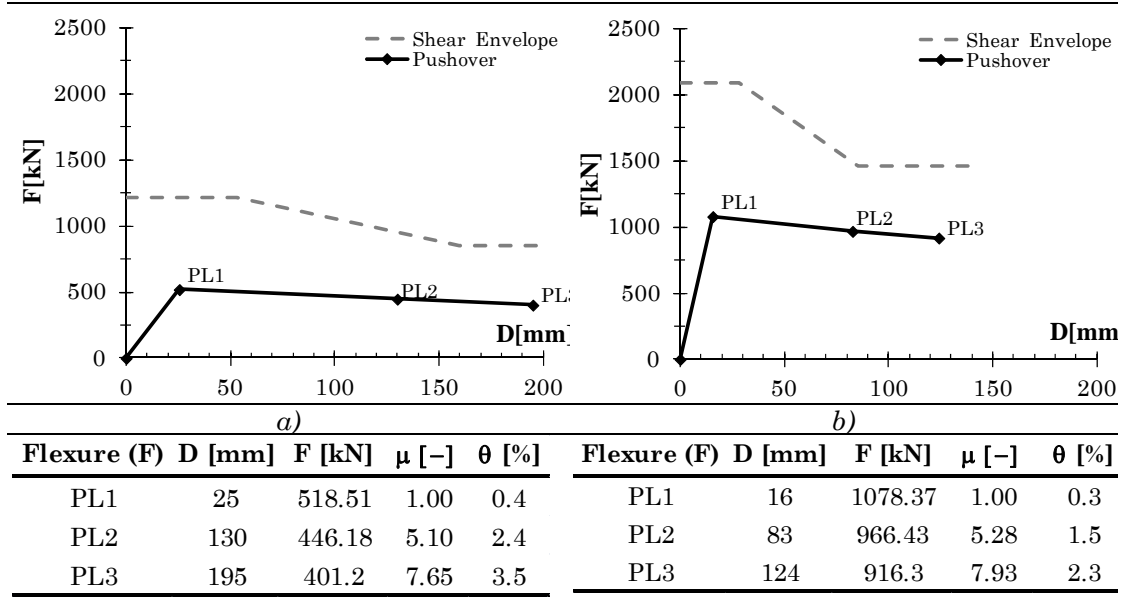
<i>DBA analysis-L</i>							
Cav. A27-L-	Δ_c [mm]	V_b [kN]	ξ_c [-]	T_c [s]	C/D	DM _{PL} =D/C	
PL1	24	438.09	0.050	0.617	0.734	1.363	
PL2	108	409.32	0.167	1.527	1.346	0.743	
PL3	162	391.89	0.175	1.911	1.073	0.932	

<i>TH verification-L</i>							
Cav. A27-L-	TH					DBA	Error
	C/D	σ	C.o.V[%]	C/D \pm σ	C/D	%	
PL1	0.726	0.060	8.319	0.666	0.786	0.734	-1.04
PL2	1.483	0.155	10.463	1.328	1.638	1.346	9.26
PL3	1.185	0.132	11.147	1.053	1.317	1.073	9.46

Tab. 6.33 – *RBs7: transverse. direction (T), comparison between DBA and TH results*

<i>DBA analysis-T</i>							
Cav. A27-T-	Δ_c	V_b [kN]	ξ_c [-]	T_c [s]	C/D	DM _{PL} =D/C	
PL1	15	901.387	0.050	0.344	0.842	1.187	
PL2	72	855.565	0.168	0.866	1.601	0.625	
PL3	109	828.074	0.176	1.078	1.281	0.780	

<i>THA verification-T</i>							
Cav. A27-T-	TH					DBA	Error
	C/D	σ	C.o.V[%]	C/D \pm σ	C/D	%	
PL1	0.959	0.139	14.494	0.820	1.098	0.842	12.20
PL2	1.897	0.182	9.579	1.716	2.079	1.601	15.65
PL3	1.569	0.133	8.493	1.436	1.702	1.281	18.33

RBs 5-Campelli Bridge
Tab. 6.34 – *RBs7: Capacity curves of a single column of the pier bent: a) longitudinal b) transverse direction*

Tab. 6.35 – *RBs5: long. direction (L), comparison between DBA and TH results*

<i>DBA analysis-L</i>						
Campelli-L-	Δ_c [mm]	V_b [kN]	ξ_c [-]	T_c [s]	C/D	$DM_{PL}=D/C$
PL1	25	518.52	0.050	0.689	0.599	1.670
PL2	130	446.18	0.164	1.676	1.075	0.931
PL3	195	401.20	0.173	2.165	0.888	1.126

<i>TH verification-L</i>							
Campelli-L-	TH			DBA		Error %	
	C/D	σ	C.o.V[%]	$C/D \pm \sigma$	C/D		
PL1	0.540	0.068	12.540	0.473	0.608	0.599	-10.79
PL2	1.201	0.090	7.499	1.111	1.291	1.075	10.54
PL3	1.006	0.134	13.282	0.872	1.139	0.888	11.67

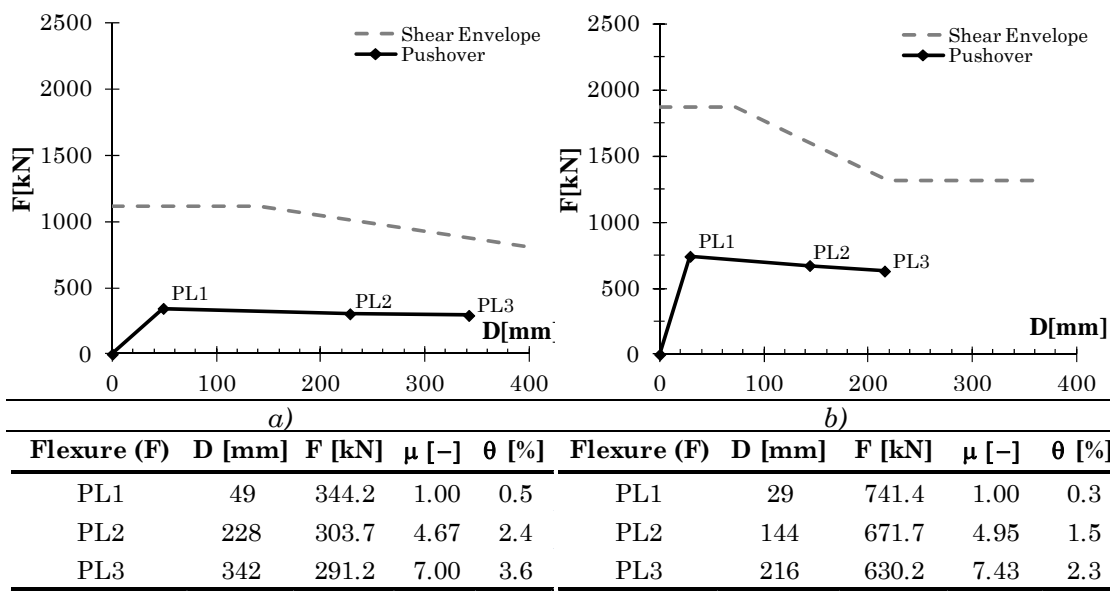
Tab. 6.36 – *RBs5: transverse direction (T), comparison between DBA and TH results*

<i>DBA analysis-T</i>						
Campelli-T-	Δ_c [mm]	V_b [kN]	ξ_c [-]	T_c [s]	C/D	$DM_{PL}=D/C$
PL1	16	1078.37	0.050	0.374	0.677	1.478
PL2	83	966.43	0.165	0.933	1.232	0.812
PL3	124	916.30	0.174	1.211	1.013	0.987

<i>THA verification-T</i>							
Campelli-T-	TH			DBA		Error %	
	C/D	σ	C.o.V[%]	$C/D \pm \sigma$	C/D		
PL1	0.699	0.034	4.861	0.665	0.733	0.677	3.20
PL2	1.326	0.133	10.048	1.193	1.459	1.232	7.11
PL3	1.265	0.066	5.250	1.199	1.332	1.013	19.95

RBs 6- Vittorio Veneto (Fener Bridge)

Tab. 6.37 – RBs7: Capacity curves of a single column of the pier bent: a) longitudinal b) transverse direction



Tab. 6.38 – RBs6: long. direction (L), comparison between DBA and TH results

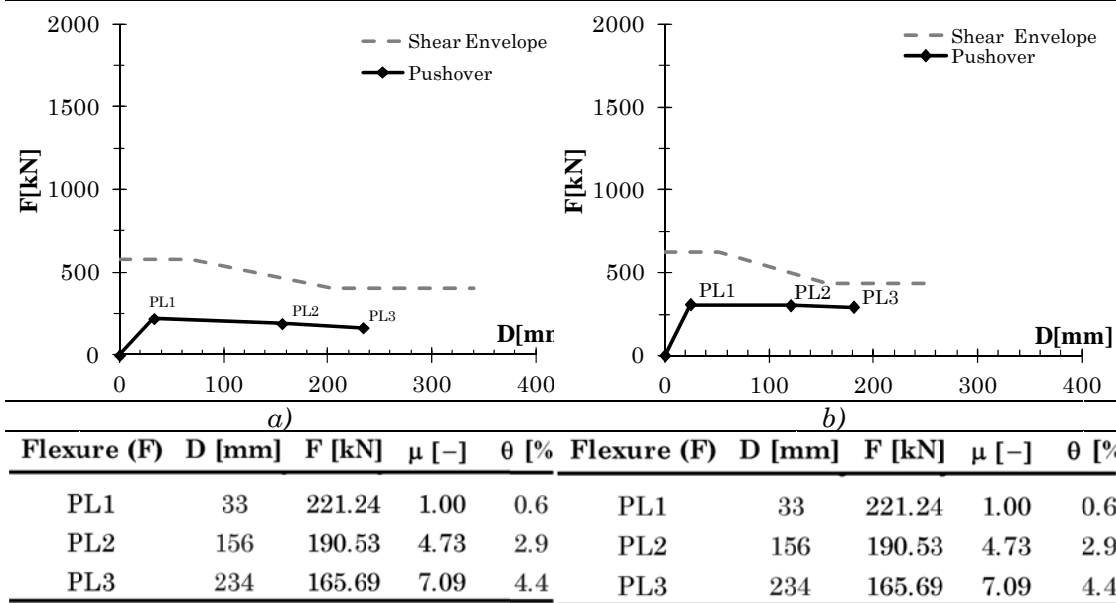
<i>DBA analysis-L</i>							
Fener-L-	Δ_c [mm]	V_b [kN]	ξ_c [-]	T_c [s]	C/D	DM _{PL} =D/C	
PL1	49	344.21	0.050	1.187	0.633	1.581	
PL2	228	303.66	0.161	2.776	1.055	0.948	
PL3	342	291.15	0.171	3.603	0.831	1.204	

<i>TH verification-L</i>							
Fener-L-	TH				DBA		Error
	C/D	σ	C.o.V[%]	C/D \pm σ	C/D	%	
PL1	0.659	0.079	11.986	0.580 0.738	0.633	3.96	
PL2	1.094	0.106	9.652	0.988 1.200	1.055	3.57	
PL3	0.939	0.130	13.889	0.809 1.070	0.831	11.56	

Tab. 6.39 – RBs6: transverse direction (T), comparison between DBA and TH results

<i>DBA analysis-T</i>							
Fener-T-	Δ_c [mm]	V_b [kN]	ξ_c [-]	T_c [s]	C/D	DM _{PL} =D/C	
PL1	29	741.36	0.050	0.623	0.715	1.398	
PL2	144	671.69	0.163	1.515	1.225	0.817	
PL3	216	630.15	0.172	1.979	0.957	1.045	

<i>THA verification-T</i>							
Fener-T-	TH				DBA		Error
	C/D	σ	C.o.V[%]	C/D \pm σ	C/D	%	
PL1	0.637	0.089	14.055	0.547 0.726	0.715	-12.36	
PL2	1.380	0.074	5.368	1.306 1.454	1.225	11.23	
PL3	1.197	0.094	7.891	1.103 1.292	0.957	20.12	

RBs 7- Schiavonesca
Tab. 6.40 – RBs7: Capacity curves of a single column of the pier bent: a) longitudinal b) transverse direction

Tab. 6.41 – RBs7: long. direction (L), comparison between DBA and TH results

<i>DBA analysis-L</i>							
Schiavonesca-L-	Δ_c [mm]	V_b [kN]	ξ_c [-]	T_c [s]	C/D	DM _{PL=D/C}	
PL1	33	221.24	0.050	0.705	0.728	1.374	
PL2	156	190.53	0.172	1.946	1.676	0.597	
PL3	234	165.69	0.179	2.397	1.370	0.730	

<i>TH verification-L</i>							
Schiavonesca-L-	TH				DBA		Error
	C/D	σ	C.o.V[%]	C/D $\pm \sigma$		C/D	%
PL1	0.658	0.077	11.637	0.582	0.735	0.728	-10.56
PL2	1.933	0.278	14.381	1.655	2.211	1.676	13.33
PL3	1.697	0.154	9.079	1.543	1.852	1.370	19.29

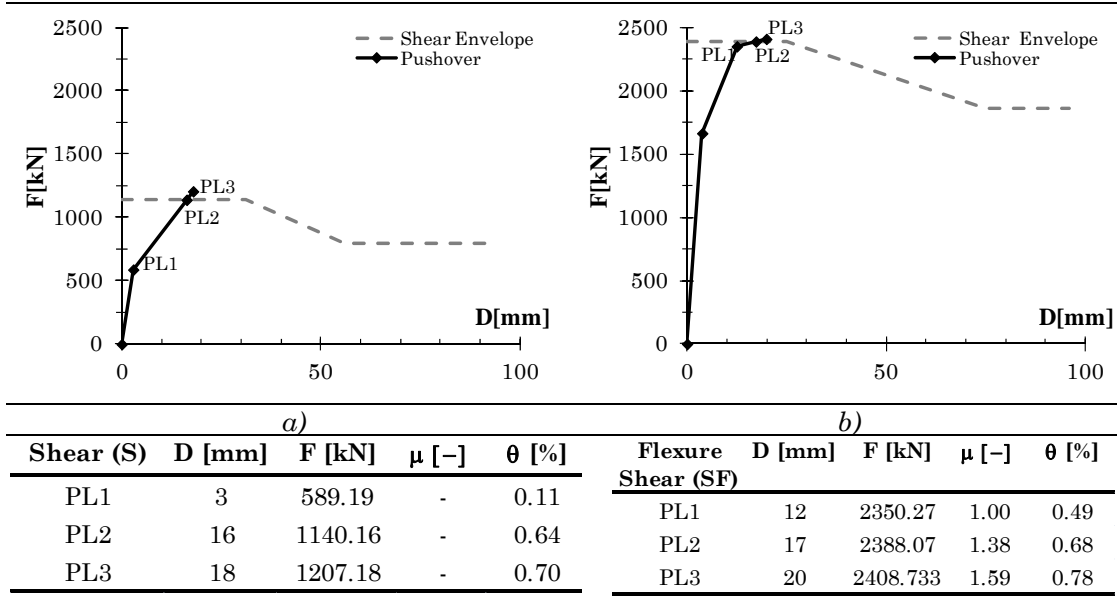
Tab. 6.42 – RBs7: transverse direction (T), comparison between DBA and TH results

<i>DBA analysis-T</i>							
Schiavonesca-T-	Δ_c [mm]	V_b [kN]	ξ_c [-]	T_c [s]	C/D	DM _{PL=D/C}	
PL1	25	308.14	0.050	0.520	0.745	1.343	
PL2	121	301.77	0.175	1.561	1.840	0.543	
PL3	181	292.43	0.180	1.934	1.492	0.670	

<i>THA verification-T</i>							
Schiavonesca -T-	TH				DBA		Error
	C/D	σ	C.o.V[%]	C/D $\pm \sigma$		C/D	%
PL1	0.665	0.066	9.984	0.599	0.732	0.745	-11.91
PL2	2.133	0.119	5.598	2.014	2.253	1.840	13.73
PL3	1.796	0.0186	1.036	1.777	1.814	1.492	16.92

RBs 8- Fiume Reghena Bridge

Tab. 6.43 – RBs7: Capacity curves of a single column of the pier bent: a) longitudinal b) transverse direction



Tab. 6.44 – RBs7: long. direction (L), comparison between DBA and TH results

DBA analysis-L							
Reghena-L-	Δ_c [mm]	V_b [kN]	ξ_c [-]	T_c [s]	C/D	DM _{PL} =D/C	
PL1	3	589.19	0.050	0.217	0.448	2.233	
PL2	16	1140.16	0.090	0.362	0.576	1.737	
PL3	18	1207.18	0.103	0.372	0.403	2.481	

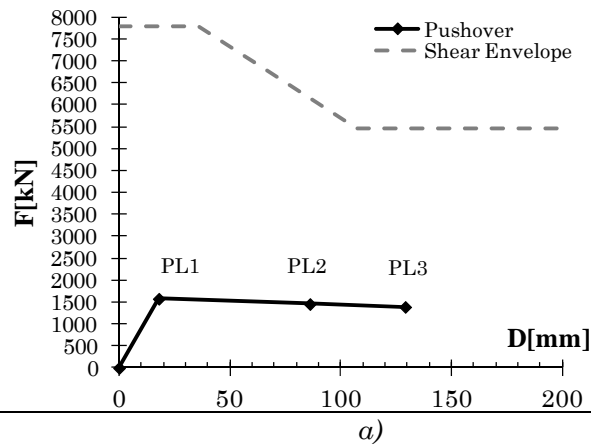
TH verification-L							
Reghena-L-	TH				DBA	Error	
	C/D	σ	C.o.V[%]	C/D $\pm \sigma$	C/D	%	
PL1	0.493	0.056	11.361	0.437 0.549	0.448	9.110	
PL2	2.180	0.055	2.523	2.125 2.235	1.737	20.33	
PL3	3.256	0.123	3.778	3.133 3.379	2.481	23.80	

Tab. 6.45 – RBs7: transverse direction (T), comparison between DBA and TH results

DBA analysis-T							
Reghena-T-	Δ_c [mm]	V_b [kN]	ξ_c [-]	T_c [s]	C/D	DM _{PL} =D/C	
PL1	12	2350.27	0.050	0.271	1.682	0.594	
PL2	17	2388.07	0.121	0.383	0.739	1.353	
PL3	20	2408.73	0.132	0.412	0.627	1.594	

THA verification-T							
Reghena-T-	TH				DBA	Error	
	C/D	σ	C.o.V[%]	C/D $\pm \sigma$	C/D	%	
PL1	1.545	0.072	4.662	1.473 1.617	1.682	-8.90	
PL2	0.661	0.113	17.106	0.548 0.774	0.739	-11.90	
PL3	0.809	0.098	12.113	0.711 0.907	0.627	22.50	

RBs 9-Canal Bianco Bridge

Tab. 6.46 – *RBs7: Capacity curve of the pier: a) longitudinal direction*


Flexure (F)	D [mm]	F [kN]	μ [-]	θ [%]
PL1	18	1575.27	1.00	0.44
PL2	86	1455.42	4.81	2.10
PL3	129	1390.05	7.21	3.15

Tab. 6.47 – *RBs7: long. direction, comparison between DBA and TH results*

<i>DBA analysis</i>						
C. BIANCO-L-	Δcap	Vbase	ξ_c	τ_c	C/D	$DM_{PL}=D/C$
	[mm]	[kN]	-	[s]	-	-
PL1	18	1575.27	0.050	0.443	0.496	2.018
PL2	86	1455.42	0.176	1.356	0.738	1.354
PL3	129	1390.05	0.181	1.661	1.155	0.866

<i>THA verification</i>							
C. BIANCO-L-	TH				DBA	Error	
	C/D	σ	C.o.V	C/D $\pm \sigma$	C/D	%	
	-	-	[%]	-	-	%	
PL1	0.503	0.031	6.167	0.472	0.534	1.33	
PL2	1.481	0.069	4.660	1.412	1.550	8.56	
PL3	0.968	0.086	8.884	0.882	1.054	10.54	

The medium error obtained by the comparison of the C/D ratios is reported in Fig.6.11. A general trend can be observed for PL1, PL2, PL3 limit states: the simplified method is generally conservative, and the error increases for the more severe limit damage states (PL2, PL3). Underestimation error is generally limited in the range [-10%, 0], while overestimation, in most of cases under the 20%, is a little bit higher for shear failure cases (Reghena Bridge), with a maximum of about 25%.

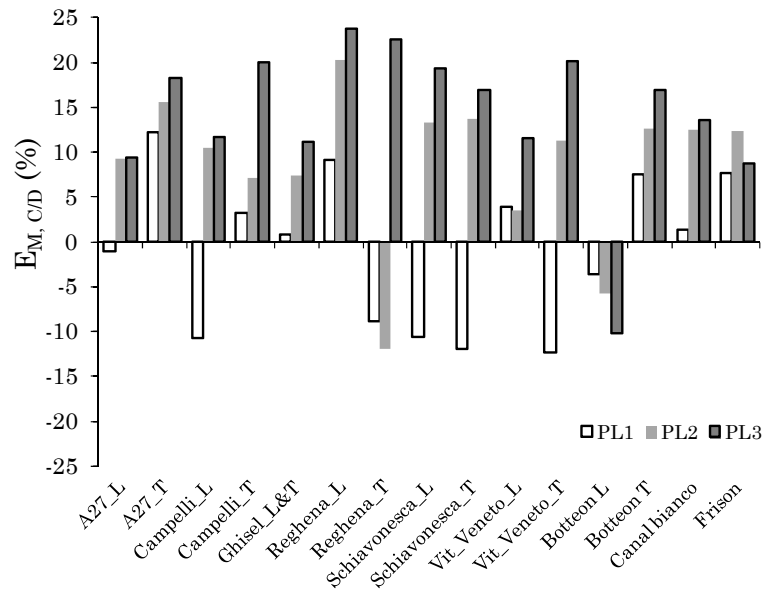


Fig. 6.12 – Medium error trend for C/D ratio calculated according to Eq. 6.7, for PL1, PL2, PL3 limit states for RBs of classes 2.1,2.2.

6.4 METHODS FOR FRAGILITY CURVE DEVELOPMENT

In evaluating the seismic risk of a structural system, in this case consisting of bridges or viaducts, it is important to identify the vulnerability of the structural components associated with various levels of damage; the probabilistic approach to the problem is due to the uncertainty of the variables involved. Characteristics of the material and structural properties, on which the overall capacity of the bridge depends, are not exact values, and neither are the intensity of earthquake action and site conditions, governing the seismic demand. It follows that the performance of the structure has to be represented by a range of values, associated to a certain probability of exceeding a pre-defined damage level.

The cumulative function representing the exceeding probability is represented by a fragility curve, traditionally individuated by a two-parameter lognormal distribution, which is function of the seismic intensity measure (*IM*). There are various methods for its determination: a first approach is empirical, based on data collected on-site as a result of seismic events (Basoz^[B5], 1994, with reference to observations after the 1994 earthquake in Northridge, and

Shinouzuka^[S4], 1998, after the earthquake in Kobe). The other fundamental approach is analytical. In the past decade different numerical approaches were used with various degrees of complexity: analysis with elastic spectrum (Hwang et al., 2000), Capacity Spectrum-based analysis (Shinouzuka et al.^[S2], 2000) and nonlinear dynamic analysis in Time History (Karim, 2001, Choi, 2003). Also hybrid approaches are possible, when there is a lack of damage at certain intensity levels, by combining post-earthquake damage statistics with simulated damage data in hybrid damage probability matrices (Barabat et al.^[B6], 1996).

A realistic structure behaviour can best be described with NLTH analysis on full three-dimensional MDOF models, but at the present there is still a problem with computation time requirements when TH is used in Monte Carlo simulation, hence simplified analysis are required for vulnerability evaluations on a large scale.

As said above, non linear static methods had a widespread diffusion for vulnerability appraisal in past decade (Hanus method, FEMA^[F4], 2003), while Displacement-Based methods were being developed, even if some applications for buildings in urban environment had already been presented (Ordaz et al., 2000, Restrepo-Velez and Magenes, 2004). These methods made use of displacement or inter-story drifts as the fundamental indicator of performance level, following the observed better correlation of these parameters to structural and non-structural damage. A full probabilistic framework for Displacement-Based Earthquake Loss Assessment (DBELA) was formulated by Crowley et al.^[C4], 2004.

The main concept of DBELA is the comparison of the displacement capacity of the building stock and the imposed displacement demand from a given scenario earthquake. In this case the probability of exceedance, which is calculated by comparing the displacement demand with the displacement capacity, is plotted against the mean spectral displacement demand to the randomly generated set of buildings, using the displacement at the fundamental vibration period of the building $S_d(T_1)$ as the Intensity Measure (*IM*), instead of the traditional PGA values. This evaluation can be repeated for a number of displacement response spectra with increasing levels of intensity (in terms of PGA or spectral displacement at a given period, for example) and plotted to produce fragility curves. Recent applications of of the DBELA method can be found in Bal et al.^[B3], 2010 and Tarque et al.^[T4], 2012.

In the present study analytical fragility curves based on simplified Displacement-Based Assessment procedures are developed, and used for the prediction of the expected damage for all multi-span rc bridges of the VR stock.

The (DBFr) curves can be obtained in two forms: one using PGA as intensity measure, the other one using the spectral displacement $S_d(T_1)$, calculated at the fundamental period of the structure. The PGA-fashion of fragility curves has the advantage that at present hazard functions are generally available in seismic codes relating PGA to annual probability of exceedance, consequently this form is to date

the most convenient for calculation of seismic risk scenarios. On the other hand the DRS-fashion of fragility curves are developed by using a parameter for intensity measure, the response spectrum displacement, that shows good correlation to damage and that accounts for the relationship between the ground motion frequency content and the fundamental period of the structure (Crowley^[C4], 2004).

6.4.1 Fragility curves obtained with NLTH analysis (THFr)

The method herein used for the calculation of fragility curves is based on the definition of fragility distribution as a log-normal CDF function, as described in Nielson^[N2], 2003.

NLTH analyses are used in this context to evaluate the reliability of the DBA method, which uses the parameter Demand/Capacity ratio (expressed in terms of elastic spectral displacements for a pre-defined Performance Level) as Damage Measure, $DM=D/C$.

1.) Representative suites of real or synthetic ground motion time histories are sorted and grouped to the nearest representative seismic intensity value a (which stands for the Intensity Measure), using appropriate scaling. The PGA range 0.05g-0.8g is considered for scaling operations.

2.) Incremental Dynamic Analysis is thus applied to the j -th sample bridge, by scaling incrementally for each a value the set of accelerograms (which have $PGA =a$), till the ultimate displacement capacity (or the PL capacity) is reached. The mean value $\bar{\alpha}_j(a)$ of the obtained seismic action scaling factors α_i is assumed for the calculation of the Demand/Capacity ratio for the structure under examination.

$$1 / \bar{\alpha}_j(a) = c_j(a) = DM_j \tag{6.11}$$

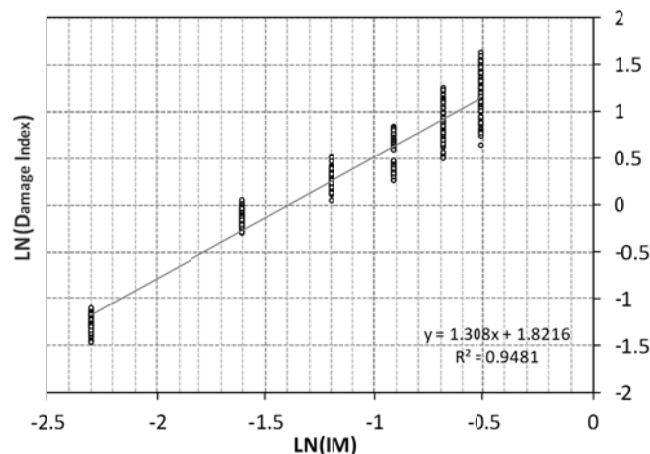


Fig. 6.13 – Linear Regression in the bi-logarithmic plane for the probabilistic model of Damage Measure (Intensity Measure is given in this case by PGA, with maximum value $PGA=1g$)

The IDA is repeated for all the j sample structures representing the real bridge for each specific value of seismic intensity a . The result is a “cluster” of data (see Fig. 6.2).

3.) The mean value of D/C ratio for each a value is described in this case by an exponential function:

$$c(a) = a^B e^A \quad (6.12)$$

represented in the bi-logarithmic plane by the line:

$$\ln(c(a)) = A + B \ln(a) \quad (6.13)$$

in which a is the seismic intensity and A, B fixed parameters, determined by a least-squares linear regression. Here the standard deviation ξ of the data cluster is calculated on the whole set of data, thus ξ is independent of seismic intensity a .

4.) Once coefficient A, B and standard deviation ξ are determined, the fragility curve is represented by a log-normal CDF function, and the conditioned exceedance probability (fragility), is calculated as:

$$P_{f,PL}(a) = P[DM > dm_{PL} | a] = \int_{DM(a) > dm_{PL}} f_{DM}(dm | a) \, ddm \quad (6.14)$$

where DM is the damage variable (e.g. D/C), dm_{PL} is a given damage level, and f_{DM} is pdf of the damage function, with a log-normal distribution:

$$f_{DM}(dm) = \frac{1}{\sqrt{2\pi}\varepsilon dm} \exp\left[-\frac{1}{2}\left(\frac{\ln dm - \lambda}{\varepsilon}\right)^2\right] \quad (6.15)$$

$\lambda = A + B \ln(a)$ is the mean value calculated on the regression line for a certain value of a , ξ is the standard deviation.

5.) According to this method the damage function $f_{DM}(dm/a)$ has a mean defined for each value of seismic intensity a , and a standard deviation independent of seismic intensity. Consequently, other fragility values can be extrapolated for any possible value of seismic intensity, the curve being a continuous function of the variable a .

6.4.2 Displacement-Based fragility curves (DBFr)

The method herein presented for the calculation of fragility curves is adapted from the procedure proposed for non-linear static analysis by Shinozuka et al.^[S2], 2000. In this method, random populations of bridges are generated using Monte Carlo simulation, each real bridge being represented by a set of sample bridges, obtained by considering the uncertainty on material and structural

properties. The displacement capacity and effective period of vibration of each sample bridge (the j -th bridge) at the different PLs is calculated on the base of the global pushover curve of the bridge (for multi-span simply supported bridges is represented by the F-s curve obtained for a single pier). The seismic demand is obtained from displacement response spectra.

6.4.2.1 DBFr curves construction: method DBFr1

The procedure used to calculate one fragility curve for a set performance level d_{PL} is summarized below:

- a) Parameter a identifying seismic intensity is set, e.g. $a=PGA[g]$.
- b) Representative suites of real or synthetic ground motion time histories are sorted and grouped to the nearest representative a value with appropriate scaling.
- c) For a defined value of a , the average spectrum DRS_m and the average spectrum plus and minus the standard deviation $DRS_{m \pm \sigma}$ of the elastic displacement response spectra for all the time histories in the group are calculated for the considered range of structure period;
- d) The DBA procedure (§2.3.2) is applied to calculate the equivalent elastic displacement capacity $\Delta_{Cap-el,j}$ for the j -th sample bridge;
- e) Three spectrum displacement demands are calculated by reading off respectively the computed DRS_m , $DRS_{m \pm \sigma}$ spectra at the effective period $T_{e,j}$ for the j -th bridge sample;

$$\Delta_{Dem-el,j}^{k=1} = \overline{\Delta}_{Dem-el,j}, \quad \Delta_{Dem-el,j}^{k=2,3} = \overline{\Delta}_{Dem-el,j} \pm \sigma_{D,j}^+ \quad (6.16)$$

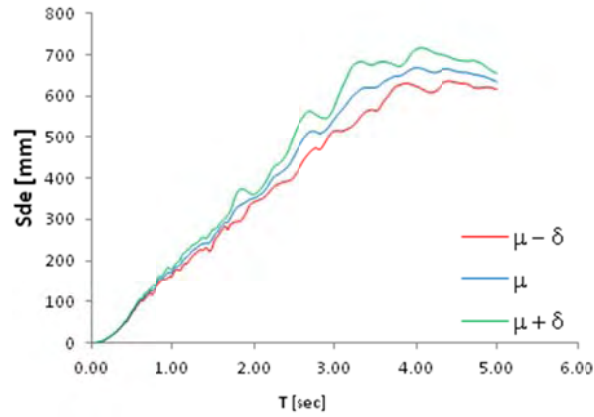


Fig. 6.14 – Mean displacement response spectrum and mean ± 1 standard deviation

- f) The corresponding three Demand/ Capacity displacement ratios (Damage Measure) are determined:

$$DM_j^k = D_{el,j}^k / C_{el,j} = \Delta_{Dem-el,j}^k / \Delta_{Cap-el,j} \quad k=1,2,3 \quad (6.17)$$

g) The log-normal distribution of damage function for the j -th bridge is generated by the mean $c_j(a)$ and standard deviation $\xi_j(a)$ parameters. These parameters are obtained inverting the associated system given by:

$$\begin{aligned} \bar{S}_d(a) &= c(a) \exp\left[\frac{\{\zeta(a)\}^2}{2}\right] \\ \{\sigma_d(a)\}^2 &= \{\bar{S}_d(a)\}^2 \left[\exp\left(\{\zeta(a)\}^2\right) - 1\right] \end{aligned} \quad (6.18)$$

h) Once $c_j(a)$ and $\xi_j(a)$ parameters are determined for the j -th bridge, the probability of exceeding the damage level is calculated as:

$$P_j[S_d(a) \geq d_l] = P_j(a, d_l) = 1 - \Phi \left[\frac{\ln\left(\frac{d_{l,j}}{c_j(a)}\right)}{\xi_j(a)} \right] \quad (6.19)$$

where Φ is the normal distribution function;

i) the procedure is repeated for each j -th sample bridge ($j=1 \dots k$), carrying out k values, where k is the total number of statistically different bridges. For the given seismic intensity a , the final fragility value for the examined real bridge is obtained as:

$$F(a, d_l) = \frac{\sum_{j=1}^K P_j(a, d_l)}{k} \quad (6.20)$$

l) the procedure a) – h) is repeated for all the values of seismic intensity a considered.

It has to be noted that with this method, the fragility distribution is obtained point to point in correspondence to each seismic intensity value a , and is not a continuous function of the variable a : linear interpolation is used between the calculated values to represent the distribution.

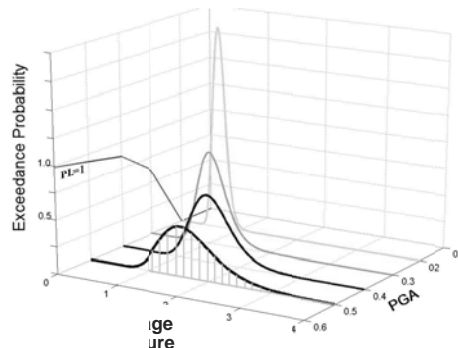


Fig. 6.15 – Pdf of damage functions for different value of IM (PGA) and lognormal CDF curve obtained, associated to a pre-defined PL

6.4.2.1 DBFr curves development: method DBFr2

This second procedure is introduced to obtain fragility curves as continuous functions of the variable a , in order to compare numerically the DBFr and THFr curves.

Displacement-Based fragility curves were approximated with cumulative log-normal functions by mean of non-linear regression analysis (as already done for TH analysis) using all the cluster of data obtained for different a values. The two parameters of cumulative log normal distribution functions (average c and standard deviation ξ) can be thus directly compared.

In this procedure only some modifications are introduced into DBFr1 method: regarding **g)-l)** steps.

a)-f): same as method DBFr1.

g) step a)-f) are repeated for each value of seismic intensity a . The result is a “cluster” of data, with three DM values for each a value of the range.

h) construction of the continuous CDF fragility curve according to step **3.)** to **5.)** of the THFr procedure, using least squares linear regression on the overall data set.

i) the procedure is repeated for each j -th sample bridge ($j=1\dots k$), carrying out k fragility curves, where k is the total number of statistically different bridges. For the given seismic intensity a , the final fragility value for the examined real bridge is obtained as:

$$F(a, d_l) = \frac{\sum_{j=1}^K P_j(a, d_l)}{k} \quad (6.21)$$

6.4.3 System fragility curves for bridges

In many studies fragility analyses assume piers as the only vulnerable components for multi-span bridge structures, and the column damage state is assumed as representative of the damage state of the entire bridge (among others, Shinozuka et al.^[S2], 2000, Karim and Yamazaki^[K6], 2001).

In the case of simply supported bridges, for which each pier’s response can be considered as statistically independent from the others’, the system fragility for the overall bridge consisting of N piers, given a pre-defined Performance Level, can be estimated as:

$$P_{f,PL,system} = 1 - \prod_{pier=1}^N (1 - P_{f,PL,pier}) \quad (6.22)$$

As regards multi-span continuous bridges, the deck connect the pier top displacements proportionally to its transversal stiffness, and the system can be regarded as an elastic element (deck), laterally and longitudinally restrained by a series of non linear springs, represented by the piers. The failure of one springs (piers) can be considered as the event leading to the failure of the overall system^[C6]: this assumption is generally acceptable because piers are the main elements of the horizontal-force resisting system, and generally a deck does not collapse before piers.

If the coupling of piers' response given by the continuous deck is effective, the vulnerable components (piers) can be assumed as fully stochastically dependent, and the system fragility is represented by:

$$P_{f,PL,system} = \max_{pier=1}^n [P_{f,PL,pier}] \quad (6.23)$$

The process described above for the development of fragility curves regards only a structural element of the lateral load resisting system, namely the piers. However, the overall fragility of multi-span bridges can be conditioned by other vulnerable structural components such as bearings, expansions joints, abutment and foundations.

In this case multiple different components are considered, an overall bridge fragility can be obtained through a crude Montecarlo simulation, but an alternative would be to combine the component fragility curves to derive the system (bridge) fragility curve. The process requires information about the stochastic dependence between the damage states of the various bridge components. Using first-order reliability theory, an upper and lower bound of the system fragility can be determined^[C6]:

$$\max_{i=1}^m [P(F_i)] \leq P(F_{sys}) \leq 1 - \prod_{i=1}^m (1 - P(F_i)) \quad (6.24)$$

The lower bound represents the probability of failure for a system whose components are all fully stochastically dependent, while the upper bound is calculated by assuming components are all statistically independent, and thus providing a conservative estimate of the overall bridge fragility.

Different works have shown that fragility bridge components other than piers affect overall bridge fragility with a variable trend of influence in dependence of the different bridge types: for example, the columns for the multi-span continuous pre-stressed concrete girder typical in Mid-America has been found to be the most fragile bridge component (Choi et al.^[C6], 2002), while for steel girder bridges steel fixed bearings seems to condition the bridge performance at different damage states (Nielson^[N2], 2003). As regards bridge typologies typical of the reference database (VR database), some considerations were drawn in a previous

study^[G5]: as for the bearings it was observed that deck unseating is unlikely in a 50 years service life, while for expansion joints fragile failures are likely to occur, but represent only a limitation to the service conditions. Also on the base of these considerations, in the present study only piers are individuated as vulnerable components of the lateral resisting system, and is the author's opinion that this restriction does not sensibly varies the seismic risk estimation for the multi-span rc bridges, in particularly for the most severe damage states.

6.5 EVALUATION OF SEISMIC RISK

6.5.1 Seismic hazard

Seismic hazard is the probability of observing a certain level of ground shaking in a defined time period at the site of observation. It is measured by the seismic hazard curve that represents the mean annual frequency by which a certain value of seismic action intensity is exceeded. It can be obtained by a conventional Probabilistic Seismic Hazard Analysis (PSHA-Cornell, 1968). Usually a distinction is made between standard and local seismic hazard, the latter obtained by micro-seismic zonation and identifying the local effects produced by the geomorphologic condition of the site and their contribution to seismic hazard.

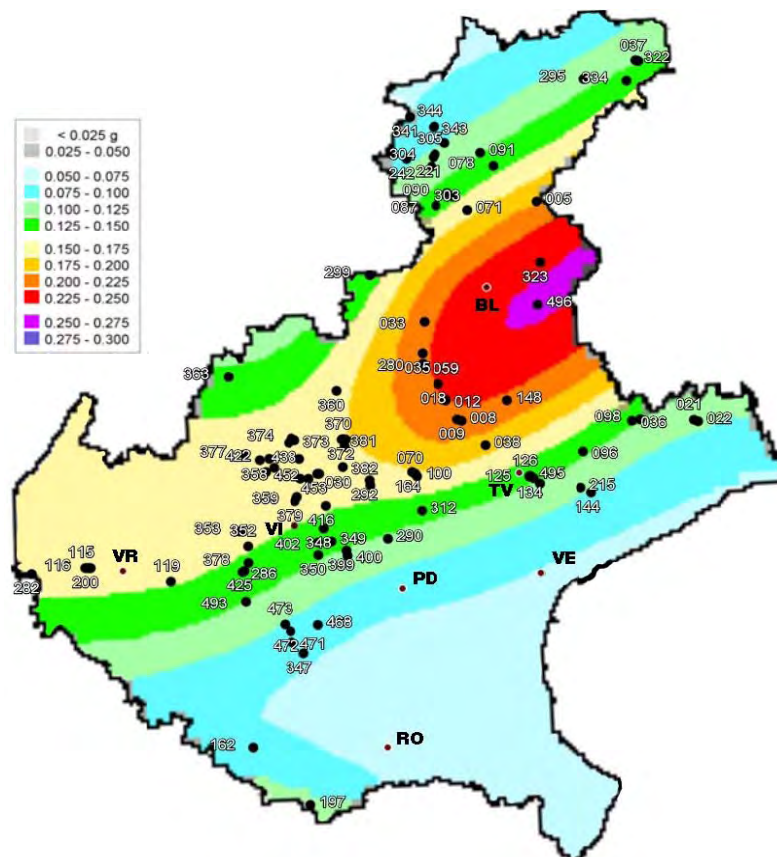


Fig. 6.16 – Hazard map of the Veneto region supplied by INGV (PGA, 10% probability of exceeding in 50 years on a soil type A) and exposure of the analyzed bridge stock

The hazard curves used in this work are directly derived from Italian seismic hazard maps obtained by INGV (Meletti and Montaldo^[M7], 2007), with reference to 50 years probability of exceedance for PGA values on rock soil (type A; $V_{s30} > 800$ m/s). The probability values are referred to 9 return period T_r : 30, 50, 72, 101, 140, 201, 475, 975, 2475 (corresponding to exceedance probability of 81%, 63%, 50%, 39%, 30, 22%, 10%, 5%, 2% respectively). The Italian hazard maps are plotted on a reference grid 10x10km, and the hazard curve for construction sites of the bridges are obtained interpolating the values of the nearest grid nodes. In Fig. 6.15 the hazard curves for four of the examined bridges are presented. For the computation of the seismic risk, a regression analysis was carried out on the nine values supplied by INGV maps, and the hazard curve functions were approximated with log-normal distributions to provide values less than 2% probability.

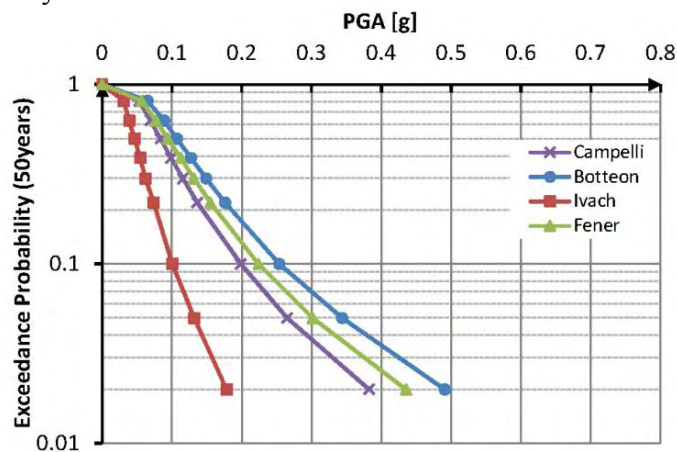


Fig. 6.17 – Hazard curve supplied by INGV: Campelli Bridge (Longarone-BL-, seismic zone 2), Botteon Bridge (Fadalto-TV- seismic zone 2), Ivach Bridge (San Tommaso Agordino-BL- seismic zone 3), Fener Bridge (Alano di Piave-BL-, seismic zone 2).

6.5.2 Seismic risk

Seismic risk is defined as the relationship between the occurrence of seismic events and socio-economic losses of the functional system being examined. The ultimate goal of loss estimation in performance-based earthquake engineering is to compute the mean annual probability, or annual rate $P(DV)$ of a decision variable (DV) to be exceeded (DV could be for example a predefined level of repair cost).

The mean annual frequency of DV is obtained by applying the theorem of total probability (Cornell & Krawinkler, 2002), using three intermediate variables:

the measure of seismic action (Intensity Measure, IM), a parameter of structural response (Engineering Demand Parameter, EDP), and the Measure of Damage level, DM .

$$P(DV) = \iiint P(DV | DM) | dP(DM | EDP) dP(EDP | IM) | d\lambda(IM) | \quad (6.25)$$

where:

- $P(DV/DM)$ is the probability DV of exceeding a specific value, given that the Damage Measure (DM) is equal to particular values;
- $P(DM/EDP)$ is the probability DM of exceeding a specific value when the parameter EDP related to structural response is equal to a certain value, and therefore $P(DM/EDP)$ is the vulnerability;
- $P(EDP/IM)$ is the probability EDP -e.g. maximum drift- exceeds a specified value, given a certain level of IM ;
- $|d\lambda(IM)|$ is the derivative absolute value of the annual rate of exceeding a given value of the intensity measure (the seismic hazard curve). The absolute value is needed because the derivative is negative.

Evaluation of seismic risk in terms of global direct and indirect economic losses is out of the goals of this work, which focuses only on the probability prediction of observing a certain damage level for the structure, with reference to a residual period of their service life, set in 50 years, considering that the reference structures are existing bridges, and most of them were built soon after the IInd World War. Thus only seismic hazard and structural vulnerability are considered, and Eq. 6.1 becomes:

$$P(DV) = \int P(DV | IM) | d\lambda(IM) | \quad (6.26)$$

where (DV), in this case, coincide with DM . Thus, the assessment of the expected damage for a set performance level PL is obtained by the convolution of the hazard probability density function:

$$P_{PL} = \int_{IM} P(D > d_{PL} | IM) \left| \frac{d\lambda(IM)}{dIM} \right| dIM \quad (6.27)$$

where $P(D > d_{PL}/IM)$ is the fragility curve associated with damage state d_{PL} and $H(IM)$ is the hazard function. The continuous IM variable can be discretely triggered at certain values, and the previous equation becomes:

$$P_{PL} = \sum_{IM} P(D > d_{PL} | IM) |\Delta\lambda(IM)| \quad (6.28)$$

With this procedure a total exceeding probability is derived, that has to be compared with acceptable values for a pre-defined Performance Level. Alternatively seismic risk can be evaluated for a certain scenario earthquake, with reference to a specified value of IM (e.g. PGA value), which means considering seismic risk associated to a seismic intensity having a certain probability of occurrence in the reference period assumed for the structure (e.g. 50 years).

6.6 DISPLACEMENT-BASED FRAGILITY CURVES FOR REFERENCE BRIDGES

In the present paragraph analytical fragility curves for the reference bridge structures (RBs), are calculated with DBFr and THFr approach and compared in terms of median values $c(a)$ and standard deviation $\xi(a)$.

Fragility analysis includes: simulation of ground motions, simulation of bridge samples to account for uncertainty in bridge properties, development of fragility curves from the seismic response data of the bridges.

6.6.1 Seismic input

As regard seismic input definition, it has to be evidenced that for a correct definition of local amplification of the ground motion intensity supplied by the seismic macro-zonation maps, soil type at the construction site has to be known.

In this context has to be evidenced that only for a limited number of structures, for which the original bridge project was recovered, informations about soil characteristics were available. No specific geotechnical on site-tests were performed in the structural survey campaign, except for masonry structures (some of these masonry arch bridges were next to other rc bridges, and in some cases it was possible to use the information obtained also for the rc structures).

In most cases other sources had to be used for the definition of soil characteristics in the vulnerability study:

- a seismic mapping- V_{s30} map- of the Treviso Province, (V_{s30} measurement is the average shear-velocity down to 30 m) is available as deliverable of a study realized by the Istituto Nazionale di Oceanografia e Geofisica Sperimentale^[F10];

- V_{s30} global maps, free downloadable from the website <http://earthquake.usgs.gov/hazards/apps/vs30/>. Wald et al.^[W1], 2007, describe a methodology for deriving maps of seismic site conditions using topographic slope as a proxy. V_{s30} measurements were correlated against topographic slope to develop two sets of coefficients for deriving V_{s30} : one for active tectonic regions that possess dynamic topographic relief, and one for stable continental regions where changes in topography are more subdued. These coefficients have been applied to the plotting of V_{s30} global maps,. These maps were applied as approximated tools for the

definition of site condition (hence local amplification due to ground properties) in the vulnerability study, when more direct information were not available.

6.6.1.1 Scaling of time history sets

Fragility analysis are often developed using a single suite of ground motions (recorded or synthetic accelerograms) progressively scaled to obtained the seismic input for all the desired PGA values in the range under exam.

The main objection to this “simple straip” approach is that the “same” record” being scaled in each step is not the same record anymore due to the fact that is scaled linearly and the ground motion parameters (i.e. frequency content, energy content, bracketed duration ecc..) are heavily changed and this is not proportional to the linear scaling factors (Bal et al.^[B3], 2010). This phenomenon may lead the structure to have increased capacity for the higher amplitudes of the acceleration in some cases, just because the altered ground motion parameters trigger a completely different mechanism of the structure (Vamvatsikos and Cornell^[V1], 2002).

For this reason a Multiple Straip Analysis was adopted in this work, choosing the 3 reference suits of 7 spectrum compatible ground motions adopted for PL1, PL2 and PL3 in the deterministic analysis (see §6.3.2), and scaling the accelerograms to values of PGA only in a narrow straip, so that the input characteristics are not heavily changed

The probabilistic input ground motion simulation was carried out in the PGA range 0.05-0.8g, generating 17 suites of ground motions for the different reference PGA:

- 0.05g, 0.10g, 0.15g, 0.2g, 0.25g reference PGA values were obtained scaling the suite of 7 ground motions referring to PL1;
- 0.2, 0.25, 0.3g, 0.35g, 0.4g, 0.45g were obtained scaling the accelerograms referring to PL2;
- 0.4g, 0.45g, 0.5g, 0.6g, 0.7g e 0.8g were obtained scaling the accelerograms referring to PL3;

A partial overlap of the ground motions suites is introduced to smooth possible abrupt change in the structure response when the seismic input set is changed skipping from a PGA value to another.

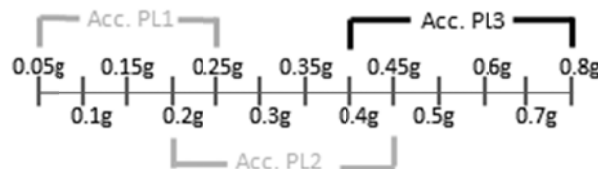


Fig. 6.18 – Generation of seismic input suites according to Multi Straip Analysis technique

6.6.2 Bridge model simulation

To represent the inherent variability in the material properties, compressive strength of unconfined concrete and the yield strength of reinforcing steel were taken as random variables, with a mean μ and standard deviation σ defined on the base of the results of the previous statistical survey.

The reference values for f_y of reinforcement bars are reported in Tab.6.14, for bars classified as Aq50-60 and FeB44k. The attribution of steel bars to these category for a bridge of the VR stock were defined on the base of lab tests or original project specification, if available, or on the base of construction year (Aq50-60 for bridges built before 1972, and FeB44k for more recent structures). In the absence of this information the reference values of Tab 6.11 were adopted for the normal distribution, with $\mu=408.5$ MPa and $\sigma=86$ MPa.

As regard concrete properties, f_{cm} was in several cases directly available from on site tests or lab tests; in these cases a standard deviation of 9 MPa was used for the normal distribution. In other cases the normal distribution reported in Tab. 6.8 was adopted ($\mu=33.6$ MPa and $\sigma=15.3$ MPa).

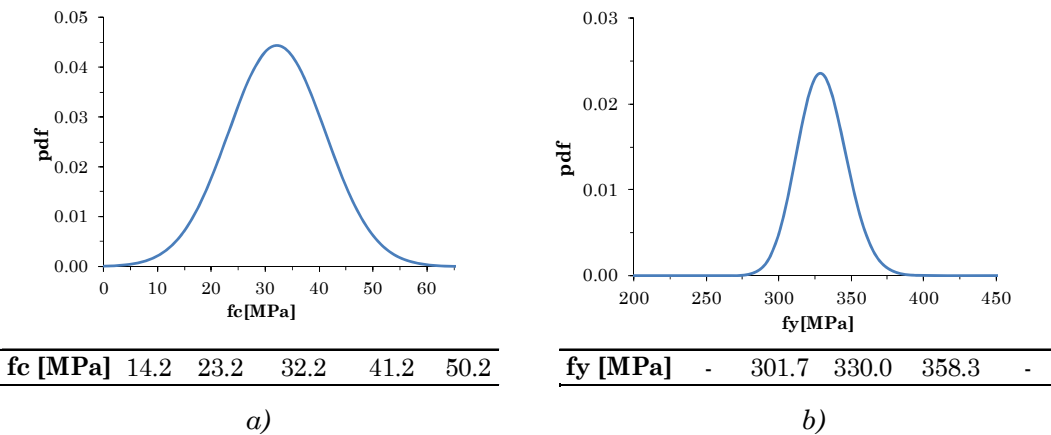


Fig. 6.19 – a) f_c normal distribution ($\mu=32.2$ MPa, $\sigma=9.0$ MPa), and corresponding 5 realizations used in bridge samples, b) f_y normal distribution for Aq50-60 steel ($\mu=330$ MPa, $\sigma=17$ MPa) and 3 realizations adopted for fragility analysis.

A sample of 15 nominally identical but statistically different bridges were created by simulating 15 realizations of f_c and f_y according to respective probability distribution functions assumed. The probabilistic distribution of strength of the two materials is also taken into account by associating a suitable weight to each of the % values of concrete strength and each of the 3 values of steel strength. Other parameters that could contribute to variability of structural response were not considered.

As regards numerical models used for fragility assessment, they were represented by single piers f.e. fiber models, with the aggregation of non linear shear behaviour, calibrated with the parametrical analysis developed in Chapter 5.

The f.e models of single bridge samples are thus similar to the models used for the previous deterministic analysis in §6.3.

As for the representation of restraint at foundation and soil-structure interaction, translational and rotational elastic spring were used, to model foundation stiffness. In most cases multi-span bridges of the VR stock have pile footings; if the Winkler modulus is known or hypothesized the foundation spring can be derived with the following simplified formulas:

$$K_v = mnk_p, \quad K_h = nk_{p,h}, \quad K_r = m \sum_{i=1}^n k_p x_i^2 \quad (6.29)$$

where:

m is the number of pile files parallel to the direction of the seismic action;

$k_p = EA/L$ is the axial stiffness of a single pile of length L ;

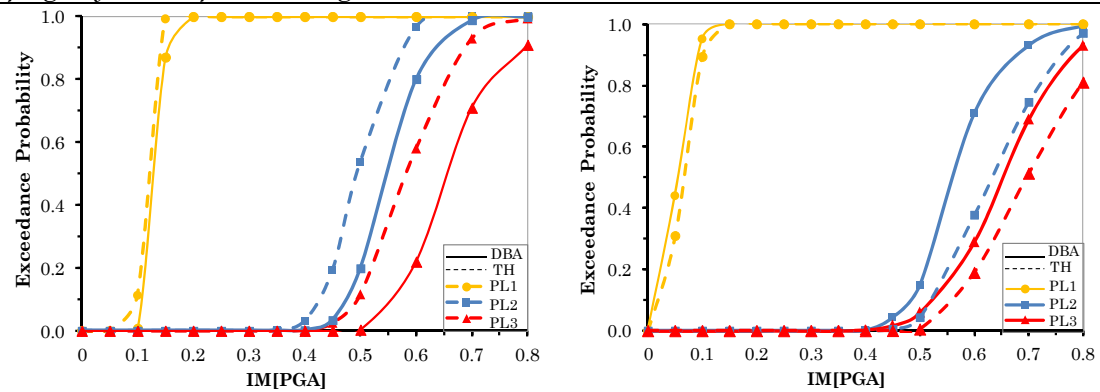
x_i is the pile distance from the plinth geometric center;

$k_{p,h}$ is the horizontal stiffness of the single pile, calculated with a f.e. model, considering the pile as vertical elastic beam subjected to unit horizontal force, with a rotational restraint on the cap, and horizontal springs k_i distributed on the length, calculated considering a linearly variable ground reaction modulus:

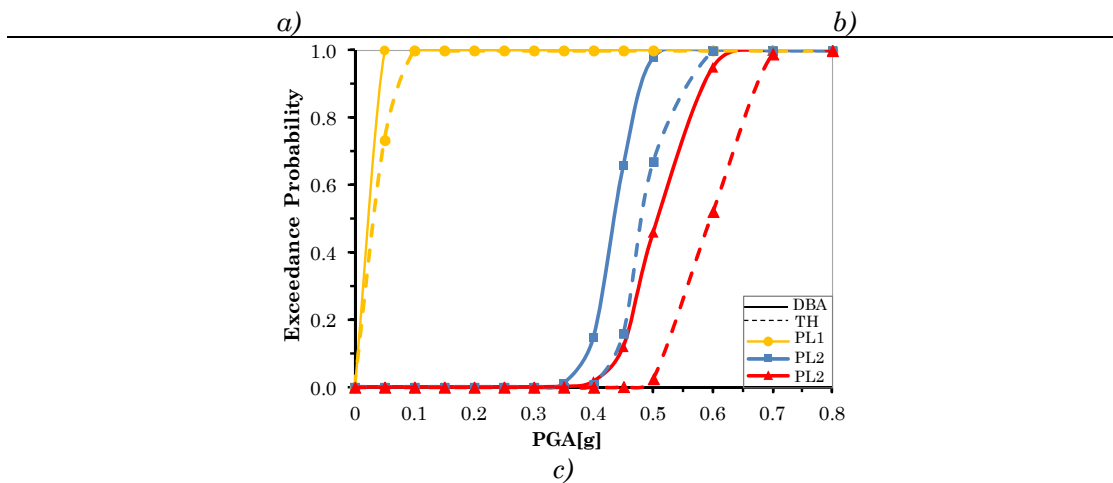
$$k_i = n_h(z/D) \quad (6.30)$$

6.6.3 Fragility curves and risk assessment for RBs: DBA and TH approach

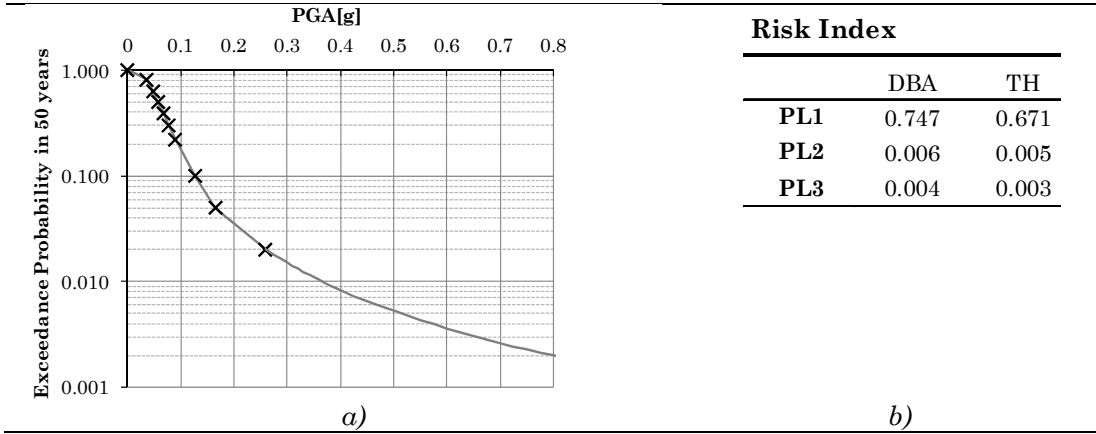
Tab. 6.48 –RBs1, Botteon Bridge. DBFr and THFr fragility curves and medium error: a) Long. Direction-single pier-, b) Transv. Direction-single pier-, c) System fragility curves for the bridge



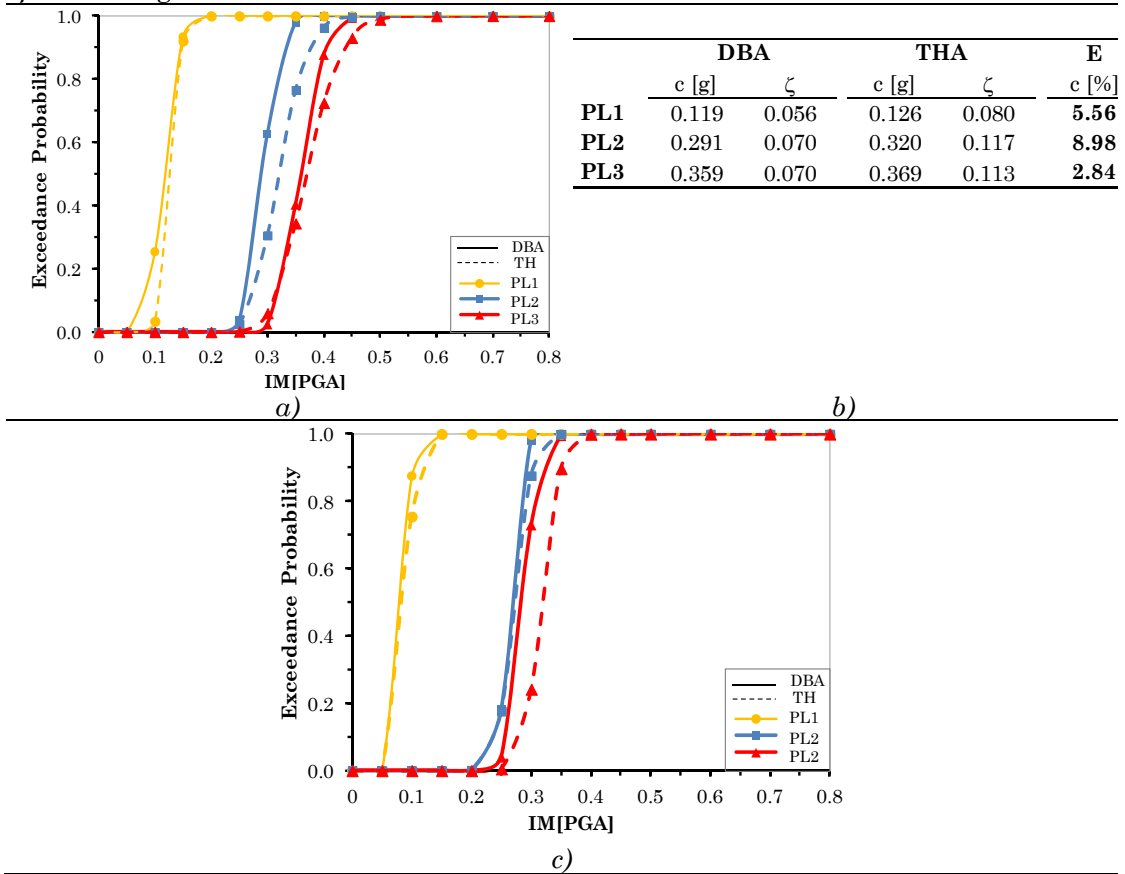
	DBA		THA		E		DBA		THA		E
	c [g]	ζ	c [g]	ζ			c [g]	ζ	c [g]	ζ	
PL1	0.129	0.082	0.121	0.061	-6.61	PL1	0.044	0.076	0.049	0.117	10.38
PL2	0.548	0.123	0.495	0.105	-10.67	PL2	0.560	0.101	0.632	0.146	11.39
PL3	0.656	0.150	0.585	0.139	-12.12	PL3	0.651	0.186	0.697	0.165	6.60



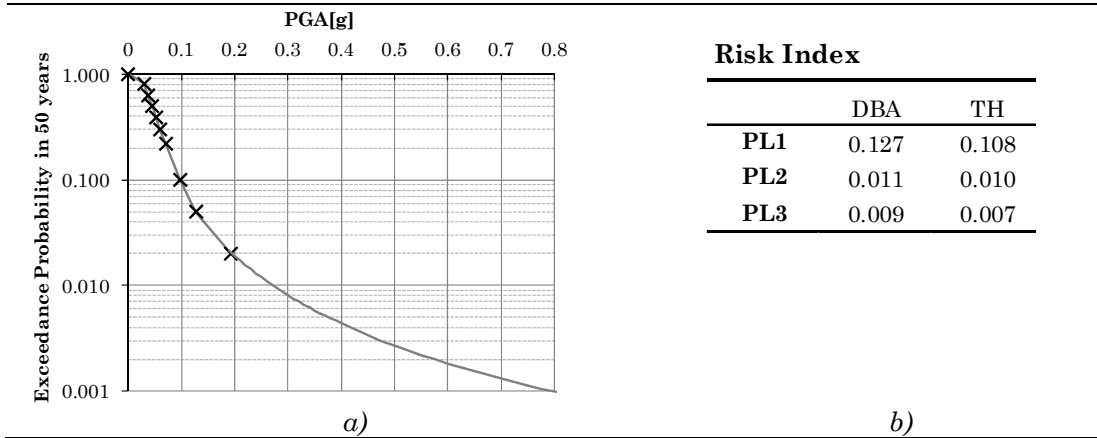
Tab. 6.49 –RBs1, Botteon Bridge: a) hazard curve b) Seismic Risk



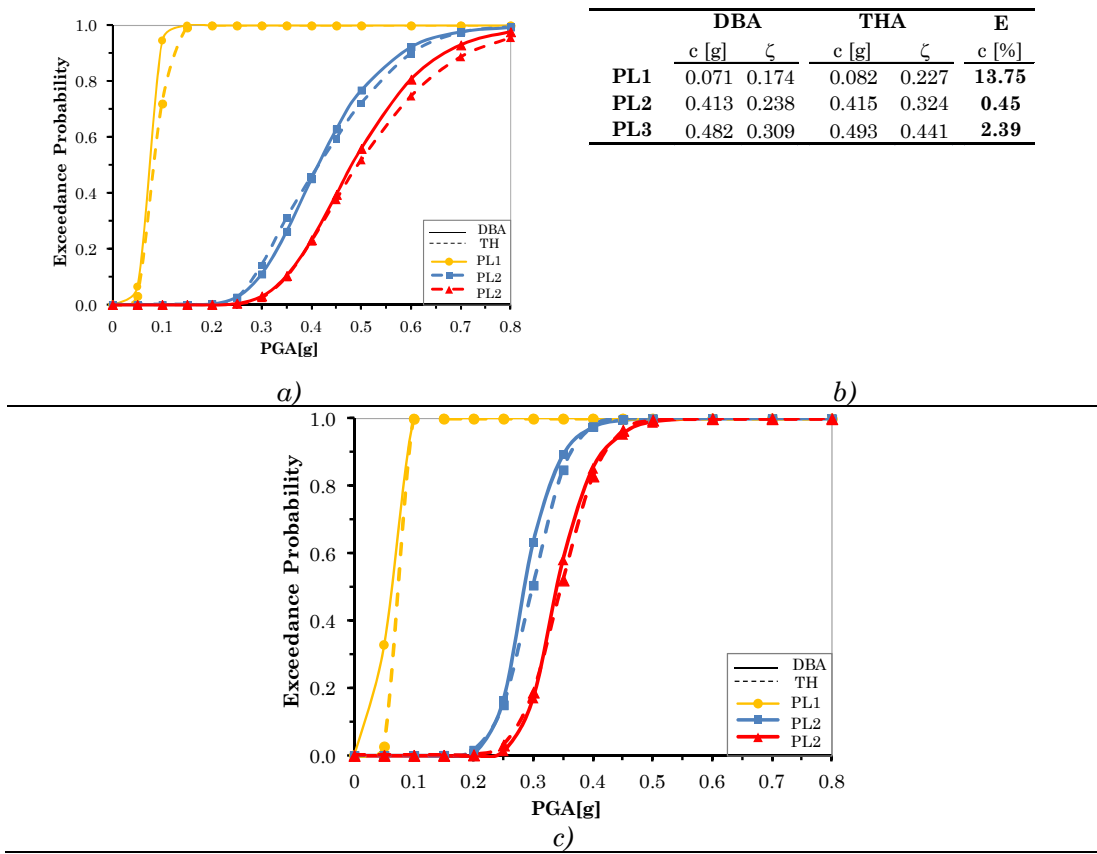
Tab. 6.50 –RBs 2, Rio Ghisel Bridge. DBFr and THFr fragility curves and medium error: a), b) Long. and Transverse Direction-single pier-, b) c) System fragility curves for the bridge.



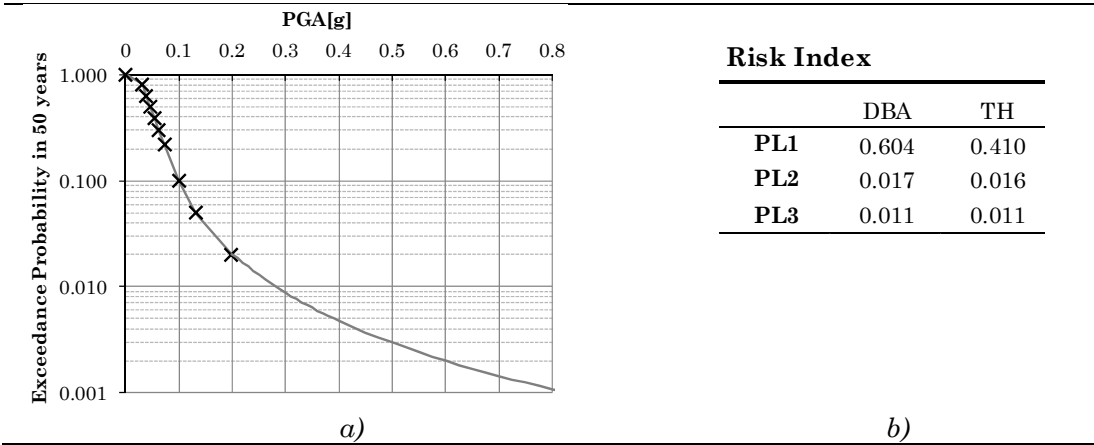
Tab. 6.51 –RBs 2, Rio Ghisel Bridge: a) hazard curve b) Seismic Risk



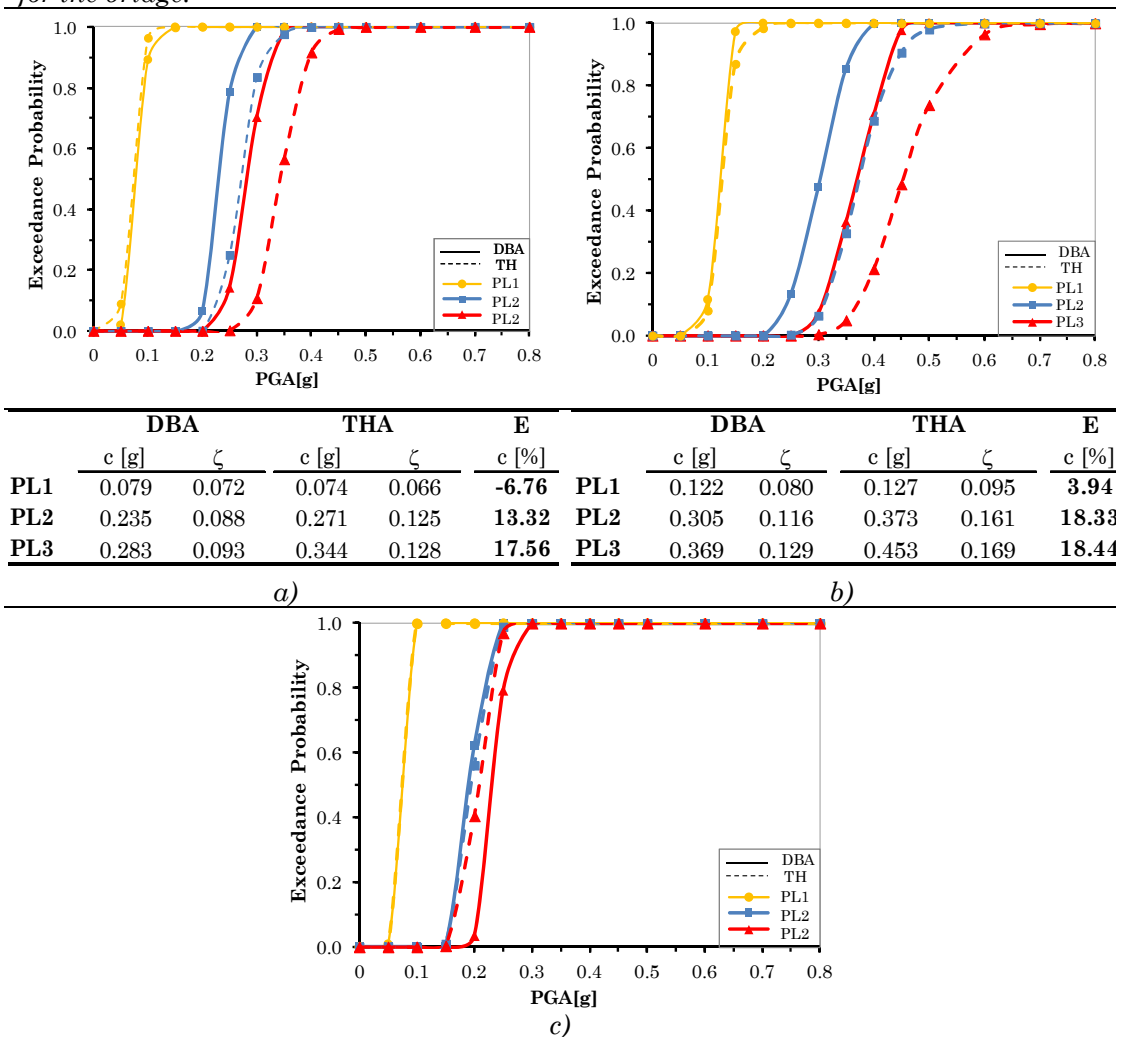
Tab. 6.52 –RBs 3, Torrente Frison Bridge. DBFr and THFr fragility curves and medium error: a), b) Long. and Transverse Direction-single pier-, c) System fragility curves for the bridge.



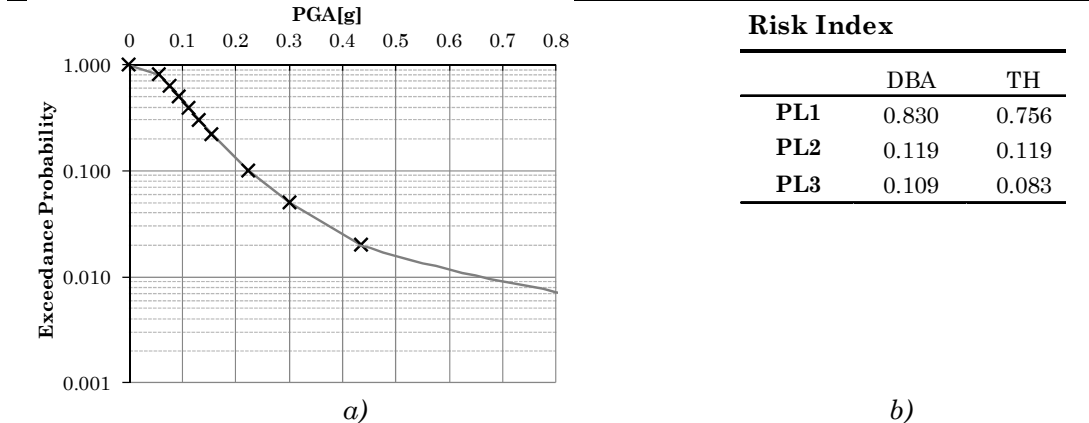
Tab. 6.53 –RBs 3, Torrente Frison Bridge: a) hazard curve b) Seismic Risk



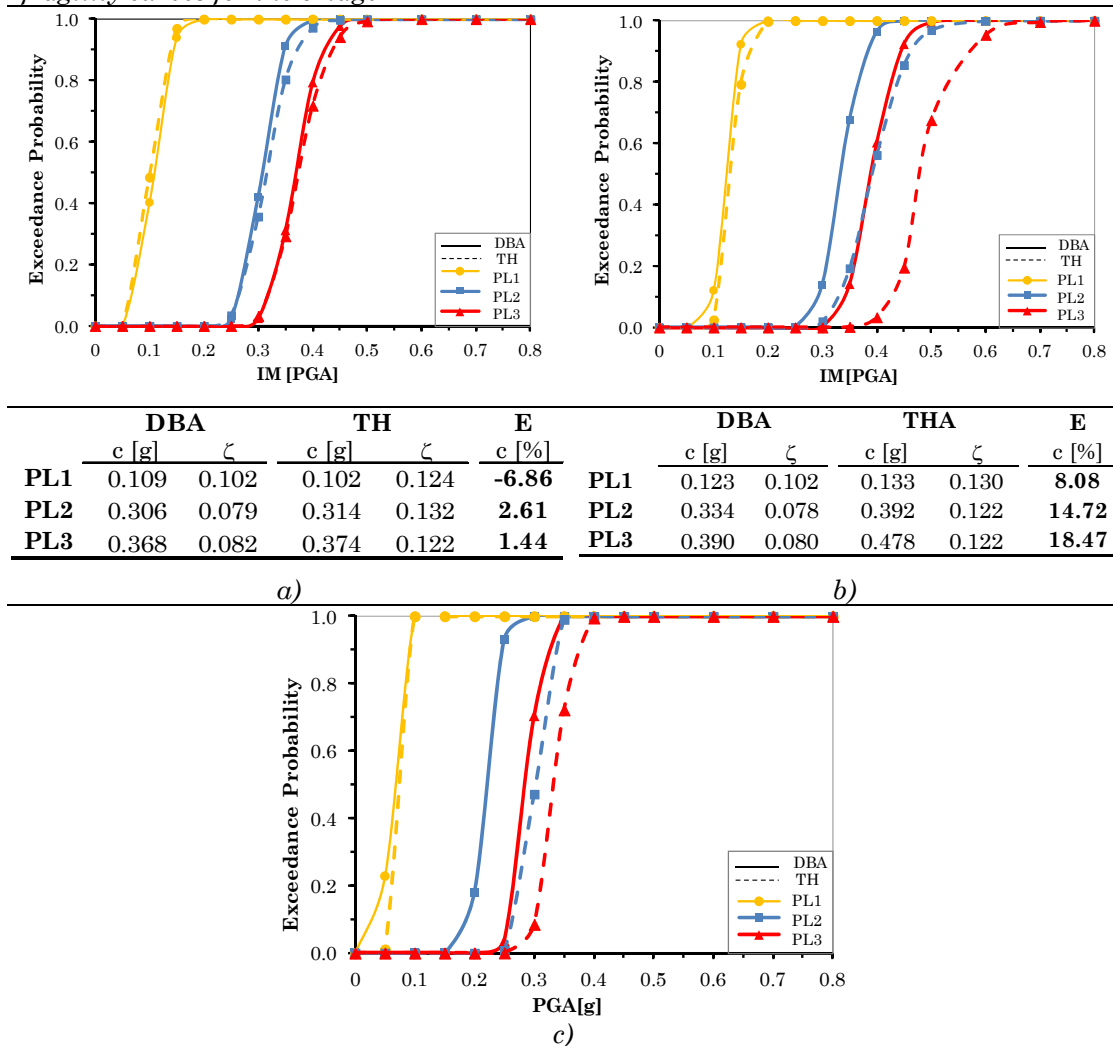
Tab. 6.54 –Rbs 4, A27 Bridge. DBFr and THFr fragility curves and medium error: a) Long. Direction-single pier-, b) Transv. Direction-single pier-, c) System fragility curves for the bridge.



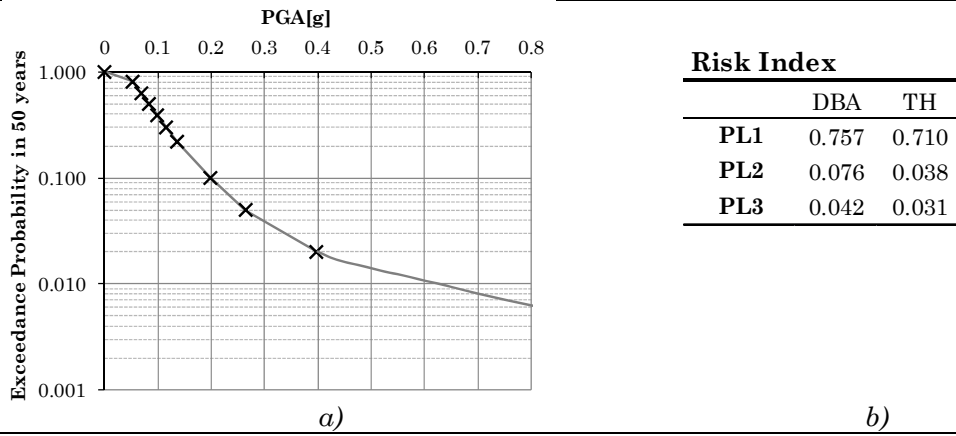
Tab. 6.55 –Rbs3, A27 Bridge: a) hazard curve b) Seismic Risk



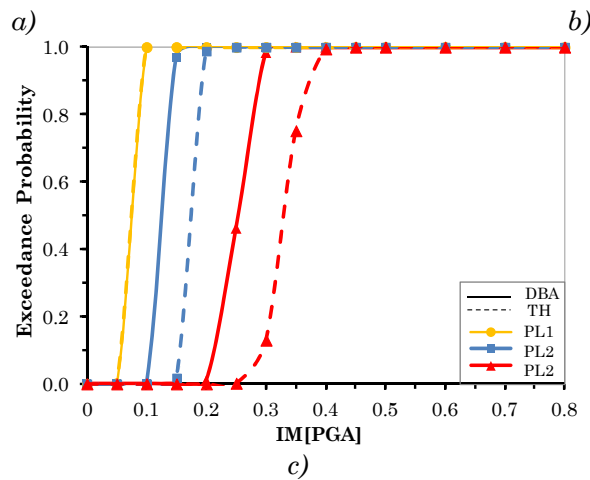
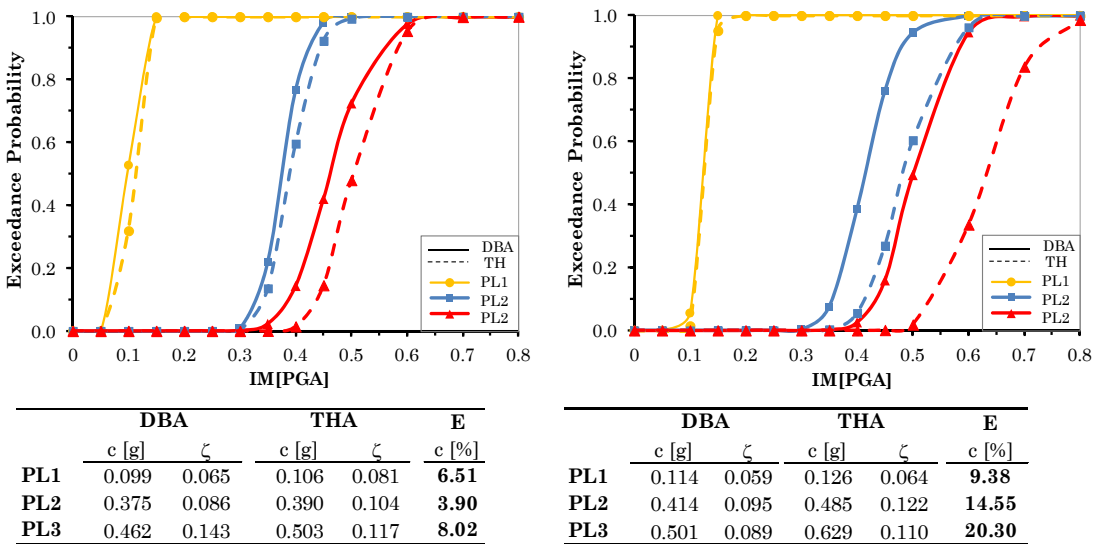
Tab. 6.56 –RB5, Campelli Bridge. DBFr and THFr fragility curves and medium error: a) Long. Direction-single pier-, b) Transv. Direction-single pier-, c) System fragility curves for the bridge



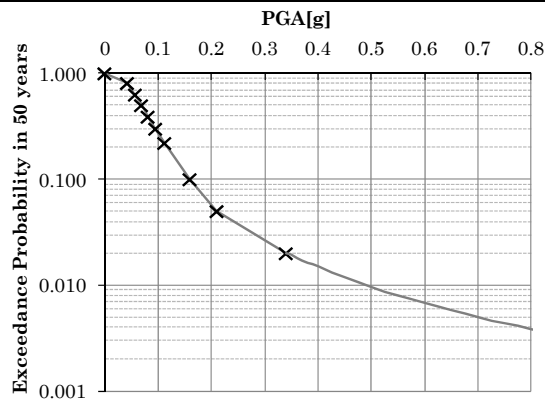
Tab. 6.57 –RBs 5, Campelli Bridge: a) hazard curve b) Seismic Risk



Tab. 6.58 –RBs6, Vittorio Veneto (Fener) Bridge. DBFr and THFr fragility curves and medium error: a) Long. Direction-single pier-, b) Transv. Direction-single pier-, c) System fragility curves for the bridge.



Tab. 6.59 –RBs 6, *FenerBridge*: a) hazard curve b) seismic risk



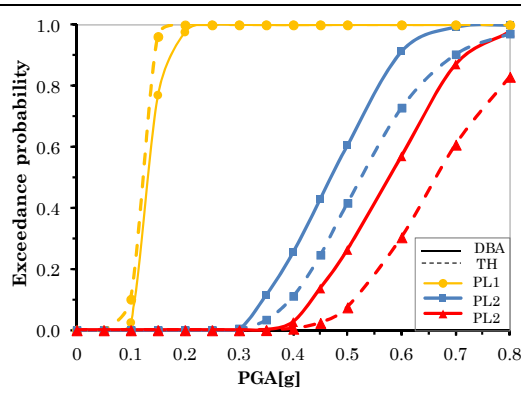
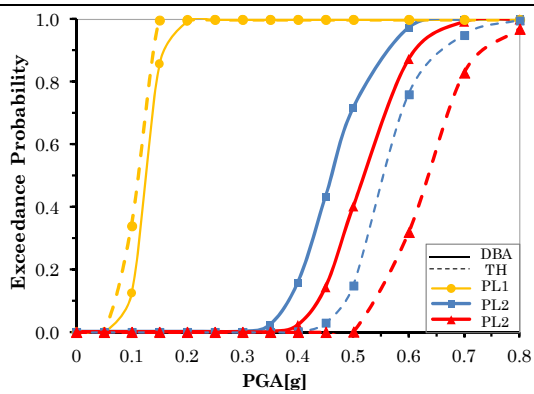
Risk Index

	DBA	TH
PL1	0.740	0.665
PL2	0.218	0.135
PL3	0.066	0.037

a)

b)

Tab. 6.60 –RBs7, *Schiavonesca Bridge*. *DBFr* and *THFr* fragility curves and medium error: a) Long. Direction-single pier-, b) Transv. Direction-single pier-, c) System fragility curves for the bridge.

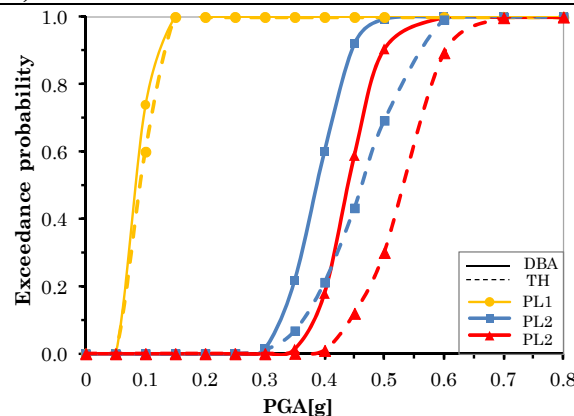


	DBA		THA		E
	c [g]	ζ	c [g]	ζ	c [%]
PL1	0.126	0.090	0.113	0.112	-11.50
PL2	0.461	0.118	0.560	0.127	17.62
PL3	0.517	0.100	0.633	0.123	18.34

	DBA		THA		E
	c [g]	ζ	c [g]	ζ	c [%]
PL1	0.131	0.087	0.126	0.113	-3.97
PL2	0.470	0.169	0.524	0.205	10.21
PL3	0.582	0.178	0.663	0.197	12.27

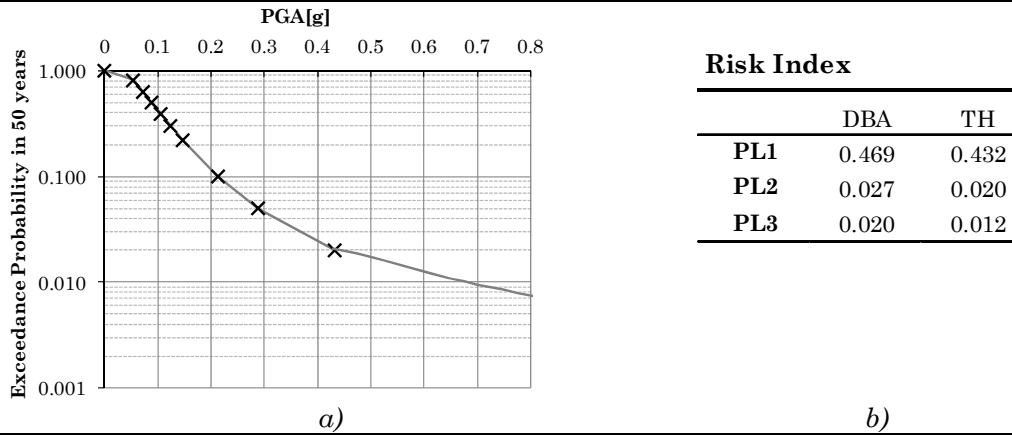
a)

b)

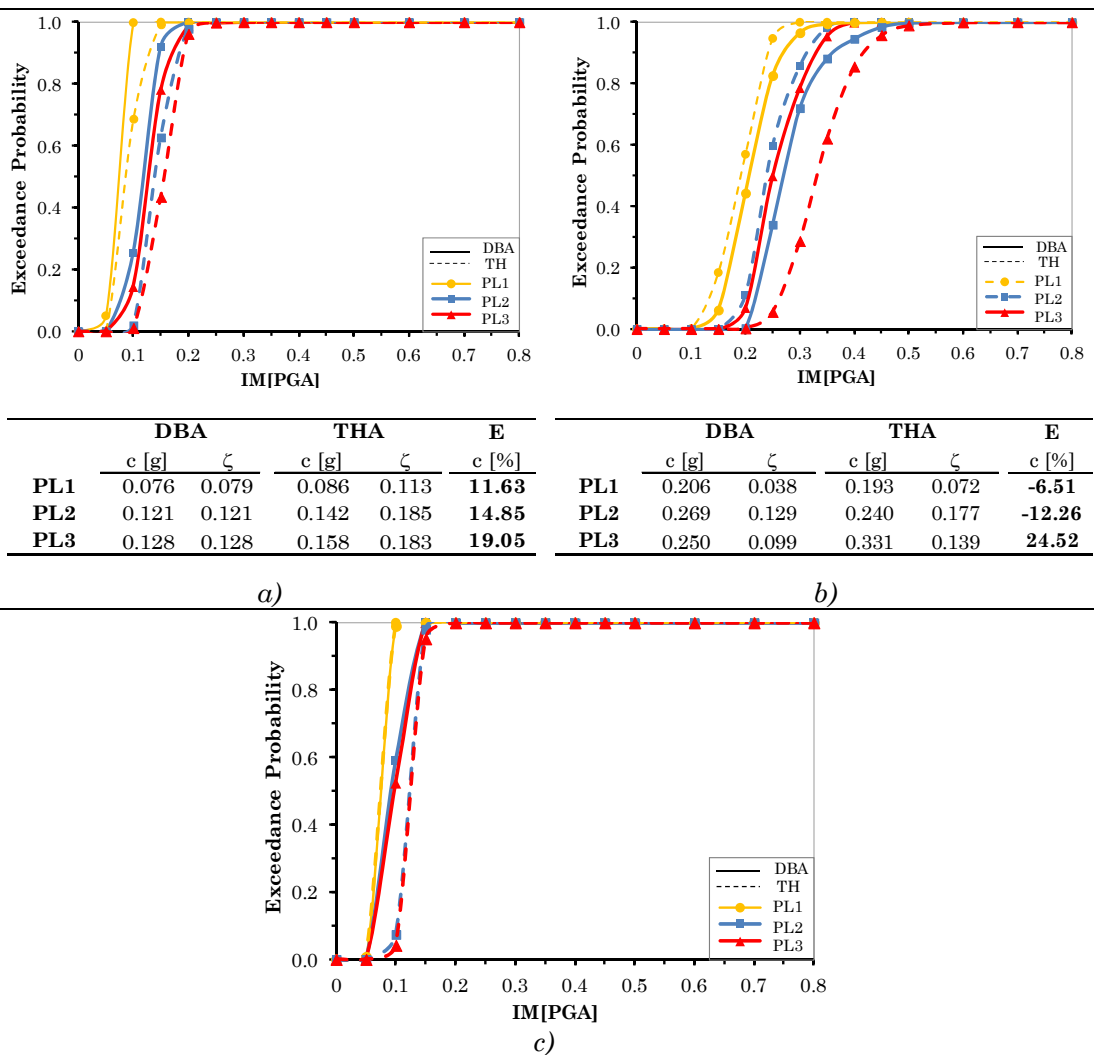


c)

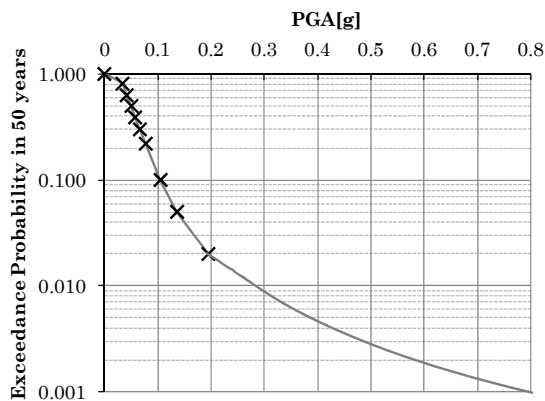
Tab. 6.61 –RBs7, Schiavonesca Bridge: a) hazard curve b) Seismic Risk



Tab. 6.62 –RBs 8, Reghena Bridge. DBFr and THFr fragility curves and medium error: a) Long. Direction-single pier-, b) Transv. Direction-single pier-, c) System fragility curves for the bridge.



Tab. 6.63 –RBs 8, Reghena Bridge: a) hazard curve b) Seismic Risk



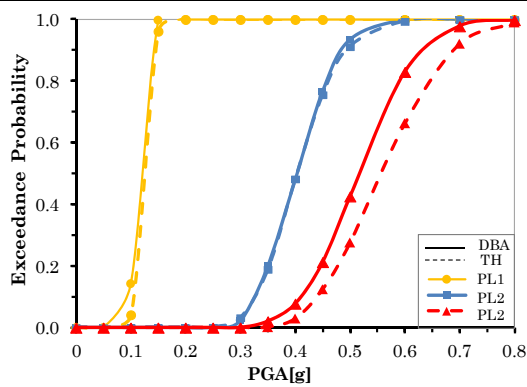
Risk Index

	DBA	TH
PL1	0.328	0.253
PL2	0.132	0.121
PL3	0.114	0.102

a)

b)

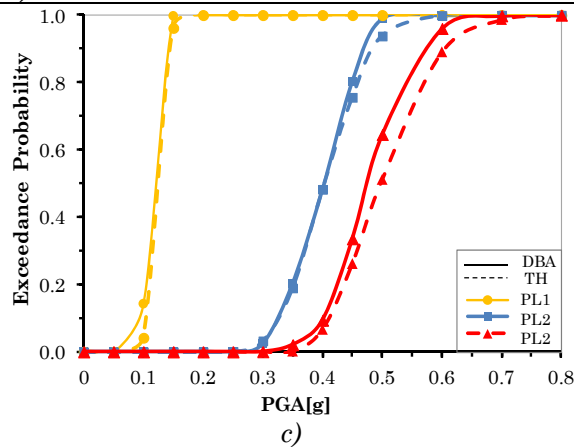
Tab. 6.64 –RBs10, Canal Bianco Bridge. DBFr and THFr fragility curves and medium error: a), b) Long. and Transverse Direction-single pier-, b) c) System fragility curves for the bridge.



	DBA		THA		E
	c [g]	ζ	c [g]	ζ	c [%]
PL1	0.121	0.072	0.124	0.101	2.42
PL2	0.403	0.113	0.403	0.171	-0.01
PL3	0.520	0.193	0.559	0.242	6.89

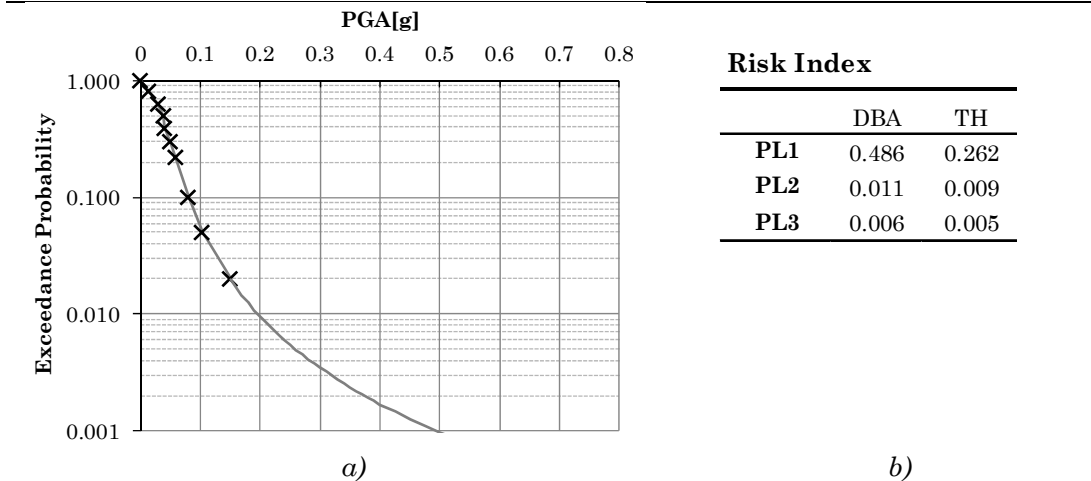
a)

b)



c)

Tab. 6.65 –RBs 10, Canal Bianco Bridge: a) hazard curve b) Seismic Risk



The medium error obtained for the reference bridges is reported in Fig.6.19; $c[g]$ is calculated in correspondence to the value $p=0.5$ of the DBFr and THFr curves, for PL1, PL2, PL3 damage states.

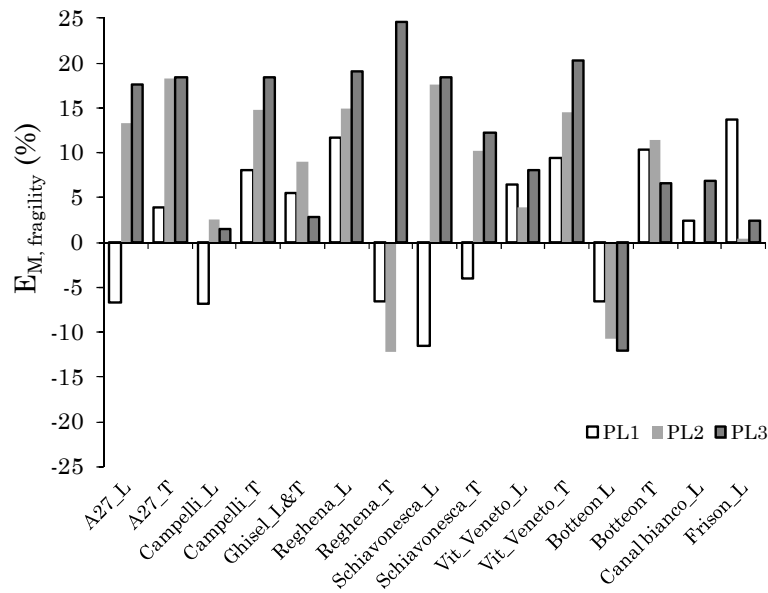


Fig. 6.20 – Error obtained by comparing the medium value $c[g]$ of DBFr and THFr curves for the Reference Bridge structures analyzed

6.6.1 Fragility curves for RBs: comparison with RISK-UE curves

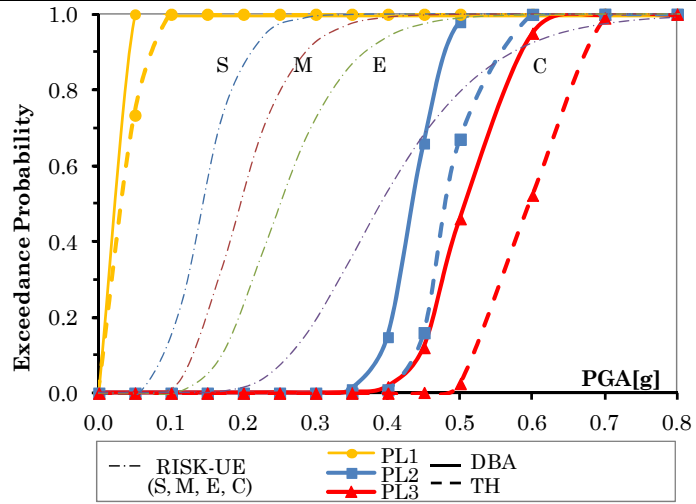
Tab. 6.66 – RISK-UE method: bridge classes individuated on the base of material, column bent type, deck static scheme, structural code adopted for design

Material	Column bent type	Span continuity	Design	Category	
All	Single Span	-	Conventional	1	
			Seismic	2	
Concrete bridges	Single	Simple Support	Conventional	3	
			Seismic	4	
		Continucus	Conventional	5	
			Seismic	6	
	Multiple	Simple Support	Conventional	7	
			Seismic	8	
		Continucus	Conventional	9	
			Seismic	10	
Steel bridges	Multiple	Simple Support	Conventional	11	
			Seismic	12	
	All	Continucus	Conventional	13	
			Seismic	14	
	Other				15

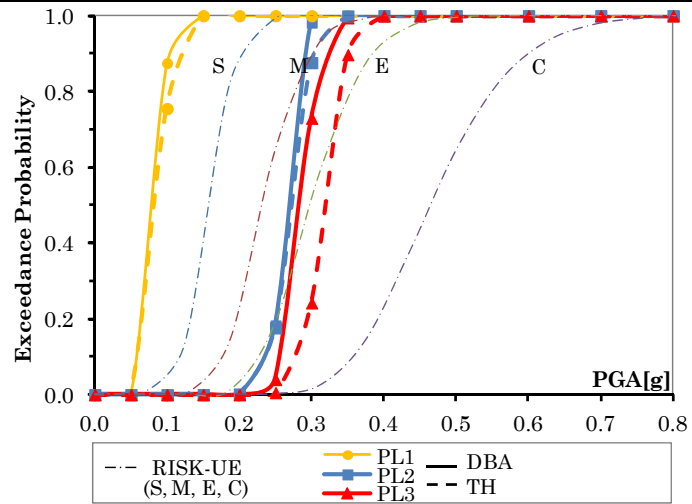
Tab. 6.67 – Parameters for fragility curves development according to RISK-UE method

Skew angle (K_{skew})	3-dimensional arch action in the deck (K_{3D})						
	EQ1	EQ2	EQ3	EQ4	EQ5	EQ6	EQ7
$\sqrt{\sin(90-\alpha)}$	$1+\frac{0.25}{N-1}$	$1+\frac{0.33}{N}$	$1+\frac{0.33}{N-1}$	$1+\frac{0.33}{N-1}$	$1+\frac{0.05}{N}$	$1+\frac{0.20}{N-1}$	$1+\frac{0.10}{N}$
Typology	Damage state						
	Minor	Moderate	Extensive	Complete			
Category	Median SA at 1.0 s (g) with $\beta=0.6$						
1-2	$0.8 \times \min\left(1; 2.5 \times \frac{SA(1.0)}{SA(0.3)}\right)$	$1.0 \times K_{skew} \times EQ1$	$1.2 \times K_{skew} \times EQ1$	$1.7 \times K_{skew} \times EQ1$			
3	0.25	$0.35 \times K_{skew} \times EQ1$	$0.45 \times K_{skew} \times EQ1$	$0.70 \times K_{skew} \times EQ1$			
4	0.50	$0.80 \times K_{skew} \times EQ1$	$1.10 \times K_{skew} \times EQ1$	$1.70 \times K_{skew} \times EQ1$			
5	0.35	$0.45 \times K_{skew} \times EQ2$	$0.55 \times K_{skew} \times EQ2$	$0.80 \times K_{skew} \times EQ2$			
6	0.60	$0.90 \times K_{skew} \times EQ3$	$1.30 \times K_{skew} \times EQ3$	$1.60 \times K_{skew} \times EQ3$			
7	0.25	$0.35 \times K_{skew} \times EQ1$	$0.45 \times K_{skew} \times EQ1$	$0.70 \times K_{skew} \times EQ1$			
8	0.50	$0.80 \times K_{skew} \times EQ1$	$1.10 \times K_{skew} \times EQ1$	$1.70 \times K_{skew} \times EQ1$			
9	$0.60 \times \min\left(1; 2.5 \times \frac{SA(1.0)}{SA(0.3)}\right)$	$0.90 \times K_{skew} \times EQ2$	$1.10 \times K_{skew} \times EQ2$	$1.50 \times K_{skew} \times EQ2$			
10	$0.90 \times \min\left(1; 2.5 \times \frac{SA(1.0)}{SA(0.3)}\right)$	$0.90 \times K_{skew} \times EQ3$	$1.10 \times K_{skew} \times EQ3$	$1.50 \times K_{skew} \times EQ3$			
11	0.25	$0.35 \times K_{skew} \times EQ4$	$0.45 \times K_{skew} \times EQ4$	$0.70 \times K_{skew} \times EQ4$			
12	0.50	$0.80 \times K_{skew} \times EQ1$	$1.10 \times K_{skew} \times EQ1$	$1.70 \times K_{skew} \times EQ1$			
13	$0.75 \times \min\left(1; 2.5 \times \frac{SA(1.0)}{SA(0.3)}\right)$	$0.75 \times K_{skew} \times EQ5$	$0.75 \times K_{skew} \times EQ5$	$1.10 \times K_{skew} \times EQ5$			
14	$0.90 \times \min\left(1; 2.5 \times \frac{SA(1.0)}{SA(0.3)}\right)$	$0.90 \times K_{skew} \times EQ3$	$1.10 \times K_{skew} \times EQ3$	$1.50 \times K_{skew} \times EQ3$			
15	0.80	1.00	1.20	1.70			

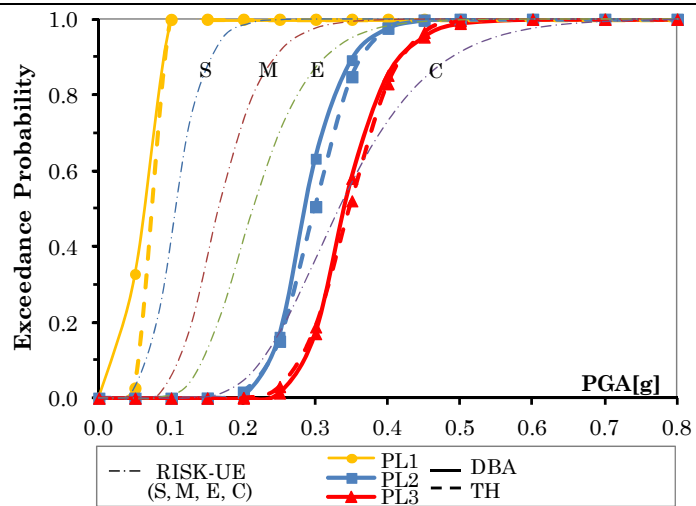
a) RBs1
Botteon Bridge



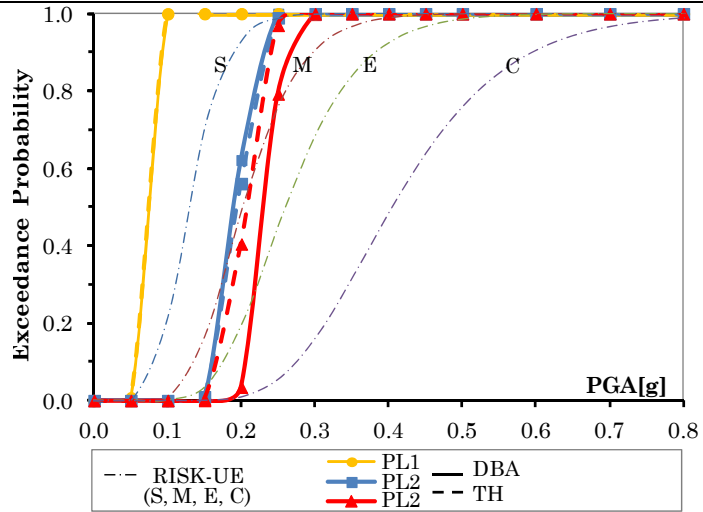
a) RBs2
Rio Ghisel Bridge



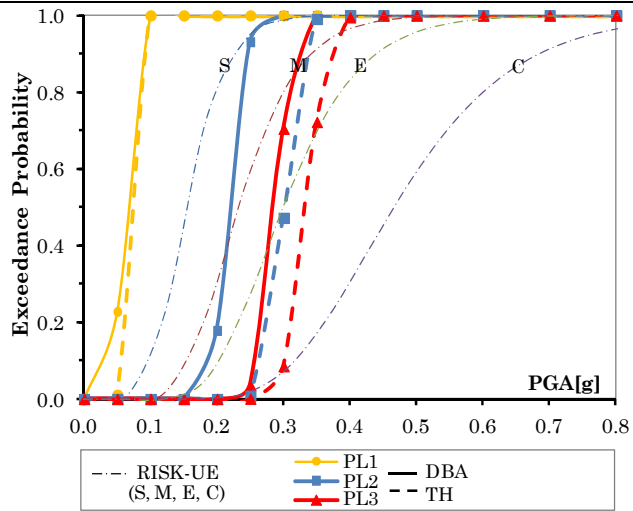
a) RBs 3
Frison Bridge



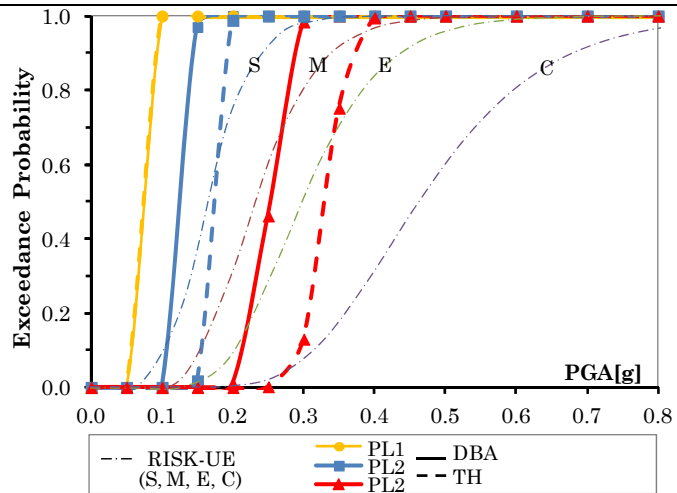
a) RBs 4-
A27 Bridge



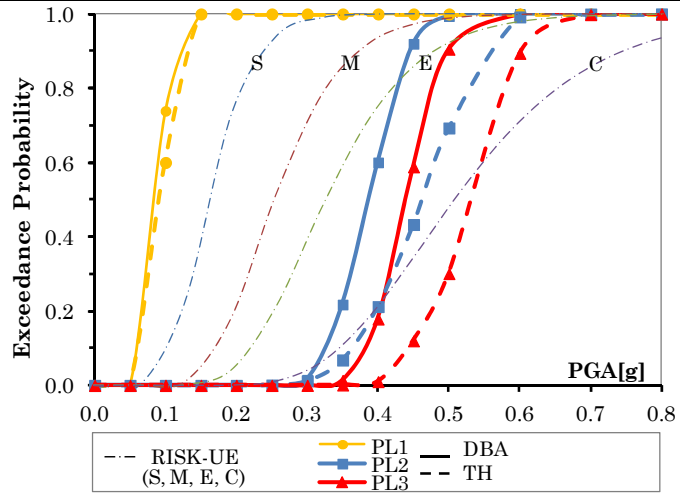
a) RBs5-
Campelli Bridge



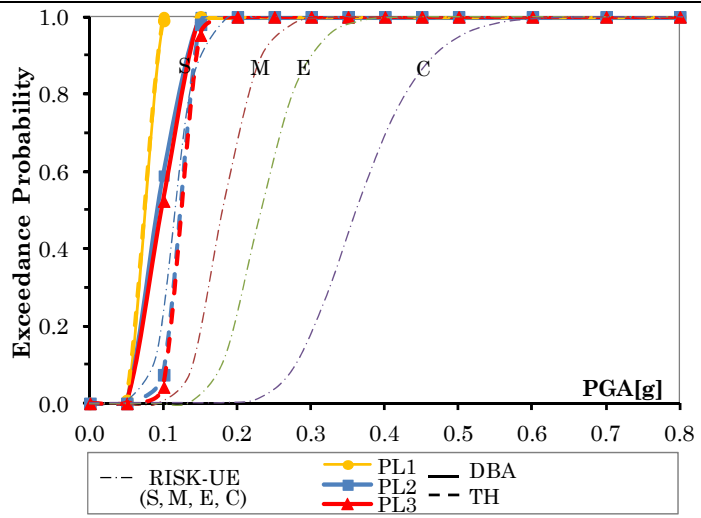
a) RBs 6-
Fener Bridge



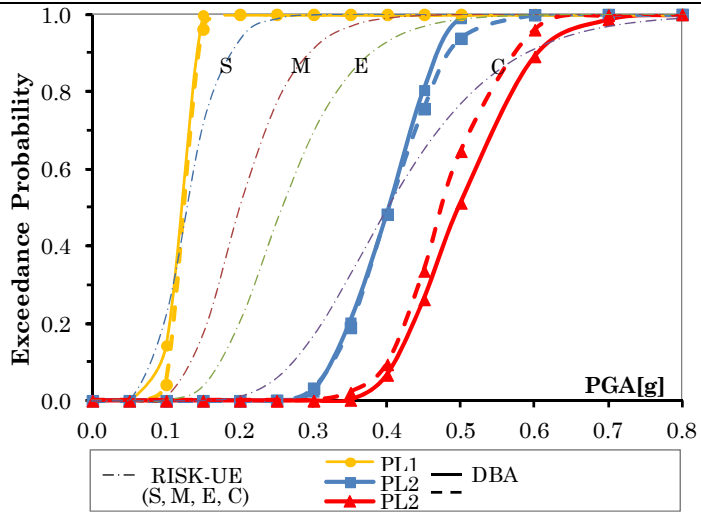
a) RBs 7-
Shiavonesca Bridge



a) RBs 8-
Reghena Bridge



a) RBs 10-
Canal Bianco Bridge



6.7 EXPECTED SEISMIC DAMAGE

In this chapter the level of expected seismic risk for all rc bridges of classes 2.1, 2.2 (multi-span bridges) is derived and the spatial distribution of expected damage is represented for the Veneto Region (VR) stock.

Fragility curves obtained with NLTH analyses (THFr) were generated only for the Reference Bridge structures as comparison with the simplified approach, and the corresponding seismic risk is calculated in §6.6.2. DBFr curves, obtained with the displacement-based approach, were carried out for all the rc multispan bridges of the VR stock (101 girder bridges in total) for the predefined Performance Levels described in §6.3.3.

6.7.1 Maps of the expected damage for the Veneto Region stock

The maps of expected damage related to Performance Levels PL_1 , PL_2 , PL_3 are shown superimposed on digital orthophoto images (Google Earth maps), in Figs 6.18, 6.19, and 6.20 respectively. The listing of the risk values obtained for all multispan rc girder bridges is reported in Tab.6.64. Bridges are denoted by dots of different colors, according to the total probability R_i (Risk index) of exceeding the limit state (not the probability of a single scenario corresponding to a pre-defined return period T_r). This value is calculated by the convolution of the hazard probability density function, using Eqs. 6.23, 6.24.

For the graphical representation, 4 categories are used, corresponding to increasing probability values: green ($R_i < 10^{-2}$), yellow ($10^{-2} < R_i < 10^{-1}$), orange ($10^{-1} < R_i < 5 \cdot 10^{-1}$) and red ($R_i > 5 \cdot 10^{-1}$).

The results show that the seismic risk characterizing the VR stock of multi-span rc bridges is generally moderate.

For limit state PL_3 only a limited number of bridges (the 11% on the whole) has high failure probability (belonging to the orange category, none to the red), as shown in Fig. 6.17, and this percentage is incremented for PL_2 till the 20%. More than the half of bridges exhibit a non negligible probability (yellow category, $10^{-2} < R_i < 10^{-1}$) of exceeding the limit states PL_3 and PL_2 (53% and 57%). Very low probability ($R_i < 10^{-2}$) are attained for collapse or severe damage limit states by the remaining part of the of the structures (22% and 36% respectively).

Although the direct seismic risk involving collapse or severe damage (PL_3 and PL_2) is moderate, complete system operation at network level could be a concern in a post earthquake situation, due to the fact that the 85% of bridges of the VR stock are supposed to sustain with high probability (orange to red categories) a light damage, associated to PL_1 limit state. This damage could also not require in most cases a repair intervention, but it could imply at least structural inspections and provisional downtime for the traffic. It is worth to evidence that in this case,

PL_1 is defined for ductile members as a condition in which a certain, even limited ductility is already developed (and not as the first yielding of the section at pier base, see Tab. 6.23).

These results can be partially explained by the seismic activity of the Veneto region, which is characterized by low-medium seismicity. From Fig. 2.11, it can be seen that for the 475 year return period (10% in 50 years), PGA values in south of the Veneto region are under the limit $0.05g$, which corresponds to the limit for lowest seismicity areas (Zone 4). On the north part of the Belluno Province corresponds in the administrative classification to Zone 3 ($0.05 < PGA < 0.15$), as well as the central part of the region, in the territory of Verona and Vicenza provinces. There are higher PGA values in the north-east part of the region, corresponding to the territory of Treviso, and Belluno (zone 2, $0.15 < PGA < 0.275$).

The other fundamental component of the seismic risk is the intrinsic fragility of the structure. No seismically designed rc structures, built in the past decades (like the most of the bridges of the VR stock), are generally affected by typical construction defects, such as low confinement of nodes (see results of statistics in §6.2.4), insufficient transversal reinforcement, poor detailing for starter bars, etc.

It can be noted that seismic vulnerability of rc multi-span bridges is substantially different for each subclass, depending on pier type.

PL1

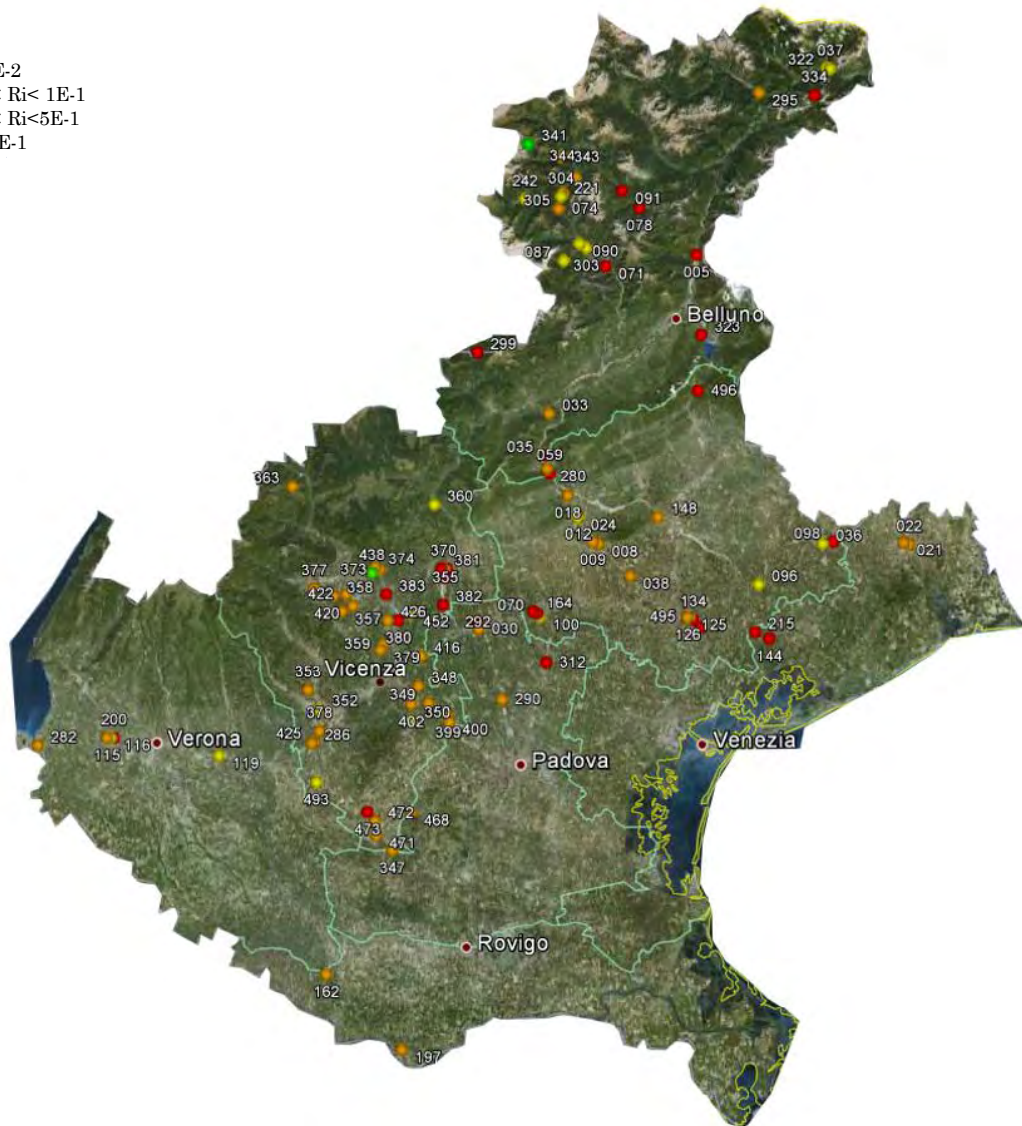
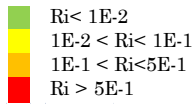
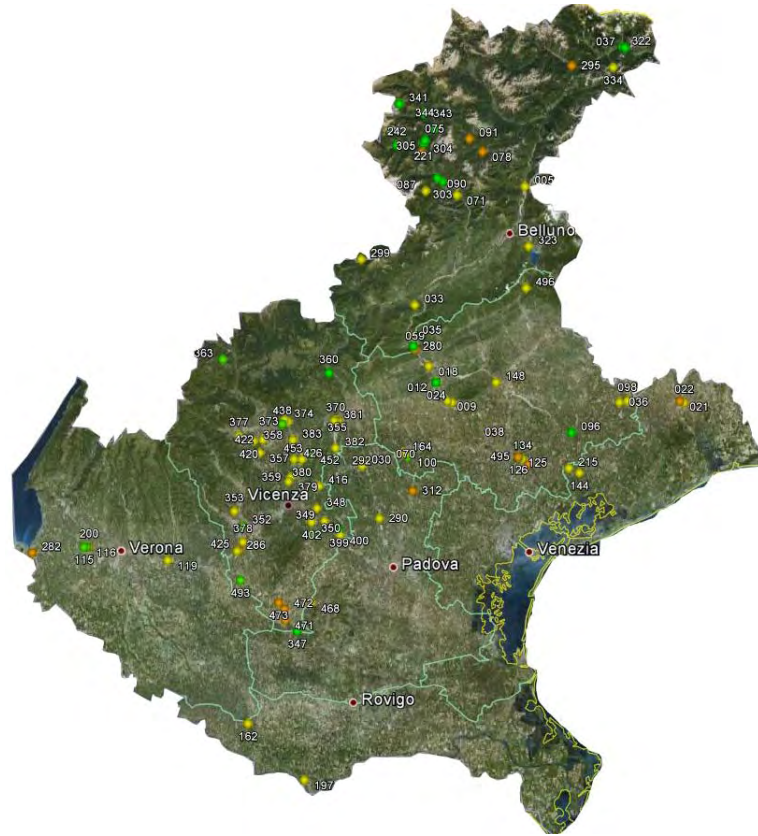


Fig. 6.21 – Seismic Risk for multi-span rc bridges (classes 2.1, 2.1) in the VR stock.
Damage state corresponding to PL1

PL2

- $R_i < 1E-2$
- $1E-2 < R_i < 1E-1$
- $1E-1 < R_i < 5E-1$
- $R_i > 5E-1$



PL3

- $R_i < 1E-2$
- $1E-2 < R_i < 1E-1$
- $1E-1 < R_i < 5E-1$
- $R_i > 5E-1$

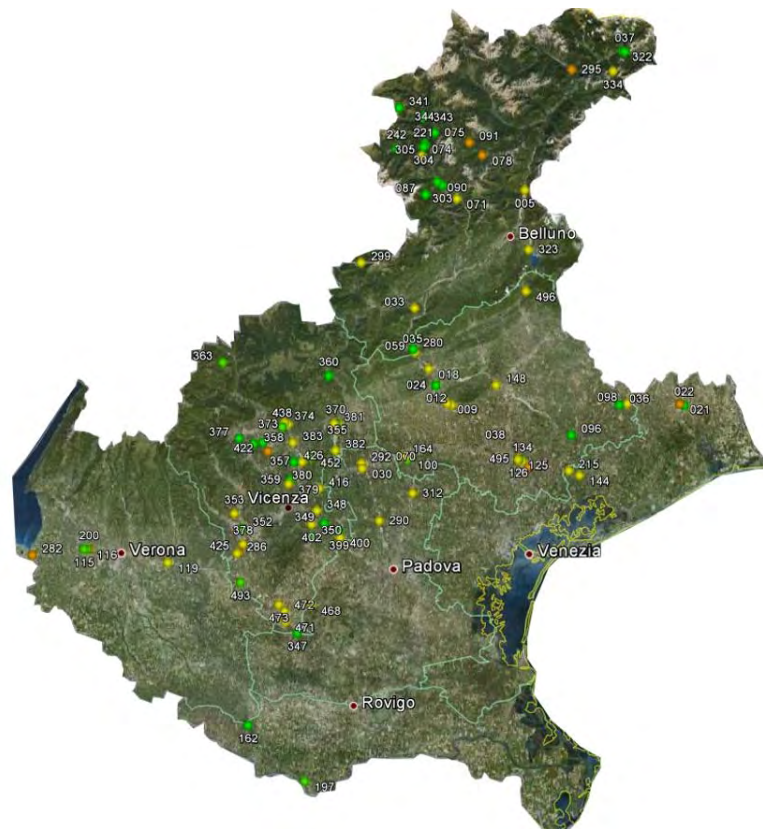


Fig. 6.22 – Seismic Risk for multi-span rc bridges (classes 2.1, 2.1) in the VR stock. Damage states corresponding to PL2 and PL3.

-Bridges with wall piers, which represent a considerable amount of the whole stock (the 38.6% of the total including also continuous bridges, see §6.2.2), are less vulnerable. Shear resistance is very high, and in longitudinal direction generally the great inertia of the section is sufficient to guarantee adequate resistance for flexural displacement demand, even with limited ductility. According to the analyses developed, none of the sample bridges of the stock belonging to class 2.1.2 (bridges with pier wall) has high probability of collapse or severe damage, and in the 84% of cases $Ri < 10^{-2}$;

-Simply supported bridges with shear (or flexure-shear) piers (typically with $H/B_T < 2.5-3$, see chapter 5) are the most vulnerable, because existing piers (cantilever and frame) have limited shear resistance and low transverse reinforcement ratio. In the 66% of cases these piers fail with high probability ($Ri > 10^{-1}$), and also complete collapse can be expected. They represent a small number of structures in the VR stock.

- Very slender cantilever and frame pier bents ($H/D > 4.5$) with flexural behaviour, are subjected to low inertia forces due to the high effective periods of vibration. Bridges equipped with this kind of piers have low seismic damage exposure. Also for this subclass always low probabilities were found for PL_2 and PL_3 (yellow and orange category, $Ri < 10^{-1}$).

- Fragility is higher for very long bridges with multiple spans, increasing with the number of vulnerable elements (number of pier bents of multi-span simply supported bridges). Vulnerability of long bridges can be incremented also by asynchronism of ground motion, that can greatly influences pounding forces and deck-pier differential displacements (not addressed in this study, see for detail Tecchio et al.^[T5], 2012).

The map of seismic risk can be used for economic loss estimation and provides also a basis for prioritization of interventions on the existing structures, aimed at lowering their intrinsic vulnerability: the listing provided in Tab. 6.58 represent a direct tool that may directly be implemented in a Bridge Management System for assigning retrofit prioritization for bridges.

Tab. 6.68 –*Seismic risk associated to PL1, PL2, PL3 for multi-span rc continuous bridges (Classes 2.1)*

N°	Location	Zone	Name	Road (S.P.- S.R.)	Km	No. of Spans	Static scheme	Pier type	Pier Cross	PL1	PL2	PL3
5	Longarone	3	Campelli	S.P. 251	103+750	5	M_SIMPLE	PF2	SC	0.757	0.076	0.042
8	Montebelluna	2	S.P.248 "Schiavonesca"	S.R. 348	17+710	3	M_SIMPLE	PFM	SR	0.469	0.027	0.02
9	Montebelluna	2	Bocca Cavalla	S.R. 348	18+929	4	M_SIMPLE	PFM	SR	0.128	0.028	0.013
12	Crocetta del Montello	2	FF.SS	S.R. 348	25+025	2	M_SIMPLE	PF2	SC	0.492	0.058	0.035
18	Pederobba	2	Torrente Courogna	S.R. 348	29+753	3	M_SIMPLE	PF2	SC	0.301	0.039	0.027
21	Portogruaro	3	Fiume Reghena	S.R. 53	113+712	4	M_SIMPLE	PFM	SC	0.328	0.132	0.114
22	Portogruaro	3	Calvacavia FF.SS.	S.R. 53	114+880	4	M_SIMPLE	PFM	SR	0.192	0.013	0.007
24	Crocetta del Montello	2	Via 4 Novembre	S.R. 348	24+838	3	M_SIMPLE	PF2	SC	0.071	0.003	0.002
30	Cittadella	3	FF.SS	S.P. 47	28+430	3	M_SIMPLE	PFM	SC	0.212	0.023	0.014
33	Feltre	2	Torrente Sonna	S.R. 348	48+925	3	M_SIMPLE	PSC	SC	0.255	0.029	0.018
35	Quero/Vas	2	Fante d'Italia	S.P. 1 bis	16+078	13	GERBER	PSC	HM	0.566	0.023	0.01
36	Motta di Livenza	3	Fiume Livenza Ramo Morto	S.R. 53	96+802	2	M_SIMPLE	PW	SR	0.088	0.012	0.007
37	San Pietro di Cadore	3	Viadotto sulla SR355	S.R. 355	41+355	6	M_SIMPLE	PF2	SC	0.044	0.003	4E-04
38	Paese	3	SP Postumia	S.R. 348	9+100	3	M_SIMPLE	PW	SR	0.322	0.011	0.005
59	Alano di Piave	2	Cav. Vittorio Veneto - Ponte Fener-	S.P. 32	0+429	21	M_SIMPLE	PF2	SC	0.74	0.218	0.066
71	La Valle Agordina	3	Torrente Cordevole	S.R. 203	19+647	3	M_SIMPLE	PW	SR	0.754	0.028	0.019
74	Cencenighe	3	Torrente Cordevole	S.R. 203	35+958	3	M_SIMPLE	PSC	SC	0.489	0.125	0.093
75	Masare	3	Torrente Cordevole	S.R. 203	44+800	2	M_SIMPLE	PW	SR	0.1	0.004	0.003
78	Forno di Zoldo	3	Torrente Mareson	S.R. 251	121+226	3	M_SIMPLE	PF2	SC	0.712	0.259	0.219
87	Voltago Agordino	3	Torrente Zoppi e Cortolei	S.R. 347	23+500	4	M_SIMPLE	PFM	SR	0.099	0.011	0.003
90	Taibon Agordo	3	Torrente Cordevole	S.R. 347	30+835	3	M_SIMPLE	PW	SR	0.099	0.005	0.003
91	Zoldo Alto	3	Torrente Moiazza	S.R. 347	48+278	3	M_SIMPLE	PF2	SC	0.663	0.166	0.143
96	San Biagio di Callalta	3	Ponte sul Piave	S.R. 53	73+260	7	M_SIMPLE	PW	SR	0.062	0.009	0.006
98	Motta di Livenza	3	Canale Malgher	S.R. 53	98+973	3	M_SIMPLE	PW	SR	0.537	0.024	0.015
134	Silea	3	Sottopasso via Sile	S.R. 89	1+030	2	M_SIMPLE	PFM	SC	0.601	0.059	0.042
144	Meolo	3	Cavalcaferrovia FF.SS. TS-VE	S.R. 89	16+350	3	M_SIMPLE	PFM	SC	0.621	0.065	0.029
148	Nervesa della Battaglia	2	Canale Vittoria	S.P. 248	76+115	2	GERBER	PW	SR	0.489	0.049	0.031
162	Ceneselli	3	Canal Bianco	S.R. 482	59+831	3	GERBER	PW	SR	0.486	0.011	0.006
196	Silea	3	Cavalcavia A27	S.R. 89	2+778	3	M_SIMPLE	PF2	SR	0.83	0.119	0.109
200	Verona	3	Cavalcavia A22 del Brennero	S.R. 11	293+435	3	M_SIMPLE	PFM	SC	0.926	0.312	0.161
215	Meolo	3	Cavalcavia Autostrada VE-TS	S.R. 89	13+312	3	GERBER	PW	SR	0.572	0.068	0.029
221	San Tomaso Agordino	3	Torrente Cordevole	S.R. 203	38+736	4	GERBER	PSC	SC	0.1	0.006	0.004
242	Falcade	3	Torrente Gavon	S.P. 346	23+230	3	M_SIMPLE	PSC	SC	0.048	0.006	0.003
280	Alano di Piave/Quero	2	Torrente Tegorzo	S.R. 348	36+313	3	M_SIMPLE	PW	SR	0.11	0.009	0.004
286	Montebello	3	Cavalcavia Autostrada BS-PD	S.R. 11	333+564	2	M_SIMPLE	PFM	SR	0.142	0.047	0.041
290	Piazzola sul Brenta	3	Fiume Brenta	S.R. 47	14+080 DX	3	M_SIMPLE	PF2	SC	0.209	0.038	0.021
295	Auronzo di Cadore	3	Torrente Diebba	S.R. 48	159+800	4	M_SIMPLE	PF2	SC	0.415	0.117	0.101
303	Agordo	3	Torrente Rovala	S.R. 203	26+387	2	M_SIMPLE	PW	SR	0.09	0.009	0.005
304	Cencenighe/San Tommaso /	3	Rio Ghisel	S.R. 203	39+056	5	M_SIMPLE	PSC	SC	0.127	0.011	0.009
305	San Tommaso Agordino	3	Torrente Ivach	S.R. 203	39+584	9	M_SIMPLE	PSC	SC	0.198	0.008	0.004
312	Loreggia	3	Fiume Muson dei Sassi	S.R. 307	20+538	3	M_SIMPLE	PFM	SR	0.71	0.134	0.054
322	San Pietro di Cadore	3	Fiume Piave	S.R. 355	42+210	2	M_SIMPLE	PW	SR	0.057	0.006	0.003
334	Santo Stefano di Cadore	3	Torrente Frison	S.R. 465	4+200	3	M_SIMPLE	PW	SR	0.604	0.017	0.011
341	Rocca Pietore	3	Pian de Lebbia I	S.P. 641	16+224	6	M_SIMPLE	PSC	SR	0.003	0.001	9E-04
343	Rocca Pietore	3	Rio Crepolba	S.P. 641	26+550	3	M_SIMPLE	PW	SR	0.153	0.002	0.001
344	Rocca Pietore	3	X	S.P. 641	26+890	4	M_SIMPLE	PSC	SR	0.032	0.002	0.001
347	lovento Vicentina - Casell	4	Ponte sul Frassin	S.P. 4	2+160	3	M_SIMPLE	PW	SR	0.145	0.008	0.003
348	orri di Quaratesolo - Maro	3	Fiume Bacchiglione	S.P. 28	1+500	3	M_SIMPLE	PF2	SC	0.212	0.018	0.011
349	Grumolo delle Abbadesse	3	Ferrovia MI-VE e strada	S.P. 26	1+307	9	M_SIMPLE	PW	SR	0.206	0.012	0.007
353	Arzignano	3	Ponte delle Tezze	S.P. 89	2+985	3	M_SIMPLE	PFM	SC	0.32	0.022	0.012
355	Cartigliano	3	Fiume Brenta	S.P. 58	5+630	16	M_SIMPLE	PF2	SC	0.672	0.057	0.031
358	Marano Vicentino	3	Torrente Timonchio	S.P. 10	4+640	2	M_SIMPLE	PW	SR	0.245	0.015	0.008
359	Dueville	3	Torrente Timonchio	S.P. 101	2+000	3	M_SIMPLE	PW	SR	0.276	0.011	0.006
360	Oliero	4	Torrente Oliero	S.P. 73	10+100	3	M_SIMPLE	PW	SR	0.03	0.006	0.003
370	Bassano del Grappa	3	Bacino imbrifero strade comunali	S.P. 248	2+946	7	M_SIMPLE	PFM	SC	0.694	0.074	0.049
372	Bassano del Grappa	3	Fiume Brenta	S.P. 248	3+535	12	M_SIMPLE	PFM	SC	0.666	0.042	0.035
373	Zugliano	3	Fiume Astico	S.P. 67	5+530	6	M_SIMPLE	PF2	SC	0.316	0.019	0.015
374	Lugo di Vicenza	3	Fiume Astico	S.P. 68	4+900	3	M_SIMPLE	PF2	SC	0.314	0.019	0.015
377	Schio	3	Torrente Leogra	S.P. 46	23+700	3	M_SIMPLE	PW	SR	0.155	0.017	0.009
379	Caldogno	3	Fiume Bacchiglione	S.P. 41	4+400	3	M_SIMPLE	PW	SR	0.352	0.021	0.011
380	Sandrigio	3	Ponte sull'Astico	S.P. 248	12+250	8	M_SIMPLE	PF2	SC	0.54	0.037	0.023
381	Bassano del Grappa	3	Torrente Longhella	S.P. 248	2+595	4	M_SIMPLE	PFM	SC	0.677	0.053	0.034
382	Pozzoleone	3	Fiume Brenta	S.P. 44	0+200	17	M_SIMPLE	PF2	SC	0.583	0.047	0.03
383	Sarcedo	3	Ponte sull'Astico	S.P. 111	5+210	6	M_SIMPLE	PF2	SC	0.613	0.058	0.037
399	Grisignano di Zocco	3	Ferrovia MI-VE	S.P. 21	3+402	2	M_SIMPLE	PW	SR	0.103	0.004	0.002
402	Torri di Quaratesolo	3	Autostrada A4	S.P. 27	1+161	3	M_SIMPLE	PFM	SR	0.313	0.025	0.013
415	Bassano del Grappa	3	Torrente Longhella	S.P. 52	3+150	3	M_SIMPLE	PW	SR	0.067	0.013	0.006
416	Bolzano Vicentino	3	Ferrovia VE - TV	S.P. 30	0+100	3	M_SIMPLE	PF2	SC	0.49	0.042	0.025
420	Malo	3	Autostrada Valdastico A31	S.P. 48	1+540	3	M_SIMPLE	PSC	SC	0.36	0.127	0.113
422	Marano Vicentino	3	Autostrada Valdastico A31	S.P. 10	7+350	3	GERBER	PSC	SC	0.247	0.012	0.006
426	Dueville	3	Autostrada Valdastico A31	S.P. 63	2+100	3	GERBER	PSC	SC	0.22	0.012	0.006
471	Noventa Vicentina	4	Fiume Alonte	S.P. XI	0+450	3	M_SIMPLE	PFM	SC	0.494	0.301	0.08
472	Pojana Maggiore	4	Scolo Alonte	S.P. XIV	12+840	3	M_SIMPLE	PFM	SC	0.499	0.219	0.084
473	Sossano	3	Scolo Alonte	S.P. 4	4+140	3	M_SIMPLE	PFM	SC	0.553	0.246	0.087
496	Fadalto	2	Botteon	S.S. 51	X	6	M_SIMPLE	PSC	SR	0.91	0.028	0.02

Tab. 6.69 –*Seismic risk associated to PL1, PL2, PL3 for multi-span rc continuous bridges (Classes 2.2)*

N°	Location	Zone	Name	Road (S.P.- S.R.)	Km	No. of Spans	Static scheme	Pier type	Pier Cross Sect.	PL1	PL2	PL3
70	Castelfranco Veneto	3	Cavalcaferrovia FF.SS	S.R. 245	2+486	12	CONT	PSC	SC	0.676	0.074	0.051
100	Castelfranco Veneto	3	SP per Treville (Torr. Muson)	S.R. 54	1+533	3	CONT	PW	SR	0.017	0.01	0.009
115	Bussolengo	3	Cavalcavia Z.I. Bussolengo	S.R. 11	292+040	2	CONT	PW	SR	0.167	0.001	3E-05
116	Bussolengo	3	Cavalcavia zona città mercato	S.R. 11	292+800	2	CONT	PFM	SR	0.012	1E-03	3E-06
119	Colognola ai Colli/Caldiero	3	Torrente Progno	S.R. 11	314+412	2	CONT	PW	SR	0.064	0.013	0.012
125	Treviso	3	Tang. Tv Ponte sul Sile	S.R. 53	63+315	3	KINEMATIC	PFM	SC	0.433	0.116	0.096
126	Treviso	3	Tang. Tv Ponte sul Sile	S.R. 53	63+387	3	KINEMATIC	PFM	SC	0.433	0.116	0.095
164	Castelfranco Veneto	3	Cavalcavia S.P. 83	S.R. 54	3+146	8	CONT	PSC	SC	0.648	0.077	0.051
197	Occhiobello	3	Cavalcavia A13	S.R. 06	4+400	3	CONT	PF2	SC	0.146	0.013	0.005
282	Peschiera del Garda	3	Ponte del fiume Mincio	S.R. 11	278+205	3	CONT	PW	SR	0.369	0.134	0.124
292	Cittadella	3	Cavalcavia Borgo Vicenza	S.R. 47	29+990	6	CONT	PW	SR	0.566	0.095	0.08
299	Sovramonte	3	Pontet I	S.R. 50	60+608	4	CONT	PSC	HS	0.645	0.078	0.065
323	Ponte nelle Alpi/Pous d'Alpago	2	Loc. La Secca	S.R. 422	0+115	3	CONT	PW	SR	0.722	0.025	0.012
350	Longare	3	Fiume Bacchiglione	S.P. 20	0+298	3	CONT	PW	SR	0.094	0.003	0.002
352	Montecchio Maggiore	3	Torrente Guà	S.P. 33	1+340	5	CONT	PW	SR	0.016	1E-08	2E-15
357	Malo	3	Ponte sul Timonchio	S.P. 48	3+850	3	CONT	PW	SR	0.417	0.01	0.005
363	Tonezza del Cimone	3	Valle	S.P. 64	5+000	3	CONT	PW	SR	0.138	0.004	0.002
378	Montebello Vicentino	3	Torrente Chiampo	S.P. 31	0+600	3	KINEMATIC	PFM	SC	0.321	0.08	0.067
400	Grisignano di Zocco	3	Autostrada A4	S.P. 21	4+846	3	CONT	PF2	SR	0.102	0.028	0.056
425	Montebello Vicentino	3	Autostrada A4	S.P. 18	5+018	3	CONT	PF2	SR	0.355	0.199	0.154
438	Grumolo Pedemonte	3	Canale	S.P. 67	2+325	2	CONT	PW	SR	3E-04	3E-07	9E-08
452	Sandrigò	3	Fiume Tesina	S.P. 46	15+336	2	CONT	PW	SR	0.014	0.003	0.002
453	Sandrigò	3	Torrente Leverda	S.P. 248	15+782	2	CONT	PW	SR	0.419	0.01	0.005
468	Agugliaro	4	Scolo Liona	S.P. 7	3+710	3	CONT	PW	SR	0.121	0.034	0.031
493	Lonigo	3	Torrente	S.P. 57	X	3	CONT	PW	SR	0.008	0.001	0.001
495	Silea	3	Cavalcavia Silea	S.R. 53	X	4	CONT	PFM	SC	0.054	0.01	0.006

6.8 CONCLUSIONS

With regard to the methods of assessment of the existing bridges, the specific interest of the use of simplified procedures is apparent when probabilistic risk analysis is carried out on a large-scale, reliable indications having to be provided in a relatively short time for a large number of structures.

Displacement-Based assessment procedures are used herein to assess the seismic vulnerability of the multi-span rc girder bridges (101) belonging to the regional road network of the Veneto region (N-E of Italy).

After a preliminary subdivision of the bridge stock into homogeneous subclasses, a detailed statistical survey of the reference VR bridge database is presented, characterizing the effective ranges of pier properties (in terms of material characteristics, geometrical properties, reinforcement ratios etc.) that can influence the pier seismic capacity.

A limited number of rc multi-span bridges are chosen as reference samples (named Reference Bridge structures, *RBs*) for each homogeneous class, and a direct comparisons of the DBA procedure with NLTH analyses are carried out on this restricted (but representative) set of structures, showing how the analytical simplified DB method allows to predict the seismic fragility with fair accuracy. A direct comparison with fragility curves obtained by the application of the tabular RISK-UE method (extensively used for large-scale fragility analyses) is also proposed for the RB structures, showing how these curves are generally very distant from the analytical ones, while the analytical DB curves catch much better the overall fragility of the structure, giving a representative value of the final seismic risk index.

Subsequently the vulnerability analysis of the entire bridge stock for multi-span rc bridges is developed. Displacement-Based fragility curves are calculated by adapting the procedure proposed for non-linear static analyses by Shinozuka et al.^[S2], 2000, using displacement elastic spectra, and calculating the damage index as the Demand/Capacity ratio, expressed in terms of elastic spectral displacements for a pre-defined Performance Level.

The seismic risk maps, show that the majority of structures are supposed to sustain with high probability a light damage, while risk involving severe damage collapse or is generally moderate, even if it is substantially negligible only for about 1/3rd of the analyzed structures (at PL₃ limit states). These results, that represent to the author's knowledge the first indication on large scale of the expected seismic damage for bridges in this region, confirm that there is an intrinsic fragility typical of these classes of bridge structures, and the related seismic risk should be lowered through retrofit interventions. To this aim, the risk maps can be used as a direct tool by managing authorities to assign prioritization for interventions.

CHAPTER 7

CONCLUSIONS

7.1 GENERAL OBSERVATIONS

The fast few years have seen the emergence of Displacement-Based (DB) design methods as the most promising basis for the future developments in a Performance-Based approach for seismic design and assessment. In these methods the capacity-demand comparison is expressed in terms of displacements and deformations, since it has been recognized that they are primary variables for seismic damage estimation.

DB methods are simplified approaches using equivalent single degree of freedom systems for response prediction. As in the case of other simplified methods the constant interest is explained by the great uncertainty characterizing the prediction of the seismic response, which makes the use of sophisticated models not always effective and warranted. This specific interest is further justified when the seismic risk evaluation is carried out in a probabilistic framework, relating to large-scale case studies, quick and reliable simplified approaches being more convenient in respect to NLTH analyses, balancing accuracy and time saving.

Displacement Based methods for seismic design and assessment of bridges in the present study are addressed from a methodological point of view: in the first part the current DB design methods for new structures with flexural ductile behaviour are evaluated, in particular with reference to the formulations of the equivalent viscous damping and the target displacement profile to be adopted in the analysis.

In the second part the calibration of the DB procedures regards the specific issues arising in the evaluation of existing structures, not seismically designed, and often not characterized by a global ductile behaviour. In particular the research focuses on the assessment of pier capacity and effective properties, piers generally representing the most vulnerable elements in the lateral resisting system of bridges.

The final outcome of the study is the supply of regional seismic risk maps for the whole class of multi-span rc bridges belonging to the Veneto regional road network. The expected seismic damage is obtained with vulnerability analyses based on the simplified analytical displacement-based procedures, previously calibrated.

7.2 INNOVATIVE ASPECTS OF THE RESEARCH

The thesis contains unpublished material, or partly, material that has recently been submitted to scientific journals or conferences in a different form. Most of the content of the work is therefore new, and the main results of the research are summarized below.

As regards the calibration of the Displacement-Based Design procedures, applied to new structures with global ductile behaviour, the following original results were obtained:

- the estimate of the medium error committed by the current DDBD method for the design of SDOF structures is derived, with specific reference to isostatic bridge piers (cantilever piers conform to the assumption of SDOF systems), through the development of an average error chart, characterizing the scatter in the results as a function of design ductility μ_{Δ}^d and effective period T_{eff} . A relation between displacement ductility and drift is also derived for cantilever piers, and a parametric chart is presented for pre-fixed values of pier height/ diameter ratio. The chart can be directly employed for design purposes;
- a comparison between the current DDBD procedure and NLTH analyses for the prediction of transverse response of continuous bridges is presented with reference to an ample set of bridge configurations, showing how the system regularity can significantly affect the reliability of the DDBD simplified procedure. An alternative direct design method (named DBD-DEM), is proposed with the aim of simplifying the current iterative procedure for everyday design use. In the DBD-DEM method the global effective stiffness of the linearized system at the target displacement is predicted by using the DBD framework, and subsequently an effective Spectrum Response Analysis (RSA) is used for the estimation of the final target displacement shape and the design of piers.

As regards the calibration of Displacement Based Assessment procedures and its application to existing bridge structures, the following results were achieved:

- the definition of the typical effective ranges of the main pier parameters, essential for the calculation of rc multi-span bridges pier capacity for multi-span bridges (longitudinal and transverse reinforcement ratio, confinement parameters, normalized axial load, etc.), obtained through the statistical analysis of the VR bridge inventory. The usual level of detail characterizing existing bridge database is generally very poor, and the definition of the ranges of structural pier characteristics as basic data for a vulnerability analysis on a large scale, represents an achievement in itself;
- the simplified non linear numerical model used for the flexural and shear interaction, gives a reliable representation of the non linear behaviour of shear critical piers, for which a new equivalent damping expression is formulated. The extensive parametrical analysis developed for pier capacity, allowed to define the collapse mechanisms, significant limit states in terms of strain and drifts, and effective properties of single bent and multiple bent piers were. A series of parametric charts, that can be directly employed for the construction of piers capacity curves are presented, and can be used within the framework of the Displacement-Based assessment method;

- direct comparisons of simplified DBA procedures with NLTH analyses are developed on a representative set of structures for the construction of analytical fragility curves in a probabilistic framework. On the same set of bridges comparisons are also made with tabular methods (RISK-UE), usually employed as tools for earthquake risk assessment on a large scale;
- seismic risk maps on a regional scale are finally plotted for all the multi-span rc bridges of the VR stock, for three different scenarios corresponding to light damage, severe damage and collapse of bridges. These maps, obtained with analytical Displacement-Based methods, represent the first indication of seismic vulnerability for the whole class of multi-span rc bridges belonging to the Veneto regional road network, and can be used by the managing authorities as a direct tool to assigning a priority of retrofitting interventions.

7.3 FUTURE DEVELOPMENTS AND RECCOMENDATIONS FOR FURTHER RESEARCH

The development of Displacement-Based Assessment (DBA) approaches has to address the specific issues of the definition of possible failure modes, limit states, hysteretic behaviour for existing structures, generally different from those characterizing new seismically designed structures.

This research contributes to the implementation of these aspects in bridge seismic Displacement-Based assessment. However, further studies are needed in order to calibrate simplified but accurate models for the interaction of shear-flexure behaviour of piers under cyclic forces, predicting the shear cracking level and individuating the point of expected collapse. Moreover the definition of adequate performance levels related to the observable damage states is still a fundamental task for a displacement-based vulnerability analysis, and research on this topic need to be progressed.

Several ideas for continuing the research presented in this thesis may be considered. An immediate extension of the research, may be represented by the development of a set of displacement-based fragility curves valid for the whole class of multi-span rc bridges. The need for analytical fragility curves representative of whole classes of bridges is apparent, if we consider that existing tabular methods (Hazus, Risk-UE) prove unreliable when applied to common Italian or European bridge typologies. A long-term development of the work may regard the extension of the simplified Displacement-Based procedures to the evaluation of different classes of bridge structures, particularly the single span rc bridges and masonry arch bridges, which represent the two other major categories of existing bridges in Italy. This could lead to completion of the scenario of seismic risk for the infrastructure network under examination (Veneto Region bridge inventory) on a regional scale. Furthermore in this context it will be possible to calibrate the seismic input for risk analysis through the use of hazard curves, obtained from micro-zonation studies in the areas of interest.

REFERENCES

- **A1** ATC, (1996). Seismic evaluation and retrofit of concrete buildings Vol.1 (ATC-40), *Applied Technology Council*, Berkeley, California, USA.
- **A2** Ayers, J.P., *Evaluation of parameters for limit states design of masonry walls*, MS Thesis, North Carolina State University, Raleigh, USA, 2000.
- **A3** Alvarez, J.C., (2004). *Displacement Based Design of Continuous Concrete Bridges under Transverse Seismic Excitation*, MSc Thesis, Rose School, IUSS, Pavia.
- **A4** Alfawakhiri, F., Bruneau, M., (2000). Flexibility of Superstructures and Supports in the Seismic Analysis of Simple Bridges, *Earthquake Engineering and Structural Dynamics*, **29**, 711 – 729.
- **A5** Adhikari, G., Petrini, L., Calvi, G.M., (2010). Application of direct displacement based design to long span bridges, *Bulletin of Earthquake Engineering*, **8**, 897-819.
- **A6** Applied Technology Council, (1981). Seismic Shear Strength of Circular Reinforced Concrete Columns, *ACI Structural Journal*, **86(1)**, 45-49
- **A7** ACI Committee 318, (2002). Building Code Requirement for Structural Concrete (ACI 318-02) and Commentary (ACI 318R-02), *American Concrete Institute*, Farmington Hills, Michigan, USA.
- **B1** Bernal, D., “Amplification Factors for Inelastic Dynamic P- Δ Effects in Earthquake Analyses”, *Earthquake Engineering and Structural Dynamics*, **15**, 1981, p. 635 – 651.
- **B2** Boore, D.N. and Bommer, J.J., (2005). Processing of Strong-Motion Accelerograms: Needs, Options and Consequences, *Soil Dynamic and Earthquake Engineering*, (**25**), 93-115.
- **B3** Bal, I.E., Crowley, H. and Pinho R. (2010). *Displacement-Based Earthquake Loss Assessment: Method development and application to Turkish Building Stock*. IUSS Press, Pavia.
- **B4** Basöz, N., and Kiremidjian, A. S. (1995). *Prioritization of bridges for seismic retrofitting*, *Technical Report NCEER-95-0007*. Multidisciplinary Center for Earthquake Engineering Research, Buffalo, New York.
- **B5** Basöz and Kiremidjian, (1997). Risk assessment of bridges and highway systems from the Northridge earthquake. *Proceedings of the National Seismic Conference on Bridge and Highways*. Progress in Research and Practice. Sacramento, California. July 8-11, 1997, pages 65-79.
- **B6** Barbat, A.H. Yezpez Moya, F., Canas, J.A., (1996). Damage scenario simulation for seismic risk assessment in urban zones, *Earthquake spectra*, **12(3)**, 371-394.
- **C1** Chopra, A.K., (2001). Direct displacement-based design: use of inelastic vs. elastic design spectra”, *Earthquake Spectra*, **17(1)**, 47 – 64.
- **C2** Calvi, G.M. and Sullivan, T.J., (2009). *A Model Code for the*

- Displacement-Based Seismic Design of Structures, DBD 09, Draft subject to public enquiry*, IUSS Press, Pavia.
- **C3** Calvi, G.M., Kingsley, G.R., (1995). Displacement-Based Seismic Design of Multi-Degree of Freedom bridge Structures, *Earthquake Engineering and Structural Dynamics*, **24**, 1247 – 1266.
 - **C4** Crowley, H., Pinho, R., and Bommer, J.J., (2004). A probabilistic displacement-based vulnerability assessment procedure for earthquake loss estimation, *Bulletin of Earthquake Engineering* **2**, 173–219.
 - **C5** Calvi, G.M., Ciampoli, M. and Pinto, P.E. (1989). Guidelines for seismic design of bridges. Background studies: Part 1 *Euro. Earthquake Eng.*, **2**, 3-16.
 - **C6** Calvi, G.M., and Pinto, P.E. (1996). Experimental and numerical investigations on the seismic response of bridges and recommendations for code provisions. ECOEST/PREC8 Rep. n4, National Laboratory for Civil Engineering, Lisbon, Portugal.
 - **C6** Choi E., R. DesRoches and B. Nielson, (2004). Seismic fragility of typical bridges in moderate seismic zones, *Engineering Structures*, **26**, 187-199.
 - **C7** Calvi, G. M. (1999). A displacement-based approach for vulnerability evaluation of classes of buildings, *Journal of Earthquake Engineering*, **3**(3), 411-438.
 - **C8** Crowley, H., Pinho, R., Bommer, J.J., Bird, J.F., (2006). Development of a Displacement-Based Method for Earthquake Loss Assessment, IUSS Press, Pavia.
 - **C9** Calvi, G. M., Pavese, A., Rasulo, A., Bolognini, D., (2005). Experimental and Numerical Studies on the Seismic Response of R.C. Hollow Bridge Piers, *Bulletin of Earthquake Engineering*, **3**, 267-297.
 - **D1** Dwairi, H.M., Kowalsky, M.J., Nau, J.M., (2007). Equivalent Damping in Support of Direct Displacement-Based Design, *Journal of Earthquake Engineering*, **11**, 512 – 530.
 - **D2** Dwairi, H.M., Kowalsky, M.J., (2006). Implementation of Inelastic Displacement Patterns in Direct Displacement-Based Design of Continuous Bridge Structures”, *Earthquake Spectra*, **22**(3), 631 – 662.
 - **F1** Faccioli, E., Paolucci, R., Rey, J., (2004). Displacement Spectra for Long Periods”, *Earthquake Spectra*, **20**(2), 347 – 376.
 - **F2** Faccioli, E., Villani, M., (2009). Seismic hazard mapping for Italy in terms of broadband Displacement Response Spectra”, *Earthquake Spectra*, **(25)**, 515.
 - **F3** FEMA, Federal Emergency Management Agency, (1997). *NEHRP Guidelines for the Seismic Rehabilitation of Buildings*, prepared by the Applied Technology Council.
 - **F4** FEMA, Federal Emergency Management Agency (2003). *Multi-hazard Loss Estimate Methodology (Earthquake Model)*. Technical Manual, Department of Homeland Security, Emergency Preparedness and Response Directorate, FEMA Mitigation Division, Washington, D.C.
 - **F5** Fajfar, P. and Krawinkler, H. (Editors), (1997). *Seismic Design Methodologies for the Next Generation of Codes*, Bled, Slovenia,

- Workshop on Seismic Design Methodologies for the Next Generation of Codes*, 436pp
- **F6** Frangopol, D. M., and Neves LC. (2004). Probabilistic performance prediction of deteriorating structures under different maintenance strategies: Condition, safety and cost. In Frangopol, D. M., Bruhwiler E, Faber MH and Adey B, (eds), *Life-Cycle Performance of Deteriorating Structures: Assessment, Design and Management*. ASCE, Reston, Virginia. 2004. 9-18.
 - **F7** Frangopol, D. M., and Liu, M. (2007). *Bridge network maintenance optimization using stochastic dynamic programming*. Journal of Structural Engineering-Asce, 133(12), 1772-1782.
 - **F8** FEMA, Federal Emergency Management Agency (1999). *HAZUS-MH Technical Manual*, Washington D.C.
 - **F9** FEMA, Federal Emergency Management Agency (2003). *HAZUS-MH Technical Manual*, Washington D.C.
 - **F10** Francese, R., Bondesan A., Centoze, J. Wardell, N., (2007). *Cartografia sismica della pianura della provincia di Treviso*, Istituto Nazionale di Oceanografia e Geofisica Sperimentale.
 - **G1** Grant, D.N., Blandon, C.A., Priestley, M.J.N., (2005). *Modelling Inelastic Response in Direct Displacement-Based Design*, Report 2005/03, IUSS Press, Pavia.
 - **G2** Gulkan, P., Sozen, M., (1974). Inelastic response of reinforced concrete structures to earthquake motion”, *ACI Journal*, **71**, 604 – 610.
 - **G3** Grendene M., Franchetti P., Tecchio G. and Modena C., (2006). Structural regularity of multi-span continuous bridges, *Proceedings of the 1st Conference on Advances in Bridge Engineering*, 26-28 June 2006, West London, UK.
 - **G4** Grendene M., Franchetti P., Modena C., (2012). Regularity Criteria for RC and PRC Multispan Continuous Bridges, *Journal of Bridge Engineering*, **17(4)**, 671-681.
 - **G4** Gasparini D. A. and Vanmarcke E.H., (1976). *Simulated earthquake motions compatible with prescribed response spectra*, MIT, pub. R76-4, 65pp.
 - **G5** Grendene, M., (2006). *Simplified Approach to expected seismic Damage for Existing RC Bridges*, Phd dissertation thesis, Padova.
 - **I1** Iwan, W.D., Gates, N.C., (1979). The effective period and damping of a class of hysteretic structures, *Earthquake Engineering and Structural Dynamics*, **7**, 199 – 211.
 - **J1** Jacobsen, L.S.,(1930). Steady forced vibrations as influenced by damping, *ASME Transactione*, **52(1)**, 169 – 181.
 - **J2** Jacobsen, L.S., “Damping in composite structures”, 1960. *Proceedings, 2nd World Conference on Earthquake Engineering*, Vol. 2, Tokyo and Kyoto, Japan, 1029 – 1044.
 - **J3** Jennings, P.C., (1968). Equivalent viscous damping for yielding structures, *ASCE Journal of Engineering Mechanics Division*, **94(1)**, 103 – 116.
 - **K1** Kowalsky, M.J., Priestley, M.J.N., Macrae, G.A., (1995), Displacement-

- based design of rc bridge columns in seismic regions, *Earthquake Engineering and Structural Dynamics*, **24**, 1623-1643.
- **K2** Kwan, W.P., Billington S.L., “Influence of hysteretic behavior on equivalent period and damping of structural system”, *ASCE Journal of Structural Engineering*, 129(5), p. 576 – 585.
 - **K3** Kowalsky, M.J., (2002). Displacement-based approach for the seismic design of continuous concrete bridges, *Earthquake Engineering and Structural Dynamics*, **31**, 719 – 747.
 - **K4** Krawinkler, H., (1999). Challenges and Progress in Performance-Based Earthquake Engineering, *Proceedings of the International Seminar on Seismic Engineering for Tomorrow*, November 26, 1999, Japan.
 - **K5** Kreslin, M. Fajfar P. (2012), The Extended N2 method considering higher mode effects in both plan and elevation, *Bulletin of Earthquake Engineering* **10(2)**, 695-715.
 - **K6** Karim K.R. and Yamazaki F., (2003). A simplified method of constructing fragility curves for highway bridges, *Earthquake Engineering and Structural Dynamics*, **32(10)**, 1603-1626.
 - **K7** Kowalsky, M. J. and Priestley, M.J.N., (2000). Improved analytical Model for Shear Strength of Circular Reinforced Concrete Columns in Seismic Regions. *ACI Structural Journal*, **97(3)**, 388-396.
 - **K8** Kent, D.C. and Park, R., (1971). Flexural members with confined concrete, *Journal of the Structural Division*, ASCE, **97**, 1969-1990.
 - **M1** Calvi, G.M., Sullivan, T.J., *A Model Code for the Displacement-Based Seismic Design of Structures*, DBD 09, Draft subject to public enquiry, IUSS Press, Pavia, 2009.
 - **M2** Miranda, E., Ruiz-García, J., (2002). Evaluation of approximate methods to estimate maximum inelastic displacement demands, *Earthquake Engineering and Structural Dynamics*, **31**, 539 – 560.
 - **M3** Mander, J.P., Priestley, M.J.N., Park, R., (1998). Theoretical stress-strain model for confined concrete, *Journal Structural Engineering ASCE*, **114(8)**, 1804 – 1826.
 - **M4** Mahin, S.A., Boroschek, R.L., “Influence of Geometric Nonlinearities on the Seismic Response of Bridge Structures”, *Proceedings, 3rd NSF Workshop on Bridge Engineering Research in Progress*, La Jolla, 1992, p. 317 – 320.
 - **M5** MacRae, G.M., Priestley, M.J.N., Tao, J., *P-Δ Design in Seismic Regions*, Report SSRP-93-05, University of California, San Diego, 1993.
 - **M6** Mouroux, P. and Le Brun Benoit, (2006). Special Issue: Earthquake Scenarios for European Cities - The RISK-UE Project, *Bulletin of Earthquake Engineering*, **4(4)**, 323-339.
 - **M7** Meletti C., Montaldo V., 2007. *Stime di pericolosità sismica per diverse probabilità di superamento in 50 anni: valori di ag*. Progetto DPC-INGV S1, Deliverable D2, <http://esse1.mi.ingv.it/d2.html>
 - **M8** Miranda, P.A., Calvi, G. M., Pinho, R. and Priestley, J.M., (2005). Displacement-Based Assessment of RC Columns with Limited Shear Resistance, IUSS Press, Pavia.

- **M9** Menegotto M. and Pinto P.E., (1973). Method of Analysis for Cyclically Loaded R.C. Plane Frames Including Change in Geometry and Non-Elements Behavior of Elements under Combined Normal Force and Bending. *Proc. of IABSE Symposium on Resistance and Ultimate Deformability of Structures Acted on by Well Defined Repeated Loads*, 13, 15-22.
- **N1** Newmark, N.M., Hall, W.J., (1982). *Earthquake Spectra and Design*, EERI Monograph, Oakland, USA,
- **N2** Nielson B., (2003). *Bridge Seismic Fragility – Functionality Relationships: A Requirement for Loss Estimation in Mid-America*, Georgia Institute of Technology – CBE Institute, Texas A&M University.
- **O1** California Office of Emergency Services, (1995). *Vision 2000: Performance Based Seismic Engineering of Buildings*, Structural Engineers Association of California, Sacramento, USA.
- **O2** Ortiz Restrepo Jc. (2006) *Displacement-based design of continuous bridge under transverse seismic excitation*. Master dissertation, ROSE School, Pavia, Italy
- **P1** Priestley, M.J.N., Calvi, G.M., Kowalsky, M.J., (2007). *Displacement-Based Seismic Design of Structures*, IUSS Press, Pavia.
- **P2** Priestley, M.J.N., (2000), Performance based seismic design, *Keynote Address, 12th world conference on earthquake engineering*, Auckland, New Zealand, Paper n. 2831
- **P3** Priestley, M.J.N., (1993), *Myths and Fallacies in Earthquake Engineering-Conflicts between Design and Reality*, *Bulletin NZSEE*, **26(3)**, 329-341.
- **P4** Priestley, M.J.N., Seible, F., Calvi, G.M., (1996). *Seismic Design and Retrofit of Bridges*, Wiley, New York.
- **P5** Priestley, M.J.N., Kowalsky, M.J., (2000), Direct Displacement-Based Seismic Design of Concrete Buildings, *Bulletin NZNSEE*, **33(4)**, 1998, 421-444.
- **P6** Priestley, M.J.N., “Brief Comments on Elastic Flexibility of Reinforced Concrete Frames, and Significance to Seismic Design”, *Bulletin NZSEE*, 31(4), 1998, p. 246 – 259.
- **P7** Paulay, T., Priestley, M.J.N., *Seismic Design of Reinforced Concrete and Masonry Building*, Wiley, New York, 1992.
- **P8** Priestley, M.J.N., Calvi, G.M., “Direct Displacement-Based Seismic Design of Bridges”, *Proceedings, ACI Special Seminar on Seismic Design of Bridges*, San Diego, 2003.
- **P9** Priestley, M.J.N., (1997). Displacement-based seismic assessment of reinforced concrete buildings, *Journal of Earthquake Engineering*, **1(1)**, 157-192.
- **P10** Park, R and Paulay, T., (1976). *Reinforced Concrete Structures*, Wiley, 800pp
- **P11** Priestley, M.J.N., (2005). Viscous damping in seismic design and analysis, *Journal of Earthquake Engineering*, **9(2)**, 229-255.
- **P14** Pampanin, S., Christopoulos, C. and Priestley, M.J.N., (2002). *Residual Deformations in the Performance-based Seismic Assessment of Frame*

- Structures*, ROSE Research Report N. 2002/2, IUSS Press, Pavia, 203pp.
- **P15** Paksoy, A.M. and Petrini L., (2012). A displacement-based procedure for seismic assessment of reinforced concrete bridges. *Proceedings of the 6th International Conference on Bridge Maintenance, Safety and management-IABMAS 2012*, Stresa, Lake Maggiore, Italy, 8-12 July 2012.
 - **S1** Shibata A. and Sozen M, (1976). Substitute-structure method for seismic design in reinforced concrete, *Journal of the structural division ASCE*, **102(1)** 1-18.
 - **S2** Shinozuka M., Feng M.Q., Kim H.-K. and Kim S.-H.,(2000). Nonlinear Static Procedure for Fragility Curve Development. *Journal of Engineering Mechanics*, **126(12)**, 1287-1295.
 - **S3** Strasser, F. O., Bommer, J. J., Sesetyan, K., Erdik, M. Cagnan, Z., Irizarry, J. Goula, X., Lucantoni, A., Sabetta, F., Bal, I.E, Crowley, H. and Lindholm, C., (2008). A comparative study of European loss estimation tools for an earthquake scenario in Istanbul. *Journal of Earthquake Engineering*, **12(S2)**, 246-256.
 - **S4** Shinozuka, M., (1998). Development of Bridge Fragility Curves. Technical report MCEER, University of Southern California.
 - **S5** Sezen, H. and Moehle, J.P., (2004). Shear Strength Model for lightly reinforced concrete columns. *Journal of Structural Engineering*, **130(11)**, 1692-1703
 - **T1** Tecchio G., Grendene M., Donà M., (2011). Predizione dell'errore del metodo DDBD applicato a ponti in c.a. isostatici, *Proceedings of the XIV-Italian Conference on Earthquake Engineering-ANIDIS*, 18-22 September 2011, Bari, Italy (in Italian).
 - **T2** Tecchio G., Donà M., da Porto F., Carturan F. and Modena C., (2012). DisplacementBasedDesign for transverse response of rc bridges: evaluation of iterative and direct procedures. *Proceedings of the 15th World Conference on Earthquake Engineering-WCEE*, 24-28 September 2012, Lisbon, Portugal.
 - **T3** Thompson P.D., Small E. P., Johnson M and Marshall AR. *The Pontis bridge management system*. *Structural Engineering International*, 1998, 8(4): 303-308.
 - **T4** Tarque N., Crowley H., Pinho R., Varum H. (2012). Displacement-Based Fragility Curves for Seismic Assessment of Adobe Buildings in Cusco, Peru. *Earthquake Spectra*, **28(2)**, 759-794.
 - **T5** Tecchio G., Grendene M., Modena C. (2012). Pounding Effects in Simply Supported Bridges Accounting for Spatial Variability of Ground Motion: A Case Study. *Advances in Civil Engineering* (**2012**), doi:10.1155/2012/267584.
 - **V1** Vamvatsikos D. and Cornell C.A., (2002). Incremental dynamic analysis, *Earthquake Engineering and Structural Dynamics*, **31(3)**, 491-514.
 - **X1** Italian Ministry of Infrastructure, (2008). *D.M. Infrastrutture 14 gennaio 2008- NTC '08, Nuove Norme Tecniche per le Costruzioni*, published on S.O. n. 30 in G.U. n. 29.
 - **X2** Comité Européen de Normalisation, (2004). *Eurocode 8 - Design of Structures for Earthquake Resistance - Part 1: General Rules, Seismic*

- Actions and Rules for Buildings*, EN 1998-1, CEN, Brussels, Belgium, 222 pp.
- **X3** Comité Européen de Normalisation, (1998). *Eurocode 8 - Design of Structures for Earthquake Resistance - Part 1: General Rules, Seismic Actions and Rules for Buildings*, prEN 1998-1, CEN, Brussels, Belgium.
 - **X4** International Code Council, (2006). *International Building Code*, Thomson Delmar Learning, 663 pp.
 - **X5** NZS-3101, (1995). *New Zealand Standard. Concrete Structures Standard, Part 1*, Wellington, New Zealand.
 - **X6** Turkish Earthquake Code, (2007). *Specifications for the buildings to be constructed in earthquake hazardous areas*, Ministry of Public Works and Settlement, Ankara, Turkey.
 - **Y1** McKenna F., Mazzoni S., Scott M. H., Fenves G. L., et al. Opensees, (2007). *Open System for Earthquake Engineering Simulation*, Pacific Earthquake Engineering Research Center, US, version 1.7.4, opensees.berkeley.edu.
 - **W1** Wald, D. J., and T. I. Allen, (2007). Topographic slope as a proxy for seismic site conditions and amplification, *Bull., Seism. Soc. Am*, **97(5)**, 1379-1395.
 - **Z1** Zhao, J. and Sritharan, S., (2007). Modeling of strain penetration effects in fiber-based analysis of reinforced concrete structures. *ACI Structural Journal*, **104(2)**, 133-141.

APPENDIX A

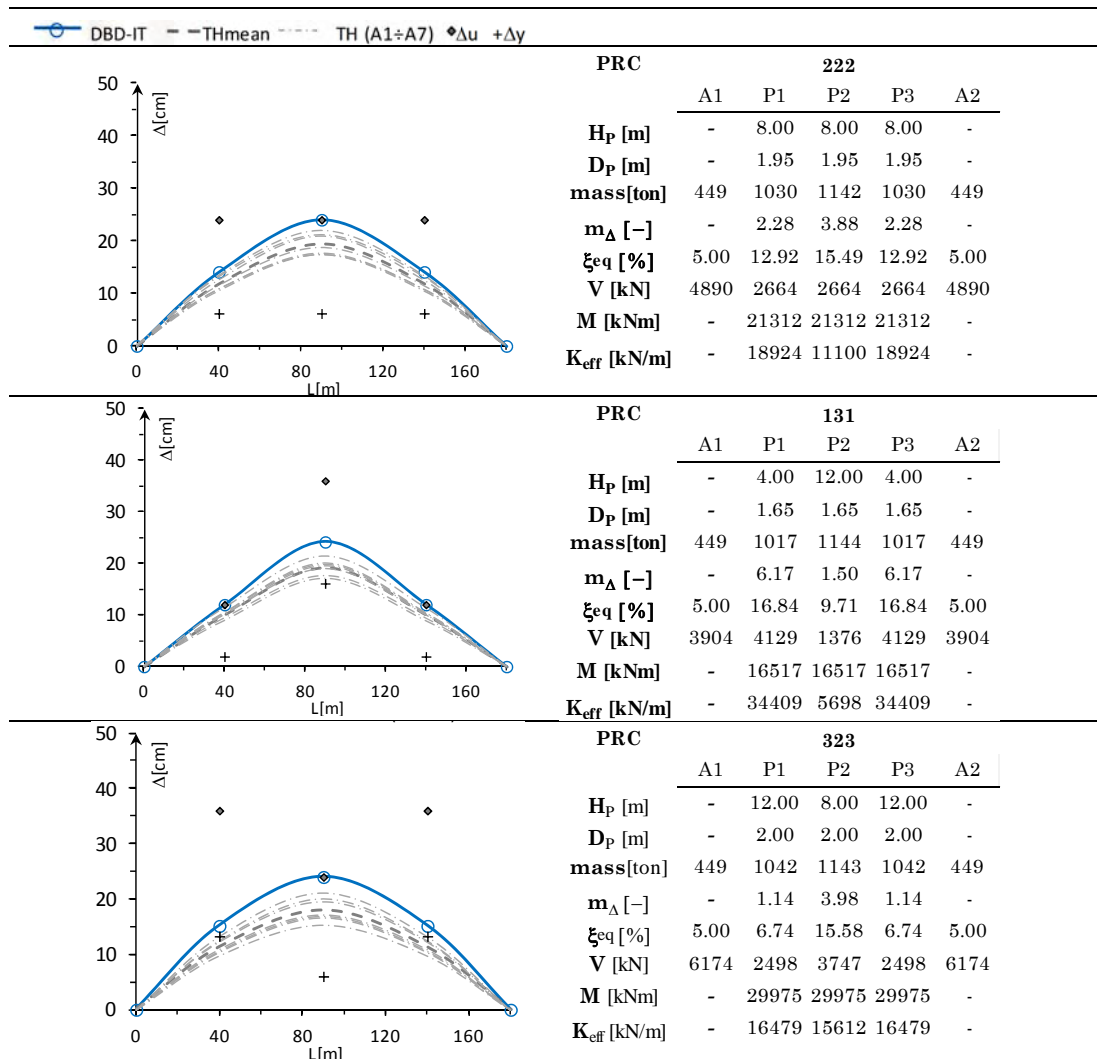
DBD PROCEDURES FOR TRANSVERSE RESPONSE OF CONTINUOUS BRIDGES: (DBD-IT) AND (DBD- DEM) RESULTS AND NLTH VERIFICATIONS.

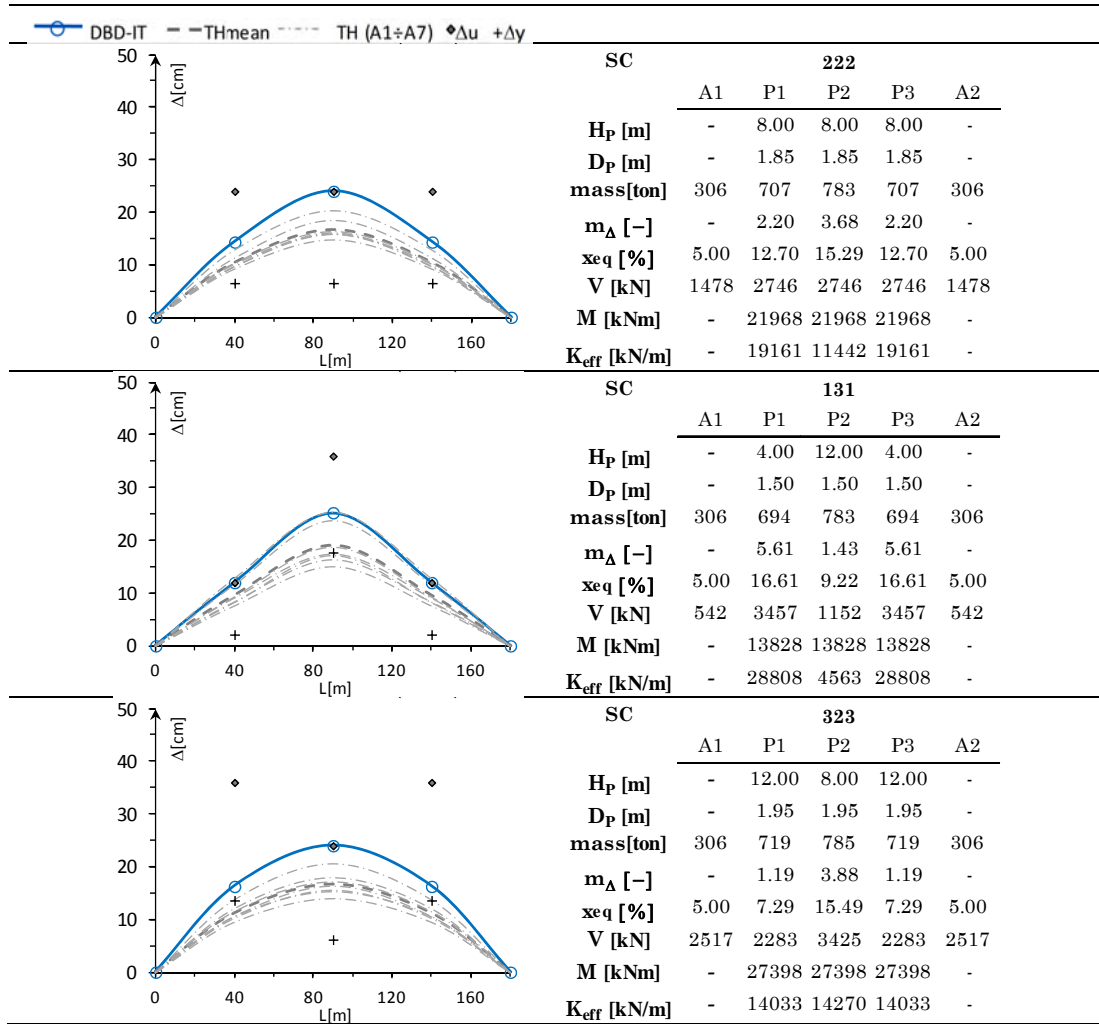
A.1 DESIGN RESULTS (DBD-IT) PROCEDURE. BRIDGES SERIES 3

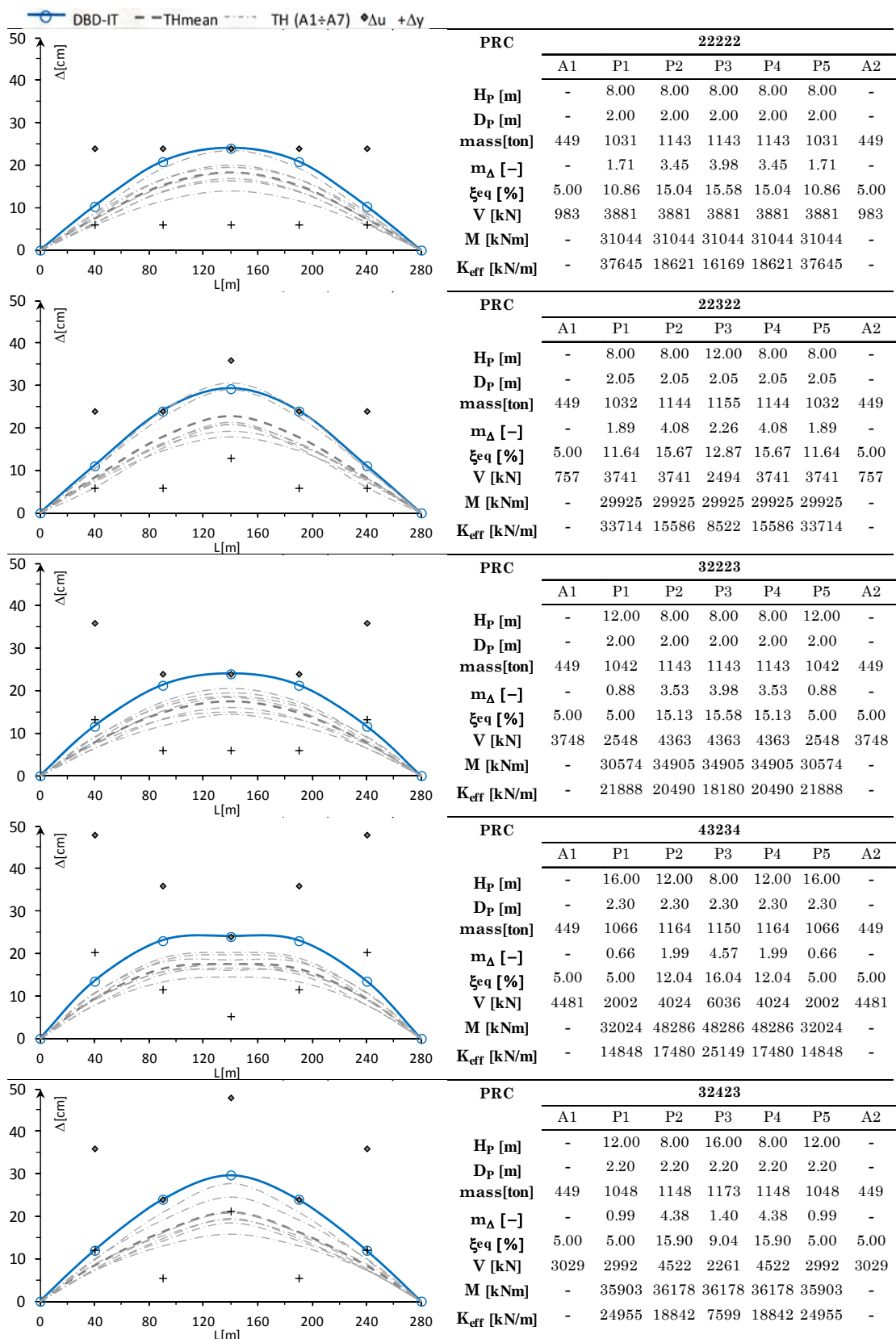
Tab. A.1 – *Substitute SDOF parameters for bridges of Series 3, $\theta_L=3\%$*

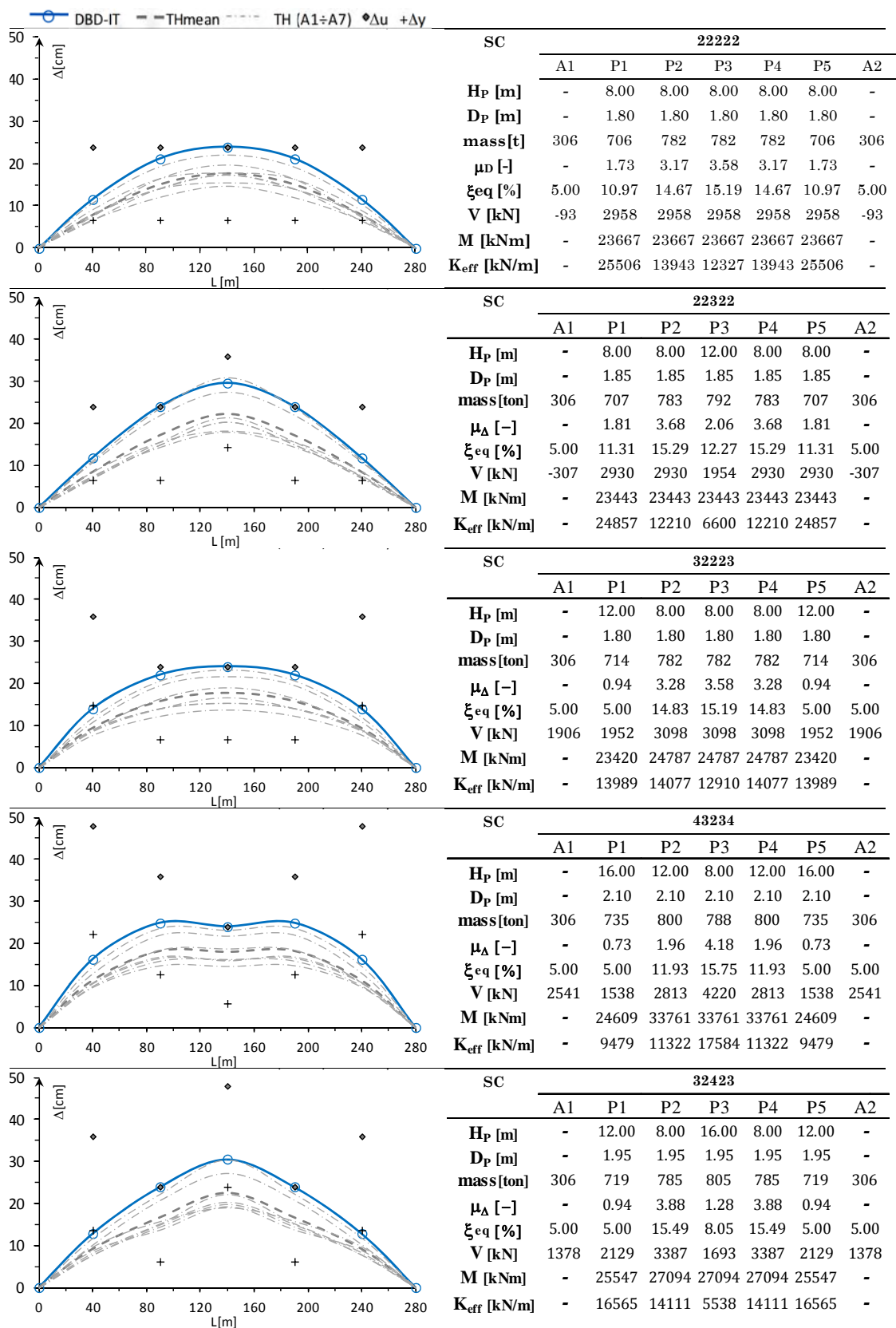
	M_{eff} [ton]	H_{eff} [m]	Δ_{eff}^d [m]	$\Delta_{y,eff}$ [m]	$\mu_{D,eff}$ [-]	ξ_{eff} [%]	T_{eff} [s]	K_{eff} [kN/m]	V_{base} [kN]	x [%]
PRC222	3424	9.16	0.23	0.157	1.50	9.68	1.35	74061	17772	55.6
PRC131	3351	8.98	0.24	0.172	1.41	9.13	1.37	69984	17442	45.2
PRC323	3467	11.22	0.23	0.182	1.25	7.82	1.22	91457	21092	59.1
SC222	2357	9.16	0.24	0.136	1.74	11.00	1.42	46283	11194	26.1
SC131	2267	9.06	0.25	0.112	2.23	12.80	1.59	35260	9151	11.8
SC323	2417	11.24	0.23	0.167	1.40	9.07	1.32	54591	13025	39.1
PRC22222	5384	9.48	0.24	0.094	2.57	13.64	1.58	85118	21368	9.3
PRC22322	5306	10.61	0.28	0.117	2.37	13.18	1.78	65824	18970	8.1
PRC32223	5455	10.46	0.24	0.146	1.66	10.62	1.44	103329	25682	29.7
PRC43234	5602	13.39	0.25	0.164	1.51	9.78	1.44	106780	27049	33.3
PRC32423	5356	12.67	0.27	0.174	1.56	10.07	1.59	83895	23347	26.3
SC22222	3735	9.46	0.25	0.103	2.44	13.34	1.62	56241	14606	-1.2
SC22322	3666	10.59	0.28	0.122	2.31	13.01	1.80	44680	13061	-4.6
SC32223	3831	10.51	0.26	0.151	1.69	10.79	1.53	64868	17011	22.5
SC43234	3950	13.51	0.27	0.178	1.50	9.68	1.53	66316	18006	27.7
SC32423	3705	12.69	0.28	0.171	1.62	10.42	1.64	54411	15481	18.1

Tab. A.2 – DBD-IT results vs TH verification for bridges of the Series 3, $\theta_L=3\%$







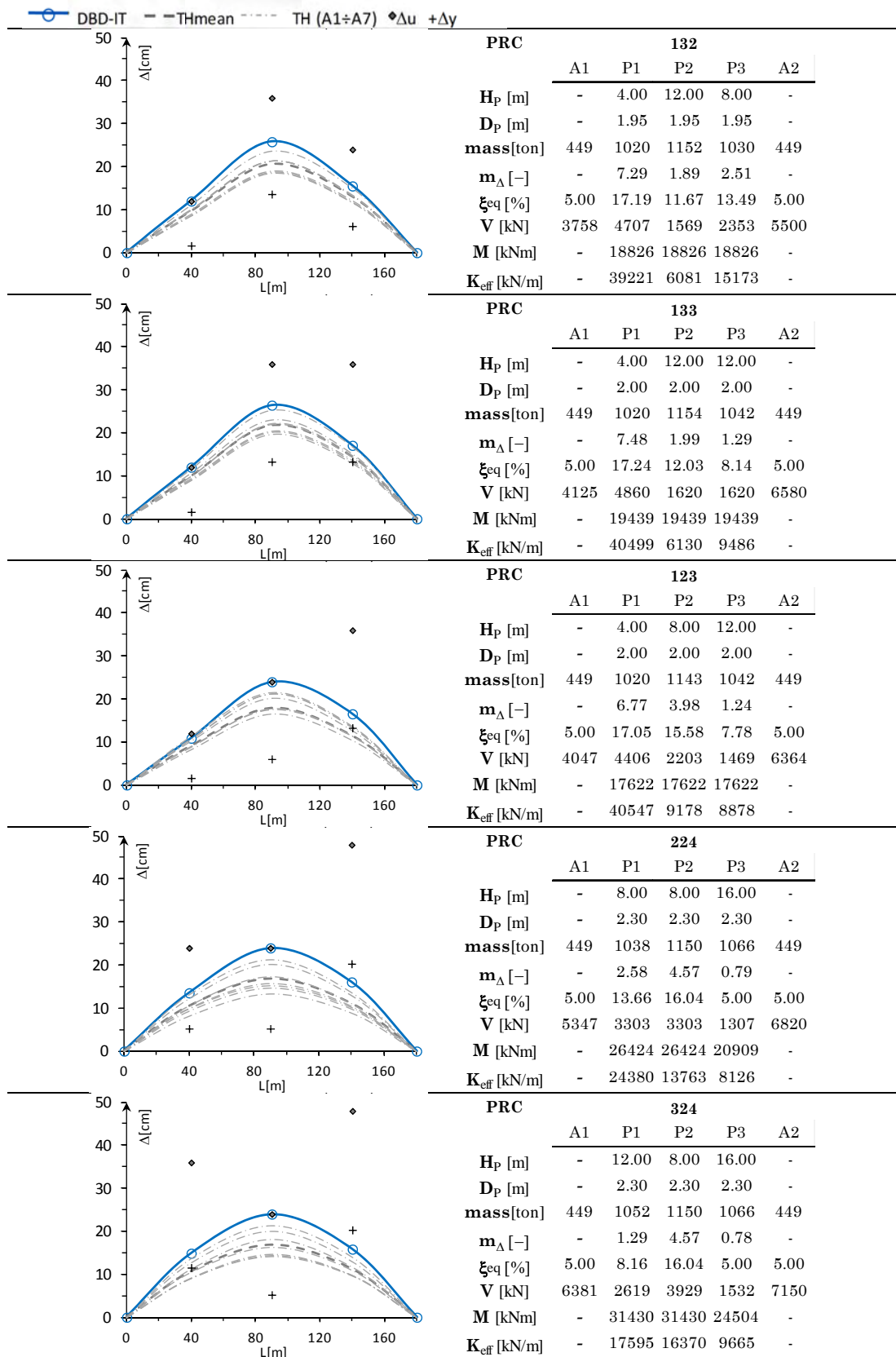


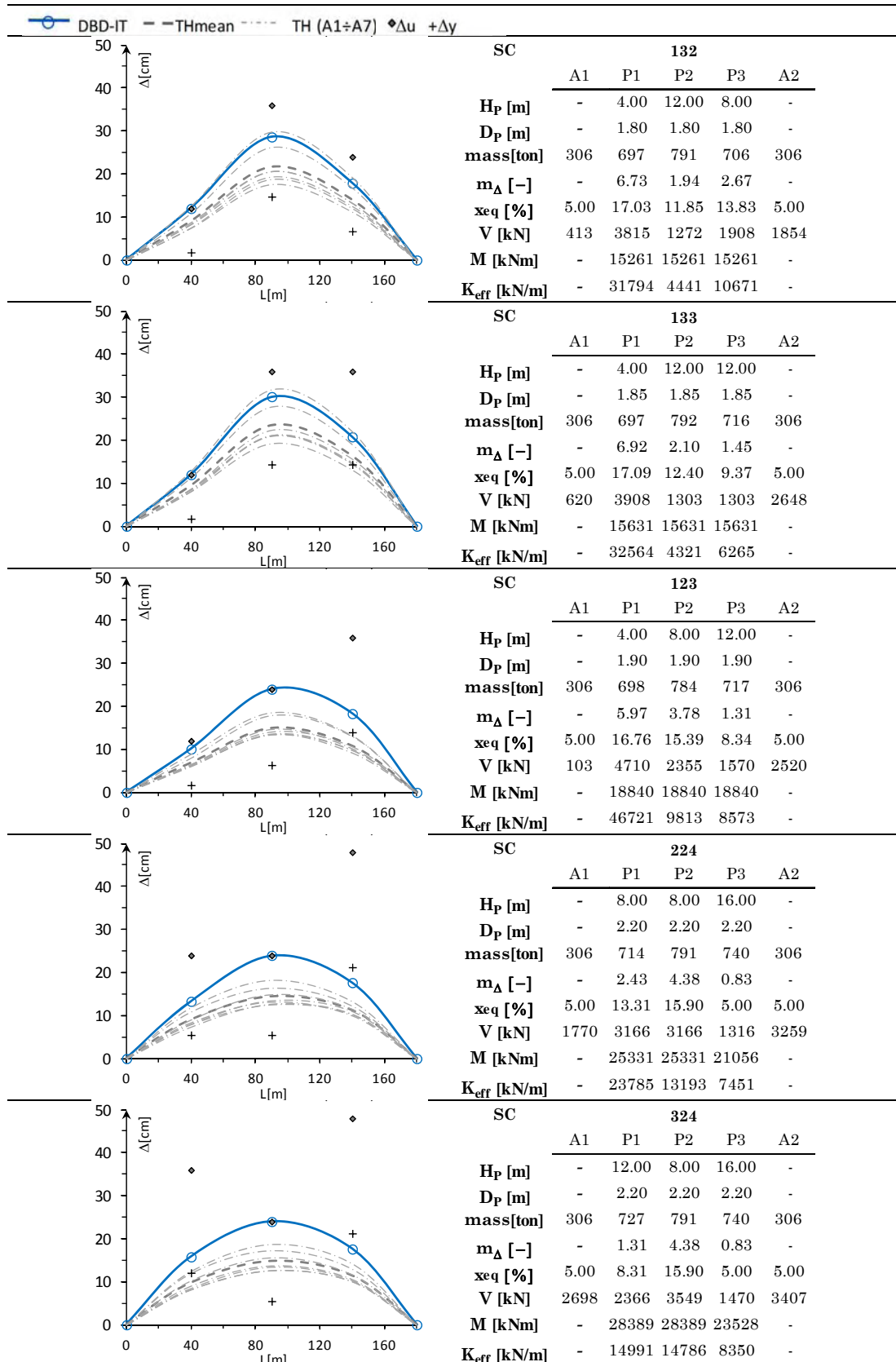
A.2 DESIGN RESULTS (DBD-IT) PROCEDURE. BRIDGES OF SERIES 4

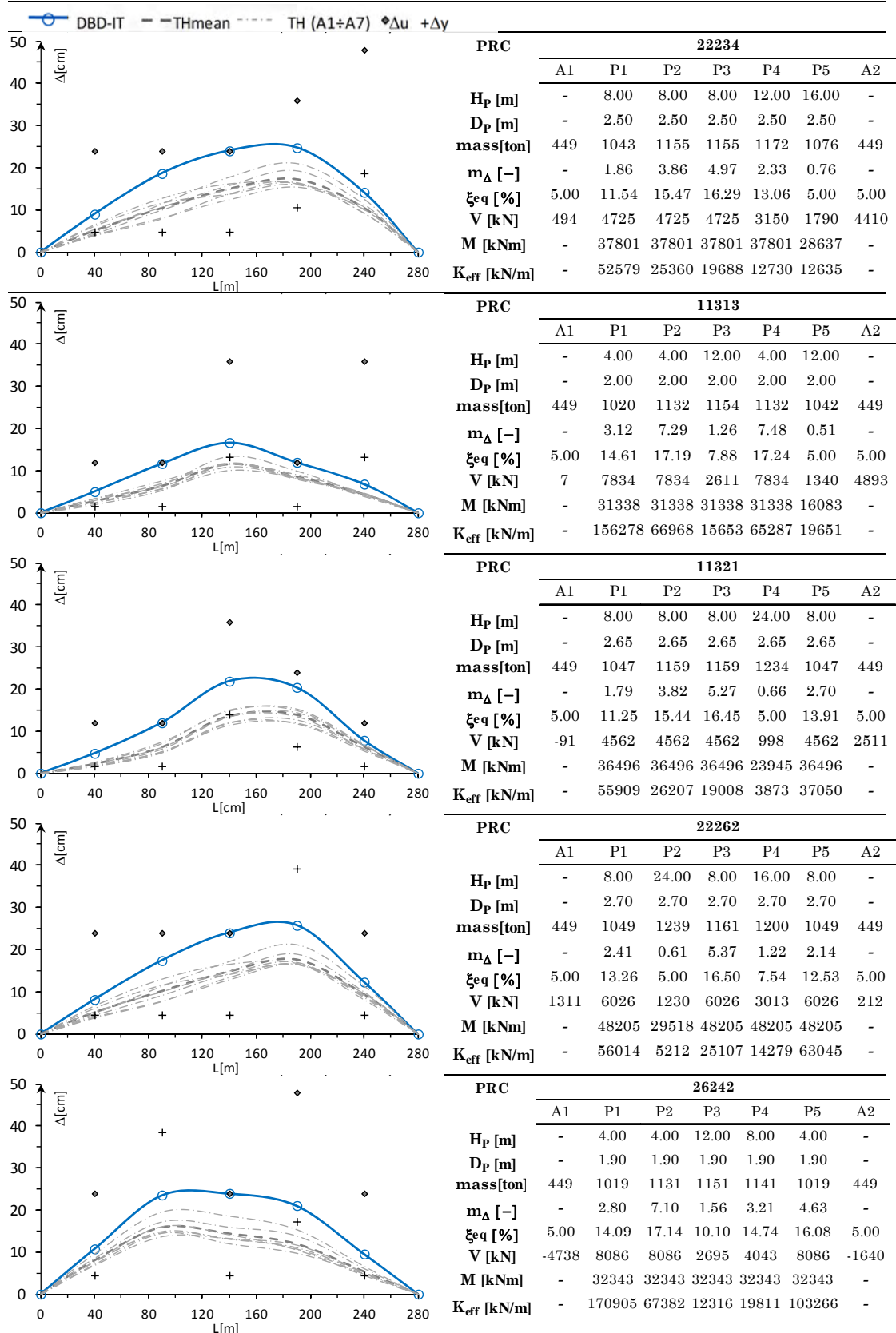
Tab. A.3 –Substitute SDOF parameters for bridges of Series 4, $\theta_L=3\%$

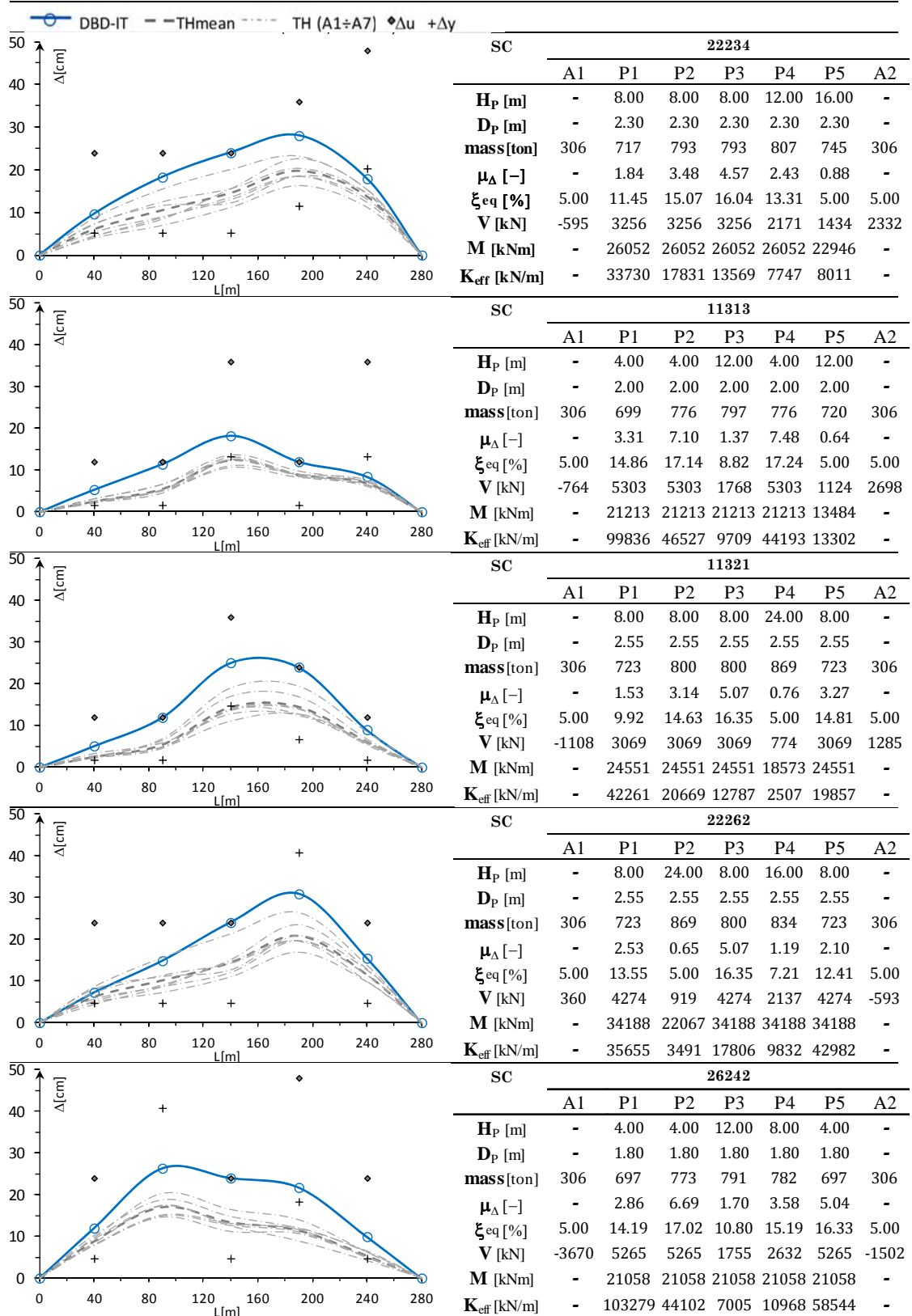
	M_{eff} [ton]	H_{eff} [m]	$\Delta^{\text{d,eff}}$ [m]	$\Delta_{y,\text{eff}}$ [m]	$\mu_{\Delta,\text{eff}}$ [-]	ξ_{eff} [%]	T_{eff} [s]	K_{eff} [kN/m]	V_{base} [kN]	\mathbf{x} [%]
PRC222	3424	9.16	0.23	0.157	1.50	9.68	1.35	74061	17772	55.6
PRC131	3351	8.98	0.24	0.172	1.41	9.13	1.37	69984	17442	45.2
PRC323	3467	11.22	0.23	0.182	1.25	7.82	1.22	91457	21092	59.1
PRC132	3379	10.03	0.25	0.188	1.33	8.48	1.38	69959	17886	51.9
PRC133	3390	11.15	0.25	0.201	1.24	7.77	1.35	73530	18805	56.8
PRC123	3403	9.38	0.24	0.174	1.37	8.79	1.33	75945	18488	56.9
SC222	2357	9.16	0.24	0.136	1.74	11.00	1.42	46283	11194	26.1
SC131	2267	9.06	0.25	0.112	2.23	12.80	1.59	35260	9151	11.8
SC323	2417	11.24	0.23	0.167	1.40	9.07	1.32	54591	13025	39.1
SC132	2293	10.12	0.28	0.156	1.77	11.16	1.67	32467	9262	24.3
PRC22234	5476	11.67	0.24	0.129	1.89	11.66	1.50	96155	24019	20.8
PRC11313	5317	8.88	0.16	0.072	2.25	12.84	1.04	195848	32355	15.4
PRC11321	5405	14.06	0.24	0.099	2.45	13.36	1.56	87789	21666	11.3
PRC22262	5497	15.54	0.24	0.116	2.05	12.23	1.48	98853	23843	6.5
PRC26242	5051	9.06	0.22	0.109	1.97	11.98	1.34	111460	24618	-26.0
SC22234	3806	11.87	0.26	0.128	2.05	12.24	1.63	56210	15111	11.7
SC11313	3687	9.04	0.17	0.069	2.48	13.43	1.10	119441	20735	9.5
SC11321	3624	14.70	0.26	0.103	2.55	13.59	1.71	49111	13227	1.4
SC22262	3821	15.76	0.25	0.120	2.08	12.33	1.57	61345	15643	-1.4
SC26242	3402	9.16	0.25	0.131	1.87	11.57	1.50	59305	15008	-35.1

Tab. A.4 – DBD-IT results vs TH verification for bridges of Series 4, $\theta_L=3\%$







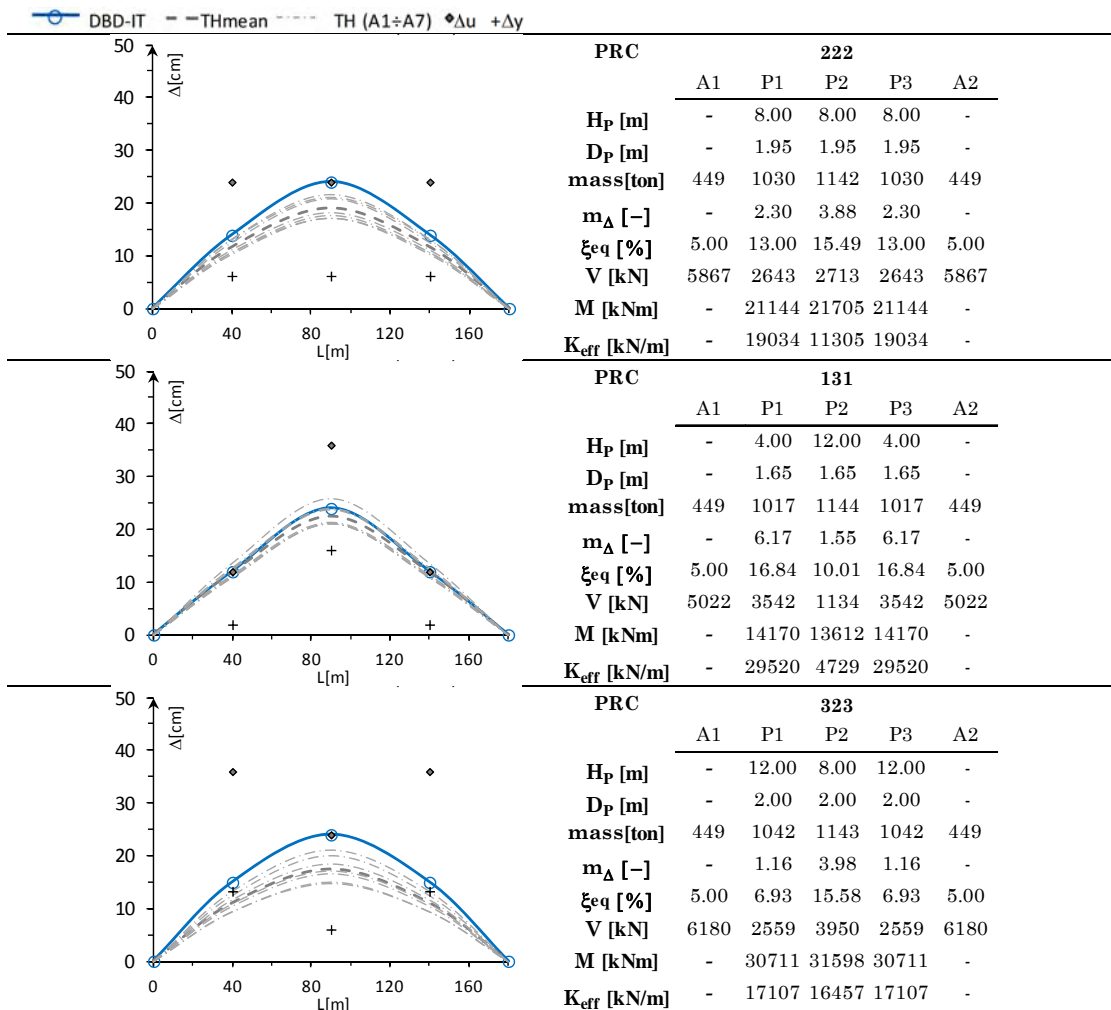


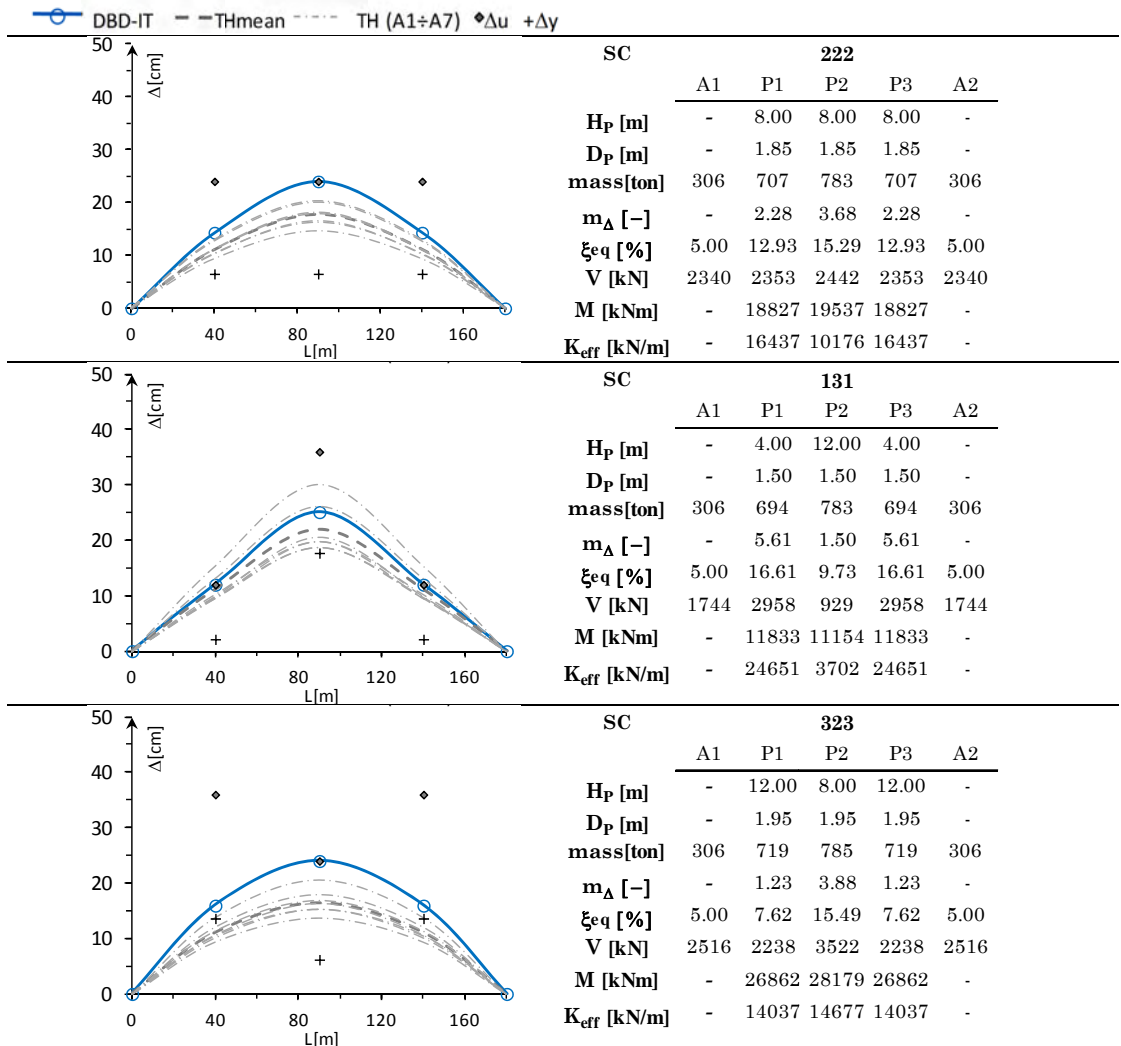
A.3 DESIGN RESULTS (DBD-DEM) PROCEDURE. BRIDGES SERIES 3

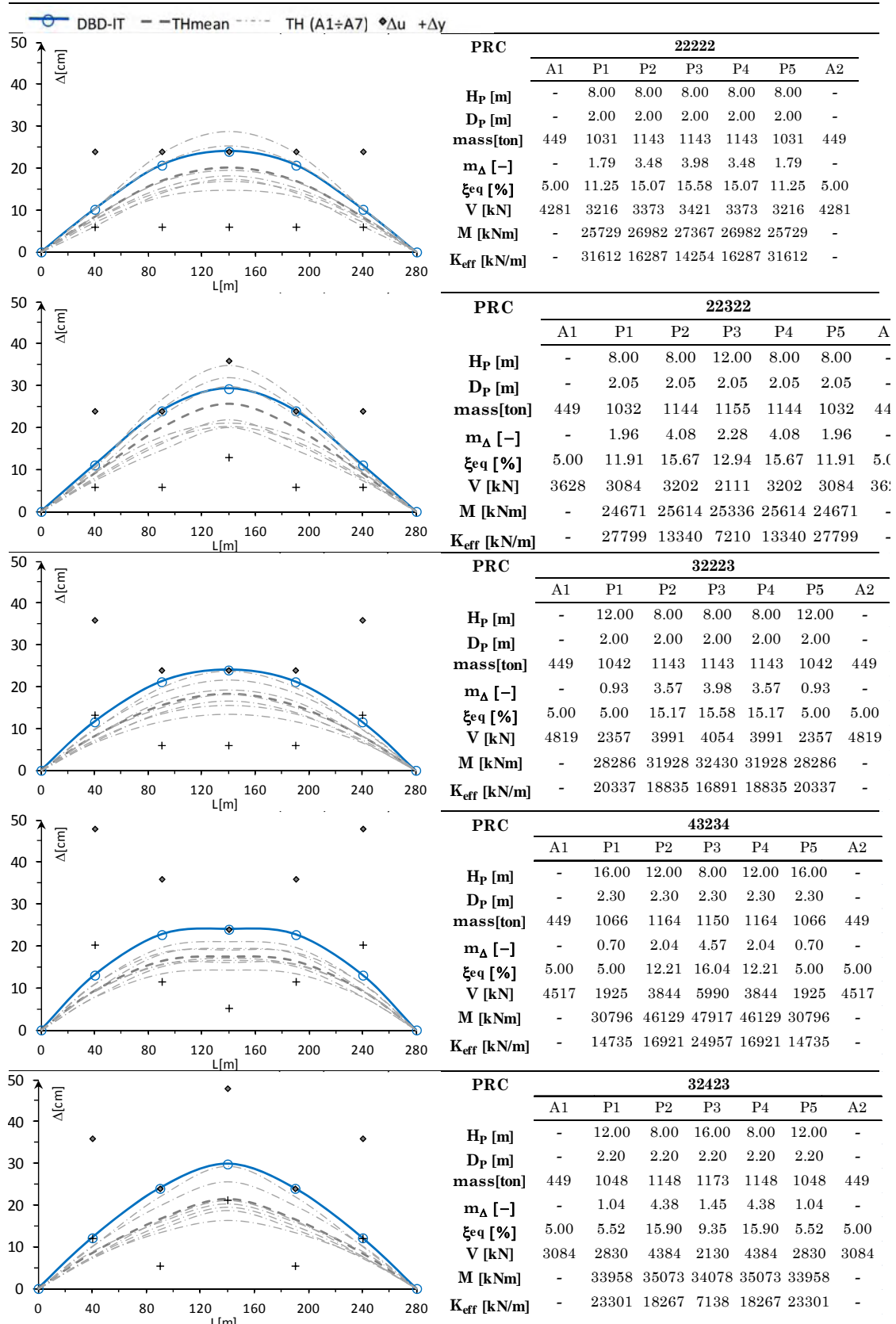
Tab. A.5 –Substitute SDOF parameters for bridges of Series 3, $\theta_L=3\%$

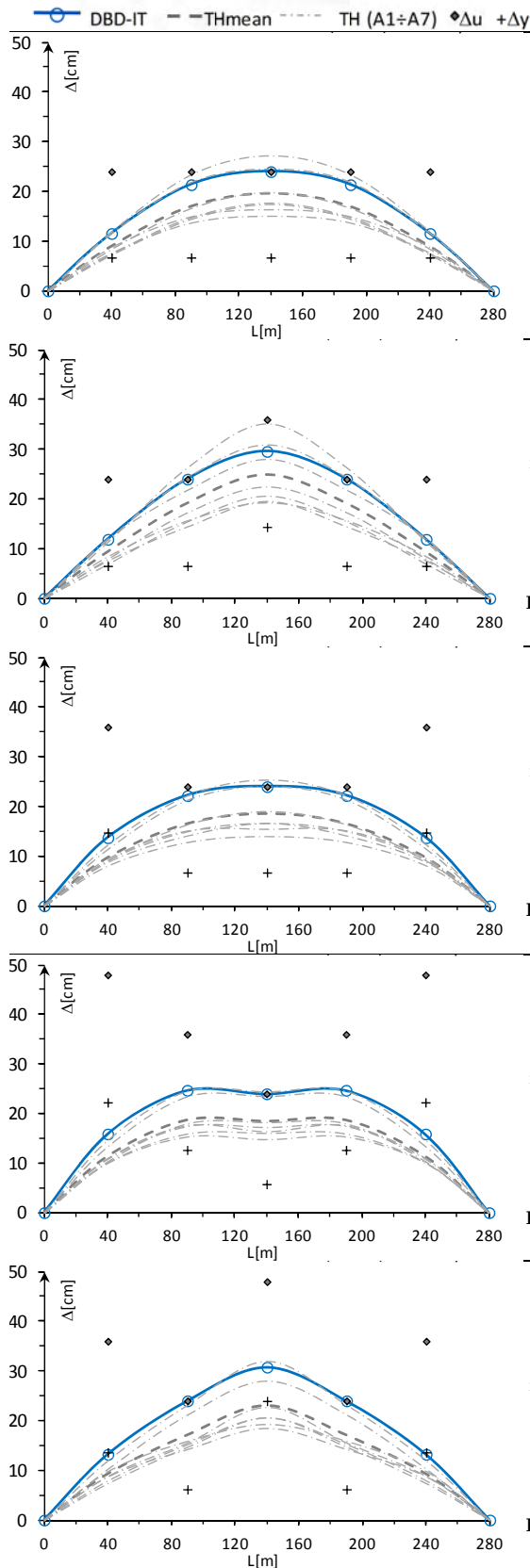
	M_{eff} [ton]	H_{eff} [m]	$\Delta^{\text{d,eff}}$ [m]	$\Delta_{y,\text{eff}}$ [m]	$\mu_{\text{D,eff}}$ [-]	ξ_{eff} [%]	T_{eff} [s]	K_{eff} [kN/m]	V_{base} [kN]	x [%]
PRC222	3424	9.16	0.23	0.157	1.50	9.68	1.35	74061	17772	55.6
PRC131	3351	8.98	0.24	0.172	1.41	9.13	1.37	69984	17442	45.2
PRC323	3467	11.22	0.23	0.182	1.25	7.82	1.22	91457	21092	59.1
SC222	2370	9.15	0.24	0.156	1.54	9.93	1.40	48063	11829	39.6
SC131	2241	9.14	0.26	0.164	1.57	10.11	1.51	38903	10333	33.7
SC323	2428	11.25	0.24	0.171	1.39	8.94	1.33	53855	13031	38.6
PRC22222	5405	9.47	0.25	0.150	1.65	10.57	1.47	99079	25161	34.0
PRC22322	5317	10.61	0.28	0.174	1.62	10.43	1.67	75227	21938	33.1
PRC32223	5492	10.47	0.25	0.160	1.55	9.99	1.44	103981	26387	36.5
PRC43234	5648	13.42	0.25	0.166	1.53	9.87	1.47	102530	26561	34.0
SC22222	3759	9.46	0.25	0.136	1.86	11.54	1.55	61517	16093	22.3
SC22322	3664	10.60	0.29	0.158	1.81	11.34	1.75	47504	14104	21.4
SC32223	3869	10.53	0.26	0.161	1.62	10.39	1.54	64190	17229	28.6
SC43234	4009	13.59	0.28	0.181	1.55	10.03	1.64	59023	16961	28.8
SC32423	3699	12.73	0.29	0.181	1.58	10.21	1.68	51800	15218	20.0

Tab. A.6 – DBD-DEM results vs TH verification for bridges of Series 3, $\theta_L=3\%$









	SC 22222						
	A1	P1	P2	P3	P4	P5	A2
H_P [m]	-	8.00	8.00	8.00	8.00	8.00	-
D_P [m]	-	1.80	1.80	1.80	1.80	1.80	-
mass[ton]	306	706	782	782	782	706	306
m_Δ [-]	-	1.79	3.21	3.58	3.21	1.79	-
ξ_{eq} [%]	5.00	11.24	14.73	15.19	14.73	11.24	5.00
V [kN]	1791	2451	2530	2550	2530	2451	1791
M [kNm]	-	19609	20238	20399	20238	19609	-
K_{eff} [kN/m]	-	21232	11840	10625	11840	21232	-

	SC 22322						
	A1	P1	P2	P3	P4	P5	A2
H_P [m]	-	8.00	8.00	12.00	8.00	8.00	-
D_P [m]	-	1.85	1.85	1.85	1.85	1.85	-
mass[ton]	306	707	783	792	783	707	306
m_Δ [-]	-	1.86	3.68	2.11	3.68	1.86	-
ξ_{eq} [%]	5.00	11.55	15.29	12.42	15.29	11.55	5.00
V [kN]	1507	2353	2407	1569	2407	2353	1507
M [kNm]	-	18826	19259	18823	19259	18826	-
K_{eff} [kN/m]	-	19810	10031	5304	10031	19810	-

	SC 32223						
	A1	P1	P2	P3	P4	P5	A2
H_P [m]	-	12.00	8.00	8.00	8.00	12.00	-
D_P [m]	-	1.80	1.80	1.80	1.80	1.80	-
mass[ton]	306	714	782	782	782	714	306
m_Δ [-]	-	1.01	3.37	3.58	3.37	1.01	-
ξ_{eq} [%]	5.00	5.13	14.94	15.19	14.94	5.13	5.00
V [kN]	2464	1801	2881	2936	2881	1801	2464
M [kNm]	-	21618	23049	23490	23049	21618	-
K_{eff} [kN/m]	-	13134	12988	12234	12988	13134	-

	SC 43234						
	A1	P1	P2	P3	P4	P5	A2
H_P [m]	-	16.00	12.00	8.00	12.00	16.00	-
D_P [m]	-	2.10	2.10	2.10	2.10	2.10	-
mass[ton]	306	735	800	788	800	735	306
m_Δ [-]	-	0.83	2.08	4.18	2.08	0.83	-
ξ_{eq} [%]	5.00	5.00	12.34	15.75	12.34	5.00	5.00
V [kN]	2439	1454	2550	4075	2550	1454	2439
M [kNm]	-	23264	30606	32603	30606	23264	-
K_{eff} [kN/m]	-	9154	10323	16981	10323	9154	-

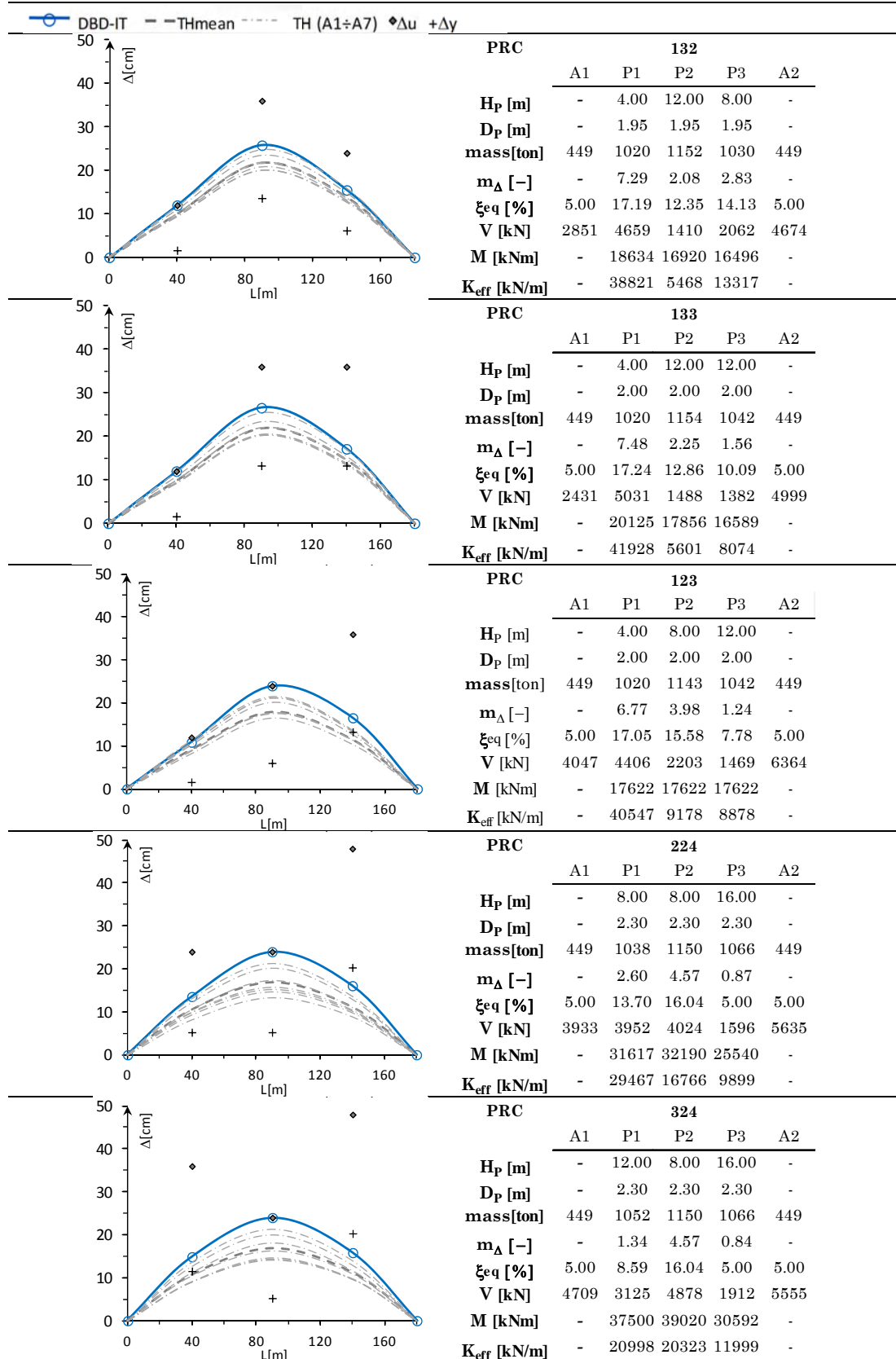
	SC 32423						
	A1	P1	P2	P3	P4	P5	A2
H_P [m]	-	12.00	8.00	16.00	8.00	12.00	-
D_P [m]	-	1.95	1.95	1.95	1.95	1.95	-
mass[ton]	306	719	785	805	785	719	306
m_Δ [-]	-	0.99	3.88	1.33	3.88	0.99	-
ξ_{eq} [%]	5.00	5.00	15.49	8.54	15.49	5.00	5.00
V [kN]	1521	2087	3225	1552	3225	2087	1521
M [kNm]	-	25048	25798	24825	25798	25048	-
K_{eff} [kN/m]	-	15773	13436	5040	13436	15773	-

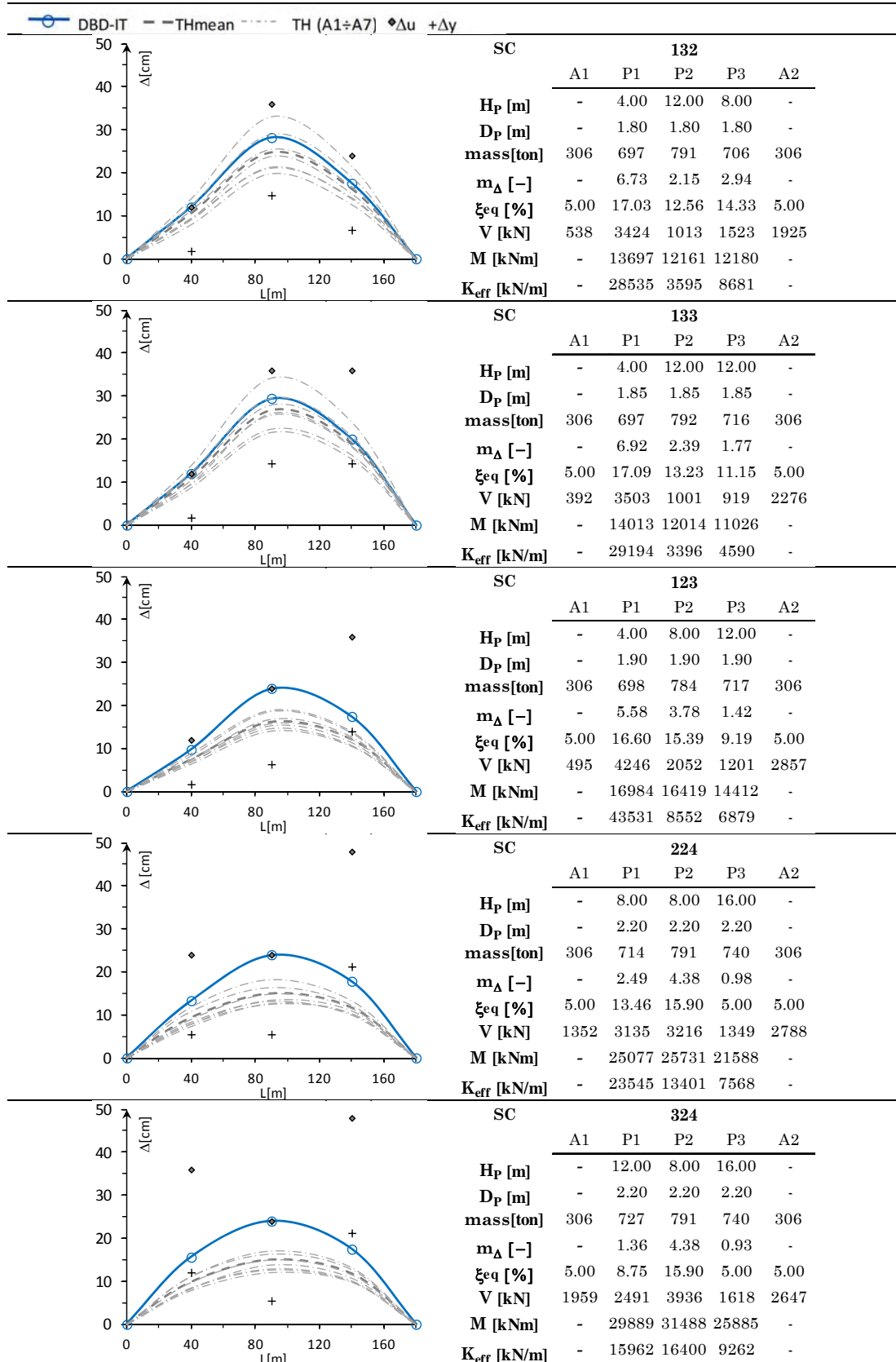
A.4 DESIGN RESULTS (DBD-DEM) PROCEDURE. BRIDGES SERIES 4

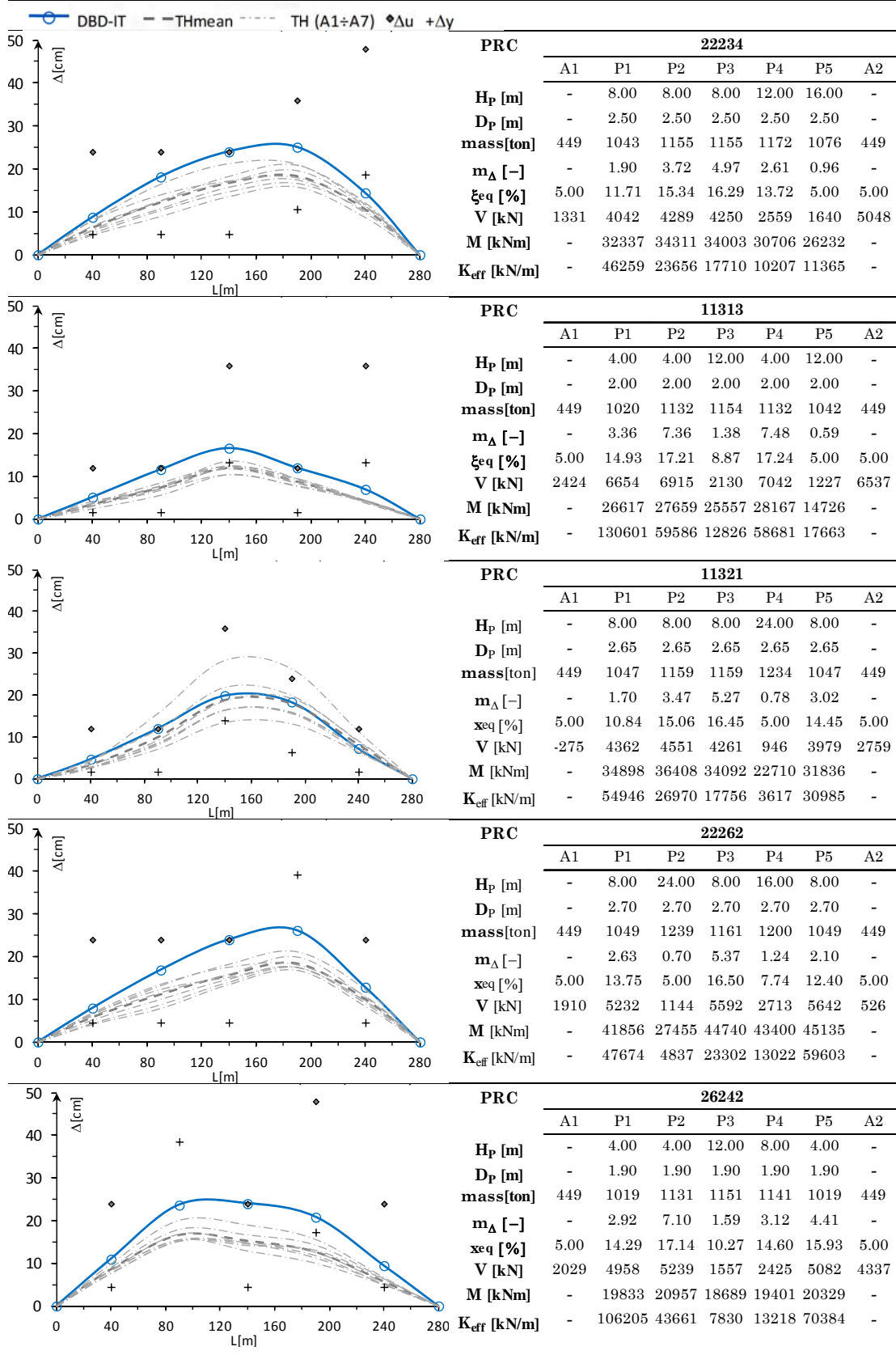
Tab. A.7 –Substitute SDOF parameters for bridges of Series 4, $\theta_L=3\%$

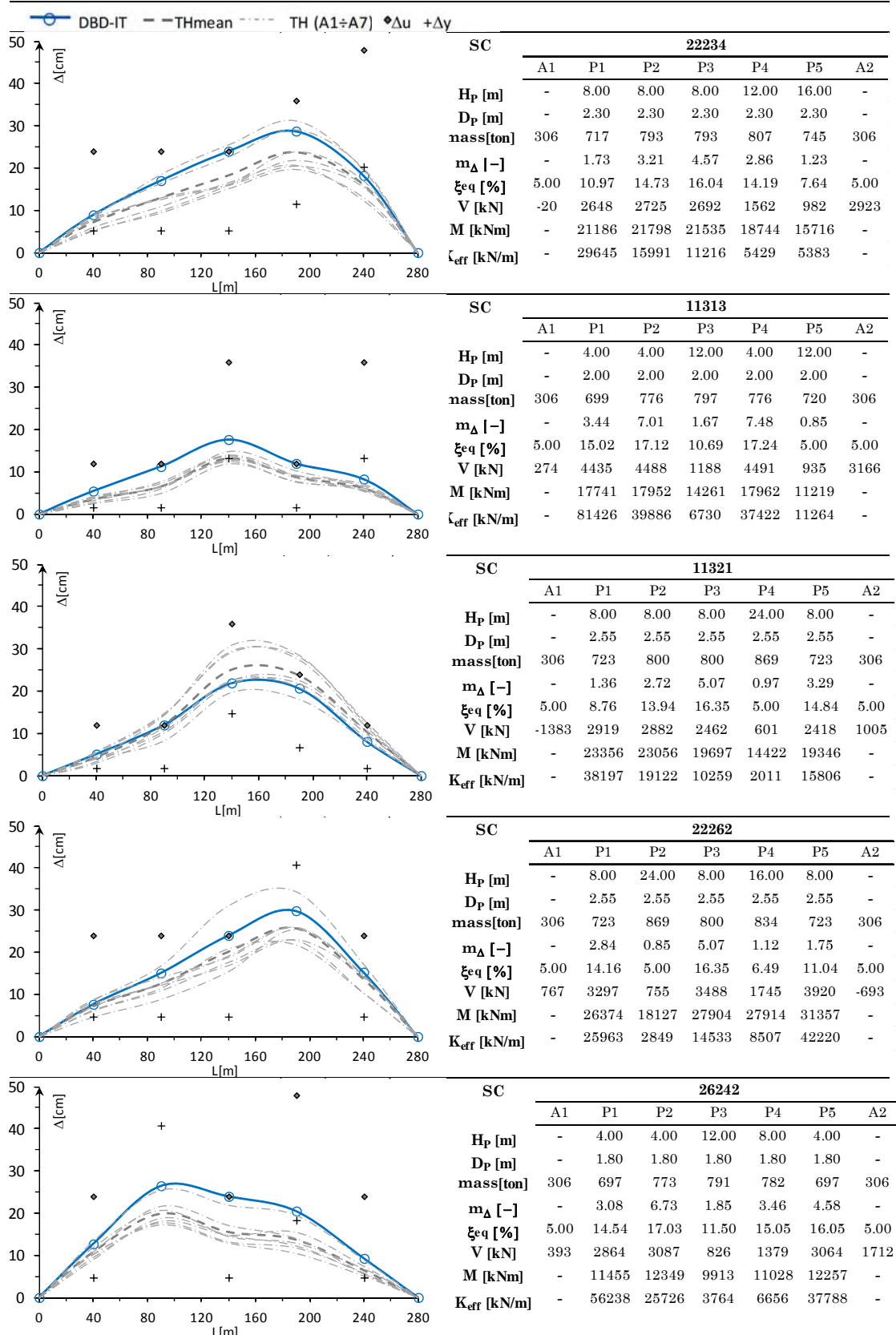
	M_{eff} [ton]	H_{eff} [m]	$\Delta^{\text{d,eff}}$ [m]	$\Delta_{y,\text{eff}}$ [m]	$\mu_{\text{D,eff}}$ [-]	ξ_{eff} [%]	T_{eff} [s]	K_{eff} [kN/m]	V_{base} [kN]	x [%]
PRC132	3379	10.03	0.25	0.188	1.33	8.48	1.38	69959	17886	51.9
PRC133	3390	11.15	0.25	0.201	1.24	7.77	1.35	73530	18805	56.8
PRC123	3403	9.38	0.24	0.174	1.37	8.79	1.33	75945	18488	56.9
SC132	2262	10.20	0.30	0.170	1.77	11.17	1.82	26912	8424	29.2
SC133	2272	11.44	0.33	0.201	1.64	10.50	1.95	23664	8091	33.0
SC123	2321	9.62	0.25	0.152	1.63	10.44	1.47	42601	10851	30.9
SC224	2438	11.61	0.25	0.161	1.53	9.89	1.43	47075	11839	35.0
SC324	2483	12.46	0.24	0.170	1.44	9.29	1.39	50927	12651	36.4
PRC22234	5471	11.86	0.26	0.151	1.75	11.04	1.59	85732	23159	27.5
PRC11313	5318	8.95	0.17	0.093	1.85	11.50	1.06	187340	32928	27.2
PRC11321	5231	14.57	0.26	0.128	2.05	12.23	1.64	76585	20585	12.1
PRC22262	5434	15.79	0.25	0.132	1.92	11.76	1.56	88339	22759	10.7
PRC26242	5054	9.08	0.22	0.119	1.81	11.31	1.31	116248	25628	24.8
SC22234	3700	12.21	0.30	0.160	1.86	11.54	1.82	43864	13512	21.5
SC11313	3627	9.31	0.19	0.092	2.11	12.43	1.22	95553	18977	18.1
SC11321	3292	15.67	0.31	0.144	2.14	12.53	1.95	34281	10905	-3.5
SC22262	3593	16.47	0.28	0.145	1.96	11.93	1.76	45567	13278	0.6
SC26242	3355	9.27	0.25	0.112	2.27	12.90	1.61	50786	13324	15.8

Tab. A.8 – DBD-DEM results vs TH verification for bridges of Series 4, $\theta_L=3\%$









APPENDIX B

PARAMETRIC STUDY FOR CAPACITY AND PIER EFFECTIVE PROPERTIES: SINGLE AND MULTIPLE BENT RECTANGULAR PIERS AND WALL PIERS

B.1 RECTANGULAR PIERS

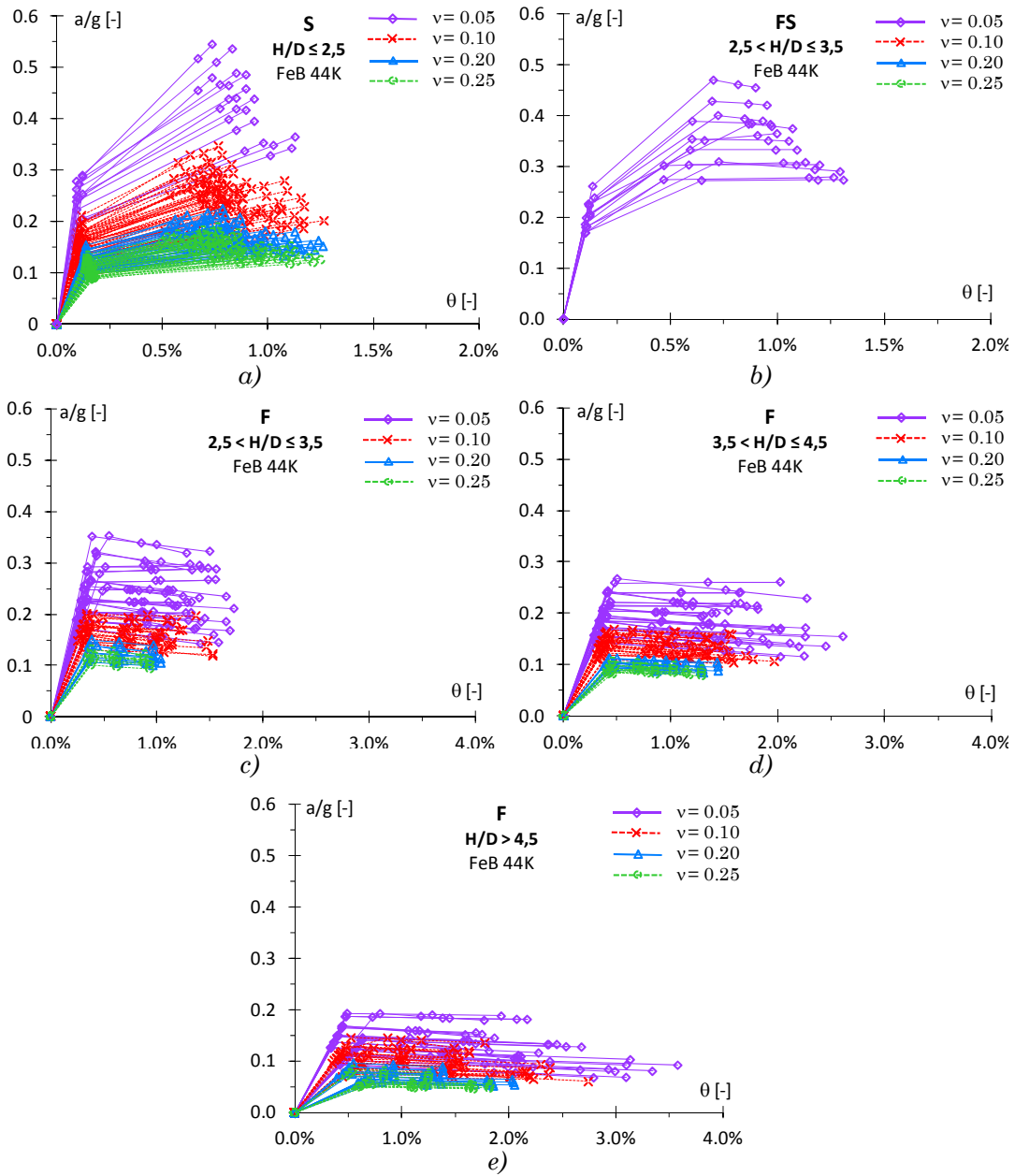


Fig. A.1 – Single bent rectangular piers: adimensional capacity curves (resistant acceleration vs drift): a) shear (S) piers, b) shear flexure (FS) piers, c),d),e) flexure (F) piers

B.1 WALL PIERS

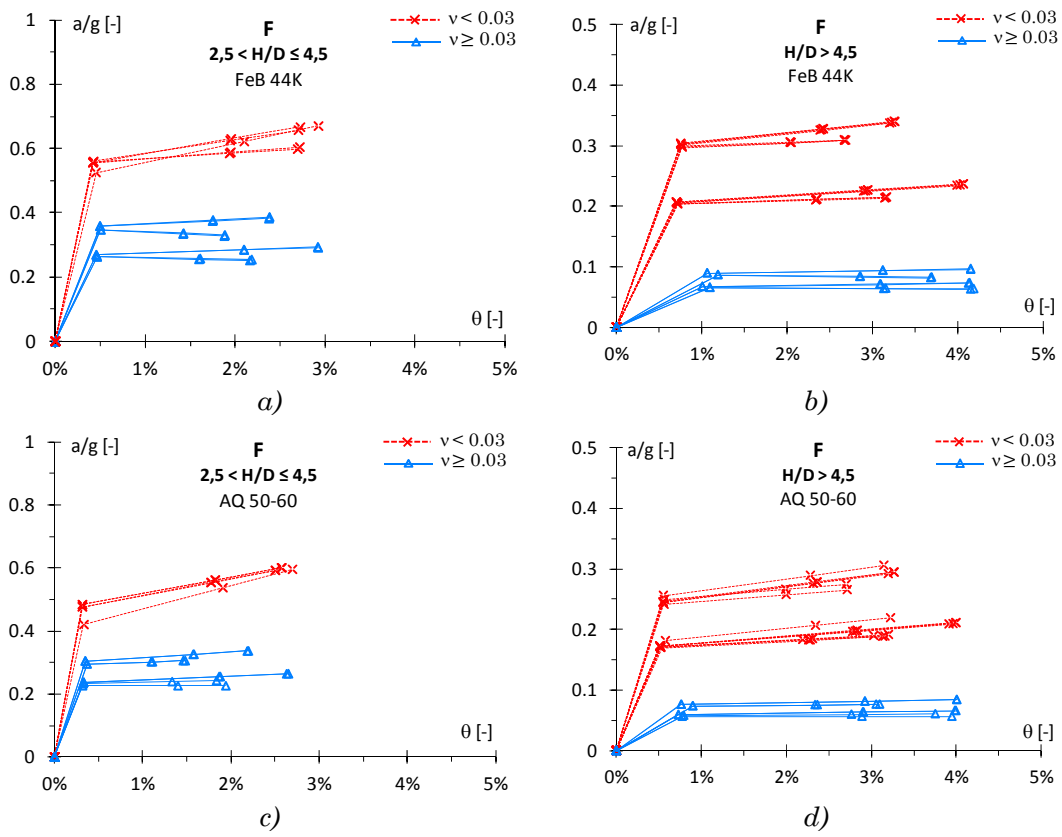


Fig. A.2 – Wall piers: adimensional capacity curves (resistant acceleration vs drift). a) shear (S) piers, b) shear flexure (FS) piers, c),d),e) flexure (F) piers

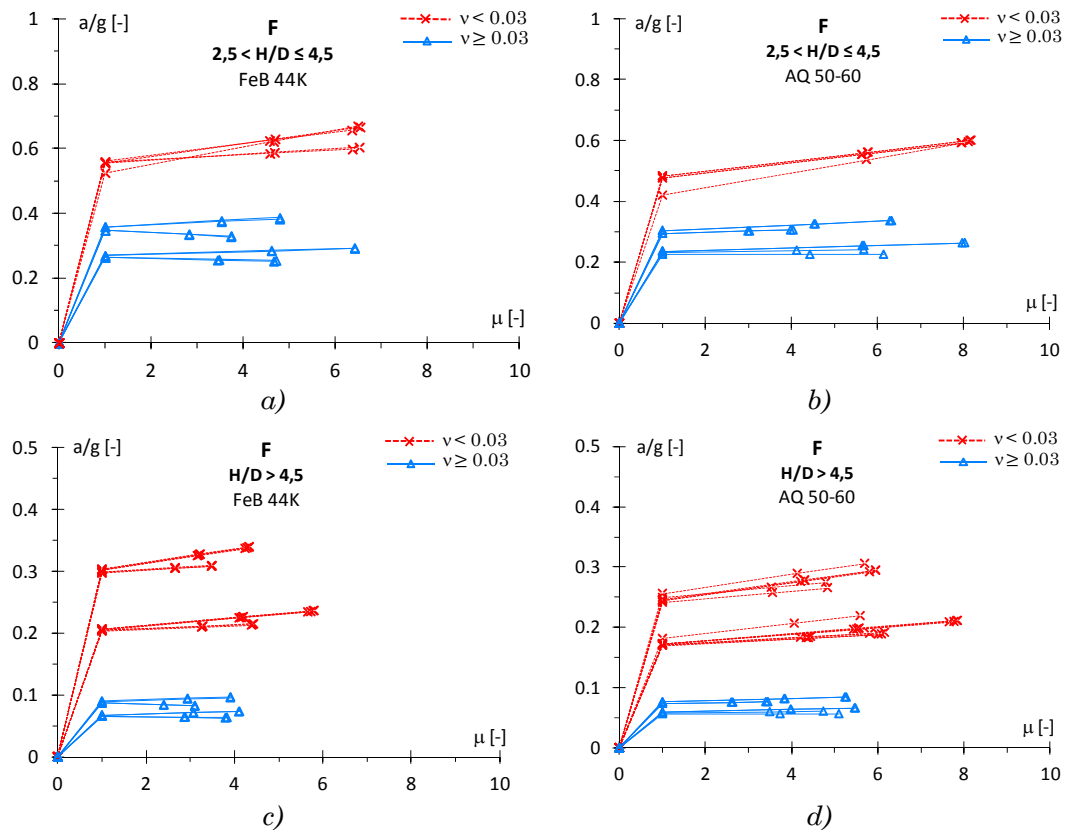


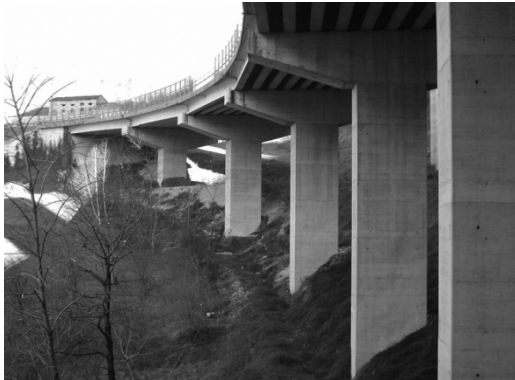
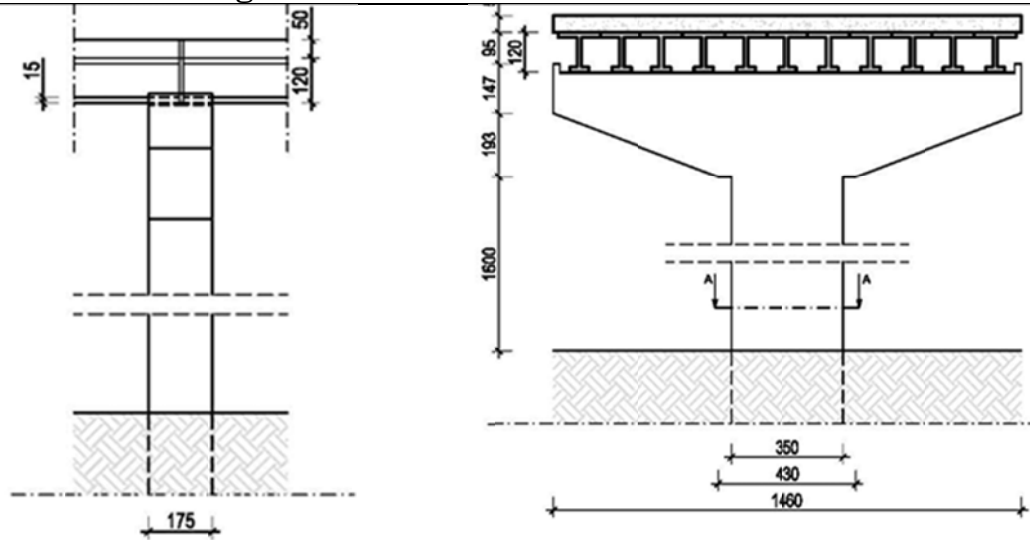
Fig. A.3 – Wall piers: adimensional capacity curves (resistant acceleration vs displacement ductility). a), b), c), d) Flexure (F) piers

APPENDIX C

VENETO REGION (VR) BRIDGE STOCK

C.1 REFERENCE BRIDGE STRUCTURES

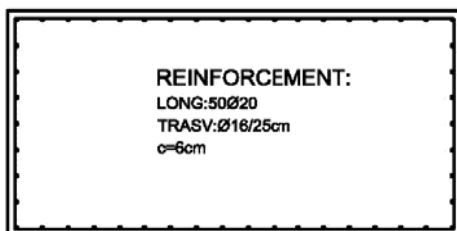
RBs1- Botteon Bridge-



LOCATION

N:	46° 02' 18"	[grad]
E:	12° 18' 35"	[grad]
City	Fadalto	[-]
Province	Treviso	[-]
Road	S.S. 51	[-]
Km	[-]	[km]

SECTION A-A



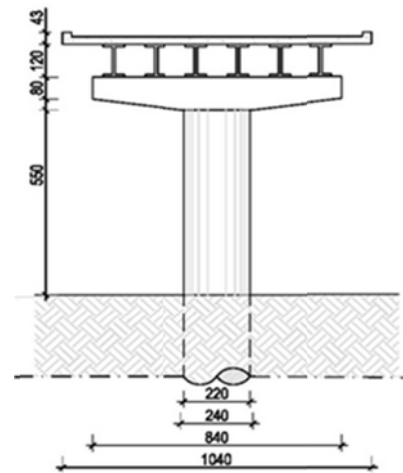
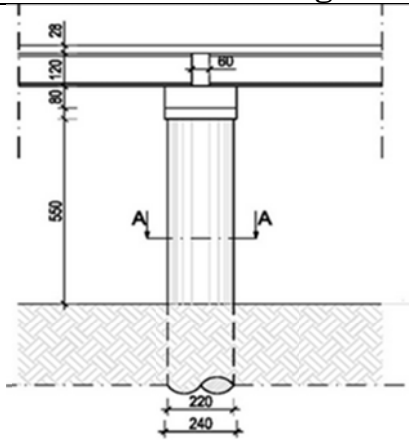
PIER

Pier Type	Single Bent	[-]
No. columns	1	[-]
BT	3.50	[m]
BL	1.75	[m]
H	16	[m]
Fcm	32.90	[MPa]
Reinf. Steel	FeB44k	[-]
Transv. Reinf.	Ø16/25cm	[-]
Long. Reinf.	50Ø20	[-]

DECK

Span Length	24.00	[m]
n° Span	7	[-]
Width	14.6	[m]
Material	DPC	[-]
Deck mass on pier	470	[t]
StaticScheme	M_SIMPLY	

RBs2- Rio Ghisel Bridge-



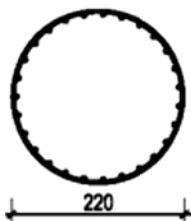
LOCATION

N:	11° 58' 39"	[grad]
E:	46° 22' 60"	[grad]
City	Cencenighe	[-]
Province	Belluno	[-]
Road	S.R. 203	[-]
Km	39+056	[km]

PIER

Pier Type	Single Bent	[-]
No. columns	1	[-]
D	2.20	[m]
H	6.50	[m]
Fcm	40.92	[MPa]
Reinf. Steel	Aq 50-60	[-]
Transv. Reinf.	Ø10/25cm	[-]
Long. Reinf.	20Ø25	[-]

SECTION A-A

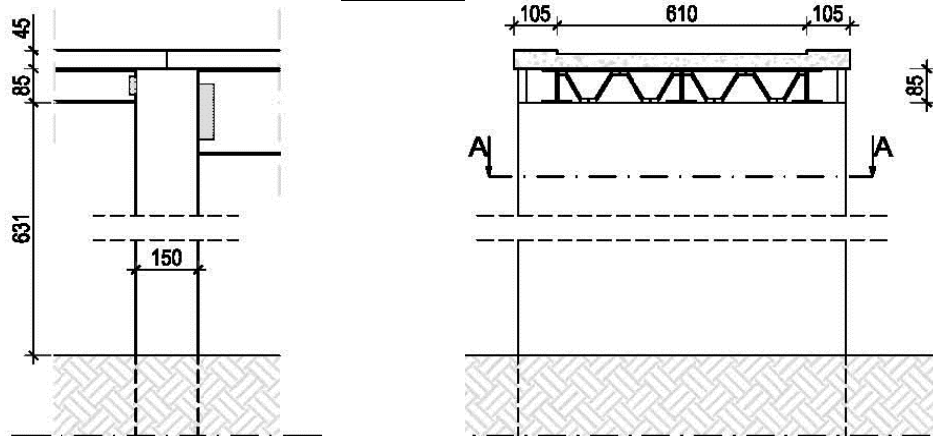


REINFORCEMENT:
LONG: 27Ø16
TRASV: Ø16/25cm
s=4cm

DECK

Span Length	16.40	[m]
n° Span	5	[-]
Width	10.00	[m]
Material	DPC	[-]
Deck mass on pier	360	[t]
StaticScheme	M_SIMPLE	

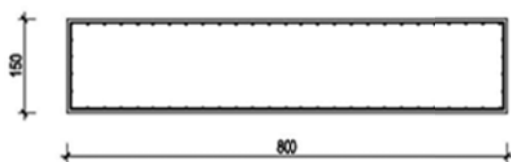
RBs3- Frison Bridge-



LOCATION

N:	46° 32' 04"	[grad]
E:	12° 35' 56"	[grad]
City	S. Stefano di Cadore	[-]
Province	Belluno	[-]
Road	S.R. 465	[-]
Km	4+200	[km]

SECTION A-A



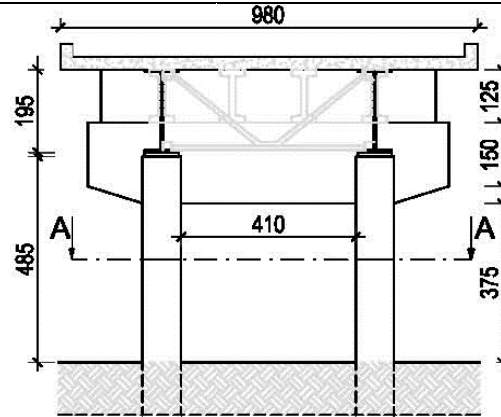
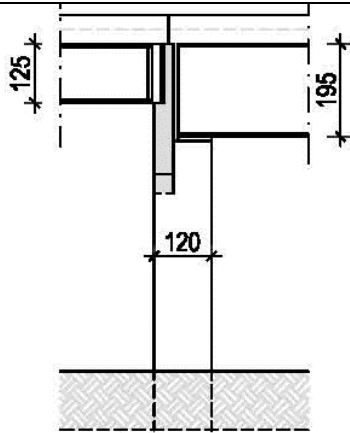
PIER

Pier Type	Wall	[-]
BT	8.00	[m]
BL	1.50	[m]
H	14.80	[m]
Fcm	24.23	[MPa]
Reinf. Steel	Aq 50-60	[-]
Transv. Reinf.	Ø12/30cm	[-]
Long. Reinf.	62Ø20	[-]

DECK

Span Length	48.6	[m]
n° Span	2-3	[-]
Width	8.00	[m]
Material	DCS	[-]
Deck mass on pier	320	[t]
StaticScheme	M_SIMPLE	

RBs4- Cavalcavia A27 Bridge-



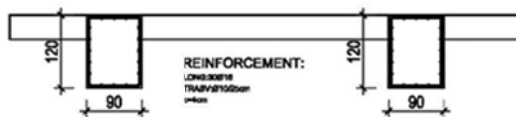
LOCATION

N:	45° 38' 52"	[grad]
E:	12° 18' 60"	[grad]
City	Silea	[-]
Province	Treviso	[-]
Road	S.R. 89	[-]
Km	2+778	[km]

PIER

Pier Type	Multiple Bent	[-]
No. of columns	2	
BT	0.90	[m]
BL	0.90	[m]
H	3.75	[m]
Fcm	26.14	[MPa]
Reinf. Steel	FeB44k	[-]
Transv. Reinf.	Ø12/30cm	[-]
Long. Reinf.	13Ø20	[-]

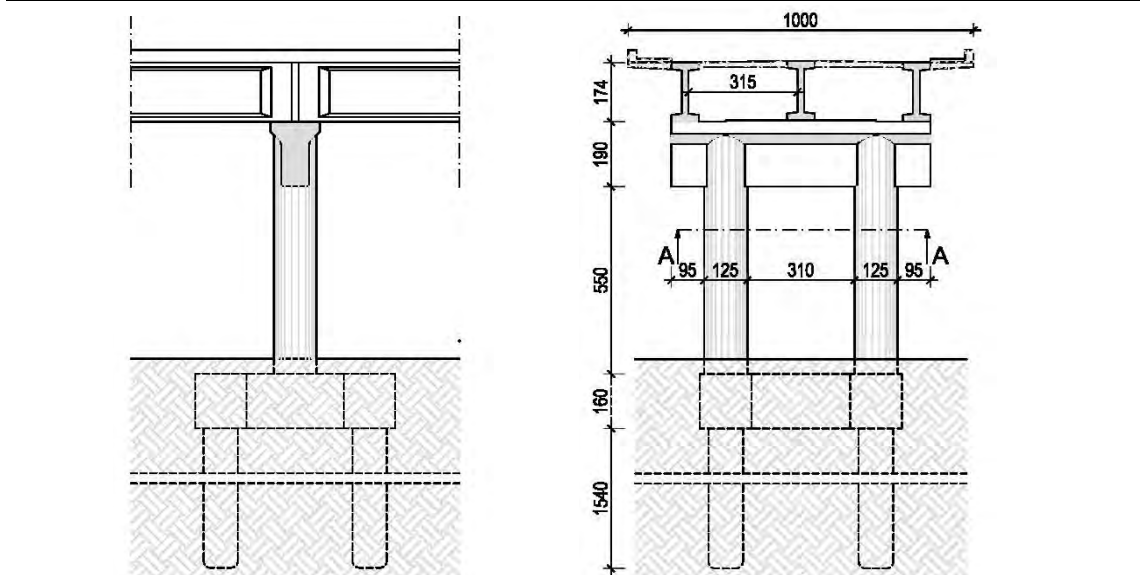
SECTION A-A



DECK

Span Length	37.50	[m]
n° Span	3	[-]
Width	10.00	[m]
Material	DCS	[-]
Deck mass on pier	290	[t]
StaticScheme	M_SIMPLE	

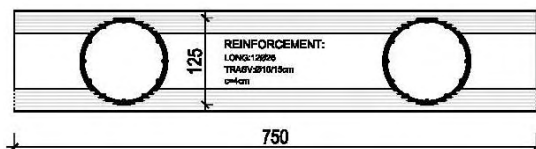
RBS5- Campelli Bridge-



LOCATION

N:	46° 16' 04"	[grad]
E:	12° 18' 27"	[grad]
City	Longarone	[-]
Province	Belluno	[-]
Road	S.P. 251	[-]
Km	103+750	[km]

SECTION A-A



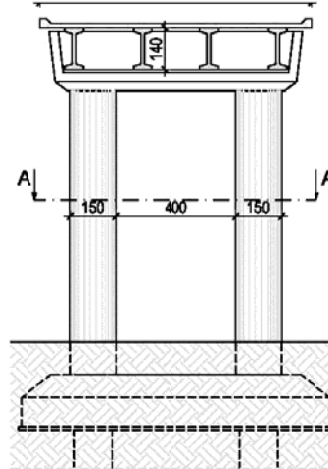
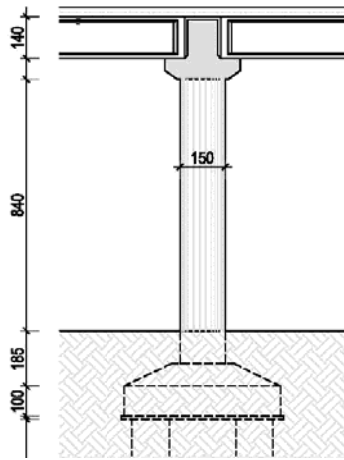
PIER

Pier Type	Multiple Bent	[-]
No. of columns	2	[-]
D	1.25	[m]
H	5.50	[m]
Fcm	64.11	[MPa]
Reinf. Steel	Aq 50-60	[-]
Transv. Reinf.	Ø10/15cm	[-]
Long. Reinf.	12Ø26	[-]

DECK

Span Length	30.33	[m]
n° Span	8	[-]
Width	9.00	[m]
Material	DPC	[-]
Deck mass on pier	312	[t]
StaticScheme	M_SIMPLE	

RBs6- Fener Bridge-



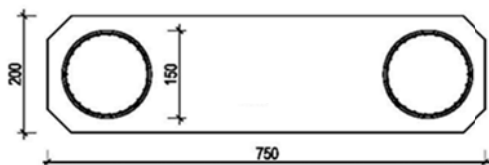
LOCATION

N:	45° 53' 59"	[grad]
E:	11° 56' 52"	[grad]
City	Alano di Piave	[-]
Province	Belluno	[-]
Road	S.P. 32	[-]
Km	0+429	[km]

PIER

Pier Type	Multiple Bent	[-]
No. of columns	2	
BT	1.50	[m]
BL	9.50	[m]
H	51.72	[m]
Fcm	Aq 50-60	[MPa]
Reinf. Steel	Ø10/20 cm	[-]
Transv. Reinf.	22Ø20	[-]
Long. Reinf.	1.50	[-]

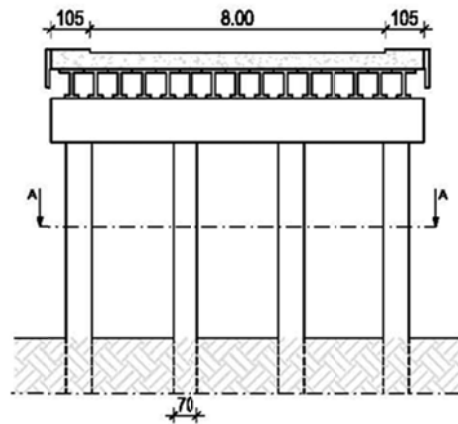
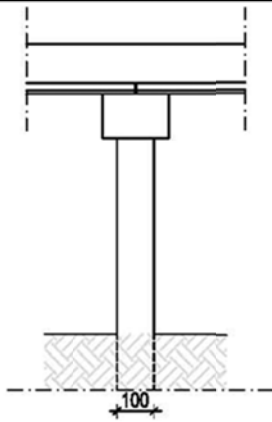
SECTION A-A



DECK

Span Length	23.73	[m]
n° Span	21	[-]
Width	9.00	[m]
Material	DPC	[-]
Deck mass on pier	320	[t]
StaticScheme	M_SIMPLE	

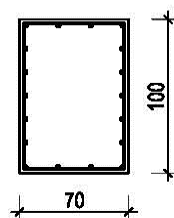
RBs7- Schiavonesca Bridge-



LOCATION

N:	45° 46' 49"	[grad]
E:	12° 04' 02"	[grad]
City	Montebelluna	[-]
Province	Treviso	[-]
Road	S.R. 348	[-]
Km	17+710	[km]

SECTION A-A



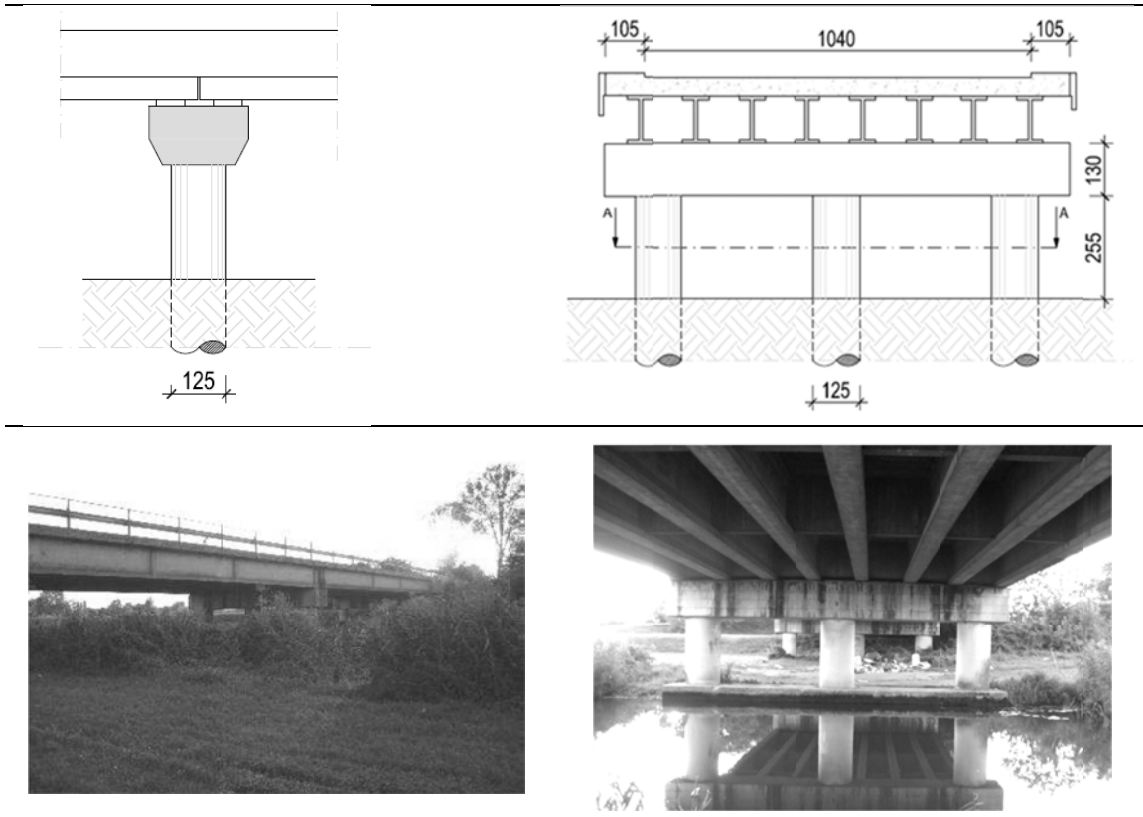
PIER

Pier Type	Multiple Bent	[-]
No. of columns	4	
BT	0.70	[m]
BL	1.00	[m]
H	5.33	[m]
Fcm	28.73	[MPa]
Reinf. Steel	FeB44k	[-]
Transv. Reinf.	Ø10/20 cm	[-]
Long. Reinf.	18Ø20	[-]

DECK

Span Length	16.14	[m]
n° Span	3	[-]
Width	10.00	[m]
Material	DPC	[-]
Deck mass on pier	225	[t]
StaticScheme	M_SIMPLE	

RBs8- Reghena Bridge-



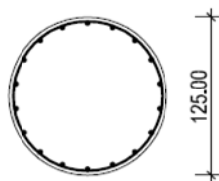
LOCATION

N:	45° 46' 48"	[grad]
E:	12° 48' 26"	[grad]
City	Portogruaro	[-]
Province	Treviso	[-]
Road	S.R. 53	[-]
Km	113+712	[km]

PIER

Pier Type	Multiple Bent	[-]
No. of columns	3	[m]
D	1.25	[m]
H	22,20	[m]
Fcm	FeB44k	[MPa]
Reinf. Steel	Ø10/25cm	[-]
Transv. Reinf.	28Ø20	[-]
Long. Reinf.	1.25	[-]

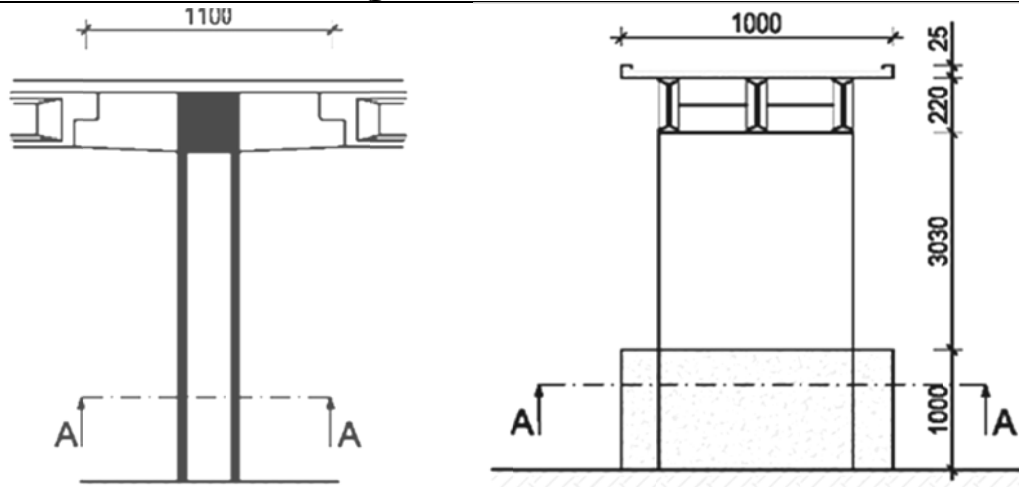
SECTION A-A



DECK

Span Length	24	[m]
n° Span	3	[-]
Width	12.5	[m]
Material	DPC	[-]
Deck mass on pier	470	[t]
StaticScheme	M_SIMPLE	

RBs9- Fante d'Italia Bridge-



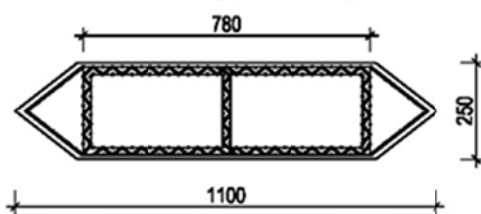
LOCATION

N:	45° 55' 48"	[grad]
E:	11° 56' 28"	[grad]
City	Quero	[-]
Province	Belluno	[-]
Road	S.P. 1 bis	[-]
Km	16+078	[km]

PIER

Pier Type	Single Bent	[-]
No. of columns	1	[-]
BT	7.80	[m]
BL	2.50	[m]
H	40.30	[m]
Fcm	28.04	[MPa]
Reinf. Steel	Aq 50-60	[-]
Transv. Reinf.	Ø8/20cm	[-]
Long. Reinf.	161Ø14	[-]

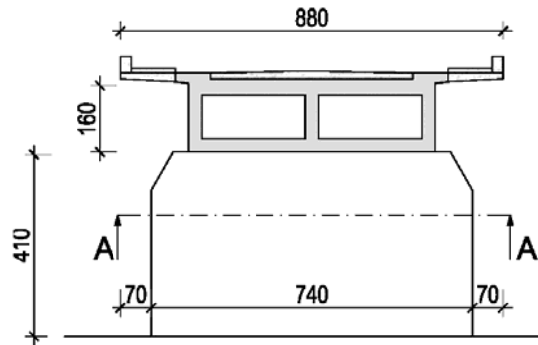
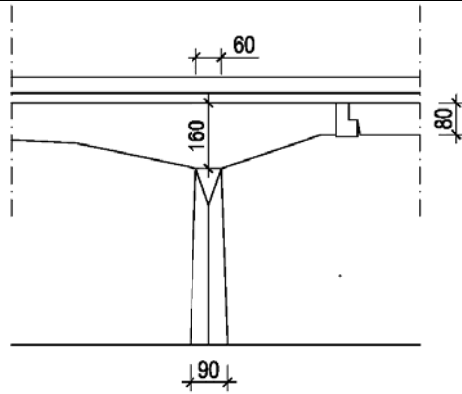
SECTION A-A



DECK

Span Length	34.50	[m]
n° Span	13	[-]
Width	10.00	[m]
Material	DPC	[-]
Deck mass on pier	414	[t]
StaticScheme	GERBER	

RBs10- Canal Bianco Bridge-

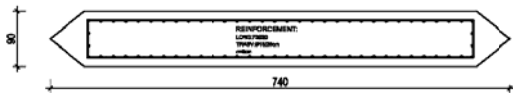


LOCATION

N:	45° 02' 59"	[grad]
E:	11° 24' 27"	[grad]
City	Ceneselli	[-]
Province	Rovigo	[-]
Road	S.R. 482	[-]
Km	59+831	[km]

SECTION A-A

SECTION A-A



PIER

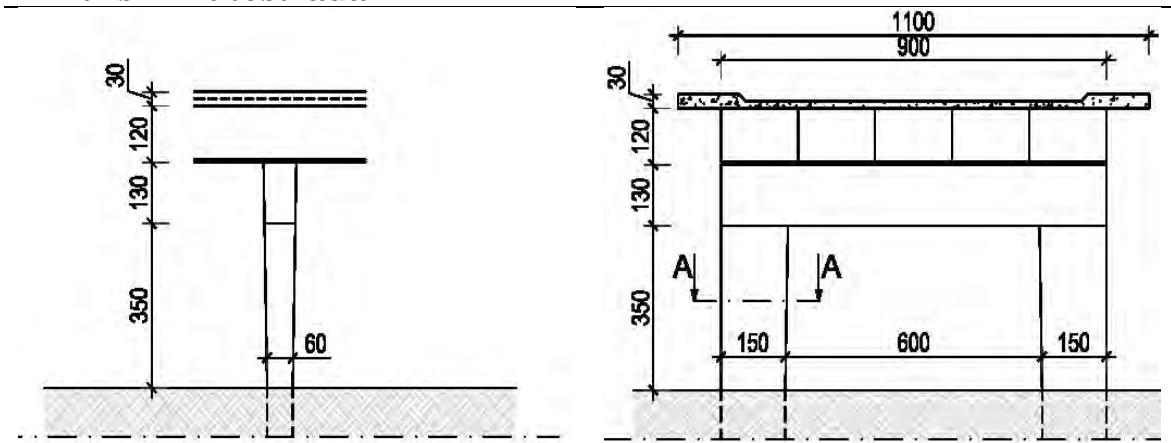
Pier Type	Wall	[-]
No. of columns	1	
BT	7.40	[m]
BL	0.90	[m]
H	4.10	[m]
Fcm	39.01	[MPa]
Reinf. Steel	Aq50	[-]
Transv. Reinf.	Ø16/25	[-]
Long. Reinf.	70Ø20	[-]

DECK

Span Length	31.35	[m]
n° Span	2-3	[-]
Width	10.00	[m]
Material	DC	[-]
Deck mass on pier	520	[t]

StaticScheme GERBER

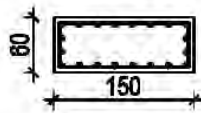
RBs11-Autostrada A4



LOCATION

N:	45° 28' 45"	[grad]
E:	11° 42' 16"	[grad]
Country	Grisignano Zocco	[-]
Province	Vicenza	[-]
Highway	S.P. 21	[-]
Km	4+846	[km]

SECTION A-A



REINFORCEMENT:

LONG: 20Ø18
TRANS: Ø12/20cm
c=8cm

PIER

n° trasv. Pier	2	[-]
Pier Type	PF2-SR	[-]
BT	1.50	[m]
BL	0.60	[m]
H	4.80	[m]
Fcm	37.05	[Mpa]
Reinf. Steel	FeB44k	[-]
Transv. Reinf.	Ø12/20cm	[-]
Long. Reinf.	20Ø18	[-]

DECK

Span Length	10.20-36.40	[m]
n° Span	2-3 (3)	[-]
Width	11.00	[m]
Material	DPC	[-]
Mass	382.26	[t]

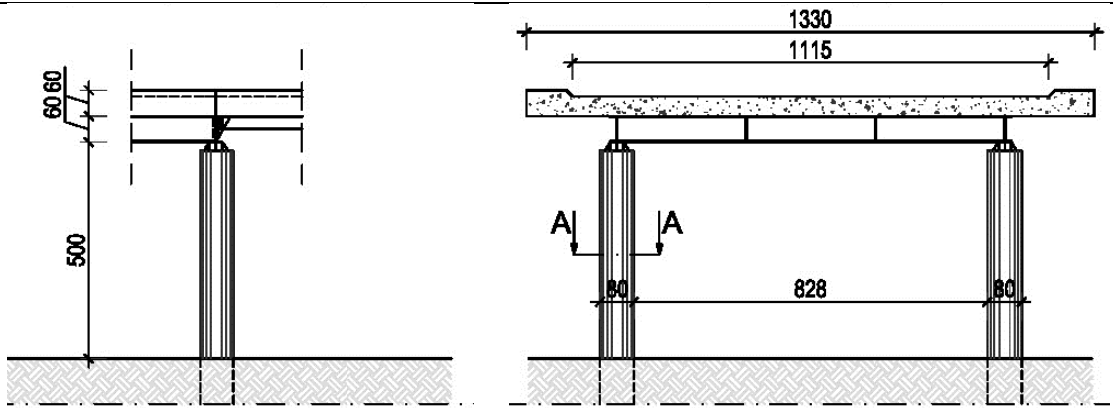
BRIGDE

StaticScheme	M_CONT	[-]
--------------	--------	-----

BEARING

Type	NEO	[-]
------	-----	-----

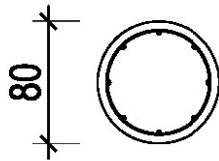
RBs12-Cavalcavia A13



LOCATION

N:	44° 55' 21"	[grad]
E:	11° 35' 24"	[grad]
Country	Occhiobello	[-]
Province	Rovigo	[-]
Highway	S.R. 06	[-]
Km	4+400	[km]

SECTION A-A



REINFORCEMENT:
LONG:8Ø22
TRANS:Ø12/25cm
c=6cm

PIER

n° trasv. Pier	2	[-]
Pier Type	PF2-SC	[-]
BT	0.80	[m]
BL	0.80	[m]
H	5.00	[m]
Fcm	26.14	[Mpa]
Reinf. Steel	Aq50	[-]
Transv. Reinf.	Ø12/25cm	[-]
Long. Reinf.	8Ø22	[-]

DECK

Span Length	8.00-26.10	[m]
n° Span	2-3 (3)	[-]
Width	9.40	[m]
Material	DPC	[-]
Mass	303.30	[t]

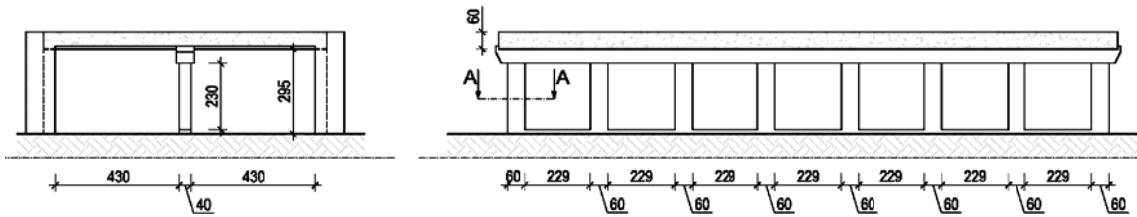
BRIGDE

StaticScheme	M_CONT	[-]
--------------	--------	-----

BEARING

Type	DEV	[-]
------	-----	-----

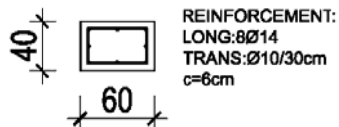
RBs13-Cavalcavia zona città



LOCATION

N:	45° 26' 47"	[grad]
E:	10° 52' 46"	[grad]
Country	Bussolengo	[-]
Province	Verona	[-]
Highway	S.R. 11	[-]
Km	292+800	[km]

SECTION A-A



PIER

n° trasv. Pier	8	[-]
Pier Type	PFM-SR	[-]
BT	0.60	[m]
BL	0.40	[m]
H	2.30	[m]
Fcm	31.21	[Mpa]
Reinf. Steel	FeB44k	[-]
Transv. Reinf.	Ø10/30cm	[-]
Long. Reinf.	8Ø14	[-]

DECK

Span Length	4.30	[m]
n° Span	2-3 (2)	[-]
Width	20.80	[m]
Material	DC	[-]
Mass	1089	[t]

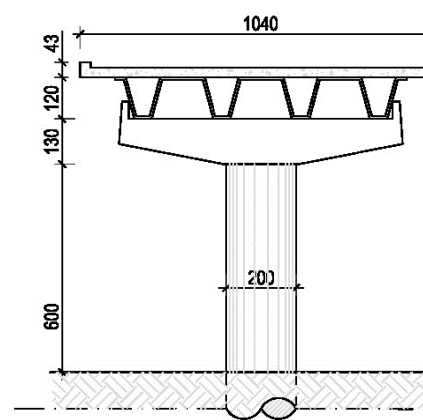
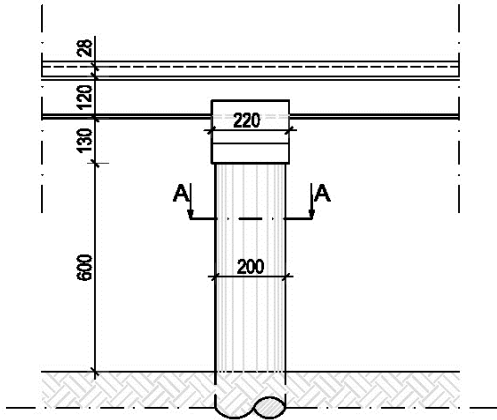
BRIGDE

StaticScheme	M_CONT	[-]
--------------	--------	-----

BEARING

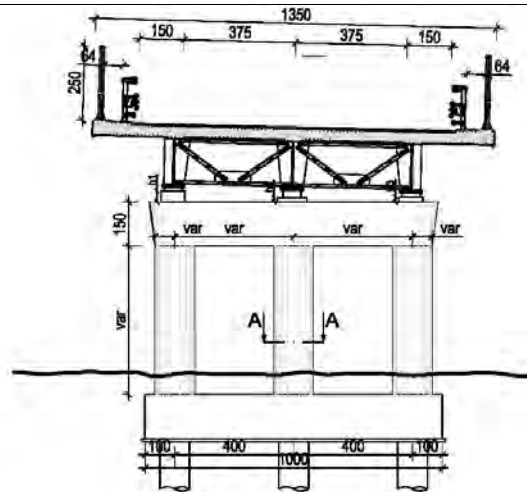
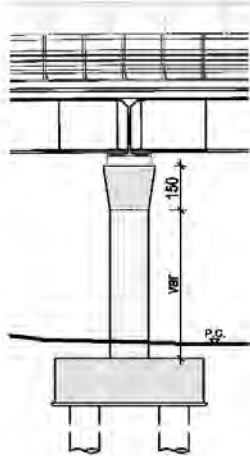
Type	FRI	[-]
------	-----	-----

RBs14-Cavalcaferrovia FF.SS.



LOCATION			PIER		
N:	45° 39' 46"	[grad]	n° trasv. Pier	1	[-]
E:	11° 55' 02"	[grad]	Pier Type	PSC-SC	[-]
Country	Castelfranco Veneto	[-]	BT	2.00	[m]
Province	Treviso	[-]	BL	2.00	[m]
Highway	S.R. 245	[-]	H	6	[m]
Km	2+486	[km]	Fcm	29.55	[Mpa]
SECTION A-A			Reinf. Steel	FeB44k	[-]
			Transv. Reinf.	Ø20/25cm	[-]
			Long. Reinf.	24Ø20	[-]
			DECK		
			Span Length	33	[m]
			n° Span	M (12)	[-]
			Width	10.40	[m]
			Material	DPC	[-]
			Mass	1089	[t]
			BRIGDE		
			StaticScheme	M_CONT	[-]
			BEARING		
			Type	DEV	[-]

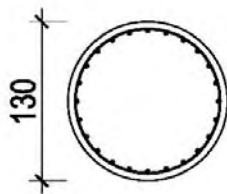
RBs17-Cavalcavia Silea



LOCATION

N:	45° 39' 25	[grad]
E:	12° 17' 06	[grad]
Country	Silea	[-]
Province	Treviso	[-]
Highway	S.R. 53	[-]
Km	nd	[km]

SECTION A-A



REINFORCEMENT:
LONG:30Ø24
TRANS:Ø10/10cm
c=6cm

PIER

n° trasv. Pier	3	[-]
Pier Type	PFM-SC	[-]
BT	1.30	[m]
BL	1.30	[m]
H	4.00-5.00	[m]
Fcm	37.05	[Mpa]
Reinf. Steel	FeB44k	[-]
Transv. Reinf.	Ø10/10cm	[-]
Long. Reinf.	30Ø24	[-]

DECK

Span Length	40.00	[m]
n° Span	M (4)	[-]
Width	13.50	[m]
Material	DCS	[-]
Mass	550.46	[t]

BRIGDE

StaticScheme	M_CONT	[-]
--------------	--------	-----

BEARING

Type	DEV	[-]
------	-----	-----